A Fundamental Study of Turbulence and Turbulent Mixing in a Small Subtropical Estuary

A thesis submitted for the degree of Doctor of Philosophy at the University of Queensland in "September" "2007"

Mark Trevethan

School of Engineering

The degree has been conferred when the Thesis has been accepted by the UQ Library

STATEMENT OF ORIGINALITY

The work presented in this thesis is, to the best of my knowledge, original, except as acknowledged in text. The candidate co-authored all publications listed, with these publications being relevant to the Thesis, but not forming part of it. The material has not been submitted, either in whole or in part, for a degree at any university.
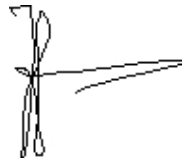
Candidate: Mark Trevethan

Division of Civil Engineering, The University of Queensland, Brisbane, QLD 4072, Australia

Principle Supervisor: Professor Hubert Chanson

Division of Civil Engineering, The University of Queensland, Brisbane, QLD 4072, Australia

LIST OF PUBLICATIONS

(Derived from this PhD Project)

Journal papers

Chanson, H. and Trevethan, M. (2007) − Turbulence in small sub-tropical estuary with semi-diurnal tides − Pearl River, Renmin Zhujiang, No. 1, Feb., pp. 16-22 (ISSN 1001-9235) (in Chinese)

Trevethan, M., Chanson, H. and Takeuchi, M. (2007) − Continuous high-frequency turbulence and suspended sediment concentration measurements in an upper estuary − Estuarine, Coastal and Shelf Science, 73(1-2), pp. 341-350

Trevethan, M. and Chanson, H. (2007) − Detailed measurements during a transient front in a small subtropical estuary − Estuarine, Coastal and Shelf Science, 73(3-4), pp. 735-742

Chanson, H., Takeuchi, M. and Trevethan, M. (2007) − Using turbidity and acoustic backscatter intensity as surrogate measures of suspended sediment concentration in a small sub-tropical estuary − Journal of Environmental Management, Vol. (DOI: 10.1016/ j.jenvman.2007.07.009) (ISSN 0301-4797)

Chanson, H., Trevethan, M. and Koch, C. (2007) − Turbulence measurements with acoustic Doppler velocimeters: Discussion − Journal of Hydraulic Engineering ASCE, 132(11), pp. 1283-1286, (ISSN 0733-9429)

Technical reports (refereed)

Trevethan, M., Chanson, H. and Brown, R. (2006) − Two series of detailed turbulence measurements in a small subtropical estuarine system − Report No. CH58/06, Division of Civil Engineering, The University of Queensland, Brisbane, Australia (ISBN 1864998520)

Chanson, H., Takeuchi, M. and Trevethan, M. (2006) − Using turbidity and acoustic backscatter intensity as surrogate measures of suspended sediment concentration. Application to a sub-tropical estuary (Eprapah Creek) − Report No. CH60/06, Division of Civil Engineering, The University of Queensland, Brisbane, Australia (ISBN 1864998628)

Conference papers (refereed)

Chanson, H., Trevethan, M. and Aoki, S. (2005) – Acoustic Doppler velocimetry (ADV) in a small estuarine system. Field experience and "de-spiking" – Proceedings of 2005 IAHR Congress Seoul Korea, Sept. 2005, pp. 3954-3966

Chanson, H. and Trevethan, M. (2006) – Turbulence in small sub-tropical estuary with semi-diurnal tides – Proceedings of 2nd Intl Conf. on Estuaries & Coasts (ICEC-2006), Guangzhou, Guangdong Province, China, November 28-30, Invited paper, Guangdong Economy Publ., Vol. I, pp. 140-151, (ISBN 7-80728-422-6)

Chanson, H., Takeuchi, M. and Trevethan, M. (2007) – High-frequency suspended sediment flux measurements in a small estuary – Proceedings of 6th International Conference on Multiphase Flow ICMF 2007, Leipzig, Germany, July 9-13, (Ed. Sommerfield, M.) Session 7, Paper No. S7_Mon_C_S7_Mon_C_5, 12 pages (CD-ROM) (ISBN 978-3-86010-913-7)

Chanson, H., Trevethan M. and Takeuchi, M. (2007) – High-frequency turbulence and suspended sediment flux measurements in an upper estuarine zone – Proceedings of 32nd IAHR Biennial Congress, Venice, Italy, (Ed. Di Silvio, G. and Lanzoni, S.) Topic D1.b, 10 pages (CD-ROM)

ABSTRACT

The flow of water in natural systems such as estuaries is a turbulent process, with Reynolds numbers greater than 10^5. Understanding the turbulence properties of an estuary is important for the investigation of mixing, dispersion and sediment transport within an estuary. This study investigates the turbulence properties in a typical small subtropical estuary (Eprapah Creek, Australia). Small coastal plain type estuaries constitute approximately 60 % of all estuaries in Australia, yet no thorough study of the turbulence properties of this type of estuary has been conducted.

To date only a limited number of turbulence studies in estuaries have been undertaken. One reason for this was the lack of appropriate instrumentation to collect turbulent velocity measurements with fine spatial and temporal resolutions. This is especially true of turbulence studies in small estuaries, with the majority of published turbulence studies being performed in relatively large systems. Previous studies of turbulence in estuaries were mostly conducted for relatively short periods (up to 6 hours) and by collecting data over long periods in bursts of several minutes. The present study showed that acoustic Doppler velocimetry (ADV) was well suited for the measurement of turbulence properties in small estuarine systems.

A unique aspect of this study was the continuous collection of turbulence data at high frequency ($f_{scan} \geq 25$ Hz) for relatively long periods (T_{study} up to 50 hours). This approach characterised the estuarine turbulence properties for up to two complete tidal cycles. The data analysis showed that continuous collection of high frequency turbulence data was essential to accurately characterise the rapid fluctuations of turbulence in an estuary.

The field data showed that the turbulence flow properties were highly fluctuating in a small estuary. All turbulence properties exhibited large and rapid fluctuations over the investigation period of each field study. The variations in time scales were related to both the instantaneous local flow properties and the tidal fluctuations. Some long period oscillations observed in the water level and velocity data also had a significant impact on the turbulence properties. These long period oscillations had periods similar to resonance periods generated both internally in and externally to the creek.

Many turbulence properties showed an asymmetrical response to the tidal forcing, especially under spring tidal conditions. Large turbulent velocity fluctuations were, however, observed throughout all investigation periods, including during the slack tides. Substantial fluctuations in the normal and tangential Reynolds stresses were observed in the middle and upper estuarine zones. The turbulent velocity data showed some non-Gaussian behaviour and the Reynolds stresses were non-Gaussian throughout all investigation periods.

Field data collected mid estuary under spring and neap tidal conditions showed two distinctly different turbulence responses for spring and neap tides. During spring tides, the magnitudes of all turbulence properties were up to an order of magnitude larger than for neap tides. The turbulence properties showed some increased tidal asymmetries under spring tidal conditions. Further two field studies were conducted under similar neap tidal conditions in the middle and upper estuarine zones. A comparison of these two data sets showed that the turbulence properties in the middle and upper estuaries differed substantially. Mid estuary, the magnitude of the turbulence properties were up to an order of magnitude larger than those observed in the upper estuary, thereby indicating that at least three distinct sets of turbulence properties existed in this small subtropical estuary.

This study included some turbulence data collected in a large tidal lake with a restricted entrance (Hamana Lake, Japan). This turbulence data was compared with the data measured in Eprapah Creek. The comparison showed similar tidal patterns in some turbulence properties were observed close to the bed despite the distinct topography and hydrodynamics of the two estuaries. Some of these patterns in turbulence properties were also observed in previous studies of turbulence in estuaries. However, the spring tide data collected in the small estuary showed an increased magnitude of turbulence and a more asymmetrical response than other estuarine turbulence studies.

The ratio of local tidal amplitude and local mean depth a_1/h_1 was used to characterise the local turbulence properties for a certain tidal range. A critical value of the ratio a_1/h_1 was 0.5, corresponding to the local tidal range being equal to the local mean depth. If the tidal range was greater than the local mean depth (i.e. $a_1/h_1 > 0.5$), a more asymmetrical tidal response and some increased turbulence property magnitudes were observed. A comparison of the turbulence properties in two distinct tidal systems (Eprapah Creek and Hamana Lake) showed similar tidal patterns for $a_1/h_1 < 0.5$.

TABLE OF CONTENTS

APPENDIX H   EFFECT OF WIND WAVES ON TURBULENCE DATA

APPENDIX I   INVESTIGATION OF CORRELATION BETWEEN WATER

LIST OF FIGURES

LIST OF TABLES

LIST OF SYMBOLS

<u>Symbols</u>

a_i instantaneous acceleration at a point (m/s^2)

a_l amplitude of tidal variation at experimental site (m)

A_Z vertical acceleration (m/s^2)

AM   acceleration magnitude between data points of vertical acceleration (m/s^2)

AMP   acoustic signal amplitude (counts, 1 count = 0.43 dB)

AVAMP   averaged signal amplitude (counts)

B_{FN} front data replacement buffer size for navigation events (s)

B_{FP} front data replacement buffer size for probe adjustment events (s)

B_{FU} front data replacement buffer size for unknown events (s)

B_{RN} rear data replacement buffer size for navigation events (s)

B_{RP} rear data replacement buffer size for probe adjustment events (s)

B_{RU} rear data replacement buffer size for unknown events (s)

C_D coefficient of friction

C_{EN} navigation event search threshold constant

C_{EP} probe adjustment event search threshold constant

C_{EU} unknown event search threshold constant

d   water depth (m)

d_H depth at extreme high tide (m)

d_L depth at extreme low tide (m)

d_{av} averaged water depth (m)

d_{range} range of water depth variation (m)

d_{50} grain diameter of 50 percentile (m)

E_{peak} peak wave energy (joules)

E_{TK} turbulent kinetic energy (m^2/s^2)

$$E_{TK} = 0.5 * (v_x^2 + v_y^2 + v_z^2)$$

f   frequency (Hz)

f_{scan} scanning frequency (Hz)

f_{waves}	frequency range for which wave-turbulence interaction occurs
g	gravity acceleration (9.80 m/s² in Brisbane) (m/s²)
h_l	mean depth at experimental site (m)
i	parameter direction tensor (x, y, z)
I_B	intensity of ADV signal backscatter
J	data point number
Ku	kurtosis
$Ku(V_x)$	kurtosis of streamwise velocity
$Ku(V_y)$	kurtosis of transverse velocity
$Ku(V_z)$	kurtosis of vertical velocity
$Ku(\rho v_x v_y)$	kurtosis of tangential Reynolds stress $\rho v_x v_y$)
$Ku(\rho v_x v_z)$	kurtosis of tangential Reynolds stress $\rho v_x v_z$
$Ku(\rho v_y v_z)$	kurtosis of tangential Reynolds stress $\rho v_y v_z$
l_m	pseudo mixing length (m)
L	horizontal distance between two topographical landmarks (m)
L	characteristic length scale
N	number of data points in data sample (data points)
q_S	suspended sediment flux per unit area (kg/s/m²)
$\overline{q_S}$	time-averaged suspended sediment flux per unit area (kg/s/m²)
r	polar coordinate representing a turbulence characteristic in polar plot
R	correlation coefficient
R_{ii}	normalised autocorrelation function
Re	Reynolds number
Ri	local Richardson number
R_{vxvy}	correlation coefficient of tangential Reynolds stress $\rho v_x v_z$
	$R_{vxvy} = \overline{v_x v_y} / (v'_x v'_y)$
R_{vxvz}	correlation coefficient of Reynolds stress $\rho v_x v_y$
	$R_{vxvz} = \overline{v_x v_z} / (v'_x v'_z)$
R_{vyvz}	correlation coefficient of Reynolds stress $\rho v_y v_z$
	$R_{vyvz} = \overline{v_y v_z} / (v'_y v'_z)$

$R_{V\xi}(\tau)$ cross-correlation function of velocity and water level data (m^2/s)

$R_{\xi\xi}(\tau)$ auto-correlation function of water level (m^2)

S_{VV} spectrum of velocity (m^2s^{-2}/Hz)

S_{VxVx} spectrum of streamwise velocity (m^2s^{-2}/Hz)

S_{VyVy} spectrum of transverse velocity (m^2s^{-2}/Hz)

S_{VzVz} spectrum of vertical velocity (m^2s^{-2}/Hz)

$S_{V\xi}(\omega)$ co-spectrum of velocity and water level (m^2s^{-1}/Hz)

$S_{\xi\xi}(\omega)$ spectrum of water level (m^2/Hz)

Sk   skewness

$Sk(V_x)$ skewness of streamwise velocity

$Sk(V_y)$ skewness of transverse velocity

$Sk(V_z)$ skewness of vertical velocity

$Sk(\rho v_x v_y)$ skewness of tangential Reynolds stress $\rho v_x v_y$

$Sk(\rho v_x v_z)$ skewness of tangential Reynolds stress $\rho v_x v_z$

$Sk(\rho v_y v_z)$ skewness of tangential Reynolds stress $\rho v_y v_z$

SR_F size of front portion of event search region (s)

SR_R size of rear portion of event search region (s)

SSC   suspended sediment concentration (g/L)

$\overline{SSC}$ time-averaged suspended sediment concentration (g/L)

$SSC^{'}$ standard deviation of suspended sediment concentration (g/L)

SW   statistical search window size (data points)

t   time (s)

T   period (s)

T_E Eulerian integral time scale (s)

T_{Essc} Eulerian integral time scale of suspended sediment concentration (s)

T_{Ex} Eulerian integral time scale of streamwise velocity (s)

T_{Ey} Eulerian integral time scale of transverse velocity (s)

T_{Ez} Eulerian integral time scale of vertical velocity (s)

T_{range} period range of long period oscillation groups (s)

T_{scan} scan duration (s)

T_{study}	duration of field study (s)
TR	tidal range (m)
u	high-pass filtered velocity data used during de-spiking (m/s)
u_i	velocity deviation at a point (m/s)
U	characteristic velocity scale
U_{xy}	horizontal velocity magnitude (m/s)
UC	universal criterion of phase-space thresholding method (m/s)
	$UC = \Lambda_U \, \sigma$
V	instantaneous velocity (m/s)
V_{range}	ADV velocity range setting (m/s)
V_W	wind speed (m/s)
V_x	instantaneous streamwise velocity (m/s)
V_y	instantaneous transverse velocity (m/s)
V_z	instantaneous vertical velocity (m/s)
$\overline{V}$	time-averaged velocity (m/s)
$\overline{V_x}$	time-averaged streamwise velocity (m/s)
$\overline{V_y}$	time-averaged transverse velocity (m/s)
$\overline{V_z}$	time-averaged vertical velocity (m/s)
v	instantaneous turbulent velocity fluctuations (m/s)
	$v = V - \overline{V}$
v_x	instantaneous streamwise turbulent velocity fluctuations (m/s)
v_y	instantaneous transverse turbulent velocity fluctuations (m/s)
v_z	instantaneous vertical turbulent velocity fluctuations (m/s)
v_x'	standard deviation of streamwise velocity (m/s)
v_y'	standard deviation of transverse velocity (m/s)
v_z'	standard deviation of vertical velocity (m/s)
W	width (m)
x	longitudinal (streamwise) distance (m)
y	transverse distance (m)
z	vertical elevation (m)

z_0 grain diameter/30 (m)

z_r vertical elevation of sampling volume above bed (m)

β slope of linear approximation

δt time scale sampling interval (s)

δt_{scan} sampling scan interval (s)

Δu surrogate first derivative of high-pass filtered velocity data (m/s^2)

$\Delta^2 u$ surrogate second derivative of high-pass filtered velocity data (m/s^3)

$\Delta \overline{V_x}$ maximum range of streamwise velocity (m/s)

$\Delta \overline{V_y}$ maximum range of transverse velocity (m/s)

θ Shields parameter

$\overline{\theta}$ time-averaged Shields parameter

κ von Karman constant

λ_a de-spiking acceleration threshold

λ_{EN} threshold value of navigation event search region (m/s)

$$\lambda_{EN} = C_{EN} \; \sigma_{SR(N)}$$

λ_{EP} threshold value of probe adjustment event search region (m/s)

$$\lambda_{EP} = C_{EP} \; \sigma_{SR(P)}$$

λ_{EU} threshold value of unknown event search region (m/s)

$$\lambda_{EU} = C_{EU} \; \sigma_{SS(U)}$$

λ_k de-spiking absolute deviation threshold

Λ_f post-processing high-pass/low-pass filtering threshold (s)

Λ_U universal threshold for phase-space thresholding method

ν kinematic viscosity of water (m^2/s)

ρ density of water (kg/m^3)

$\rho v_x v_y$ instantaneous tangential Reynolds stress (Pa)

$\rho v_x v_z$ instantaneous tangential Reynolds stress (Pa)

$\rho v_y v_z$ instantaneous tangential Reynolds stress (Pa)

$\rho \overline{v_x v_x}$ time-averaged normal streamwise Reynolds stress (Pa)

$\rho \overline{v_x v_y}$ time-averaged tangential Reynolds stress (Pa)

$\rho\overline{v_x v_z}$	time-averaged tangential Reynolds stress (Pa)
$\rho\overline{v_y v_z}$	time-averaged tangential Reynolds stress (Pa)
$(\rho v_x v_y)'$	standard deviation of tangential Reynolds stress (Pa)
$(\rho v_x v_z)'$	standard deviation of tangential Reynolds stress (Pa)
$(\rho v_y v_z)'$	standard deviation of tangential Reynolds stress (Pa)
σ	standard deviation of entire data set being de-spiked (m/s)
$\sigma_{SR(N)}$	standard deviation of the navigation event search region (m/s)
$\sigma_{SR(P)}$	standard deviation of probe adjustment event search region (m/s)
$\sigma_{SS(U)}$	standard deviation of unknown event search region (m/s)
ξ	fluctuations in water level (m)
τ	time lag (s)
τ_b	instantaneous bed shear stress (Pa)
$\overline{\tau_b}$	time-averaged bed shear stress (Pa)
τ_E	Eulerian dissipation time scale (s)
τ_{Ex}	Eulerian dissipation time scale of streamwise velocity (s)
τ_{Ey}	Eulerian dissipation time scale of transverse velocity (s)
τ_{Ez}	Eulerian dissipation time scale of vertical velocity (s)
υ_T	pseudo eddy viscosity (m^2/s)
ω	angular frequency (rad/s)

Subscripts

av	averaged value
x	streamwise direction positive downwards
y	transverse direction positive towards left bank
z	vertical direction positive upwards

Superscripts

T	current induced turbulence data
W	wave induced turbulence data

Abbreviations

ADV	Acoustic Doppler Velocimeter
AHD	Australian Height Datum
AMP	signal amplitude of ADV receiver
AMTD	Australian Middle Thread Distance (upstream from mouth)
AVAMP	average signal amplitude of ADV receivers
BI	bisector of ADV beams
Cond	conductivity
COR	signal correlation of ADV receivers
DO	dissolved oxygen
E	East
EMCM	Electromagnetic Current Meter
EPA	Environmental Protection Agency
HLJ	Hamana Lake Japan
HW	High Water
LDA	Laser Doppler Anemometer
LTS	In-Situ Troll9000 probe
LW	Low Water
max	maximum value
min	minimum value
N	North
NE	navigation event
NL	Noise Level of ADV signal
NTU	Nephelometric Turbidity Units
PA	probe adjustment
QLD	Queensland
RS	Reynolds stress
S	South
SNR	Signal to Noise Ratio
SSC	Suspended Sediment Concentration
STP	Sewage Treatment Plant
TC	Tidal Cycle
TEDP	total number of erroneous data points in data set
Temp	temperature
TNDP	total number of data points in data set

TOT	total for pre-processing stage
Turb	turbidity
UW	Under Water
W	West

1   INTRODUCTION

1.1   DESCRIPTION

An estuary occurs when a river or stream intersects with the open waters of the ocean. The estuarine zone is that section of the river in which the mixing of salt and freshwater occurs. Each estuary is distinctly unique, with the freshwater inflow, tidal forcing and topography influencing the shape, flow properties and mixing that occur locally. The shape of an estuary is continuously changing because of the erosion, transportation and deposition of sediment and other objects such as trees about the estuary. This continuous variation in the bathymetry of an estuary, along with the seasonal changes in weather conditions and tidal forcing make the flow properties of each estuary unique in space and time.

Estuaries are important to the health and well-being of the local flora, fauna and humans that live in and about these systems, while estuaries also support a large range of industrial and recreational activities vital to the local community. If the health of an estuary should suffer, then so will the many life forms that depend on these systems. Therefore it is important to understand the natural estuarine processes and the impact that changes could have on these sensitive systems to ensure the health of the local and global environment into the future.

Humans have utilised estuaries for thousands of years, for activities including fishing, aquaculture, recreation, trade and harbouring boats. The calmer waters of estuaries have provided sailors with a safe place from which to enter the oceans, to shelter from storms and swells or conduct repairs on damaged vessels since ocean navigation first began. Figure 1.1 shows a boat repair yard located in Eprapah Creek, Australia.

Figure 1.1 – Boat repair yard located in Eprapah Creek, Australia. Photograph taken mid ebb tide (09:41) on 7/06/06 during field study E7 (5-7/06/06).

Estuaries are also commonly used by humans to disperse treated and/or waste fluids into the ocean. One example of a treated fluid is the treated sewage water from sewage treatment plants. These introduced fluids can have a large effect on the water quality and flow properties within the estuary. As cities grow and increasingly encroach on estuarine zones, the quantity of pollutants entering the estuaries increases. One source of pollution entering estuaries is from the natural runoff in the estuarine catchment areas (Figure 1.2). As the rainwater flows across the dirty roads, shopping centres and other man made structures, it collects man made substances left behind by the polluting existence of modern humans. These substances are in turn carried into the estuarine system. Figure 1.2 shows the natural runoff for a small rainstorm entering the upper estuary of Eprapah Creek.

Figure 1.2 – Storm water runoff entering upper estuary of Eprapah Creek through mangrove swamps. Photograph taken by H. Chanson at 07:29 on 28/08/06 (field study E8), approximately 2 hours after 30 mm of rain fell in catchment of Eprapah Creek.

If the impact of these introduced fluids and pollutants is not properly investigated through modelling, then the health of estuary and subsequently the local environment could be compromised. Estuarine systems are important to the local environment in several ways: firstly to provide a safe breeding ground and/or nursery for marine animals (e.g. Figure 1.3C); secondly, the land surrounding estuaries is usually not ideal for human settlement making this land one of the last refuges for natural flora and fauna to flourish along the coasts of most populated regions. In Southeast Queensland, the estuarine zones of many creeks and rivers are home to endangered species such as koalas (Figure 1.3A); brahminy kites; azure kingfishers (Figure 1.3B); and swamp wallabies. Figure 1.3 shows examples of flora and fauna that rely on estuaries. Flora such as mangroves (Figure 1.3D) thrive in the brackish waters of these estuaries, using the waters to disperse their seeds, while the roots of the mangroves provide a safe haven for small marine creatures.

2

(A) Koala.

(B) Azure kingfisher.

(C) Small school of young mullet.

(D) Mangrove trees.

Figure 1.3 – Examples of flora and fauna that rely on estuaries.

As the community around an estuary grows, the impact of human life threatens the ability of the estuaries to support the flora and fauna that rely on the estuaries to exist. By straining the health of the estuaries humans are placing their own health and well-being at risk. Government bodies such as the Queensland Environmental Protection Agency (EPA (QLD)) are interested in ensuring the health of these estuaries through a thorough monitoring and modelling program. Monitoring allows the current health of the waterways to be determined and provides data for calibrating the models used. Modelling is used to estimate the present health of local waterways and to predict the impact of future development on the health of these waterways. The accuracy of these models is dependent on the physical understanding of the mixing and dispersion processes within these estuarine systems.

At present the current understanding of the mixing and dispersion processes within estuaries is extremely limited. Estuarine hydrodynamics are extremely complex because of the unsteady flow conditions, varying water density and complex variations of bathymetry within each system. The flow in estuaries is turbulent, and mixing and dispersion in estuaries are turbulent processes. At present little is understood about turbulent processes in estuaries,

especially small subtropical estuarine systems. One of the main reasons for the limited understanding of the flow of turbulence in estuaries is the lack of appropriate instrumentation. More recently, instrumentation capable of measuring flow turbulence in estuaries has been developed. To date, the study of estuarine turbulence has been limited to mainly larger estuaries (Section 2.4.2). Small subtropical/tropical estuaries constitute approximately 60 % of all estuaries in Australia (Digby et al. (1999)). The knowledge of the flow turbulence governing the mixing and dispersion processes in subtropical estuaries must be improved. Once a more complete understanding of the turbulence in these small estuaries is established, models that better represent the true mixing and dispersion processes in small estuaries can be developed.

1.2   OBJECTIVES

The main objective of this project is to improve the understanding of the flow turbulence and turbulent mixing processes in small subtropical estuaries. This project aims to achieve this objective through the continuous collection of high frequency velocity and water quality data for relatively long periods. The field data collected are then used to look for possible patterns in key turbulence properties related to the variation of the tidal amplitude, phase of a tidal cycle and the location within the estuarine zone of a typical small subtropical estuary. Further field data were collected in a distinctly different estuary type (large tidal lake with a restricted entrance in Japan) to investigate common turbulence properties and patterns, and those unique to small subtropical estuaries. After an improved understanding of the turbulence properties in small subtropical estuaries is established, this project aims to investigate some initial links between turbulence and some water quality properties. It is conceivable that the understanding of turbulence and turbulent mixing in small subtropical estuaries gained through this investigation could be used to assist in the modelling of these estuaries. However small an impact this project will have on the understanding of estuarine processes, the author is satisfied with his role in the process of ensuring the existence and quality of life on the planet Earth for future generations.

1.3 OUTLINE

The work presented in each chapter of this thesis is outlined in Table 1.1, while the contents of each Appendix are outlined in Table 1.2.

Table 1.1 – Outline of work presented in each chapter.

Chapter	Description
1	**INTRODUCTION**
2	**TURBULENT MIXING IN ESTUARIES: A BIBLIOGRAPHIC REVIEW** Overview of turbulence and turbulent mixing. Outlining importance of turbulence in understanding mixing in turbulent systems. Review of previous studies on turbulence and turbulence in estuaries.
3	**FIELD STUDIES AND INSTRUMENTATION** Detailed description of field site, experimental techniques and instruments used for field studies.
4	**ADV DATA PROCESSING** Description of post-processing technique and analysis methodology used in processing data collected by an acoustic Doppler velocimeter (ADV).
5	**FIELD OBSERVATIONS: TURBULENCE** Presentation of turbulence field data collected at Eprapah Creek. Outlines tidal patterns and values observed for key turbulence properties.
6	**FIELD OBSERVATIONS: WATER PROPERTIES** Presentation of water property field data collected at Eprapah Creek. Outlines tidal patterns and values observed for key water properties measured.
7	**DISCUSSION OF ESTUARINE TURBULENCE** Investigation of turbulence properties under influence of spring and neap tidal forcing and long period oscillations. Study showed distinct turbulence properties under spring and neap tidal conditions.
8	**A COMPARISON OF TURBULENT PROPERTIES IN MIDDLE AND UPPER ESTUARINE ZONES** Comparison of turbulence properties observed in middle and upper estuarine zones. Discussion of relationship between long period oscillations and some transverse velocity events and associate secondary currents. Study showed different turbulence properties in middle and upper estuarine zones.
9	**A COMPARISON OF TURBULENCE PROPERTIES BETWEEN EPRAPAH CREEK (AUSTRALIA) AND HAMANA LAKE (JAPAN)** Comparison of field studies conducted at Eprapah Creek and Hamana Lake (a large tidal lake in Japan). Presents Hamana Lake field site, field studies conducted and instruments used. Comparison of general hydrodynamics and turbulence properties of these two estuaries. Despite distinct bathymetry and forcing conditions some similar turbulence patterns were observed close to bed.
10	**RELATIONSHIPS BETWEEN TURBULENCE AND WATER PROPERTIES** Investigation of relationship between turbulence and mixing of key water properties such as suspended sediment concentration and conductivity. Discussion on effect of natural freshwater inflow on physio-chemistry and variability of turbulent mixing parameters in Eprapah Creek also included.
11	**CONCLUSION** Summary of work presented in this thesis and outlines ideas for future research.

Table 1.2 – Outline of work contained in Appendices.

Appendix	Description
A	**POST-PROCESSING OF ADV DATA** Detailed description of post-processing technique used in this investigation to process acoustic Doppler velocimetry data.
B	**DATA ANALYSIS TECHNIQUES** Description of statistical sampling and analysis techniques used in this study.
C	**FIELD DATA COLLECTED AT EPRAPAH CREEK (AUSTRALIA)** Graphical presentation of instantaneous velocity and physio-chemistry data collected continuously for field studies E1 through E7, along with vertical physio-chemistry profiles measured for all field studies at Eprapah Creek.
D	**LABORATORY EXPERIMENT – RELATIONSHIP BETWEEN SUSPENDED SEDIMENT CONCENTRATION AND ADV BACKSCATTER INTENSITY** Description of laboratory experiments conducted to calibrate ADV backscatter intensity with suspended sediment concentration at Eprapah Creek.
E	**INVESTIGATION OF LONG PERIOD OSCILLATIONS OBSERVED AT EPRAPAH CREEK** Detailed investigation of long period oscillations in velocity and water level observed during field studies conducted at Eprapah Creek.
F	**WAVE-TURBULENCE SEPARATION TECHNIQUE** In-depth description of theory and technique used to separate the wave induced and current induced turbulence data collected at Hamana Lake.
G	**FIELD STUDIES CONDUCTED AT HAMANA LAKE IN 2005** Description of field studies conducted at Hamana Lake (Japan) during 2005 and presents main observations from gross and current induced velocity data sets.
H	**EFFECT OF WIND WAVES ON TURBULENCE DATA COLLECTED AT HAMANA LAKE (JAPAN)** Investigation of effect of wind waves observed during field studies at Hamana Lake had on turbulence data collected above bed.
I	**INVESTIGATION OF CORRELATION BETWEEN WATER QUALITY PROPERTIES AND MOMENTUM** Description of study using cross-correlation of velocity and physio-chemistry spectra performed to investigate possible links between variation of each water quality and momentum mixing.
Digital	**DIGITAL APPENDIX** The Digital appendix can be found on CD attached to last page of this Thesis. It presents all turbulence and water quality properties collected continuously at high frequency and vertical profile physio-chemistry profiles collected at Eprapah Creek and Hamana Lake analysed as part of this investigation. Digital Appendix also includes tabular data in text file format of the calculated turbulence properties for this investigation and DPlot graph files of instantaneous velocity and suspended sediment concentration data for inspection by readers. The Digital Appendix also contains a digital copies of this Thesis and the journal/conference publications co-authored as part of this investigation.

2 TURBULENT MIXING IN ESTUARIES: A BIBLIOGRAPHIC REVIEW

2.1 PRESENTATION

The flow of water in natural waterways such as estuaries is a turbulent process, with Reynolds numbers greater than 10^5. In order to properly understand the mixing and dispersion processes in estuaries it is first necessary to understand the turbulence properties of these systems. Section 2.2 outlines the current understanding of turbulence and its effects on the mixing processes in turbulent flows through a general review of turbulence theory in all flows. However, estuaries and other natural waterways belong to a specific category of fluid mechanics known as open channel flow. Section 2.3 investigates the history and developments of research into turbulence in open channels and the difference between turbulence properties in man made and natural channels. The present understanding of estuarine processes is outlined in Section 2.4.1, while Section 2.4.2 discusses some of the key studies conducted on turbulence and turbulent mixing in estuaries. Section 2.4.2 concludes by summarising the key differences between these previous studies into estuarine turbulence and the present study undertaken in a small subtropical estuary.

2.2 TURBULENCE

Turbulence is the chaotic fluctuations of a property (e.g. velocity) occurring in both the space and time coordinates. Figure 2.1 shows an example of the fluctuations in turbulent velocity data. Bradshaw (1971) provided the definition: "Turbulence is a three-dimensional time-dependent motion in which vortex stretching causes velocity fluctuations to spread to all wavelengths between a minimum determined by viscous forces, and a maximum determined by the boundary conditions of the flow". In Nature the majority of fluid flows whether liquid or gas, are turbulent. Turbulent flows have a much greater ability to transfer momentum (Monin and Yaglom (1971)). The mixing processes in turbulent flows are therefore dominated by the turbulence. To better understand the mixing processes in natural systems we must first understand the turbulence properties of that system.

In-depth study of turbulence only began in modern times with the ground breaking works of Osborne Reynolds (1842-1912). While studying the transformation of a fluid from laminar to turbulent properties, Reynolds developed a general criterion for dynamic similarity in an incompressible, viscous fluid. With geometric similarity and an absence of external forces this criterion is represented by the values of the so-called Reynolds number $\mathrm{Re} = UL/\nu$, where L and U are the characteristic length and velocity scales and ν is the kinematic viscosity of the fluid. Monin and Yaglom (1971) stated that the Reynolds number can be

used to describe a ratio between the inertial and viscous forces acting on a fluid. The inertial forces produce mixing of different volumes of fluid moving with different velocities through inertia. This produces an energy transfer from the large to small scale components of the motion, and hence assists in the creation of the sharp, small scale in-homogeneities within the flow. These small scale in-homogeneities characterise turbulent flow. Viscous forces, on the other hand, help to smooth out the small scale in-homogeneities of the flow.
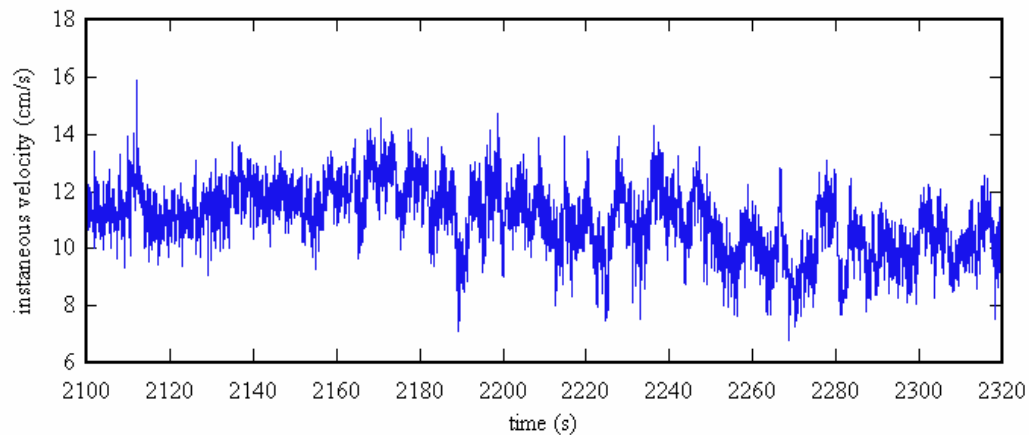
Figure 2.1 – Example of turbulent fluctuations in streamwise velocity. Data shown measured at 25 Hz during a field study conducted at Eprapah Creek.

The random and chaotic nature of turbulence makes the study and modelling of turbulence extremely difficult. Fortunately, the "random" nature of turbulence means that it is possible to describe it using the laws of probability. Hinze (1975) defined turbulence as: "Turbulent fluid motion is an irregular condition of flow in which the various quantities show a random variation with time and space coordinates, so that statistically distinct average values can be discerned". In the early 20th century the major advances in turbulence theory were of a semi-empirical nature. Key semi-empirical theories were developed by L. Prandtl (1875-1953), G.I. Taylor (1886-1975), T. von Karman (1881-1963) and A. Kolmogorov (1903-1987). These included boundary layer theory and the theory of homogeneous and isotropic turbulence. In the mid to late 20th century, flow visualisation experiments provided some of the most notable advances in the understanding of turbulence. These experiments allowed researchers to investigate the structure of turbulence within the boundary layers and isolate phenomena such as bursting (Kline et al. (1967)), that are crucial to understanding turbulence and turbulent mixing. Earlier texts such as Hinze (1959), Monin and Yaglom (1971) and Bradshaw (1971) provide a good explanation of the fundamentals of turbulence theory, while more recent texts such as Piquet (1999) and Pope (2000) include more recent advances in turbulence theory.

8

2.3 TURBULENCE IN OPEN CHANNELS

Some of the earliest known studies into turbulence were conducted in natural open channels such as rivers and estuaries. For example, Leonardo da Vinci (1452-1519) made observations and sketches of the water motion around piers in a river, noting the coherent structure of the vortices. However, it was not until the later part of the 20th century that boundary layer and turbulence theories were fully applied to hydraulic applications (Nezu and Nakagawa (1993)). Nezu and Nakagawa stated that one reason for this was that turbulence measurements of air flows are easier than water flows. This changed in the last 40 to 20 years with the development of new instrumentation and a concerted effort to understand the turbulence properties of natural and man made open channels. Figure 2.2 shows some turbulence measurements being undertaken in an open channel flume at the University of Queensland.
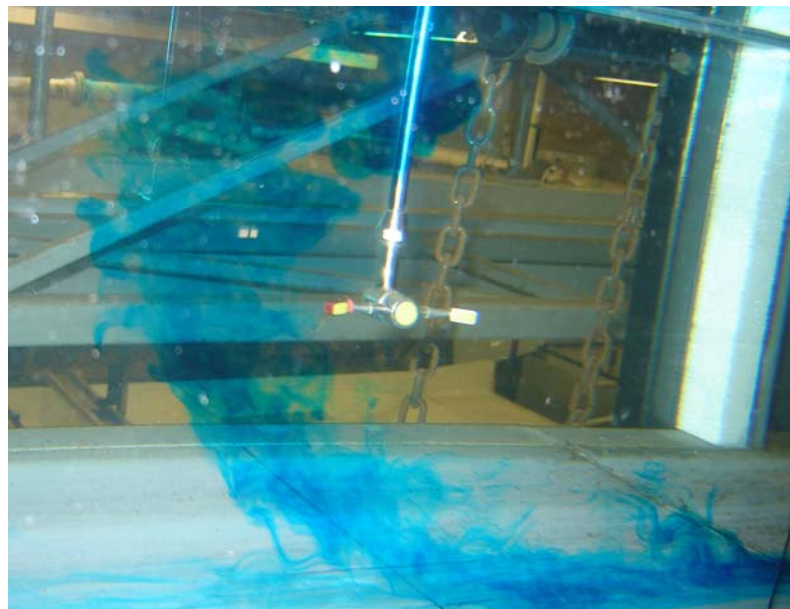
Figure 2.2 – Turbulence measurements conducted in an open channel flume at University of Queensland. Photograph shows blue dye passing sampling volume of acoustic Doppler velocimeter (ADV) located mid channel 0.12 m above bed. Note free surface visible in top right-hand corner.

2.3.1 Turbulence in laboratory channels

Since the 1970s, researchers have begun to study turbulence in open channels. One of the main reasons for this renewed interest was the invention of new instruments (e.g. Laser Doppler Anemometer (LDA)) that were better suited to turbulence measurements in water. A LDA uses a non-intrusive sampling technique to measure turbulence with high spatial and temporal resolution. Nezu (2005) provides a good review of the research conducted into turbulence in open channels to date. These studies have found that many of the turbulence

theories developed for the boundary layers in air are also valid in open channel flows. However, the three-dimensional characteristics of the turbulence flows are distinctly different in pipes and open channels, because of the free surface boundary. Nezu and Nakagawa (1993) detail the three-dimensional structure of turbulence in open channel flows.

The understanding of turbulence in open channels has advanced tremendously since the 1970s, to the extent that turbulence in man made channels is relatively well understood. This is not necessarily the case in natural channels, especially not estuaries. Nezu (2005) noted several complex areas of turbulence research that need further investigation in the future. These included: the effects of fluid density and temperature stratification; the effects of complex channel geometry; and turbulence in unsteady flow conditions. All three of these phenomena are found in natural estuarine channels.

2.3.2 Turbulence in natural channels

Unlike man made channels, the geometry of natural channels such as rivers and estuaries is complex, with the width, depth, slope and cross-section shape being unique at each point in the channel. Figure 2.3 shows an example of these variations in channel geometry as observed in a small subtropical estuary (Eprapah Creek, Australia). The geometry of the channel also varies with time because of erosion and deposition of sediment and other objects (e.g. trees) along the stream. Extreme weather events such as a storm can rapidly change the hydrodynamic properties experienced in the channel. The turbulence properties of each natural channel are therefore unique in time and space.

Figure 2.3 – Example of bathymetry observed in a natural channel. Photograph taken mid estuary at Eprapah Creek (Australia), about low tide (06:20) on 11/10/06.

Natural channels come in three types: freshwater channels such as rivers; tidal channels in oceans and bays; and estuarine channels which are a hybrid of the freshwater and tidal channels. Field investigations have been conducted in all three natural channel types to study their turbulence properties. Nezu (2005) stated that turbulence data collected in the laboratory can be appropriately scaled up to be applied to rivers with high Reynolds numbers. Turbulence field studies performed in natural freshwater channels showed that river turbulence did behave in a similar fashion to that in man made open channels (e.g. Yokosi (1967)).

The unsteady flow conditions generated in tidal channels have also been reasonably well investigated since the 1950s. Studies such as those undertaken by Bowden (1962) and Osonphasop (1984) have provided a reasonable understanding of the turbulence properties observed in natural tidal channels. Nakagawa and Hinwood (1978) summarised the previous studies of turbulence in tidal channels. However, the turbulence properties observed in estuarine channels have not been thoroughly studied to date (Section 2.4.2).

2.3.3 Turbulent mixing in natural channels

The main physical mechanisms driving the mixing processes in natural channels are described in texts such as Fischer et al. (1979). The turbulent mixing properties of rivers are reasonably well understood (e.g. Fischer et al. (1979) and Rutherford (1994)). However, those in estuaries are not as well understood. Several texts (e.g. Fischer et al. (1979) and Lewis (1997)) have described some of the most prominent mixing mechanisms in estuaries. A more recent text, (Savenije (2005)) updated the mixing mechanisms described in Fischer et al. (1979), but stated that more research is required to fully understand all mixing mechanisms in estuaries.

2.4 TURBULENCE IN ESTUARINE SYSTEMS

2.4.1 Estuarine systems

The simplest definition for an estuary is "an area in which saltwater and freshwater interact". As such, estuaries form along the coastal regions where rivers, creeks and freshwater runoff meet the ocean. Each estuary is distinctly unique, with the freshwater inflow, tidal forcing and topography influencing the shape and mixing that occur locally. Estuaries are classified by two main schemes based on topography and salinity structure. The classification schemes were reviewed in Pritchard (1952), Dyer (1973) and Lewis (1997). Classically, both the topography and salinity structure classification schemes contain three main types. For the topographical classification of estuaries, the three main types are: coastal plain type estuaries;

fjord type estuaries; and bar-built type estuaries. The three salinity structure classification type definitions are: stratified (salt wedge and fjord types); partially-mixed; and well-mixed. The salinity structure of an estuary can change depending on the proportions of fresh and salt water entering the estuary.

One method for estimating the salinity structure in an estuary is the local Richardson number (Ri):

$$Ri = \frac{g}{\rho} \frac{\left(\partial\overline{\rho}/\partial z\right)}{\left(\partial\overline{V_x}/\partial z\right)^2}$$

(2.1)

where g is gravitational acceleration; ρ is the density of water; z is the vertical elevation; and $\overline{V_x}$ is the time-averaged streamwise velocity. Previous studies (e.g. West and Shiono (1985)) used the local Richardson number to classify the salinity structure of the estuaries being investigated. Officer (1976) classified the transition region between well-mixed and substantially stratified salinity profiles to be 0.1 > Ri >10, while Dyer (1997) noted that the level of stratification begins to affect the local mixing and turbulence when Ri > 0.25. The local Richardson number was used here to provide an approximation of the level of stratification within the estuary.

The interaction of the ocean tides and the freshwater inflow creates a distinctly different set of hydrodynamic and physio-chemical conditions than those experienced in oceans or rivers. Much research has been conducted into the physical processes in estuaries, which have been described in classical texts such as Ippen (1966) and Dyer (1973). Recent advances in the understanding of estuarine processes have been updated in reviews (e.g. Uncles (2002), Savenije (2005)). However, the complexity of estuarine dynamics and the uniqueness of each estuary means that there is still much to be understood about the dynamic processes in estuaries. This is especially true of the turbulent processes in estuaries.

2.4.2   Key studies of turbulence in estuaries

At present, published studies on the turbulent properties in estuaries are limited. This is especially true of studies undertaken in small estuaries. One reason for the lack of attention into the study of estuarine turbulence was the lack of appropriate instrumentation for the measurement of fine scale turbulence. Recently, instruments such as electromagnetic current meters and acoustic Doppler velocimeters were developed, which allowed for the study of estuarine turbulence. Nevertheless, long duration studies of estuarine turbulence conducted at high frequency are extremely rare. Most studies were performed in relatively large estuaries for short durations or bursts, and lacked spatial or temporal resolution detailed enough to

study fine scale turbulence. Table 2.1 summarises some of the published studies of turbulence in estuaries. In Table 2.1 no previous studies collected continuous high frequency turbulence data for relatively long periods (T_{study} > 25 hours). A study period of greater than 25 hours is required to establish whether diurnal or semi-diurnal tidal conditions exist, and allows the analysis of turbulence properties over multiple tidal cycles.

The focus of this study was the collection of continuous high frequency (f_{scan} ≥ 25 Hz) for relatively long periods (T_{study} up to 50 hours). Analysis of the field data collected at Eprapah Creek showed that large and rapid fluctuations in turbulence properties occurred over the investigation period (see Chapter 5). Such large and rapid fluctuations could be missed by sampling in bursts (e.g. 20 minutes every hour) over a similar investigation period, while an investigation period of several tidal cycles (e.g. 25 > T_{study} > 50 hours) allows tidal trends in the fluctuations of turbulence properties to be established.

Turbulence studies in small shallow estuarine systems are extremely limited, yet small coastal plain type estuaries constitute approximately 60 % of all estuaries in Australia. This study analyses a significant number of turbulence properties extracted from field data measured in multiple locations over several field studies in a typical small subtropical estuary, Eprapah Creek, Australia (Table 2.2). Several of these turbulence properties have not been applied to published estuarine turbulence data investigations before. To assist in the study of estuarine turbulence properties, the same number of turbulence properties were extracted from field data collected in a large bar-built estuary at Hamana Lake, Japan.

Many of the studies summarised in Table 2.1 have made some important insights into the turbulence properties in estuaries, however, these studies were limited by the instrumentation and/or sampling techniques used. For example, most studies in Table 2.1 discussed the turbulence of the streamwise and vertical velocity components, but not the turbulence from the transverse velocity component (Table 2.2). Table 2.2 outlines the turbulence properties analysed in some of the estuarine studies presented in Table 2.1 and the present study.

Turbulence data from all three velocity components are required to get the correct energy balance at all scales. Data collected as part of this study showed significant fluctuations in the transverse velocity and its associated turbulence properties (see Chapter 5), indicating that transverse velocity data should be included in any comprehensive study of estuarine turbulence. This investigation will try to present all turbulence data recorded, because this increases the quantity and type of turbulence properties that can be studied, thereby allowing a better understanding of the turbulence in a small subtropical estuary.

Table 2.1 – Summary of some published studies of turbulence in estuaries.

Reference	Flow conditions	Instrumentation	Remarks
Bowden and Howe (1963)	Mersey Estuary (UK) d_{range} : 4-13 m	Electromagnetic flow meters, f_{scan} : 1 Hz, T_{scan} : 5 min., T_{study} : 3 h	
Shiono and West (1987)	Conway estuary (UK) d_{range} : 2-3 m	Electromagnetic flow meters, f_{scan} : 15 Hz, T_{scan} : 10 min., T_{study} : 3 h	
West and Shiono (1988)	Teign estuary (UK) d_{range} : 1-5 m, W: 600 m	Electromagnetic current meters, f_{scan} : 10 Hz, T_{scan} : 205 or 410 s	
West and Oduyemi (1989)	Conway estuary (UK) d_{range} : 1-5 m Tamar estuary (UK) d_{range} : 1-5 m	Electromagnetic current meters, f_{scan} : 10 Hz, T_{scan} : 51 & 102 s	
French and Clifford (1992)	Hut Creek (Norfolk) d_{av} : 2.6 m, W: 30 m, TR : 4 -6 m	Electromagnetic current meters, f_{scan} : 10 Hz, T_{scan} : 5 to 7 min., T_{study} : 6 h	Spring tide
Kawanisi and Yokosi (1994)	Ota river estuary (Japan) d_{av} : 3 m, W: 320 m, TR : 4m	Electromagnetic current meters, f_{scan} : 3 Hz, T_{scan} : continuous, T_{study} : 26 h	Spring tides
Kawanisi and Yokosi (1997)	Ota river estuary (Japan) d_{av} : 3 m, W: 320 m, TR : 4m	ADV, T_{scan} : 300 s, T_{study} : 12 h	Spring tides
van der Haam et al. (2001)	Ems estuary (Holland) d_{av} : 3.3 m, W: 600 m, TR : 3 m	Electromagnetic flow meters, f_{scan} : 20 Hz, T_{scan} : 10 min., T_{study} : up to 5 tidal cycles	2 spring tides and 2 neap tides
Nikora et al. (2002)	Beatrix Bay (New Zealand) d_{av} : 38.2 m, W: 4 km	Sontek ADVs, f_{scan} : 10 & 25 Hz, T_{scan} : 300 s, T_{study} : 7 days	
Kawanisi (2004)	Ota river estuary (Japan) d_{av} : 3 m, W: 320 m, TR : 4m	Nortek high resolution current profiler (1.5 MHz), f_{scan} : 0.33 Hz, T_{study} : 24 h	Spring tides
Voulgaris and Meyers (2004)	Bly Creek, North Inlet (USA) d_{av} : 1 m, W: 30 m, TR_{av} : 1.4 m	Sontek ADV (10 MHz), f_{scan} : 10 Hz, T_{scan} : 12 min., T_{study} : up to 7 days	
Trevethan et al. (2007)	Eprapah Creek (Australia) d_{av} : 1.6 m, W: 15 m, TR_{av} : 1.24 m	2D-microADV (16 MHz), f_{scan} : 50 Hz, T_{scan} : continuous, T_{study} : 50 h	Upper estuary, neap tides

Note: f_{scan} : scan rate; T_{scan} : scan duration; T_{study} : study duration; d: depth; W: width; TR: tidal range.

14

Table 2.2 – Turbulence measurements analysed in some estuarine turbulence studies.

Source	Measured data			Velocity data (V)				Reynolds stress data (RS)				Turbulent time scales	
	V_x	V_y	V_z	$\overline{V}$	v'	Sk	Ku	$\overline{RS}$	$(RS)'$	Sk	Ku	T_E	τ_E
Bowden and Howe (1963)	x		x	1	2			1				2	
Shiono and West (1987)	x		x	1	2	2	2	2	1	1	1	2	
West and Shiono (1988)	x		x	1	1			1					
West and Oduyemi (1989)	x		x	1	1			1					
Kawanisi and Yokosi (1994)	x		x	1	2			1				2	
Van der Haam et al. (2001)	x		x	1	1			1					
Nikora et al. (2002)	x	x	x	3	3	1	1	6					
Present Study	x	x	x	3	3	3	3	6	3	3	3	3	3

Note: numerals indicate number of parameters analysed in study.

3 FIELD STUDIES AND INSTRUMENTATION

3.1 PRESENTATION

This study is focused on turbulence and turbulent mixing in the small subtropical estuaries of Southeast Queensland. The typical topographical and hydrological characteristics of small subtropical estuaries are described in Section 3.1.1. Section 3.2 describes Eprapah Creek, a small subtropical estuary chosen for the field experiments. The field studies at Eprapah Creek and the experimental techniques are described in Section 3.3. Section 3.4 presents the instrumentation used. A brief description of the issues that arose from the practical experiences during these field investigations is presented in Section 3.5.

3.1.1 Characteristics of small subtropical estuaries

Each estuary is distinctly unique because of the topography, freshwater inflow and tidal forcing, which all influence the local bathymetry and mixing processes. Estuaries are classified by two main schemes based on topography and salinity structure (Section 2.4.1). These classification schemes were reviewed in Pritchard (1952), Dyer (1973) and Lewis (1997). Topographically, the vast majority of the estuaries in Southeast Queensland were found to be of the drowned river valley (coastal plain) type (Digby et al. (1999)). The following topographical characteristics are attributed to a coastal plain estuary: (a) shallow, with large width to depth ratio; (b) cross-sections that deepen and widen towards the mouth; (c) ratio of freshwater inflow to tidal prism volume is small; (d) large variation of sediment type and size found in estuary; (e) surrounded by extensive mud flats; and (f) sinuous central channel. Figure 3.1 shows the main topographical features that are typical of coastal plain estuaries.
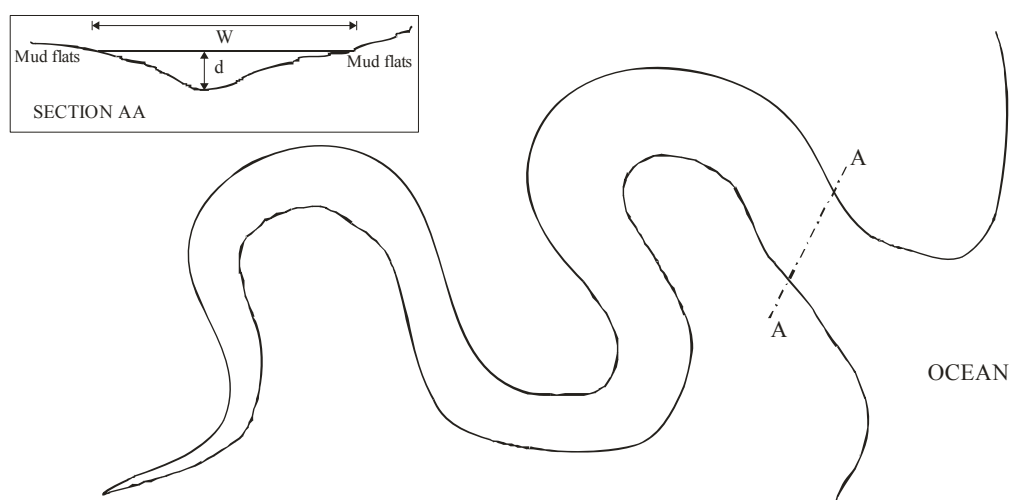
Figure 3.1 – Sketch outlining some topographical features of a coastal plain type estuary.

16

Digby et al. (1999) classified the estuaries of Southeast Queensland as wet and dry tropical/subtropical estuaries in terms of their hydrology. The "wet and dry tropical/subtropical estuary" type accounts for 68 % of the estuaries in Australia. These estuaries are characterised by short-lived episodic freshwater inflows during the wet season and very little or no flow during the dry season. During high inflow situations the estuary is flushed to the mouth with freshwater. After a flushing event, the estuary quickly recovers because of the tidal forcing. The hydrological conditions of a small estuary change from fully flushed to partially-mixed (well stratified) back to vertically homogeneous within a few days of the high flow event ending (Digby et al. (1999)).

3.2   FIELD SITE: EPRAPAH CREEK

Eprapah Creek (153.30°E, 27.567°S) is a small subtropical stream located on the East coast of Australia, near the city of Brisbane. The creek is approximately 12.6 km long with an estuarine zone of approximately 3.8 km. Figure 3.2 shows an aerial photograph of Eprapah Creek and the surrounding area. In the estuary, the mean water depth is typically 1 to 2 m mid-stream and the mean width is approximately 20 to 40 m. The meandering channel of this relatively small estuary is predominantly bordered by trees. This vegetation acts as a wind buffer, minimising the effect of wind on the water surface. At Eprapah Creek there are mixed semi-diurnal tides, with a tidal range of 1 to 2.5 m (i.e. "micro-tidal" conditions). The catchment area of Eprapah Creek is approximately 39 km^2.

Figure 3.2 – Aerial photograph of Eprapah Creek (courtesy of Queensland Department of Natural Resources and Mines, 2001).

The land surrounding Eprapah Creek includes several conservation areas that are home to endangered species such as koalas, swamp wallabies, azure kingfishers and brahminy kites. A sewage treatment plant (STP) is located next to Eprapah Creek and discharges treated water into the creek mid estuary, 2.5 km from the mouth. The sewage treatment facilities were upgraded in 2005-2006 to improve the quality of the water discharged. Each day, the treated water is discharged into the creek with an average outflow of approximately 0.07 m^3/s. There are two daily peak discharges into Eprapah Creek, when the discharge flow rates reach about 0.11 to 0.17 m^3/s. Figure 3.3 shows the averaged daily volumetric flow rate over the sewage treatment plant outflow weir for 10 days of the study E9 (Table 3.1). In Figure 3.3, two peaks in volumetric flow rate were observed, corresponding to the increased discharge from the STP. The largest of these discharges occurred between 08:00 and 11:00 each day.
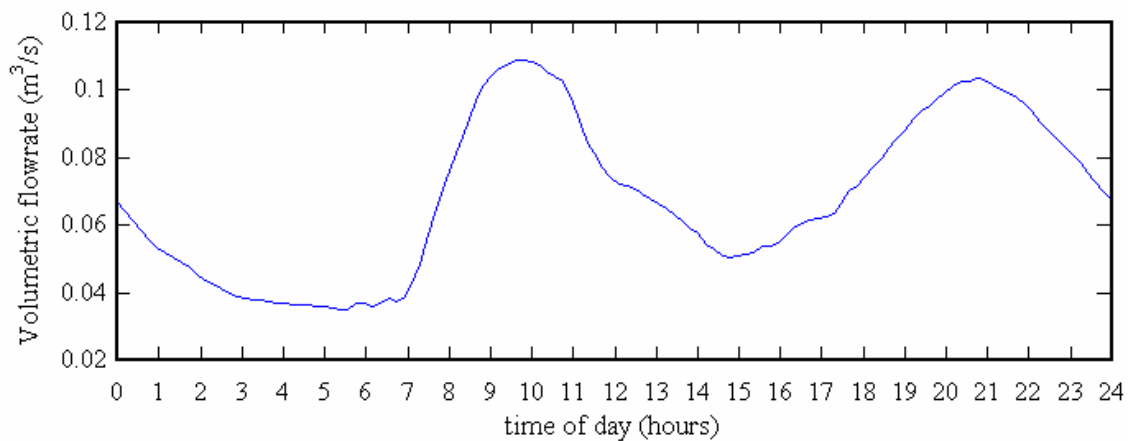
Figure 3.3 – Averaged daily volumetric flow rate over STP outflow weir during field study E9 (2-13/10/06). Data shown was averaged every 10 minutes along entire data set and then divided into 24 hour sections and averaged over 10 full days of study E9.

The freshwater runoff from the local shopping centres surrounding the upper estuarine zone flows into the mangrove swamps of the upper estuary. During periods of rainfall this freshwater runoff enters the creek at numerous locations the upper estuary. For the majority of the year there is no natural freshwater inflow into the estuarine zone.

Eprapah Creek is a typical small subtropical estuary. It has a single unconstricted mouth, an unbranched channel, and no off channel embayment. This type of estuary constitutes approximately 28 % of all estuaries in Australia (Digby et al. (1999)). Eprapah Creek would be classified as a coastal plain estuary type (Section 3.1.1). Figure 3.2 shows that Eprapah Creek contains a sinusoidal central channel that widens and deepens towards the mouth. It banks are encapsulated by extensive mud flats (e.g. Figure 3.4). The sediment observed

ranges from fine silt of less than 0.02 mm in diameter to some sharp rocks with a diameter of up to 0.2 to 0.4 m (highlighted in Figure 3.4).

Figure 3.4 – Eprapah Creek looking downstream from Site 2, showing exposed mud flats at beginning of flood tide (14:31) on 10/03/06.

There is minimal natural freshwater inflow entering Eprapah Creek for the majority of the year. Figure 3.5 shows the median monthly rainfall recorded over 50 years at the Redlands meteorological station (153.250°E, 27.528°S). The Redlands meteorological station is located approximately 10 km from the Eprapah Creek catchment area. In Figure 3.5 the majority of rainfall (55 %) falls in just four months (December to March). The majority of the rainfall for these months falls in storms of a short duration (less than one day). Eprapah Creek experiences similar hydrological characteristics to those of a wet and dry tropical and subtropical estuary as typified by Digby et al. (1999).
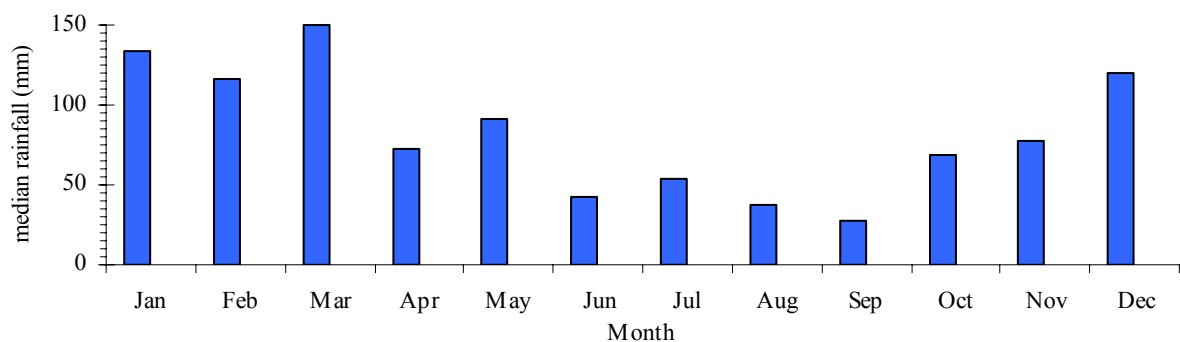
Figure 3.5 – Averaged monthly rainfall recorded at Redlands meteorological station approximately 10 km from Eprapah Creek. Rainfall averaged over a 50 year period.

3.3 FIELD STUDIES AND EXPERIMENTAL TECHNIQUES

Nine field investigations were conducted at Eprapah Creek in the period 2003 to 2007. During this period three different types of experiments were performed at six locations along Eprapah Creek. Figure 3.6 shows the location of the field sites used at Eprapah Creek and the type of field experiments undertaken at each site.

At Eprapah Creek several experimental techniques were used. These were:

A   The collection of continuous high frequency turbulence and water quality data.

B   Simultaneous collection of simple hydrodynamic and physio-chemistry measurements and surveying of fauna populations at multiple locations along Eprapah Creek.

C   Collection of continuous high frequency water level, temperature and conductivity data simultaneously at multiple locations along Eprapah Creek.

Table 3.1 outlines the field investigations conducted at Eprapah Creek and the experimental techniques used during each study. The experimental techniques A, B and C are described in Sections 3.3.1, 3.3.2 and 3.3.3 respectively. For each field study vertical profiles of physio-chemistry were measured from a boat at several longitudinal locations along the estuary.

Table 3.1 – Summary of field investigations at Eprapah Creek between 2003 and 2007.

Field study	Date	Duration (hours)	Rainfall (mm)	Tidal range (m)	Site of research	Experimental technique type
E1	4/04/03	12	10 (18:00 on 3/04/03)	1.61	2B 1,2,3,4	A B
E2	17/07/03	8	0	1.32	2	A
E3	24/11/03	7	0	2.49	2B	A
E4	2/09/04	12	0	1.76	2B 1,2,3	A B
E5	8-9/03/05	25	0	2.33	2B	A
E6	16-18/05/05	48	0	1.32	2B	A
E7	5-7/06/06	50	0	1.34	3,STP,3B	A
E8	28/08/06	12	30 (05:30 on 28/08/06)	1.53	1,2,3	B
E9	2-4/10/06 11-13/10/06	50 50	0	1.89 1.81	1,2B,2C,3,STP, 3B,4	C

Note: STP: sewage treatment plant; Tidal range: maximum observed at Victoria Point; Rainfall: observed immediately before or during field study (time and date).
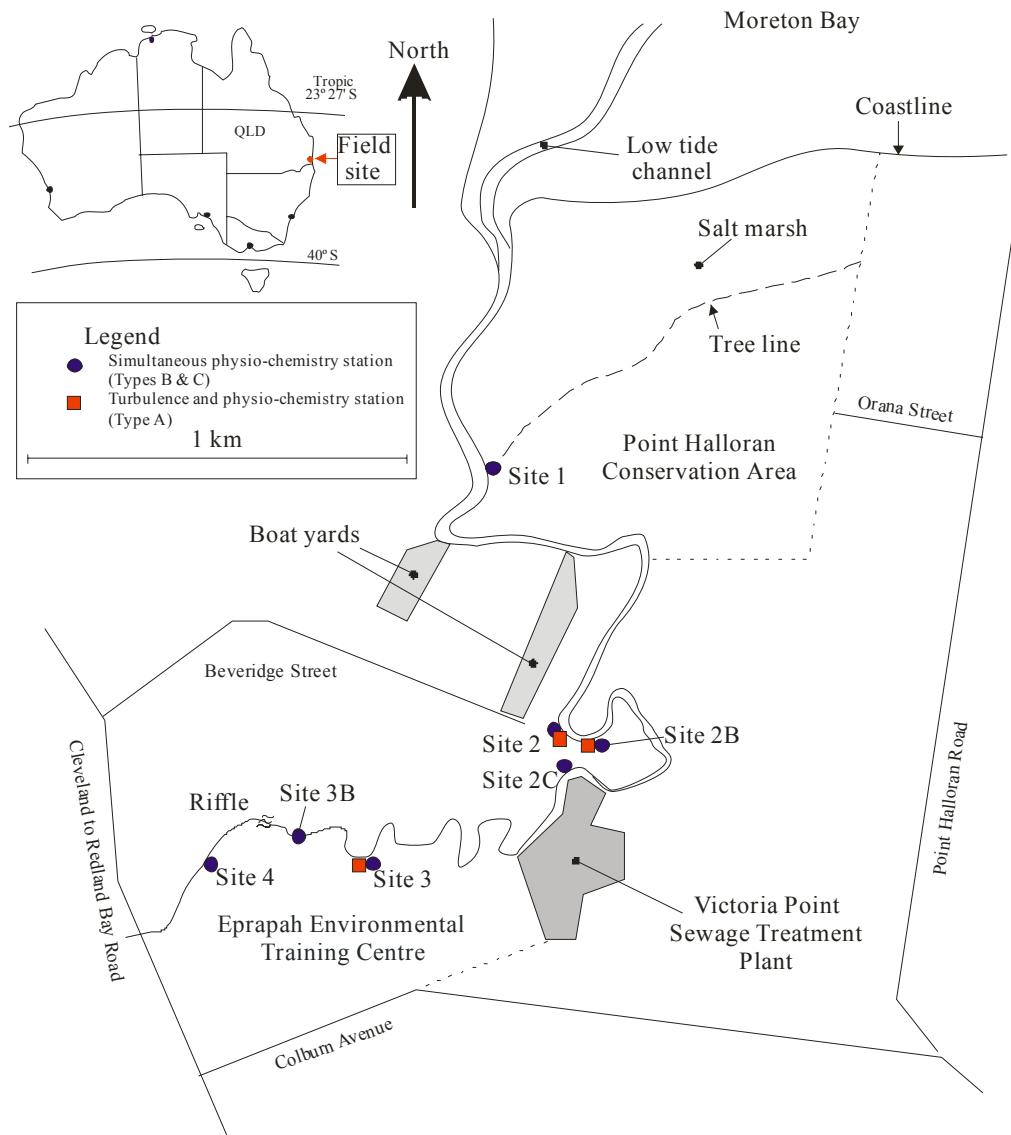
Figure 3.6 – Sketch of Eprapah Creek (153.30°E, 27.567°S) located near Brisbane Australia. Field sites and type of experiments conducted at each site are presented.

3.3.1 <u>Continuous high frequency turbulence and water quality measurements</u>

One focus of this project were the continuous high frequency turbulence and water quality data collected over a relatively long period. In estuarine dynamics a relatively long period is considered larger than the diurnal tidal period (approximately 25 hours). A study of at least 25 hours shows whether the estuary experiences diurnal or semi-diurnal tidal conditions. Continuous high frequency measurements over a period which includes several tidal cycles allows the researcher to observe the variation of the turbulence and water quality properties of the estuary.

The turbulent velocity measurements within Eprapah Creek were performed with two acoustic Doppler velocimeters: (1) a Sontek UW ADV (10 MHz, serial 0510) with a three-dimensional down-looking head; and (2) a Sontek microADV (16 MHz, serial number A641F) with a two-dimensional side-looking head. For both ADVs, the sampling volume

was located 5 cm from its sensor, with the sensor heads being mounted on rigid stems. In this report these ADVs are referred to as the 3D-ADV (10 MHz) and 2D-microADV (16 MHz) respectively. For all "type A" field studies, the physio-chemistry data were collected using a YSI6600 probe. The YSI6600 probe measured water depth, water temperature, conductivity, turbidity, pH, dissolved oxygen and chlorophyll a levels. The standard configuration (Figure 3.7A) for data collection used in all "type A" field studies was to have the sampling volume of the 3D-ADV and YSI6600 probes horizontally aligned, with the YSI6600 probe 0.3 m towards the bank.
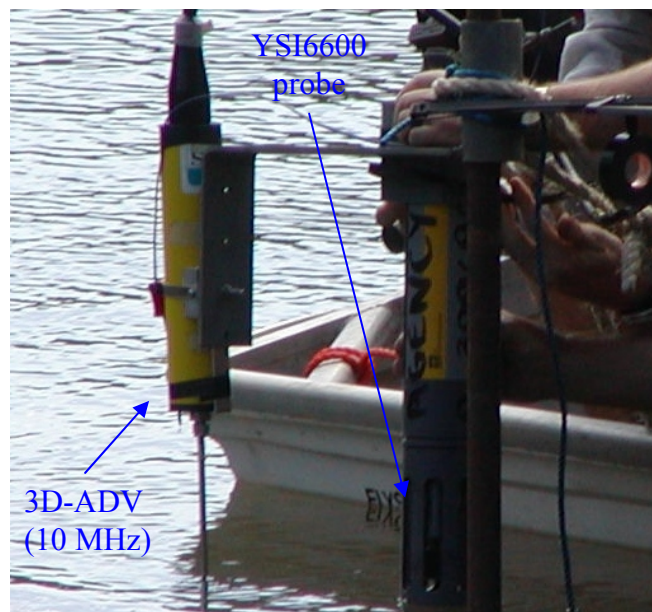
(A) Standard configuration for 3D-ADV (10 MHz) and YSI6600 probe for collecting turbulence and physio-chemistry data during field studies. Photograph by H. Chanson during installation of study E2 (17/07/03).

(B) Configuration of 3D-ADV and 2D-microADV used during field studies E6 and E7. Photograph by H. Chanson during preparation for study E6 (16-18/05/05).

Figure 3.7 – Configurations used for collection of high frequency turbulence and physio-chemistry data during field studies conducted at Eprapah Creek.

For the later "type A" field trips (studies E6 and E7), additional turbulence and physio-chemistry probes were used in conjunction with the standard configuration to collect additional information. During the field studies E6 and E7 two ADVs were deployed with the sampling volumes vertically aligned. Figure 3.7B shows that the sampling volume of the 2D-microADV was positioned 0.2 m below the sampling volume of the 3D-ADV. As with earlier field studies the YSI6600 probe was horizontally aligned with the 3D-ADV, 0.3 m towards the bank. The field studies E6 and E7 were conducted with additional physio-chemistry probes located transversely (Figure 3.8A) or longitudinally (Figure 3.8B) about the sampling site. Table 3.2 describes the field investigations in which continuous high frequency turbulence and water quality data were collected and the equipment deployed. For each study, all data sets from the individual probes were synchronised by converting each instruments start time to GPS time (s) since midnight on Day 1 of that study. Before and after each field deployment the clock of each instrument/computer was compared to GPS time, which allowed the start time of each data set to be synchronised relative 00:00 on Day 1.
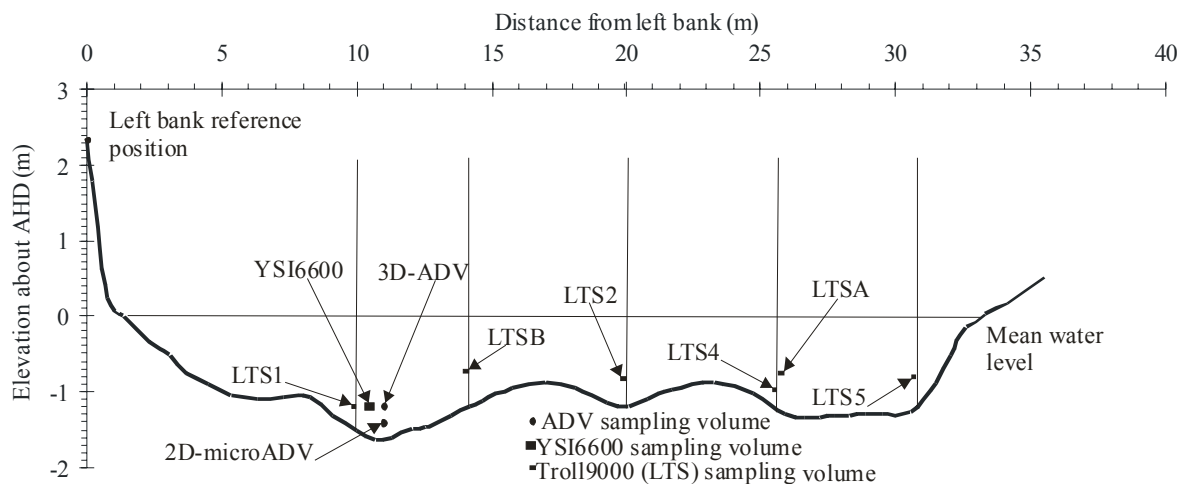
(A) Transverse location of physio-chemistry probes deployed at Site 2B for study E6.
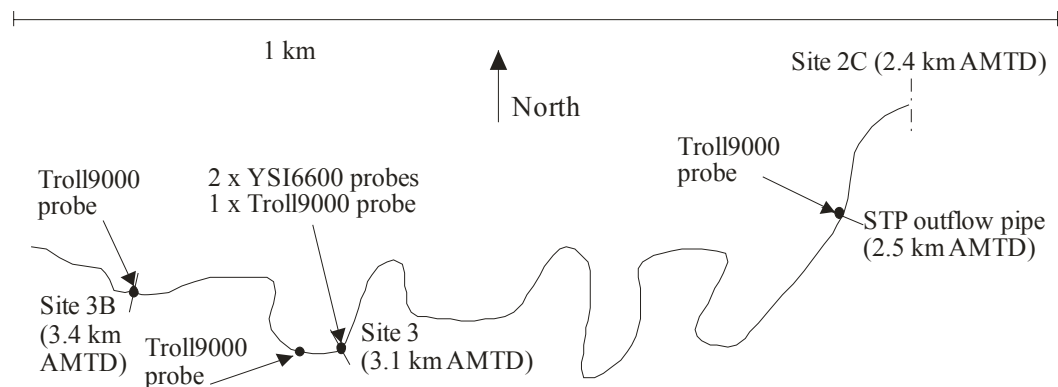
(B) Longitudinal location of physio-chemistry probes deployed for study E7.

Figure 3.8 – Locations of additional physio-chemistry probes. Note: AHD: Australian height datum; AMTD: Australian middle thread distance (distance upstream of mouth).

Table 3.2 – Summary of field studies with continuous high frequency data collection.

Field study	E1	E2	E3	E4
Date	4/04/03	17/07/03	24/11/03	2/09/04
Study focus	Near free surface	Near free surface	Near free surface	Near bed
Site	2B	2	2B	2B
ADV sampling location	~0.5 m below free surface, 14.2 m from left bank	~0.5 m below free surface, 8.0 m from left bank	~0.5 m below free surface, 10.7 m from left bank	0.05 m above bed, 10.7 m from left bank
ADV f_{scan} (Hz)	25	25	25	25
V_{range} (m/s)	1.0 and 0.3	0.3	1.0	0.3
YSI6600 sampling location	~0.5 m below free surface, 13.9 m from left bank	~0.5 m below free surface, 7.7 m from left bank	~0.5 m below free surface, 10.4 m from left bank	0.05 m above bed, 10.4 m from left bank
YSI6600 f_{scan} (Hz)	0.2	0.2	0.5	0.3

Field study	E5	E6	E7
Date	8-9/03/05	16-18/05/05	5-7/06/06
Study focus	Near bed – mid estuary – spring tide	Near bed – mid estuary – neap tide	Near bed – upper estuary – neap tide
Site	2B	2B	3
ADV sampling location	0.1 m above bed, 10.7 m from left bank	0.2 (#) and 0.4 m above bed, 10.7 m from left bank	0.2 (#) and 0.4 m above bed, 4.2 m from right bank
ADV f_{scan} (Hz)	25	25 / 25 (#)	25 / 50 (#)
V_{range} (m/s)	1.0	1.0 / 1.0 (#)	0.3 / 0.3 (#)
YSI6600 sampling location	0.1 m above bed, 10.4 m from left bank	0.4 m above bed, 10.4 m from left bank	0.4 m above bed, and 0.3 m below free surface, 3.9 m from right bank
YSI6600 f_{scan} (Hz)	0.167	0.083	0.083
Troll9000 f_{scan} (Hz)		0.167	0.167

Note: f_{scan} : sampling frequency; V_{range} : ADV velocity range; [#]: indicates information pertaining to 2D-microADV (16 MHz).

The field trips E5, E6 and E7 were all conducted over investigation periods larger than 25 hours, and are the focus of this study. The field trips E1, E2, E3 and E4 were undertaken prior to the commencement of this project. Each had an investigation period of less than 12.5 hours. These field studies were not the main data sets of this study, but were used to validate and confirm the observations made during the studies E5, E6 and E7. The turbulence and

water quality data collected during all field investigations listed in Table 3.2 are presented in Chapters 5 and 6 respectively.

3.3.2 Simultaneous physio-chemistry, hydrodynamic and fauna sampling

During the field studies E1 (4/04/2003), E4 (2/09/2004) and E8 (28/08/2006), three to four groups of undergraduate students from the University of Queensland were located at different field sites in the lower (Site 1), middle (Site 2 or 2B) and upper estuarine zones (Site 3). The students sampled physio-chemistry and hydrodynamic data simultaneously and also surveyed the fauna at each site for a period of twelve hours. During each field study students measured air and water temperatures, conductivity, turbidity, dissolved oxygen, pH, water depth and surface velocity data every 15 to 30 minutes.

For these field investigations vertical profiles of physio-chemistry data were collected at each site by a member of the EPA (QLD) using a YSI6920 probe. The vertical profiles were measured 3 to 4 times at each site throughout the investigation. About 30 minutes before the field study E8 started, approximately 30 mm of rain fell in the Eprapah catchment. During the field trip E1 a small rainstorm occurred at about 18:00 the night before the field study, while the study E4 was conducted during a severe drought period.

3.3.3 Simultaneous high frequency continuous tidal measurements at multiple locations

A series of simultaneous continuous high frequency tidal measurements were performed in October 2006. The aim was to determine the variation in tidal amplitude and phase at several longitudinal locations along the estuary. These field studies were undertaken to assist with the understanding of the basic hydrodynamics of the estuary. This information helped in the comparison of the turbulence and physio-chemistry data collected in the lower, middle and upper estuarine zones. The field study E9 consisted of two 50 hour studies approximately 10 days apart during tidal conditions close to spring and neap tides. Water depth and temperature data were measured simultaneously at Sites 1, 2B, 2C, 3, 3B and 4 (Figure 3.6) by six In-Situ mini-Troll probes continuously logged at 1 Hz. At Sites 2B and 3 water depth, temperature and conductivity data were collected every 6 s by two In-Situ Troll9000 probes. A mini-Troll probe was also placed in the outflow weir of the sewage treatment plant. It gathered water depth and temperature data every 6 s for the 13 days of the field study E9 (note that the former was related to the STP outflow discharge (Figure 3.3)).

3.4 INSTRUMENTATION

3.4.1 <u>Turbulence measurement with an acoustic Doppler velocimeter (ADV)</u>

As already noted the measurement of high frequency turbulence data in natural systems such as rivers and estuaries was until recently limited by the lack of appropriate instrumentation. Instruments which could successfully measure high frequency turbulence data in controlled laboratory conditions (e.g. laser Doppler anemometer, hot film anemometer) were unsuitable in natural waterways. The suspended sediment, flora and fauna found in estuary and river flows interfered with the turbulence measurements of these sensitive devices and rendered them impractical. Devices like the electromagnetic current meter (EMCM) are more suited to measurements in natural waterways, but could only measure over a limited sampling frequency and generally in only two dimensions. Sontek developed the acoustic Doppler velocimeter (ADV) to overcome some shortcomings of the field instrumentation. The acoustic Doppler velocimeter measures three-dimensional turbulent velocity fluctuations at a relatively high sampling frequency (up to 100 Hz) in a small remote sampling volume (e.g. Kraus et al. (1994)).

3.4.1.1 Principles of operation

Acoustic Doppler velocimetry is based upon the acoustic Doppler principle. It measures the three-dimensional particle velocities within a small sampling volume of less than 1 cm^3 and the sampling volume is located 5 to 15 cm from the probe head to reduce flow interference. An ADV sensor usually contains a transmitter and 2 to 4 signal receivers. Figure 3.9 demonstrates the principles of operation of an acoustic Doppler velocimeter. The transmitter sends out short acoustic pulses at a frequency determined by the device. Small proportions of the pulse are scattered by particles in the sampling volume and detected by the receivers. The scattered "echoes" of the pulse undergo a Doppler shift due to the relative velocity of the flow. Doppler shifts at each receiver are proportional to the velocity component (e.g. V_A, V_B and V_C) along the bisector (BI) of the transmitter and receiver beams (Figure 3.9). The number of receivers determines the number of flow velocity components that can then be resolved.

The radial velocity components (V_A, V_B and V_C) are transformed into a Cartesian coordinate system (V_1, V_2 and V_3) using a transformation matrix. This first transformation matrix is unique for each probe and is determined empirically by the manufacturer (Lohrmann et al. (1995)). The orthogonal velocities then need to be transformed into a local coordinate system, with the velocities orientated in the streamwise (V_x), transverse (V_y) and vertical (V_z) directions. For a 3D-ADV this transformation is described by the matrix B (Equation 3.1):

$$B = \begin{bmatrix} \cos\beta_3\cos\beta_2 & -\sin\beta_3\cos\beta_2 & -\sin\beta_2 \\ \sin\beta_3\cos\beta_1 - \cos\beta_3\sin\beta_2\sin\beta_1 & \cos\beta_3\cos\beta_1 + \sin\beta_3\sin\beta_2\sin\beta_1 & -\cos\beta_2\sin\beta_1 \\ \sin\beta_3\sin\beta_1 - \cos\beta_3\sin\beta_2\cos\beta_1 & \cos\beta_3\sin\beta_1 - \sin\beta_3\sin\beta_2\cos\beta_1 & \cos\beta_2\cos\beta_1 \end{bmatrix}$$

$$\begin{bmatrix} V_x \\ V_y \\ V_z \end{bmatrix} = B \bullet \begin{bmatrix} V_1 \\ V_2 \\ V_3 \end{bmatrix} \qquad (3.1)$$

where β_1, β_2 and β_3 are angles of rotation around the axes V_1, V_2 and V_3 respectively (McLelland and Nicholas (2000)). The angles β_1, β_2 and β_3 are the angles between the Cartesian coordinates and the local coordinates. Along with the three velocity components the ADV records the signal amplitude of each receiver and the correlation between each of the receivers.
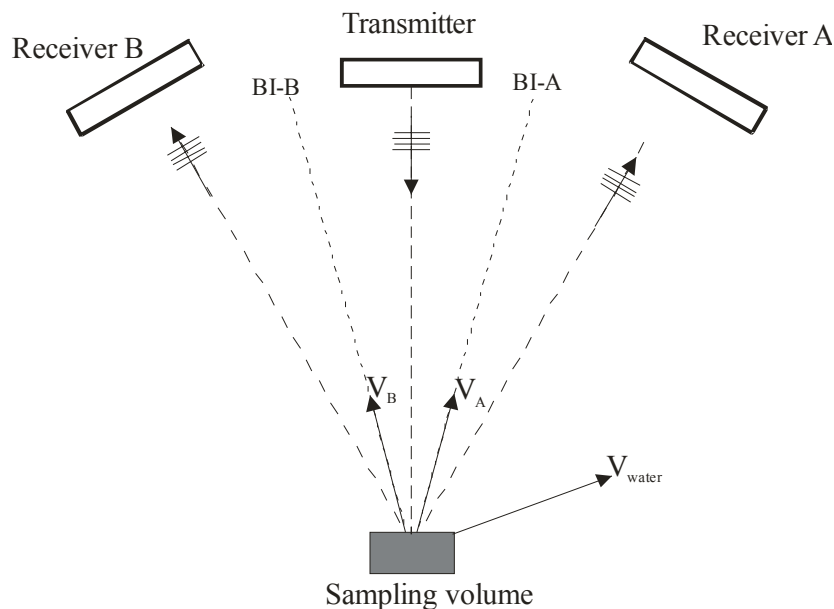
Figure 3.9 – Sketch of ADV sensor Doppler measurement technique.

In this project, the marked (e.g. coloured red in Figure 3.7B) V_1 receiver was aligned closely in the streamwise direction of the flow (i.e. parallel to the bank at the sampling location). By aligning the V_1 receiver with the streamwise direction the Cartesian coordinates are the local coordinates.

3.4.1.2   *ADV backscatter intensity as a proxy for suspended sediment concentration*

Acoustic Doppler devices perform high frequency velocity measurements, but a further output is the signal backscatter intensity (I_B). This intensity I_B is the acoustic signal that is backscattered from small particles within the sampling volume. The backscatter intensity relates to the suspended sediment concentration (Lohrmann et al. (1994), Sontek (1997)).

Thus acoustic Doppler devices can measure at high frequency (up to 100 Hz) an estimate of the sediment concentration. The backscatter intensity is calculated from the signal amplitude (AMP) of each receiver of the ADV. Measured in counts (one count equals 0.43 dB), the amplitude (AMP) represents the signal strength of the receiver. A count is the number of particles for which the transmitted signal is reflected back to the individual receiver. Lohrmann et al. (1994) outlined a simplified relationship between the acoustic signal scatter and the concentration of particles in the sampling volume (Equation 3.2):

$$I = I_0 \ C_s \ S_f \ S_a \left(\frac{e^{-2(a_w + a_s)r}}{r^2} \right) \tag{3.2}$$

where I = backscatter intensity; I_0 = transmitted intensity; a_w = water absorption; a_s = absorption due to particle scattering; r = acoustic propagation path; S_a = holds all particle specific parameters (size, elasticity, and density); S_f = all system specific parameters (transducer size, efficiency, probe geometry, receive sensitivity); and C_s = suspended sediment concentration. For low concentrations (C_s < 1 g/L) and a known particle size distribution, Equation 3.2 presents a linear relationship between sediment concentration and ADV backscatter intensity.

Lohrmann et al. (1994) calculated the backscatter intensity (I) from the ADV signal to noise ratio (SNR):

$$SNR = 10 \ log_{10} \left(\frac{I}{NL} \right) \tag{3.3}$$

Sontek (1997) recommended against calculating backscatter intensity from the signal to noise ratio. The backscatter intensity can be calculated from the signal amplitude by substituting SNR = 0.43(SL - NL), where SL is the signal amplitude (AMP); and NL is the noise level into Equation 3.3. Kawanisi and Yokosi (1997) outlined a relationship between backscatter intensity and signal amplitude:

$$I = 10^{0.043 \ SL} - 10^{0.043 \ NL} \tag{3.4}$$

Since ADVs operate at high frequencies (10 to 16 MHz) the noise level is small compared to the signal amplitude (Kawanisi and Yokosi (1997)). Kawanisi and Yokosi (1997) deduced the backscatter intensity from the averaged intensity of the three receivers. Nikora and Goring (2002) neglected the effect of noise level (NL) and used:

$$I_a \ \propto \ 10^{0.0434 \ SL_a} \tag{3.5}$$

where I_a = individual backscatter intensity for the amplitude of receiver a (SL_a). The sum of the individual amplitudes of the three receivers was multiplied by 0.00003 to estimate backscatter intensity $I_M = 0.00003 \ (I_a + I_b + I_c)$. The use of 0.00003 provided Nikora and

Goring (2002) with a pseudo intensity average from the three receivers. Other studies, such as Voulgaris and Meyers (2004) and Fugate and Friedrichs (2002) also found linear relationships between suspended sediment concentration and ADV backscatter intensity.

3.4.1.2.1 Method used

Since the signal amplitude is a scalar property of the sampling volume, the backscatter intensity I_B of an ADV signal was estimated by using the averaged amplitude of the ADV signal (AVAMP) measured in counts:

$$I_B = 0.00001 * (10^{0.043 \, \mathrm{AVAMP}}) \tag{3.6}$$

where AVAMP is the averaged amplitude output from the post-processing software (e.g. WinADV). The coefficient 0.00001 was a value introduced to avoid large values of backscatter intensity. Nikora and Goring (2002) used a constant of similar magnitude (0.00003) to "avoid too large numbers". A relationship between ADV backscatter intensity and suspended sediment concentration for this study was developed through calibration experiments (Chanson et al. (2006)). This laboratory calibration experiment is detailed in Appendix D. The relationship between backscatter intensity of the 2D-microADV (16 MHz, serial no. A641F) and the suspended sediment concentration at Eprapah Creek used in this study is:

$$SSC = 0.943 \, (1 - \exp^{(-\,0.111\,I_B)}) \qquad R = 0.996 \tag{3.7}$$

where I_B = ADV backscatter intensity; and SSC = suspended sediment concentration (g/L).

3.4.1.3 *Errors in ADV measurements*

The ADV is a robust device that is well suited to shallow-water systems such as small estuaries. However, the accuracy and reliability of the device are still under investigation. The ADV has some inherent problems, and velocity data may be adversely affected by "spike events" caused by a combination of the inherent measurement errors to the ADV instrumentation (e.g. Lemmin and Lhermitte (1999), Goring and Nikora (2002)). There are three sources of inherent measurement errors in ADV instruments (McLelland and Nicholas (2000)): sampling errors that are hardware controlled; noise that is intrinsic to the Doppler measurement technique; and errors because of velocity shear in the sampling volume.

The sampling errors may bias the mean velocity, but the velocity gradient will not affect the mean velocity if the shear is uniform across the sampling volume. Doppler noise is "white noise" and thus does not bias the mean velocity (Lohrmann et al. (1995)). Voulgaris and Trowbridge (1998) showed that the ADV sensor measured mean velocity and Reynolds stress

within 1 % of the true value, but the inherent measurement errors could influence the higher statistical moments of the velocity.

The sampling errors such as communication errors, low signal to noise ratio and low signal correlation can be found and replaced using industrial software (e.g. WinADV). Goring and Nikora (2002) proposed several methods for removing the "spikes" caused by Doppler noise from the ADV signal. Of these, the phase-space thresholding technique was found to be the most appropriate for the flow conditions in small estuaries (Chanson et al. (2005b)).

Continuous ADV measurements over long periods in natural systems may also be affected by larger disturbances not related to the natural flow conditions. The types of large disturbances observed in estuaries include: probe adjustments; navigation events near the probe; and flora and fauna passing through the sampling volume or bumping the ADV sensor. The effect of these large disturbances has not been investigated in-depth to date, the exception being navigation events (e.g. Schoellhamer (1996), Verney et al. (2007)). However, these disturbances need to be removed and replaced in the data set before a proper turbulence analysis can be undertaken.

A post-processing technique was developed to remove the errors caused by both small (e.g. Doppler noise) and large disturbances (e.g. navigation events) from the ADV velocity data. This post-processing technique was first described in Chanson et al. (2005b) and it is comprehensively described in Section 4.2 and Appendix A.

3.4.1.4 *Specifications of the Sontek 3D-ADV (10 MHz) and 2D-microADV (16 MHz)*

Two acoustic Doppler velocimeters were used in the field studies at Eprapah Creek. These were: (1) a Sontek UW ADV (10 MHz, serial 0510) with a three-dimensional down-looking head; and (2) a Sontek microADV (16 MHz, serial number A641F) with a two-dimensional side-looking head. Table 3.3 presents the factory specifications for the two instruments. The 3D-ADV (10 MHz) was used in all field trips until the study E7 (i.e. studies E1 to E7, Table 3.2), while the 2D-microADV (16 MHz) was used in the field trips E6 and E7.

Table 3.3 – Specifications of ADVs used for field investigations in Eprapah Creek.

	2D-microADV (16 MHz)	3D-ADV (10 MHz)
Sampling rate (Hz)	0.1 to 50	0.1 to 25
Sampling volume (cc)	0.09	0.25
Distance to sampling volume (cm)	5	5
Resolution (cm/s)	0.01	0.01
Programmed velocity range (cm/s)	3, 10, 30, 100, 250	3, 10, 30, 100, 250
Accuracy	1 % of measured velocity	
Measured velocity components	V_x , V_y	V_x , V_y , V_z

3.4.2   Collection of physio-chemistry data

During the field studies conducted at Eprapah Creek four different physio-chemistry probes were used, depending on the investigation.   These were: YSI6600; YSI6920; In-Situ Troll9000; and In-Situ mini-Troll probes.

3.4.2.1   YSI6600 probe

A YSI6600 probe (Figure 3.10) is a multi-port probe capable of long term monitoring (up to 75 days) and will sample each of the physio-chemical properties at the programmed interval. The sampling frequency is limited by the system memory, which stores 1500,000 readings and the duration of investigation period. For the field studies at Eprapah Creek (Table 3.1), the YSI6600 probe was used to monitor water depth, water temperature, conductivity, dissolved oxygen, pH, turbidity and chlorophyll a levels.

For each field study a YSI6600 probe was aligned horizontally with the sampling volume of the 3D-ADV, 0.3 m towards the bank. In the study E7 a second YSI6600 probe was deployed on a float 10 m upstream of the ADV sampling location. The second YSI6600 probe sampled continuously at approximately 0.3 m below the free surface. Table 3.4 outlines the factory specifications of the sensors used in the YSI6600 probe for the field studies conducted at Eprapah Creek. The YSI6600 probes used in this project were provided and calibrated by the Queensland Environmental Protection Agency (EPA (QLD)).

Figure 3.10 – YSI6600 probe with sensors exposed.

Table 3.4 – Sensor specifications for YSI6600 and YSI6920 probes.

Sensor for:	Range	Resolution	Accuracy YSI6600	Accuracy YSI6920
depth (m)	0 to 9	0.001	± 0.02	± 0.02
temperature (C)	- 5 to + 45	0.01	± 0.15	± 0.15
conductivity (mS/cm)	0 to 100	0.001 to 0.1	± 0.5 %	± 0.5 %
dissolved oxygen (mg/L)	0 to 50	0.01	0 to 20: ± 2 % 20 to 50: ± 6 %	0 to 20: ± 2 % 20 to 50: ± 6 %
pH (unit)	0 to 14	0.01	± 0.2	± 0.2
turbidity (NTU)	0 to 1,000	0.1	± 5 %	± 5 %
chlorophyll a (µg/L)	0 to 400	0.1	Not available	Not measured

3.4.2.2 _YSI6920 probe_

The YSI6920 probe measures water depth, temperature, conductivity, pH, turbidity and dissolved oxygen. YSI6920 probes are used by the EPA (QLD) to conduct the monthly monitoring of estuaries in Southeast Queensland. During or about the time of the field investigations at Eprapah Creek, the EPA (QLD) conducted its monthly monitoring program. The monthly monitoring program measured vertical profiles of key physio-chemical properties (outlined in Table 3.4) at certain locations along the creek. For the field studies E1, E4 and E8, multiple vertical profiles were collected along Eprapah Creek in conjunction with the student field trips (Section 3.3.2). Figure 3.11 shows the EPA (QLD) collecting physio-chemistry samples at Eprapah Creek using a YSI6920 probe.

YSI6920 probe

Figure 3.11 – EPA (QLD) monthly monitoring conducted at Eprapah Creek during study E6 on 17/05/05. Photograph by H. Chanson looking upstream from Site 2.

3.4.2.3 *In-Situ Troll9000 probe*

The In-Situ Troll9000 probe (Figure 3.12) is a thin multi-port probe that was used to measure water pressure, temperature and conductivity for the field studies E6, E7 and E9. During these studies a number of Troll9000 probes were placed longitudinally or transversely in the creek in conjunction with other physio-chemistry probes (Figure 3.8). A Troll9000 probe is capable of storing up to 240,000 readings. The specification of the sensors used in the Troll9000 probes during field studies at Eprapah Creek are presented in Table 3.5.

Table 3.5 – Specifications of sensors used in Troll9000 and mini-Troll probes.

Sensor for:	Troll9000			mini-Troll	
	Range	Resolution	Accuracy	Range	Accuracy
water level (m)	0 to 11	0.001	± 0.1 %	0 to 11	± 0.2 %
temperature (C)	- 5 to + 50	0.01	± 0.1 %	- 5 to + 50	± 0.25
conductivity (mS/cm)	0 to 60	Range dependent	± 2 %	Not measured	

Figure 3.12 – In-Situ Troll9000 probe.

3.4.2.4 *In-Situ mini-Troll probe*

The In-Situ mini-Troll probe (Figure 3.13) measures water level and temperature at a sampling frequency up to 2 Hz, with the specifications outlined in Table 3.5. It is capable of storing up to 240,000 samples. Seven mini-Troll probes were used during the field trip E9 (2-13/10/06) to measure water level and temperature variation at 1 Hz for selected locations along Eprapah Creek (Section 3.3.3).

Figure 3.13 – In-Situ mini-Troll probe.

3.5   PRACTICAL EXPERIENCES

The study of natural systems raises some interesting challenges for the researcher. Weather, tidal and freshwater inflow conditions change continuously and can only be predicted with a limited accuracy. Local flora, fauna and human activities can interfere with experimentation in natural systems such as estuaries. These natural factors make each field experiment unique, and impossible to replicate. It is for these reasons that the importance of careful and thorough preparation of the field investigations can not be emphasised enough. In particular, all instrumentation must be thoroughly calibrated before and after each field study. Manual readings are an essential part of a successful field investigation. The manual measurement of properties such as water depth, temperature, surface velocity and turbidity all assist in the validation of the data collected by digital instrumentation. Along with these manual readings, observations of peculiar flow events, navigation and fauna activity about the experimental region should be recorded in a manual log of the experiment. These manual entries assist with the post-processing of the ADV signal (Section 4.2 and Appendix A), which ensures the quality of the data analysed.

3.5.1   <u>Vertical velocity component</u>

With the 3D-ADV system, some possible problems were encountered with the vertical velocity component (e.g. Chanson (2003)). It is believed that the ADV emitter, stem and body created some form of wake which adversely affected the vertical velocity. Chanson (2003) stated that the time-averaged vertical velocity should be approximately zero, but this was not found with vertical velocity data measured with the 3D-ADV (10 MHz). A similar experience was noted during field studies at Hamana Lake, Japan, by Aoki (personal communication, 2005). It is worth noting that the vertical velocity data measured with a Nortek Vector 3D-ADV for the field studies at Hamana Lake during November and

December 2005 did not have a mean of zero over the entire data sets (Appendix G). This indicated that the same possible fault occurred in this piece of equipment, and therefore may conceivably be common to all 3D-ADV with down-looking heads. The vertical velocity data collected at Eprapah Creek and Hamana Lake are presented with this in mind and are discussed with caution, due to this possible error. No adjustment of the vertical velocity data were attempted in this project. It is not known whether the observed anomaly in the vertical velocity is caused by erroneous data or is just a natural phenomenon. Since the probe was mounted vertically with a down-looking head and the vertical velocities were small, the effects on the horizontal velocity components were deemed negligible.

3.5.2   Hardware fault in 3D-ADV (10 MHz) during the field study E7

After a thorough inspection of the data set measured with the 3D-ADV (10 MHz, serial 0510) during the field trip E7 (5-7/06/06), it was determined that a hardware fault in the ADV system occurred. The 3D-ADV (10 MHz) signal was very noisy, with uncharacteristically lower signal to noise ratios observed on two of the three sensors. These two sensors consistently had signal to noise ratios half the strength of those of the third sensor of the 3D-ADV (10 MHz) and the two sensors of the 2D-microADV (16 MHz) throughout the field study E7. This hardware fault affected the high-pass filtered data collected, with the noise generated dominating the ADV signal between 25 and 0.1 Hz. This meant that only the time-averaged velocity data could be used. All other turbulence data were not used within this project because of the influence of the hardware fault on the higher statistical moments.

4 ADV DATA PROCESSING

4.1 PRESENTATION

Before analysis of any data recorded by an ADV, the signal must undergo several layers of processing. This chapter outlines the processing techniques and analysis methods used for the ADV data collected at Eprapah Creek. The raw ADV data must first undergo a post-processing procedure (outlined in Section 4.2), to find and remove erroneous and/or corrupted data points. Section 4.2 notes that the ADV data measured in natural systems contain small disturbances inherent to ADV measurements, and large disturbances caused by humans, flora and/or fauna interacting with the instrumentation. In Section 4.2 the details of the signal processing to find and repair the erroneous and corrupted data generated by these large and small disturbances to the ADV signal. The post-processed data are then used for the turbulence analyses. Section 4.3 outlines the methods applied to the post-processed ADV data to calculate the turbulence properties.

4.2 ADV SIGNAL POST-PROCESSING

The ADV is a robust device that is well suited to shallow-water systems such as small estuaries. However, and as previously noted, the accuracy and reliability of the device are still under investigation. The ADV has some inherent problems and velocity data may be adversely affected by "spike events" caused by a combination of aliasing of the Doppler signal, velocity shear, intrinsic Doppler noise and hardware errors (e.g. Lemmin and Lhermitte (1999), Goring and Nikora (2002)). Continuous ADV measurements over long periods in natural systems may be affected by larger disturbances, such as probe adjustments and navigation events.

Both small and large disturbances must be found and the data replaced prior to turbulence statistical analysis. A procedure known as "post-processing" was applied to the raw acoustic Doppler velocimeter data. After a velocity signal check (e.g. WinADV), the post-processing procedure finds large disturbances and replaces the corrupted data, then the post-processing procedure finds the small disturbances and the corresponding erroneous data are replaced.

4.2.1 <u>Post-processing technique</u>

After collection the ADV data were processed in several stages. Firstly, data points containing communication errors, low signal to noise ratio (SNR < 5 dB) and low signal correlation (COR < 60 %) were found and replaced. This was usually done by an industrial software (e.g. WinADV). Two further stages called "pre-processing" and "de-spiking" were also used to process the data. The former stage (pre-processing) was designed to find and

replace data corrupted by large disturbances (e.g. probe adjustments). The latter stage (de-spiking) was developed to find and replace data corrupted by "spike events" and other small disturbances.

All stages of post-processing involved two steps: i.e., detection and replacement of erroneous data. Both steps were performed in each stage before the start of the next stage. Each detection step was performed on the high-pass filtered data (e.g. $f > 0.1$ Hz for Eprapah Creek data). Erroneous data were replaced using a technique based upon the mean of the endpoints. The mean of the endpoints technique reduced distortion of statistical values, while not inferring trends on the replaced data.

In the pre-processing stage, large disturbances were searched for with a minimum of 3,500 data points replaced per event. Replacement was conducted on the original data, to avoid inferring a trend that would occur if the replacement process was undertaken on the high-pass filtered data.

The de-spiking stage searched for small disturbances, usually less than 10 data points in size. In the de-spiking stage data replacement was conducted on the high-pass filtered data. After the completion of the iterative de-spiking process, the high-pass filtered data were added to the low-pass filtered component. Minimal trend was inferred when the low-pass and high-pass filtered data were added, since only a small quantity of data were replaced.

4.2.2 Pre-processing stage

This stage was developed as part of this study. It finds and replaces events that cause large disturbances to the measured velocity data. In small subtropical estuarine systems, large disturbances can be caused by a probe adjustment, navigation event, fish or bird activity, floating debris and wind. It was found that the probe adjustments and navigation events caused the largest disturbances. Both types of events could conceivably cause disturbances with a magnitude much larger than the natural velocity fluctuations (Chanson et al. (2005b)). Figure 4.1 presents an example of a probe adjustment and a navigation event.

(A) Probe adjustment.   (B) Navigation event.

Figure 4.1 – Example of a probe adjustment and a navigation event at Eprapah Creek for study E2 (17/07/03). Photographs by H. Chanson.

4.2.2.1   *Probe adjustment event search*

During data acquisition, it was found that any probe motion caused large disturbances. Vertical probe adjustments may be applied at regular intervals to maintain the probe sampling volume within a certain distance of the free surface in an estuary, for example. Figure 4.2 shows the increased velocity fluctuations in all three velocity components during a probe adjustment. In the detection step the high-pass filtered data ($f > 0.1$ Hz for Eprapah Creek studies) were used to locate the probe adjustments.
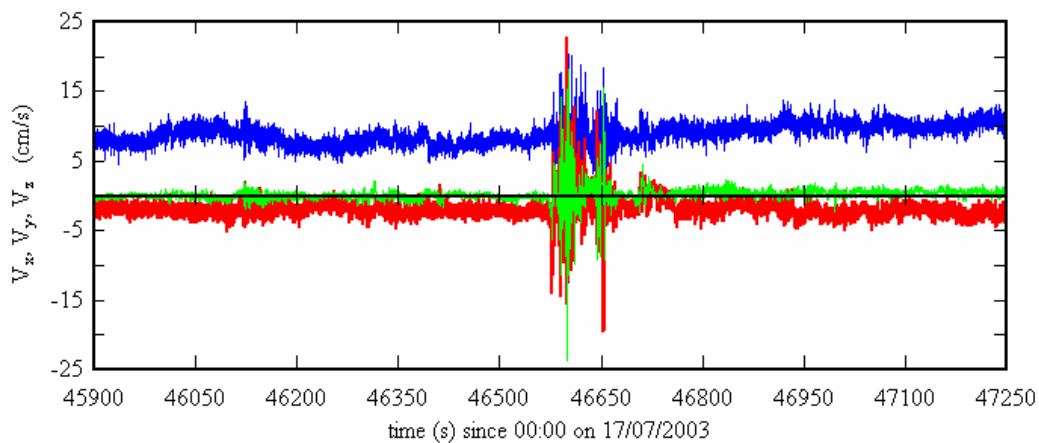
Figure 4.2 – Example of velocity signal during a probe adjustment. Data collected during study E2 (17/07/03) at Eprapah Creek. Probe adjustment occurred at start of ebb tide. Legend: — streamwise velocity V_x ; — transverse velocity V_y ; — vertical velocity V_z .

A search region is generated around the position of a known probe adjustment. For each velocity component the standard deviation ($\sigma_{SR(P)}$) of the velocity over the search region was

calculated and multiplied by a dimensionless threshold constant (C_{EP}). This provided the event threshold (λ_{EP}, Equation 4.1) for that component:

$$\lambda_{EP} = C_{EP} \times \sigma_{SR(P)} \tag{4.1}$$

Within the search region, the velocity component standard deviations in smaller statistical data "windows" were compared to the event threshold λ_{EP}. If the standard deviation of the smaller statistical window exceeded the event threshold λ_{EP} in two or more of the velocity components, the data points in that window were deemed "disturbed". These data points were then replaced.

4.2.2.2 *Navigation event search*

Navigation events may affect the data for several minutes after the passage of a boat (e.g. Chanson (2003), Verney et al. (2007)). Figure 4.3A shows the effect of a navigation event on the velocity data. The detection of navigation events was performed on the high-pass filtered data. A search region was generated about a known event position. Within the search region the vertical acceleration (A_Z) was calculated (Equation 4.2). The acceleration magnitude (AM) between data points of the vertical acceleration data was calculated using Equation 4.3 (where j is the data point number):

$$A_Z(j) = \frac{\left(V_Z(j) - V_Z(j-1)\right)}{\partial t} \tag{4.2}$$

$$AM = \left|A_Z(j)\right| + \left|A_Z(j-1)\right| \tag{4.3}$$

$$\lambda_{EN} = C_{EN} \times \sigma_{SR(N)} \tag{4.4}$$

where $\partial t = 1/f_{scan}$; with f_{scan} = ADV sampling frequency (25 or 50 Hz herein). Navigation events caused large fluctuations in the vertical acceleration magnitude, typically associated with the propagation of the bow wave (Schoellhamer (1996)). An event threshold (λ_{EN}, Equation 4.4) was determined by multiplying the standard deviation of the acceleration magnitude ($\sigma_{SR(N)}$) in the search region by a threshold constant (C_{EN}). Standard deviations of smaller statistical data samples within the search region were compared to the event threshold λ_{EN}. If the sample standard deviation of vertical acceleration was greater than the event threshold λ_{EN}, that data sample was "flagged" and the data replaced.

The maximum value of acceleration magnitude within the "disturbed" region indicates the vertical acceleration induced by the first bow wave when its impact reaches the probe location. Figure 4.3B shows the acceleration magnitude of the data set shown in Figure 4.3A. In

Figure 4.3B the maximum acceleration magnitude coincides with the start of the disturbance induced by the boat passage.
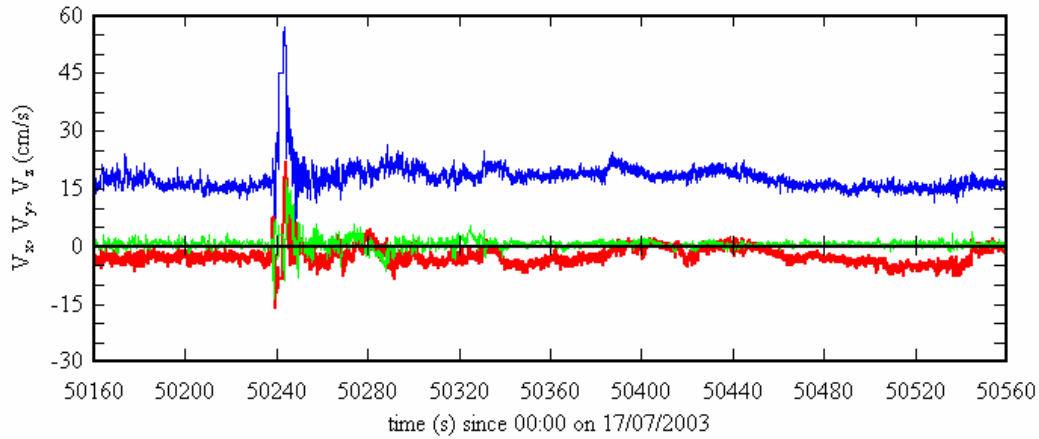
(A) Example of a navigation event and its effect on three velocity components.
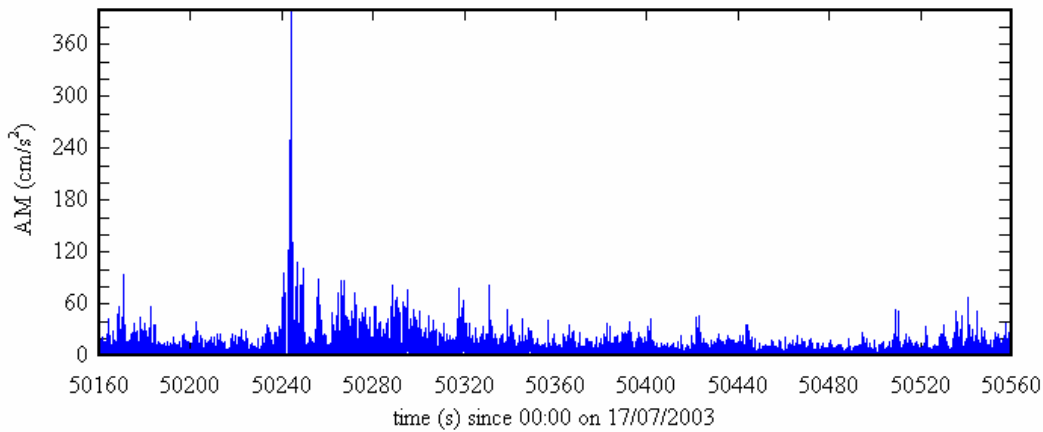
(B) Acceleration magnitude (AM) data for navigation event shown.

Figure 4.3 – Example of a navigation event that occurred close to ADV. Data collected during field study E2 (17/07/03) about 0.5 m below surface at Site 2, Eprapah Creek. Navigation event occurred on mid ebb tide.

Legend: — streamwise velocity V_x ; — transverse velocity V_y ; — vertical velocity V_z .

4.2.2.3 *Unknown event search*

The detection of large disturbances was dependent upon the manual recording of the time that such an event occurred. There were however some other events which might not have been observed and not recorded manually.

After all probe adjustments and navigation events were processed a final check of the data was conducted. The data set was checked for any large disturbances such as un-logged probe adjustments and navigation events, or flora/fauna interfering with the ADV. Localised searches were performed on each velocity component using 15 minute long sections

throughout the entire data set. For each section the event threshold (λ_{EU}, Equation 4.5) was calculated by multiplying the section standard deviation ($\sigma_{SS(U)}$) of a velocity component by the threshold constant C_{EU}:

$$\lambda_{EU} = C_{EU} \times \sigma_{SS(U)} \qquad (4.5)$$

The standard deviations of the smaller statistical data samples of each section were compared to the event threshold λ_{EU}. If the standard deviation of the data sample were larger than the event threshold λ_{EU}, the data in that sample were "flagged" but not replaced.

Data were only replaced during this stage if the "unknown events" found occurred within the known limits at the beginning and end of the field study. During these times people were known to be around the probe, setting up or dismantling the experiment. The beginning and end of these periods were manually recorded. Any unknown events found during these periods were considered to be similar to probe adjustments (i.e. human interference) and were therefore replaced.

4.2.3   De-spiking stage

Two de-spiking methods were investigated in this study. These were the acceleration thresholding method and the phase-space thresholding method (Goring and Nikora (2002)). Initial investigations showed that the acceleration thresholding method was inappropriate for the low velocity unsteady flows under investigation (Appendix A). The phase-space thresholding method was found suitable and was used here.

4.2.3.1   Phase-space thresholding method

The phase-space thresholding method uses a three-dimensional Poincaré map (phase space plot) to plot a variable and its derivatives against each other (Goring and Nikora (2002)). Here the variable was the high-pass filtered data of an individual velocity component. An ellipsoid generated using the Universal Criterion (UC, Equation 4.6) determined which data points were contaminated by "spike events". The Universal criterion was calculated for each velocity component from the standard deviation σ and the number of data points N within the entire data set:

$$UC = \Lambda_U \, \sigma \qquad (4.6)$$

where $\Lambda_U = \sqrt{2 \, Ln(N)}$ is the Universal threshold. A slightly enhanced version of this method was used here, where data points found outside the ellipse of a single velocity component were deemed erroneous and replaced in all components.

41

For each velocity component, the "surrogate" first and second derivatives (Equations 4.7 and 4.8 respectively) were calculated:

$$\Delta u_j = \left(u_{j-1} - u_{j+1} \right)/2 \tag{4.7}$$

$$\Delta^2 u_j = \left(\Delta u_{j-1} - \Delta u_{j+1} \right)/2 \tag{4.8}$$

where u = individual velocity component ($u = U - \overline{U}$); and j = data point number. These form the dimensions of the investigation phase space (Figure 4.4). Figure 4.4 shows a section of streamwise velocity data from the field study E2 in phase space.

The Universal Criterion (UC) of each derivative provides the major and minor ellipse threshold values. Any data points outside the three-dimensional ellipse were deemed erroneous. Erroneous data were replaced on the high-pass filtered data before the next iteration was performed. The iteration process then continued until no new erroneous data points were found.
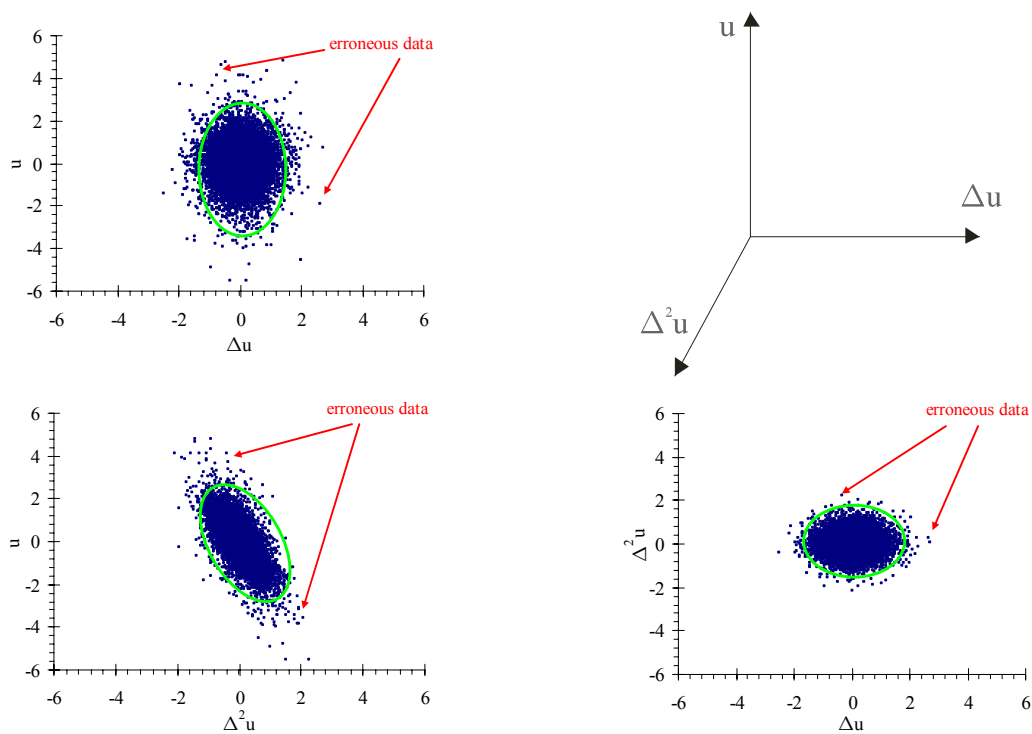
Figure 4.4 – Streamwise velocity component and its "surrogate" derivatives in phase space. Data in example are first 10,000 data points from study E2.

The phase-space thresholding method does not require calibration to the velocity data set. But, as a new technique, some questions remain regarding the best way to apply the technique. Wahl (2003) questioned the use of the Universal threshold criterion for generating the boundaries of the ellipse. In response, Goring and Nikora (2003) defended the use of this criterion. Wahl (2003) also suggested the use of the median and the median of absolute

deviation instead of the mean and standard deviation. Wahl suggested that these would improve the method's ability to detect spike events and eliminate the need to iterate. Goring and Nikora (2003) agreed that the use of the median improved the robustness of the method, but disputed that it eliminated the need to iterate.

4.2.4 Discussion

A sensitivity analysis was undertaken before this post-processing technique was applied to the ADV data sets collected at Eprapah Creek (Appendix A). This sensitivity analysis investigated all variables in the post-processing procedure using the data measured during the field studies E2, E3 and E4. It found that the standard values used for the sensitivity analysis (Appendix A) provided robust results. However, an independent velocity data set recorded simultaneously with ADV measurements would assist in the optimisation of all post-processing parameter values. The key parameters of the post-processing procedure were found to be:

High-pass/low-pass filtering threshold (Λ_f), with a standard value = 10 s

Event threshold parameters (C_{EP}, C_{EN}), with a standard value = 1.5

Statistical search window size (SW), with a standard value = 1,000 data points

where Λ_f is the frequency that separates the low-pass and high-pass filtered data, defining the frequency ranges of each, with the extreme upper limit being $2 \times \partial t$ (time step size (s)), while the extreme lower limit is 0 Hz. The post-processing technique was then applied to all ADV data sets collected at Eprapah Creek. Table 4.1 outlines the number erroneous data points detected in the ADV data sets of the studies E1 through E7. The post-processing technique found that 6.3 % of all data collected were corrupted by large or small disturbances to the ADV signal. This highlights the importance of post-processing the ADV data before analysis.

The ADV data set for the field trip E2, before and after the application of the post-processing procedure is shown in Figure 4.5. Figure 4.5 shows the instantaneous velocity components of the study E2 as functions of time since midnight on 17/07/03. This ADV data set was one of the best for illustrating the effectiveness of the post-processing technique, as it contained a period of large noise corruption (t = 38,000 to 42,000 s) and numerous large disturbances. It was conducted near the free surface, so numerous probe adjustments occurred and experimental boat passes were undertaken as part of the investigation. Appendix A details the effectiveness of the post-processing technique in removing the data corrupted by small and large disturbances, primarily using the data set of the field study E2.

Table 4.1 – Number of erroneous data points detected and removed from ADV data sets.

Field study	ADV type	Total data points	Number of erroneous data points			Total erroneous data points	%
			Velocity signal check	Pre-processing	De-spiking		
E1	3D-ADV	332,567	1,358	53,471	76,968	132,067	40
E2	3D-ADV	696,129	5,580	78,005	53,596	137,181	20
E3	3D-ADV	596,297	12,762	54,058	9,118	75,938	13
E4	3D-ADV	841,807	441	25,131	61,207	86,779	10
E5	3D-ADV	2,246,210	138,203	0	23,950	162,153	7
E6	3D-ADV	4,362,222	357	189,574	62,003	251,934	6
	2D-microADV	4,342,930	706	175,291	94,657	270,654	6
E7	3D-ADV	4,496,595	data set corrupted due to instrumentation fault (Section 3.5.2)				--
	2D-microADV	8,994,684	1,678	200,430	93,414	295,522	3
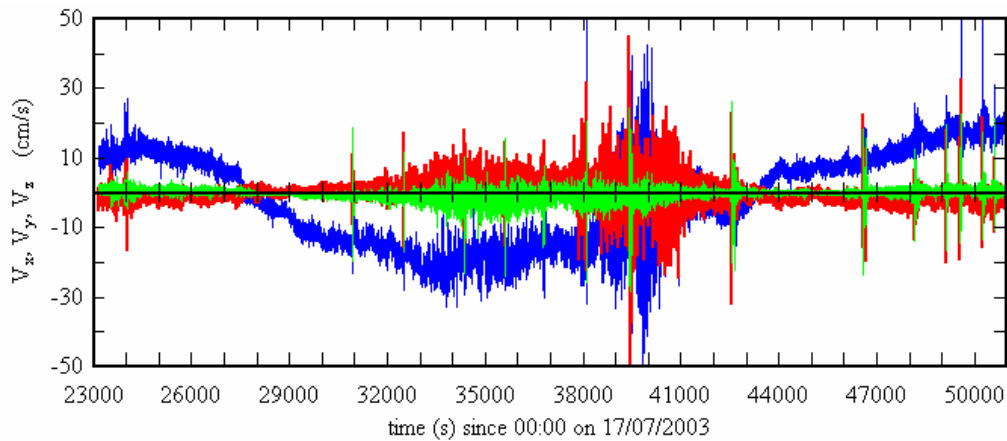
(A) Instantaneous velocity data before post-processing.
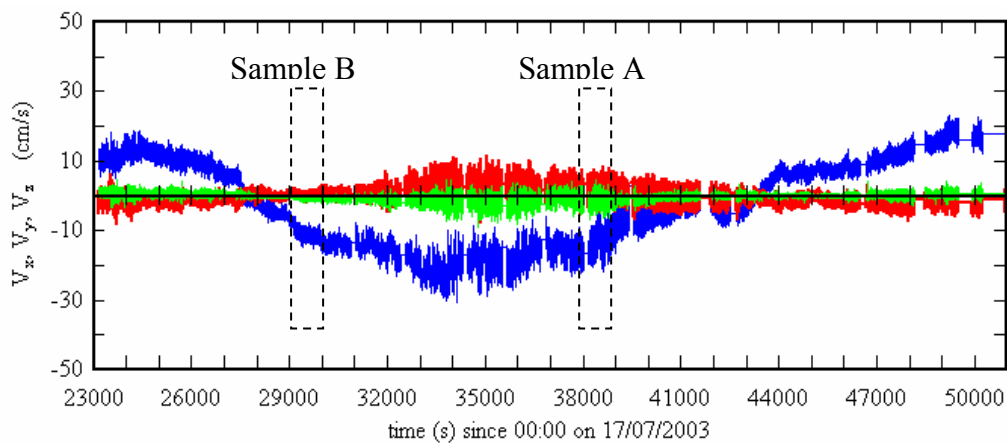
(B) Instantaneous velocity data after post-processing.

Figure 4.5 – Instantaneous velocity data of field study E2 (17/07/03). Data collected at 25 Hz about 0.5 m below surface at Site 2, Eprapah Creek.

Legend: — streamwise velocity V_x ; — transverse velocity V_y ; — vertical velocity V_z .

Table 4.2 illustrates and example of the impact of post-processing on the turbulence statistics. In Table 4.2 the statistics of Sample A (high noise sample) and Sample B (low noise sample) before and after post-processing are shown. Both Sample A and Sample B (starting at t = 38,000 and 29,000 s since midnight on 17/07/03 respectively) are highlighted in Figure 4.5B. Sample A contained 62 % erroneous data points caused by "spike events", while Sample B contained no erroneous data points. For Sample A there was a large difference in turbulence statistics before and after post-processing. Whereas for Sample B the difference between the turbulence statistics before and after post-processing was small.

Table 4.2 – Comparison of statistics for two data samples of streamwise velocity (study E2). Sample A (high noise region, t = 38,000 s) and Sample B (low noise region, t = 29,000 s). Both data samples contain 5,000 data points.

	$\overline{V}_x$ (cm/s)	v'_x (cm/s)	$Sk(V_x)$	$Ku(V_x)$
Sample A before de-spiking	-4.39	3.39	0.002	5.91
Sample A after de-spiking	-4.59	1.66	-0.095	-0.246
Sample B before de-spiking	-10.17	0.83	0.005	-0.066
Sample B after de-spiking	-10.17	0.83	0.005	-0.066

Note: $\overline{V}_x$: time-averaged streamwise velocity; v'_x : standard deviation of streamwise velocity; $Sk(V_x)$: skewness of streamwise velocity; and $Ku(V_x)$: kurtosis of streamwise velocity.

4.3   CALCULATION OF TURBULENCE PROPERTIES

Each post-processed data set contained the three instantaneous velocity components V_x, V_y and V_z, where x is the streamwise direction (positive downstream); y is the transverse direction (positive towards left bank); and z is the vertical direction (positive upwards). A basic turbulence analysis yielded the first four statistical moments of each velocity component, and the respective integral and dissipation time scales. From the velocity data, the instantaneous Reynolds stress tensor was extracted and the first four statistical moments of the tangential Reynolds stresses were calculated. The analysis also yielded the correlation coefficients of Reynolds stress and the horizontal and vertical turbulence intensity ratios.

All turbulence properties were calculated using the sampling size and sampling technique described in Section 4.3.1. Note that a data sample was considered corrupted if more than 20 % of the data points in that sample were erroneous. Corrupted data samples were not analysed (i.e. left blank), so as not to influence the turbulence properties analysed.

4.3.1 Sampling size of turbulence properties

In natural estuaries the flow is unsteady and gradually time-variable. The sample size for the calculation of the time-averaged velocity ($\overline{V}$) effectively acts as a low-pass filter threshold. The cut-off frequency affects the calculation of the turbulent velocity fluctuations v ($v = V - \overline{V}$) for a given data set. This cut-off frequency is critical and must provide a sample size that yields statistically meaningful results, and it must be larger than the turbulent velocity fluctuations, yet smaller than the variation of the tides.

For the present study, all the turbulence properties were processed over 200 s (5,000 data points at 25 Hz and 10,000 data points at 50 Hz). A sensitivity analysis found that a sampling period of 200 s allowed 95 % of all data samples to be statistically stationary over several tidal cycles (Appendix B). Turbulent properties were calculated every 10 s along the entire data set to limit the number of samples to be analysed. As the "10 s" interval was smaller than the sample size (200 s), the data points within neighbouring samples overlapped (Figure 4.6). Figure 4.6 illustrates the data sampling technique.
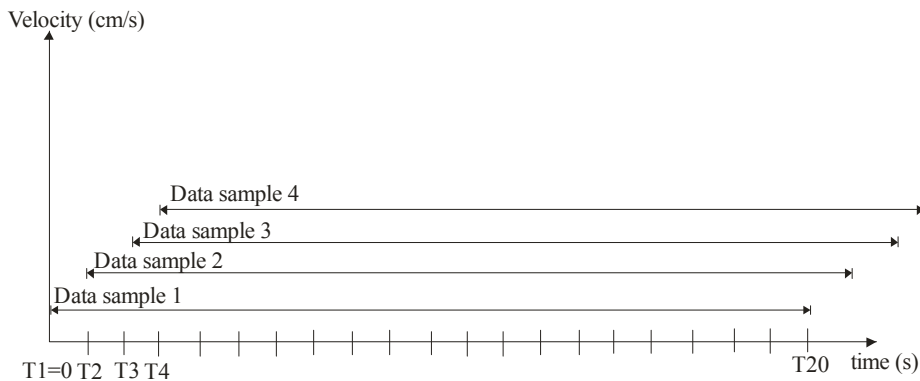
Figure 4.6 – Data sampling technique used for calculation of turbulence properties.

4.3.2 Instantaneous Reynolds stresses

The Reynolds stress tensor included the normal stresses and tangential stresses. A Reynolds stress describes a transport effect resulting from the turbulent motion induced by velocity fluctuations, with its subsequent increase of momentum exchange and mixing (Piquet (1999)). The instantaneous Reynolds stress is defined as:

$$\rho v_l v_m = \rho \left(V_l(j) - \overline{V_l} \right) \left(V_m(j) - \overline{V_m} \right) \tag{4.9}$$

The instantaneous values of $\overline{V_l}$, $\overline{V_m}$ (l, m = direction tensors: x, y, z) were calculated using 200 s samples from the data point being calculated. The first four statistical moments of each tangential Reynolds stress were calculated from this instantaneous Reynolds stress data.

4.3.3 Statistical moments

The first four statistical moments (time-averaged mean, standard deviation, skewness and kurtosis) of the velocity and tangential Reynolds stresses were used. These were calculated using the definition of the statistical moments provided in Press et al. (1992). Press et al. defined the time-averaged mean ($\overline{X}$), standard deviation ($x^{'}$), skewness ($Sk(X)$) and kurtosis ($Ku(X)$) of the instantaneous random variable X as:

$$\overline{X} = \frac{1}{N}\sum_{j=1}^{N} X_{j} \tag{4.10}$$

$$x^{'} = \sqrt{\frac{1}{N-1}\sum_{j=1}^{N}\left(X_{j} - \overline{X}\right)^{2}} \tag{4.11}$$

$$Sk(X) = \frac{1}{N}\sum_{j=1}^{N}\left[\frac{X_{j} - \overline{X}}{x^{'}}\right]^{3} \tag{4.12}$$

$$Ku(X) = \left\{\frac{1}{N}\sum_{j=1}^{N}\left[\frac{X_{j} - \overline{X}}{x^{'}}\right]^{4}\right\} - 3 \tag{4.13}$$

where N = number of data points in a sample; j = data point number; and X_{j} = data value at sample number j. The kurtosis is zero for a Gaussian distribution and this definition is known as "excess kurtosis" (Kenney and Keeping (1951)).

The standard deviation characterises the magnitude of fluctuations about the time-averaged mean. Skewness and kurtosis provide some information regarding the temporal distribution of fluctuations around its mean value and the deviations from a Gaussian distribution. Non-zero skewness indicates some degree of temporal asymmetry of the turbulence fluctuations (e.g. sweep versus ejection). A kurtosis larger than zero is associated with a peaky signal (e.g. produced by intermittent turbulent events). Although turbulence is a "random" process, and hence Gaussian, Bradshaw (1971) stated that: "the small departures from a Gaussian probability distribution are the most interesting features of the turbulence".

4.3.4 Eulerian time scales

An autocorrelation analysis was used to calculate the Eulerian integral and dissipation time scales. The normalised autocorrelation function R_{ii} for a point measurement was defined as:

$$R_{ii}(\tau) = \frac{R(v_{i}(t), v_{i}(t + \tau))}{v_{i}^{'2}} \tag{4.14}$$

where v is the instantaneous velocity fluctuation ($v = V - \overline{V}$); $v^{'}$ is the standard deviation of velocity; i is a direction tensor ($i = x, y, z$); τ is the time lag; and R is the covariance

function. Figure 4.7 shows an autocorrelation function and demonstrates how the Eulerian integral and dissipation time scales were calculated from it.
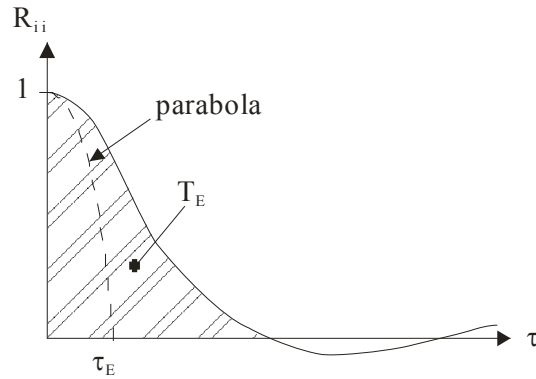
Figure 4.7 – Sketch defining an autocorrelation function and Eulerian integral T_E and dissipation τ_E time scales.

4.3.4.1 *Integral time scales*

The integral time scale represents the longest connection in the turbulent velocity fluctuations. Piquet (1999) defined the integral time scale T_E as:

$$T_E = \int_{\tau=0}^{\tau(R_{ii}(\tau)=0)} R_{ii}(\tau)\,d\tau \tag{4.15}$$

where τ is the time lag; R_{ii} is the normalised autocorrelation function; i is a direction tensor $(i = x, y, z)$; and $\tau(R_{ii}(\tau) = 0)$ is the time lag for which $R_{ii} = 0$ (Figure 4.8). Integral time scales are equal to the area under the normalised autocorrelation curve up to $R_{ii}(\tau) = 0$. Figure 4.8 illustrates the calculation of the integral time scale.
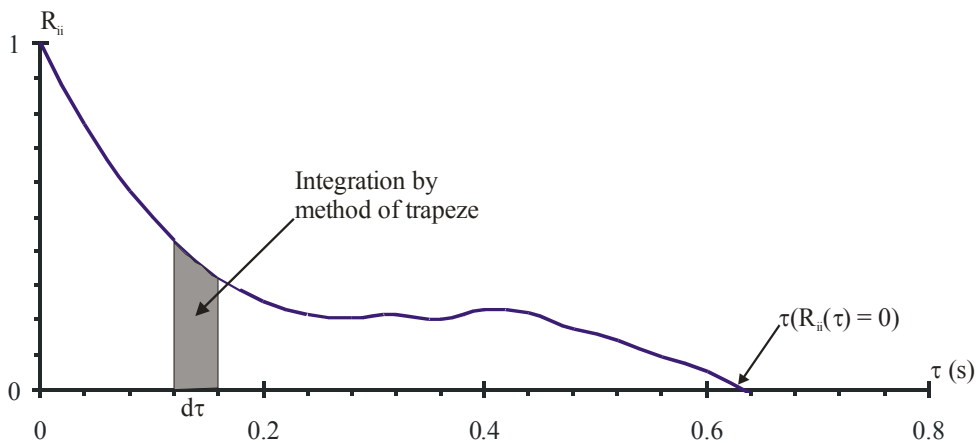
Figure 4.8 – Calculation of integral time scale using area under autocorrelation function until $R_{ii}(\tau) = 0$. Data in example from field study E2 (17/07/03) for data sample of 200 s.

For each data sample of 200 s (5,000 (25 Hz) and 10,000 (50 Hz) data points), the integral time scale was calculated for each correlation window of 10 s (250 (25 Hz) and 500 (50 Hz) data points). The overall integral time scale of the data sample was calculated by averaging the individual integral time scales of the correlation windows within that data sample. At present the individual correlation windows within a statistical data sample window do not overlap. If $\tau\left(R_{ii}(\tau) = 0\right) < 1/f_{scan}$ then the value of that sample was ignored.

4.3.4.2 *Dissipation time scales*

The dissipation time scale τ_E is a measure of the most rapid changes that occur in the turbulent fluctuations of velocity v(t) (Hinze (1975)). It is related to the curvature of the autocorrelation function at the origin ($\tau = 0$). Using the Taylor series expansion of the autocorrelation function, the dissipation time scale τ_E may be expressed as:

$$\tau_E = \sqrt{\frac{2\,v'^2}{\overline{\left(\dfrac{\partial v}{\partial t}\right)^2}}} \tag{4.16}$$

Hallback et al. (1989), Fransson et al. (2005) and Koch and Chanson (2005) used the above formula to obtain a measured time scale $\tau_E(\delta t)$ based upon the time increment δt:

$$\tau_E(\delta t) = \sqrt{\frac{2\,v'^2}{\overline{\left(\dfrac{\delta v}{\delta t}\right)^2}}} \tag{4.17}$$

where v' is the standard deviation of velocity component; δt_{scan} is the experimental scan rate ($1/f_{scan}$, f_{scan} = 25 or 50 Hz); and δt is a time increment ($\delta t_{scan} \leq \delta t \leq 4\,\delta t_{scan}$). Following Koch and Chanson (2005), several time increments $\delta t = \delta t_{scan}$, $2\,\delta t_{scan}$ and $4\,\delta t_{scan}$ were used to calculate $\tau_E(\delta t)$ with the results fitted by a quadratic expression:

$$\tau_E(\delta t) = \tau_E(0) + a\,\delta t^2 + b\,\delta t \tag{4.18}$$

where $\tau_E(0)$ is the estimated dissipation time scale; and a and b are constants calculated from best data fit. Figure 4.9 explains the calculation of the dissipation time scale through quadratic interpolation.

Within the data sample of 200 s (5,000 (25 Hz) and 10,000 (50 Hz) data points), an overlapping correlation window of 10 s (250 (25 Hz) and 500 (50 Hz) data points) in size was used to calculate numerous values of $\tau_E(\delta t)$. These values of $\tau_E(\delta t)$ were averaged to

provide a value of $\tau_E(\delta t)$ most representative of that statistical data sample. If during quadratic interpolation $\tau_E(0)$ was negative, that sample was ignored.
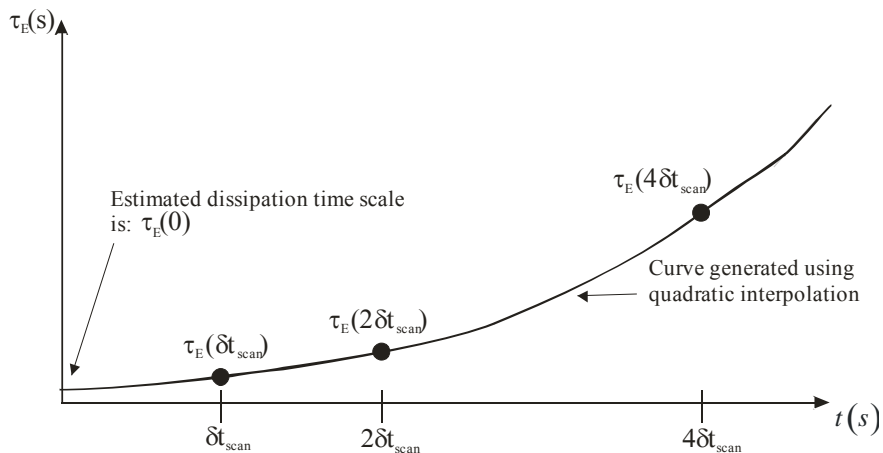
Figure 4.9 – Definition sketch for dissipation time scales.

4.3.5   Dimensionless turbulence parameters

Some dimensionless turbulence properties were investigated during this report. These were the relative horizontal and vertical turbulence intensity ratios (v_y'/v_x' and v_z'/v_x') and the correlation coefficients of tangential Reynolds stresses (R_{vxvy}, R_{vxvz} and R_{vyvz}). The turbulence intensity ratios are dimensionless parameters that describe the structure of the turbulence (Nezu and Nakagawa (1993)). A correlation coefficient of tangential Reynolds stress (e.g. $R_{vxvy} = \overline{v_x v_y}/(v_x' v_y')$) indicate the degree of similarity of the turbulence (Nezu and Nakagawa (1993)).

5   FIELD OBSERVATIONS: TURBULENCE

5.1   PRESENTATION

This section presents some basic turbulence data collected during the field investigations conducted in the estuary of Eprapah Creek. High frequency turbulence data were measured during the first seven field studies undertaken at Eprapah Creek. Table 5.1 outlines the field studies at Eprapah Creek in which high frequency turbulence data were collected.

Table 5.1 – Field studies at Eprapah Creek during which high frequency turbulence data were collected.

Field study	Date	Duration (hours)	Rainfall (mm)	Tidal range (m)	Sampling location
E1	4/04/03	12	10 (at 18:00 3/04/03)	1.61	Site 2B, 0.5 m below free surface, 14.2 m from left bank
E2	17/07/03	8	0	1.32	Site 2, 0.5 m below free surface, 8.0 m from left bank
E3	24/11/03	10	0	2.49	Site 2B, 0.5 m below free surface, 10.7 m from left bank
E4	2/09/04	12	0	1.76	Site 2B, 0.05 m above bed, 10.7 m from left bank
E5	8-9/03/05	25	0	2.33	Site 2B, 0.1 m above bed, 10.7 m from left bank
E6	16-18/05/05	48	0	1.32	Site 2B, 0.2 and 0.4 m above bed, 10.7 m from left bank
E7	5-7/06/06	50	0	1.34	Site 3, 0.2 and 0.4 m above bed, 4.2 m from right bank

Note: Tidal range: maximum tidal range during field study at Victoria Point; Rainfall: recorded in catchment immediately before or during field study.

The field investigations were performed at three different locations in the creek, these being: Site 2, Site 2B (two different transverse locations) and Site 3 (Figure 3.6). Figure 5.1 shows the surveyed experimental cross-sections at Site 2, Site 2B and Site 3, with the transverse sampling location(s) indicated. Sites 2 and 2B are located mid estuary approximately 2.0 and 2.1 km from the mouth respectively, while Site 3 is located in the upper estuary approximately 3.1 km from the mouth.
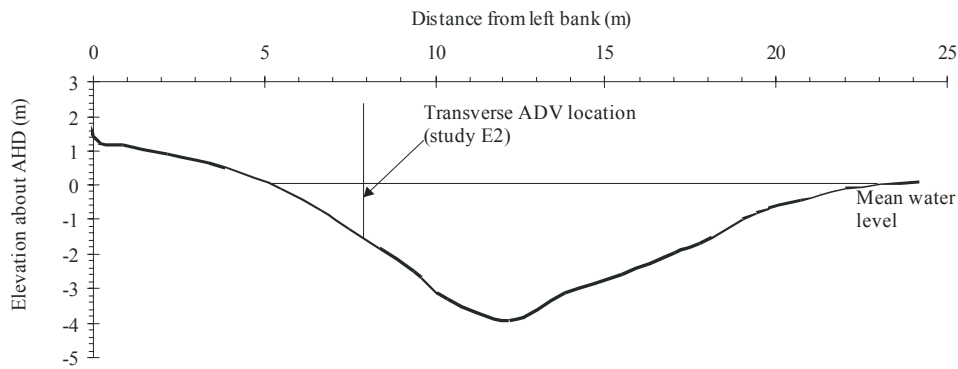
(A) Cross-section at Site 2, located 2.0 km from mouth.
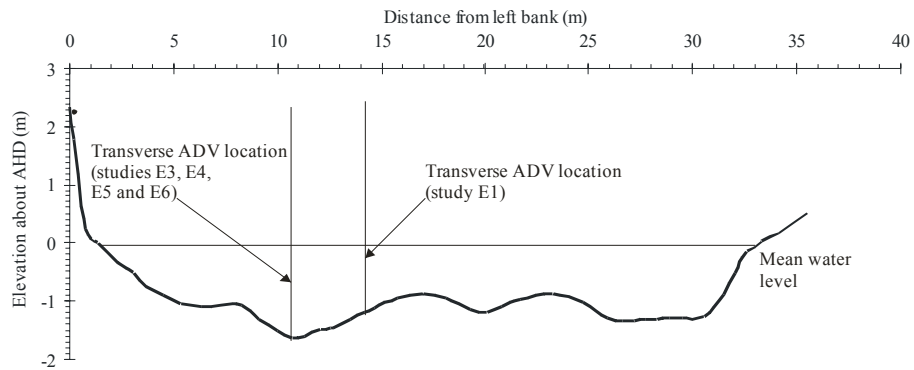
(B) Cross-section at Site 2B, located 2.1 km from mouth.
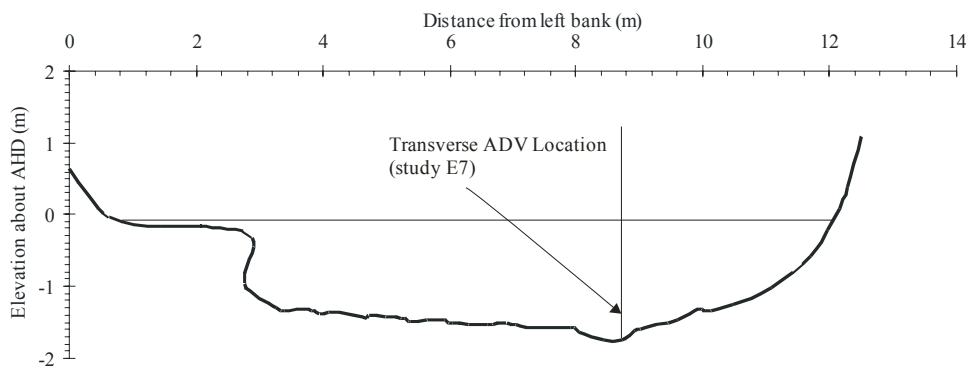
(C) Cross-section at Site 3, located 3.1 km from mouth.

Figure 5.1 – Surveyed data of experimental cross-sections and transverse ADV locations used at Eprapah Creek, looking downstream.

The high frequency turbulence data are analysed here. For all field studies, the streamwise velocity component V_x is positive downstream; the transverse velocity component V_y is positive towards the left bank; and the vertical velocity component V_z is positive upwards. Turbulence properties are presented herein and include: the first four statistical moments of velocity (Section 5.2) and tangential Reynolds stresses (Section 5.4); turbulence intensity ratios (Section 5.3); correlation coefficients of Reynolds stresses (Section 5.5); and turbulence time scales (integral and dissipation) (Section 5.6). All the ADV velocity data were post-

processed using the technique outlined in Section 4.2. Time series plots for all turbulence properties analysed from the Eprapah Creek field studies are presented in Digital Appendix.

5.2   TURBULENCE PROPERTIES: STATISTICAL MOMENTS OF VELOCITY

For all field studies conducted at Eprapah Creek the time-averaged streamwise velocity varied with the tides. Mid estuary, the field measurements of the studies E5 and E6 (25 and 48 hours respectively) showed that the streamwise velocity maxima of the flood and ebb tides occurred about low water (Figure 5.2). Kawanisi and Yokosi (1994) observed similar flood and ebb velocity maxima about low tide in an estuarine channel in Japan. Figure 5.2 shows the time-averaged streamwise velocity and water depth at Site 2B for the studies E5 and E6 as functions of time. Some influence from "long period oscillations" was present during both spring (Figure 5.2A) and neap (Figure 5.2B) tidal conditions. Figure 5.2B shows that the effect of these long period oscillations was significant during neap tidal conditions. In the upper estuary (study E7), velocity maxima seemed also to occur about low tides, but the low frequency fluctuations dominated the tidal fluctuations making confirmation difficult. For all field studies the streamwise velocity was larger during the flood tide than during the ebb tide (Figure 5.2).

For the field trips E4, E5, E6 and E7, the velocity data were collected close to the bed and multiple flow reversals were observed about most high tides (e.g. Figure 5.2B). Here a multiple flow reversal is defined as a rapid succession of changes in the streamwise velocity direction. An exception was the second tidal cycle during the study E5 recorded under large spring tidal forcing (tidal range at Site 2B = 2.48 m) (t = 100,000 to 150,000 s, Figure 5.2A). These multiple flow reversals about high tide seemed related to the long period oscillations (Section 7.3 and Appendix E) observed in Eprapah Creek and Moreton Bay. Multiple flow reversals were not observed during the field studies E2 and E3, when measurements were conducted approximately 0.5 m below the free surface.

During the field studies E5, E6 and E7, the time-averaged transverse velocity varied consistently with the tides. The sampling sites at both Site 2B and Site 3 were located close to the outer banks of meanders. In both the middle (studies E5 and E6) and upper (study E7) estuarine zones, the time-averaged transverse velocity was predominantly towards the inner bank during the flood tide and towards the outer bank during the ebb tide (Figure 5.3). Figure 5.3 shows the time-averaged transverse velocity (positive towards left bank) as a function of the time-averaged streamwise velocity (positive downstream). In Figure 5.3A, the transverse velocity is predominantly negative during the flood tide and positive during the ebb tide mid estuary, while in the upper estuary (Figure 5.3B), the opposite trend was observed. This trend

53

seemed to be caused by the meandering profile of the estuary that curved in the opposite directions at Site 2B and Site 3 (Figure 3.6). The magnitude of time-averaged transverse velocity was largest during the flood tide for all field studies.
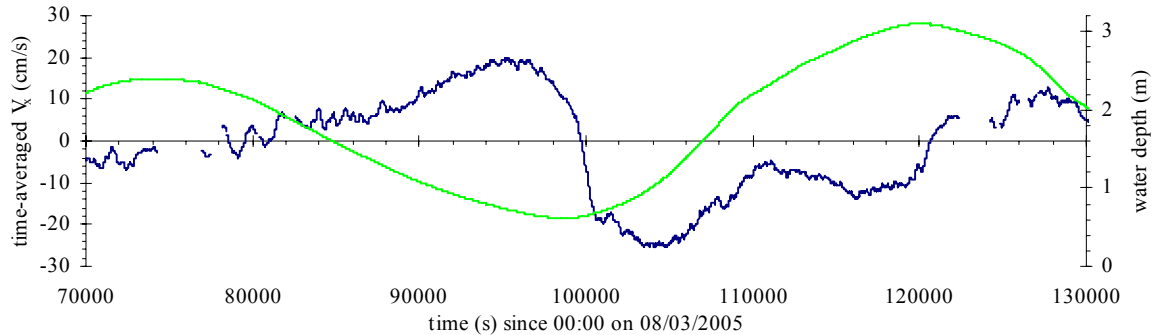
(A) Spring tide data collected by 3D-ADV at 0.1 m above bed, 10.7 m from left bank at Site 2B, Eprapah Creek for study E5 (8-9/03/05).
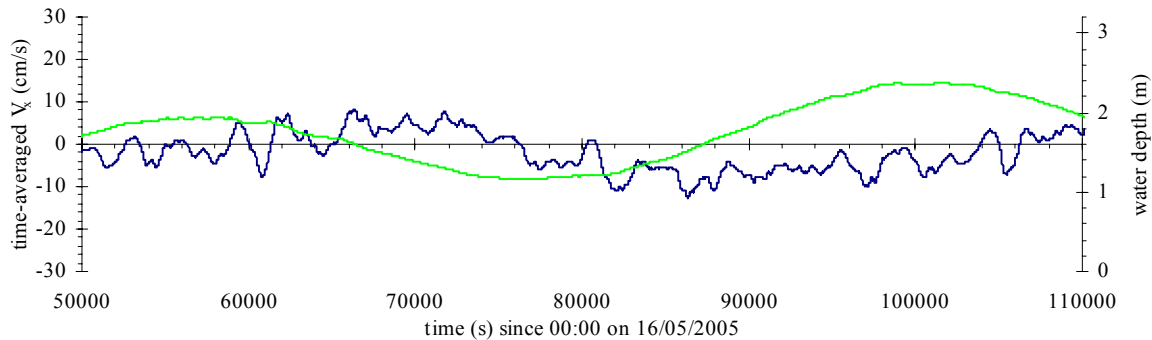
(B) Neap tide data collected by 3D-ADV at 0.4 m above bed, 10.7 m from left bank at Site 2B, Eprapah Creek for study E6 (16-18/05/05).

Figure 5.2 – Time-averaged streamwise velocity and water depth as functions of time for field studies E5 and E6. Data averaged over 200 s every 10 s along entire data set.

Legend: — water depth; — time-averaged streamwise velocity.

The time-averaged vertical velocity was predominantly negative (downwards) during the flood tide for all field investigations undertaken at Eprapah Creek. Figure 5.4 shows the time-averaged vertical velocity (positive upwards) as a function of the time-averaged streamwise velocity (positive downstream). In Figure 5.4, the magnitude of the downwards velocity increased as the streamwise velocity of the flood tide ($\overline{V_x} < 0$) increased. These negative or downwards velocities during the flood tide are thought to be an anomaly. During the ebb tide no tidal pattern for the vertical velocity was consistently observed for all field studies. As mentioned in Section 3.5.1, some questions remain about the quality of the vertical velocity data measured with a down-looking 3D-ADV, and this data must be considered with caution.

54
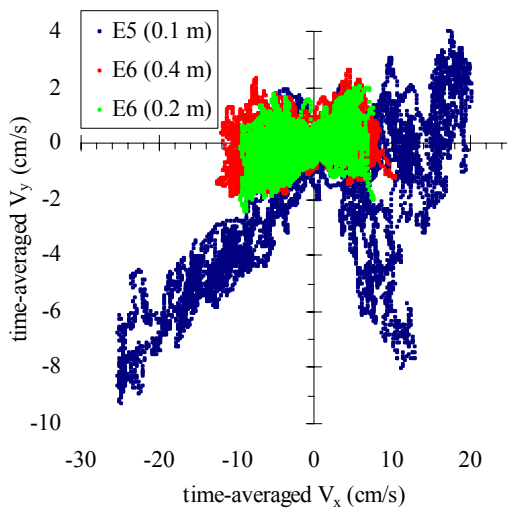
(A) Mid estuary data for studies E5 (8-9/03/05) and E6 (16-18/05/05).
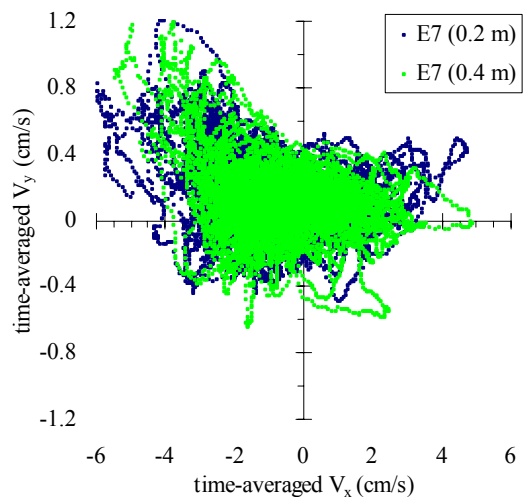
(B) Upper estuary data for study E7 (5-7/06/06).

Figure 5.3 – Time-averaged transverse velocity $\overline{V_y}$ (positive towards left bank) as a function of time-averaged streamwise velocity (positive downstream). Velocity data averaged over 200 s every 10 s along entire data set.
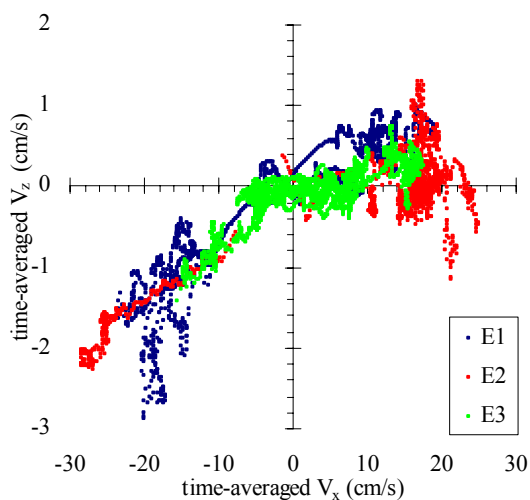
(A) Data collected 0.5 m below free surface at Site 2 (study E2) and Site 2B (studies E1 and E3).
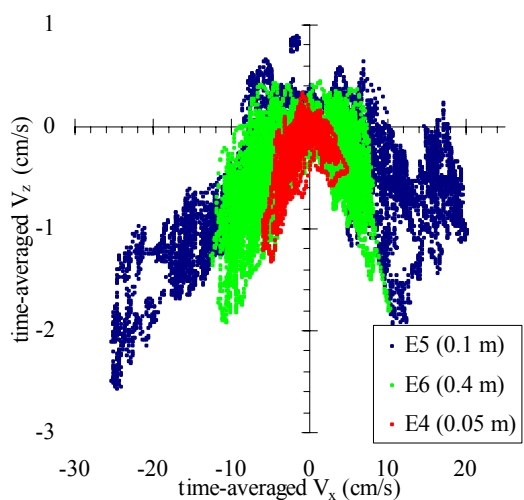
(B) Data collected close to bed at Site 2B for studies E4, E5 and E6.

Figure 5.4 – Time-averaged vertical velocity $\overline{V_z}$ (positive upwards) as a function of time-averaged streamwise velocity (positive downstream). Velocity data averaged over 200 s every 10 s along entire data set.

The standard deviations of all velocity components tended to vary with the tides for all field studies at Eprapah Creek. Figure 5.5 shows the standard deviations of streamwise velocity as functions of the time-averaged streamwise velocity (positive downstream). In Figure 5.5, the

55

standard deviations of streamwise velocity v_x' increased with the streamwise velocity magnitude. Similar tidal patterns were observed in the standard deviations of transverse and vertical velocity components. The values of the standard deviations of transverse velocity were of similar magnitude to those of the streamwise velocity, while the standard deviations of vertical velocity were slightly smaller.
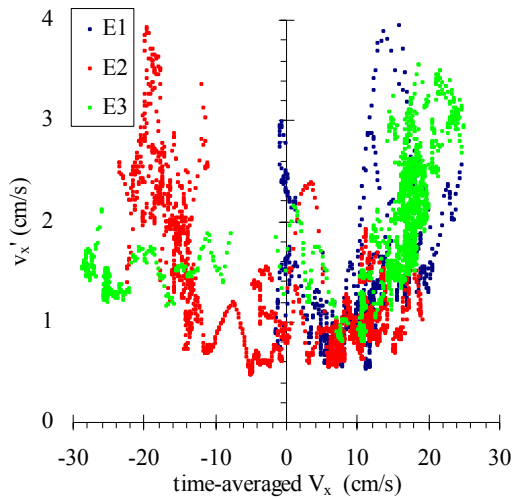
(A) Data collected mid estuary at 0.5 m below surface for studies E1, E2 and E3 (3D-ADV).
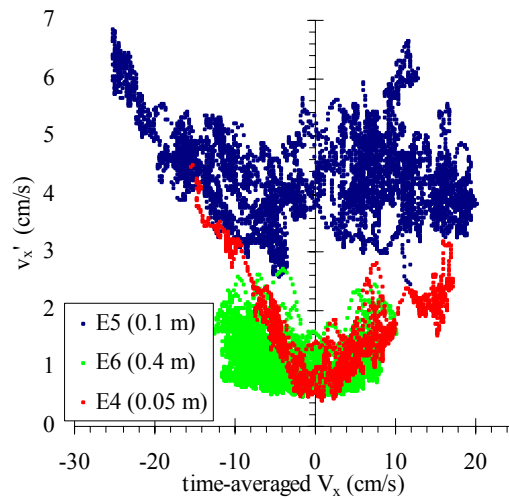
(B) Data collected mid estuary close to bed for studies E4, E5 and E6 (3D-ADV).
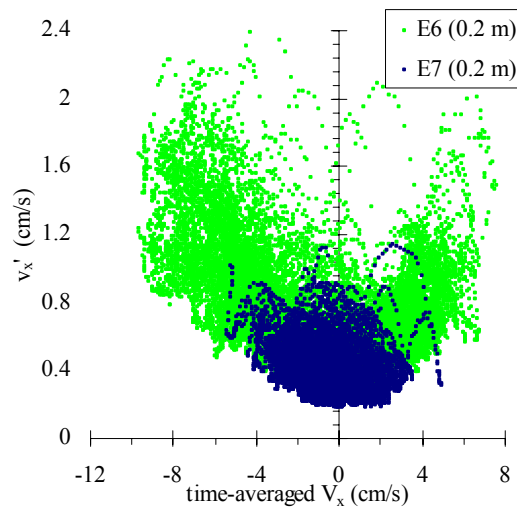
(C) Data collected close to bed in middle (study E6) and upper (study E7) estuary (2D-microADV).

Figure 5.5 – Standard deviations of streamwise velocity v_x' as functions of time-averaged streamwise velocity (positive downstream). Standard deviations calculated over 200 s every 10 s along entire data set.

For all field studies, with the exception of field works E1 and E3 because of limited flood tide data, the standard deviations of all velocity components were larger during the flood tide than the ebb tide (Figure 5.5). This trend was observed by Kawanisi and Yokosi (1994) in an estuarine channel, and during the "rising" phase of unsteady open channel flow laboratory experiments of Song and Graf (1996) and Nezu et al. (1997).

The standard deviations of velocity can represent the intensity of the turbulent velocity fluctuations. At Eprapah Creek, all velocity standard deviations were larger mid estuary under spring tides (study E5, Figure 5.5B), which indicated increased mixing under spring tidal conditions. Equally the smaller velocity standard deviations observed in the upper estuary (study E7, Figure 5.5C) seemed to indicate reduced mixing in the upper estuary.

The skewness and kurtosis of a data sample show how that data varies from a Gaussian distribution. For an infinite number of samples the skewness and "excess" kurtosis of a Gaussian distribution are both zero. In a finite data set, the reasonable limits for the expected deviations from a Gaussian distribution are: $|Sk| < 4*\sqrt{15/N}$ and $|Ku| < 4*\sqrt{96/N}$, where N is the number of data points per sample (Press et al. (1992)). Skewness and kurtosis values within these limits represent a distribution with skewness and kurtosis close to Gaussian values, while values outside these limits indicate a non-Gaussian velocity distribution. For this analysis, a total of 161,501 velocity data samples (64,903 samples for V_x data, 64,903 samples for V_y data and 31,695 samples for V_z data) were analysed for the field studies E1 to E7. Of these 161,501 samples, 45 % (73,160 samples) could be considered within the reasonable Gaussian limits in terms of both skewness and kurtosis. Approximately 18 % (29,716 samples) were outside the reasonable Gaussian limits for both skewness and kurtosis (i.e. $|Sk| > 4*\sqrt{15/N}$ and $|Ku| > 4*\sqrt{96/N}$). For all field studies at Eprapah Creek, the majority of skewness and kurtosis values for all velocity components ranged between -0.6 < Sk < 0.6 and -1 < Ku < +3 respectively. Shiono and West (1987) observed similar skewness and kurtosis values in a larger estuarine channel in England.

5.3   TURBULENCE PROPERTIES: TURBULENCE INTENSITY RATIOS

The turbulence intensity ratio is a dimensionless parameter that characterises the structure of the turbulence rather than its absolute values. For all field studies conducted mid estuary, the vertical turbulence intensity ratio v'_z/v'_x showed some variation with the tidal phase (Figure 5.6). Figure 5.6 shows the vertical turbulence intensity ratio v'_z/v'_x as a function of the time-averaged streamwise velocity (positive downstream). In Figure 5.6 v'_z/v'_x increased with the magnitude of the streamwise velocity in all field studies conducted mid estuary. The values

of vertical turbulence intensity ratio were v_z'/v_x' = 0.2 to 0.7, with median values mostly between 0.37 to 0.52 mid estuary. These were similar to those observed in estuarine field studies by Shiono and West (1987), West and Shiono (1988) and Kawanisi and Yokosi (1994). Interestingly, the magnitude of the vertical turbulence intensity ratio observed during all these field studies was comparable to that observed in turbulent open channel flow experiments v_z'/v_x' = 0.5 to 0.6 (e.g. Nezu and Nakagawa (1993)).
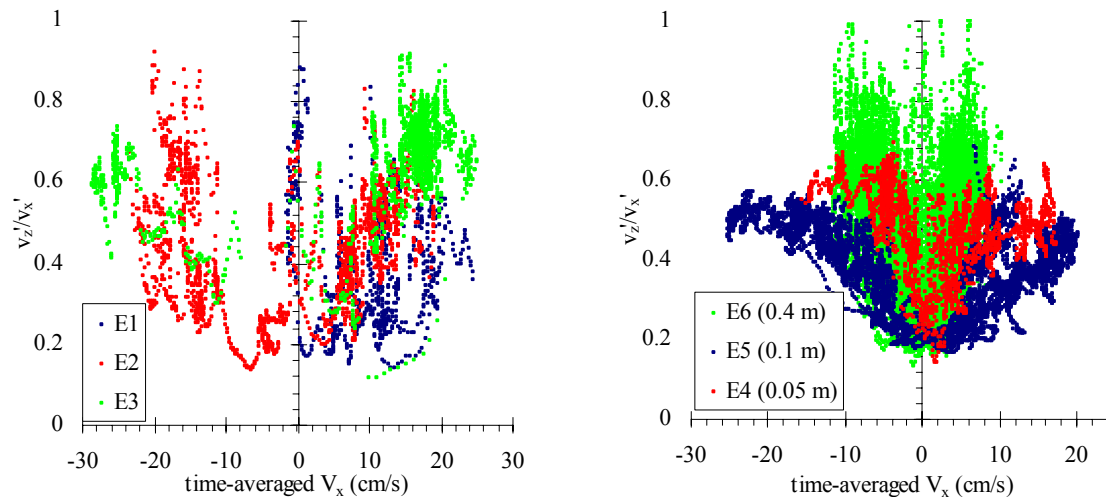
(A) Data collected at 0.5 m below free surface at Site 2 (study E2) and Site 2B (studies E1 and E3).

(B) Data collected close to bed at Site 2B for studies E4, E5 and E6.

Figure 5.6 – Vertical turbulence intensity ratio v_z'/v_x' as a function of time-averaged streamwise velocity (positive downstream). Values calculated over 200 s every 10 s along entire data set.

For the limited data (less than one tidal cycle) collected close to the free surface (studies E1, E2 and E3), the horizontal turbulence intensity ratio v_y'/v_x' seemed to vary with the tides (Figure 5.7A). Figure 5.7 shows the horizontal turbulence intensity ratio v_y'/v_x' as a function of the time-averaged streamwise velocity (positive downstream). In Figure 5.7A, the horizontal turbulence intensity ratio v_y'/v_x' close to the free surface increased with increasing streamwise velocity magnitude. For the data measured close to the bed (studies E4, E5, E6 and E7) no easily discernible tidal trend was observed (Figure 5.7B).

The horizontal turbulence intensity ratios for the mid estuary field studies were approximately twice as large as the vertical turbulence intensity ratios, inferring some form of turbulence

anisotropy. The median values of v'_y/v'_x observed were between 0.8 and 1.0 during the field studies in the middle estuarine zone. Simply, the turbulent fluctuations in the transverse and streamwise directions were of a similar magnitude. These observations mid estuary were higher than those observed for laboratory experiments in rectangular channels, which yielded v'_y/v'_x = 0.5 to 0.7 (e.g. Nezu and Nakagawa (1993), Koch and Chanson (2005)). In the upper estuarine zone, the median value of the horizontal turbulence intensity ratio observed at 0.2 m above the bed was 0.44, which seemed to indicate reduced transverse velocity fluctuations in the upper estuarine zone.
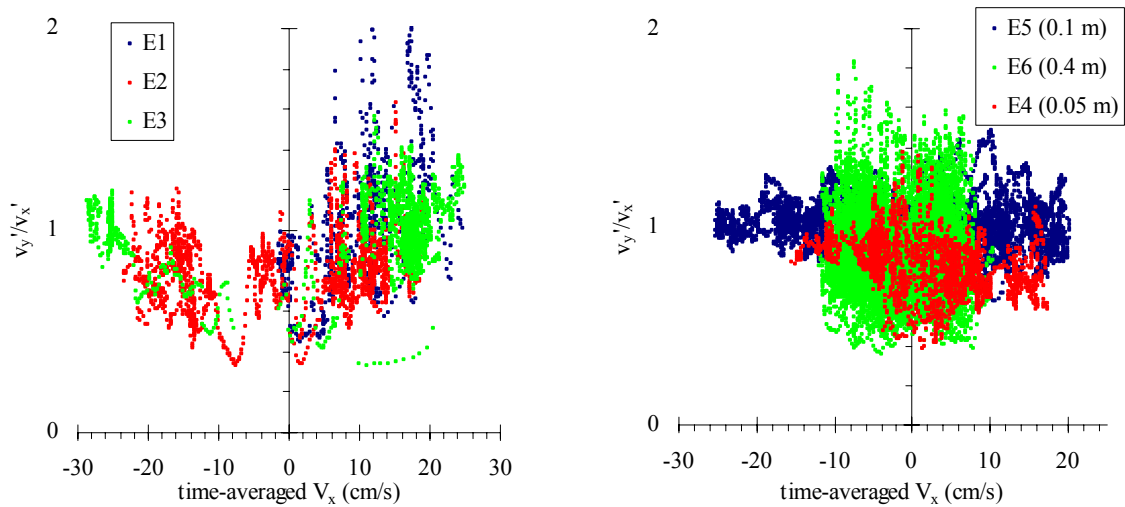
(A) Data collected at 0.5 m below free surface at Site 2 (study E2) and Site 2B (studies E1 and E3).

(B) Data collected close to bed at Site 2B for studies E4, E5 and E6.

Figure 5.7 – Horizontal turbulence intensity ratio v'_y/v'_x as a function of time-averaged streamwise velocity (positive downstream). Values calculated over 200 s every 10 s along entire data set.

5.4 TURBULENCE PROPERTIES: STATISTICAL MOMENTS OF TANGENTIAL REYNOLDS STRESSES

Tangential Reynolds stresses are important turbulence properties in the study of turbulent mixing and sediment transport. The Reynolds stresses $\rho v_x v_y$ and $\rho v_x v_z$ represent the transverse and vertical shear generated by the high frequency fluctuations in streamwise velocity respectively, while $\rho v_y v_z$ represents the vertical shear generated by fluctuations in the transverse velocity. For the field experiments conducted close to the bed (e.g. studies E4,

E5 and E6) the time-averaged Reynolds stress $\rho\overline{v_x v_z}$ varied with the tides. Figure 5.8 shows the time-averaged Reynolds stress $\rho\overline{v_x v_z}$ as a function of the time-averaged streamwise velocity (positive downstream). In Figure 5.8B, the time-average Reynolds stress $\rho\overline{v_x v_z}$ was predominantly positive during the flood tide and negative during the ebb tide. A similar tidal trend was observed by Osonphasop (1983) and Kawanisi and Yokosi (1993, 1994) in natural tidal channels, and van der Ham et al. (2001) in a shallow semi-enclosed bay.

During the field studies E1, E2 and E3 performed near the free surface no easily discernible tidal trends in $\rho\overline{v_x v_z}$ were observed (Figure 5.8A). The time-averaged Reynolds stresses $\rho\overline{v_x v_y}$ and $\rho\overline{v_y v_z}$ showed no easily discernible tidal trends for all field studies undertaken at Eprapah Creek to date.
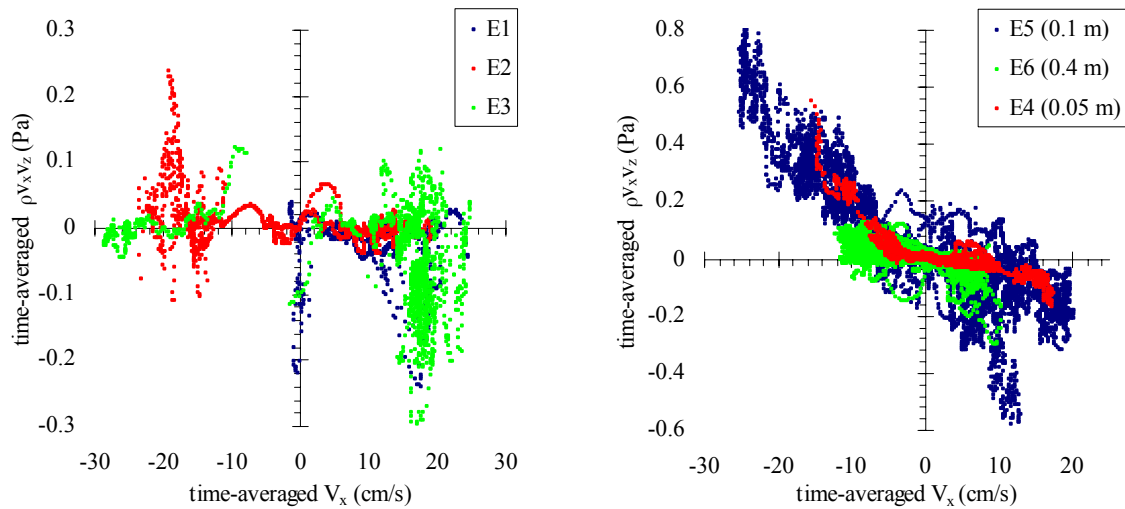
(A) Data collected at 0.5 m below surface at Site 2 (study E2) and Site 2B (studies E1 and E3).

(B) Data collected close to bed at Site 2B for studies E4, E5 and E6.

Figure 5.8 – Time-averaged Reynolds stress $\rho\overline{v_x v_z}$ as a function of time-averaged streamwise velocity (positive downstream). Reynolds stresses averaged over 200 s every 10 s along entire data set.

For all field studies conducted at Eprapah Creek the standard deviations of all Reynolds stresses varied with the tides. Figure 5.9 shows the standard deviations $(\rho v_x v_y)'$ of Reynolds stress $\rho v_x v_y$ as functions of the time-averaged streamwise velocity (positive downstream). In Figure 5.9, the magnitude of standard deviations $(\rho v_x v_y)'$ increased with the magnitude of the time-averaged streamwise velocity. The standard deviations of both $\rho v_x v_z$ and $\rho v_y v_z$

also increased with the magnitude of streamwise velocity. At Eprapah Creek, the standard deviations of all tangential Reynolds stresses observed during the flood tide were larger than those during the ebb tide. Under spring tidal forcing larger standard deviations of all Reynolds stresses were observed (study E5, Figure 5.9B), while under neap tidal conditions smaller values were observed in the upper estuary (study E7, Figure 5.9C). These results seemed to indicate increased mixing for spring tides and reduced mixing in the upper estuary.
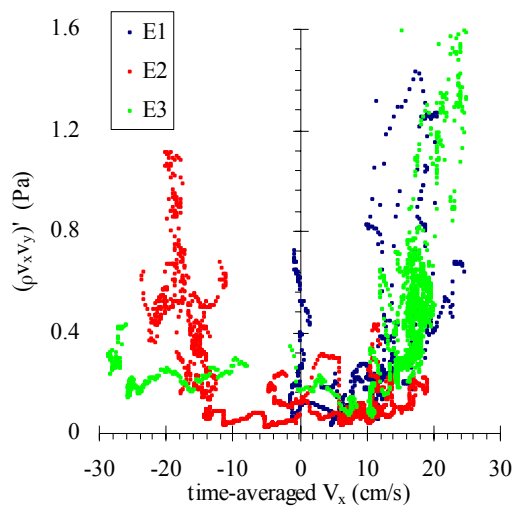
(A) Data collected with 3D-ADV mid estuary at 0.5 m below surface (studies E1, E2 and E3).
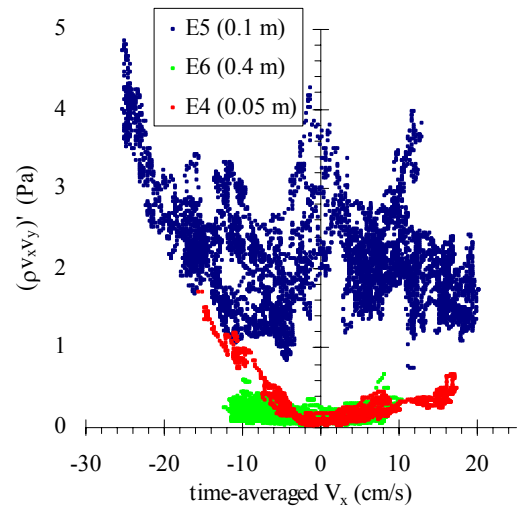
(B) Data collected with 3D-ADV mid estuary close to bed (studies E4, E5 and E6).
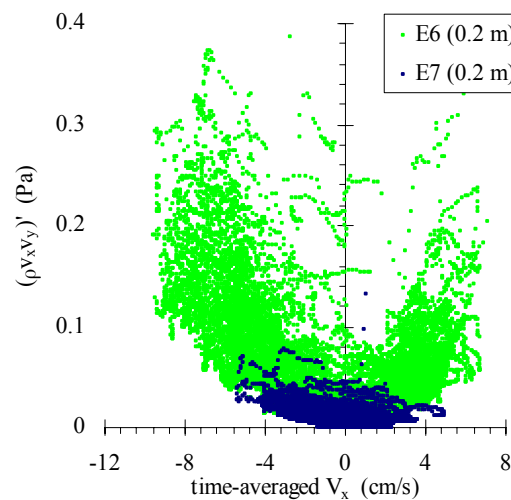
(C) Data collected with 2D-microADV close to bed in middle (study E6) and upper (study E7) estuary.

Figure 5.9 – Standard deviations of Reynolds stress $(\rho v_x v_y)'$ as functions of time-averaged streamwise velocity (positive downstream). Standard deviations calculated over 200 s every 10 s along entire data set.

For the field studies close to the bed in the middle estuarine zone (studies E4, E5 and E6), the skewness $Sk(\rho v_x v_z)$ of Reynolds stress $\rho v_x v_z$ varied with the tides (Figure 5.10B). Figure 5.10 shows the skewness $Sk(\rho v_x v_z)$ as a function of the time-averaged streamwise velocity (positive downstream). In Figure 5.10B the skewness $Sk(\rho v_x v_z)$ was predominantly positive during the flood tide and negative during the ebb tide. This tidal trend in $Sk(\rho v_x v_z)$ was not observed for the field trips E1, E2 and E3 conducted near the free surface (Figure 5.10A). No easily discernible trends were observed for the skewness values $Sk(\rho v_x v_y)$ and $Sk(\rho v_y v_z)$ in any of the field studies undertaken at Eprapah Creek. The Kurtosis values of all tangential Reynolds stresses showed no easily discernible tidal patterns that were consistent for all field studies at Eprapah Creek.
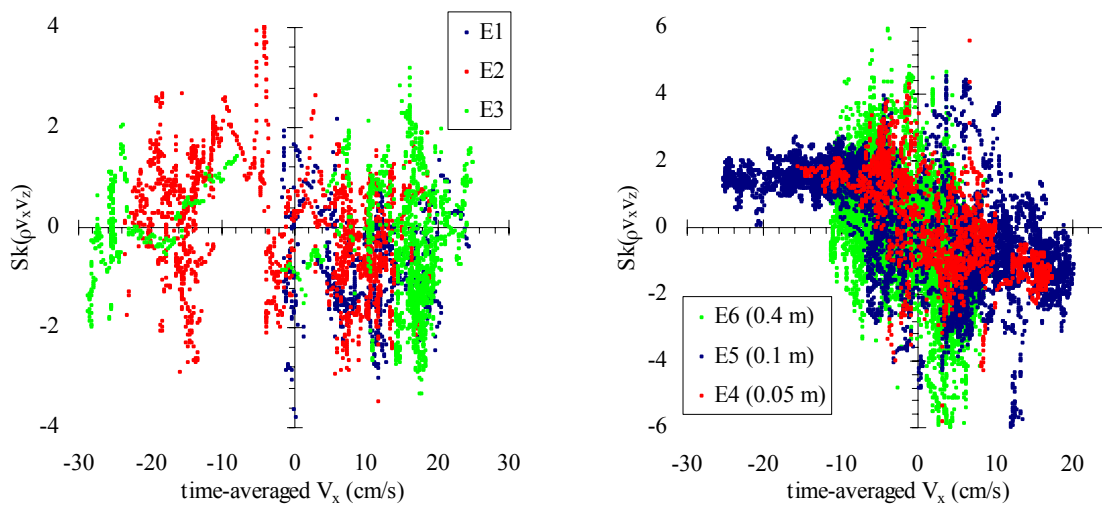
(A) Data collected 0.5 m below surface at Site 2 (study E2) and Site 2B (studies E1 and E3).

(B) Data collected close to bed at Site 2B (studies E4, E5 and E6).

Figure 5.10 – Skewness $Sk(\rho v_x v_z)$ as a function of time-averaged streamwise velocity (positive downstream). Skewness calculated over 200 s every 10 s along entire data set.

For the 128,293 tangential Reynolds stress data samples (64,903 samples for $\rho v_x v_y$, 31,695 samples of $\rho v_x v_z$ and 31,695 samples of $\rho v_y v_z$) collected at Eprapah Creek, 86 % (110,204 samples) could be considered non-Gaussian in terms of both skewness and kurtosis (i.e. $|Sk| > 4*\sqrt{15/N}$ and $|Ku| > 4*\sqrt{96/N}$). The majority of skewness and kurtosis values of all tangential Reynolds stresses for all field studies performed at Eprapah Creek were found to be between $-3.0 < Sk < 3.0$ and $3 < Ku < 18$. These results agree well with those of the

tangential Reynolds stress $\rho v_x v_z$ observed by Shiono and West (1987) in an estuarine channel and Osonphasop (1983) in a tidal channel.

5.5 TURBULENCE PROPERTIES: CORRELATION COEFFICIENTS OF REYNOLDS STRESS

The correlation coefficient of Reynolds stress is a dimensionless parameter that indicates the degree of similarity of the turbulence fluctuations. It is defined as: $R_{vxvy} = \overline{v_x v_y}/(v_x' v_y')$. For all field studies conducted close to the bed the dimensionless Reynolds stress R_{vxvz} varied with the tides (Figure 5.11B). Figure 5.11 shows the correlation coefficient R_{vxvz} as a function of the time-averaged streamwise velocity (positive downstream). In Figure 5.11B, the values of R_{vxvz} were predominantly positive during the flood tides and negative during the ebb tides for the studies E4, E5 and E6. A similar trend for R_{vxvz} was observed by Kawanisi and Yokosi (1993, 1994) during some field measurements close to the bed in an estuarine tidal channel in Japan. No tidal trend for R_{vxvz} was observed during the studies E1, E2 and E3, performed approximately 0.5 m below the free surface (Figure 5.11A).
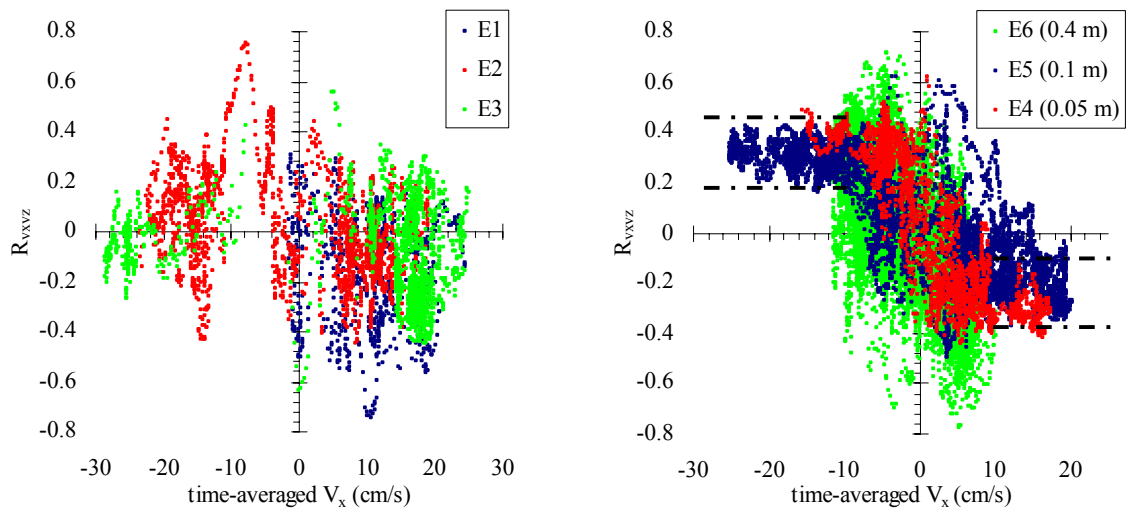
(A) Data collected at 0.5 m below free surface at Site 2 (study E2) and Site 2B (studies E1 and E3).

(B) Data collected close to bed at Site 2B (studies E4, E5 and E6).

Figure 5.11 – Correlation coefficient R_{vxvz} as a function of time-averaged streamwise velocity (positive downstream). Correlation coefficients calculated over 200 s every 10 s along entire data set.

Figure 5.11 shows that for the field studies conducted close to the bed the values of R_{vxvz} seemed larger during the flood tide than the ebb tide. This tidal asymmetry in terms of R_{vxvz} was also reported by Kawanisi and Yokosi (1994). Close to the bed the correlation coefficient R_{vxvz} seemed to obtain a near constant value of $\left|R_{vxvz}\right| \sim 0.3 \pm 0.1$ when $\left|\overline{V_x}\right| > 12$ cm/s (highlighted in Figure 5.11B), while for $\left|\overline{V_x}\right| < 12$ cm/s the magnitude of correlation coefficient R_{vxvz} seemed to vary directly with the magnitude of streamwise velocity. The correlation coefficients R_{vxvy} and R_{vyvz} showed no easily discernible tidal trend for any field trip undertaken at Eprapah Creek.

For all field studies performed mid estuary at Eprapah Creek, the observed values of the correlation coefficient ($R_{vxvz} = $ -0.6 to 0.6) were similar to those observed by West and Shiono (1988), West and Oduyemi (1989) and Kawanisi and Yokosi (1994). These values were also similar to those observed in laboratory flume experiments by Nezu and Nakagawa (1993). The observed values of the correlation coefficients R_{vxvy} and R_{vyvz} were within the same range of values as R_{vxvz}.

5.6   TURBULENCE PROPERTIES: TURBULENCE TIME SCALES

5.6.1   Integral time scales

The integral time scale of a velocity component is a measure of the longest connection in the turbulent behaviour of that component. For all field studies conducted at Eprapah Creek the integral time scales of all velocity components varied over the tidal cycle (Figure 5.12). Figure 5.12 shows a turbulence property (herein T_{Ex}) relative to the position in the tidal cycle presented. Here the data for a tidal cycle is collected from one low water to the next, and is then represented in a circular plot. The polar coordinates are r = turbulence characteristic (e.g. r = T_{Ex} (Figure 5.12)) and $\theta = 2\pi\, t/T$, where T = period of tidal cycle from first low water (LW1) to second low water (LW2); and t = position in tidal cycle (t = 0 at LW1 and t = T at LW2). From the first low water on the plot (y = 0 on positive x-axis), the data progresses anticlockwise around the plot until the second low water (y = 0 on positive x-axis). Note that in Figure 5.12 the axes have a logarithmic scale and the units are in milliseconds (ms). In Figure 5.12 the streamwise integral time scales were observed to vary over the tidal cycle, but there was no consistent tidal pattern for all integral time scales at Eprapah Creek.

For the field studies undertaken at Eprapah Creek the integral time scales of all velocity components were between 0.01 and 3.30 s. The median values of streamwise, transverse and

vertical integral time scales for all field studies mid estuary were 0.46, 0.47 and 0.58 s respectively. West and Shiono (1985) observed a similar magnitude for the vertical integral time scales, but slightly larger streamwise integral time scales during some ebb tide measurements in an estuarine tidal channel in the UK.
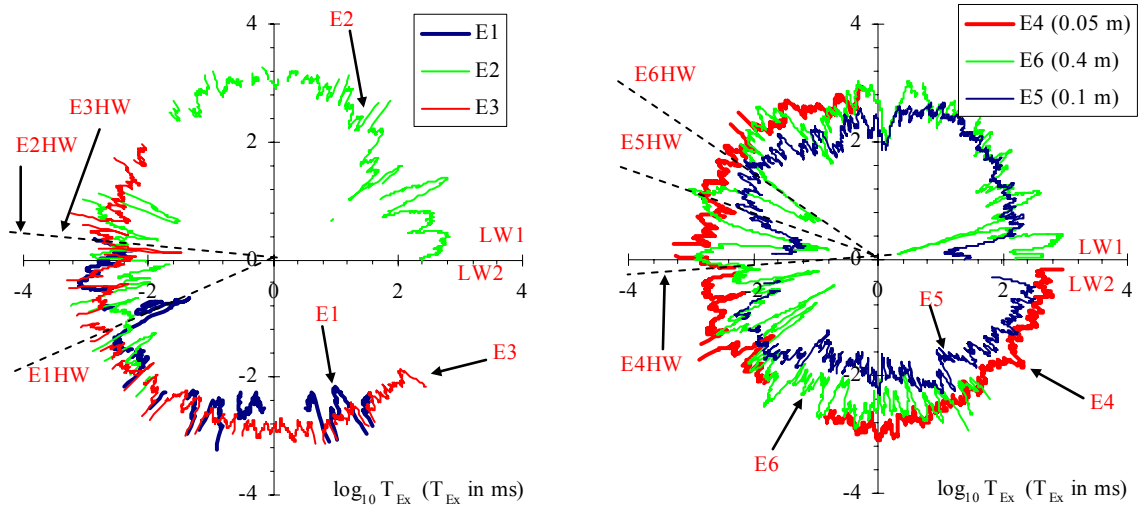
(A) Data collected with 3D-ADV mid estuary at 0.5 m below surface (studies E1, E2 and E3).

(B) Data collected with 3D-ADV mid estuary close to bed (studies E4, E5 and E6).
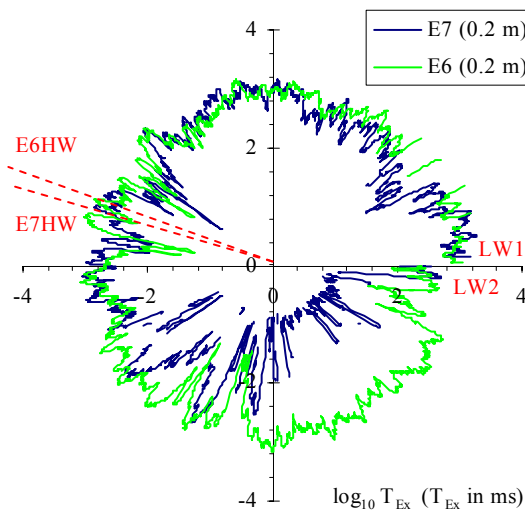
(C) Data collected with 2D-microADV close to bed in middle (study E6) and upper (study E7) estuary.

Figure 5.12 – Variation of integral time scales T_{Ex} for streamwise velocity (in milliseconds) over an observed tidal cycle. Time scales calculated over 200 s every 10 s along entire data set.

The median values of the horizontal and vertical dimensionless integral time scales recorded with the 3D-ADV (10 MHz) were $T_{Ey}/T_{Ex} = 0.8$ to 1.3 and $T_{Ez}/T_{Ex} = 0.7$ to 2.8 respectively. The former seemed to differ from the median values of T_{Ey}/T_{Ex} measured with the 2D-microADV (16 MHz) during the field trips E6 and E7, which were $T_{Ey}/T_{Ex} = 1.4$ and 3.6 respectively.

5.6.2   Dissipation time scales

The dissipation time scale is a measure of the most rapid changes that occur in the fluctuations of a velocity component. Physically, it represents the time scales of the smaller eddies that are responsible for the dissipation of energy. For all field studies performed at Eprapah Creek the dissipation time scales of all velocity components seemed independent of the tidal phase. The dissipation time scales of all velocity components showed no easily discernible tidal pattern for all field studies conducted at Eprapah Creek. Figure 5.13 shows the variation of dissipation time scales for streamwise velocity over the presented tidal cycle in a circular plot.   Note that the axes have a logarithmic scale and the units are in microseconds (μs).   In Figure 5.13, the streamwise dissipation time scales showed little variation over the presented tidal cycle for each field investigation.

For all field studies undertaken at Eprapah Creek the dissipation time scales of the horizontal velocity components were between 0.000001 and 0.06 s, while the vertical dissipation time scales ranged between 0.000001 and 0.2 s.   The median values of the streamwise τ_{Ex} , transverse τ_{Ey} and vertical τ_{Ez} dissipation time scales recorded for all field studies performed mid estuary were 0.0081, 0.0061 and 0.057 s respectively.

The median values of the horizontal and vertical dimensionless dissipation time scales measured with the 3D-ADV (10 MHz) were $\tau_{Ey}/\tau_{Ex} = 0.8$ to 1.3 and $\tau_{Ez}/\tau_{Ex} = 3.8$ to 10.6 respectively.   Median values of τ_{Ey}/τ_{Ex} measured with the 2D-microADV (16 MHz) were larger than those observed with the 3D-ADV (10 MHz).   The median values of τ_{Ey}/τ_{Ex} recorded with the 2D-microADV (16 MHz) were approximately 9.0 and 2.0 for the field works E6 and E7 respectively.

5.7   DISCUSSION

From the initial analysis of the data collected at Eprapah Creek several tidal patterns were found in the turbulence properties.   However, some key differences in the turbulence properties were observed: 1) mid estuary under spring and neap tidal forcing; 2) under neap tidal conditions in the middle and upper estuarine zones. The different tidal responses to

spring and neap tidal forcing are discussed further using the studies E5 and E6 in Chapter 7. Chapter 8 compares the data sets collected during the field studies E6 and E7 and discusses the difference in turbulence properties in the middle and upper estuary. Finally it is important to determine which of the turbulence properties observed at Eprapah Creek are unique to small subtropical estuaries. Therefore Chapter 9 compares the turbulence properties collected at Eprapah Creek to those at Hamana Lake (a large tidal lake) to study common tidal patterns.
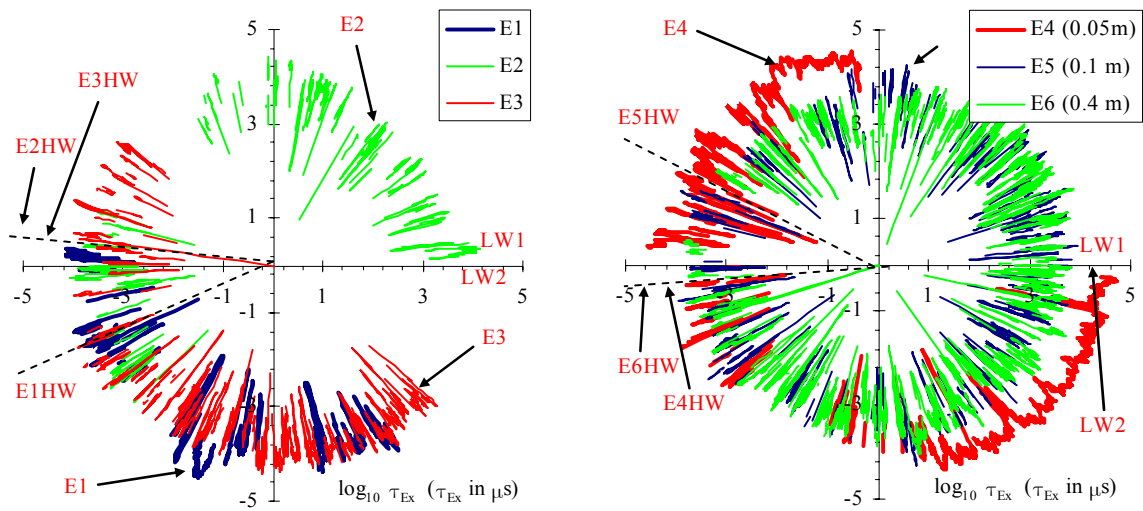
(A) Data collected with 3D-ADV mid estuary at 0.5 m below surface (studies E1, E2 and E3).

(B) Data collected with 3D-ADV mid estuary close to bed (studies E4, E5 and E6).
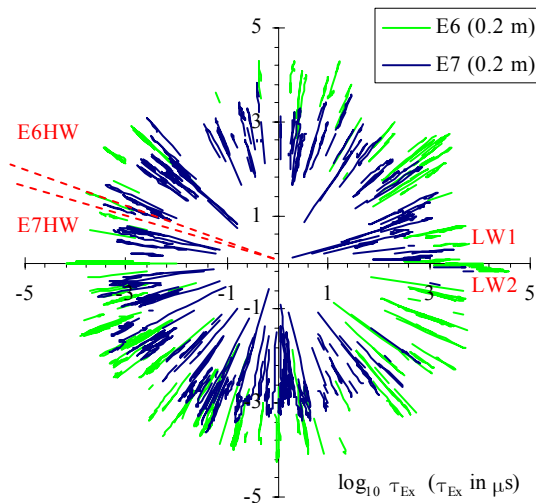
(C) Data collected with 2D-microADV close to bed in middle (study E6) and upper (study E7) estuary.

Figure 5.13 – Variation of dissipation time scales τ_{Ex} for streamwise velocity (in microseconds) over an observed tidal cycle. Time scales calculated over 200 s every 10 s along entire data set.

6 FIELD OBSERVATIONS: WATER PROPERTIES

6.1 PRESENTATION

Some water properties were measured as part of this investigation to help define the physical characteristics of the estuary, to asses the water quality, and to investigate the impact of turbulent mixing. These properties included common water quality parameters such as water temperature, conductivity, pH, turbidity, dissolved oxygen and chlorophyll a levels measured with physio-chemistry probes (e.g. YSI6600) and the suspended sediment concentration. Physio-chemistry data were collected during all field studies conducted at Eprapah Creek. High frequency suspended sediment concentration measurements were recorded during the field studies E6 and E7 using the 2D-microADV (16 MHz). Table 6.1 outlines the field investigations at Eprapah Creek during which some water properties were measured and the type of sampling undertaken.

Table 6.1 – Field studies at Eprapah Creek in which water quality data were collected.

Field study	Date	Duration (hours)	Rainfall (mm)	Tidal range (m)	Field site(s)	Sampling type
E1	4/04/03	12	10 (18:00 on 3/04/03)	1.61	1,2,3 2B	Surface sampling from bank YSI6600 probe
E2	17/07/03	8	0	1.32	2	YSI6600 probe
E3	24/11/03	10	0	2.49	2B	YSI6600 probe
E4	2/09/04	12	0	1.76	1,2,3 2B	Surface sampling from bank YSI6600 probe
E5	8-9/03/05	25	0	2.33	2B	YSI6600 probe
E6	16-18/05/05	48	0	1.32	2B	YSI6600 probe 6 LTS9000 probes (*)2D-microADV
E7	5-7/06/06	50	0	1.34	3 3,3B,STP 3	2 YSI6600 probes 4 LTS9000 probes (*)2D-microADV
E8	28/08/06	12	30 (05:30 on 28/08/06)	1.53	1,2B,3	Surface sampling from bank
E9	2-4/10/06 11-13/10/06	50 50	0 0	1.89 1.81	1,2B,2C,3 3B,4,STP	7 mini-Troll probes 2 LTS9000 probes

Note: Tidal range: maximum tidal range during field study at Victoria Point; Rainfall: observed immediately before or during field study (time and date); (*): instrument used to collect suspended sediment concentration.

The field studies were performed at four main locations in the estuary. These were: Site 1; Site 2; Site 2B; and Site 3 (Figure 3.6). Figure 6.1 compares the surveyed experimental cross-sections at Sites 1, 2, 2B and 3. Site 1 was located in the lower estuary approximately 1.0 km from the mouth. Mid estuary, Sites 2 and 2B were located about 2.0 and 2.1 km from the mouth respectively. Site 3 was located in the upper estuary approximately 3.1 km from the mouth.

(A) Site 1 (1.0 km from mouth).

(B) Site 2 (2.0 km from mouth).

(C) Site 2B (2.1 km from mouth).

(D) Site 3 (3.1 km from mouth).
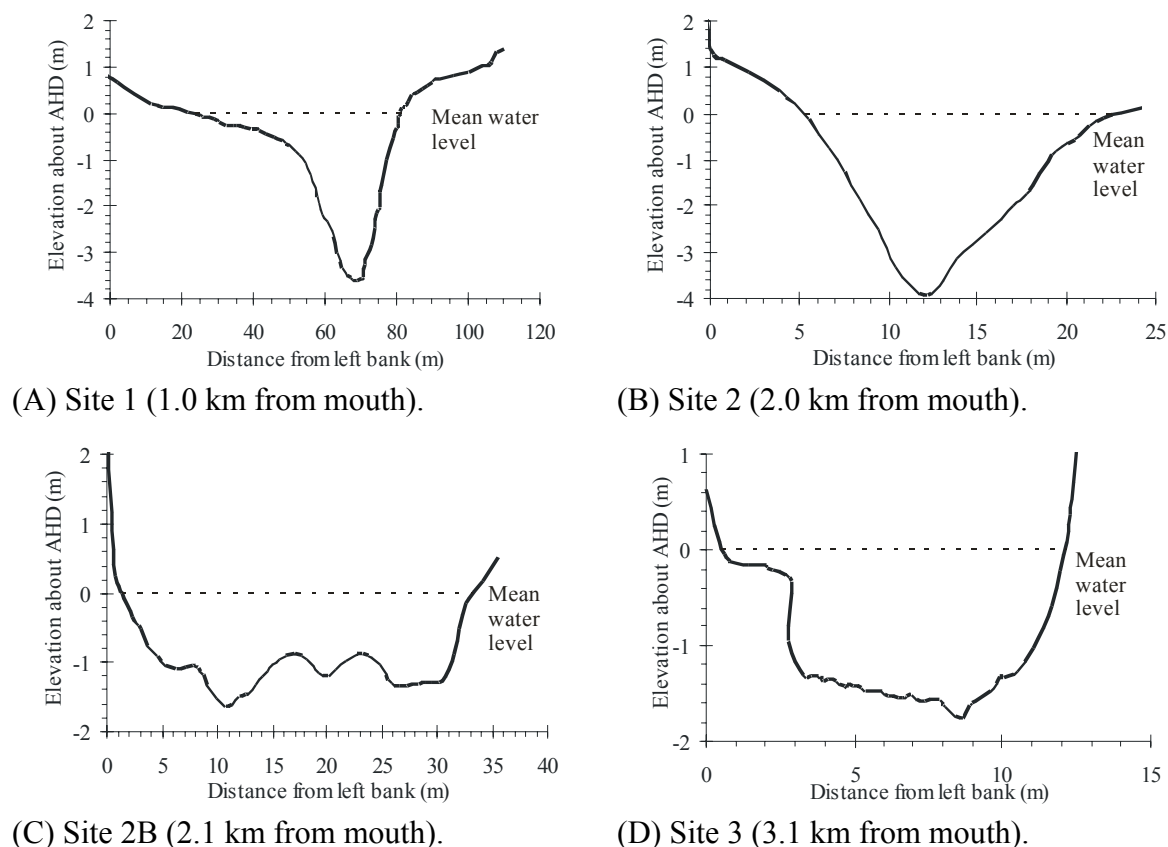
Figure 6.1 – Surveyed experimental cross-sections used at Eprapah Creek. Note different horizontal and vertical scales of figures.

Section 6.2 defines the physio-chemistry properties used in this investigation and presents some key observations from the physio-chemistry data measured at Eprapah Creek. The suspended sediment concentration data collected during the field studies E6 and E7 are presented in Section 6.3. Section 6.4 discusses the implications of the measured physio-chemistry data on the physical characteristics and water quality of Eprapah Creek. The effects of turbulence on the mixing of the water properties in Eprapah Creek are discussed in Chapter 10. Time series and vertical profiles plots of all water quality data from the field studies at Eprapah Creek are presented in Digital Appendix.

6.2 PHYSIO-CHEMISTRY OBSERVATIONS

Section 6.2 presents some key findings from the analysis of the physio-chemistry data collected at Eprapah. These include observations from the continuous data measured by YSI6600 probes (Section 6.2.2) and the additional LTS9000 probes deployed for the studies E6 and E7 (Sections 6.2.3 and 6.2.4). Key observations from the study E9 are presented in Section 6.2.5. Lastly, Section 6.2.6 presents some key observations from the vertical profile conductivity data collected as part of the field studies at Eprapah Creek.

6.2.1 Water quality properties investigated

Physio-chemical indicators are commonly used to assess the water quality in the fresh and marine waterways of Australia and New Zealand (e.g. ANZECC (2000)). This investigation focused on the "high frequency" collection of physio-chemistry data for relatively long periods. One instrument capable of performing this type of measurements was the YSI6600 probe (provided by the EPA (QLD)). The physio-chemical properties measured by the YSI6600 probes and therefore those properties investigated, were:

Conductivity (mS/cm) – A measure of the ratio of fresh and sea water in the estuary. The conductivity values of fresh and sea water being approximately 0 and 60 mS/cm respectively. Water conductivity is an important water parameter for assessing the level of stratification in an estuary caused by the interaction of fresh and sea water. Previous studies have found that water density stratification can have a substantial impact on the turbulent mixing processes in estuaries (e.g. Dyer (1997)). Section 6.4.1 presents some approximations of the stratification levels in Eprapah Creek from the conductivity data collected.

Temperature (C) – Water temperature affects the rate of all chemical and biological processes. The local water temperature in estuaries is affected by the interaction of the fresh and sea water and the variations in the ambient air temperature. In Eprapah Creek the water temperature ranged between 10 and 30 C.

Dissolved oxygen (% saturation) – Measures the amount of oxygen in the water and defines the living conditions of aquatic organisms that require oxygen. Dissolved oxygen can have units of mg/L or % saturation. For the estuaries of Southeast Australia, the water quality is considered healthy if 80 < DO < 110 % saturation (ANZECC (2000)).

pH – Measures the acidity or alkalinity level of a substance. In water quality pH is important for defining the waters health and ability to support aquatic organisms. It is measured on a logarithmic scale from 0 (extremely acidic) through 7 (neutral) to 14 (extremely alkaline). The water quality would be considered healthy if 7.0 < pH < 8.5 for the estuaries of Southeast Australia (ANZECC (2000)).

Chlorophyll a levels (μg/L) – An indicator of phytoplankton biomass within the water. It can be measured by optical sensor (fluorometry) in the field or by spectrophotometry in a laboratory. The YSI6600 probe uses fluorometry to directly measure the level of chlorophyll a in the water. For the estuaries of Southeast Australia chlorophyll a levels < 5 μg/L are recommended (ANZECC (2000)).

Turbidity (NTU) – A measure of the water transparency, which can be used to estimate the quantity of suspended matter in the water column. Water clarity is important for determining the productivity and condition of an aquatic system. Turbidity is measured by Secchi disk or optical backscatter meters (e.g. YSI6600 probe). For the estuaries of Southeast Australia turbidity between 0.5 < turbidity < 10 NTU is recommended (ANZECC (2000)).

6.2.2 Physio-chemistry point measurements with a YSI6600 probe (field studies E1 to E7)

For the field studies E1 to E7 a YSI6600 probe was deployed 0.3 m beside the 3D-ADV position (Table 6.2). During the study E7 a second YSI6600 probe was deployed on a float to sample next to the free surface. Table 6.2 lists the locations of the YSI6600 probes for each field study. The YSI6600 probes continuously measured at "high frequency" water temperature, conductivity, pH, turbidity, dissolved oxygen and chlorophyll a levels throughout the period of each field study.

Table 6.2 – Location of YSI6600 probes in Eprapah Creek.

Field study	Date	Duration (hours)	f_{scan} (Hz)	Sampling location
E1	4/04/03	12	0.20	Site 2B, 0.5 m below free surface, 13.9 m from left bank
E2	17/07/03	8	0.20	Site 2, 0.5 m below free surface, 7.7 m from left bank
E3	24/11/03	10	0.50	Site 2B, 0.5 m below free surface, 10.4 m from left bank
E4	2/09/04	12	0.30	Site 2B, 0.05 m above bed, 10.4 m from left bank
E5	8-9/03/05	25	0.16	Site 2B, 0.1 m above bed, 10.4 m from left bank
E6	16-18/05/05	48	0.08	Site 2B, 0.4 m above bed, 10.4 m from left bank
E7	5-7/06/06	50	0.08	Site 3, 0.4 m above bed and 0.3 m below free surface, 3.9 m from right bank

Note: f_{scan} : sampling frequency.

Table 6.3 summarises the median, maximum and minimum values for each physio-chemistry property observed during the field studies E1 to E7. During the field study E5, some

potentially irregular values of turbidity, dissolved oxygen and chlorophyll a levels were observed. These data were irregularly high and were thought to be related to a possible instrumentation fault.

Table 6.3 – Summary of data measured by YSI6600 probes at Eprapah Creek.

Field study	E1	E2	E3	E4
Date	4/04/03	17/07/03	24/11/03	2/09/04
Duration (hours)	12	8	10	12
f_{scan} (Hz)	0.2	0.2	0.5	0.3
Notes	Site 2B near surface	Site 2 near surface	Site 2B near surface	Site 2B close to bed
Water temperature (C)	24.18 [24.15-24.96]	17.5 [16.6-19.76]	25.59 [24.85-25.97]	17.19 [16.35-18.07]
Conductivity (mS/cm)	35.08 [28.11-42.27]	39.2 [30.49-43.63]	49.28 [42.71-55.13]	49.57 [41.11-53.42]
pH	7.51 [7.14-7.83]	7.53 [7.1-7.77]	7.71 [7.4-8.04]	7.41 [6.78-7.79]
Turbidity (NTU)	9.5 [5.8-14.8]	9.8 [7.3-90.8]	18.9 [7.1-43.0]	21.4 [7.2-864.1]
Dissolved oxygen (% saturation)	60.2 [48.8-91.4]	87.1 [66.7-94.0]	81.3 [76.2-84.8]	71.8 [35.1-95.5]
Chlorophyll a (µg/L)	1.7 [0.1-3.6]	3.0 [0.4-5.5]	17.2 [2.9-27.5]	6.1 [2.3-8.4]

Field study	E5	E6	E7Bed	E7Surface
Date	8-9/03/05	16-18/05/05	5-7/06/06	5-7/06/06
Duration (hours)	25	48	50	50
f_{scan} (Hz)	0.167	0.083	0.083	0.083
Notes	Site 2B close to bed	Site 2B close to bed	Site 3 close to bed	Site 3 near surface
Water temperature (C)	26.06 [24.07-26.94]	21.09 [20.20-21.80]	18.87 [18.24-19.28]	17.4 [16.19-19.51]
Conductivity (mS/cm)	50.85 [44.32-55.96]	47.27 [44.05-50.25]	47.26 [46.05-47.94]	37.92 [25.5-45.54]
pH	8.12 [7.7-8.35]	7.83 [7.45-8.05]	7.32 [7.01-7.58]	6.98 [6.78-7.35]
Turbidity (NTU)	315.5* [6.5-1849.3*]	12.1 [3.4-747.3]	8.6 [3.4-175.9]	3.0 [1.3-188.6]
Dissolved oxygen (% saturation)	135.1* [85.6-219.3*]	64.2 [45.5-84.9]	39.7 [20.4-54.8]	26.7 [11.2-56.8]
Chlorophyll a (µg/L)	45.2* [2.9-108.5*]	5.9 [1.5-13.9]	5.4 [3.6-9.6]	3.2 [1.3-7.3]

Note: median value [minimum value-maximum value]; (*): possibly unrealistic value; f_{scan}: sampling frequency; E7Bed and E7Surface were measured near bed and free surface respectively.

All physio-chemical properties showed some variation with the tides for all field studies at Eprapah Creek (e.g. Figure 6.2). Figure 6.2 shows the variation of physio-chemistry properties of the YSI6600 probe at sampling 0.4 m above the bed during the study E6 (16-18/05/05) as functions of time. Similar tidal trends were observed in all field studies conducted at Eprapah Creek (Appendix C). For all field studies at Eprapah Creek, the conductivity, pH and dissolved oxygen values were the largest at high tide, while the water temperature, turbidity and chlorophyll a levels were the largest at low tide.
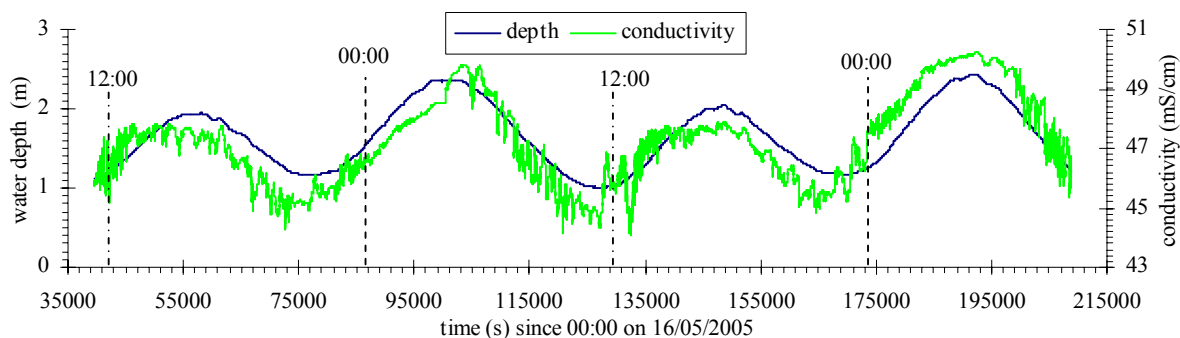
(A) Water depth and conductivity.
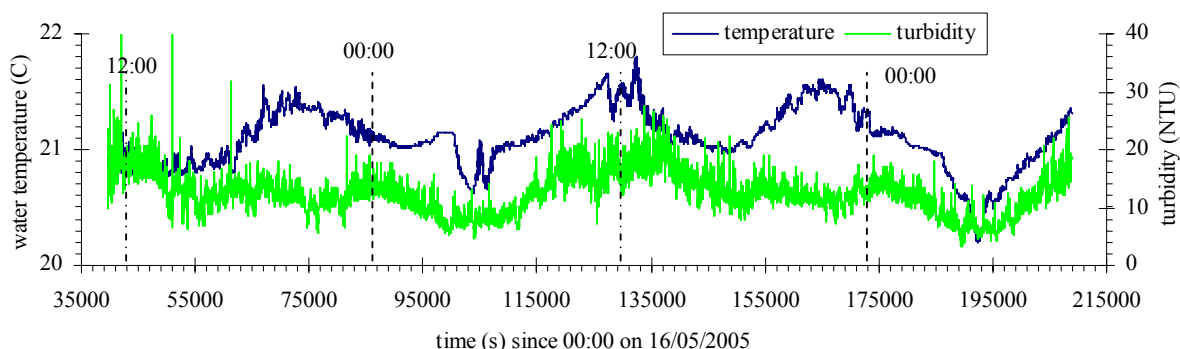
(B) Water temperature and turbidity.
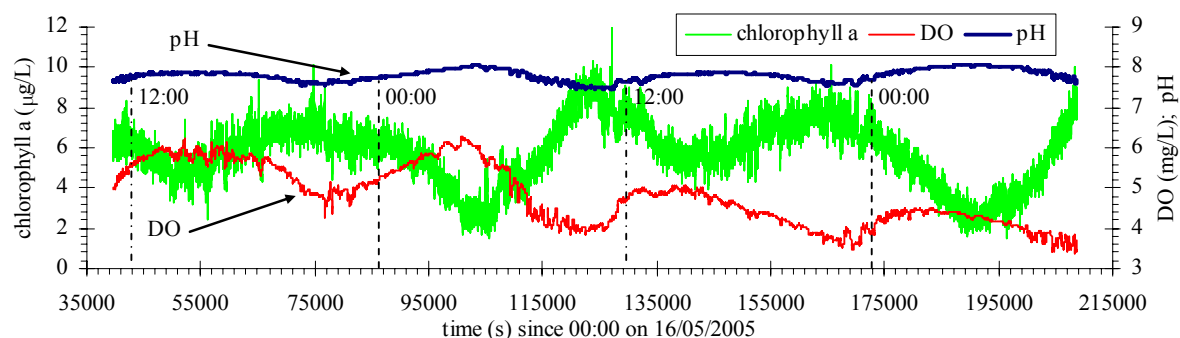
(C) Chlorophyll a, dissolved oxygen and pH.

Figure 6.2 – Physio-chemistry data as functions of time since midnight on 16/05/05. Data collected with a YSI6600 probe located 0.4 m above bed at Site 2B, Eprapah Creek for field study E6 (16-18/05/05).

A more detailed series of physio-chemistry measurements were performed in the upper estuary (Site 3) during the study E7 when two YSI6600 probes were deployed. The first YSI6600 probe was fixed 0.4 m above the bed next to the ADVs, while the second YSI6600 probe was deployed on a float with its sampling volume approximately 0.3 m below the free surface. Close to the bed only minor changes in all physio-chemical properties were observed throughout the entire study. This was not the case close to the free surface where the variation of all physio-chemistry properties was larger (Figure 6.3, Table 6.3). Figure 6.3 shows the water temperature and conductivity data close to the bed and near the surface at Site 3 as functions of time. Note that this data set was collected in the upper estuary (Site 3), while the data shown in Figure 6.2 were measured in the middle estuary (Site 2B). In Figure 6.3, the difference in conductivity and temperature close to the bed and free surface seemed to indicate that some stratification occurred in the upper estuary for the study E7. This was possibly related to the freshwater discharge from the STP, because no natural freshwater inflow or rainfall was observed before or during the study E7.
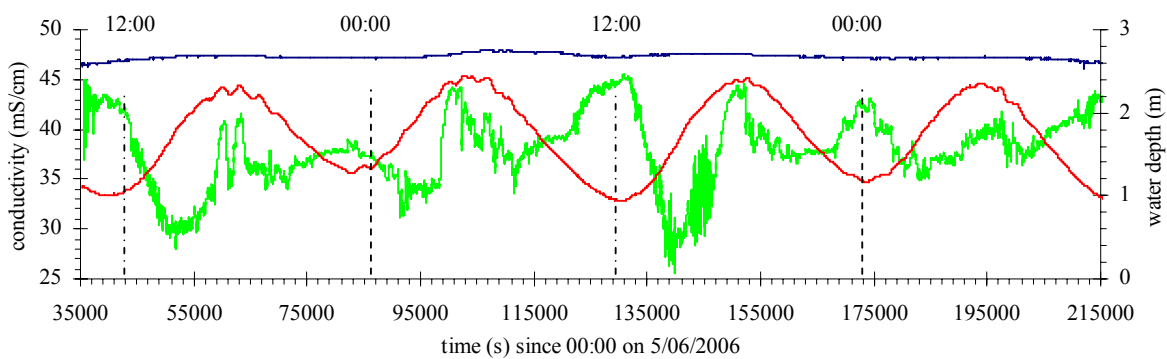
(A) Conductivity and water depth.
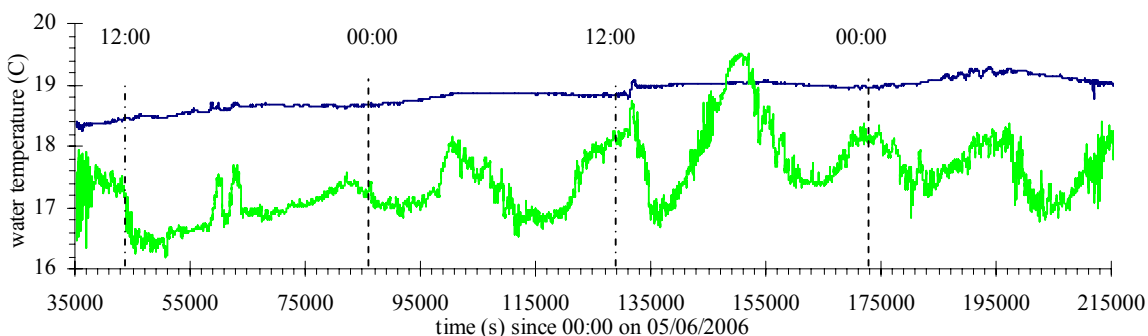
(B) Water temperature.

Figure 6.3 – Water depth, temperature and conductivity as functions of time. Data collected 0.4 m above bed and 0.3 m below surface at Site 3, Eprapah Creek for study E7 (5-7/06/06). Legend: — sampled 0.4 m above bed; — sampled 0.3 m below surface; — water depth.

6.2.3   Simultaneous cross-sectional measurements of physio-chemistry (field study E6)

For the field study E6 (16-18/05/05), six In-Situ Troll9000 probes (LTS9000) were installed transversely across the experimental cross-section of Site 2B with a YSI6600 probe (Figure 6.4). Figure 6.4 shows the location of the LTS9000 and YSI6600 probes in the Site 2B experimental cross-section for the study E6. Table 6.4 outlines the transverse and vertical locations of the probes in the cross-section. The median, maximum and minimum values of the water temperature and conductivity data collected by the six LTS9000 probes and the YSI6600 probe deployed are presented in Table 6.4.
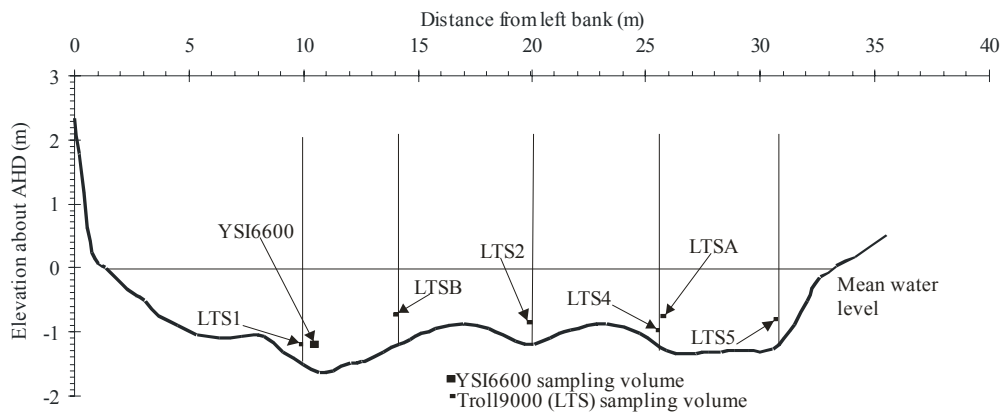
Figure 6.4 – Location of probes in cross-section at Site 2B, Eprapah Creek for field study E6.

Table 6.4 – Location and median, maximum and minimum water temperature and conductivity values collected by physio-chemistry probes for field study E6.

Probe code	Transverse location (m)	Vertical elevation (m.a.b.)	Water temperature (C)	Conductivity (mS/cm)
LTS1	10.1	0.29	21.16 [20.28-21.83]	49.79 [48.13-51.95]
LTS2	20.0	0.41	21.15 [20.22-22.65]	47.45 [51.90-50.54]
LTS4	25.6	0.15	21.10 [20.37-21.86]	47.16 [43.43-49.68]
LTS5	31.0	0.36	21.11 [20.32-22.17]	52.69 [36.41-56.09]
LTSA	25.6	0.59	21.16 [20.36-22.30]	45.36 [35.28-48.29]
LTSB	14.0	0.59	21.24 [20.28-22.59]	47.50 [33.47-50.70]
YSI6600	10.4	0.40	21.09 [20.20-21.80]	47.26 [46.05-47.94]

Note: Transverse location is from left bank (Figure 6.4); Vertical elevation is distance of sensor above bed; m.a.b.: metres above bed; median value [minimum value-maximum value].

Figure 6.5 shows the variation of water temperature and conductivity measured by the LTS9000 probes as functions of time for the study E6. The tidal patterns and median values of the water temperature data were similar for all probes in the experimental cross-section. Over the 48 hours of the investigation the water temperature varied by only 2.5 C, whereas the air temperature varied by 14 C during the same period. The median values of conductivity varied by 15 % transversely across the cross-section at Site 2B. Any cause for this difference in conductivity is presently unknown. The trends in conductivity observed were similar for all physio-chemistry probes deployed at Site 2B for the field study E6.

In Figure 6.5, a large fluctuation in water temperature and conductivity data was observed between t = 120,000 and 135,000 s (approximately 10:00 to 13:00 on 17/05/05). During this period a significant decrease in conductivity was observed, which indicated the presence of freshwater and was therefore possibly related to the daily maximum of STP outflow discharge which seemed to occur about this time (Section 3.2). However, it is inappropriate to speculate without more data on the discharge from the sewage treatment plant.
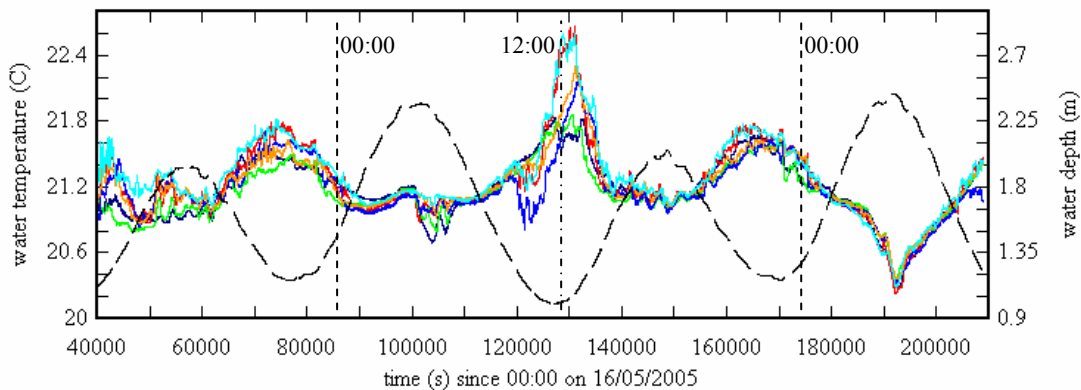
(A) Water temperature and depth data.
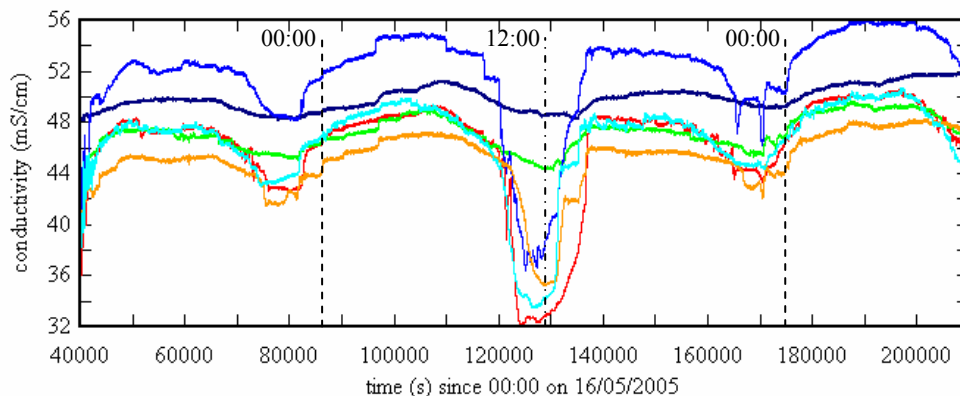
(B) Conductivity data.

Figure 6.5 – Water temperature and conductivity data collected at Site 2B for field study E6.

Legend: — data from LTS1; — data from LTS2; — data from LTS4; — data from LTS5; — data from LTSA; — data from LTSB; − − water depth.

6.2.4   Simultaneous longitudinal measurements in the upper estuary (field study E7)

For the field study E7, four LTS9000 probes were deployed longitudinally in the upper estuarine zone about the main investigation site, located at Site 3. The LTS9000 probes were deployed on the bank opposite the STP (2.5 km from mouth); at Site 3; approximately 50 m upstream of Site 3; and at Site 3B (3.4 km from mouth). Figure 6.6 shows the location of the LTS9000 and YSI6600 probes in the upper estuarine zone.   Table 6.5 provides the longitudinal and vertical elevations along with the medium, maximum and minimum values of the observed water temperature and conductivity data from the LTS9000 probes.
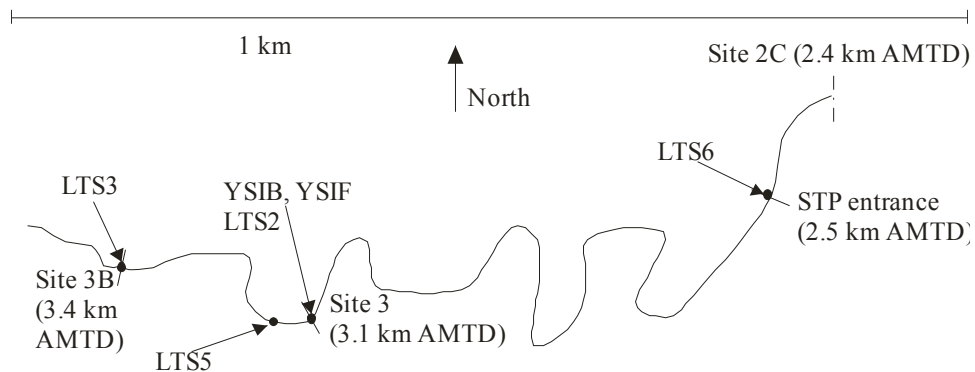
Figure 6.6 – Location of physio-chemistry probes in upper estuary for study E7 (5-7/06/06).

Table 6.5 – Location of LTS9000 probes and median, maximum and minimum water temperature and conductivity values measured for study E7.

Probe code	Longitudinal location (km)	Vertical elevation (m.a.b.)	Water temperature (C)	Conductivity (mS/cm)	Remarks
LTS2	3.10	0.40	19.02 [18.51-19.46]	45.30 [44.68-45.98]	Site 3, next to ADV
LTS3	3.40	0.40	18.45 [18.00-18.75]	44.62 [41.78-45.79]	Site 3B
LTS5	3.15	0.23	18.85 [17.68-19.35]	48.33 [40.55-49.40]	50 m upstream of Site 3
LTS6	2.5	0.33	19.10 [16.93-22.97]	47.51 [6.46-49.50]	Left bank, opposite STP outfall

Note: Longitudinal distance along creek from mouth; Vertical elevation is distance of probe above bed; m.a.b.: metres above bed; median value [minimum value-maximum value].

The water temperature seemed to increase over the 50 hours of observation at all sampling locations in the upper estuarine zone (Figure 6.7A). Figure 6.7 shows the water temperature and conductivity measured in the upper estuarine zone by the four LTS9000 probes as functions of time. In Figure 6.7 the tidal trends in water temperature and conductivity were

different at Site 3B than those of the other sampling locations in the upper estuary. One possible explanation for these different tidal trends was that Site 3B seemed to be located at the edge of the estuarine zone at Eprapah Creek. The water level data indicated that Site 3B was cut off from the rest of the estuary at low tide with the water level being constant at Site 3B about low water (e.g. Figure 6.9).
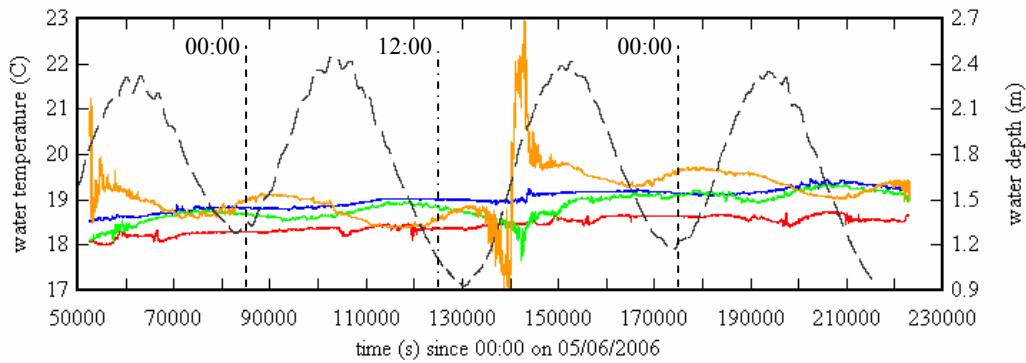
(A) Water temperature and water depth data.
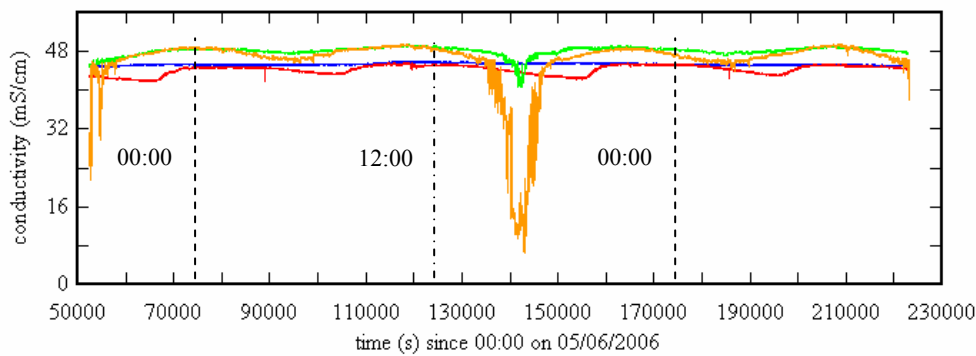
(B) Conductivity data.

Figure 6.7 – Water temperature and conductivity data collected in upper estuary for study E7. Legend: — data from LTS6; — data from LTS2; — data from LTS5; — data from LTS3; − − water depth.

A large change in water temperature and conductivity was observed near the STP between $t = 135,000$ and $150,000$ s since midnight on 5/06/06 (approximately 13:00 to 17:00 on 6/06/06). The probes about Site 3 observed smaller variations in water temperature and conductivity around the same period. This anomaly was similar to that observed during the study E6 (Section 6.2.3). The anomaly was possibly related to the discharge from the STP, because the substantial decrease in conductivity seemed to indicate increased quantities of freshwater in the upper estuary. Note that no natural freshwater inflow was observed during the study E7.

6.2.5   Simultaneous high frequency measurements along Eprapah Creek (field study E9)

Two studies were performed in October 2006 collecting high frequency water level, temperature and conductivity data at selected longitudinal locations along Eprapah Creek. The two field studies were conducted in near spring (study E9A, 2-4/10/06) and near neap (study E9B, 11-13/10/06) tidal conditions. In-Situ mini-Troll (mini-Troll) probes were placed at Sites 1, 2B, 2C, 3, 3B and 4, which measured water level and temperature samples at 1 Hz for 50 hours. Figure 6.8 shows the location of the mini-Troll probes in Eprapah Creek for the field study E9. Table 6.6 summarises the physio-chemistry data measured by the mini-Troll probes in Eprapah Creek for the studies E9A and E9B.   In Table 6.6 the variation of temperature seemed smallest in the upper estuary.
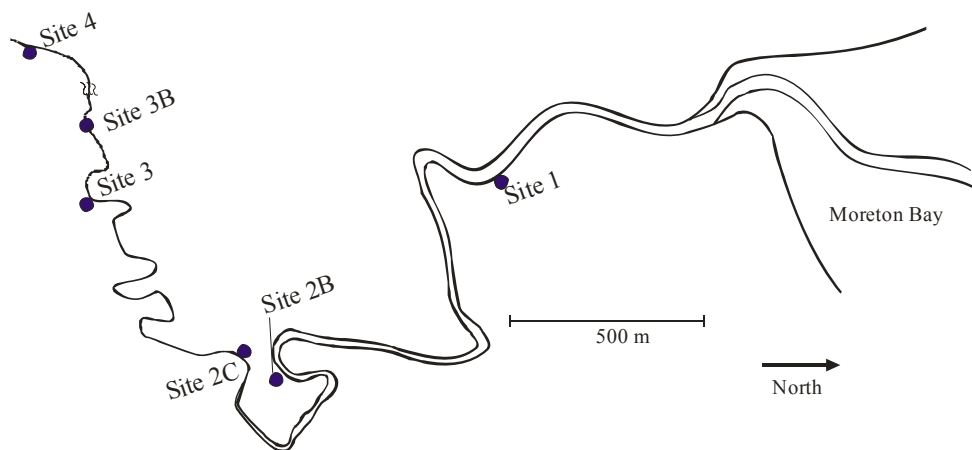
Figure 6.8 – Location of mini-Troll probes in Eprapah Creek for field study E9.

Two LTS9000 probes were installed at Sites 2B and 3.   These recorded water level, temperature and conductivity samples every 6 s for the 50 hours of the two studies. Table 6.7 summarises the water temperature and conductivity data collected by the LTS9000 probes for the studies E9A and E9B. For the field studies E9A and E9B the water temperature and conductivity ranges of the LTS9000 probes were larger mid estuary (Site 2B) than in the upper estuary (Site3).

Figure 6.9 shows the water level about the Australian Height Datum (AHD) at the observation points along the Eprapah Creek estuarine zone used for the studies E9A and E9B. In Figure 6.9, the tidal variations about high water were similar in phase and amplitude throughout the estuarine zone. This was possibly because the length of the Eprapah estuarine zone is less than the wavelength of the semi-diurnal tides and the water level along the length of Eprapah Creek changed in relative unison.

In Figure 6.9 the water level at Site 3B was constant during the low tides, which suggested that Site 3B separated from the rest of the estuary during these periods. This indicated that

Site 3B represents the upper extent of the estuarine zone. For the last section of some ebb tides (e.g. t = 170,000 to 185,000 s, Figure 6.9A), the water levels observed at Site 3 differed from those observed in the lower (Site 1) and middle (Sites 2B and 2C) estuarine zones. One possible explanation for this was that the natural weir near the STP acted as a hydraulic control during extreme low tides.

Table 6.6 – Data collected by mini-Trolls probes at Eprapah Creek (studies E9A and E9B).

Site	AMTD (km)	Study E9A (near spring tides)		Study E9B (near neap tides)	
		Temp (C)	Tidal range (m)	Temp (C)	Tidal range (m)
1	1.0	24.2 [21.3-26.8]	1.88	21.0 [19.7-22.5]	1.61
2B	2.1	24.8 [21.9-27.5]	1.89	20.9 [19.5-21.6]	1.62
2C	2.4	24.9 [23.3-27.2]	1.88	20.9 [19.4-21.4]	1.62
3	3.1	24.7 [24.1-25.9]	1.79	21.2 [20.9-21.4]	1.62
3B	3.4	23.3 [22.1-25.2]	1.31	23.3 [22.1-25.2]	1.33
4	3.7	20.2 [19.4-20.9]	0.04	20.2 [19.4-20.9]	0.03

Note: AMTD: Australian Middle Thread Distance (upstream of mouth); Temp: water temperature; median value [minimum value-maximum value]; Tidal range: largest averaged tidal range at site; tidal range averaged over tidal cycle (e.g. LW1 to HW and HW to LW2).

Table 6.7 – Data from LTS9000 probes for field studies E9A and E9B.

Site	AMTD (km)	Study E9A (spring tides)		Study E9B (neap tides)	
		Temp (C)	Cond (mS/cm)	Temp (C)	Cond (mS/cm)
2B	2.1	24.7 [21.9-27.5]	52.8 [37.1-57.8]	21.0 [19.4-21.7]	52.6 [38.0-59.8]
3	3.1	24.7 [24.2-26.0]	47.8 [44.7-50.3]	21.1 [20.7-21.4]	47.2 [42.2-50.4]

Note: AMTD: Australian Middle Thread Distance (upstream of mouth); Temp: water temperature; Cond: conductivity; median value [minimum value-maximum value].
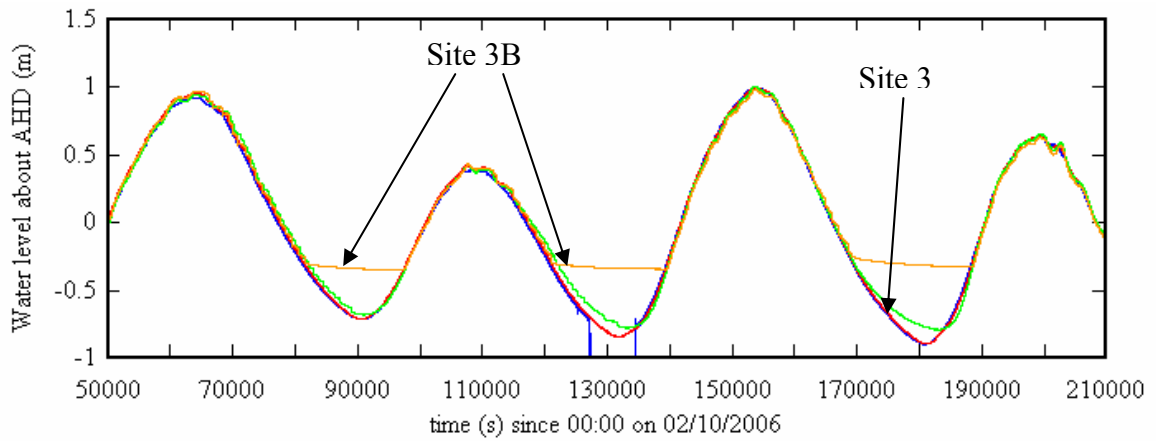
(A) Water level observed under near spring tidal conditions for study E9A.
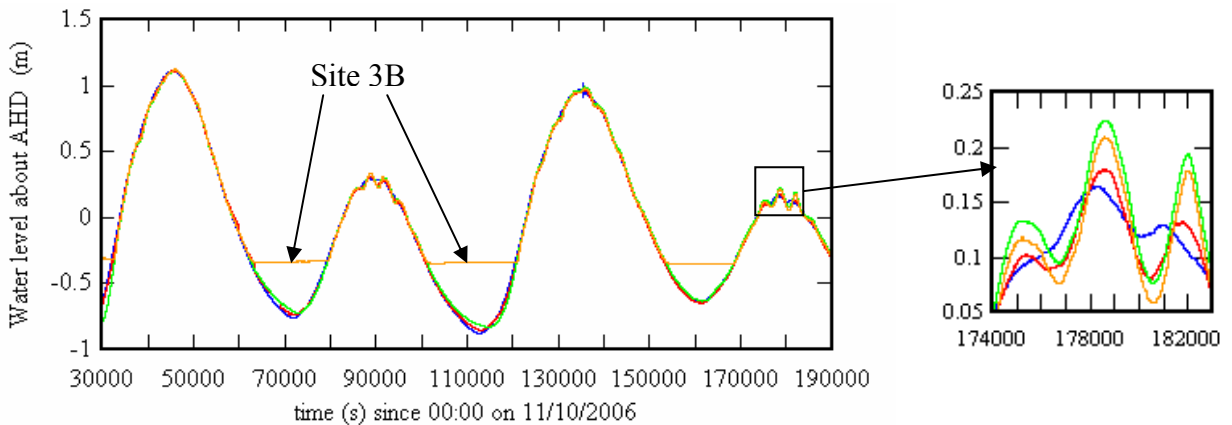
(B) Water level observed under near neap tidal conditions for study E9B.

Figure 6.9 – Water levels along Eprapah Creek as functions of time for field studies E9A (2-4/10/06) and E9B (11-13/10/06).

Legend: — data from Site1; — data from Site 2B; — data from Site 3; — data from Site 3B.

The presence of "long period oscillations" was observed in both spring (study E9A, Figure 6.9A) and neap (study E9B, Figure 6.9B) tidal studies. These long period oscillations were more prevalent on the minor (smaller) tidal cycles during neap tidal conditions (Insert, Figure 6.9B). For both spring and neap tidal conditions the amplitude of the long waves increased as they progressed upstream. In Figure 6.9 the long period oscillations were out of phase along Eprapah Creek, most likely because the wavelength of these oscillations were smaller than the length of the estuarine zone.

6.2.6   Vertical profiles collected along Eprapah Creek

Vertical profiles of key physio-chemical properties were measured with a YSI6920 probe at some longitudinal locations along Eprapah Creek, during or in the days following each field study. The data were collected from a boat drifting with the current. A YSI6920 probe measured water temperature, conductivity, turbidity, pH, dissolved oxygen and sampling

depth for each vertical elevation. All vertical profiles collected during the field studies at Eprapah Creek are presented in Appendix C.

Figure 6.10 presents the conductivity vertical profiles for a select number of field studies, these being the field studies E5 (spring tide), E7 (neap tide) and E8 (after a rainstorm). The vertical profiles for the field studies E5 (Figure 6.10A) and E7 (Figure 6.10B) were collected on the ebb tides as part of the monthly monitoring program. For the spring tidal conditions of the study E5, the vertical profiles of conductivity showed the estuary to be well-mixed throughout most of the estuarine zone (Figure 6.10A). However, under the neap tidal conditions of the field study E7, the level of stratification seemed to increase from well-mixed near the mouth, to slightly stratified mid estuary through to substantially stratified in the upper estuary. The freshwater discharge from the STP was one possible cause of this stratification since no natural freshwater inflow was observed for the study E7.
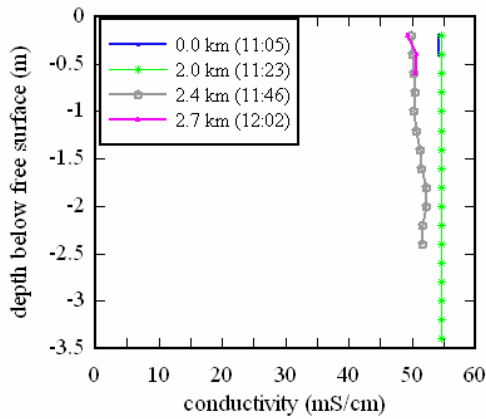
(A) Spring tide on 10/03/05 (study E5).
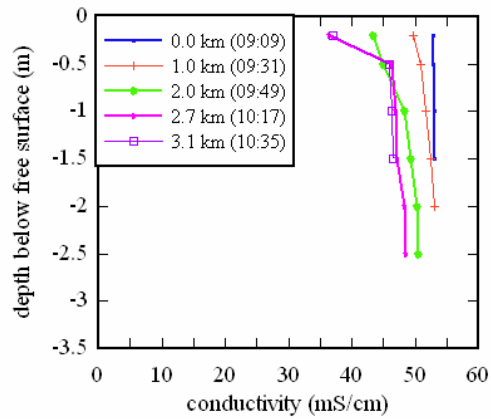
(B) Neap tide on 7/06/06 (study E7).
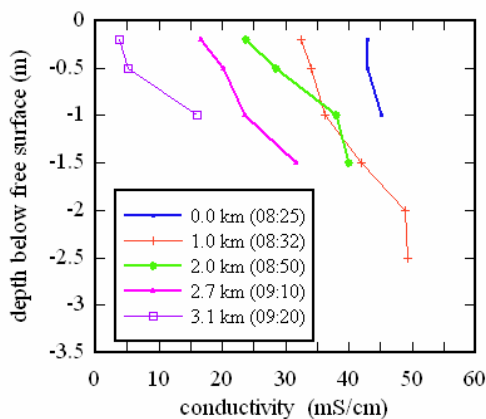
(C) 3.5 hours after rainstorm on 28/08/06 (study E8).
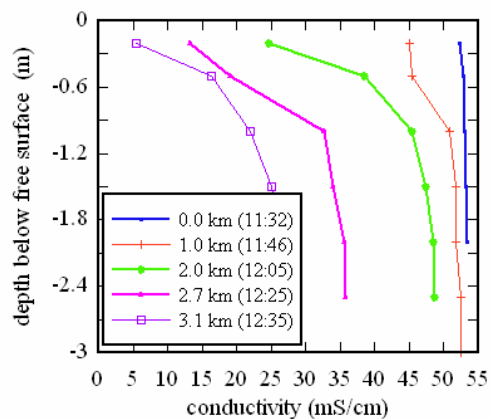
(D) 6 hours after rainstorm on 28/08/06 (study E8).

Figure 6.10 – Conductivity vertical profiles measured along Eprapah Creek. Profiles collected at 0.0, 1.0, 2.0 & 2.7 km from mouth by EPA (QLD) as part of monthly monitoring program, and 2.4 & 3.1 km from mouth as part of field studies.

Figures 6.10C and 6.10D show the effect of 30 mm of rain, 3.5 and 6 hours after it was observed at 05:30 on 28/08/06 (study E8). In Figure 6.10C, low conductivities and some substantial stratification were observed at all sampling locations (including the mouth) 3.5 hours after the rainfall. However, the vertical profiles collected 6 hours after the rainfall showed that the conductivity values close to the bed had increased at all sampling locations (Figure 6.10D). In Figure 6.10D the vertical profiles at 0.0 and 1.0 km seemed well-mixed, while the profiles at 2.0, 2.7 and 3.1 km were partially stratified. This indicated that 6 hours after the 30 mm of rain the estuary was beginning to return to a state similar to that observed in Figures 6.10A and 6.10B. The effect of this rainfall event on all physio-chemistry properties measured for the field study E8 are discussed in Section 10.4.

6.3   SUSPENDED SEDIMENT CONCENTRATION

For the field studies E6 and E7, the suspended sediment concentration (SSC) was derived from the backscatter intensity of the 2D-microADV (16 MHz). A laboratory experiment was performed using water and sediment collected at Eprapah Creek to calibrate the backscatter intensity of the 2D-microADV (16 MHz, serial no. A641F) and turbidity measured by a YSI6600 probe with suspended sediment concentration (Chanson et al. (2006)). This laboratory calibration experiment is detailed in Appendix D. The relationship between backscatter intensity of the 2D-microADV (16 MHz, serial no. A641F) and the suspended sediment concentration (Equation 3.7) is outlined in Section 3.4.1.2.1.

Suspended sediment concentration is a scalar property that measures the concentration of particles suspended in the ADV sampling volume. The suspended sediment concentration is measured in the same sampling volume as the turbulent velocity data and is sampled at the same frequency. This allows for the investigation of the interaction between the turbulent velocity fluctuations and a scalar property (SSC) within the same small sampling volume (Section 10.2). In Section 10.2 the relationship between the suspended sediment concentration and velocity is investigated: through a comparison of the integral time scales of SSC and the horizontal velocity components (Section 10.2.2); and the relationship between the suspended sediment flux within the sampling volume and the bed shear stress (Section 10.2.3).

For the studies E6 (Site 2B, 16-18/05/05) and E7 (Site 3, 5-7/06/06) the 2D-microADV was deployed at 0.2 m above the bed. Figure 6.11 shows the time-averaged suspended sediment concentration $\overline{SSC}$ and water depth as functions of time. Note that the suspended sediment concentration data are presented on a logarithmic scale (left vertical axes). In Figure 6.11, suspended sediment concentration variation periods of approximately 25 and 12.5 hours

seemed present at 0.2 m above the bed in the middle (study E6) and upper (study E7) estuaries. The variation in suspended sediment concentration was larger mid estuary (Figure 6.11A) than in the upper estuary (Figure 6.12B). For the field studies E6 and E7, the median values of suspended sediment concentration were 0.018 and 0.007 g/L respectively.
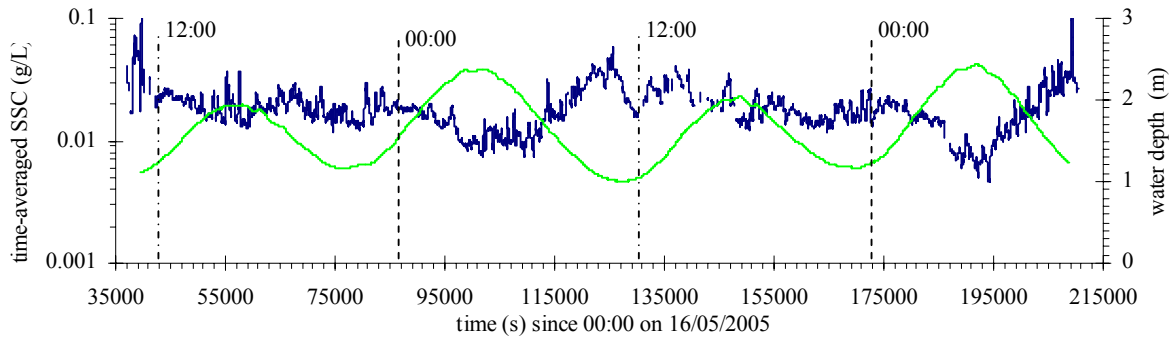
(A) Data collected at 25 Hz in middle estuary (Site 2B) for study E6 (16-18/05/05).
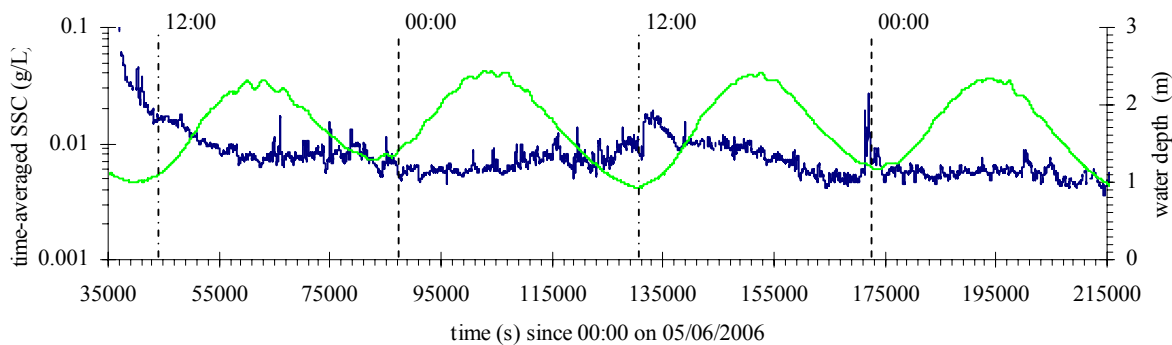
(B) Data collected at 50 Hz in upper estuary (Site 3) for study E7 (5-7/06/06).

Figure 6.11 − Water depth and time-averaged suspended sediment concentration $\overline{SSC}$ as functions of time. Data measured at 0.2 m above bed for field studies E6 and E7. Statistics calculated over 200 s every 10 s along entire data set.

Legend: — $\overline{SSC}$; — water depth.

6.4   DISCUSSION

The analyses of the physio-chemistry data collected at Eprapah Creek revealed that all physio-chemistry properties measured varied with the tides, with the conductivity, pH and dissolved oxygen values largest at high tide, and the water temperature, turbidity and chlorophyll a levels largest at low tide. The suspended sediment concentration was also largest about low tide. In the study of water chemistry, properties such as conductivity, pH and dissolved oxygen are considered solute properties, while turbidity, suspended sediment concentration and chlorophyll a levels are thought of as particulate properties. The water quality data from Eprapah Creek showed that the all solute properties had a similar tidal trend,

while all particulate properties varied in an inverse tidal pattern to the solute properties. This seemed to validate the common assumption made in water quality modelling that all solute properties vary in a similar fashion to the conductivity, while particulate properties vary in a similar fashion to the suspended sediment concentration.

Long period water level oscillations were observed throughout the estuarine zone, with the magnitude increasing with distance upstream of the mouth. These long period oscillations seemed to cause some significant fluctuations in most water quality properties. Significant fluctuations in the measured water level and velocity data caused by long period oscillations were observed for all field studies at Eprapah Creek. A comparison undertaken in Section 10.3 found common oscillation periods between the measured physio-chemistry properties and time-averaged velocity. This seemed to indicate that momentum mixing could have a significant impact on the variation of the water quality properties.

Some physio-chemistry properties (e.g. conductivity) were not vertically and/or transversely well-mixed over the cross-section. In both the middle and upper estuary, a reduced variation of the physio-chemistry properties was observed near the outer bank of the channel meander. Conversely, it seemed that the largest variations occurred close to the inner bank of the meander. These findings indicate that some caution should be used when assuming the physio-chemical properties to be well-mixed over the cross-section.

The possible influence of the freshwater discharge from the sewage treatment plant on the physio-chemistry data was measured under neap tides in the middle and upper estuarine zones. Under neap tidal conditions some stratification was observed in the middle and upper estuarine zones, with the level of stratification being largest in the upper estuary. This stratification may be related to the STP discharge, because no natural freshwater inflow was observed for most field investigations. However, it is inappropriate to speculate on the influence of the STP discharge without more data. Since stratification can influence turbulent mixing, the level of stratification in Eprapah Creek was quantified in Section 6.4.1.

6.4.1   Level of stratification in Eprapah Creek

The level of stratification was approximated for several field investigations using the local Richardson number (Equation 2.1). A "pseudo" approximation of the local Richardson number was used here because field data were not specifically collected for the calculation of the Richardson number. Two methods were used to approximate the local Richardson number from the data available. The first used the vertical profile data recorded during each field study and the ADV velocity data at the time of measurement, while the additional physio-chemistry probes deployed for the field studies E6 and E7 allowed a continuous

approximation of the local Richardson number over the investigation period. For both techniques the variation of velocity and water density were not measured over the same vertical elevation and as such could only be considered "pseudo" values of the local Richardson number. However, these "pseudo" Richardson number values provide a reasonable approximation of the level of stratification during the field studies.

Table 6.8 presents the "pseudo" Richardson number calculated for several field studies undertaken at Eprapah Creek. In Table 6.8, the field studies presented were performed under spring (studies E3 and E5) and neap (study E6) tides at Site 2B and neap tidal conditions at Site 3 in the upper estuary (study E7). Note that the probes used in the calculation of the continuous "pseudo" Richardson number are indicated in Table 6.8. Here the transition between well-mixed and fully stratified is represented as $0.1 < Ri < 10.0$ (Officer (1976)). Table 6.8 shows that Site 2B seemed well-mixed for spring tides and some slight stratification under neap tides, while under neap tidal conditions in the upper estuary the "pseudo" Richardson number indicated significant levels of stratification at Site 3.

Figure 6.12 shows the variation of the continuous "pseudo" Richardson number as a function of time for the field studies E6 and E7. In Figure 6.12 the local Richardson number varied by several orders of magnitude with the tides in the middle (study E6) and upper (study E7) estuarine zones. For both studies, the "pseudo" Richardson number seemed to increase during the ebb tide and decrease during the flood tide. However, long period oscillations seemed to also have a substantial influence on the local Richardson number in both the middle and upper estuary.

Table 6.8 – "Pseudo" Richardson number values for some field studies at Eprapah Creek.

Tidal conditions	Study	Site	Ri	Notes
Spring	E5	2B	0.003	Vertical profile – mid ebb tide (11:23-10/03/05)
	E3	2B	0.0003	Vertical profile – high tide (09:45-23/11/03)
			0.0009	Vertical profile – mid ebb tide (11:41-23/11/03)
			0.004	Vertical profile – end ebb tide (13:24-23/11/03)
Neap	E6	2B	0.37	Vertical profile – mid ebb tide (08:53-17/05/05)
			0.17 #	Continuous – LTS1 and LTSB
	E7	3	35.2	Vertical profile – mid ebb tide (10:35-7/06/06)
			1.35 #	Continuous – YSIB and YSIS

Note: [#]: median Richardson number value for entire study period; LTS: In-SituTroll9000 probe (probe location shown in Figure 6.4); YSIB and YSIS are YSI6600 probes located close to bed and surface respectfully (Table 6.2).

The level of stratification mid estuary under neap tidal conditions (study E6) seemed to vary between well-mixed (some flood tides) and slightly stratified over the investigation period. In the upper estuary under similar neap tides (study E7) the level of stratification varied between partially and fully stratified over the investigation period. From the limited spring tide data collected mid estuary (Site 2B) at the beginning end, middle and end of the ebb tide it seemed reasonable to assume that at Site 2B the water was well-mixed under spring tidal conditions (e.g. study E5).
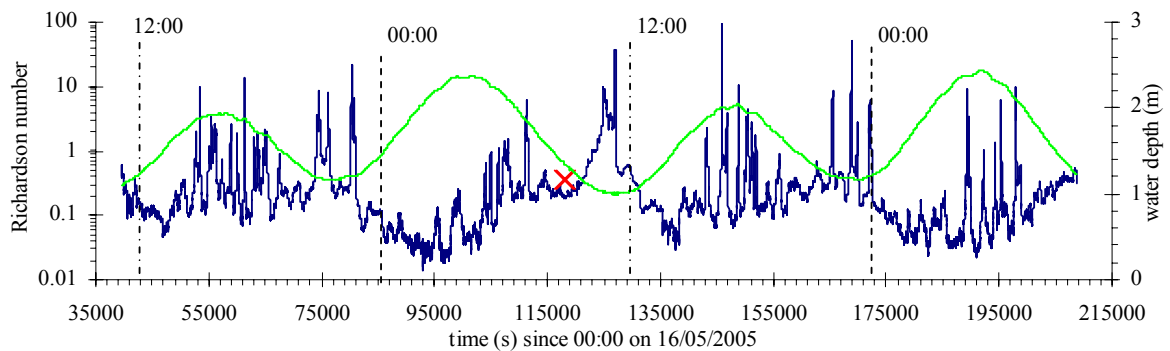
(A) Data collected in middle estuary (Site 2B) for study E6 (16-18/05/05).
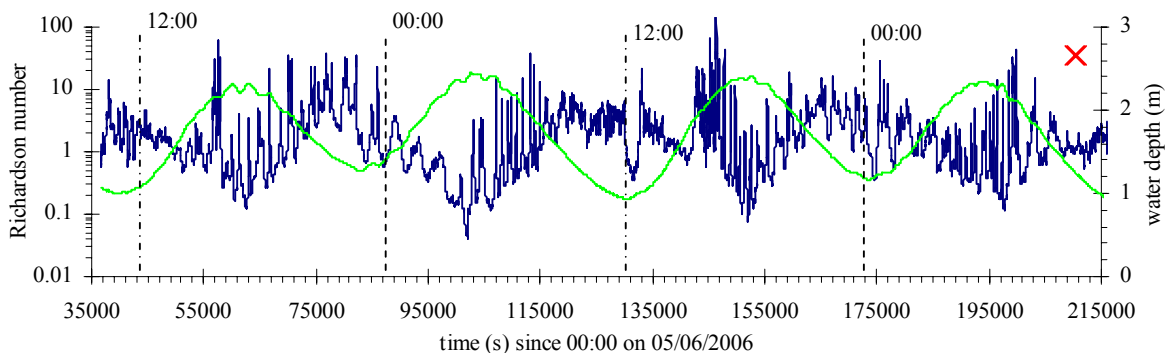
(B) Data collected in upper estuary (Site 3) for study E7 (5-7/06/06).

Figure 6.12 – Water depth and "pseudo" Richardson number Ri as functions of time for field studies E6 and E7. For study E6 Richardson number was approximated using conductivity data collected by probes LTS1 and LTSB. In study E7 Richardson number calculated from conductivity data collected by YSI6600 probes located near bed and surface.

Legend: — local Richardson number Ri ; — water depth; x: value from vertical profile.

7 DISCUSSION OF ESTUARINE TURBULENCE

7.1 PRESENTATION

What are the main influences on the turbulence properties in a small subtropical estuary such as Eprapah Creek? The dominant influences are tidal forcing and freshwater inflow. Since no significant rainstorm occurred during the field studies when the high frequency turbulence and physio-chemistry measurements were conducted, the impact of natural freshwater inflow on the turbulence are not discussed here. Some impact of natural freshwater inflow on the water quality properties will be discussed briefly in Section 10.4.

Section 7.2 compares the effects of the difference in spring and neap tidal forcing on the turbulence properties observed mid estuary at Site 2B. In Section 7.2, the fluctuations in streamwise and transverse velocities, tangential Reynolds stresses $\rho v_x v_z$ and $\rho v_x v_y$ and turbulence time scales are used to illustrate the impact of tidal forcing. During the field studies at Eprapah Creek some "long period oscillations" were observed. The long period oscillations observed during the studies E5 and E6 (spring and neap tides) are discussed in Section 7.3. Section 7.3 outlines the predominant frequencies of these oscillations and their impact on the estuarine turbulence. In Section 7.4, the ratio of the local tidal amplitude and the local mean water depth (a_1/h_1) is introduced as an indicator for the impact of the tidal conditions on the local turbulence properties.

7.1.1 Tidal fluctuations

The tides about Southeast Queensland are mixed semi-diurnal tides, with the tidal range varying between 0.5 m and almost 3.0 m. In Moreton Bay and Eprapah Creek, the predominant tidal constituents were the M2, S1 and O1 components which have tidal periods of 12.42, 24.00 and 24.50 hours respectively. Diurnal inequalities were observed in Moreton Bay and Eprapah Creek under both spring and neap tidal conditions. A diurnal inequality occurs when the two tidal cycles that occur within the 25 hour period of the semi-diurnal tide have different tidal amplitudes and periods. Figure 7.1 shows the water depth at Site 2B as a function of time for the study E5. In this study the terms minor tide and major tide refer to the smallest and largest of the two tidal cycles respectively, and an individual "tide cycle" starts at low water (LW1) and ends at low water (LW2) (e.g. Figure 7.1).
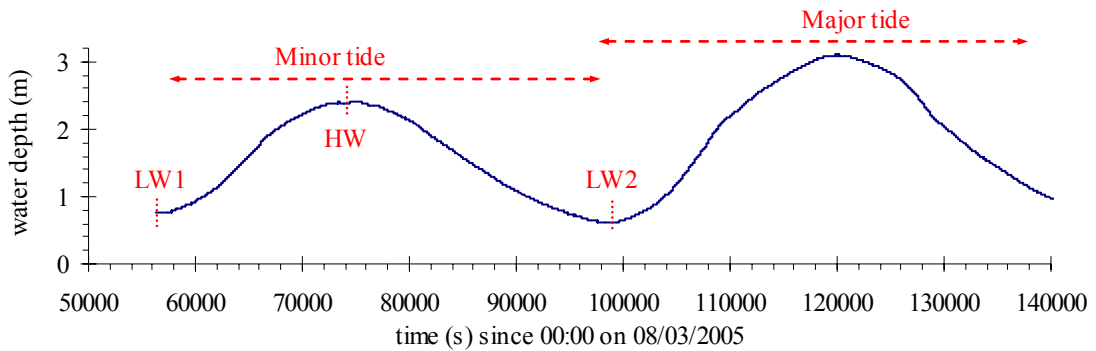
Figure 7.1 – A diurnal inequality observed at Site 2B during field study E5 (8-9/03/05).

7.1.2 Field investigations

High frequency turbulence data were collected continuously close to the bed in the middle estuary (Site 2B) under spring and neap tidal conditions. Table 7.1 describes the tidal conditions observed for the field studies E5 and E6 and lists the instrumentation. The field studies E5 and E6 were both performed with the ADV sampling volume located at 10.7 m from the left bank at Site 2B and the data sets are suitable for comparing the differences in the turbulence properties observed under spring and neap tidal conditions. Figure 7.2 shows the transverse location of the ADV sampling volumes and maximum tidal variations observed at Site 2B. The comparison between the spring and neap tides is focused on the data measured with the 3D-ADV (10 MHz), which sampled at 0.1 and 0.4 m above the bed for the studies E5 and E6 respectively. The effects on the turbulence properties of the different ADV sampling elevations were assumed to be smaller than the impact of the tidal forcing.
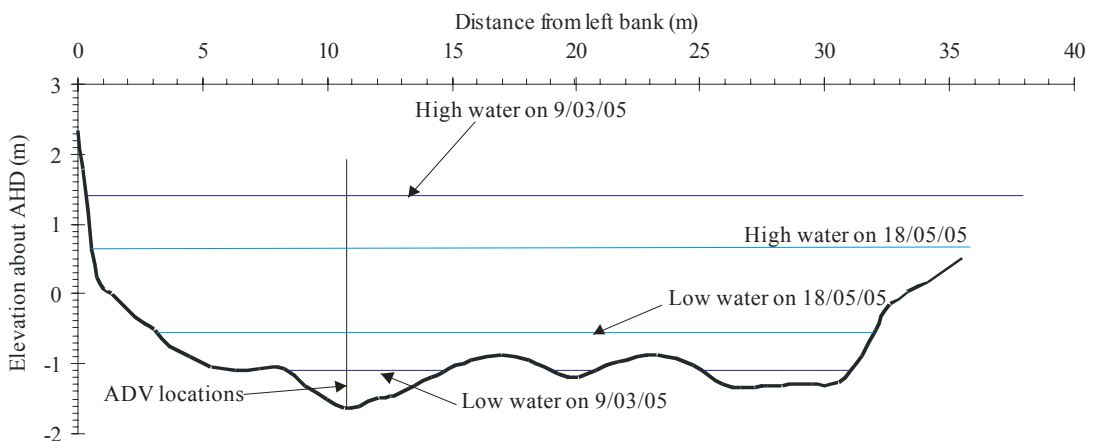
Figure 7.2 – Surveyed cross-section at Site 2B with ADV sampling location and tidal maxima for studies E5 and E6 shown, looking downstream.

Some vertical conductivity profiles were collected near Site 2B during the field studies E5 and E6. These vertical profiles indicated that some slight stratification occurred on the ebb

89

tides under neap tidal conditions, while the water was well-mixed under spring tidal conditions (Section 6.2.6). Further investigations showed that the "pseudo" local Richardson number (Ri) was mostly between $0.01 < Ri < 1$ with a median value of $Ri = 0.17$ for the neap tides of the study E6 and that $Ri < 0.01$ for spring tides (e.g. study E5) (Section 6.4.1). For the study E6 the water seemed well-mixed for most of the flood tides observed and slightly stratified over the rest of the investigation period with the largest levels of stratification on the ebb tides. All data recorded under spring tidal conditions at Site 2B seemed to indicate that the water at Site 2B was well-mixed throughout the investigation period of the study E5. For both studies the median grain size was approximately 0.02 mm.

Table 7.1 – Details of field studies E5 and E6 and instrumentation.

Field study	**E5**	**E6**
Date	8-9/03/05	16-18/05/05
Focus (tidal conditions)	Spring	Neap
Duration (hours)	25	48
Tides: TR (m) [LW1 to LW2 s]	TC1 1.71 m [56,880 to 98,880 s] TC2 2.44 m [98,880 to 146,280 s]	TC1 0.81 m [37,560 to 76,380 s] TC2 1.28 m [76,380 to 127,500 s] TC3 0.97 m [127,500 to 170,148 s] TC4 1.19 m [170,148 to 217,320 s]
Rainfall (mm)	0	0
Mean water depth (m)	1.6	1.6
Site	2B	2B
Longitudinal location (km)	2.1	2.1
Transverse location (m)	10.7 m from left bank	10.7 m from left bank
d_{SV} (m.a.b.) 3D-ADV 2D-microADV	0.1 *	0.4 0.2
f_{scan} (Hz) 3D-ADV 2D-microADV	25 *	25 25
V_{range} (m/s) 3D-ADV 2D-microADV	1.0 *	1.0 1.0

Note: d_{SV} : vertical elevation of ADV sampling volume; m.a.b.: metres above bed; f_{scan} : sampling frequency; V_{range} : ADV maximum velocity range; Tidal information provided defines each tidal cycle (TC), by averaged tidal range (TR) at site and times of LW1 and LW2 since midnight of first day of study; [*]: instrument not deployed.

7.2 VARIATIONS IN TIDAL FORCING (SPRING VS NEAP TIDES)

The two tidal cycles of the field study E5 (spring tides) are compared here to the first two tidal cycles of the field study E6 (neap tides). The first two tidal cycles of the study E6 were chosen because these were the smallest and largest tidal ranges observed. Here, the tidal cycles of the studies E5 and E6 investigated are referred to as tidal cycles E5TC1, E5TC2, E6TC1 and E6TC2 and the averaged tidal range and period of each tidal cycle are listed in Table 7.2. For both field studies the mean water depth observed at 10.7 m from the left bank at Site 2B was approximately 1.6 m. The data were collected with the same 3D-ADV (10 MHz) whose sampling volume was located at 0.1 and 0.4 m above the bed for the studies E5 and E6 respectively. The variations and magnitudes of the streamwise and transverse velocities, tangential Reynolds stresses and turbulence time scales are discussed below.

Table 7.2 – Tidal range and period of tidal cycles E5TC1, E5TC2, E6TC1 and E6TC2.

Tidal cycle	Description	Tidal range (m)	Tidal period (s)
E5TC1	Minor spring	1.71	42,000
E5TC2	Major spring	2.44	47,400
E6TC1	Minor neap	0.81	38,820
E6TC2	Major neap	1.28	51,120

Note: Tidal range at site averaged over tidal cycle; Tidal period time between LW1 and LW2.

7.2.1 Horizontal velocity components at Site 2B, Eprapah Creek

The time-averaged streamwise velocity varied with the tides under both spring (study E5) and neap (study E6) tidal conditions (Section 5.2). Figure 7.3 shows the variation of the time-averaged streamwise velocity $\overline{V_x}$ (positive downstream) over the tidal cycles E5TC1, E5TC2, E6TC1 and E6TC2. In Figure 7.3, the variation of a time-averaged parameter (e.g. $\overline{V_x}$ in Figure 7.3) is shown in relation to the proportion of the period between LW1 and LW2 for the individual tidal cycles. On the horizontal axis 0 represents the start time of tidal cycle (LW1) and 1 represents the end of the tidal cycle (LW2), with the approximate transition between the flood and ebb tides indicated by a dashed line.

In Figure 7.3A, the low water slack tide occurred at the same single position (0.02 on x-axis) in both tidal cycles under the spring tidal conditions (study E5). This was not observed under neap tidal conditions (study E6, Figure 7.3B). With the neap tides multiple flow reversals were observed about both the high and low water slacks (Figure 7.3B). Under spring tidal conditions (study E5) the flood and ebb velocity maxima were approximately two to three

times larger than those observed for neap tidal conditions (study E6). In Figure 7.3A the flood velocity maximum of the major cycle (E5TC2) was slightly larger than that of the minor cycle (E5TC1). This was not the case for the neap tidal cycles (E6TC1 and E6TC2) with the flood and ebb maxima being similar despite the different tidal ranges (Figure 7.3B).
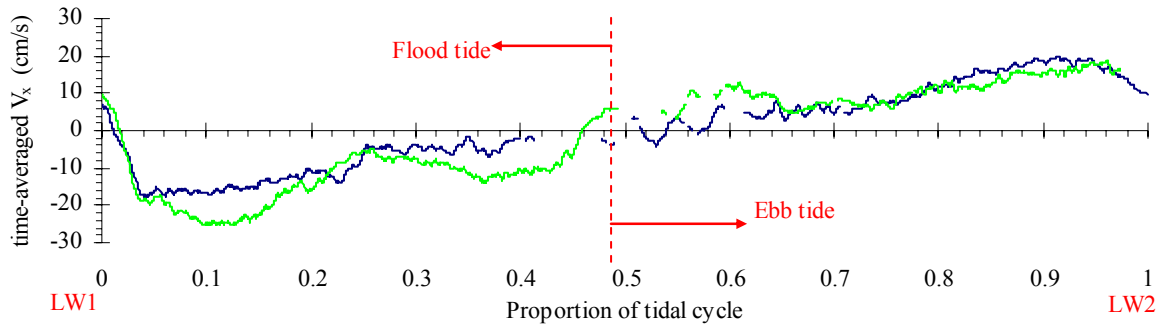
(A) Spring tide data collected at 0.1 m above bed for study E5 (8-9/03/05).
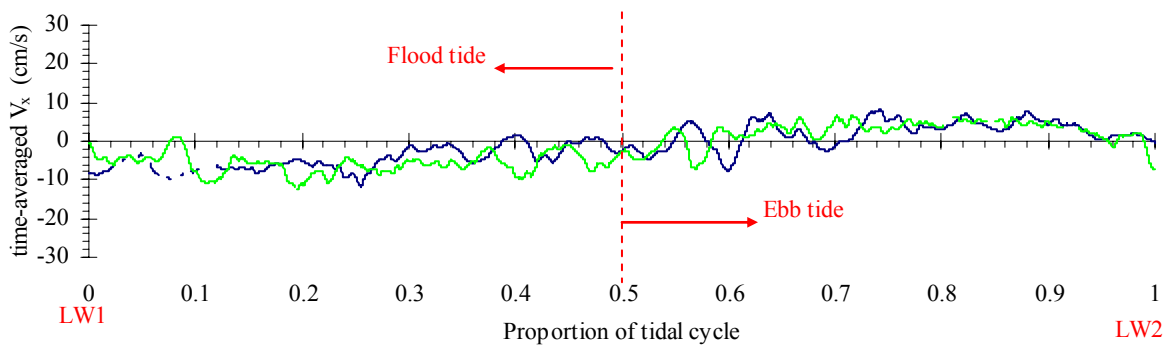
(B) Neap tidal data collected at 0.4 m above bed for study E6 (16-18/05/05).

Figure 7.3 − Variation of time-averaged streamwise velocity $\overline{V_x}$ relative to position in individual tidal cycle. Data collected at Site 2B, 10.7 m from left bank for field studies E5 and E6. Time-averaged data calculated over 200 s every 10 s along entire data set.

Legend: — minor tidal cycle; — major tidal cycle.

For spring tidal conditions (study E5) the flood and ebb velocity maxima occurred close to low tides (0.1 and 0.9 on x-axis respectively, Figure 7.3A). Under neap tidal conditions (study E6) the flood and ebb velocity maxima occurred closer to the middle of the flood and ebb tides (approximately 0.2 and 0.8 on x-axis respectively, Figure 7.3B). This difference in velocity maxima tended to suggest that the larger tidal range of the study E5 (spring tides) induced a more asymmetric response in the streamwise velocity.

For spring and neap tidal conditions the transverse velocity varied with the tides (Section 5.2). Figure 7.4 shows the variation of the time-averaged transverse velocity $\overline{V_y}$ (positive towards left bank) over the tidal cycles E5TC1, E5TC2, E6TC1 and E6TC2. For the spring tides, the

92

transverse velocities showed a predominance towards the inside of the bend ($\overline{V_y} < 0$, Figure 7.4A). However, in Figure 7.4B the transverse velocities were predominantly negative (towards inside of bend) during the flood and positive during the ebb tide for the neap tides. A long period oscillation with a period of approximately 3.5 hours observed during the spring tides of the study E5 might cause this variation away from some "standard" tidal trend.

During the flood tide the magnitudes of the spring tide transverse velocities were up to one order of magnitude larger than those of the neap tidal cycles. This difference in transverse velocities could strongly affect the entire estuarine mixing process. A large variation in the transverse velocity between spring and neap tides possibly indicated two different types of processes for turbulent transverse mixing, with increased transverse mixing occurring when the tidal range was large.
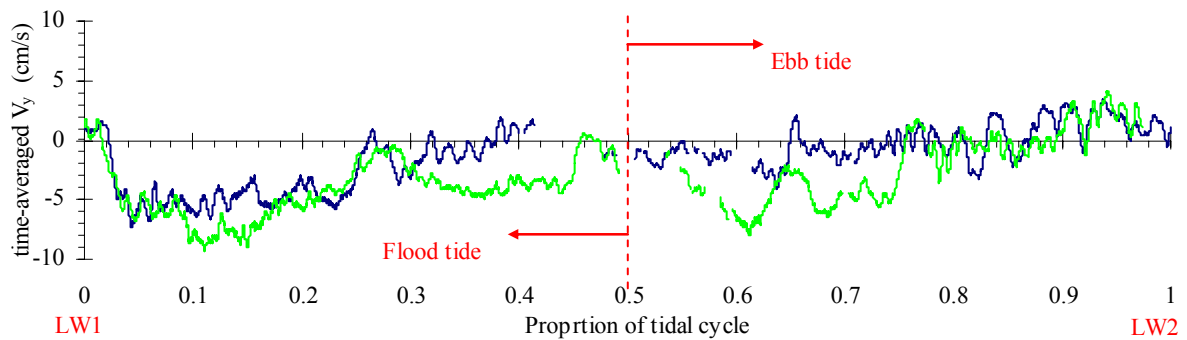
(A) Spring tide data collected at 0.1 m above bed for study E5 (8-9/03/05).
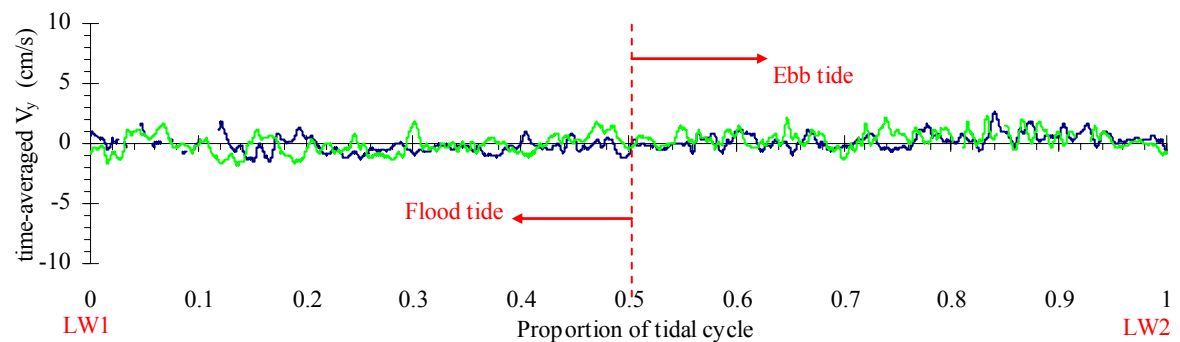
(B) Neap tidal data collected at 0.4 m above bed for study E6 (16-18/05/05).

Figure 7.4 – Variation of time-averaged transverse velocity $\overline{V_y}$ relative to position in individual tidal cycle. Data collected at Site 2B, 10.7 m from left bank for field studies E5 and E6. Time-averaged data calculated over 200 s every 10 s along entire data set.

Legend: — minor tidal cycle; — major tidal cycle.

The standard deviations of the velocity can represent the intensity of turbulent velocity fluctuations. For all field studies conducted at Eprapah Creek, the standard deviations of all

velocity components increased with the magnitude of streamwise velocity (Section 5.2). Figure 7.5 shows the variation of the standard deviations of streamwise velocity $v_x^{'}$ over the tidal cycles E5TC1, E5TC2, E6TC1 and E6TC2. In Figure 7.5 the data for a tidal cycle is collected from one low water to the next and it is presented in a circular plot. The polar coordinates are r = turbulence characteristic (e.g. r = $v_x^{'}$ (Figure 7.5)) and $\theta = 2\pi\, t/T$, where T = period of tidal cycle from first low water (LW1) to second low water (LW2); and t = position in tidal cycle (t = 0 at LW1 and t = T at LW2). From the first low water on the plot (y = 0 on positive x-axis) the data progresses anticlockwise around the plot until the second low water (y = 0 on positive x-axis).

The standard deviations of streamwise velocity for the spring tidal cycles were up to five times larger than those of the neap tidal cycles (Figure 7.5). This difference was also observed with the transverse and vertical velocity components. The increased magnitude of the velocity standard deviations for the study E5 indicated that the intensity of turbulence fluctuations increased under spring tidal conditions, and that increased mixing would occur.
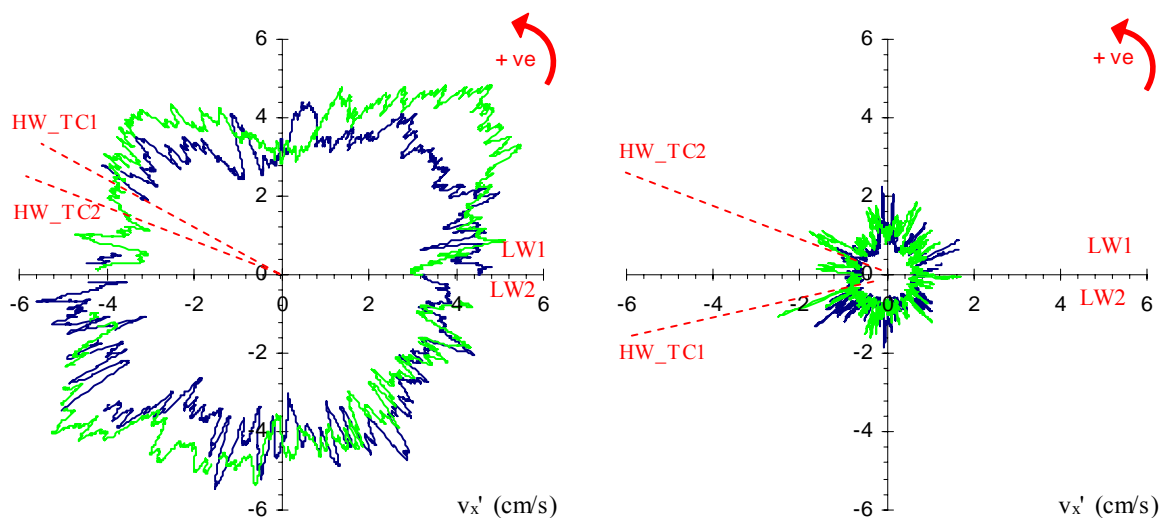
(A) Spring tide data collected at 0.1 m above bed for E5TC1 and E5TC2 (study E5).

(B) Neap tide data collected at 0.4 m above bed for E6TC1 and E6TC2 (study E6).

Figure 7.5 – Variation of standard deviations for streamwise velocity $v_x^{'}$ over some tidal cycles of field studies E5 and E6. Standard deviations calculated over 200 s every 10 s along entire data set.

Legend: — minor tidal cycle; — major tidal cycle.

7.2.2   Tangential Reynolds stresses

The tangential Reynolds stresses $\rho v_x v_y$ and $\rho v_x v_z$ are important turbulence properties in the study of turbulent mixing and sediment transport: these represent the transverse and vertical

shear generated by the high frequency fluctuations in streamwise velocity respectively. Previous studies (e.g. Kawanisi and Yokosi (1997)) found that $\rho v_x v_z$ was strongly related to some fluctuations in suspended sediment concentration. The Reynolds stress $\rho v_x v_y$ represents the horizontal shear stress in the sampling volume and the high frequency fluctuations in the horizontal velocity magnitude. The horizontal velocity magnitude is important for determining the bed shear stress and Shields parameter, both of which characterise the flows ability to move sediment (Nielsen (1992)).

For all field studies conducted at Eprapah Creek, the Reynolds stress $\rho \overline{v_x v_z}$ varied with the tides close to the bed, being predominantly positive and negative for the flood and ebb tides respectively (Section 5.4). Figure 7.6 shows the variation of the time-averaged Reynolds stress $\rho \overline{v_x v_z}$ over the tidal cycles E5TC1, E5TC2, E6TC1 and E6TC2. In Figure 7.6, the flood tide maxima of $\rho \overline{v_x v_z}$ during the spring tidal cycles were up to an order magnitude larger than those observed during the neap tides.
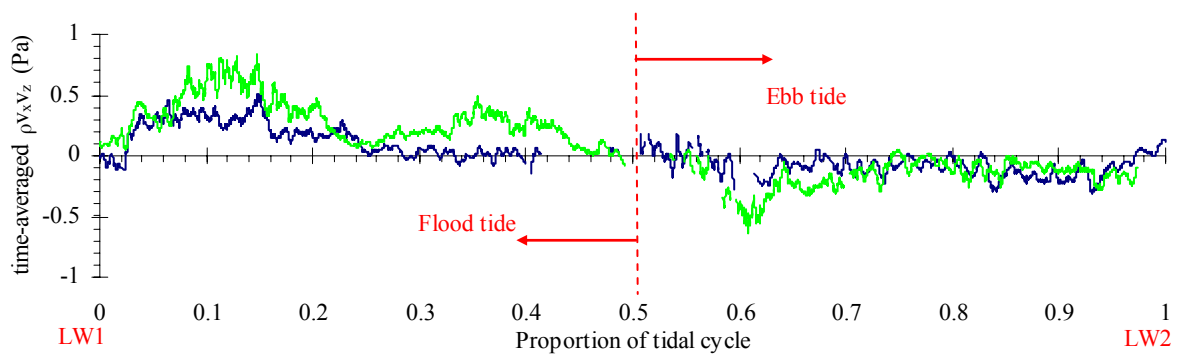
(A) Spring tide data collected 0.1 m above bed for study E5 (8-9/03/05).
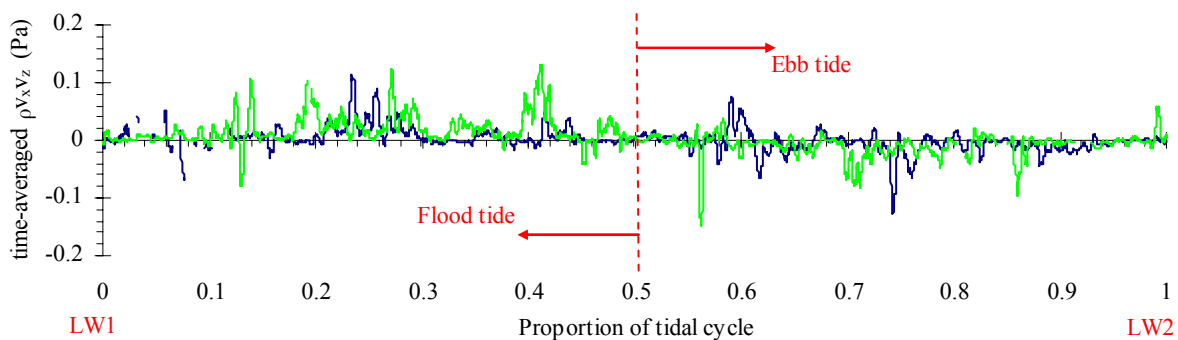
(B) Neap tidal data collected 0.4 m above bed for study E6 (16-18/05/05).

Figure 7.6 – Variation of time-averaged Reynolds stress $\rho \overline{v_x v_z}$ relative to position in individual tidal cycle. Data collected at Site 2B, 10.7 m from left bank for field studies E5 and E6. Time-averaged data calculated over 200 s every 10 s along entire data set.

Legend: — minor tidal cycle; — major tidal cycle.

95

Figure 7.7 shows the variation of time-averaged Reynolds stress $\rho \overline{v_x v_y}$ over the tidal cycles E5TC1, E5TC2, E6TC1 and E6TC2. In Figure 7.7 the time-averaged Reynolds stress $\rho \overline{v_x v_y}$ showed no easily discernible tidal trend. The maxima of $\rho \overline{v_x v_y}$ observed during the spring tides (study E5) were also an order of magnitude larger than those of the neap tides (study E6).
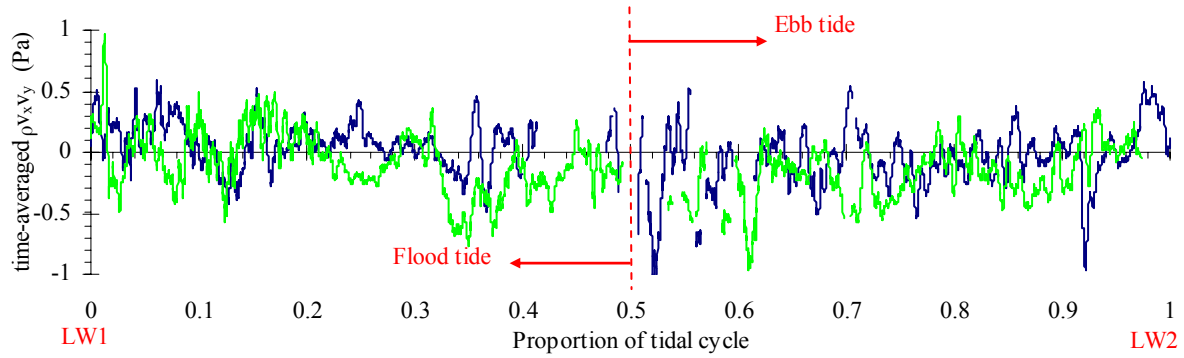
(A) Spring tide data collected 0.1 m above bed for study E5 (8-9/03/05).
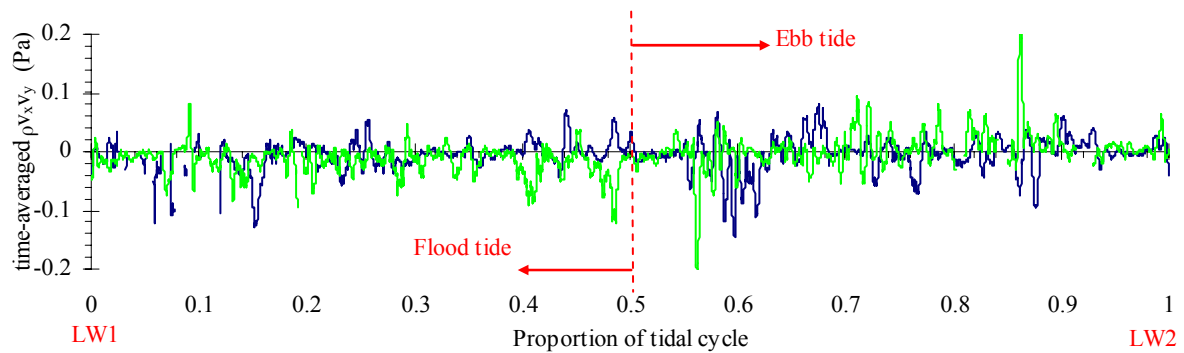
(B) Neap tidal data collected 0.4 m above bed for study E6 (16-18/05/05).

Figure 7.7 – Variation of time-averaged Reynolds stress $\rho \overline{v_x v_y}$ relative to position in individual tidal cycle. Data collected at Site 2B, 10.7 m from left bank for field studies E5 and E6. Time-averaged data calculated over 200 s every 10 s along entire data set.

Legend: — minor tidal cycle; — major tidal cycle.

The standard deviations of tangential Reynolds stresses represent the intensity of fluctuations of the Reynolds stresses. For all field studies the standard deviations of all Reynolds stresses increased with the magnitude of streamwise velocity (Section 5.4). Figure 7.8 shows the variation of standard deviations $(\rho v_x v_z)'$ for the Reynolds stress $\rho v_x v_z$ in a circular plot. In Figure 7.8A, the spring tidal conditions produced a highly asymmetrical response in $(\rho v_x v_z)'$ which was not observed for the neap tidal cycles (Figure 7.8B). For the neap tidal cycles the magnitude of $(\rho v_x v_z)'$ for the minor (E6TC1) and major (E6TC2) tides were similar (Figure 7.8B); this was not the case for the spring tidal conditions (Figure 7.8A). For spring tidal

conditions, the magnitude of $(\rho v_x v_z)'$ during the major tide (E5TC2) could be up to twice as large as those observed during the minor tide (E5TC1).
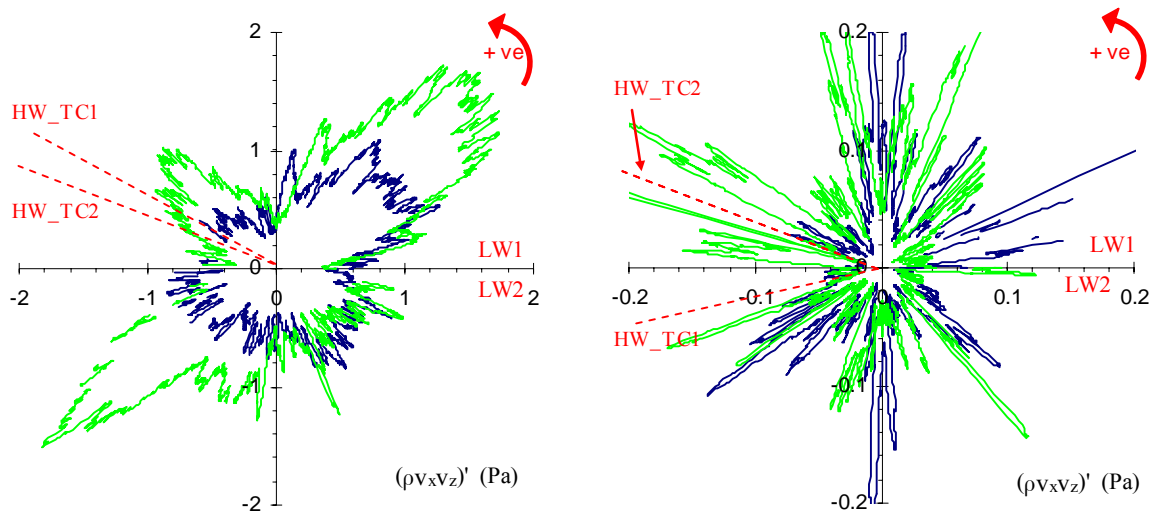
(A) Spring tide data collected at 0.1 m above bed for E5TC1 and E5TC2 (study E5).

(B) Neap tide data collected at 0.4 m above bed for E6TC1 and E6TC2 (study E6).

Figure 7.8 – Variation of standard deviations $(\rho v_x v_z)'$ over some tidal cycles of field studies E5 and E6. Standard deviations calculated over 200 s every 10 s along entire data set. Legend: — minor tidal cycle; — major tidal cycle.

The increased magnitude and fluctuation intensity of the Reynolds stresses $\rho v_x v_y$ and $\rho v_x v_z$ under spring tidal conditions tended to indicate some enhanced sediment transport and mixing processes during spring tides. This increase in the magnitude and fluctuation intensity of Reynolds stresses would also impact the type of sediment suspended and transported. Conversely, the decreased magnitude and fluctuation intensity of Reynolds stresses under neap tidal conditions could be responsible for an increased levels of stratification, because of the decreased mixing in the estuary.

7.2.3   Turbulence time scales

7.2.3.1   *Integral time scales*

The integral time scale represents the longest connection between turbulent velocity fluctuations. The integral time scales of all velocity components varied with the tides for all field studies conducted at Eprapah Creek (Section 5.6.1). Figure 7.9 shows the variation of the streamwise integral time scales T_{Ex} in a circular plot. In Figure 7.9 the integral time scales T_{Ex} observed during the spring tidal cycles were smaller than those observed for the neap tidal cycles. The transverse integral time scales of the spring tidal cycles were also

smaller than those of the neap tidal cycles. This conceivably indicated that the size of the vortices represented by the horizontal integral time scales was restricted by the larger tidal forcing and increased velocities observed under spring tides. The maximum horizontal time scales observed for the studies E5 and E6 were 1.02 and 2.35 s respectively, while the median values were between 0.1 and 0.4 s (Table 7.3).
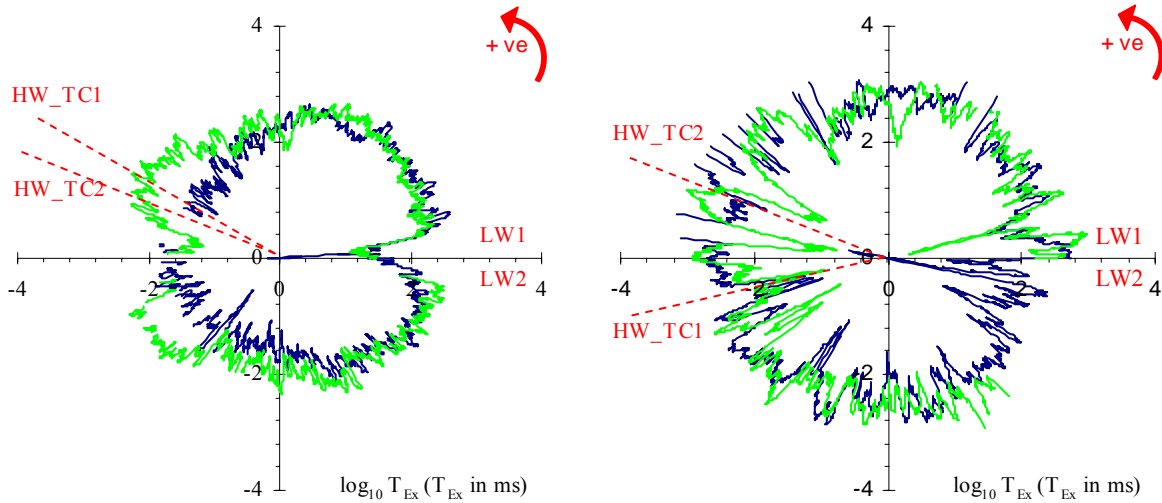
(A) Spring tide data collected at 0.1 m above bed for E5TC1 and E5TC2 (study E5).

(B) Neap tide data collected at 0.4 m above bed for E6TC1 and E6TC2 (study E6).

Figure 7.9 – Variation of streamwise integral time scales T_{Ex} (in milliseconds) over some tidal cycles of field studies E5 and E6. Time scales calculated over 200 s every 10 s along entire data set.

Legend: — minor tidal cycle; — major tidal cycle.

Table 7.3 – Median values of integral and dissipation time scales for studies E5 and E6.

Field study	Tides	T_{Ex} (s)	T_{Ey} (s)	T_{Ez} (s)	τ_{Ex} (s)	τ_{Ey} (s)	τ_{Ez} (s)
E5	Spring	0.17	0.13	0.31	0.003	0.003	0.021
E6	Neap	0.32	0.38	0.83	0.002	0.002	0.029

7.2.3.2 *Dissipation time scales*

The dissipation time scales represent the most rapid fluctuations in the turbulent velocity components. For all field studies undertaken at Eprapah Creek, the dissipation time scales of all velocity components seemed independent of the tidal phase (Section 5.6.2). The median values of the horizontal dissipation time scales observed for all spring and neap tidal cycles of the studies E5 and E6 were between 0.002 and 0.003 s (Table 7.3). This indicated that mid

estuary the dissipation time scales were independent of the tidal amplitude and vertical sampling elevation as well as independent of the tidal phase.

7.3   LONG PERIOD OSCILLATIONS

Some long period oscillations were observed in the water levels and horizontal velocities for most field studies conducted at Eprapah Creek (Figure 7.10). Figure 7.10 shows the water depth and time-averaged streamwise velocity as functions of time for the field studies E6 and E7 (Tables 3.2 and 5.1). In Figure 7.10 the period of these fluctuations in water depth and velocity were similar, indicating that these long period velocity oscillations were related to the long period water level oscillations. About high water under neap tidal conditions these long period oscillations created multiple flow reversals (Figure 7.10). Here a multiple flow reversal is defined as a rapid succession of changes in the streamwise velocity direction.
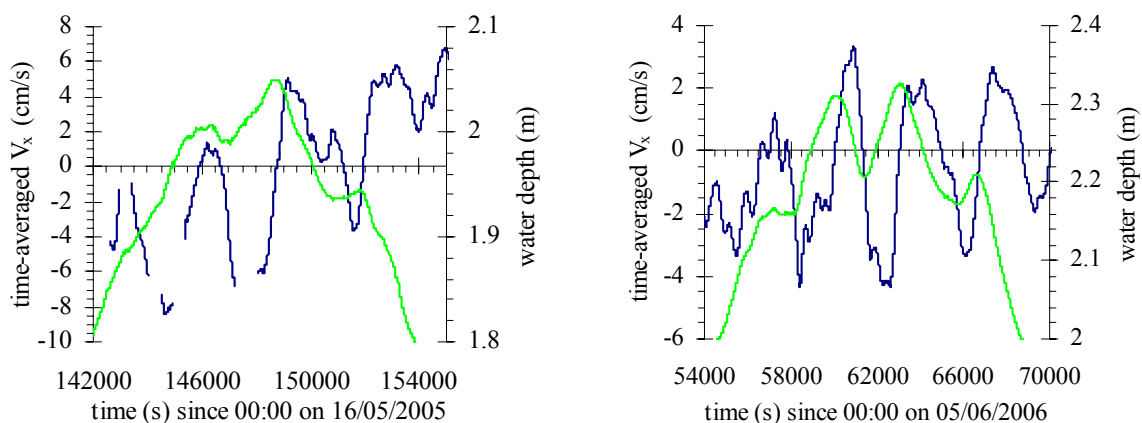
(A) Data collected in middle estuary (Site 2B) during study E6 (16-18/05/05).

(B) Data collected in upper estuary (Site 3) during study E7 (5-7/06/06).

Figure 7.10 – Water depth and time-averaged streamwise velocity as functions of time. Data collected by YSI6600 and 3D-ADV (10 MHz) respectively, located 0.4 m above bed for field studies E6 and E7. Velocity data averaged over 200 s every 10 s along entire data set. Legend: — time-averaged streamwise velocity; — water depth.

The periods and impact of these long period oscillations differed under spring and neap tidal conditions. For the spring tidal conditions (studies E5 and E3), large velocity fluctuations with a period of approximately 3.5 hours were observed. Under neap tidal conditions (studies E6 and E7), long period oscillations with periods of about 1 hour ($2,000 < T < 5,000$ s) caused velocity fluctuations with a magnitude similar to that of the tidal forcing. This section investigates the different long period oscillations observed mid estuary during the spring and neap tides (studies E5 and E6). The velocity fluctuations were divided into groups of certain

periods based on physical and tidal characteristics both internal and external to Eprapah Creek (Table 7.4). Table 7.4 presents the period ranges investigated and the physical characteristics used for the choice of that range. Appendix E justifies the selection of the groups used in this discussion.

A spectrum analysis was conducted on the water depth and horizontal velocity data collected at Site 2B for the field studies E5 and E6. Because of a lack of resolution in the larger period ranges from the 25 hour investigation window of the study E5 it is prudent to only discuss oscillation periods smaller than 7,200 s. A complete listing of the 20 most prominent peaks in the spectra of the streamwise and transverse velocities of the field studies E5 and E6 are shown in Appendix E. The predominant peaks in a frequency spectrum indicated the oscillation periods that contributed the most energy to the fluctuations of the measured data.

Table 7.4 – Period ranges of tidal and physical characteristics investigated.

Group	Period range (s)	Tidal and/or physical characteristics
A	$T_{range} > 14,400$	Tidal constituents
B	$14,400 > T_{range} > 2,200$	Possible external resonance sources (e.g. Moreton Bay)
C	$2,200 > T_{range} > 1,200$	Extreme range of entire estuary length resonance ($d_L = 1.2$ m, $d_H = 4.0$ m)
D	$1,200 > T_{range} > 200$	Range of smaller possible longitudinal resonance (e.g. Site 2B to upper limits of estuary)
E	$200 > T_{range} > 2$	Smaller resonances caused by meander lengths or cross-section widths
F	$2 > T_{range}$	Related to turbulence (Section 5.6)

Note: d_L and d_H are approximate mean depth of entire estuary for extreme low and high tides; T_{range}: period range for oscillation groups investigated.

Table 7.5 summarises the oscillation groups (Table 7.4) in which the 20 predominant oscillation periods (T < 7,200 s) occurred for the field studies E5 and E6. In Table 7.5, the most prominent long period oscillations observed under neap tides (study E6) were from external sources (e.g. group B, Table 7.4). For spring tides (study E5), predominant oscillation periods (T < 7,200 s) from groups B, C and D were observed (Table 7.5). These were possibly caused by a combination of internal sources (resonance within Eprapah Creek) and external sources (e.g. resonance in Moreton Bay). One explanation may be the increased tidal energy observed during the spring tides (study E5) induced stronger internal resonance fluctuations.

The streamwise and transverse velocity data of the field studies E5 and E6 were filtered using a band-pass filter based upon the period ranges defined in Table 7.4. The velocity magnitude and standard deviations were used to assess the impact of each oscillation group on the turbulence. Figure 7.11 shows the median values of the magnitude and standard deviations of the streamwise and transverse velocities as functions of frequency for each oscillation group. Median values of the velocity magnitude and standard deviations are presented on the high frequency cut-off for each oscillation group (e.g. 0.005 Hz for group D).

Table 7.5 – Groupings of 20 most prominent oscillation periods (T < 7,200 s) of field studies E5 and E6.

Group	Period range (s)	Study E5		Study E6	
		V_x	V_y	V_x	V_y
A	$T_{range} > 14,400$	--	--	--	--
B	$14,400 > T_{range} > 2,200$	13	13	18	18
C	$2,200 > T_{range} > 1,200$	5	5	2	2
D	$1,200 > T_{range} > 200$	2	2	0	0
E	$200 > T_{range} > 2$	0	0	0	0
F	$2 > T_{range}$	0	0	0	0
Range of predominant oscillation periods (T < 7,200 s)		950-5,990 s	600-6,710 s	2,020-4,930 s	1,260-7,200s

Note: T_{range} : period range for oscillation groups investigated; smallest-largest: smallest and largest of 20 most predominant oscillation periods observed for studies E5 and E6 (listed in Appendix E).

In Figure 7.11A the median values of streamwise and transverse velocity magnitude decreased rapidly with increasing frequencies. This indicated that the predominant influence on the velocity oscillations mid estuary in Eprapah Creek came from external sources (T > 2,200 s). For the field study E6 the transverse velocity magnitudes of oscillation groups C and D (internal sources) were similar to those of the external sources (groups A and B). This indicated that oscillation sources internal to Eprapah Creek (e.g. internal resonance) could conceivably have a significant influence on the observed transverse velocity fluctuations. A similar phenomenon was observed at Site 3 (upper estuary) under similar neap tidal conditions for the study E7 (Appendix E).

Figure 7.11B shows that the median values of streamwise and transverse velocity fluctuations (v_x' and v_y') increased with increasing frequency under spring tidal forcing (study E5). This was not the case for the field trip E6 (neap tides), when the streamwise and transverse velocity standard deviations were almost constant for the oscillation periods of groups D, E and F (T < 1,200 s). A similar process was observed in the turbulence fluctuation intensities of the study E7 conducted under neap tides in the upper estuary (Appendix E). The two different patterns in turbulent velocity fluctuations indicated two different types of energy transfer processes driving the velocity fluctuations.
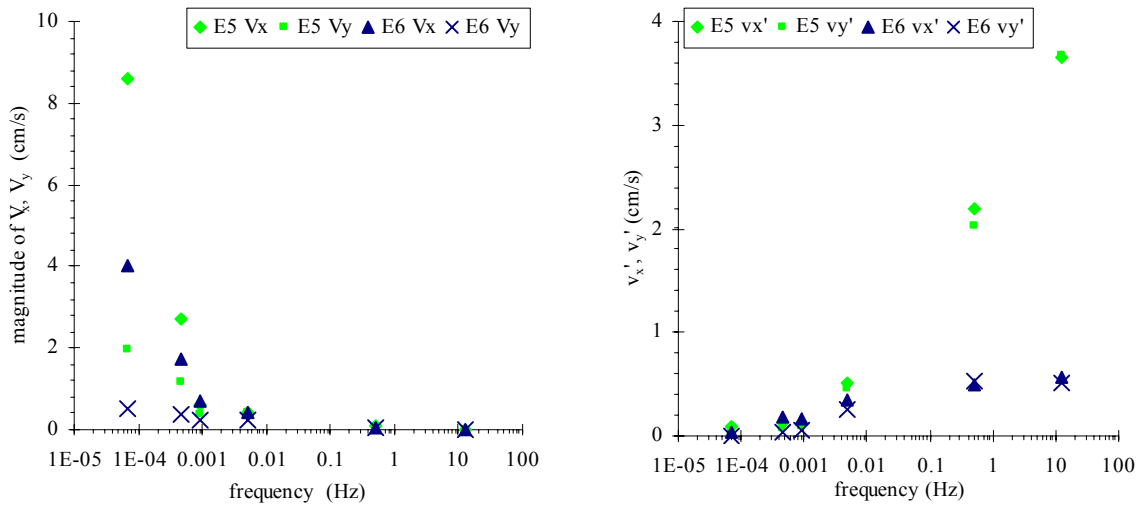
(A) Velocity magnitude of V_x and V_y, collected for spring (study E5) and neap (study E6) tides.

(B) Standard deviations v_x' and v_y', collected for spring (study E5) and neap (study E6) tides.

Figure 7.11 – Median values of magnitude and standard deviations for streamwise and transverse velocity as functions of high frequency cut-off for each oscillation group. Data collected at Site 2B, Eprapah Creek for field studies E5 and E6.

Figure 7.12 shows the smoothed spectrum of streamwise velocity for the field studies E5 and E6. These spectra were smoothed using a window of 128 data points, because the large quantity of noise at high frequency made interpretation difficult. Appendix E shows these spectra before the smoothing process. In Figure 7.12 the tidal forcing of the spring tides (study E5) seemed to dominate the velocity fluctuations throughout all frequency ranges. This allowed a strong boundary layer to form and energy to be passed through all frequency ranges leading to the increased energy observed in high frequency region. Alternatively, under neap tidal conditions (study E6), the long period oscillations of groups B and C (5,000 > T > 2,000 s) had an increased influence (increased intensity) on the velocity

fluctuations. This increased intensity caused by the long period oscillations $(2{,}000 < T < 5{,}000\ \text{s})$ seemed to correspond to reduced energy in the smaller period velocity oscillations $(T < 1{,}200\ \text{s})$ under neap tidal conditions (Figure 7.12).
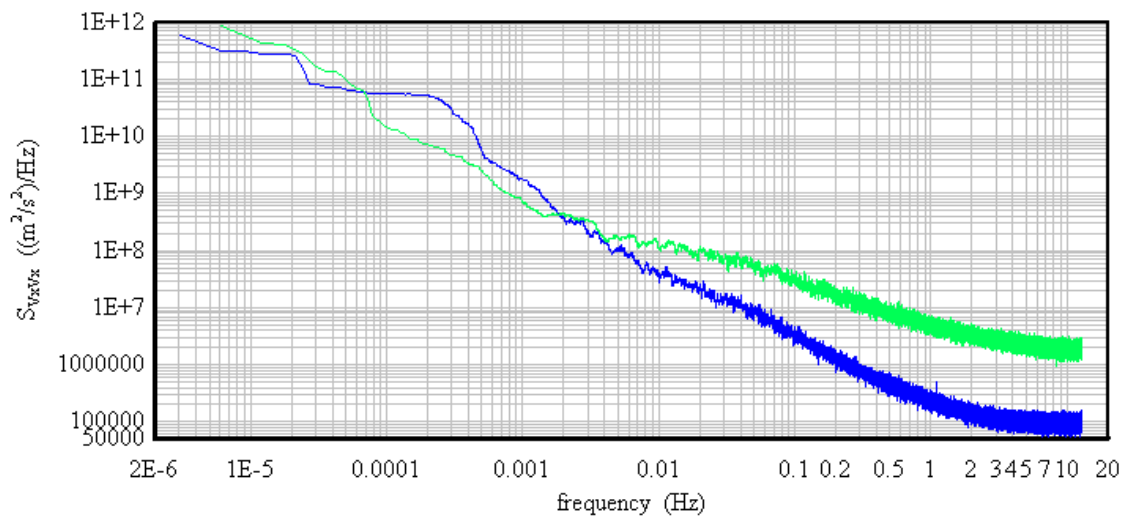
Figure 7.12 – Smoothed spectrum of streamwise velocity $S_{V_xV_x}$ for field studies E5 and E6. Spectrum smoothed using smoothing window of 128 data points.

Legend: — $S_{V_xV_x}$ for study E5; — $S_{V_xV_x}$ for study E6.

7.4 DISCUSSION

This section has shown that two different sets of turbulence properties exist in Eprapah Creek: one set for neap tidal conditions and a different more energetic set for spring tidal conditions. The turbulent mixing under these two distinct turbulence property cases would be completely different. Calculations for the dispersal and mixing of discharge using spring tide velocity and turbulence properties may drastically overestimate the mixing efficiency of the estuarine system. The tidal conditions of Southeast Queensland have in the past been classified as micro-tidal (tidal range < 2 m), but the tidal variations are regularly greater than 2 m. Here the ratio of the "local" tidal amplitude and the "local" mean depth a_1/h_1 is proposed as one method to assess some differences in the turbulence properties between spring and neap tidal conditions. The term "local" refers to the tidal amplitude and mean water depth observed at a specific site in the estuary. However, this ratio could be averaged over many sites in the estuary to assess the impact of the varying tidal range on the turbulence properties of the estuarine system as a whole.

7.4.1   Ratio of local tidal amplitude and local mean depth a_1/h_1

Previous studies (e.g. Speer and Aubrey (1985), Hinwood et al. (2003, 2005)) investigated a similar ratio of the ocean tidal amplitude to the mean depth of the entrance channel of a restricted entrance estuary. Both studies found this ratio important to assess the asymmetric response of the estuary to tidal forcing. Savenije (2005) suggested that the ratio of the tidal amplitude to the mean water level could be used to assess whether gravitational or turbulence mixing was the dominant mixing process in an alluvial estuary. In this study it is suggested that the ratio of the local tidal amplitude to the local mean depth a_1/h_1 could be used to assess the effect of tidal range on the turbulence properties at a specific sampling location. The data sets of the field studies E5 (spring tide) and E6 (neap tide) were used to evaluate the influence of ratio a_1/h_1 . The sampling locations used for the studies E5 and E6 were situated 10.7 m from the left bank at Site 2B (2.1 km from mouth). The mean water depth observed at 10.7 m from the left bank was approximately 1.6 m for both field studies. Table 7.6 presents the tidal range and a_1/h_1 for each tidal cycle of the studies E5 and E6 (defined in Table 7.1).

In Table 7.6 the ratio a_1/h_1 was greater than 0.5 for the tidal cycles of study E5, and less than 0.5 for the tidal cycles of study E6. For $a_1/h_1 = 0.5$ the local tidal range is equal to the local mean depth at the sampling location. The value of $a_1/h_1 = 0.5$ seemed to be a critical value that separated the two distinct sets of turbulence properties.

Table 7.6 – Values of ratio a_1/h_1 for tidal cycles of field studies E5 and E6.

Field study	Tidal cycle	Tidal range (m)	a_1/h_1
E5	E5TC1	1.71	0.53
	E5TC2	2.44	0.76
E6	E6TC1	0.81	0.25
	E6TC2	1.28	0.40
	E6TC3	0.97	0.30
	E6TC4	1.19	0.37

Note: Tidal range averaged variation over tidal cycle at site; Tidal cycles of studies E5 and E6 defined in Table 7.1.

Figure 7.13 shows the median tidal cycle values of some turbulence parameters (v_x' ; v_y' ; $(\rho v_x v_z)'$; $(\rho v_x v_y)'$; T_{Ex} ; T_{Ey}) as functions of the ratio a_1/h_1 . In Figures 7.13A and 7.13B the standard deviations of the velocity components and tangential Reynolds stresses increased

considerably for the tidal cycles when $a_1/h_1 > 0.5$. When $a_1/h_1 < 0.5$ the median values of all turbulent properties were of a similar magnitude (Figures 7.13A and 7.13B). In Figure 7.13C the median values of the horizontal integral time scales were relatively similar despite the value of a_1/h_1, yet, the maximum values of the horizontal integral time scales were smaller when $a_1/h_1 > 0.5$ than when $a_1/h_1 < 0.5$ (Figure 7.13D). All these observations were discussed in Section 7.2, confirming that the ratio a_1/h_1 could be a useful parameter in assessing the range of turbulence properties observed in an individual estuary.
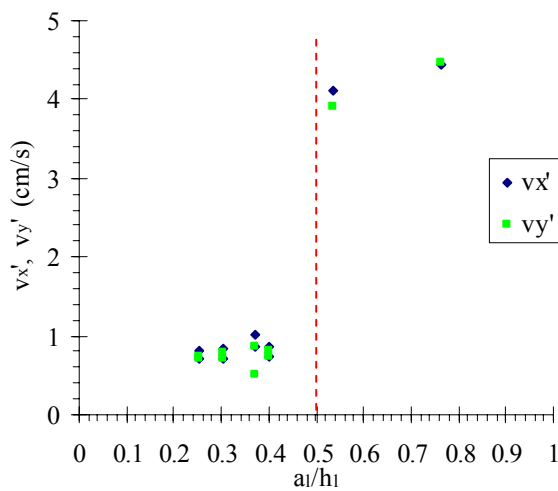
(A) Median values of $v_x^{'}$ and $v_y^{'}$. (B) Median values of $(\rho v_x v_z)^{'}$ and $(\rho v_x v_y)^{'}$.
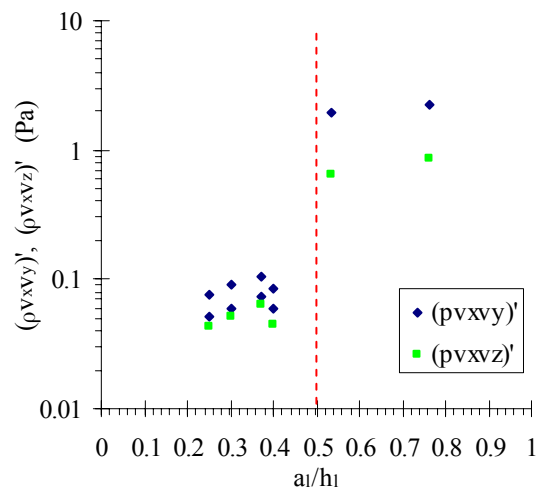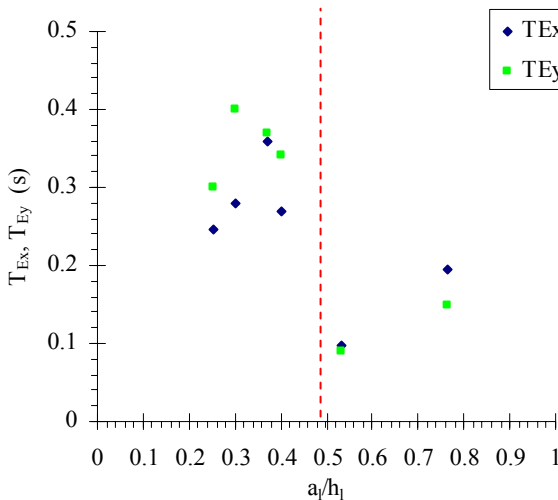
(C) Median values of T_{Ex} and T_{Ey}. (D) Maximum values of T_{Ex} and T_{Ey}.
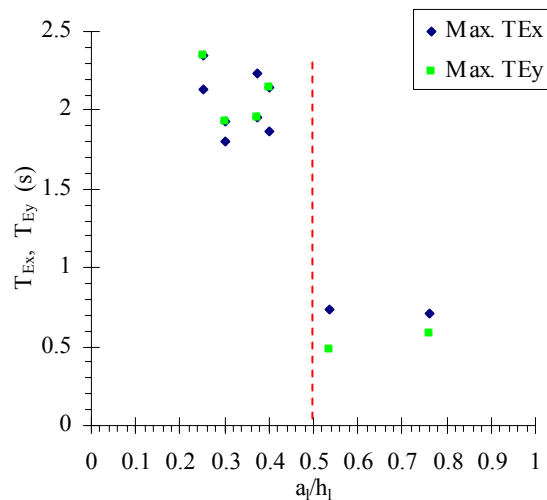
Figure 7.13 – Values of turbulence properties for individual tidal cycles as functions of ratio a_1/h_1 for field studies E5 and E6.

8 A COMPARISON OF TURBULENT PROPERTIES IN MIDDLE AND UPPER ESTUARINE ZONES

8.1 PRESENTATION

Two field investigations were conducted for 50 hours under neap tidal conditions in the middle (study E6) and upper (study E7) estuarine zones of Eprapah Creek. This Chapter compares the turbulence properties of field studies E6 (16-18/05/2005) and E7 (5-7/06/2006). Figure 8.1 shows some photographs of the study sites at Site 2B and Site 3 which were used for the field studies E6 and E7 respectively. Both field studies were performed close to the outer bank of the meanders at Site 2B and Site 3 (Figures 3.6 and 8.1). For the studies E6 and E7 the maximum tidal range observed at Victoria Point was approximately 1.33 m and no natural freshwater inflow was observed. However, some stratification was observed at Sites 2B and 3 during the studies E6 and E7 (Section 6.4.1). These conditions allowed a thorough comparison of the turbulence properties in the middle and upper estuarine zones.

(A) Experimental set up at Site 2B for study E6 (16-18/05/05), looking upstream. Photograph by M. Takahashi.

(B) Experimental set up at Site 3 for study E7 (5-7/06/06), looking downstream.

Figure 8.1 – Photographs of Experimental cross-sections used at Eprapah Creek for field studies E6 and E7.

For both field studies two ADVs were deployed: a 2D-microADV (16 MHz) and a 3D-ADV (10 MHz) at 0.2 and 0.4 m above the bed respectively. The sampling volumes of the two ADVs were vertically aligned. Figure 8.2 shows the location of the ADVs at Site 2B (study E6) and Site 3 (study E7). Note that the horizontal and vertical scales of Figures 8.2A and 8.2B are different. Table 8.1 outlines the longitudinal and transverse location of the ADVs and tidal conditions observed for the studies E6 and E7.

Table 8.1 – Investigations and ADV information for field studies E6 and E7.

Field study	**E6**	**E7**
Date	16-18/05/05	5-7/06/06
Focus (estuarine zone)	Middle	Upper
Duration (hours)	48	50
Tides: TR (m) [LW1 to LW2 s]	TC1 0.81 m [37,560 to 76,380 s] TC2 1.28 m [76,380 to 127,500 s] TC3 0.97 m [127,500 to 170,148 s] TC4 1.19 m [170,148 to 217,320 s]	TC1 1.24 m [39,660 to 83,280 s] TC2 1.28 m [83,280 to 128,880 s] TC3 1.28 m [128,880 to 173,760 s] TC4 1.25 m [173,760 to 217,980 s]
Rainfall (mm)	0	0
Site	2B	3
Longitudinal location (km)	2.1	3.1
Transverse location (m)	10.7 m from left bank	4.2 m from right bank
f_{scan} (Hz): 3D-ADV 2D-microADV	25 25	25 50
V_{range} (m/s): 3D-ADV 2D-microADV	1.0 1.0	0.3 0.3

Note: f_{scan} : ADV sampling frequency; V_{range} : ADV velocity range; Tidal information defines tidal cycles by averaged tidal range (TR) and time from first low water (LW1) to second low water (LW2); averaged tidal range is average of tidal variations at site between LW1 to HW and HW to LW2.

A hardware fault with the 3D-ADV (10 MHz) system was observed during the field study E7 (Section 3.5.2). All turbulence properties recorded with the 2D-microADV (16 MHz) were analysed, but only the time-averaged velocities collected by the 3D-ADV system for both studies E6 and E7 are discussed. Section 8.2 compares the time-averaged streamwise and transverse velocities observed in the middle (study E6) and upper (study E7) estuarine zones of Eprapah Creek. The turbulence properties of the middle and upper estuarine zones are

discussed in Section 8.3. In Section 8.3 the higher statistical moments, Reynolds stresses and turbulence time scales are discussed using the data measured by the 2D-microADV for the studies E6 and E7. Section 8.4 investigates the possible relationship between the long period oscillations and some secondary current events observed in both middle (study E6) and upper (study E7) estuarine zones. The possible differences in turbulent mixing regimes for the middle and upper estuary are discussed in Section 8.5.
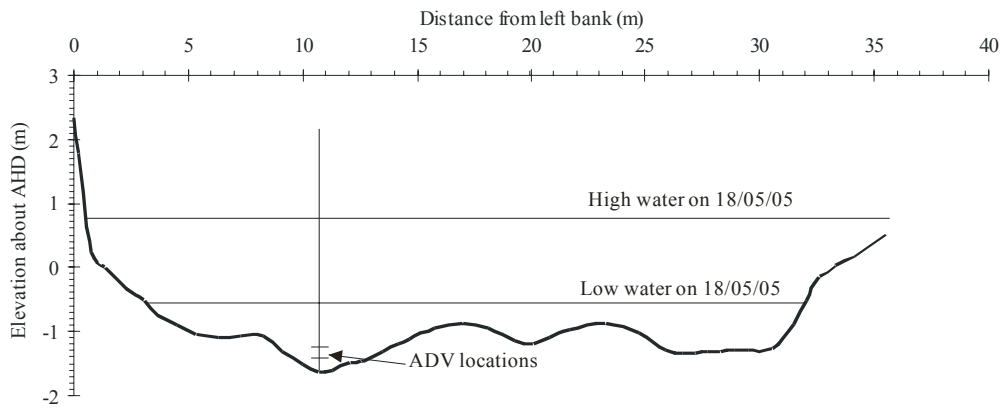
(A) Site 2B for study E6 (16-18/05/05).
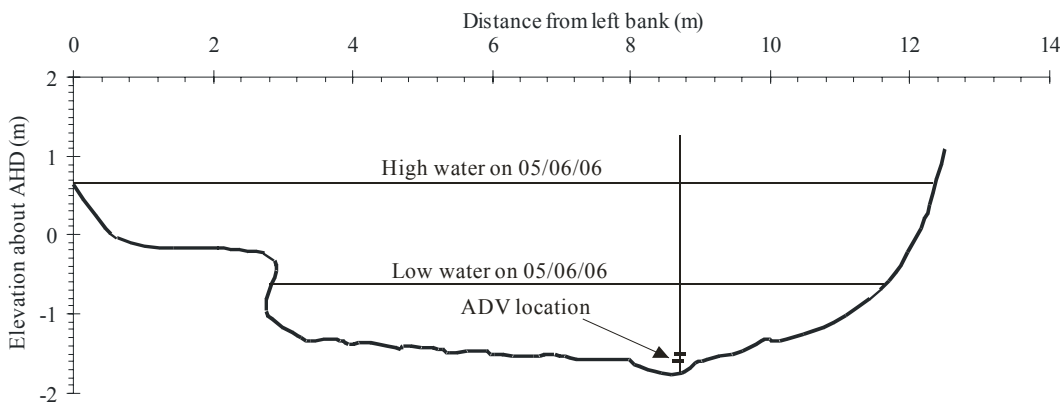
(B) Site 3 for study E7 (5-7/06/06).

Figure 8.2 – ADV locations for field studies E6 and E7 conducted at Eprapah Creek.

8.2   TIME-AVERAGED VELOCITY

8.2.1   Streamwise velocity

The time-averaged streamwise velocity varied with the tides in both the middle and upper estuarine zones (Section 5.2). Figure 8.3 shows the time-averaged streamwise velocities at 0.2 and 0.4 m above the bed and water depth as functions of time. In Figure 8.3A the streamwise velocity maxima of the flood and ebb tides mid estuary occurred either side of low water. A similar tidal trend seemed to occur in the upper estuarine zone for the field study E7 (Figure 8.3B). However, in the upper estuarine zone the effect of the long period oscillations on streamwise velocity seemed to dominate the tidal forcing.
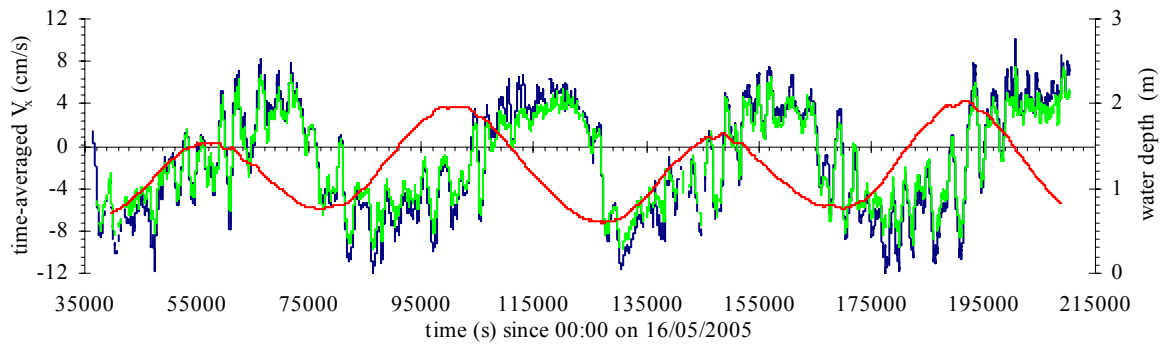
(A) Data collected mid estuary at Site 2B, Eprapah Creek for study E6 (16-18/05/05).
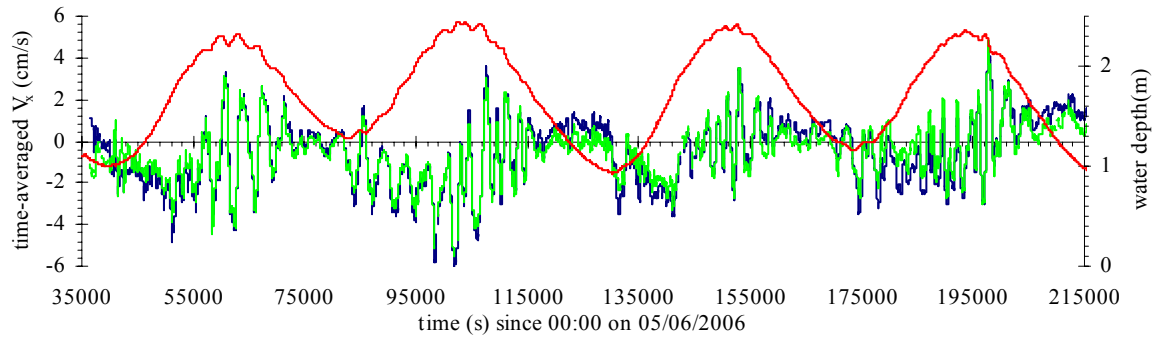
(B) Data collected in upper estuary at Site 3, Eprapah Creek for study E7 (5-7/06/06).

Figure 8.3 – Time-averaged streamwise velocity $\overline{V_x}$ and water depth as functions of time. Velocity data collected at 0.2 and 0.4 m above bed by 2D-microADV and 3D-ADV respectively. Water depth collected by YSI6600 probe located 0.3 m from 3D-ADV. Velocities averaged over 200 s every 10 s along entire data set.

Legend: — $\overline{V_x}$ at 0.2 m above bed; — $\overline{V_x}$ at 0.4 m above bed; — water depth.

In both middle and upper estuarine zones, the flood tide velocity maxima were approximately 1.5 times larger than the ebb tide maxima for the neap tidal conditions of these field studies. This suggested that the entire estuarine zone of Eprapah Creek was heavily influenced by the flood tide, which implied that the net flux of discharged waters was towards the upper estuary, rather than out to Moreton Bay. The flood and ebb time-averaged streamwise velocity maxima observed mid estuary (study E6) were about 12 and 8 cm/s respectively. These mid estuary velocity maxima were approximately twice those observed in the upper estuary (study E7).

8.2.2   Transverse velocity

For the field studies E6 and E7 the time-averaged transverse velocity varied with the tides. Figure 8.4 shows the time-averaged transverse velocities observed at 0.2 and 0.4 m above the bed and water depth as functions of time. At both Site 2B (study E6) and Site 3 (study E7),

109

the transverse velocities flowed predominantly towards the inner bank during the flood tides and towards the outer bank during the ebb tides (Section 5.2). In Figure 8.4A the magnitudes of the flood and ebb transverse velocity maxima observed mid estuary (study E6) were similar (approximately 2 cm/s). However, in the upper estuary, the magnitudes of transverse velocity maxima during the flood tide were approximately three times larger than the ebb tide maxima (Figure 8.4B). At Site 3 the flood and ebb tide transverse velocity maxima were 1.2 and 0.4 cm/s respectively. The small ebb tide transverse velocities (towards outer bank) observed at Site 3 seemed to reduce the mixing close to the bed near the outer bank. Some evidence of reduced mixing was observed with the small variation of physio-chemical properties at 0.4 m above the bed, next to the ADVs at Site 3 (Sections 6.2.2 and 6.2.4).
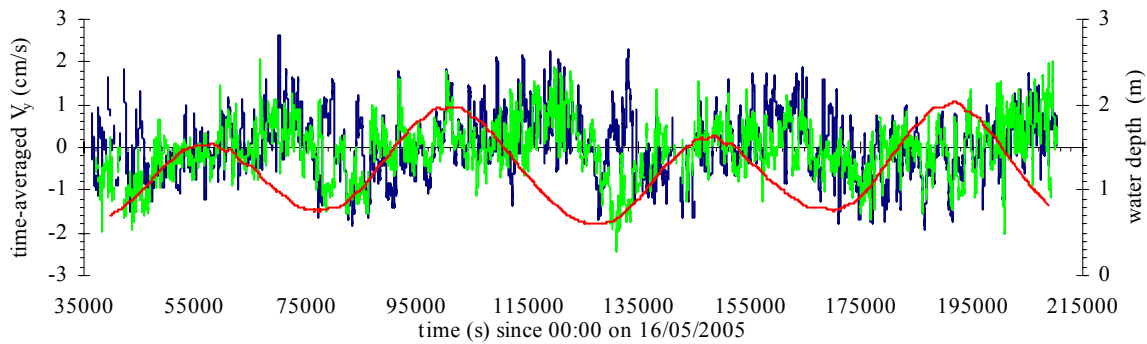
(A) Data collected mid estuary at Site 2B Eprapah Creek for study E6 (16-18/05/05).
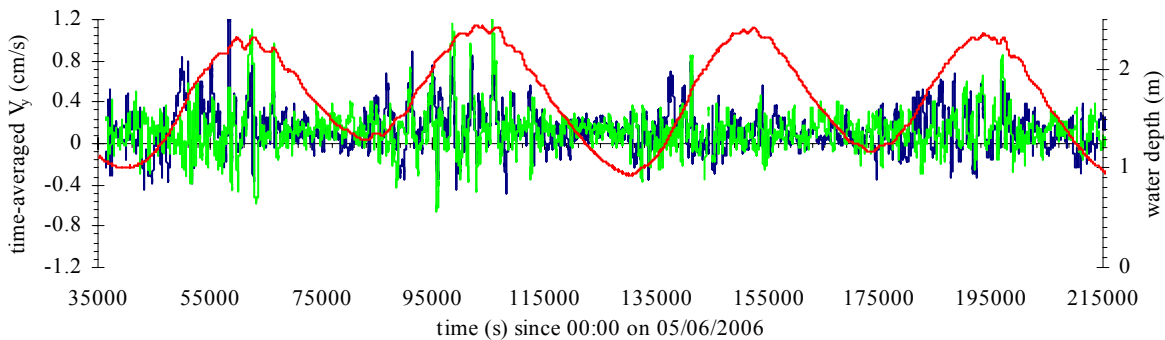
(B) Data collected in upper estuary at Site 3 Eprapah Creek for study E7 (5-7/06/06).

Figure 8.4 – Time-averaged transverse velocity $\overline{V_y}$ and water depth as functions of time. Velocity data collected at 0.2 and 0.4 m above bed by 2D-microADV and 3D-ADV respectively. Water depth collected by YSI6600 probe located 0.3 m from 3D-ADV. Velocity averaged over 200 s every 10 s along entire data set.

Legend: — $\overline{V_y}$ at 0.2 m above bed; — $\overline{V_y}$ at 0.4 m above bed; — water depth.

8.3   COMPARATIVE TURBULENT PROPERTIES

This section focuses on the horizontal turbulence properties in the middle and upper estuarine zones collected with the 2D-microADV (16 MHz). For both field investigations the 2D-microADV was located at 0.2 m above the bed, close to the outer bank of the meanders at Site 2B and Site 3 (Figure 8.1). The turbulence properties of the tidal cycles E6TC2 and E7TC2 (Table 8.1) are used to illustrate the findings. These tidal cycles (E6TC2 and E7TC2) had an averaged tidal range of 1.28 m with no natural freshwater inflow observed. However, some stratification seemed present during the tidal cycles E6TC2 and E7TC2. The median values of the "pseudo" Richardson number over these tidal cycles were Ri = 0.19 and 0.98 respectively (Section 6.4.1). These median values of "pseudo" Richardson number seemed to indicate that partially stratified conditions were observed during the tidal cycles E6TC2 and E7TC2. Since no natural freshwater inflow was observed, one possible cause of these stratified conditions was the freshwater discharge from the STP. Fortunately, both tidal cycles occurred between approximately 22:00 and 12:00, therefore any influence from the STP discharge should be comparable. For both studies the median grain size at Sites 2B and 3 was approximately 0.02 mm. This approach allowed a systematic comparison of the turbulence properties in the middle (Site 2B) and upper (Site 3) estuaries under neap tidal conditions. The turbulence properties observed in the other tidal cycles of the studies E6 and E7 were similar to those of E6TC2 and E7TC2.

8.3.1   <u>Statistical moments of horizontal velocities</u>

The standard deviations of a velocity component are representative of the turbulent velocity fluctuations. In both middle and upper estuarine zones the standard deviations of streamwise and transverse velocities varied with the tides (Section 5.2). For the neap tidal conditions the turbulence fluctuations of streamwise and transverse velocities observed mid estuary (study E6) were larger than those observed in the upper estuary (study E7) (Figure 8.5). Median values of the standard deviations for streamwise and transverse velocities were v_x' = 0.76 and 0.33 cm/s and v_y' = 0.64 and 0.14 cm/s in the middle and upper estuarine zones respectively. The decreased magnitude of streamwise and transverse velocity standard deviations at Site 3 seemed to indicate decreased mixing occurred in the upper estuary.

Figure 8.5 shows the variation of streamwise and transverse velocity standard deviations over the tidal cycles E6TC2 and E7TC2. In Figure 8.5 the variations of a turbulence property (e.g. v_x' in Figure 8.5A) are represented in a circular plot and relative to the position in the tidal cycle. The data for a tidal cycle are collected from one low water to the next. The polar

coordinates are r = turbulence characteristic (e.g. r = v_x' (Figure 8.5A)) and $\theta = 2\pi\,t/T$, where T = period of tidal cycle from first low water (LW1) to second low water (LW2); and t = position in tidal cycle (t = 0 at LW1 and t = T at LW2). From the first low water on the plot (y = 0 on positive x-axis) the data progresses anticlockwise around the plot until the second low water (y = 0 on positive x-axis).

In Figure 8.5 the streamwise and transverse standard deviations (v_x' and v_y' respectively) observed mid estuary were of similar magnitude, while in the upper estuary v_x' was approximately twice as large as v_y'. This difference was reflected in the dimensionless horizontal turbulence intensity ratio v_y'/v_x'. For the studies E6 and E7, the median values of the horizontal turbulence intensity ratio were v_y'/v_x' = 0.85 and 0.44 respectively.
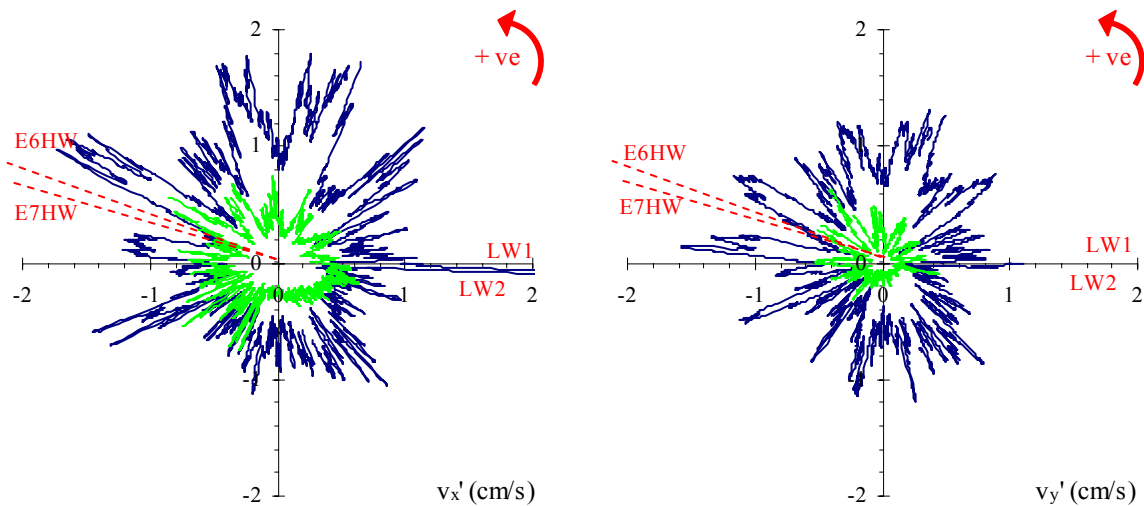
(A) v_x' data collected at Site 2B (study E6) and Site 3 (study E7).

(B) v_y' data collected at Site 2B (study E6) and Site 3 (study E7).

Figure 8.5 – Variation of standard deviations for streamwise and transverse velocities over tidal cycles E6TC2 and E7TC2. Standard deviations calculated over 200 s every 10 s along entire data set.

Legend: — field study E6; — field study E7.

The Gaussian behaviour of the horizontal velocity components represented by the skewness (Sk) and kurtosis (Ku) differed between the middle and upper estuarine zones for the field studies E6 and E7. In this study a data sample was considered to behave in a Gaussian fashion if: $|Sk| < 4*\sqrt{15/N}$ and $|Ku| < 4*\sqrt{96/N}$, where N is the number of data points per sample. The percentage of horizontal velocity data samples that could be considered within

reasonable Gaussian limits for both skewness and kurtosis were 40 and 20 % for the studies E6 and E7 respectively. This seemed to indicate an increased level of non-Gaussian turbulence behaviour in the upper estuary.

8.3.2 Statistical moments of Reynolds stress $\rho v_x v_y$

The Reynolds stress $\rho v_x v_y$ is an important turbulence property in the study of turbulent mixing and sediment transport, it represents the horizontal shear stress in the sampling volume and the high frequency fluctuations in the horizontal velocity magnitude. For the field studies E6 and E7 the time-averaged Reynolds stress $\rho \overline{v_x v_y}$ showed no easily discernible tidal trend (Section 5.4). The magnitudes of the Reynolds stress $\rho \overline{v_x v_y}$ maxima observed at Site 2B (study E6) were approximately an order of magnitude larger than those observed at Site 3 (study E7). Figure 8.6 shows the variation of time-averaged Reynolds stress $\rho \overline{v_x v_y}$ as a proportion of the tidal cycles E6TC2 and E7TC2. In Figure 8.6 the variation of the time-averaged parameter (e.g. $\rho \overline{v_x v_y}$ in Figure 8.6) is shown in relation to the proportion of the period between a low water LW1 and the next low water LW2. On the horizontal axis, 0 represents the start time of tidal cycle (LW1) and 1 represents the end of the tidal cycle (LW2), with the transition between the flood and ebb tides indicated (dashed line). In Figure 8.6 the fluctuations of the horizontal shear stress $\rho \overline{v_x v_y}$ at Site 2B were significantly larger than at Site 3. This increased magnitude of the Reynolds stress $\rho v_x v_y$ would tend to indicate increased sediment transport activity mid estuary, which seemed to be confirmed by the suspended sediment concentration data (Section 6.3).
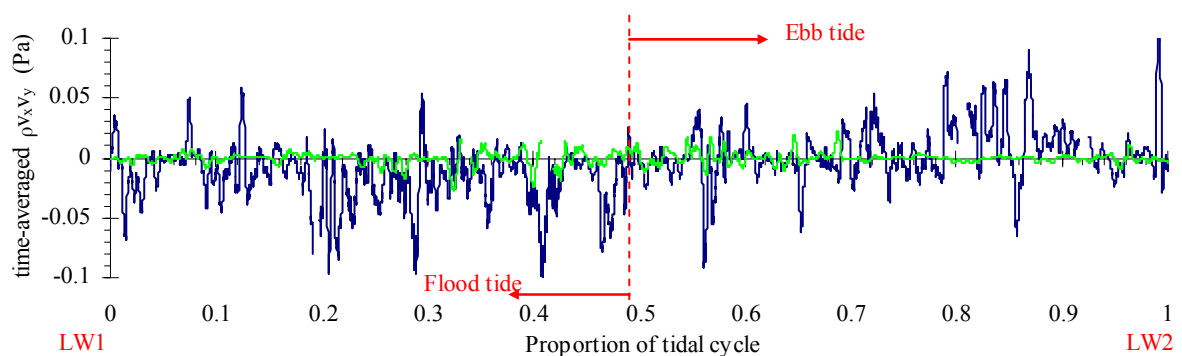
Figure 8.6 – Variation of time-averaged Reynolds stress $\rho \overline{v_x v_y}$ as a proportion of tidal cycles E6TC2 and E7TC2. Reynolds stress averaged over 200 s every 10 s along entire data set. Legend: — field study E6; — field study E7.

113

The standard deviations $(\rho v_x v_y)'$ of Reynolds stress $\rho v_x v_y$ were approximately an order of magnitude larger mid estuary (Site 2B) than those in the upper estuary (Site 3). Figure 8.7 shows the variation of standard deviations $(\rho v_x v_y)'$ over the tidal cycles E6TC2 and E7TC2. Note the enlarged scale in Figure 8.7B. In Figure 8.7 large fluctuations in $(\rho v_x v_y)'$ with periods of between 2,000 and 4,000 s were observed in both E6TC2 and E7TC2. The periods of these fluctuations were similar to those of the long period oscillations discussed in Sections 7.3 and 8.4. In both middle and upper estuarine zones, roughly 80 % of the 33,208 data samples for Reynolds stress $\rho v_x v_y$ at 0.2 m above the bed could be consider non-Gaussian in both skewness and kurtosis. In this study a data sample was considered non-Gaussian if: $|Sk > 4*\sqrt{15/N}$ and $|Ku| > 4*\sqrt{96/N}$, where N is the number of data points per sample.
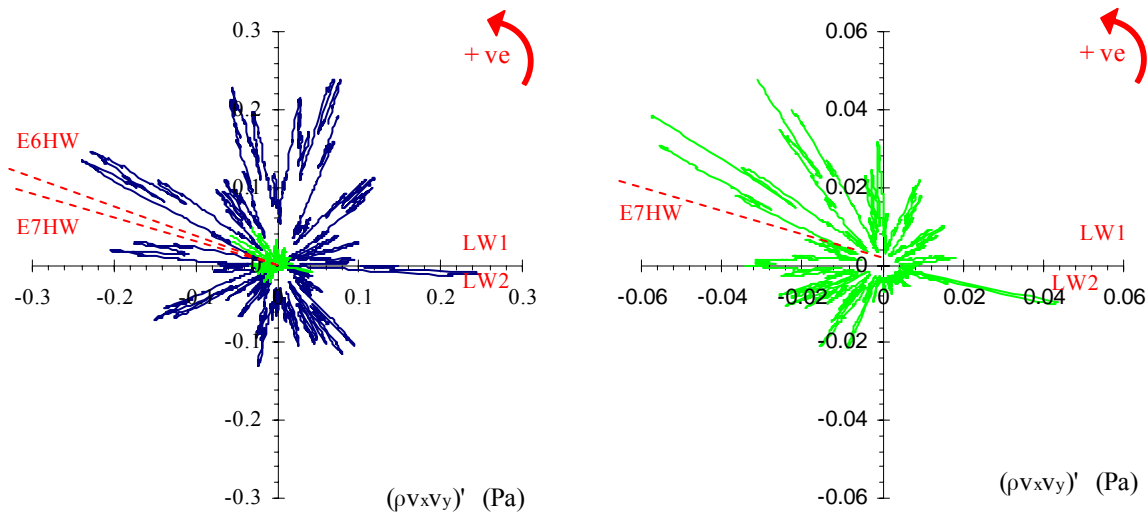
(A) Data collected at Site 2B (study E6) and Site 3 (study E7).

(B) Data collected at Site 3 (study E7).

Figure 8.7 – Variation of standard deviations $(\rho v_x v_y)'$ over tidal cycles E6TC2 and E7TC2. Standard deviations calculated over 200 s every 10 s along entire data set.

Legend: — field study E6; — field study E7.

8.3.3   Turbulence time scales

8.3.3.1   *Integral time scales*

The integral time scale represents the longest connection in the turbulent behaviour of a velocity component. In the middle and upper estuarine zones the integral time scales of streamwise and transverse velocities varied with the tide (Section 5.6.1). Figure 8.8 shows the variation of the streamwise and transverse integral time scales over the tidal cycles E6TC2 and E7TC2. In Figure 8.8A the streamwise integral time scales in the middle and upper estuary were of a similar magnitude during the flood tide. However, in the upper estuary

(study E7), the magnitude of streamwise integral time scales decreased during the ebb tides. The median values of streamwise integral time scales were T_{Ex} = 0.74 and 0.34 s for the studies E6 and E7 respectively. In Figure 8.8B the transverse integral time scales observed in the middle and upper estuary were of similar magnitude throughout the tidal cycle. The median values of transverse integral time scales observed for the studies E6 and E7 were T_{Ey} = 1.07 and 1.04 s respectively.
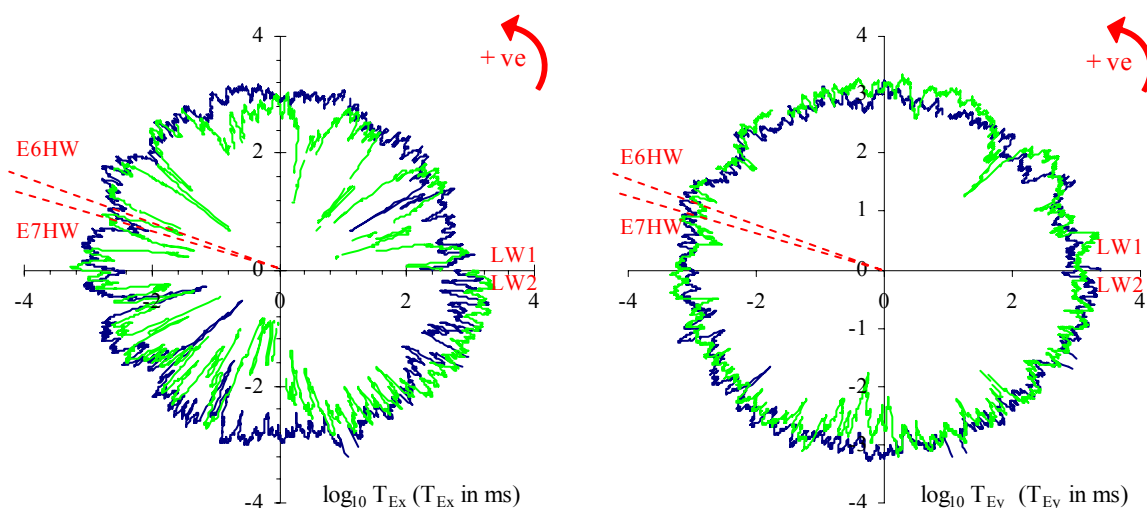
(A) T_{Ex} data collected at Site 2B (study E6) and Site 3 (study E7).

(B) T_{Ey} data collected at Site 2B (study E6) and Site 3 (study E7).

Figure 8.8 – Variation of streamwise T_{Ex} and transverse T_{Ey} integral time scales (in milliseconds) over tidal cycles E6TC2 and E7TC2. Time scales calculated over 200 s every 10 s along entire data set.

Legend: — field study E6; — field study E7.

8.3.3.2 *Dissipation time scales*

The dissipation time scale is a measure of the most rapid changes that occur in the fluctuations of a velocity component. In both middle and upper estuarine zones the dissipation time scales seemed independent of the tidal phase (Section 5.6.2). However, in the middle estuary (study E6), the transverse dissipation time scales measured with the 2D-microADV (16 MHz) at 0.2 m above the bed were approximately an order of magnitude larger than those observed in the upper estuary (study E7). The median values of streamwise and transverse dissipation time scales observed at 0.2 m above the bed for the studies E6 and E7 were τ_{Ex} = 0.003 and 0.001 s and τ_{Ey} = 0.059 and 0.002 s respectively. For the study E6, the median value of the transverse dissipation time scale at 0.4 m above the bed was

τ_{Ey} = 0.002 s. This seemed to indicate that an anomaly occurred in the transverse dissipation time scales collected at 0.2 m above the bed for the study E6. At present no reasonable explanation is available for this anomaly.

8.4   LONG PERIOD OSCILLATIONS AND SECONDARY CURRENTS

Long period oscillations were observed in the streamwise and transverse velocities in both middle (study E6) and upper (study E7) estuarine zones under neap tidal conditions (Figures 8.3 and 8.4). Under neap tidal conditions these long period oscillations caused streamwise and transverse velocity fluctuations of a similar or larger magnitude than those caused by the tides. A spectrum analysis of the streamwise and transverse velocity data collected at 0.2 and 0.4 m above the bed during the studies E6 and E7 was undertaken to study the predominant oscillation periods (Appendix E).   The predominant peaks in a spectrum indicate the oscillation periods that contributed the most energy to the measured data. Table 8.2 presents the 10 most prominent oscillation periods T < 14,400 s observed at 0.2 and 0.4 m above the bed for the field studies E6 and E7. Here, the study of the predominant oscillation periods was limited to T < 14,400 s by the 48 and 50 hour investigation periods of the studies E6 and E7.

Table 8.2 – Predominant oscillation periods (T < 14,400 s) for field studies E6 and E7.

Study E6 Oscillation periods (s)				Study E7 Oscillation periods (s)			
0.2 m above bed		0.4 m above bed		0.2 m above bed		0.4 m above bed	
V_x	V_y	V_x	V_y	V_x	V_y	V_x	V_y
3,355	9,869	3,355	4,944	3,608	13,421	3,608	2,642
3,902	11,983	3,902	4,415	3,290	12,427	3,995	3,995
2,330	8,830	3,608	2,298	3,995	11,570	3,728	3,647
4,043	5,687	3,495	10,168	1,794	10,824	3,290	3,532
9,869	6,453	2,330	2,449	2,820	3,948	2,110	8,830
12,905	2,124	4,043	2,684	1,730	7,989	3,107	11,184
2,969	6,711	2,969	4,247	2,208	8,830	1,730	3,136
3,495	1,291	9,869	6,579	2,110	6,579	1,794	1,864
2,844	4,043	4,934	13,980	3,107	9,587	2,208	2,414
4,934	1,824	2,844	3,258	12,905	3,290	4,302	4,143

Note: Oscillation periods T > 2,200 s possibly created by external resonance, while T < 2,200 s possibly created by resonance within Eprapah Creek (Appendix E).

In Table 8.2 none of the 10 most predominant transverse oscillations periods (T < 14,400 s) at 0.2 and 0.4 m above the bed were similar for the studies E6 and E7. This was not the case for the predominant streamwise oscillation periods at 0.2 and 0.4 m above the bed, with at least 8/10 of the predominant oscillation periods the same (Table 8.2). The difference in transverse velocity oscillation periods at 0.2 and 0.4 m above the bed could lead to the formation of transverse velocity events and the associated secondary currents.

8.4.1   Long period oscillations in transverse velocity and secondary currents

Transverse velocity events and the associated secondary currents of various periods were observed in both upper and middle estuarine zones during the studies E6 and E7. These transverse velocity events seemed to have periods similar to those of the long period oscillations of transverse velocity. This section investigates the relationship between the long period oscillations of transverse velocity and these transverse velocity events.

One particular transverse velocity event was observed when the transverse velocities at 0.2 and 0.4 m above the bed were in opposite directions. This type of transverse velocity event is often associated with a specific type of secondary current known as a "reverse cell". Reverse cell secondary currents commonly form near the outer bank of meanders and rotate in the opposite direction to the main transverse flow direction (Bathurst et al. (1977)). In channel meanders the main transverse velocity direction (secondary current) is towards the outer bank at the bed and towards the inner bank near the surface. Here, the largest of these transverse velocity events were observed at the beginning of the flood tide (e.g. t = 129,000 and 135,000 s of the study E6, Figures 8.4A and 8.9B) in both middle and upper estuarine zones (studies E6 and E7). This is consistent with the findings of West et al. (1984) in a study of the flow patterns of an UK estuary, which found that shear induced instabilities and secondary flow events were more likely to form on the flood tide.

The effect of the long period oscillations on the formation of transverse velocity cells (e.g. reverse cells) in the middle and upper estuaries was investigated using two of the largest transverse velocity events for the studies E6 and E7. Figure 8.9 shows these two largest transverse velocity events observed for the field studies E6 and E7. The possible reverse cell secondary currents observed are indicated for each transverse velocity event shown in Figure 8.9. In Figure 8.9 the period and magnitude of the transverse velocity events observed mid estuary (study E6) were larger than those in the upper estuary (study E7).

For both middle (study E6) and upper (study E7) estuarine zones, the individual transverse velocity cells were not uni-directional (e.g. Figures 8.9A, C and D). In Figure 8.9A, the transverse velocity cells for t = 77,160 to 77,860 s and t = 78,010 to 80,240 s seemed to rotate

in the opposite directions, (i.e. ($\overline{V_y}$ (0.2 m) > 0; $\overline{V_y}$ (0.4 m) < 0) and ($\overline{V_y}$ (0.2 m) < 0; $\overline{V_y}$ (0.4 m) > 0) respectively). These reversals in the transverse velocity cell direction had periods similar to the long period oscillations observed in Table 8.2. This seemed to indicate that the interaction of the long period oscillations (not the tides) with the local bathymetry formed these transverse velocity events observed under neap tidal conditions (studies E6 and E7).
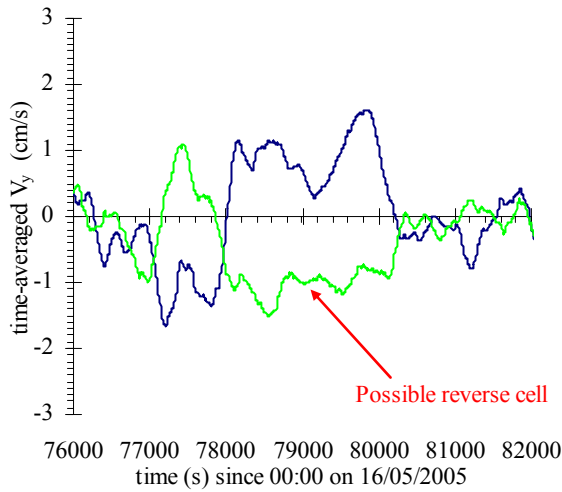
(A) Event E6a (t = 76,000 to 82,000 s, study E6).
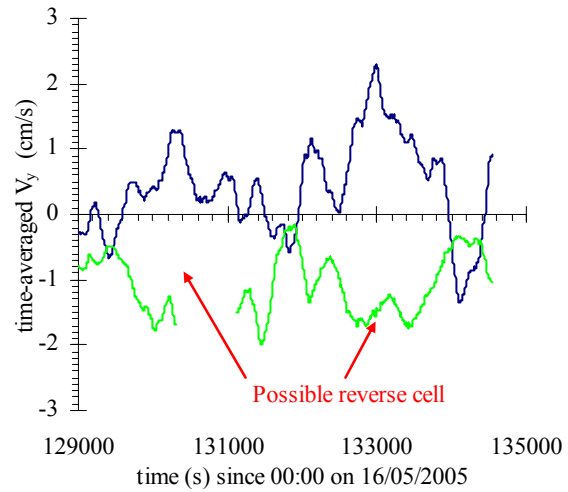
(B) Event E6b (t = 129,000 to 135,000 s, study E6).
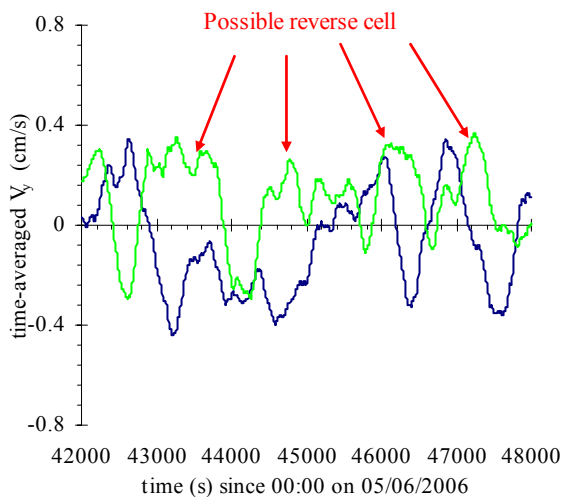
(C) Event E7a (t = 42,000 to 48,000 s, study E7).
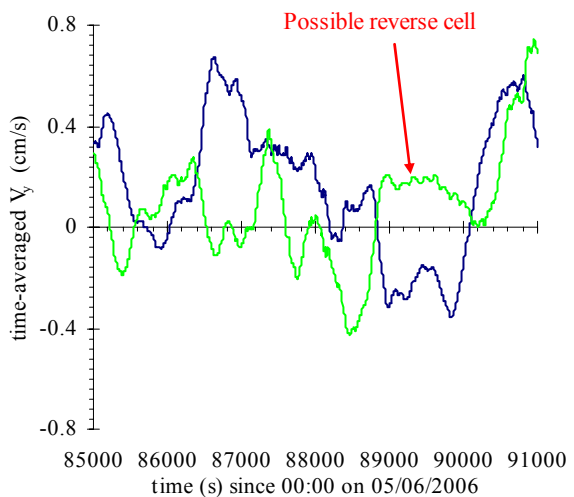
(D) Event E7b (t = 85,000 to 91,000 s, study E7).

Figure 8.9 – Time-averaged transverse velocity $\overline{V_y}$ at 0.2 and 0.4 m above bed as functions of time for some transverse velocity events observed during field studies E6 and E7. Velocity averaged over 200 s every 10 s along entire data set.

Legend: —— $\overline{V_y}$ 0.2 m above bed; —— $\overline{V_y}$ 0.4 m above bed.

118

The number of individual transverse velocity cells, their maximum and minimum durations and the median transverse velocity magnitudes are listed in Table 8.3. Table 8.3 shows that the duration of these transverse velocity events were similar to the half periods of long period oscillations in groups B, C and D (Table 7.4). This indicated that the long period oscillations from these groups were a primary cause of these larger transverse velocity events and the associated secondary currents observed in the field studies E6 and E7.

Table 8.3 – Description of some transverse velocity events from field studies E6 and E7.

Field study	Event number	Number of events	Maximum event duration (s)	Minimum event duration (s)	$\left\|\overline{V_y}\right\|$ at 0.2 m.a.b. (cm/s)	$\left\|\overline{V_y}\right\|$ at 0.4 m.a.b. (cm/s)
E6	E6a	3	2,230	460	0.81	0.66
	E6b	3	2,000	210	0.63	0.71
E7	E7a	7	970	140	0.17	0.18
	E7b	7	1,270	170	0.17	0.26

Note: Event duration refers to period in which $\overline{V_y}$ at 0.2 and 0.4 m were in opposite directions; m.a.b.: metres above bed; $\left|\overline{V_y}\right|$: median value of time-averaged transverse velocity magnitude for 6,000 s of event shown in Figure 8.9.

The median values of the transverse velocity magnitudes $\left|\overline{V_y}\right|$ for the data sets of the studies E6 and E7 were approximately 0.55 and 0.17 cm/s respectively. For each 6,000 s section of data (Figure 8.9), the median values of transverse velocity magnitude were equal to or larger than that of the entire data set for the field studies E6 and E7 (Table 8.3). This indicated that during these larger transverse velocity events there was an increased transverse velocity magnitude.

8.5 DISCUSSION

The data presented in Sections 8.2 and 8.3 showed that the horizontal velocity and turbulence properties observed in the middle (study E6) and upper (study E7) estuarine zones were distinctly different during similar neap tidal conditions. This would suggest that the mixing processes in the upper and middle estuarine zones are significantly different. In turn, this finding may have some implications in terms of estuary modelling. The upper and middle estuarine zones have distinct characteristics, and their modelling must be based upon these distinct properties. It is unclear at present whether the different turbulence conditions in the

middle and upper estuarine zones were caused by the dissipation of the tidal energy between the middle and upper estuarine zones.

For neap tidal conditions, the long period oscillations observed in streamwise and transverse velocity influenced the turbulence and mixing properties in both the middle and upper estuaries. The data collected at 0.2 and 0.4 m above the bed showed that these long period oscillations affected the fluctuations of streamwise and transverse velocities. These fluctuations in streamwise and transverse velocities were equal to or even larger than the tidal variations. This has some serious implications for the longitudinal mixing and dispersion of substances within the middle and upper estuarine zones. Section 8.4 showed that these long period oscillations caused large transverse velocity "cells" to form in one direction, collapse, and then reform rotating in the opposite direction. This rapid swapping of transverse velocity "cell" directions could greatly impact on the turbulent mixing.

At present few studies have investigated the turbulence properties in the upper estuarine zone. However, the results of the study E7 showed that the turbulent mixing in the upper estuarine zone could vary substantially from that mid estuary. All turbulence properties discussed in Section 8.3 indicated a large reduction in the turbulent energy observed in the upper estuary. The horizontal turbulence fluctuations (v_x' and v_y') and Reynolds were up to an order of magnitude smaller in the upper estuarine zone of Eprapah Creek. This reduction in energy close to the bed in the upper estuary would in theory lead to a reduction in the mixing observed close to the bed. The physio-chemistry data collected in the upper estuarine zone for the study E7 seemed to confirm this (Sections 6.2.2 and 6.2.4). The YSI6600 probe close the bed (0.3 m from the ADVs) showed only minor variations in all physio-chemistry parameters compared to that observed by the YSI6600 probe close to the free surface. Unfortunately, turbulence data could not be measured close to the free surface in that field study.

One major factor that may influence the turbulence and water quality properties in the middle and upper estuarine zone is the discharge from the sewage treatment plant. The STP discharge enters Eprapah Creek at 2.5 km AMTD between Sites 2B and 3, and could conceivably influenced the propagation of the tides from Site 2B to Site 3. In both field studies E6 and E7 the possible influence of the STP discharge was noted. However, it was not discussed here, because of a lack of information concerning the movement of this discharge during these investigations. Field studies specifically investigating the movements of the STP discharge would greatly assist the EPA (QLD) to understand the impact of such discharges on the health of the numerous small subtropical estuaries in Southeast Queensland.

9 A COMPARISON OF TURBULENCE PROPERTIES BETWEEN EPRAPAH CREEK (AUSTRALIA) AND HAMANA LAKE (JAPAN)

9.1 PRESENTATION

In late 2005, the writer participated in some field investigations at Hamana Lake conducted by Toyohashi University of Technology. Hamana Lake is located in the Shizuoka prefecture on the Southeast coast of Honshu Island, Japan (Insert, Figure 9.1). This section compares the turbulence data collected during two field studies performed at Hamana Lake with the studies E5 and E6 undertaken at Eprapah Creek. All field studies were conducted continuously at high frequency for an investigation period of at least 25 hours. This allowed a comparison of the turbulence properties in these two distinct types of estuaries, thereby isolating any commonalities or differences in the turbulence properties and behaviour of the two estuaries.

9.2 FIELD SITE: HAMANA LAKE

Hamana Lake (Figure 9.1) is a relatively large tidal lake with a small opening to the Pacific Ocean. It extends approximately 15 km inland and has a surface area of 7.4×10^7 m^2. The width of the entrance is about 200 m and it is controlled by man made structures. The entrance channel is regularly dredged to keep the channel open. The depth of Hamana Lake increases landwards, from less than 1 m near the entrance, to more than 12 m further inland.
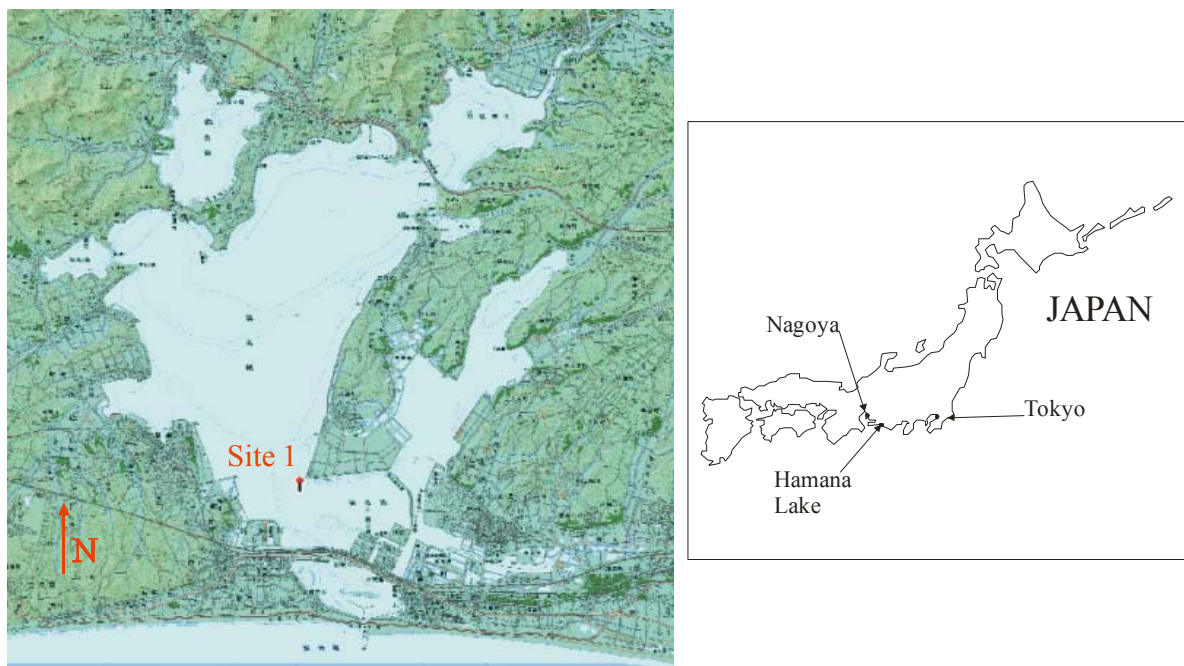
Figure 9.1 – Picture of Hamana Lake Japan (courtesy of S. Aoki). Insert shows location of Hamana Lake in Japan.

Two field studies were undertaken at Site 1 Hamana Lake (Figures 9.1 and 9.2). Site 1 (N34° 42' 27.3", E137° 34' 50.3") was located in a shallow area near the estuary mouth. This type of shallow region is typical of restricted entrance (bar-built) type estuaries (Dyer (1997)). It was located approximately 600 m Northeast of the main navigation channel, 450 m South of the nearest bank and approximately 3.5 km NNW of the entrance (Figure 9.2). Figure 9.2 shows the shallow region near the entrance of Hamana Lake. In Figure 9.2, the directions of positive streamwise and transverse velocity used for the Hamana Lake studies are defined ($V_x > 0$ to South and $V_y > 0$ to East). The location of the experimental cross-section is indicated in Figure 9.2. Figure 9.3 shows the experimental cross-section through Site 1. At Site 1 the mean depth was approximately 0.9 m during the two field studies. The maximum tidal range during the field studies were 0.39 and 0.56 m. Throughout the investigations wind waves were observed as a result of wind speeds $V_W > 1$ m/s.
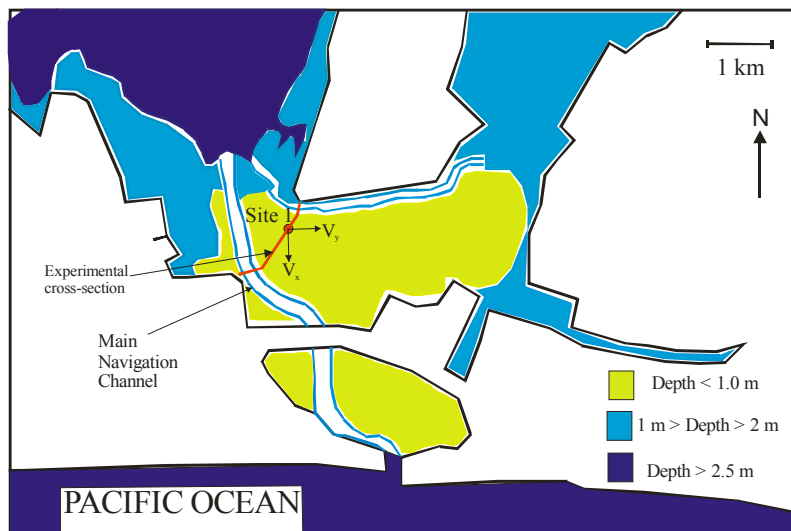
Figure 9.2 – Sketch of Hamana Lake near entrance.
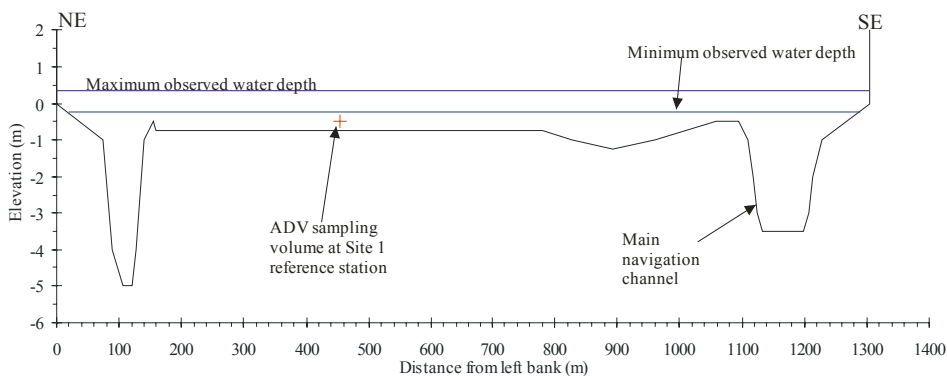
Figure 9.3 – Experimental cross-section through Site 1 Hamana Lake, looking downstream to South.

9.3 FIELD STUDIES AND INSTRUMENTATION

Two field studies at Hamana Lake (studies HLJ1 and HLJ2) were chosen for comparison with the field trips E6 and E5 (Table 3.1). The field studies HLJ1 (24-25/11/2005) and HLJ2 (30/11-1/12/2005) were conducted under neap and spring tidal conditions respectively. Wind waves were observed at Hamana Lake during both experiments. The turbulence data were processed using a wave-turbulence separation technique described in Section 9.4. This technique allowed the separation of the current induced turbulence data and wave induced turbulence data. The current induced turbulence data were compared to the post-processed data of the field studies E5 and E6, at Eprapah Creek. Table 9.1 outlines the field investigations performed at Eprapah Creek and Hamana Lake.

Table 9.1 – Description of field studies conducted at Hamana Lake and Eprapah Creek.

Estuary	Hamana Lake		Eprapah Creek	
Field study	**HLJ1**	**HLJ2**	**E5**	**E6**
Date	24-25/11/05	30/11-1/12/05	8-9/03/05	16-18/05/05
Tidal conditions	Neap	Spring	Spring	Neap
TR (m)	0.39	0.56	2.44	1.37
ADV type	Nortek 3D-ADV	Nortek 3D-ADV	Sontek 3D-ADV	Sontek 3D-ADV
T_{study} (hrs)	28	27	25	48
f_{scan} (Hz)	32	32	25	25
Sampling location	Site 1, 0.25 m above bed, 454 m from left bank	Site 1, 0.25 m above bed, 454 m from left bank	Site 2B, 0.1 m above bed, 10.7 m from left bank	Site 2B, 0.4 m above bed, 10.7 m from left bank
Site cross-section width (m)	1,476	1,476	32	32
Mean depth at site (m)	0.9	0.9	1.6	1.6
Wind waves	Moderate	Moderate	Not observed	Not observed
Wind speed (m/s)	1.2 to 6.5	1.0 to 6.0	--	--

Note: Left bank: bank on left hand side of observer when looking downstream; f_{scan} : ADV sampling frequency; T_{study} : study duration (hours); TR: maximum tidal range at site.

Two different types of acoustic Doppler velocimeters were used to measure the turbulent velocity data at Hamana Lake and Eprapah Creek. At Eprapah Creek, a Sontek 3D-ADV (10 MHz) with a down-looking head (serial 0510) was used for the field trips E5 and E6. A Nortek 3D-Vector field ADV (serial no. VEC1445) was used at Hamana Lake for the field

studies HLJ1 and HLJ2. The turbulent velocity sampling details for each field investigation are presented in Table 9.1. Some physio-chemistry data were also collected at Hamana Lake and Eprapah Creek during each field study and these are discussed in Section 9.5.2.

For the statistical analysis of the turbulence data of both Hamana Lake and Eprapah Creek a sample size of 5,000 data points was selected for statistical similarity. The sampling frequencies of the ADVs were slightly different (32 and 25 Hz respectively) because of the different brands of ADVs. A data sample containing 5,000 data points corresponds to a sample time of 200.0 and 156.25 s for the field studies conducted at Eprapah Creek and Hamana Lake respectively. The turbulence data were calculated every 10 s along each data set. If more than 20 % of the 5,000 data points of a sample were deemed erroneous, that data sample was not included in the turbulence analysis.

9.4   WAVE-TURBULENCE SEPARATION TECHNIQUE

Wind waves were observed at Hamana Lake (e.g. Figure 9.4). The wind waves interacted with the current induced turbulence: this will change the turbulence characteristics under the surface (Benilov and Filyushkin (1970), Thais and Magnaudet (1996)). Previous studies (e.g. Benilov and Filyushkin (1970), Thais and Magnaudet (1995) and Trowbridge (1998)) developed techniques for separating the current induced turbulence data from the wave induced turbulence data. A simple method derived from the linear filtration method (Benilov and Filyushkin (1970)) was used in this study. The linear filtration method required that the fluctuations in water level and the turbulent property (e.g. velocity) be sampled at the same frequency. At Hamana Lake, the Nortek Vector 3D-ADV collected the variations in water level above the sensor at the same frequency as the instantaneous velocity. The linear filtration method was applied to separate the current induced data from the wave induced data.

Figure 9.4 – Photograph of wind waves observed at Site 1 Hamana Lake taken during installation for study HLJ1 on 24/11/05, with poles holding ADV on far left.

This separation technique was based upon the water level spectrum and the spectra of the three velocity components. These spectra were visually inspected to determine the characteristic frequencies for which the velocity and water level spectra were correlated. The wave induced frequency band was selected so that the water level spectra contained more than 3 % of the energy of the dominant wave period. Appendix F provides a detailed description of the wave-turbulence separation technique used and the frequency bands of wave induced data separated for the field studies HLJ1 and HLJ2.

9.5   ESTUARINE DYNAMICS

9.5.1   Tidal variations

At Hamana Lake the tidal range was small during both spring and neap tidal conditions because of the restricted entrance of the lake (Table 9.1). The constriction reduced the tidal range observed in the estuary by dampening the ocean tidal oscillations (e.g. Keulegan (1951), van de Kreeke (1967), Hinwood et al. (2003)). The difference in tidal range was less than 0.2 m for the neap and spring tide studies (Table 9.1). At Eprapah Creek the sampling site was exposed to the full tidal range of both spring and neap tides. The difference between the maximum observed spring and neap tidal ranges was about 1.1 m (Table 9.1).

At both Hamana Lake and Eprapah Creek the tidal data showed some diurnal inequalities. Diurnal inequality occurs when the two tidal cycles observed within the 25 hour diurnal period have different tidal amplitudes and periods. Figure 9.5 shows the spring tidal variations of water depth and conductivity observed during the study HLJ2 at Hamana Lake and the study E5 at Eprapah Creek. Note that the vertical scales differ between Figures 9.5A and 9.5B.

9.5.2   Physio-chemistry

Several physio-chemistry properties were measured at both Hamana Lake and Eprapah Creek during the field studies. These included the water temperature and conductivity. Table 9.2 presents the range and median values of the water temperature and conductivity measurements. The water temperature and conductivity data were collected with an Alec Electronics compact-CT probe at Hamana Lake and with a YSI6600 probe at Eprapah Creek. At Hamana Lake the conductivity data responded differently to the tidal forcing than the conductivity readings at Eprapah Creek for both spring and neap tidal conditions. In Figure 9.5A, the phase difference between the variation of water depth and conductivity at Eprapah Creek was small. At Hamana Lake, the change in conductivity lagged behind the water depth by approximately 3 hours (Figure 9.5B). The response of the conductivity to tidal forcing at

Hamana Lake (Figure 9.5B) was more asymmetric than that observed at Eprapah Creek (Figure 9.5A). The restricted entrance of Hamana Lake seemed responsible for this asymmetric response.
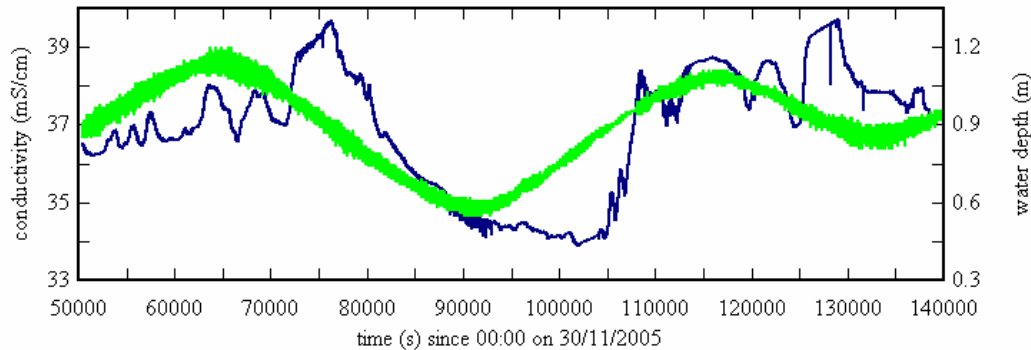
(A) Data collected at Site 1, Hamana Lake for study HLJ2 (30/11-1/12/05).
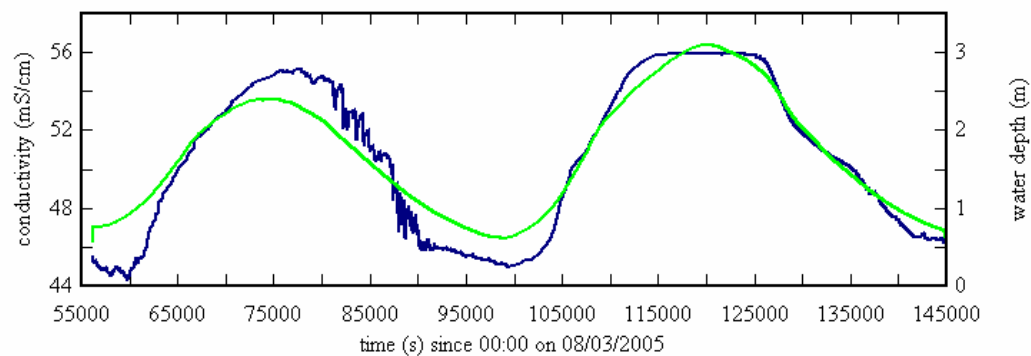
(B) Data collected at Site 2B, Eprapah Creek for study E5 (8-9/03/05).

Figure 9.5 – Variation of water depth and conductivity as functions of time since midnight on 30/11/05 (study HLJ2) and 8/03/05 (study E5). Data collected 0.1 m above bed at Site 2B, Eprapah Creek and on bed at Site1, Hamana Lake.

Legend: —— water depth; —— conductivity data.

Table 9.2 – Sample range and median values of water temperature and conductivity observed during field studies performed at Hamana Lake and Eprapah Creek.

Estuary	Field study	Instrument	f_{scan} (Hz)	Range		Median	
				Temp (C)	Cond (mS/cm)	Temp (C)	Cond (mS/cm)
Hamana Lake	HLJ1	Alec Electronics Compact-CT	1	13.7 to 18.2	38.6 to 45.3	15.5	41.1
	HLJ2	Alec Electronics Compact-CT	1	12.5 to 16.9	33.9 to 39.7	15.0	37.3
Eprapah Creek	E5	YSI6600	0.167	24.1 to 26.9	44.3 to 56.0	26.1	50.9
	E6	YSI6600	0.083	20.2 to 21.8	43.9 to 50.2	21.1	47.3

Note: f_{scan} : scanning frequency; Cond: conductivity; Temp: water temperature.

126

9.5.3   Time-averaged velocities

The distinct bathymetry and tidal forcing conditions between Hamana Lake and Eprapah Creek produced two different velocity patterns.   This section focuses on the horizontal velocity patterns, since some question remains as to the quality of the vertical velocity data of all 3D-ADVs equipped with a down-looking head (Section 3.5.1).

9.5.3.1   Streamwise velocity

The response of the time-averaged streamwise velocity to the tidal forcing was different at Eprapah Creek and Hamana Lake. Figure 9.6 shows the time-averaged streamwise velocity and water depth as functions of time for the field studies HLJ2 and E5. In Figure 9.6 the streamwise velocity is on the left vertical axis and the water depth is on the right vertical axis. At Hamana Lake, the streamwise velocity flowed along the North-South axis (Figure 9.2), with the mouth being downstream of Site 1. For both the Eprapah Creek and Hamana Lake studies the streamwise velocity was positive downstream.

In Figure 9.6A the maximum flood and ebb velocities at Hamana Lake were observed in the middle of the tide under spring and neap tidal forcing. Van der Ham et al. (2001) observed a similar tidal trend in a shallow semi-enclosed bay. For the study HLJ1, conducted during neap tidal conditions the maximum flood and ebb velocity suggested a neutral tidal bias. However, under spring tidal forcing (study HLJ2) the maximum ebb velocity at Hamana Lake was larger than the maximum flood velocity (Figure 9.6A).

At Eprapah Creek the maximum ebb and flood velocity occurred just before and just after low water, under both spring and neap tidal conditions (Figure 9.6B).   The time-averaged streamwise velocity at Eprapah Creek was largest at the beginning of the flood tide, for all tidal cycles of the studies E5 and E6. Kawanisi and Yokosi (1994) observed similar maximum flood and ebb velocities about low water in an estuarine tidal channel in Japan.
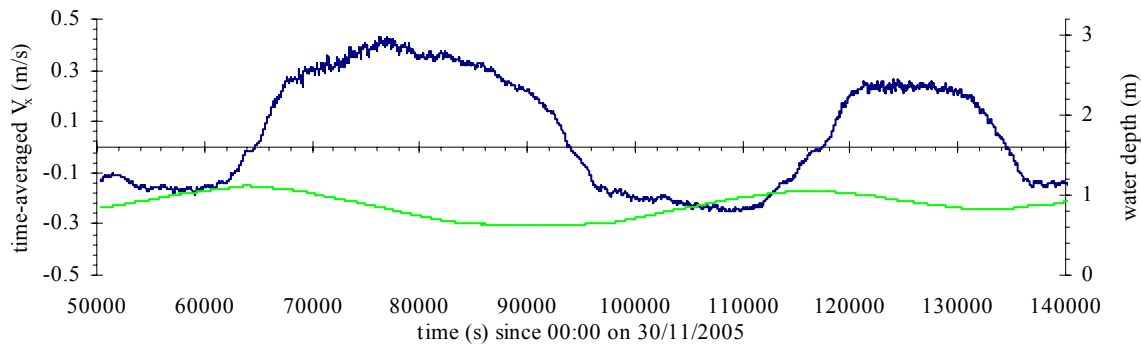
(A) Data of study HLJ2 conducted 0.25 m above bed at Hamana Lake (Site 1).
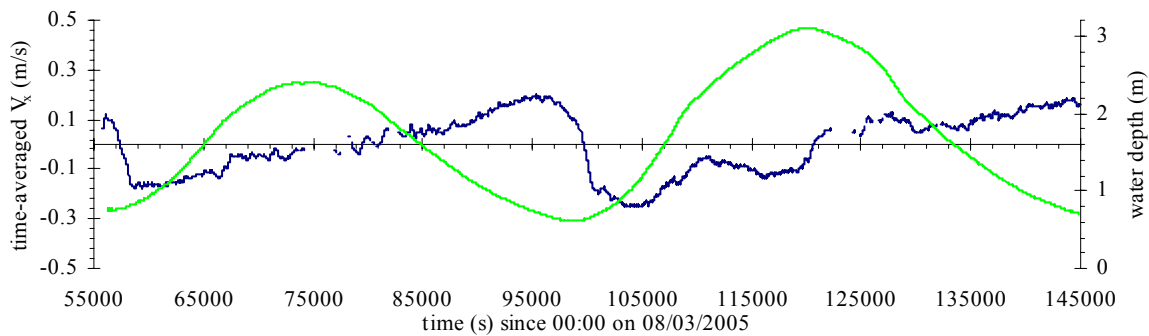
(B) Data of study E5 conducted 0.1 m above bed at Eprapah Creek (Site 2B).

Figure 9.6 – Time-averaged streamwise velocity and water depth as functions of time for spring tides of studies HLJ2 (30/11-1/12/05) and E5 (8-9/03/05). Time-averaged velocity calculated for 5,000 data points every 10 s along entire data set.

Legend: — water depth; — time-averaged streamwise velocity.

9.5.3.2 *Transverse velocity*

Different tidal patterns of transverse velocity were observed at Hamana Lake and Eprapah Creek. Figure 9.7 shows the time-averaged transverse velocity (positive towards left bank) as a function of time-averaged streamwise velocity (positive downstream) under spring and neap tidal conditions. In Figure 9.7 the magnitude of transverse velocity was much larger at Hamana Lake than at Eprapah Creek. Let us consider the ratio $\Delta \overline{V_y}/\Delta \overline{V_x}$, where $\Delta \overline{V_y}$ is the maximum range of transverse velocity and $\Delta \overline{V_x}$ is the maximum range of streamwise velocity. For spring and neap tidal conditions, this ratio was $\Delta \overline{V_y}/\Delta \overline{V_x} \sim 0.55$ at Hamana Lake and $\Delta \overline{V_y}/\Delta \overline{V_x} \sim 0.24$ at Eprapah Creek. The difference in relative transverse velocity could be related to the difference in the transverse dimensions of Site 1, Hamana Lake and Site 2B, Eprapah Creek. Figure 9.8 presents two photographs demonstrating the different transverse dimensions around Site 1 Hamana Lake and Site 2B Eprapah Creek.
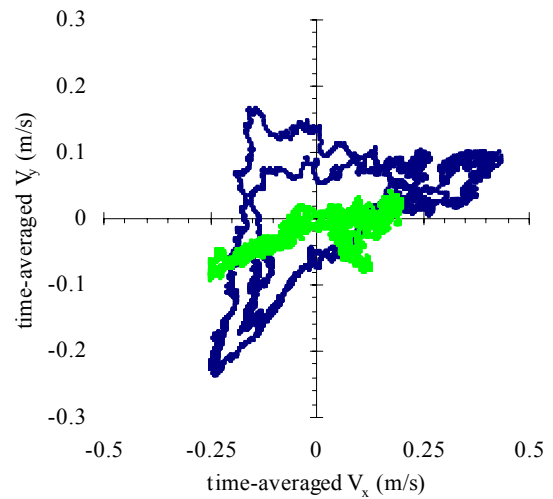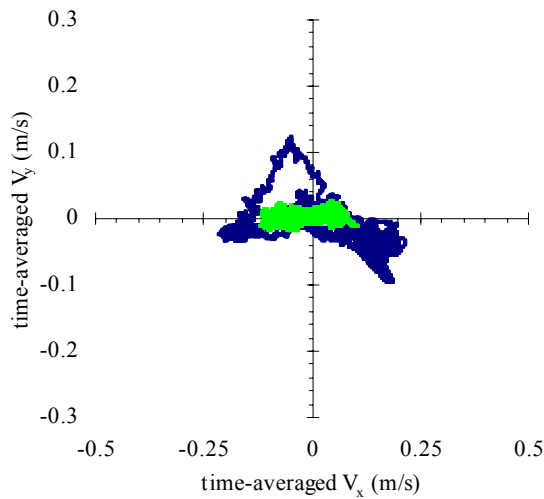
(A) Neap tide data collected 0.25 m above bed at Hamana Lake (study HLJ1) and 0.4 m above bed at Eprapah Creek (study E6).

(B) Spring tide data collected 0.25 m above bed at Hamana Lake (study HLJ2) and 0.1 m above bed at Eprapah Creek (study E5).

Figure 9.7 – Time-averaged transverse velocity $\overline{V_y}$ (positive towards left bank) as a function of time-averaged streamwise velocity (positive downstream). Data time-averaged over 5,000 data points every 10 s along entire data set.

Legend: [•] data collected at Eprapah Creek; [•] data collected at Hamana Lake.

(A) Site 1 Hamana Lake, looking North to nearest bank about 450 m away. Taken on 24/11/05 during setup of study HLJ1.

(B) Site 2B Eprapah Creek, looking downstream from left bank. Taken mid flood tide on 16/05/05 during study E6.

Figure 9.8 – Photographs demonstrating transverse dimensions about experimental sites at Hamana Lake (Site 1) and Eprapah Creek (Site 2B).

The response of the time-averaged transverse velocity at Hamana Lake was different under spring and neap tidal conditions (Figure 9.7). For spring tides, the transverse velocity of the ebb tide ($V_x > 0$) flowed towards the East ($V_y > 0$, Figure 9.7B), while for the neap tides the transverse ebb velocity predominantly flowed to the West (Figure 9.7A). It is unknown at present whether this phenomenon was caused by a physical process or by a fault in the ADV setup (see Appendix G).

At Eprapah Creek, the response of the time-averaged transverse velocity was slightly different between the spring and neap tide field studies. For the neap tidal conditions (study E6), the transverse velocity was predominantly towards the left bank during the ebb tide and towards the right bank during the flood tide, in a quasi-linear relationship between $\overline{V_x}$ and $\overline{V_y}$. However, for the study E5 (spring tides), the transverse velocity response was more asymmetric, as the magnitude of transverse velocity increased with increasing streamwise flood velocity (Figure 9.7B).

9.6 TURBULENCE PROPERTIES

Despite Hamana Lake and Eprapah Creek being different estuarine types which contained distinctly different estuarine dynamics, some similar patterns in turbulence properties were observed. These patterns were related to the changes that occurred in a turbulence property because of changes in velocity magnitude, water level and/or the tides. Only definitive patterns are discussed herein. Further, the Hamana Lake turbulence data refers to the current induced turbulence data (Section 9.4).

9.6.1 Standard deviations of velocity components

The standard deviations of all velocity components varied with the tides at Eprapah Creek and Hamana Lake. Figure 9.9 shows the standard deviations of streamwise velocity as functions of the time-averaged streamwise velocity during neap (Figure 9.9A) and spring (Figure 9.9B) tidal conditions. For the data collected at Hamana Lake and Eprapah Creek, the standard deviations of streamwise velocity increased with the magnitude of streamwise velocity. Similar trends were also observed in the standard deviations of transverse and vertical velocities in both estuaries.

Under neap tidal conditions the standard deviations of all velocity components showed a similar tidal trend at both Hamana Lake and Eprapah Creek (e.g. Figure 9.9A). The median values of standard deviations for all velocity components under neap tidal conditions were 0.005 to 0.01 m/s at Eprapah Creek and 0.01 to 0.02 m/s at Hamana Lake.

For spring tidal forcing the standard deviations of all velocity components did not show the same tidal pattern (e.g. Figure 9.9B). The median values of standard deviations for horizontal velocity components were about 0.04 and 0.02 m/s under spring tidal forcing at Eprapah Creek and Hamana Lake respectively. This difference did not seem related to the velocity magnitude as the streamwise velocity maxima were larger at Hamana Lake.

At Hamana Lake the tidal trend and median values of all velocity standard deviations were about the same for spring and neap tidal conditions. This was not so at Eprapah Creek, where different tidal trends were observed for the spring and neap tides. At Eprapah Creek the median values of all velocity standard deviations were four times larger for the spring tides.
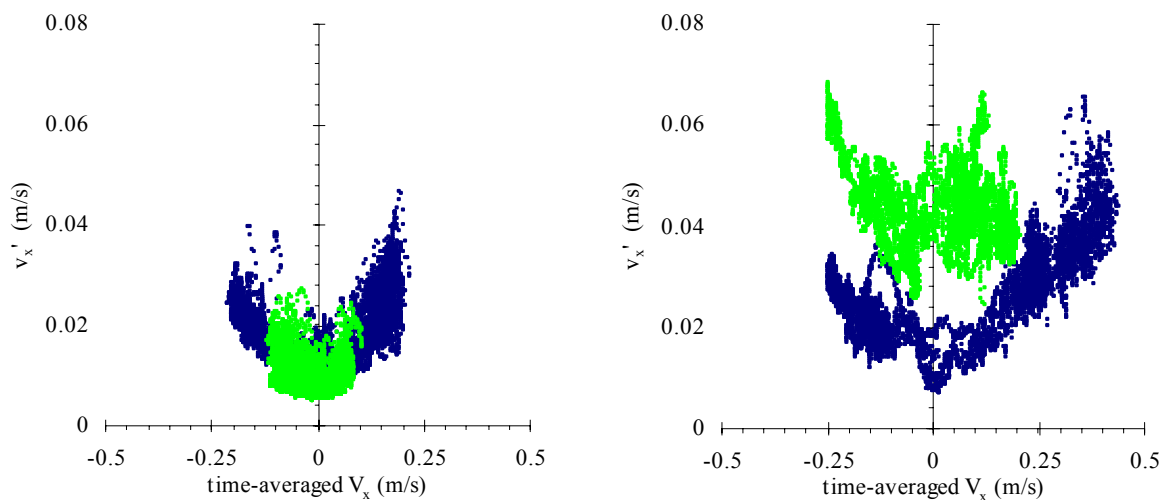
(A) Neap tide data collected 0.25 m above bed at Hamana Lake (study HLJ1) and 0.4 m above bed at Eprapah Creek (study E6).

(B) Spring tide data collected 0.25 m above bed at Hamana Lake (study HLJ2) and 0.1 m above bed at Eprapah Creek (study E5).

Figure 9.9 – Standard deviations of streamwise velocity v_x' as functions of time-averaged streamwise velocity (positive downstream). Standard deviations calculated for 5,000 data points every 10 s along entire data set.

Legend: [•] data collected at Eprapah Creek; [•] data collected at Hamana Lake.

9.6.2 Turbulence intensity ratios

The turbulence intensity ratios are dimensionless parameters that characterise the turbulence structure (Nezu and Nakagawa (1993)). For the field studies conducted under neap tidal conditions at Eprapah Creek (study E6), and spring and neap tidal conditions at Hamana Lake (studies HLJ1 and HLJ2), the median values of the vertical and horizontal turbulence intensity ratios were $v_z'/v_x' = 0.5$ to 0.6 and $v_y'/v_x' = 0.8$ to 0.9. However, for spring tidal conditions at Eprapah Creek (study E5), the median value of the turbulence intensity ratios

differed from the other field studies. For the study E5, the median value of the horizontal and vertical turbulence intensity ratios were $v_y'/v_x' = 1.0$ and $v_z'/v_x' = 0.39$. One possible cause of these different turbulence intensity ratios was that the tidal range at Site 2B (2.44 m) during the study E5 was larger than the mean water level (1.6 m). This was not observed in the studies HLJ1, HLJ2 and E6.

9.6.3 <u>Statistical moments of Reynolds stress $\rho v_x v_z$</u>

The tangential Reynolds stress $\rho v_x v_z$ represents the fluctuations in vertical velocity generated by the fluctuations of the streamwise velocity. It is an important property in the study of turbulent mixing in estuaries, because it can represent the vertical shear stress generated by the streamwise velocity. Previous studies have also noted some strong correlation between the time-averaged Reynolds stress $\rho \overline{v_x v_z}$ and suspended sediment concentration (e.g. West and Oduyemi (1989), Kawanisi and Yokosi (1997)).

At Eprapah Creek and Hamana Lake the time-averaged Reynolds stress $\rho \overline{v_x v_z}$ varied with the tides. Figure 9.10 shows the time-averaged Reynolds stress $\rho \overline{v_x v_z}$ as a function of the time-averaged streamwise velocity (positive downstream). In Figure 9.10 the time-averaged Reynolds stress was predominantly positive during the flood tide and negative during the ebb tide for both spring and neap tidal forcing. This pattern was consistent with that observed by the earlier field investigations of Osonphasop (1983) and Kawanisi and Yokosi (1994) in natural tidal channels and van der Ham et al. (2001) in a large, shallow semi-enclosed bay. Linear approximations shown in Figure 9.10 assist in highlighting some key observations of the relationship between time-averaged Reynolds stress $\rho \overline{v_x v_z}$ and time-averaged streamwise velocity $\overline{V_x}$. Table 9.3 presents the slope (β) and regression coefficient (R) values of the linear approximations $\rho \overline{v_x v_z}$ (Pa) $= \beta \overline{V_x}$ (m/s) for each study.

Table 9.3 – Properties of linear relationship between $\rho \overline{v_x v_z}$ and $\overline{V_x}$.

Estuary	Field study	Tidal conditions	$\beta = \rho \overline{v_x v_z}/\overline{V_x}$ (kgm^{-2}s^{-1})	R
Hamana Lake	HLJ1	Neap	- 0.56	0.99
	HLJ2	Spring	- 0.61	0.99
Eprapah Creek	E5	Spring	- 1.73	0.99
	E6	Neap	- 0.33	0.99

For neap tidal conditions the tidal response of the time-averaged Reynolds stress $\overline{\rho v_x v_z}$ to the streamwise velocity were relatively similar at Hamana Lake and Eprapah Creek (Figure 9.10A). This was not the case under spring tidal forcing, with a more asymmetrical response observed at Eprapah Creek (Figure 9.10B). Note that at Hamana Lake, the tidal response of the time-averaged Reynolds stress $\overline{\rho v_x v_z}$ under spring and neap tides was about the same.
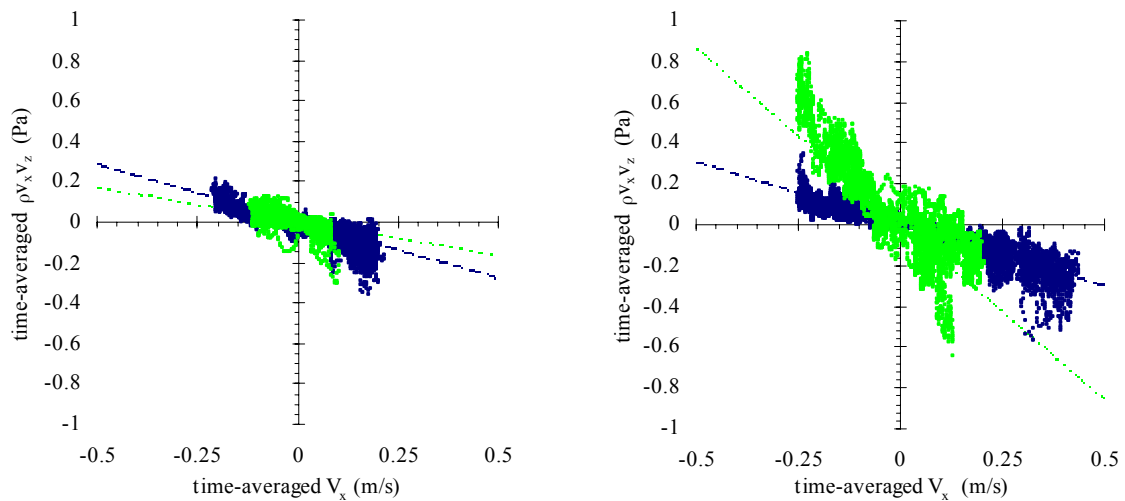
(A) Neap tide data collected 0.25 m above bed at Hamana Lake (study HLJ1) and 0.4 m above bed at Eprapah Creek (study E6).

(B) Spring tide data collected 0.25 m above bed at Hamana Lake (study HLJ2) and 0.1 m above bed at Eprapah Creek (study E5).

Figure 9.10 – Time-averaged Reynolds stress $\overline{\rho v_x v_z}$ as a function of time-averaged streamwise velocity (positive downstream). Data averaged over 5,000 data points every 10 s along entire data set.

Legend: [•] data collected at Eprapah Creek; [•] data collected Hamana Lake; [····] linear approximation for Eprapah Creek data; [– – –] linear approximation for Hamana Lake data.

The standard deviations of all Reynolds stresses varied with the tides at Hamana Lake and Eprapah Creek. The standard deviations of all Reynolds stresses varied with tide in a similar fashion to the standard deviations of velocity. Figure 9.11 shows the standard deviations of Reynolds stress $(\rho v_x v_z)'$ as functions of the time-averaged streamwise velocity (positive downstream) under spring and neap tidal conditions. The standard deviations of Reynolds stress $(\rho v_x v_z)'$ increased with the magnitude of the streamwise velocity. This pattern was also observed with the standard deviations $(\rho v_x v_y)'$ and $(\rho v_y v_z)'$ at Hamana Lake and Eprapah Creek. The standard deviations of all tangential Reynolds stresses for Eprapah

Creek and Hamana Lake showed similar tidal trends during neap tidal conditions (Figure 9.11A). This was not observed under spring tidal forcing (Figure 9.11B), when the tidal trends differed. Under spring tidal forcing, the standard deviations of all Reynolds stresses at Eprapah Creek were three to four times larger than those at Hamana Lake.
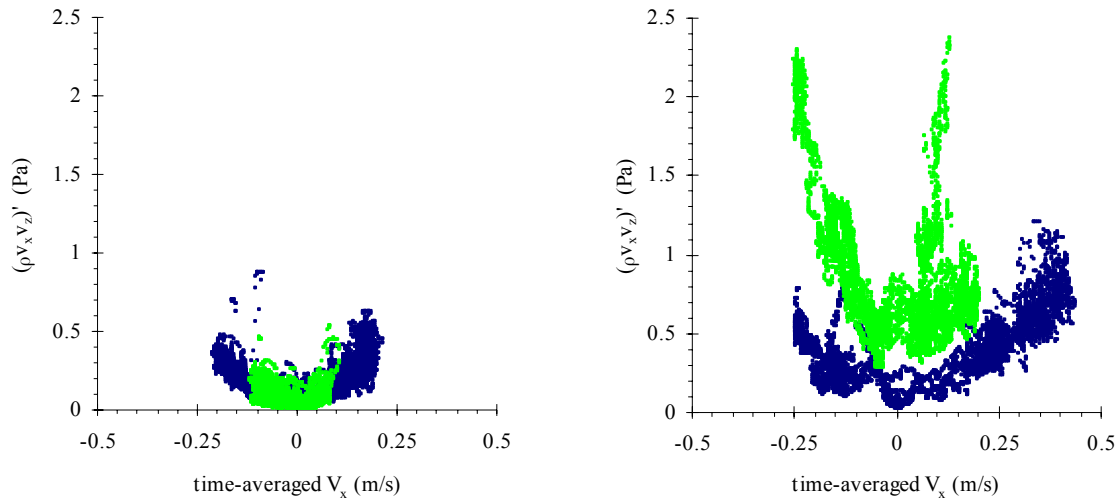
(A) Neap tide data collected 0.25 m above bed at Hamana Lake (study HLJ1) and 0.4 m above bed at Eprapah Creek (study E6).

(B) Spring tide data collected 0.25 m above bed at Hamana Lake (study HLJ2) and 0.1 m above bed at Eprapah Creek (study E5).

Figure 9.11 – Standard deviations of Reynolds stress $(\rho v_x v_z)'$ as functions of time-averaged streamwise velocity (positive downstream). Standard deviations calculated over 5,000 data points every 10 s along entire data set.

Legend: [•] data collected at Eprapah Creek; [•] data collected at Hamana Lake.

The skewness of Reynolds stress $Sk(\rho v_x v_z)$ varied with the tides at both Hamana Lake and Eprapah Creek under spring and neap tidal forcing. Figure 9.12 shows the skewness of Reynolds stress $Sk(\rho v_x v_z)$ as a function of the time-averaged streamwise velocity (positive downstream). In Figure 9.12, the skewness $Sk(\rho v_x v_z)$ was predominantly positive during the flood tide and negative during the ebb tide in both estuaries. A tidal trend was not observed in the skewness of the other tangential Reynolds stresses $Sk(\rho v_x v_y)$ and $Sk(\rho v_y v_z)$ at either Hamana Lake or Eprapah Creek. Kurtosis values of all tangential Reynolds stresses showed no easily discernible tidal trend at Hamana Lake or Eprapah Creek. The skewness and kurtosis values of all tangential Reynolds stresses at Eprapah Creek and Hamana Lake were between $-2 < Sk < 2$ and $3 < Ku < 15$ respectively and as such were considered non-Gaussian.
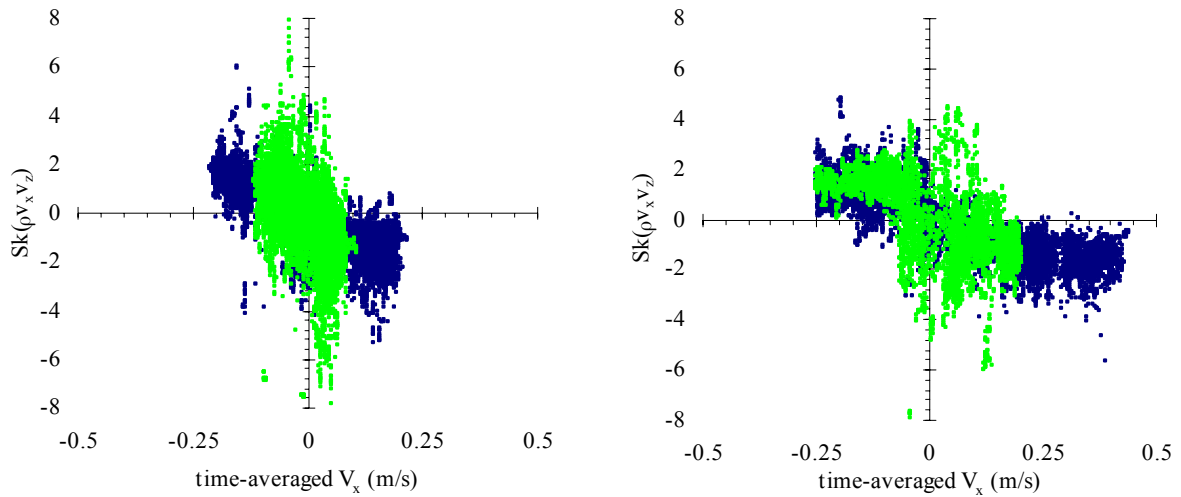
(A) Neap tide data collected 0.25 m above bed at Hamana Lake (study HLJ1) and 0.4 m above bed at Eprapah Creek (study E6).

(B) Spring tide data collected 0.25 m above bed at Hamana Lake (study HLJ2) and 0.1 m above bed at Eprapah Creek (study E5).

Figure 9.12 – Skewness of Reynolds stress $Sk(\rho v_x v_z)$ as a function of time-averaged streamwise velocity (positive downstream). Skewness values calculated over 5,000 data points every 10 s along entire data set.

Legend: [•] data collected at Eprapah Creek; [•] data collected at Hamana Lake.

9.6.4 Correlation coefficient of Reynolds stress R_{vxvz}

A correlation coefficient of Reynolds stress is a dimensionless Reynolds stress, defined as $R_{vxvz} = \overline{v_x v_z} / (v_x' v_z')$. The dimensionless Reynolds stress R_{vxvz} varied with tides during all field studies at Hamana Lake and Eprapah Creek. Figure 9.13 shows the dimensionless Reynolds stress R_{vxvz} as a function of the time-averaged streamwise velocity (positive downstream). In Figure 9.13, the correlation coefficient R_{vxvz} was predominantly positive during the flood tide and negative during the ebb tide at both Eprapah Creek and Hamana Lake. A similar trend was observed by Kawanisi and Yokosi (1993, 1994) in an estuarine tidal channel. Figure 9.13 shows further that the range of R_{vxvz} were similar at Hamana Lake and Eprapah Creek during spring and neap tidal conditions. In Figure 9.13B, the correlation coefficient R_{vxvz} seemed constant ($|R_{vxvz}| \sim 0.3 \pm 0.1$) for $|\overline{V_x}| > 0.12$ m/s for spring tides at both Hamana Lake and Eprapah Creek.
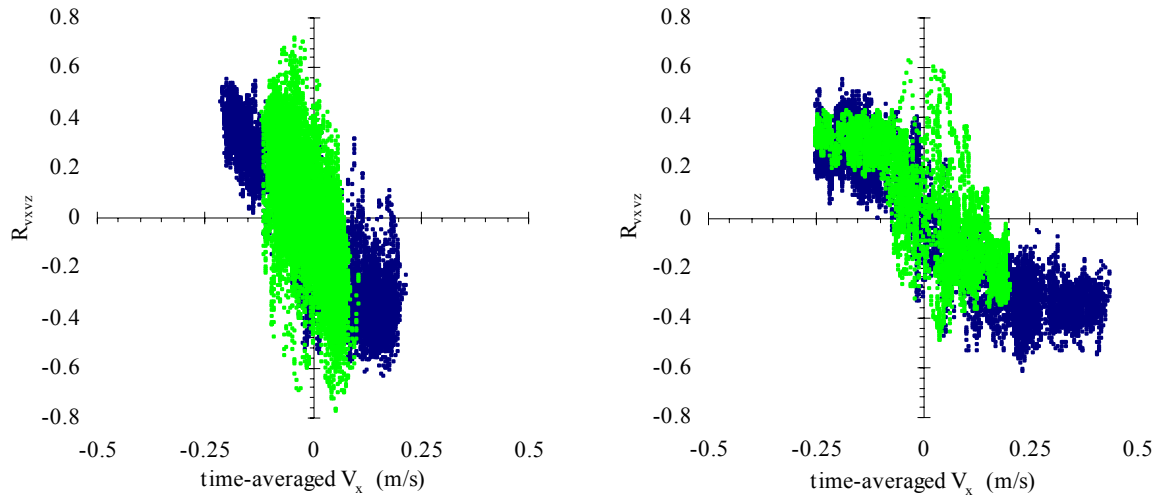
135

(A) Neap tide data collected 0.25 m above
bed at Hamana Lake (study HLJ1) and 0.4
m above bed at Eprapah Creek (study E6).

(B) Spring tide data collected 0.25 m above
bed at Hamana Lake (study HLJ2) and 0.1
m above bed at Eprapah Creek (study E5).

Figure 9.13 – Correlation coefficient R_{vxvz} as a function of time-averaged streamwise velocity (positive downstream).   Correlation coefficients calculated over 5,000 data points every 10 s along entire data set.

Legend: [•] data collected at Eprapah Creek; [•] data collected at Hamana Lake.

9.6.5   Turbulence time scales

9.6.5.1   *Integral time scales*

The integral time scales of a velocity component are the longest connection in the turbulent fluctuations of that velocity component. The median values of the horizontal integral time scales (T_{Ex} and T_{Ey}) were between 0.56 and 0.76 s at Hamana Lake and between 0.13 and 0.38 s at Eprapah Creek. Table 9.4 presents the median values of the integral time scales.

Table 9.4 – Median values of integral time scales at Hamana Lake and Eprapah Creek.

Estuary	Study	Tidal conditions	T_{Ex} (s)	T_{Ey} (s)	T_{Ez} (s)
Hamana Lake	HLJ1	Neap	0.74	0.56	0.60
	HLJ2	Spring	0.76	0.59	0.42
Eprapah Creek	E5	Spring	0.17	0.13	0.31
	E6	Neap	0.32	0.38	0.83

At Hamana Lake, the median values of streamwise and transverse integral time scales were similar under spring and neap tidal conditions ($T_{Ex} \sim 0.75$ s and $T_{Ey} \sim 0.58$ s). At Eprapah Creek, the median values of all integral time scales were larger under neap conditions (e.g.

136

$T_{Ex} \sim 0.32$ s) than spring tidal forcing (e.g. $T_{Ex} \sim 0.17$ s). Median values of the vertical integral time scales were larger under neap tidal conditions than under spring tidal conditions at both Eprapah Creek and Hamana Lake.

9.6.5.2 Dissipation time scales

The dissipation time scale is an estimate of the most rapid changes that occur in the fluctuations of a velocity component. At Eprapah Creek, the median values of the horizontal dissipation time scales were between 0.002 and 0.003 s for both spring and neap tidal conditions. This seemed to indicate that the dissipation time scales at Eprapah Creek were independent of the magnitude of tidal forcing. Table 9.5 presents the median values of the dissipation time scales.

At Hamana Lake, the median values of the horizontal dissipation time scales (τ_{Ex} and τ_{Ey}) were between 0.007 and 0.011 s for spring tidal conditions and between 0.004 and 0.006 s during neap tidal conditions. The horizontal dissipation time scales at Hamana Lake were not independent of tidal magnitude. At Hamana Lake, the median values of transverse dissipation time scales τ_{Ey} were larger than the median values of streamwise dissipation time scales τ_{Ex} under spring and neap tidal forcing.

Table 9.5 – Median values of dissipation time scales at Hamana Lake and Eprapah Creek.

Estuary	Study	Tidal conditions	τ_{Ex} (s)	τ_{Ey} (s)	τ_{Ez} (s)
Hamana Lake	HLJ1	Neap	0.004	0.006	0.058
	HLJ2	Spring	0.007	0.011	0.058
Eprapah Creek	E5	Spring	0.003	0.003	0.027
	E6	Neap	0.002	0.002	0.029

9.7 DISCUSSION

The comparison of a typical small subtropical estuary (Eprapah Creek) to a distinctly different type of estuary (e.g. Hamana Lake) is important as it allows the study of commonalities in the hydrodynamics and turbulence properties of these estuaries. If the turbulence properties of a small subtropical estuary were similar to those of a larger system (e.g. Hamana Lake), then this could indicate that a common set of turbulence parameters and assumptions could be applied to the models of most estuaries. However, as important as these commonalities, are the differences which are to be found in the turbulence properties of a small subtropical

estuary compared to those of larger estuaries, because these would indicate that a common set of turbulence parameters and assumptions should not be applied to all estuaries.

This comparison of Eprapah Creek and Hamana Lake showed that many of the hydrodynamics properties were distinctly different. For example, two distinct tidal patterns of the streamwise and transverse velocities were observed at Eprapah Creek and Hamana Lake. At Eprapah Creek the flood and ebb streamwise velocity maxima occurred about low tide, while the velocity maxima occurred about the mid tides at Hamana Lake. Similar tidal patterns of streamwise velocity were observed in previous studies of coastal plain type estuaries and semi-enclosed tidal bays. Despite the many differences between the two field sites, some similar patterns were observed close to the bed at Hamana Lake and Eprapah Creek. These included: the standard deviations of all velocities and tangential Reynolds stresses; the time-averaged Reynolds stress $\rho \overline{v_x v_z}$; the skewness $Sk(\rho v_x v_z)$ of Reynolds stress $\rho v_x v_z$; and the dimensionless Reynolds stress R_{vxvz}.

For most of the turbulence patterns observed at both Hamana Lake and Eprapah Creek, the spring tidal data at Eprapah Creek showed a more asymmetrical response. For example, the standard deviations of streamwise velocity under spring tidal conditions were larger at Eprapah Creek than at Hamana Lake, despite the larger streamwise velocity observed at Hamana Lake. The ratio of local tidal amplitude and local mean depth at the experimental site a_1/h_1 (introduced in Section 7.4.1) may assist in explaining this phenomenon.

Table 9.6 shows the maximum tidal range and values of the ratio a_1/h_1 for the field studies E5, E6, HLJ1 and HLJ2. Also shown in Table 9.6 are the maximum tidal range and values of a_1/h_1 for Kawanisi and Yokosi (1994) in the Ota River, Japan (Table 2.1). Data from this study were used to support the findings from the data collected during the field studies E5, E6, HLJ1 and HLJ2, at Eprapah Creek and Hamana Lake. Unfortunately, this study seemed to be the only one that sufficient data could be extracted from to estimate a_1/h_1 and some of the turbulence properties discussed here.

For the study E5 a value of $a_1/h_1 > 0.5$ was observed, while for the studies E6, HLJ1 and HLJ2 a value of $a_1/h_1 < 0.5$ occurred. This indicated that when $a_1/h_1 > 0.5$ the response of the turbulence properties to the tidal forcing was more asymmetric and different from that when $a_1/h_1 < 0.5$. The comparison of the Hamana Lake and Eprapah Creek data seemed to indicate that the tidal patterns of some turbulence properties are similar when $a_1/h_1 < 0.5$ at different sites.

Table 9.6 – Values of a_1/h_1 for field studies at Eprapah Creek (studies E5 and E6), Hamana Lake (studies HLJ1 and HLJ2) and Ota River (Kawanisi and Yokosi (1994)).

Estuary	Study	Tidal conditions	Mean depth (m)	Tidal range (m)	a_1/h_1
Eprapah Creek (Site 2B)	E5	spring	1.6	2.44	0.76
	E6	neap	1.6	1.37	0.43
Hamana Lake (Site 1)	HLJ1	neap	0.9	0.39	0.22
	HLJ2	spring	0.9	0.56	0.31
Ota River (Japan)	Kawanisi and Yokosi (1994)	spring	3.3	3.2	0.48

Note: Tidal range: maximum tidal range observed at site for field study.

Figure 9.14 presents the median values of some common dimensionless turbulence properties as functions of ratio a_1/h_1. These dimensionless turbulence parameters include the relative turbulence intensities of the streamwise, transverse and vertical velocity fluctuations ($v'_x/|\overline{V_x}|$; $v'_y/|\overline{V_x}|$; $v'_z/|\overline{V_x}|$), the normalised tangential Reynolds stresses ($|\overline{v_x v_z}|/\overline{V_x}^2$; $|\overline{v_x v_y}|/\overline{V_x}^2$; $|\overline{v_y v_z}|/\overline{V_x}^2$), the magnitude of correlation coefficients of Reynolds stresses ($|R_{vxvz}|$; $|R_{vxvy}|$; $|R_{vyvz}|$) and the dimensionless integral time scales ($T_{Ex}\sqrt{g/h_1}$; $T_{Ey}\sqrt{g/h_1}$; $T_{Ez}\sqrt{g/h_1}$). Some of the dimensionless parameters were commonly presented in previous turbulence studies in estuaries and tidal channels (e.g. Osonphasop (1983), West and Oduyemi (1989)). Figure 9.14 presents the dimensionless turbulence parameters of each individual tidal cycle in the field studies E5 and E6 with the a_1/h_1, details of these tidal cycles presented in Table 7.6.

In Figures 9.14A and 9.14B the relative turbulence intensities of the streamwise $v'_x/|\overline{V_x}|$ and transverse $v'_y/|\overline{V_x}|$ velocities and normalised Reynolds stresses $|\overline{v_x v_z}|/\overline{V_x}^2$ and $|\overline{v_x v_y}|/\overline{V_x}^2$ were twice as large when $a_1/h_1 > 0.5$. When $a_1/h_1 < 0.5$, the median values of all dimensionless turbulence parameters were of a similar magnitude for the three different estuaries presented (Figures 9.14A and 9.14B). In Figure 9.14C, the median values of $T_{Ex}\sqrt{g/h_1}$, $T_{Ey}\sqrt{g/h_1}$ and $T_{Ez}\sqrt{g/h_1}$ were smallest when $a_1/h_1 > 0.5$ and seemed to increase as a_1/h_1 decreased. The median values of the correlation coefficients $|R_{vxvy}|$ and $|R_{vyvz}|$ seemed to decrease as a_1/h_1 increased for the studies HLJ1, HLJ2, E5 and E6, while no

easily discernible trend was observed for the correlation coefficient $|R_{vxvz}|$ for the three estuaries shown (Figure 9.14D).

The dimensionless turbulence parameters presented in Figure 9.14 indicated that a different set of turbulence and mixing properties exist when $a_1/h_1 > 0.5$, while the magnitudes of the relative turbulence intensities and normalised Reynolds stresses were similar when $a_1/h_1 < 0.5$. These results indicated that the turbulence properties of estuaries where $a_1/h_1 < 0.5$ could not be applied to small estuaries where $a_1/h_1 > 0.5$. This further highlights the usefulness of the ratio a_1/h_1 in evaluating the local turbulence properties of estuaries.
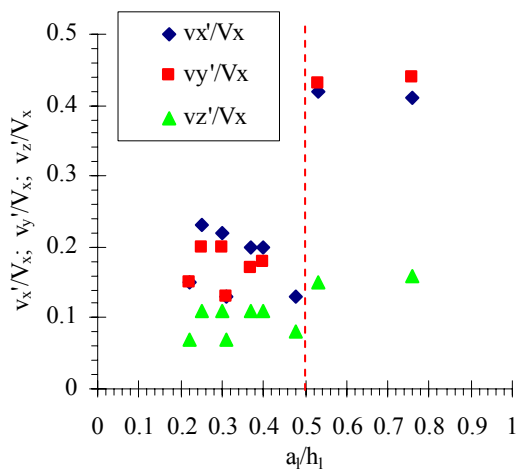
(A) $v'_x/|\overline{V_x}|$, $v'_y/|\overline{V_x}|$ and $v'_z/|\overline{V_x}|$.
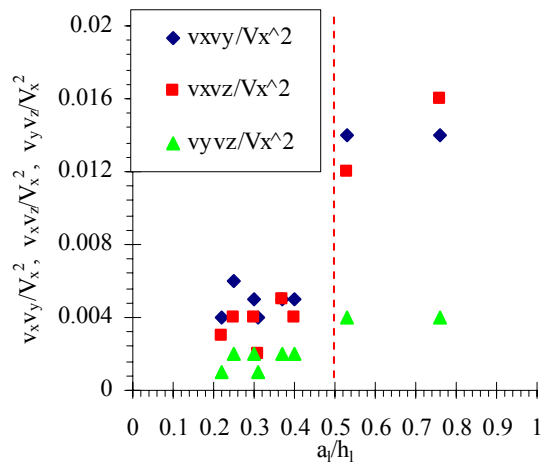
(B) $|\overline{v_x v_z}|/\overline{V_x}^2$, $|\overline{v_x v_y}|/\overline{V_x}^2$ and $|\overline{v_y v_z}|/\overline{V_x}^2$.
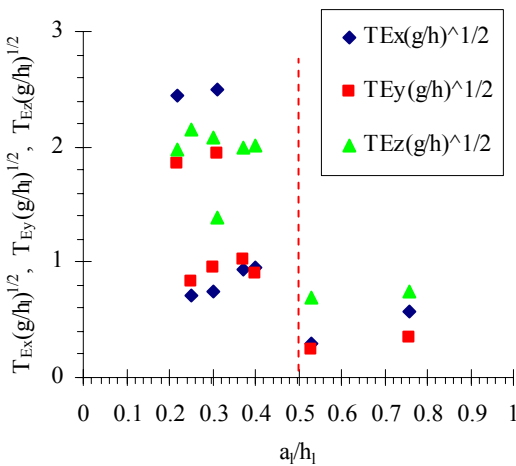
(C) $T_{Ex}\sqrt{g/h_1}$, $T_{Ey}\sqrt{g/h_1}$ and $T_{Ez}\sqrt{g/h_1}$.
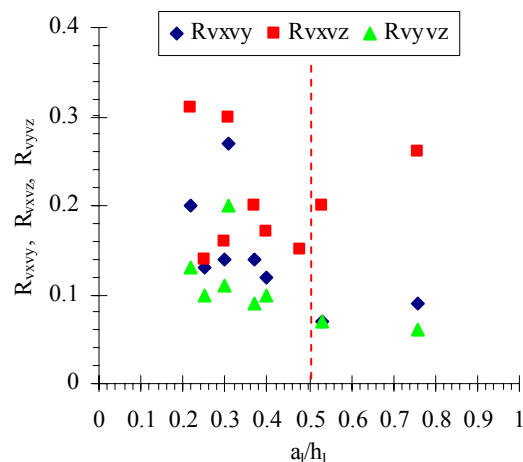
(D) $|R_{vxvz}|$, $|R_{vxvy}|$ and $|R_{vyvz}|$.

Figure 9.14 – Dimensionless turbulence parameters as functions of ratio a_1/h_1. For studies E5, E6, HLJ1 and HLJ2, parameters calculated over 5,000 data points every 10 s along entire data sets. Values from Kawanisi and Yokosi (1994) were estimated from graphs presented.

10   RELATIONSHIPS BETWEEN TURBULENCE AND WATER PROPERTIES

10.1 PRESENTATION

This chapter looks into the possible influence of turbulence properties on the mixing of water properties, which include the physio-chemistry parameters measured by the YSI6600 probe and the suspended sediment concentration.   Previous studies have found relationships between the turbulent velocity fluctuations and the fluctuations in salinity (e.g. West and Shiono (1985)) and fluctuations in suspended sediment concentrations (e.g. Kawanisi and Yokosi (1997)).   Understanding the relationship between turbulence and the variations of water properties is important to the modelling of mixing of these water properties within an estuary.   The turbulent mixing properties of an estuary also influence the ability of an introduced substance to disperse within that estuary.

Previous investigations into the relationship between turbulence and the variation of the water properties have mainly been conducted in larger estuaries (e.g. West and Oduyemi (1989)). Little research has been published on the relationships between turbulence and water properties in small estuarine systems. This section investigates some relationships between the turbulence and water properties observed during the field studies performed at Eprapah Creek. Section 10.2 investigates the relationship between suspended sediment concentration and turbulence for the field studies E6 and E7. The relationships between physio-chemistry and turbulence data collected during the field studies E5, E6 and E7 are discussed in Section 10.3. In Section 10.4 the possible influences of natural freshwater inflow from a rainstorm event are briefly discussed. Section 10.5 discusses some implications of the turbulence properties observed in Eprapah Creek on the modelling of mixing and dispersion in small subtropical estuaries.

10.2 SUSPENDED SEDIMENT CONCENTRATION AND TURBULENCE

A laboratory experiment was conducted to calibrate the backscatter intensity of the 2D-microADV (16 MHz) with the suspended sediment concentration (SSC), using water and sediment collected in the estuary of Eprapah Creek (Appendix D). The resulting relationship between backscatter intensity and SSC provided detailed measurements of instantaneous SSC during the field studies E6 and E7 (Table 10.1). Table 10.1 details the location and sampling frequencies of the 2D-microADV for these studies.

The relationship between suspended sediment concentration and turbulence was tested using data collected for the field studies E6 and E7. The first four statistical moments of the suspended sediment concentration are presented in Section 10.2.1. Section 10.2.2 presents the

integral time scales of the suspended sediment concentration. In Section 10.2.3, the suspended sediment flux per unit area ($q_S = SSC\ V_x$) at 0.2 m above the bed and its relationship to bed shear stress τ_b for the studies E6 and E7 are discussed.

Table 10.1 – Details of suspended sediment concentration data collected at Eprapah Creek.

Study	E6	E7
Date	16-18/05/05	5-7/06/06
T_{study} (hours)	48	50
Site	2B	3
Distance from mouth (km)	2.1	3.1
Transverse location (m)	10.7 (from left bank)	4.2 (from right bank)
Sampling elevation (m)	0.2	0.2
f_{scan} (Hz)	25	50
V_{range} (m/s)	1.0	0.3

Note: f_{scan} : ADV sampling frequency; V_{range} : ADV velocity range; T_{study} : study duration.

10.2.1 <u>Statistical moments of suspended sediment concentration</u>

Figure 10.1 shows the time-average $\overline{SSC}$ and standard deviations SSC' of suspended sediment concentration and water depth as functions of time. Note the logarithmic scale of the left vertical axis for $\overline{SSC}$ and SSC'. In Figure 10.1 the time-averaged suspended sediment concentration was largest about the low tides and smallest about the high tides. Larger variations in suspended sediment concentration with a period of about 24 hours were observed at a similar time of day in the middle (study E6) and upper (study E7) estuarine zones. The 24 hour variations in SSC were larger than those with the tides and occurred approximately from 10:00 to 13:00 each day of the studies E6 and E7.

In Figure 10.1 the suspended sediment fluctuations SSC' varied directly with the suspended sediment concentration (studies E6 and E7). The median values of SSC' were 0.01 and 0.004 g/L for the studies E6 and E7 respectively. For both studies the median value of the ratio $SSC'/\overline{SSC}$ was 0.57. This seemed to indicate that the larger turbulence intensities observed mid estuary under similar neap tidal conditions (Chapter 8) generated the bigger fluctuations of SSC observed in the study E6. Skewness and kurtosis values of the suspended sediment concentration showed non-Gaussian behaviour ($|Sk| > 4*\sqrt{15/N}$ and $|Ku| > 4*\sqrt{96/N}$, where N is the number of data points per sample) throughout the studies E6 and E7. The deviation of suspended sediment concentration data from Gaussian behaviour in terms of skewness and kurtosis was larger in the middle (study E6) than in the upper (study E7) estuary.
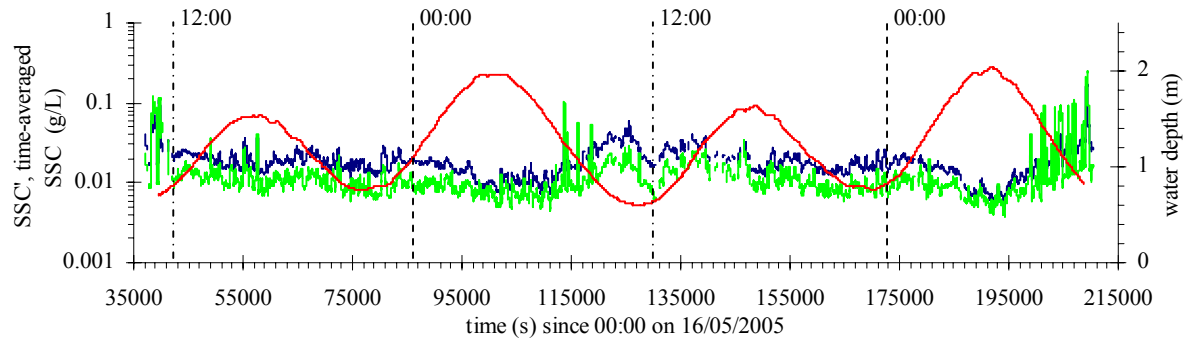
(A) Data collected in mid estuary (Site 2B) at 25 Hz for study E6 (16-18/05/05).
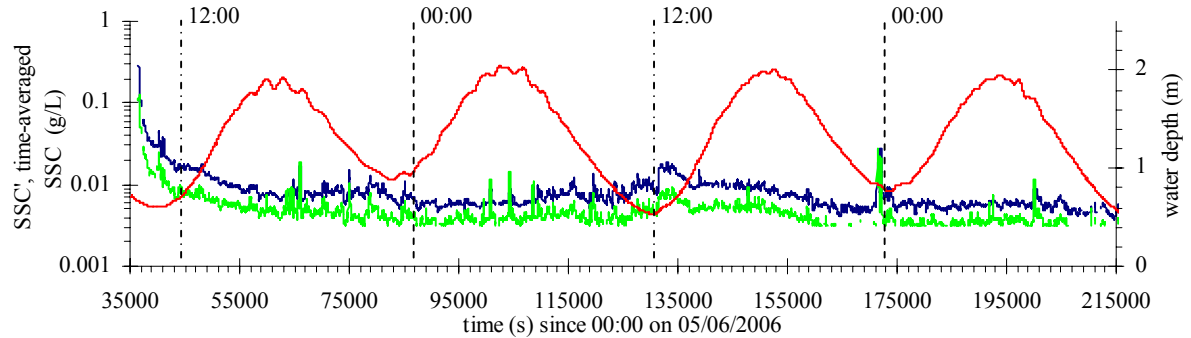
(B) Data collected in upper estuary (Site 3) at 50 Hz for study E7 (5-7/06/06).

Figure 10.1 – Water depth and time-average $\overline{SSC}$ and standard deviations SSC' of suspended sediment concentration as functions of time. Data measured at 0.2 m above bed for field studies E6 and E7. Statistics calculated over 200 s every 10 s along entire data set.

Legend: — $\overline{SSC}$; — SSC' ; — water depth.

10.2.2 Integral time scales of suspended sediment concentration

The integral time scale of suspended sediment concentration (T_{Essc}) data represents the time of turbid suspension observed at a location in the creek (Jackson (1976)). In both middle (study E6) and upper (study E7) estuarine zones, the integral time scales T_{Essc} seemed relatively independent of tidal phase under neap tidal conditions (Figure 10.2). However, the integral time scales T_{Essc} were larger during the ebb tide than the flood tide (studies E6 and E7). Figure 10.2 shows the variation of T_{Essc} and the integral time scales of streamwise velocity T_{Ex} over the tidal cycle E6TC2 (t = 76,380 to 127,500 s) and E7TC2 (t = 83,280 to 128,880 s). In Figure 10.2 the variation of a turbulence property (e.g. T_{Essc} in Figure 10.2) relative to the position in the tidal cycle are presented. Data for a tidal cycle are collected from one low water to the next and are then presented in a circular plot. The polar coordinates are r = turbulence characteristic (e.g. r = T_{Essc} (Figure 10.2)) and $\theta = 2\pi t/T$, where T = period of tidal cycle from first low water (LW1) to second low water (LW2); and

143

t = position in tidal cycle (t = 0 at LW1 and t = T at LW2). From LW1 (y = 0 on positive x-axis) the data progresses anticlockwise around the plot until LW2 (y = 0 on positive x-axis).

In Figure 10.2 the integral time scales T_{Essc} observed in the upper estuary (study E7) were slightly larger than those observed mid estuary (study E6). This was reflected in the median values of T_{Essc} = 0.065 and 0.109 s for the studies E6 and E7 respectively.
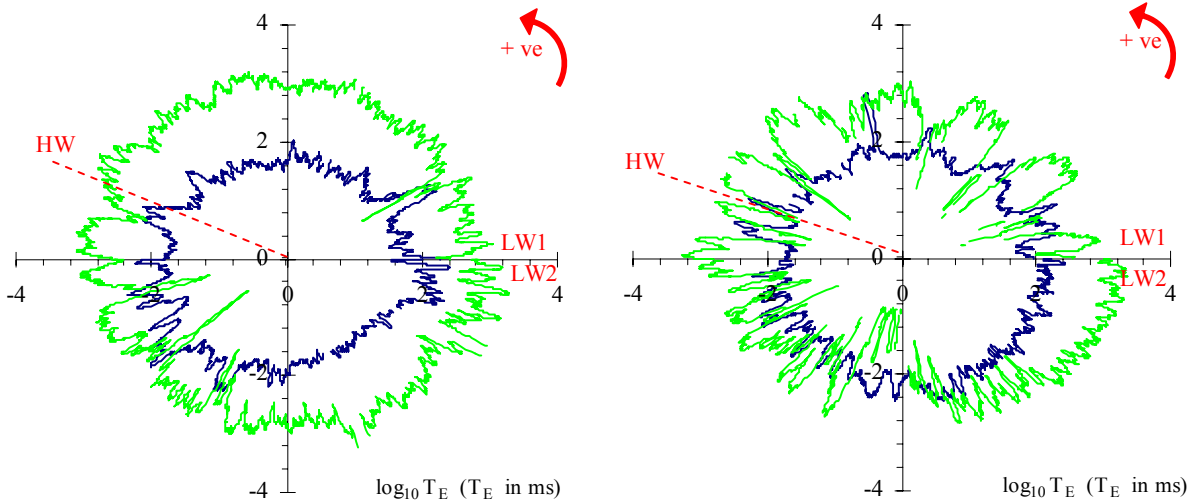
(A) Data collected for E6TC2 (t = 76,380 to 127,500 s) Site 2B (study E6).

(B) Data collected for E7TC2 (t = 83,280 to 128,880 s) Site 3 (study E7).

Figure 10.2 – Variation of integral time scales T_{Essc} and T_{Ex} (in milliseconds) at 0.2 m above bed for tidal cycles E6TC2 and E7TC2. Time scales calculated over 200 every 10 s along entire data set.

Legend: — Integral time scale of SSC T_{Essc}; — Streamwise integral time scale T_{Ex}.

A comparison of the integral time scale T_{Essc} to the integral time scales of horizontal velocities (T_{Ex} and T_{Ey}) showed that the variations of horizontal velocity and SSC integral time scales were out phase (e.g. Figure 10.2). For the field studies E6 and E7 the integral time scales of horizontal velocity were generally larger during the flood tide than the ebb tide. However, the integral time scales of SSC were generally larger during the ebb tide. This comparison also yielded the dimensionless time scales T_{Essc}/T_{Ex} and T_{Essc}/T_{Ey}. Table 10.2 presents the median values of T_{Essc}/T_{Ex} and T_{Essc}/T_{Ey} for the studies E6 and E7. These observations seemed to imply that the mixing coefficients of velocity and suspended sediment concentration could not be approximated by the same momentum exchange coefficient.

Table 10.2 – Median values of T_{Essc}/T_{Ex} and T_{Essc}/T_{Ey} for field studies E6 and E7.

Study	Estuarine zone	T_{Essc}/T_{Ex}	T_{Essc}/T_{Ey}
E6	middle (Site 2B)	0.09	0.06
E7	upper (Site 3)	0.31	0.11

10.2.3 Suspended sediment flux per unit area

The instantaneous suspended sediment flux per unit area ($q_S = SSC\ V_x$; q_S is positive downstream) in the ADV sampling volume (0.2 m above the bed) was calculated for the field studies E6 and E7. Figure 10.3 shows the time-averaged suspended sediment flux per unit area $\overline{q_S}$ and water depth as functions of time. In Figure 10.3 the tidal variations in $\overline{q_S}$ were an order of magnitude larger mid estuary (study E6) than those observed in the upper estuary (study E7).
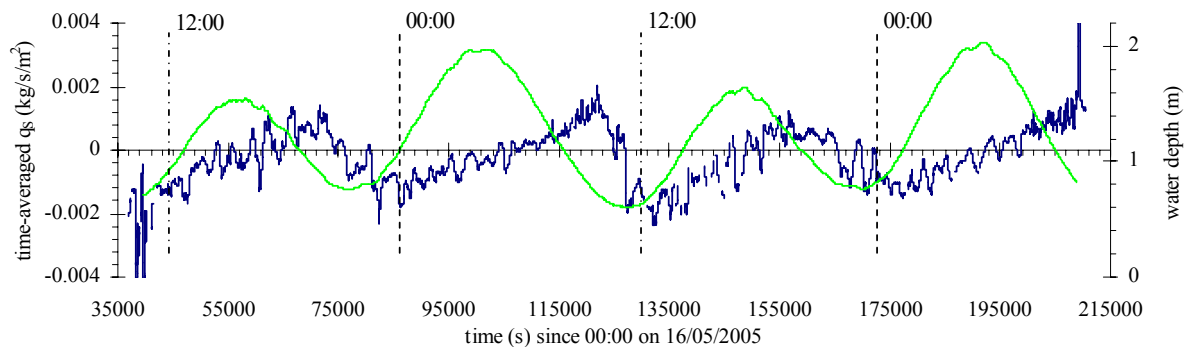
(A) Data collected at Site 2B, 10.7 m from left bank for study E6 (16-18/05/05).
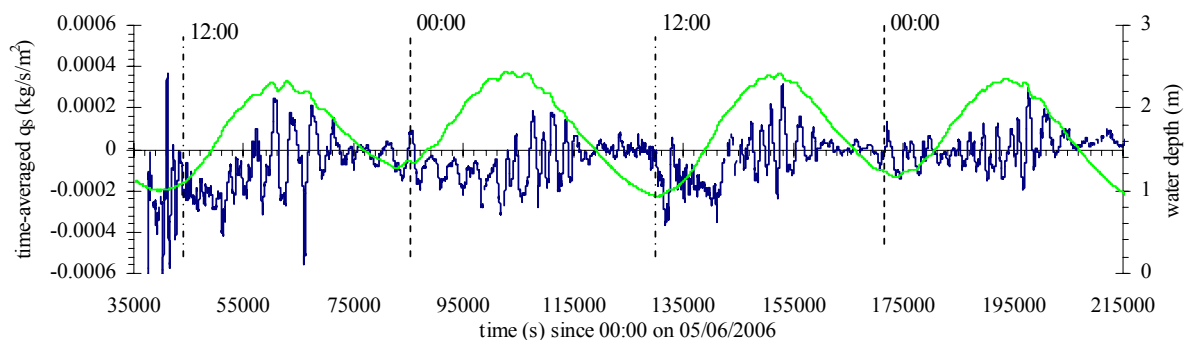
(B) Data collected at Site 3, 4.2 m from right bank for study E7 (5-7/06/06).

Figure 10.3 – Water depth and time-averaged suspended sediment flux per unit area $\overline{q_S}$ in ADV sampling volume 0.2 m above bed as functions of time. Data averaged over 200 s every 10 s along entire data set.

Legend: — water depth; — time-averaged suspended sediment flux per unit area $\overline{q_S}$.

The suspended sediment flux per unit area at 0.2 m above the bed seemed to vary with the long period oscillations observed for neap tidal conditions (studies E6 and E7). Figure 10.3 showed some oscillation periods of $\overline{q_S}$ between 2,000 to 5,000 s, which were similar to long period oscillations of velocity and water level discussed in Sections 7.3 and 8.4. In both middle and upper estuarine zones, the magnitude of $\overline{q_S}$ was larger during the flood tide than that of the ebb tide. This was reflected in the median values of $\overline{q_S}$ = –0.0002 and –0.00003 kg/s/m^2 for the studies E6 and E7 respectively.

10.2.3.1 *Suspended sediment flux per unit area and bed shear stress*

For the field studies E6 and E7, the variations of the time-averaged suspended sediment flux per unit area $\overline{q_S}$ were similar to those of the time-averaged bed shear stress $\overline{\tau_b}$. The bed shear stress is an important property in the study of sediment transport as it determines the quantity and size of sediment suspended (e.g. Fredsoe and Diegaard (1992)). Here, the bed shear stress was approximated using the magnitude of the horizontal velocity U_{xy} at 0.2 m above the bed (Appendix B):

$$\tau_b = 0.5 \, \rho \, C_D \, U_{xy}^2 \tag{10.1}$$

$$C_D = (\kappa / \ln(z_r / z_o))^2 \tag{10.2}$$

where ρ = water density; C_D = coefficient of friction (C_D = 0.00106 for studies E6 and E7); $U_{xy} = \sqrt{V_x^2 + V_y^2}$ is the horizontal velocity magnitude in the ADV sampling volume 0.2 m above bed; κ = von Karman constant (κ = 0.41); z_r = sampling elevation above the bed; z_o = (grain diameter)/30; and median grain diameter at Sites 2B and 3 was approximately 0.02 mm for the studies E6 and E7. For these calculations a logarithmic velocity profile was assumed and C_D is approximated by Equation 10.2 (Bricker et al. (2005)). Figure 10.4 shows the bed shear stress $\overline{\tau_b}$ and magnitude of suspended sediment flux per unit area $\left|\overline{q_S}\right|$ as functions of time. In Figure 10.4 the magnitude of suspended sediment flux per unit area $\left|\overline{q_S}\right|$ seemed to vary with the magnitude of the bed shear stress for the studies E6 and E7. Mid estuary (study E6) the correlation between $\left|\overline{q_S}\right|$ and $\overline{\tau_b}$ was R = 0.66, while the correlation in the upper estuary (study E6) was slightly lower (R = 0.50). This lower correlation between $\left|\overline{q_S}\right|$ and $\overline{\tau_b}$ observed for the field study E7 was possibly related to the lower velocities, greater stratification and/or increased influence of the long period oscillations observed in the
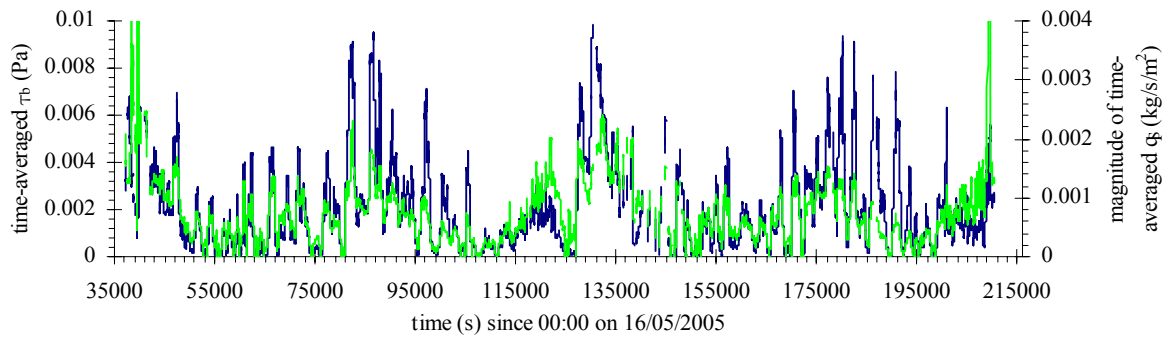
upper estuary.

(A) Data collected at Site 2B, 10.7 m from left bank for study E6 (16-18/05/05).
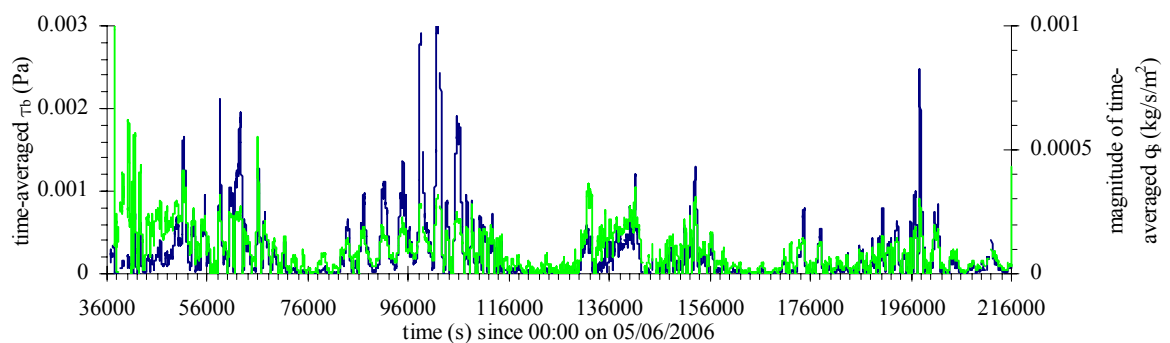
(B) Data collected at Site 3, 4.2 m from right bank for study E7 (5-7/06/06).

Figure 10.4 – Time-averaged bed shear stress $\overline{\tau_b}$ and magnitude of suspended sediment flux per unit area $\left|\overline{q_S}\right|$ in ADV sampling volume 0.2 m above bed as functions of time. Data time-averaged over 200 s every 10 s along entire data set.

Legend: — magnitude of sediment flux per unit area $\left|\overline{q_S}\right|$; — bed shear stress $\overline{\tau_b}$.

10.3 CORRELATION BETWEEN PHYSIO-CHEMISTRY AND TURBULENCE

A spectrum analysis was undertaken on the physio-chemistry data measured by a YSI6600 probe for the field studies E5, E6 and E7. In each field study the probe sensor was 0.1 or 0.4 m above the bed and 0.3 m beside the 3D-ADV. These physio-chemistry spectra were compared to the spectra of the time-averaged velocity data collected by the 3D-ADV (10 MHz). The aim of this comparison was to investigate similar oscillation periods within the velocity and physio-chemistry data. The comparison of the velocity and physio-chemistry spectra was performed by the cross-correlation of two spectra, using a technique outlined in Appendix I. Previous scientific studies (e.g. Coy et al. (1997), Arnold and Reilly (1998)) used the cross-correlation of spectra to isolate common peaks in energy spectral density. These studies showed that good correlation in the spectra of two independent data sets

147

indicated a common chemical or oscillation frequency within these data sets. In this study some correlation between the spectrum of the velocity component and spectrum of the physio-chemistry property might indicate that turbulent momentum mixing of that water quality property occurred within that frequency range. A possible correlation between two spectra was defined as $|R| > 0.5$. No large negative correlations (R < - 0.5) were observed for the field studies E5, E6 and E7.

In this study, only oscillation periods between 7,200 and 240 s are discussed because of a lack of resolution outside this range. The lower limit (7,200 s) was restricted by the 25 hour investigation period of the study E5, while the higher limit (240 s) was set by the 12 s sampling frequency of the YSI6600 probe during the studies E6 and E7. Velocity data were averaged over 200 s and sampled every 6 s (study E5) and 12 s (studies E6 and E7) along the entire data set. This approach provided time-averaged velocity data sampled at the same frequency as the physio-chemistry data. Figure 10.5 shows some examples of the cross-correlation analysis for the spectra of time-averaged velocity and some physio-chemistry properties in the field studies E5, E6 and E7. In Figure 10.5 the horizontal axis presents the frequency in Hz with a logarithmic scale and the correlation coefficient R is on the vertical axis. Further examples of the correlation between the spectra of water level and each velocity component with the spectra of the measured physio-chemistry properties are shown in Appendix I.

Figure 10.5 shows that some correlation occurred between the oscillations in time-averaged streamwise velocity and the oscillations of physio-chemistry properties shown. For example, in Figure 10.5A some correlation was observed between time-averaged streamwise velocity and chlorophyll a level oscillations for the period ranges of 5,300 to 3,200 s and 600 to 420 s for the field study E7. The stronger correlation between the time-averaged streamwise velocity and the physio-chemistry spectra about the frequency of 0.00002 Hz (highlighted in Figure 10.5A) indicated that the physio-chemical properties shown should vary with the tides. The variation of water temperature, pH, dissolved oxygen and chlorophyll a levels with the tides was noted in Section 6.2.2.

Table 10.3 lists the oscillation period ranges of each physio-chemistry property between 7,200 and 240 s which showed some correlation with momentum. In Table 10.3, some correlation between the momentum fluctuations and oscillations in all physio-chemistry properties was observed for oscillation periods between 7,200 and 240 s. This indicated that for the studies E5, E6 and E7, turbulent momentum mixing seemed to be associated with variations in most physio-chemistry properties for oscillation periods as small as 240 s.
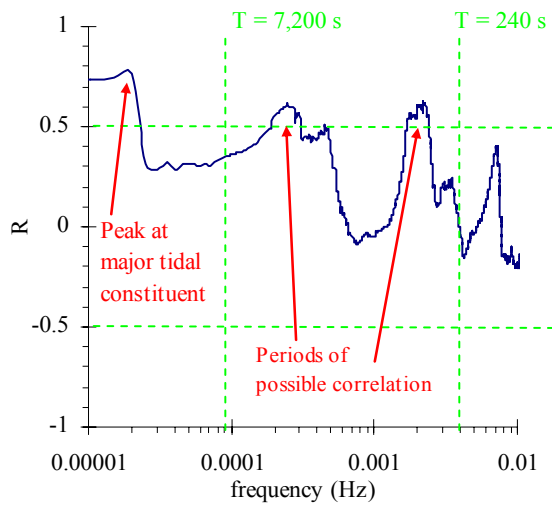
(A) $\overline{V_x}$ and chlorophyll a levels (study E7).
Data collected 0.4 m above bed at Site 3.
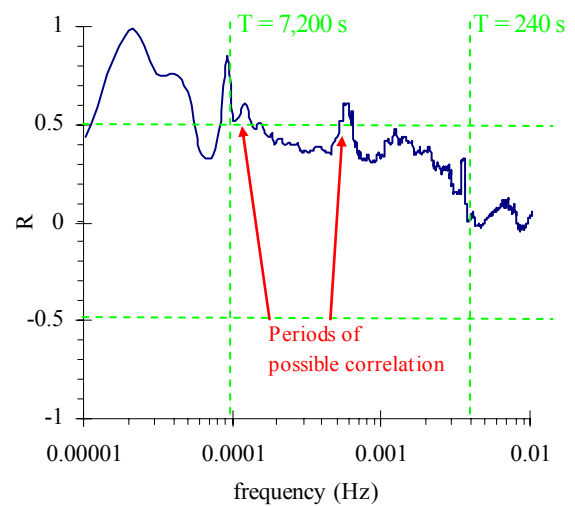
(B) $\overline{V_x}$ and dissolved oxygen (study E5).
Data collected 0.1 m above bed at Site 2B.
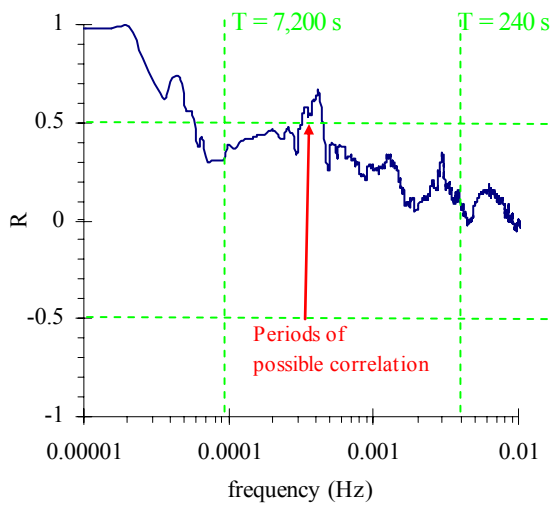
(C) $\overline{V_x}$ and water temperature (study E6).
Data collected 0.4 m above bed at Site 2B.
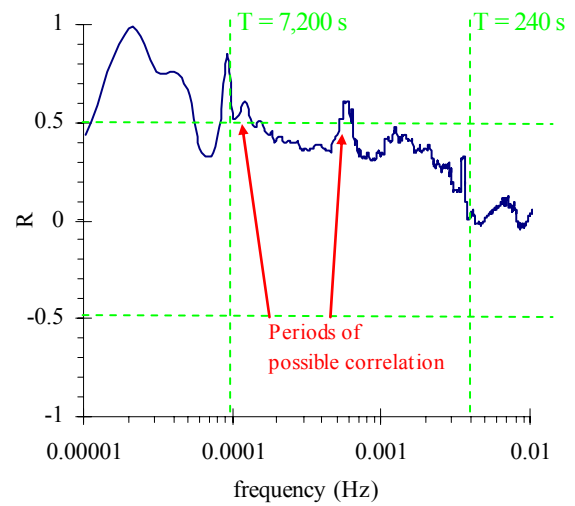
(D) $\overline{V_x}$ and pH (study E5). Data collected
0.1 m above bed at Site 2B.

Figure 10.5 – Some cross-correlation values for spectra of time-averaged velocity and physio-chemistry for field study E5 (8-9/03/05), E6 (16-18/05/05) and E7 (5-7/06/06). Cross-correlation window size was 512 data points.

The impact of turbulent momentum on the mixing of physio-chemistry properties could exist for smaller oscillation periods. However, this investigation was limited by the sampling frequency of the YSI6600 probe. Theoretically, turbulent momentum could influence the variation of physio-chemical properties down to the viscous level through turbulent energy dissipation.

Table 10.3 – Oscillation periods with some correlation between momentum and physio-chemistry for field studies E5, E6 and E7.

Momentum correlates with:	Study E5 Oscillation periods (s)	Study E6 Oscillation periods (s)	Study E7 Oscillation periods (s)
water temperature	7,200 to 4,510 3,460 to 1,720 450 to 420	3,310 to 2,240	5,780 to 1,850 1,710 to 1,320 580 to 500
conductivity	7,200 to 1,000 900 to 700 500 to 280	4,570 to 2,830 1,340 to 1,240	4,650 to 1,790
chlorophyll a levels	7,200 to 500	##	7,200 to 2,600 620 to 400
dissolved oxygen	7,200 to 610	7,200 to 2,490 980 to 840	4,950 to 3,880 2,240 to 1,400 680 to 580
pH	6,900 to 1,460 450 to 380	4,830 to 2,710 1,360 to 1,250	5,760 to 1,350 590 to 500
turbidity	5,010 to 580	##	2,270 to 560

Note: Momentum from fluctuations in time-averaged velocity components and water level; ##: not correlated for oscillation periods between 7,200 and 240 s.

10.4 IMPACT OF A RAINSTORM ON WATER QUALITY

Freshwater inflow into subtropical estuaries can come from two main sources. These are: natural sources such as stream flow and rainstorms; and man made sources such as discharges from sewage treatment plants or industry. The most significant impact on the water quality and turbulence should come from large rainstorms. In a small subtropical estuary however, significant rainfall is limited to a small number of days each year (Section 3.2). When a rainstorm does occur, the hydrodynamics and water quality of small subtropical estuaries are altered for a period of up to several days after the rainstorm (Digby et al. (1993)).

For the field study E8 (28/08/06), 30 mm of rain fell just before the commencement of the field study E8. This section uses the vertical profiles of the study E8 to discuss some of the possible influences this relatively small rainstorm event had on the water quality at Eprapah Creek. For the study E8 the only obvious change in physio-chemistry was to the conductivity (Section 6.2.6). However, the vertical profile data collected during the study E8 differed from that measured on 7/06/06 for the study E7 several months earlier. Table 10.4 presents the water quality properties recorded by the YSI6920 probe at Sites 1, 2 and 3 for the studies E7 and E8. In Table 10.4 the water quality properties presented were averaged over the depth profile.

Table 10.4 – Depth-averaged water quality data collected during field studies E7 and E8.

Site	Water quality property	Study E7	Study E8		
			A (RF+ 3.5 hrs)	B (RF+ 4.5 hrs)	C (RF+ 6 hrs)
1	Temperature (C)	17.5	19.5	20.1	20.8
	Conductivity (mS/cm)	51.6	40.5	48.7	50.0
	pH	8.1	7.9	8.2	8.2
	DO (% saturation)	88.7	81.7	84.6	90.2
	Turbidity (NTU)	7.5	20.0	12.4	7.1
2	Temperature (C)	18.8	19.2	19.5	20.1
	Conductivity (mS/cm)	47.8	32.6	36.9	42.2
	pH	7.9	7.6	7.8	7.9
	DO (% saturation)	80.2	79.9	82.5	86.6
	Turbidity (NTU)	10.5	31.3	20.7	14.3
3	Temperature (C)	18.5	18.0	18.4	18.6
	Conductivity (mS/cm)	44.0	8.3	16.5	19.0
	pH	6.9	7.0	8.2	7.0
	DO (% saturation)	25.9	80.9	72.0	67.7
	Turbidity (NTU)	6.3	29.3	25.6	26.6

Note: RF: time of rainfall event (05:30 on 28/08/06); DO: dissolved oxygen.

The three sets of vertical profile data (E8A, E8B and E8C) presented in Table 10.4 were collected 3.5, 4.5 and 6 hours after the rainfall event occurred at 05:30 on 28/08/06. In Table 10.4 the conductivity decreased and the turbidity increased throughout the estuary after the rainstorm. However, as the time passed after the rainstorm the water quality properties at Site 1, followed by those at Site 2, began to return to values similar to those observed in study E7. The physio-chemistry at Site 3 seemed to take the longest time to recover after the rainstorm event. Of special note was the increased dissolved oxygen levels observed at Site 3 for the study E8. The dissolved oxygen levels at Site 3 were low during all other field studies at Eprapah Creek. This could indicate that the freshwater inflow from the rainstorm flushed the upper estuary, improving the water quality in the upper estuary for at least a small duration.

10.5 DISCUSSION

Some similarities in the fluctuations of the turbulence properties and water properties (e.g. SSC and chlorophyll a levels) were observed at Eprapah Creek. This indicated that all water properties investigated at Eprapah Creek underwent some turbulent mixing. The turbulent mixing of the measured physio-chemistry properties and mixing and dispersion of scalar properties (e.g. SSC) is dependent on the turbulence properties observed. If the turbulence properties observed vary drastically from the assumptions used in the modelling of turbulent

mixing, then these models will not provide reliable results.

The measurement of suspended sediment concentration using an ADV provided the opportunity to study the fluctuations of velocity and SSC in the same small sampling volume. Here the suspended sediment concentration could be used as a proxy to investigate the mixing and dispersion of some scalar properties. For the neap tide data collected in the middle and upper estuarine zones of Eprapah Creek the integral time scales of velocity and suspended sediment concentration were different in the same sampling volume (Section 10.2.2). This seemed to imply that the mixing coefficients of velocity and suspended sediment concentration could not be approximated by the same momentum exchange coefficient. Section 10.5.1 highlights that turbulent mixing parameters such as the momentum exchange coefficient should also not be assumed constant over the tidal cycle.

This study in a typical small subtropical estuary (Eprapah Creek) found two distinct sets of turbulence properties mid estuary under spring and neap tidal conditions, with the magnitude of many turbulence properties up to an order of magnitude larger for spring tides. Further, substantial differences in the turbulence properties in the middle and upper estuaries under similar neap tidal conditions were observed, with reduced turbulence in the upper estuary. Cross-correlation of the spectra of time-averaged velocities and physio-chemistry properties showed similar fluctuation periods in the velocity and physio-chemistry properties. This seemed to indicate that some momentum mixing of the water properties occurred at Eprapah Creek. Therefore the different turbulent properties observed under spring and neap tidal conditions, and in the middle and upper estuarine zones, could have a substantial influence on the mixing of the water properties in small subtropical estuaries. These different turbulence properties must be considered when modelling the mixing and dispersion in small subtropical estuaries.

10.5.1 Turbulent mixing parameters

Some estimates of the momentum exchange coefficient υ_T and mixing length l_m were derived for the field studies E4 and E5. These provide some information on the turbulent mixing mid estuary in Eprapah Creek. The "eddy viscosity" υ_T is the coefficient of momentum exchange between the streamwise and vertical directions (Equation 10.3). During momentum exchanges, the mixing length l_m is a local property that characterises the dimensions for the lumps of fluid which move in the normal direction (Equation 10.4). The momentum exchange coefficient and mixing length were approximated here by:

$$\upsilon_T \approx \left| \frac{\overline{v_x v_z}}{\left(\partial \overline{V_x} / \partial z \right)^2} \right| \qquad\qquad (10.3)$$

$$l_m \approx \sqrt{\left| \frac{\overline{v_x v_z}}{\left(\partial \overline{V_x} / \partial z \right)^2} \right|} \qquad\qquad (10.4)$$

where z = vertical elevation; $\overline{V_x}$ = time-averaged streamwise velocity; v_x = instantaneous fluctuations of streamwise velocity; and v_z = instantaneous fluctuations of vertical velocity. If the sampling volume is close to the bed then it is reasonable to assume that $\partial \overline{V_x} / \partial z \equiv \overline{V_x} / z$ since $\overline{V_x}(z=0) = 0$. For the field studies E4 and E5 the sampling volume of the 3D-ADV (10 MHz) were located at 0.05 and 0.10 m above the bed respectively (Table 3.2). Similar estimates for the field studies E6 and E7 could not be undertaken because the 2D-microADV (16 MHz) was located closest to the bed and did not sample the vertical velocity.

Figure 10.6 shows the momentum exchange coefficient υ_T and the dimensionless mixing length l_m / z as a function of time-averaged streamwise velocity (positive downstream). In Figure 10.6A, the momentum exchange coefficient υ_T seemed a function of the time-averaged streamwise velocity, despite some scatter during the ebb tides. For the studies E4 and E5, the values of momentum exchange coefficient were generally larger on the flood tide than the ebb tide. Kawanisi (2004) also observed larger values of the "eddy viscosity" during the flood tide in an estuarine tidal channel in Japan. For the field trips E4 and E5 the values of the momentum exchange coefficient were typically between 0.00001 and 0.001 m^2/s. These values were comparable to momentum exchange coefficient values observed in estuarine tidal channels by Kawanisi (2004) and Ralston and Stacey (2005).

In Figure 10.6B the mixing length seemed to be an inverse function of the streamwise velocity, with l_m largest about $\overline{V_x}$ = 0. For the studies E4 and E5 the mixing length seemed larger during the flood than ebb tides. The mixing length l_m data were between 0.002 and 0.06 m for both studies.

For the field studies E4 and E5 the observations of these turbulent mixing parameters showed a large scatter of data values spread over several orders of magnitude and were associated with relatively rapid fluctuations with time. This has some serious implications for the modelling of momentum mixing in estuaries when the "mixing coefficients" are assumed to be constant. In the Eprapah Creek estuarine zone such an assumption is simply untrue.
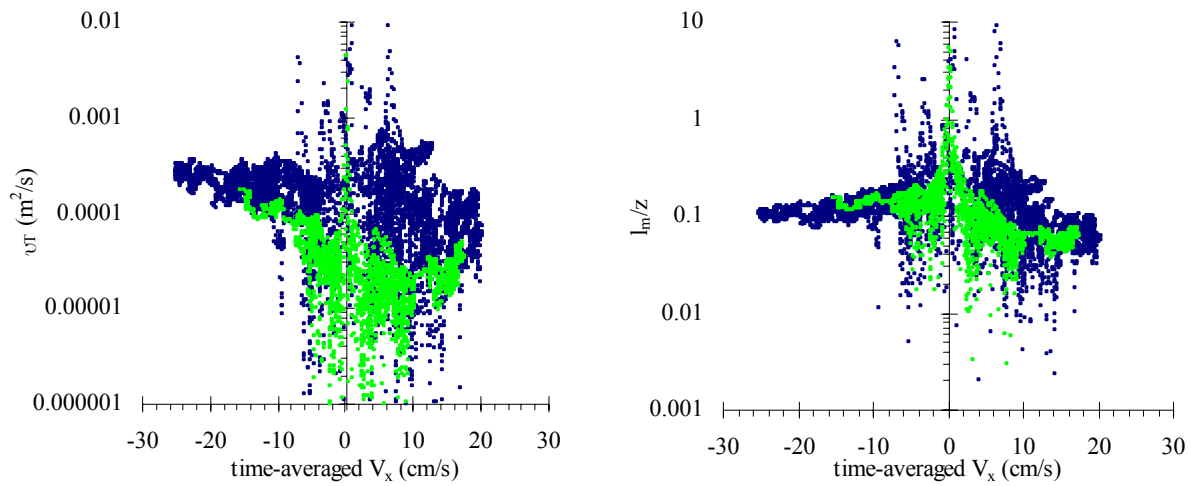
(A) Momentum exchange coefficient υ_T.   (B) Dimensionless mixing length l_m/z.

Figure 10.6 – Momentum exchange coefficient υ_T and dimensionless mixing length l_m/z as functions of time-averaged streamwise velocity (positive downstream). Data collected by 3D-ADV (10 MHz) located 0.05 m (study E4) and 0.1 m (study E5) above bed, 10.7 m from left bank at Site 2B Eprapah Creek for field studies E4 and E5. Values calculated over 5,000 data points every 10 s along entire length of data sets.

Legend: [•] data from study E4; [•] data from study E5.

11 CONCLUSION

11.1 KEY OUTCOMES

To date the limited number of studies into the turbulence properties of estuaries have been linked with a lack of suitable instrumentation to collect turbulent velocity measurements with fine spatial and temporal resolutions. The present study showed that the acoustic Doppler velocimetry was well suited for the measurement of turbulence properties in small estuarine systems. Acoustic Doppler velocimeters enabled turbulence measurements in shallow waters (depth < 0.5 m at low tides) for a range of field conditions. However, acoustic Doppler velocimetry data must undergo a thorough post-processing procedure before any turbulence analysis is undertaken.

Previous studies of turbulence in estuaries were mostly conducted for relatively short periods (up to 6 hours) and by collecting data over long periods in bursts of several minutes. A unique aspect of this study was the continuous collection of turbulence data at high frequency ($f_{scan} \geq 25$ Hz) for relatively long periods (T_{study} up to 50 hours). This approach characterised the estuarine turbulence properties for up to two complete semi-diurnal tidal cycles. The data analysis showed that the continuous measurement of high frequency turbulence data was essential to characterise accurately the rapid fluctuations of turbulence in an estuary.

The field data showed that the turbulence flow properties were highly fluctuating in a small estuary. All turbulence properties exhibited large and rapid fluctuations over the investigation period of each field study. The variations in time scales were related to both the instantaneous local flow properties and the tidal fluctuations. Many turbulence properties showed an asymmetrical response to the tidal forcing, especially under spring tidal conditions. Large turbulent velocity fluctuations were however observed throughout all investigation periods, including during the slack tides. Substantial fluctuations in the normal and tangential Reynolds stresses were observed in the middle and upper estuarine zones. The turbulent velocity data showed some non-Gaussian behaviour and the Reynolds stresses were non-Gaussian throughout all investigation periods.

The turbulence properties in two distinct estuarine types were compared: a small coastal plain type, Eprapah Creek in Australia, and a large tidal lake with a restricted entrance, Hamana Lake in Japan. Variations of the water depth, and streamwise and transverse velocities were different in the two estuarine types, yet some similar tidal patterns were observed in terms of the turbulence properties close to the bed. This suggested that the turbulence properties observed in one small subtropical estuary may be representative of those found in similar small subtropical estuaries.

Some field studies were performed mid estuary under spring and neap tidal conditions. The data showed two distinctly different turbulence responses for spring and neap tides. During spring tides, the magnitudes of all turbulence properties were up to an order of magnitude larger than for neap tides. The turbulence properties showed some increased tidal asymmetries under spring tidal conditions. This finding (i.e. the difference between spring and neap tides) does have some serious implications for the modelling of small subtropical estuaries and the predictive calculations of mixing. For example, the estimate of discharge dispersal and mixing using spring tidal conditions may drastically over predict the mixing efficiency of the estuarine system.

The ratio of local tidal amplitude and local mean depth a_1/h_1 was introduced in order to characterise the local turbulence properties for a certain tidal range. A critical value of the ratio a_1/h_1 was 0.5, which corresponds to the local tidal range being equal to the local mean depth. If the tidal range was greater than the local mean depth (i.e. $a_1/h_1 > 0.5$), a more asymmetrical tidal response and increased turbulence property magnitudes were observed. A comparison of the turbulence properties in Eprapah Creek and Hamana Lake showed similar tidal patterns for $a_1/h_1 < 0.5$.

Two field studies were conducted for approximately 50 hours under neap tidal conditions in the middle and upper estuarine zones. A comparison of these two data sets showed that the turbulence properties in the middle and upper estuaries differed substantially. In the middle estuary the magnitude of turbulence properties were up to an order of magnitude larger than those observed in the upper estuary. In the upper estuary, the influence of the tides on the variation of the turbulence properties was smaller than that mid estuary. The distinct turbulence characteristics in the middle and upper estuarine zones does have some implications for the modelling in small subtropical estuaries, suggesting some drastically weaker mixing characteristics in the upper estuarine zone.

For all field studies conducted at Eprapah Creek some long period oscillations were observed in the water level and velocity data. These long period oscillations had periods similar to resonance periods generated both internally and externally. The period and magnitude of these long period fluctuations differed between spring and neap tidal conditions. Under both spring and neap tidal conditions, the long period oscillations had a significant impact on the velocity fluctuations and turbulence properties. These long period oscillations seemed responsible for the formation of large transverse velocity cells (e.g. reverse cell secondary currents) in the middle and upper estuarine zones.

11.2 APPLICATIONS AND MODELLING

The modelling of the mixing and dispersion processes in estuaries is difficult because of the complexity of these systems. Certain assumptions are commonly used in estuarine models to simplify the calculations. Typically the most common assumptions are that:

- The flow is one-dimensional, which implies that the velocity direction and magnitude are uniform over each cross-section and secondary currents are neglected.
- The water density is constant.
- The variation of bed friction is small along the length of the estuary.
- Water quality properties are well-mixed over the cross-section.
- Mixing and dispersion coefficients are constant and independent of time and tidal conditions.
- The tidal variation is sinusoidal.
- Solute water quality properties such as dissolved oxygen, pH vary in a similar fashion to the conductivity.
- Particulate water quality properties such as chlorophyll a levels vary in a similar fashion to the suspended sediment concentration.
- Mixing coefficients are approximated by the momentum exchange coefficient.

The field studies at Eprapah Creek suggested that most of these assumptions were untrue. At Eprapah Creek the velocities in the cross-section were not uni-directional. Significant variations of the transverse velocity were observed under spring and neap tidal conditions. For example, with two measurement points (0.2 and 0.4 m above the bed), large differences in the direction and magnitude of the horizontal velocity components were observed in both middle and upper estuarine zones.

The water density in small estuarine systems was not constant in the water column. This seemed especially true in the upper estuarine zone of Eprapah Creek where some stratification was observed. For all field studies the water density varied with the tides and some smaller time scales related to momentum fluctuations. In Southeast Queensland many small subtropical estuaries are used to disperse reprocessed water (e.g. sewage treatment plant discharge) and water density variations will occur as the freshwater interacts with the estuarine waters.

In small subtropical estuaries the bottom composition and shape vary substantially throughout the estuary. Along the estuary, the bed composition can change rapidly from fine silt to relatively large and rough rocks, then to gravel within 1 to 10 metres. The mean depth and width of each cross-section along the estuary are distinct and can vary substantially within a

small longitudinal distance. These different bed compositions and shapes along a small subtropical estuary substantially change the local friction factors.

A field study conducted mid estuary under neap tidal conditions showed both transverse and vertical gradients of water temperature and conductivity data. In the upper estuarine zone vertical stratification of all physio-chemistry properties was observed. These field results showed that the assumption of well-mixed physio-chemistry properties was not valid for the upper estuarine zone in a small subtropical estuary and should only be used with extreme caution in the lower and middle estuaries.

Many river and estuarine models assume that mixing coefficient parameters such as eddy viscosity and mixing length are constant. This study showed that in small subtropical estuaries these mixing parameters varied by up to three orders of magnitude during the tidal cycle. Mid estuary, both the eddy viscosity and mixing length varied with the tides, therefore the assumption that the mixing coefficient parameters are constant over the tidal cycle in a small subtropical estuary is simply untrue.

In this study the suspended sediment concentration data were used as a proxy to investigate the mixing and dispersion of some scalar properties. For the data collected in a small subtropical estuary the integral time scales of the velocity and suspended sediment concentration were different in the same sampling volume. This seemed to imply that the mixing coefficients of velocity and suspended sediment concentration could not be approximated by the same momentum exchange coefficient.

The use of a simple sinusoidal model for the variations of the tides in Southeast Queensland seemed unreasonable because the tides of this region showed some asymmetries in amplitude and period. In Southeast Queensland, diurnal inequalities were observed in both the spring and neap tides. Water level measurements in both Moreton Bay and Eprapah Creek showed long period oscillations in the water level that seemed related to the resonance of the tides within Moreton Bay. These long period oscillations of the water level caused large fluctuations in the horizontal velocities, which then had a significant impact on the turbulence flow properties in the middle and upper estuarine zones. Water level variations based on field data collected in and around the estuary under investigation should be used to accurately model the turbulence and mixing properties in subtropical estuaries.

For all field studies at Eprapah Creek the flow motion was characterised by a strong flood tide. In small subtropical estuaries, the flow properties are dominated by the tides for the majority of the year, because of a lack of natural freshwater inflow. This has serious implications for the dispersion of introduced substances within the estuary, which need to be incorporated into models of small subtropical estuaries.

Field data collected in this investigation seemed to validate the assumptions that the solute and particulate water quality properties vary with the conductivity and suspended sediment concentration respectively. In all field studies at Eprapah Creek the values of dissolved oxygen, pH and conductivity (solute properties) were largest about high tide and smallest about low tides. This suggested that these solute water quality properties varied in a similar fashion over the tidal cycle. The measured particulate properties such as suspended sediment concentration, turbidity and chlorophyll a levels were all largest about the low tides and smallest about the high tides. This indicated that these particulate water quality properties showed similar tidal trends.

11.3 FUTURE STUDIES

The present study showed the complex and highly fluctuating nature of the turbulent flow properties in small subtropical estuarine systems. Many tidal trends in the turbulence properties observed close to the bed were similar for several estuarine types. However, the scope of the present study was limited by the period of the project (3 years) and the conditions provided by Nature during the field studies.

For the field studies performed under neap tidal conditions in the middle and upper estuarine zones, some anomalies were observed in the measured water quality and turbulence properties. These anomalies seemed to occur about the same time as the morning and evening peak discharges from the sewage treatment plant. It is unclear at present whether these anomalies were related to the freshwater discharged from the treatment plant, because no comprehensive data on the dispersion behaviour has been collected. This study showed that the flow properties in small subtropical estuaries were different to those of larger coastal plain systems and therefore these smaller estuaries need to be modelled differently. An in-depth study of the dispersion behaviour of man made substances such as STP discharge in small subtropical estuaries is therefore required in order to understand and model the impact of such discharges.

This study showed some understanding on the impact of tidal forcing on the turbulence properties in a small subtropical estuary. However, the influence of natural freshwater inflow on the turbulence properties was not studied, because a rainstorm did not occur while the high frequency turbulence and physio-chemistry instrumentation were deployed. Some data collected during a student field study showed that a small rainstorm event had a significant impact on the physio-chemistry in a small subtropical estuary, therefore an investigation into the turbulence properties of a small estuary during and after a rainstorm is required.

159

The turbulence properties observed under spring tidal conditions in small subtropical estuaries were distinctly different from those observed for neap tides. These turbulence properties were also different from those observed under spring tidal conditions in other estuaries. To date only a few turbulence investigations were conducted mid estuary under spring tidal conditions. More field investigations during spring tidal conditions are required to study in-depth the mechanisms behind the distinct turbulence properties observed when $a_1/h_1 > 0.5$.

No spring tide field study was undertaken in the upper estuarine zone of small subtropical estuaries. More studies are required there.

The study of the turbulence properties of small subtropical estuaries was limited to one system Eprapah Creek. A comparative study of the turbulence properties in Eprapah Creek and Hamana Lake showed the tidal trends in turbulence to be similar, despite the distinct bathymetry and hydrodynamics of each system. Some field studies in other small subtropical estuaries are therefore required in order to validate the observations made in Eprapah Creek.

A comparative field study between the turbulent velocity data collected by an acoustic Doppler velocimeter and by independent velocity instrumentation is recommended. Such a study would allow further validation of the turbulence data collected using acoustic Doppler velocimetry. This data set could also be used to optimise the technique for post-processing the ADV turbulence data.

BIBLIOGRAPHY

ANZECC (2000) – <u>Australia and New Zealand Guidelines for Fresh and Marine Water Quality</u> – Australia and New Zealand Environment and Conservation Council (ANZECC) and Agriculture and Resource Management Council of Australia and New Zealand (ARMCANZ), Paper No. 4, October 2000

Arnold, R.J. and Reilly, J.P. (1998) – <u>Fingerprint matching of E. Coli strains with matrix assisted laser desorption/ionization time-of-flight mass spectrometry of whole cells using a modified correlation approach</u> – Rapid Communications in Mass Spectrometry, 12, pp. 630-636

Bathurst, J.C., Thorne, C.R. and Hey, R.D. (1977) – <u>Direct measurements of secondary currents in river bends</u> – Nature, 269, pp. 504-506

Bendat, J.S. and Piersol, A.G. (1971) – <u>Random Data: Analysis and Measurement Procedures</u> – Wiley-Interscience, Jon Wiley & sons, New York, USA, 407 pages

Bendat, J.S. and Piersol, A.G. (1993) – <u>Engineering Applications of Correlation and Spectral Analysis</u> – Second edition, Wiley-Interscience, Jon Wiley & sons, New York, 458 pages

Benilov, A.Y. and Filyushkin, B.N. (1970) – <u>Application of methods of linear filtration to an analysis of fluctuations in the surface layer of the sea</u> – Izv., Atmospheric and Oceanic Physics, (trans, Kaufman, A.B.), 6(8), pp. 810-819

Bowden, K.F. (1962) – <u>Measurements of turbulence near the sea bed in a tidal current</u> – Journal of Geophysical Research, 67(8), pp. 3183-3186

Bowden, K.F. and Howe, M.R. (1963) – <u>Observations of turbulence in a tidal current</u> – Journal of Fluid Mechanics, 17(2), pp. 271-284

Bowden, K.F. and White, R.A. (1966) – <u>Measurements of the orbital velocities of sea waves and their use in determining the directional spectrum</u> – Geophysical Journal of the Royal Astronomical Society, 12, pp. 33-54

Bradshaw, P. (1971) – <u>An Introduction to Turbulence and its Measurement</u> − Pergamon Press, Oxford, UK, 218 pages

Bricker, J.D., Inagaki, S. and Monismith, S.G. (2005) – <u>Bed drag coefficient variability under wind waves in a tidal estuary</u> – Journal of Hydraulic Engineering, 131(6), pp. 497-508

Chanson, H. (2003) – <u>A hydraulic, environmental and ecological assessment of a sub-tropical stream in Eastern Australia: Eprapah Creek, Victoria Point QLD on 4 April 2003</u> – Report CH52/03, Department of Civil Engineering, University of Queensland, Australia, June, 189 pages, (ISBN 1864997044)

Chanson, H., Brown, R., Ferris, J., Ramsay, I. and Warburton, K. (2005a) – <u>Preliminary measurements of turbulence and environmental parameters in a sub-tropical estuary of eastern Australia</u> – Environmental Fluid Mechanics, 5, pp. 553-575

Chanson, H., Trevethan, M. and Aoki, S. (2005b) – <u>Acoustic Doppler velocimetry (ADV) in a small estuarine system. Field experience and "de-spiking"</u> – Proceedings of 2005 IAHR Congress, Seoul Korea, Sept. 2005, pp. 3954-3966

Chanson, H., Takeuchi, M. and Trevethan, M. (2006) – <u>Using turbidity and acoustic backscatter intensity as surrogate measures of suspended sediment concentration. Application to a sub-tropical estuary (Eprapah Creek)</u> − Report No. CH60/06, Division of Civil Engineering, The University of Queensland, Brisbane, Australia, 26 pages, (ISBN 1864998628)

Cioffi, F., Gallerano, F. and Troiani, G. (2006) – <u>An experimental study of turbulence statistics in a lagoon</u> – Journal of Hydraulic Research, 44(2), pp. 155-169

Coy, S.L., Jacobson, M.P. and Field, R.W. (1997) – <u>Identifying patterns in multicomponent signals by extended crosscorrelation</u> – Journal of Chemical Physics, 107(20), pp. 8357-8369

Dean, R.G. (1965) – <u>Stream function representation of nonlinear ocean waves</u> – Journal of Geophysical Research, 70(18), pp. 4561-4572

Digby, M.J., Saenger, P., Whelan, M.B., McConchie, D., Eyre, B., Holmes, N. and Bucher, D. (1999) − <u>A Physical Classification of Australian Estuaries</u> − National River Health Program, Urban sub-program, Report No. 9, LWRRDC, Occasional Paper, 16/99

Dyer, K. R. (1973) – <u>Estuaries: A Physical Introduction</u> – John Wiley and Sons, New York, USA, 140 pages

Dyer, K.R. (1997) – <u>Estuaries: A Physical Introduction</u> – Second Edition, John Wiley and Sons, New York, USA, 195 pages

Fischer, H.B., List, E.J., Koh, R.C.Y., Imberger, J. and Brooks, N.H. (1979) – <u>Mixing in Inland and Coastal Waters</u> – Academic Press, New York, USA, 483 pages

Fransson, J.H.M., Matsubara, M. and Alfredsson, P.H. (2005) – <u>Transition induced by free-stream turbulence</u> – Journal of Fluid Mechanics, 527, pp. 1-25

Fredsoe, J. and Deigaard, R. (1992) – <u>Mechanics of Coastal Sediment Transport</u> – Advanced Series on Ocean Engineering, Volume 3, World Scientific, Singapore, 369 pages

French, J.R. and Clifford, N.J. (1992) – <u>Characteristics and 'event structure' of near-bed turbulence in a macrotidal saltmarsh channel</u> – Estuarine, Coastal and Shelf Science, 34(1), pp. 49-69

Fugate, D.C. and Friedrichs, C.T. (2002) – <u>Determining concentration and fall velocity of estuarine particle populations using ADV, OBS and LISST</u> – Continental Shelf Research, 22(13), pp. 1867-1886

Goring, D.G. and Nikora, V.I. (2002) − <u>Despiking acoustic Doppler velocimeter data</u> − Journal of Hydraulic Engineering, 128(1), pp. 117-126

Goring, D.G. and Nikora, V.I. (2003) − <u>Despiking acoustic Doppler velocimeter data: Closure</u> − Journal of Hydraulic Engineering, 129(6), pp. 487-488

Hallback, M., Groth, J. and Johansson, A.V. (1989) – <u>A Reynolds stress closure for the dissipation in anisotropic turbulent flow</u> – Proceeding of 7th Symposium on Turbulent Shear Flows, Stanford University, Aug. 1989, pp. 17.2.1-17.2.6

Hinwood, J.B., Trevethan, M.G.B. and McLean, E.J. (2003) – <u>The effects of entrance parameters on tides in inlets</u> – Proceedings of Coasts and Ports Australasian Conference, Auckland, New Zealand, September 2003, Paper 155, (CD-ROM)

Hinwood, J.B., McLean, E.J. and Trevethan, M.G.B. (2005) – <u>Spring tidal pumping</u> – Proceedings of Coasts and Ports Australasian Conference, Adelaide, Australia, September 2005, pp. 601-606

Hinze, J.O. (1975) – <u>Turbulence</u> – Second Edition, McGraw-Hill Inc, USA, 790 pages

Ippen, A.T. (1966) – <u>Estuary and Coastline Hydrodynamics</u> – McGraw-Hill Inc, New York, USA, 744 pages

Jackson, R.G. (1976) – <u>Sedimentological and fluid-dynamic implications of the turbulent bursting phenomenon in geophysical flows</u> – Journal of Fluid Mechanics, 77(3), pp. 531-560

Jiang, J.Y, Street, R.L. and Klotz, S.P. (1990) – <u>A study of wave-turbulence interaction by use of a nonlinear water wave decomposition technique</u> – Journal of Geophysical Research, 95(C9), pp. 16,037-16,054

Kawanisi, K. (2004) – <u>Structure of turbulent flow in a shallow tidal estuary</u> – Journal of Hydraulic Engineering ASCE, 130(4), pp. 360-370

Kawanisi, K. and Yokosi, S. (1993) – <u>Measurement of turbulence and suspended sediment in tidal rivers</u> – Journal of Hydraulic Engineering, 119(6), pp.704-724

Kawanisi, K. and Yokosi, S. (1994) – <u>Mean and turbulence characteristics in a tidal river</u> – Estuarine, Coastal and Shelf Science, 38(5), pp. 447-469

Kawansi, K. and Yokosi, S. (1997) − <u>Characteristics of suspended sediment and turbulence in a tidal boundary layer</u> − Coastal Shelf Science, 17(8), pp.859-875

Kenney, J.F. and Keeping, E.S. (1951) – <u>Mathematics of Statistics (part 2)</u> – Second Edition, D. Van Nostrand Company Inc., New York, USA, 429 pages

Keulegan, G.H. (1951) – <u>Third Progress Report on Tidal Flow in Estuaries</u> – Technical Report No. 1146, National Bureau of Standards, Washington D.C.

Kitaigorodskii, S.A., Donelan, M.A., Lumely, J.L. and Terray, E.A. (1983) – <u>Wave-turbulence interactions in the upper ocean. Part 2: statistical characteristics of wave and turbulent components of the random velocity field in the marine surface layer</u> – Journal of Physical Oceanography, 13, pp. 1988-1999

Kline, S.J., Reynolds, W.C., Schraub, F.A. and Runstaller, P.W. (1967) – <u>The structure of turbulent boundary layers</u> – Journal of Fluid Mechanics, 30(4), pp. 741-773

Koch, C. and Chanson, H. (2005) – <u>An experimental study of tidal bores and positive surges: hydrodynamics and turbulence of the bore front</u> – Report No. 56/05. Department of Civil Engineering, The University of Queensland, Brisbane, Australia, 97 pages (ISBN 1864998245)

Kraus, N.C., Lohrmann, A. and Cabrera, R. (1994) – <u>New acoustic meter for measuring 3D laboratory flows</u> – Journal of Hydraulic Engineering, 120(3), pp. 406-412

Lemmin, U. and Lhermitte, R. (1999) – <u>Discussion: ADV measurements of turbulence: can we improve their interpretation?</u> – Journal of Hydraulic Engineering ASCE, 125(6), pp. 987-988

Lewis, R. (1997) – <u>Dispersion in Estuaries and Coastal Waters</u> – John Wiley & Sons, New York, USA, 312 pages

Lohrmann, A., Cabrera, R. and Kraus, N. (1994) – <u>Acoustic Doppler velocimeter (ADV) for laboratory use</u> – Proceedings of Symposium on Fundamentals and Advancements in Hydraulic Measurements and experimentation, (Ed. Pugh, C.A.) ASCE, New York, pp. 351-365

Lohrmann, A., Cabrera, R., Gelfenbaum, G. and Haines, J. (1995) – <u>Direct measurements of Reynolds stress with an acoustic Doppler velocimeter</u> – Proceedings of IEEE 5th Working Conference on Current Measurement Feb. 1995, pp. 205-210

McLelland, S.J. and Nicholas, A.P. (2000) – <u>A new method for evaluating errors in high-frequency ADV measurements</u> – Hydrological Processes, 14(2), pp. 351-366

Monin, A.S. and Yaglom, A.M. (1971) – <u>Statistical Fluid Mechanics: Mechanics of Turbulence, Volume 1</u> – (Ed. Lumley J.L.), The MIT Press, Cambridge, USA, 769 pages

Nakagawa, T. and Hinwood, J.B. (1978) – <u>On measurements of turbulence in tidal channels</u> – Monash University Report, MMEL34

Nezu, I. And Nakagawa, H. (1993) – <u>Turbulence in Open Channel Flows</u> – IAHR Monograph, IAHR Fluid Mechanics Section, Balkema Publ., Rotterdam, The Netherlands, 281 pages

Nezu, I., Kadota, A. and Nakagawa, H. (1997) − <u>Turbulence structure in unsteady depth-varying open channel flows</u> – Journal of Hydraulic Engineering ASCE, 123(9), pp. 752-763

Nezu, I. (2005) – <u>Open-channel flow turbulence and its research prospect in the 21st century</u> – Journal of Hydraulic Engineering ASCE, 131(4), pp. 229-246

Nielsen, P. (1992) – <u>Coastal Bottom Boundary Layers and Sediment Transport</u> − Advanced Series on Ocean Engineering, Volume 4, World Scientific, Singapore, 324 pages

Nikora, V.I. and Goring, D.G. (2002) − <u>Fluctuation of suspended sediment concentration and turbulent sediment fluxes in an open-channel flow</u> − Journal of Hydraulic Engineering ASCE, 128(2), pp. 214-224

Nikora, V., Goring, D. and Ross, A. (2002) – <u>The structure and dynamics of the thin near bed layer in a complex marine environment: A case study in Beatrix Bay, New Zealand</u> – Estuarine, Coastal and Shelf Science, 54(5), pp. 915-926

Officer, C.B. (1976) – <u>Physical Oceanography of Estuaries (and Associated Coastal Waters)</u> – John Wiley & Sons, New York, USA, 465 pages

Osonphasop, C. (1983) – <u>The measurement of Turbulence in Tidal Currents</u> – PhD thesis, Monash University, Australia, 233 pages

Piquet, J. (1999) – <u>Turbulent Flows – Models and Physics</u> – Springer-Verlag Berlin, Germany, 761 pages

Pope, S. B. (2000) – <u>Turbulent Flows</u> – Cambridge University Press, UK, 771 pages

Press, W. H., Teukolsky, S. A., Veterling, W. T. and Flannery, B. P. (1992) – <u>Numerical Recipes in FORTRAN</u> − Second Edition, Cambridge University Press, UK, 963 pages

Priestley, M.B. (1981) – <u>Spectral Analysis and Time Series</u> – Academic Press, London, 890 pages

Pritchard, D. W. (1952) – <u>Estuarine hydrography</u> – Advances in Geophysics, 1, pp. 243-280

Ralston, D.K. and Stacey, M. T. (2005) – <u>Stratification and turbulence in sub-tidal channels through intertidal mudflats</u> – Journal of Geophysical Research, Oceans, 110(C8), Paper C08009, 16 pages

Rutherford, J.C. (1994) – <u>River Mixing</u> – John Wiley & Sons, Chichester, USA, 347 pages

Savenije, H.H.G. (2005) − <u>Salinity and Tides in Alluvial Estuaries</u> – Elsevier, Amsterdam, The Netherlands, 193 pages

Schoellhamer, D.H. (1996) – <u>Anthropogenic sediment resuspension mechanisms in a shallow microtidal estuary</u> – Estuarine, Coastal and Shelf Science, 43(5), pp. 533-548

Shiono, K. and West, J.R. (1987) – <u>Turbulent perturbations of velocity in the Conway estuary</u> – Estuarine, Coastal and Shelf Science, 25(5), pp. 533-553

Song, T. and Graf, W.H. (1996) − Velocity and turbulence distribution in unsteady open channel flows – Journal of Hydraulic Engineering ASCE, 122(3), pp. 141-154

Sontek Application Notes (1997) – Sontek Doppler current meters – Using signal strength data to monitor suspended sediment concentration – Sontek, San Diego, USA, 7 pages

Speer, P.E. and Aubrey, D.G. (1985) – A study of non-linear tidal propagation in shallow inlet/estuarine systems part II: Theory – Estuarine, Coastal and Shelf Science, 21(2), pp. 207-224

Thais, L. and Magnaudet, J. (1995) – A triple decomposition of the fluctuating motion below laboratory wind water waves – Journal of Geophysical Research, 100(C1), pp. 741-755

Thais, L. and Magnaudet, J. (1996) – Turbulent structure beneath surface gravity waves sheared by the wind – Journal of Fluid Mechanics, 328, pp. 313-344

Trevethan, M., Chanson, H. and Brown, R. (2006) – Two series of detailed turbulence measurements in a small subtropical estuarine system – Report No. CH58/06, Division of Civil Engineering, The University of Queensland, Brisbane, Australia (ISBN 1864998520)

Trevethan, M., Chanson, H. and Takeuchi, M. (2007) – Continuous high-frequency turbulence and suspended sediment concentration measurements in an upper estuary – Estuarine, Coastal and Shelf Science, 73(1-2), pp. 341-350

Trowbridge, J.H. (1998) – On a technique for measurement of turbulent shear stress in the presence of surface waves – Journal of Atmospheric and Oceanic Technology, 15(1), pp. 290-298

Uncles, R.J. (2002) − Estuarine physical processes research: some recent studies and progress – Estuarine, Coastal and Shelf Science, 55(6), pp. 829-858

van de Kreeke, J. (1967) − Water-level fluctuations and flow in tidal inlets – Journal of Waterways and Harbours Division, ASCE, 93, pp. 97-106

van der Ham, R., Fontijn, H.L., Kranenburg, C. and Winterwerp, J.C. (2001) – <u>Turbulent exchange of fine sediments in a tidal channel in the Ems/Dollard estuary. Part 1: turbulence measurements</u> – Continental Shelf Research, 21(15), pp. 1606-1628

Varghese, T., Konofagou, E.E., Ophir, J., Alam, S.K. and Bilgen, M. (2000) – <u>Direct strain estimation in elastography using spectral cross-correlation</u> – Ultrasound in Medicine and Biology, 26(9), pp. 1525-1537

Verney, R., Deloffre, J. Brun-Cottan, J.C. and Lafite, R. (2007) – <u>The effect of wave-induced turbulence on intertidal mudflats: Impact of boat traffic and wind</u> – Continental Shelf Research, 27(5), pp. 594-612

Voulgaris, G. and Meyers, S.T. (2004) – <u>Temporal variability of hydrodynamics, sediment concentrations and sediment settling velocity in a tidal creek</u> – Continental Shelf Research, 24(15), pp. 1659-1683

Voulgaris, G. and Trowbridge, J. (1998) – <u>Evaluation of the acoustic Doppler velocimeter (ADV) for turbulence measurements</u> – Journal of Atmospheric and Oceanic Technology, 15(1), pp. 272-289

Wahl, T.L. (2003) – <u>Despiking acoustic Doppler velocimeter data: Discussion</u> – Journal of Hydraulic Engineering ASCE, 129(6), pp. 484-487

West, J.R., Knight, D.W. and Shiono, K. (1984) – <u>A note on flow structure in the Great Ouse estuary</u> – Estuarine, Coastal and Shelf Science, 19(3), pp. 271-290

West, J.R. and Oduyemi, K.O.K. (1989) – <u>Turbulence measurements of suspended solids concentration in estuaries</u> – Journal of Hydraulic Engineering ASCE, 115(4), pp. 457-473

West, J.R. and Shiono, K. (1985) – <u>A note on turbulent perturbations of salinity in a partially mixed estuary</u> – Estuarine, Coastal and Shelf Science, 20(1), pp. 55-78

West, J.R. and Shiono, K. (1988) – <u>Vertical turbulent mixing processes on ebb tides in partially mixed estuaries</u> – Estuarine, Coastal and Shelf Science, 26(1), pp. 51-66

Yokosi, S. (1967) – <u>The structure of river turbulence</u> – Bulletin of the Disaster Prevention Research Institute, 17(2), Oct. 1967, pp. 1-29

APPENDIX A   POST-PROCESSING OF ADV DATA

A.1   PRESENTATION

The acoustic Doppler velocimeter (ADV) is a robust device that is well suited to shallow-water systems such as small estuaries. However, the accuracy and reliability of the device are still under investigation. The ADV has some inherent problems and velocity data may be adversely affected by "spike events" caused by a combination of aliasing of the Doppler signal, velocity shear, intrinsic Doppler noise and hardware errors (e.g. Lemmin and Lhermitte (1999), Goring and Nikora (2002)). Continuous ADV measurements over long periods in natural systems may be affected by larger disturbances, such as probe adjustments and navigation events. Section A.2 details the various stages of the post-processing technique developed as part of this study. A sensitivity analysis of the parameters of the post-processing technique was performed as part of this study, with the results presented in Section A.3. Section A.4 discusses the effectiveness of the post-processing technique in finding and replacing "erroneous" data points in the ADV data.

A.2   POST-PROCESSING TECHNIQUE

Both small disturbances, caused by spike events and large disturbances must be removed prior to a turbulence statistical analysis. Such disturbances must be found and the data replaced before analysis. A procedure, called here "post-processing" was applied to raw acoustic Doppler velocimeter data. After a velocity signal check (e.g. WinADV), the post-processing procedure found large disturbances and replaced the corrupted data. Then the post-processing procedure found small disturbances and the corresponding erroneous data were replaced. Figure A.1 illustrates the various stages of the post-processing technique for this investigation.

After collection the ADV data were processed in several stages. First, data points that contained communication errors, low signal to noise ratio (SNR < 5 dB) and low signal correlation (COR < 60 %) were found and replaced. This was usually done by an industrial software (e.g. WinADV). Two further stages, "pre-processing" and "de-spiking" were used to process the data. The former stage (pre-processing) was designed to find and replace data corrupted by large events such as probe adjustments and navigation events. The latter stage (de-spiking) was developed to find and replace data corrupted by "spike events" and other small disturbances.

```
                    ┌─────────────────┐
                    │   Raw ADV data  │
                    └─────────────────┘
                             │
                             ▼
            ┌──────────────────────────────────┐
            │    Velocity Signal Error Check    │
            │         (e.g. WinADV)             │
            └──────────────────────────────────┘
                             │
┌────────────────────────────────────────────────────────────┐
│  POST-PROCESSING                                             │
│                                                              │
│   ┌──────────────────────────────────────────────────┐      │
│   │  PRE-PROCESSING                                    │      │
│   │                                                    │      │
│   │     ┌──────────────────────────────────────┐      │      │
│   │     │  Search for KNOWN probe adjustments   │      │      │
│   │     └──────────────────────────────────────┘      │      │
│   │                      │                             │      │
│   │                      ▼                             │      │
│   │     ┌──────────────────────────────────────┐      │      │
│   │     │  Search for KNOWN navigation events   │      │      │
│   │     └──────────────────────────────────────┘      │      │
│   │                      │                             │      │
│   │                      ▼                             │      │
│   │     ┌──────────────────────────────────────┐      │      │
│   │     │     Search for UNKNOWN events         │      │      │
│   │     └──────────────────────────────────────┘      │      │
│   └──────────────────────────────────────────────────┘      │
│                          │                                   │
│   ┌──────────────────────────────────────────────────┐      │
│   │  DE-SPIKING          │                             │      │
│   │                      ▼                             │      │
│   │     ┌──────────────────────────────────────┐      │      │
│   │     │  Search for spike events using PHASE  │      │      │
│   │     │   SPACE THRESHOLDING method           │      │      │
│   │     └──────────────────────────────────────┘      │      │
│   └──────────────────────────────────────────────────┘      │
│                          │                                   │
└────────────────────────────────────────────────────────────┘
                           ▼
            ┌──────────────────────────────────┐
            │  Processed data ready to be analysed │
            └──────────────────────────────────┘
```
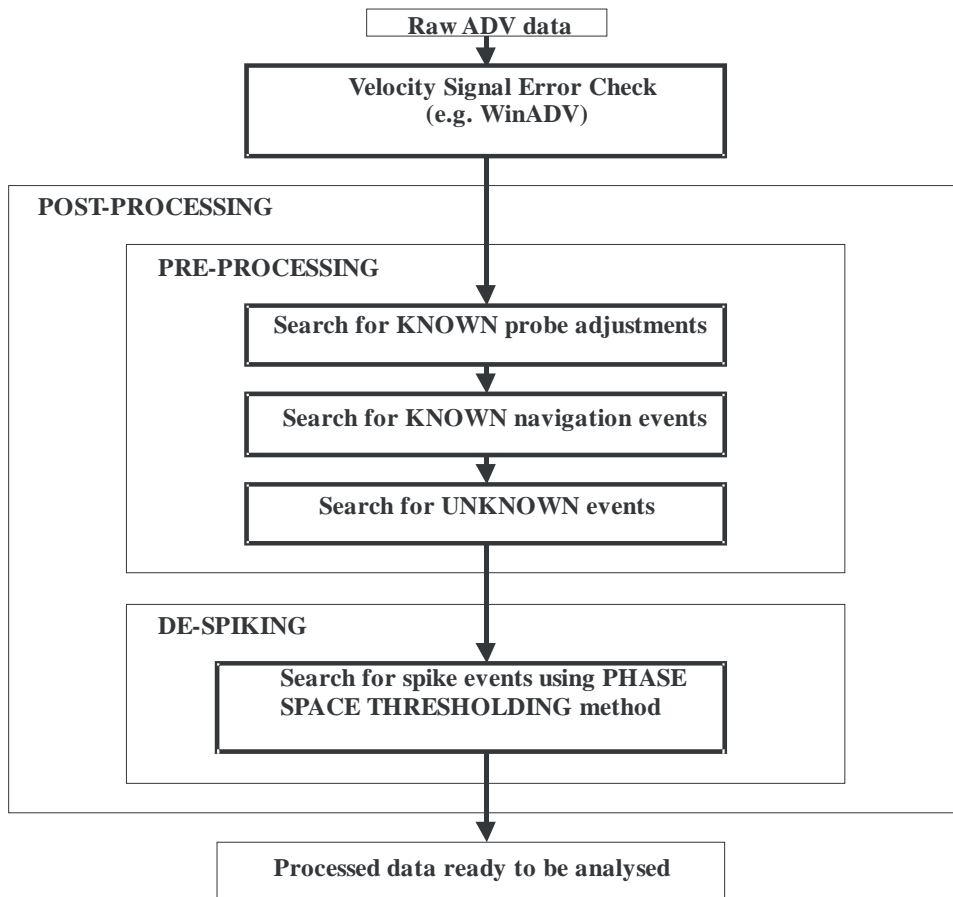
Figure A.1 – Flow chart of post-processing procedure.

All stages of the post-processing involved two steps: i.e., detection and replacement of erroneous data. Both steps were performed in each stage, before the start of the next stage. The detection step was undertaken on the high-pass filtered data. Erroneous data were replaced using a technique based upon the mean of the endpoints. The mean of the endpoints technique reduced the distortion of statistical values, while not inferring trends on the replaced data. Figure A.2 shows a section of data repaired using the mean of the endpoints technique and linear interpolation. In Figure A.2A the mean of the endpoints technique provides a constant value to all data points replaced when replacing large sections of erroneous data. For single data point replacement the mean of the endpoints is equivalent to linear interpolation. But, when interpolating over a large section of erroneous data, linear interpolation infers a trend on the replaced data (Figure A.2B).

In the pre-processing stage large disturbances were searched for, with a minimum of 3,500 data points replaced per event. Replacement was undertaken on the original data, to avoid inferring a trend that would occur if the replacement process was conducted on the high-pass filtered data. The de-spiking stage searched for small disturbances, usually less than 10 data points in size. The de-spiking replacement was undertaken on the high-pass filtered data. After the completion of the iterative de-spiking process the high-pass filtered data was added

to the low-pass filtered component. Minimal trend was inferred when the low-pass and high-pass filtered data were added, since only a small quantity of data were replaced.
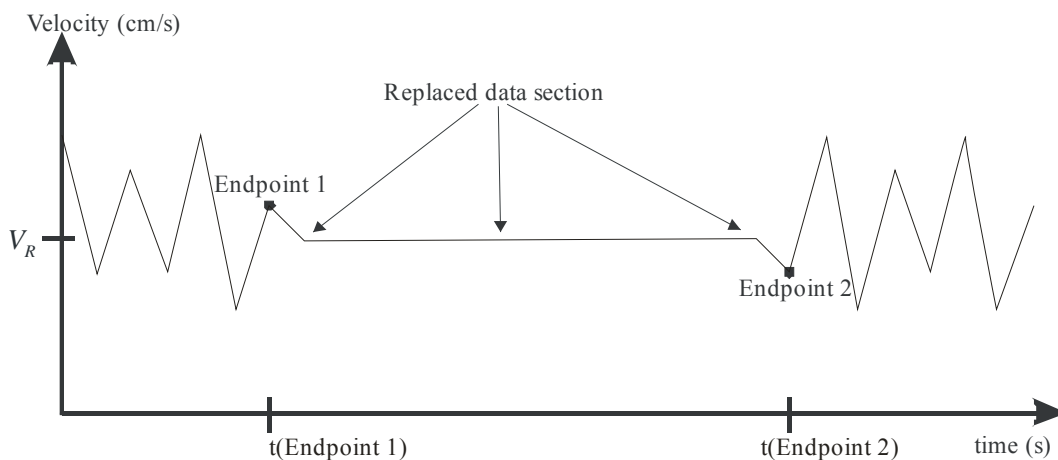
(A) Mean of endpoints technique.
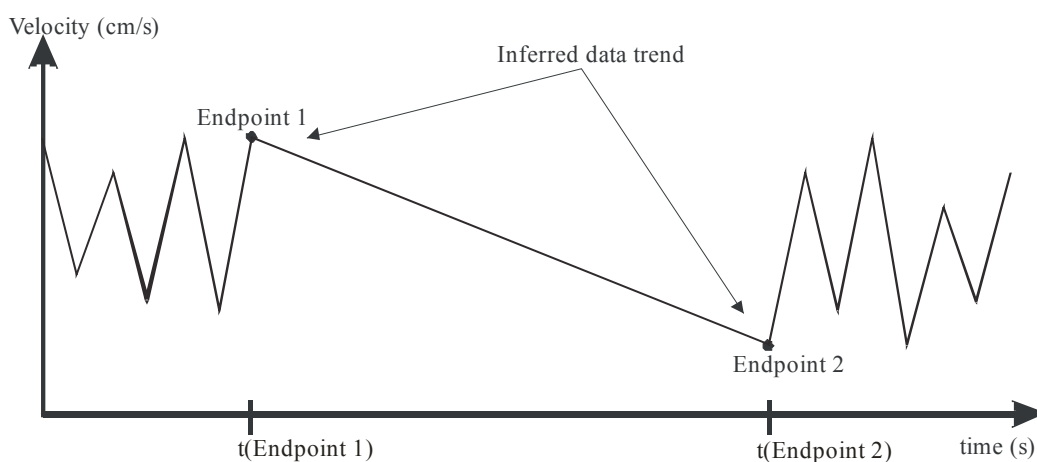
(B) Linear interpolation.

Figure A.2 – Comparison of some erroneous data replacement techniques. Data replacement conducted for approximately 3,500 erroneous data points.

A.2.1 Pre-processing stage

This stage of post-processing was developed as part of this study. It finds and replaces events that cause large disturbances to the measured velocity data. In small subtropical estuarine systems large disturbances can be caused by a probe adjustment; navigation event; fish or bird activity; floating debris; and wind. The probe adjustments and navigation events caused the largest disturbance to the recorded velocity fluctuations. Both types of events have the potential to cause disturbances several orders of magnitude larger than the natural velocity fluctuations. Figure A.3 shows some examples of probe adjustment and navigation events.

(A) Probe adjustment (4/04/03).   (B) Navigation event (17/05/05).

Figure A.3 – Example of a probe adjustment and a navigation event at Eprapah Creek. Probe adjustment was performed at high tide during field study E1 (4/04/03), while navigation event occurred on flood tide during study E6 (16-18/05/05). Photographs taken by H. Chanson.

A.2.1.1 *Probe adjustment event search*

During data acquisition it was found that any probe motion caused a large disturbance. Vertical probe adjustments may be applied at regular intervals to maintain the probe sampling volume within a certain distance of the free surface in an estuary, for example. Figure A.4 shows the increased velocity fluctuations in all three velocity components during a probe adjustment. In the detection step the high-pass filtered data were used to locate the probe adjustments.
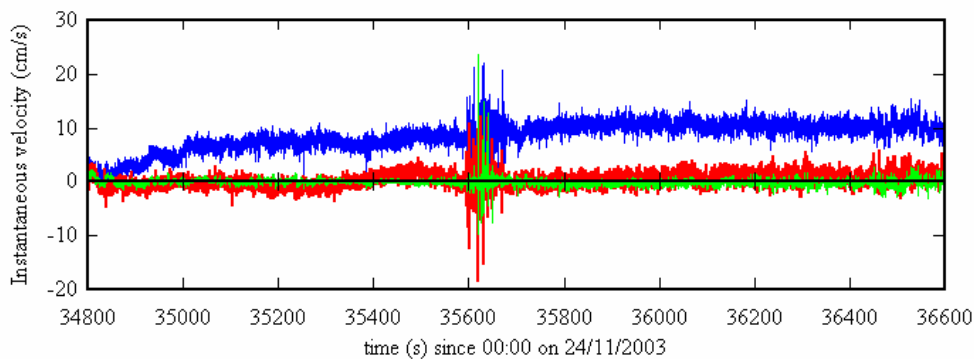
Figure A.4 – Example of velocity signal during a probe adjustment. Data collected at Site 2B during study E3 (24/11/03) at Eprapah Creek. Probe adjustment was at beginning of ebb tide. Legend: — streamwise velocity V_x ; — transverse velocity V_y ; — vertical velocity V_z .

A search region is generated around the position of known probe adjustments. For each velocity component the standard deviation ($\sigma_{SR(P)}$) of the velocity over the search region is

calculated and multiplied by a dimensionless threshold constant (C_{EP}). This provides the event threshold (λ_{EP}, Equation A.1) for that component:

$$\lambda_{EP} = C_{EP} \times \sigma_{SR(P)} \tag{A.1}$$

Within the search region the velocity component standard deviations in smaller statistical data "windows" were compared to the event threshold λ_{EP}. If the standard deviation of the smaller statistical window exceeded the event threshold λ_{EP} in at least two of the velocity components, the data points in that window were deemed "disturbed" and replaced. This detection method is demonstrated in Figure A.5.
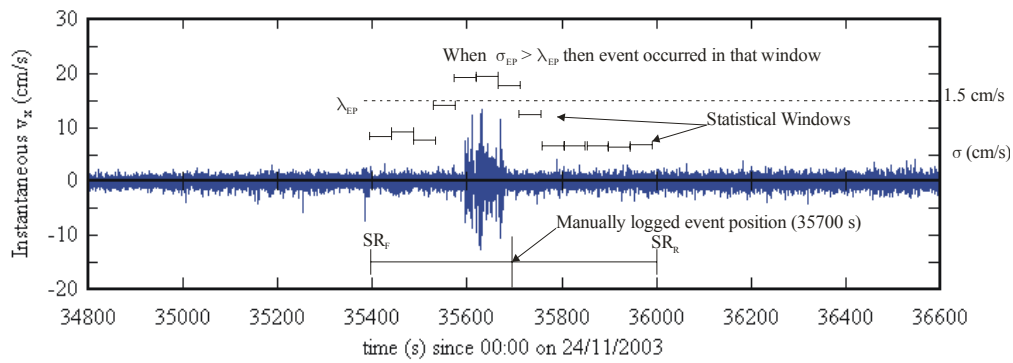
Figure A.5 – Demonstration of isolating time of known probe adjustment event on high-pass filtered velocity data. Event occurred at start of ebb tide for study E3 (Figure A.4).

A.2.1.2 *Navigation event search*

Navigation events may affect the data for several minutes after a boat passage (e.g. Chanson (2003), Verney et al. (2007)). Figure A.6A shows the effect of a navigation event on the velocity data. The detection of navigation events was performed on the high-pass filtered data. A search region was generated about a known event position. Within the search region, the vertical acceleration (A_Z) was calculated (Equation A.2). The acceleration magnitude (AM) between data points of the vertical acceleration data was calculated using Equation A.3 (where j is the data point number):

$$A_Z(j) = \frac{\left(V_Z(j) - V_Z(j-1)\right)}{\partial t} \tag{A.2}$$

$$AM = \left|A_Z(j)\right| + \left|A_Z(j-1)\right| \tag{A.3}$$

$$\lambda_{EN} = C_{EN} \times \sigma_{SR(N)} \tag{A.4}$$

where $\partial t = 1/f_{scan}$; with f_{scan} = ADV scanning frequency (25 or 50 Hz here).

Navigation events cause large fluctuations in the vertical acceleration magnitude, usually associated with the propagation of the bow wave. An event threshold (λ_{EN}, Equation A.4) was determined by multiplying the standard deviation of the acceleration magnitude ($\sigma_{SR(N)}$) in the search region by a threshold constant (C_{EN}). Standard deviations of smaller statistical data samples within the search region were compared to the event threshold λ_{EN}. If the sample standard deviation of vertical acceleration was greater than the event threshold λ_{EN} that data sample was "flagged".

The maximum value of the acceleration magnitude within the "disturbed" region indicates the vertical acceleration induced by the first bow wave when its impact reaches the probe location. Figure A.6B shows the acceleration magnitude of the data set shown in Figure A.6A. In Figure A.6B the maximum acceleration magnitude coincides with the start of the disturbance induced by the boat passage.
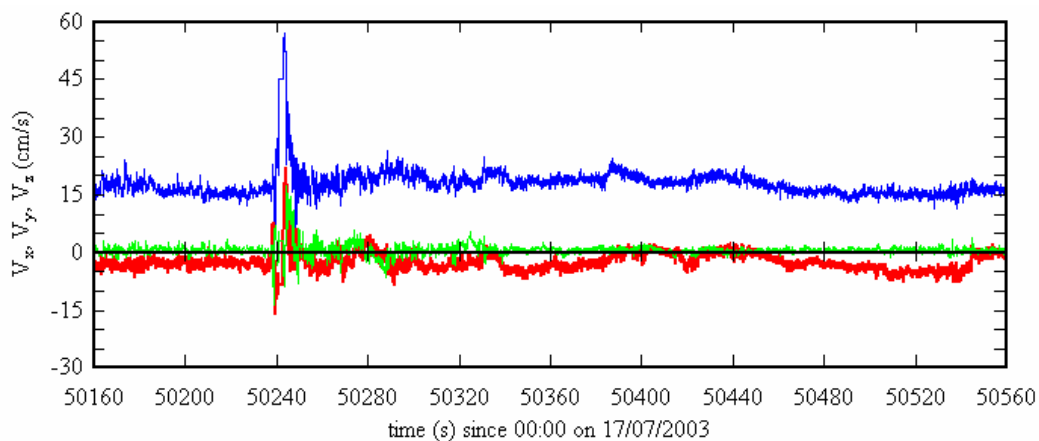
(A) Example of a navigation event and its effect on three velocity components.
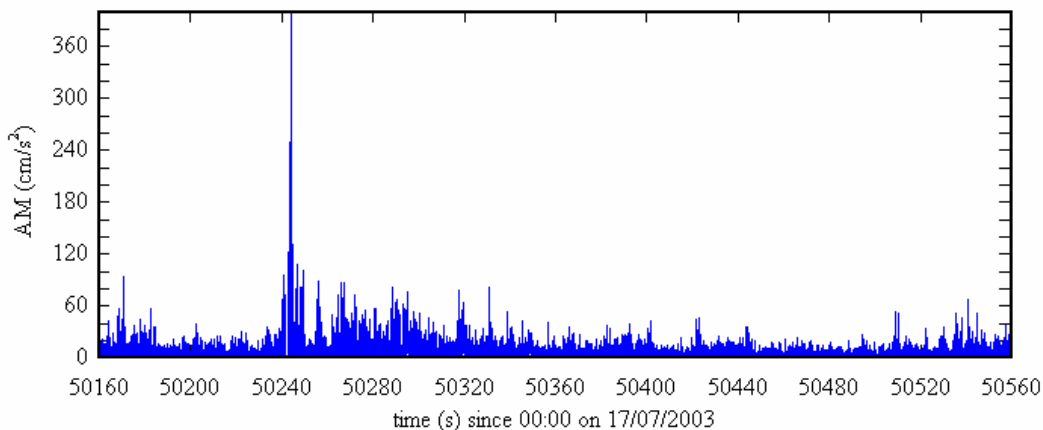
 (B) Acceleration magnitude (AM) data for navigation event shown.

Figure A.6 – Example of a navigation event close to ADV. Data collected during study E2 (17/07/03) about 0.5 m below surface at Site 2, Eprapah Creek. Event occurred mid ebb tide. Legend: — streamwise velocity V_x ; — transverse velocity V_y ; — vertical velocity V_z .

A.2.1.3 Unknown event search

The detection of large disturbances was dependent upon the manual recording of the time that such an event occurred. There were however some other events which might not have been observed and not recorded manually. After all probe adjustments and navigation events were processed a final check of the data was conducted. The data set was checked for any large disturbances such as un-logged probe adjustments and navigation events, or flora/fauna interfering with the ADV. Localised searches were performed on each velocity component with 15 minute long sections throughout the entire data set. For each section the event threshold (λ_{EU}) was calculated by multiplying the section standard deviation ($\sigma_{SS(U)}$) of the velocity component by a threshold constant C_{EU} .

$$\lambda_{EU} = C_{EU} \times \sigma_{SR(U)} \qquad\qquad\qquad (A.5)$$

The standard deviations of the smaller statistical data samples of each section were compared to the event threshold λ_{EU} . If the standard deviation of the data sample was larger than the event threshold λ_{EU} the data in that data sample was "flagged" but not replaced.

Data were only replaced during this stage if the "unknown events" found occurred within the known limits at the beginning and end of the field trip. During these times people were known to be around the probe setting up or dismantling the experiment. The beginning and end of these periods were recorded. Any unknown events found during these periods were considered similar to probe adjustments (human interference) and therefore replaced.

A.2.2 De-spiking stage

Two de-spiking methods were investigated as part of this study. These were the acceleration thresholding method and the phase-space thresholding method (Goring and Nikora (2002)). Initial investigations showed that the acceleration thresholding method was inappropriate for the low velocity unsteady flows under investigation. The phase-space thresholding method was found suitable and used for this study.

A.2.2.1 Phase-space thresholding method

The phase-space thresholding method uses a three-dimensional Poincaré map (phase space plot) to plot a variable and its derivatives against each other (Goring and Nikora (2002)). Here the variable is the high-pass filtered data of an individual velocity component. An ellipsoid generated using the Universal criterion (UC, Equation A.6) determined which data points were contaminated by "spike events". The Universal criterion was calculated for each

velocity component from the standard deviation σ and the number of data points N within the entire data set:

$$UC = \Lambda_U \, \sigma \qquad\qquad\qquad\qquad (A.6)$$

where $\Lambda_U = \sqrt{2 \, \text{Ln}(N)}$ is the Universal threshold. A slightly enhanced version of this method was used, where data points found outside the ellipse of a single velocity component were deemed erroneous and replaced in all components.

For each velocity component the "surrogate" first and second derivatives (Equations A.7 and A.8 respectively) were calculated:

$$\Delta u_j = \left(u_{j-1} - u_{j+1}\right)/2 \qquad\qquad\qquad (A.7)$$

$$\Delta^2 u_j = \left(\Delta u_{j-1} - \Delta u_{j+1}\right)/2 \qquad\qquad\qquad (A.8)$$

where u = individual velocity component ($u = U - \overline{U}$); and j = data point number. These form the dimensions of the investigation phase space (Figure A.7). Figure A.7 shows a section of streamwise velocity data from the field study E2 in phase space.

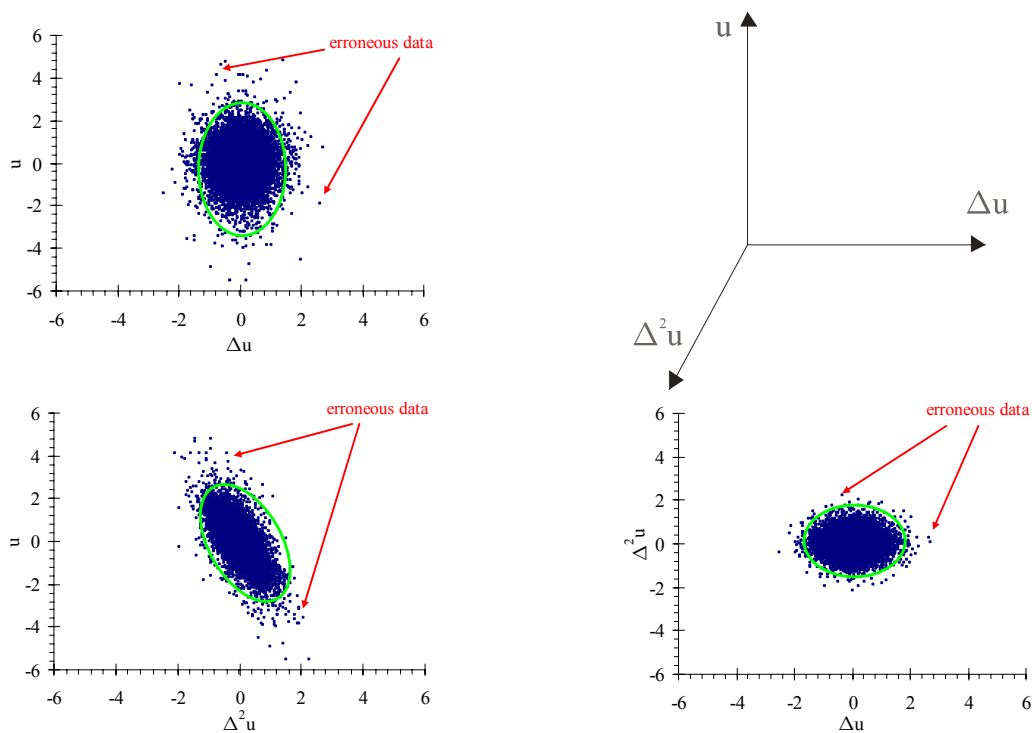Figure A.7 – Streamwise velocity component and its "surrogate" derivatives in phase space. Data in example are first 10,000 data points from field study E2 (17/07/03).

The Universal criterion (UC) of each derivative provides the major and minor ellipse threshold values. Any data points outside the three-dimensional ellipse were deemed erroneous. Erroneous data is replaced on the high-pass filtered data before the next iteration

was conducted. The iteration process continues until no new erroneous data points were found.

A.2.2.2 *Acceleration thresholding method*

A slightly enhanced version of the acceleration thresholding method (Goring and Nikora (2002)) was tested. Enhancements included searching for and then replacing erroneous data in all three velocity components simultaneously, and different threshold constants for testing vertical and horizontal velocity components.

The "pre-processed" data set was filtered and only the high-pass filtered data were used. The filtered data were exposed to two tests simultaneously (Equations A.9 and A.10):

$$\left| a_i \right| > \lambda_a \; g \tag{A.9}$$

$$\left| u_i \right| > \lambda_k \; \sigma \tag{A.10}$$

where a_i = instantaneous acceleration at a point (cm/s^2); u_i = velocity deviation at a point (cm/s); λ_a = de-spiking acceleration threshold; g = gravity acceleration (9.80 m/s^2 in Brisbane); σ = standard deviation of entire data set (cm/s); λ_k = de-spiking absolute deviation threshold; and i = parameter direction (x, y, z).

One test compared the instantaneous acceleration at a point to the acceleration threshold limit of gravity. The second test compared the absolute deviation of a point to the threshold limit of the standard deviation of the entire data set. If Equations A.9 and A.10 were satisfied for any velocity component, then those data points were deemed erroneous for all velocity components and replaced before the next iteration. The de-spiking process iterated until the number of erroneous data points found equalled zero. After the completion of the iteration process the de-spiked high-pass filtered data were added to the low-pass filtered data of initial "pre-processed" data set.

A.2.2.3 *Preferred de-spiking method*

The acceleration thresholding method was found to not be affective for de-spiking the slow unsteady flows of the estuarine systems under investigation. Goring and Nikora (2002) indicated that a de-spiking acceleration threshold parameter λ_a between 1 and 1.5. In the type of flows recorded during this experimentation λ_a of this magnitude found no spikes even in high noise areas, and values of λ_a down to 0.015 were tested.

Without a data set containing a known number of spike events finding the appropriate value of λ_a was extremely difficult. The use of the acceleration thresholding method without a

calibrated acceleration threshold does not allow confidence in the results of de-spiking provided. Therefore, the acceleration thresholding method was not used during this investigation.

The phase-space thresholding method does not require calibration to the velocity data set. But, as a new technique some questions remain regarding the best way to apply the technique. Wahl (2003) questioned the use of the universal threshold criterion for generating the boundaries of the ellipse. Goring and Nikora (2003) in response defended the use of this criterion. Wahl also suggested the use of the median and median of absolute deviation instead of the mean and standard deviation. These Wahl suggested would improve the methods ability to detect spike events and eliminate the need to iterate. Goring and Nikora agreed that the use of the median improved the robustness of the method, but disputed that it eliminated the need to iterate.

A.3   SENSITIVITY ANALYSIS

A sensitivity analysis was performed to assess the impact of each parameter of the post-processing technique and to optimise the relevant coefficients. During the sensitivity analysis two investigations were undertaken. Investigation One was an in-depth sensitivity analysis of all post-processing parameters. Its aim was to determine the effect of each parameter on the outcome of post-processing including the pre-processing and de-spiking stages. Each parameter was investigated for seven values within a typical variation range.

Investigation Two focused on the parameters that had the greatest effect on the results of post-processing. This sensitivity analysis investigated result consistency under different experimental conditions. The number of parameter values investigated was reduced to the minimum required to produce some trend. For Investigations One and Two, each parameter was varied individually, while all other parameters were kept constant. The parameters (Table A.1) were regrouped around similar tasks during post-processing. These were:

1/ – <u>High-pass/low-pass filter parameters</u> (Λ_f): Filtering of data was used throughout post-processing. The basic parameters define the frequency range for which the data was filtered. The extreme upper limit is $2\partial t$ (time step size (s)), while the extreme lower limit is 0 Hz. A time scale related to physical aspects of the system determined the threshold between high-pass and low-pass filtered data. This filtering threshold (Λ_f) was investigated through a range between 1 and 1,000 s, with a standard value of 10 s. The standard value is a value deemed the least biased through experimentation prior to the sensitivity analysis.

2/ – <u>Event threshold parameters</u> (C_{EP}, C_{EN}, C_{EU}): Event thresholds were used during the pre-processing stage to find specific events (e.g. probe adjustments). The constant event threshold (C_{EP}, C_{EN}, C_{EU}) was multiplied by the standard deviation ($\sigma_{SR(P)}$, $\sigma_{SR(N)}$, $\sigma_{SS(U)}$) of the event search region to find the individual event threshold (λ_{EP}, λ_{EN}, λ_{EU}). Each threshold (λ_{EP}, λ_{EN}, λ_{EU}) isolated when an individual event occurred within the search region. All event threshold parameters were varied through a range of 1.2 to 1.8, with a standard value of 1.5.

3/ – <u>Event search region parameters</u> (SR_F, SR_R): Search region parameters define the forward and aft extents of each event search region. The search region reduced the quantity of data processed by isolating the search around a "known" event position (Figure A.8). A known event was one whose time of occurrence was recorded during experimentation. The front and rear search region parameters were varied between 180 and 420 s, each with a standard value of 300 s.
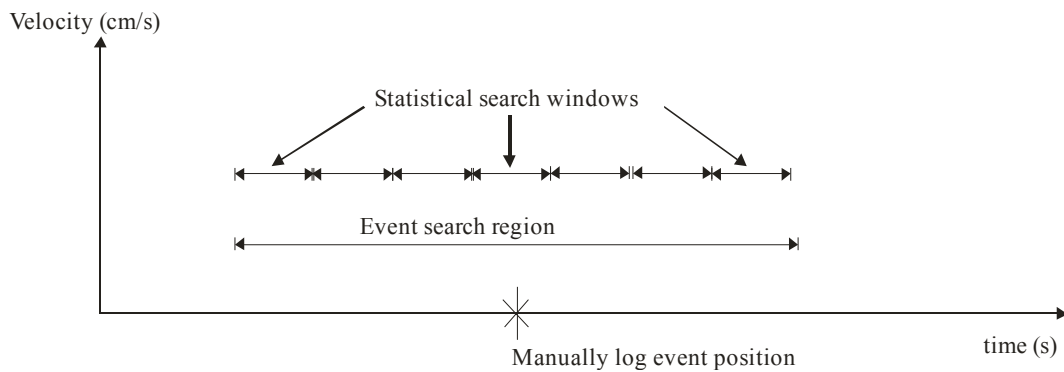
Figure A.8 – Sketch of event search region and statistical search window used during pre-processing stage.

4/ – <u>Statistical search window parameter</u> (SW): The statistical search window was used within an event search region to isolate the exact position of an event (Figure A.8). This parameter governs the size of the statistical search window used. The standard deviations of these windows were compared to the event threshold (λ_{EP}, λ_{EN}, λ_{EU}) of the search region. The statistical search window size was varied between 100 and 5,000 data points, with a standard value of 1,000 data points.

5/ – <u>Data replacement buffer parameters</u> (B_{FP}, B_{RP}, B_{FN}, B_{RN}, B_{FU}, B_{RU}): Data replacement buffers ensure that the optimal quantity of corrupted data about a found event was replaced. This buffer of time was placed either side of the event. The size of buffer depends on type of event being sought. For probe adjustments and unknown events a front and rear buffer with a

standard value of 50 s was used, and both were varied between 20 and 100 s. Navigation events affect data for up to five minutes after a boat passage. Therefore, the navigation event front and rear buffers were different. The front buffer had a range between 10 and 60 s, and a standard value of 35 s. The rear buffer included post-event effects and was varied between 180 and 420 s, with a standard value of 300 s. Values used for front and rear values were found through manual analysis of the event impact on ADV data for each type of event.

Table A.1 – Post-processing parameters investigated in sensitivity analysis.

Symbol	Description	Units	Range/Standard Value (SV)
C_{EP}	Constant threshold value used to locate position of known probe adjustment events.	--	$1.2 \leq C_{EP} \leq 1.8$ SV=1.5
C_{EN}	Constant threshold value used to locate position of known navigation events.	--	$1.2 \leq C_{EN} \leq 1.8$ SV=1.5
C_{EU}	Constant threshold value used to position of un-logged events.	--	$1.2 \leq C_{EU} \leq 1.8$ SV=1.5
B_{FP}	Front time buffer when replacing probe adjustment events.	s	$20\ s \leq B_{FP} \leq 100\ s$ SV=50 s
B_{RP}	Rear time buffer when replacing probe adjustment events.	s	$20\ s \leq B_{RP} \leq 100\ s$ SV=50 s
B_{FN}	Front time buffer when replacing navigation events.	s	$10\ s \leq B_{FN} \leq 60\ s$ SV=35 s
B_{RN}	Rear time buffer when replacing navigation events.	s	$180\ s \leq B_{RN} \leq 420\ s$ SV=300 s
B_{FU}	Front time buffer when flagging un-logged events that may cause data corruption.	s	$20\ s \leq B_{FU} \leq 100\ s$ SV=50 s
B_{RU}	Rear time buffer when flagging un-logged events that may cause data corruption.	s	$20\ s \leq B_{RU} \leq 100\ s$ SV=50 s
SR_F	Front search region about a manually logged event position for locating actual position of event in data set.	s	$180\ s \leq SR_F \leq 420\ s$ SV=300 s
SR_R	Rear search region about a manually logged event position for locating actual position of event in data set.	s	$180\ s \leq SR_R \leq 420\ s$ SV=300 s
SW	Analysis window size used for comparing window standard deviations with search region standard deviation to locate events.	dp	$100\ dp \leq SW \leq 240\ s$ SV=1,000 dp
Λ_f	The threshold between high-pass and low-pass filtering, determined by time scale related to geometry of system under investigation.	s	Between 0 and $2\partial t$ $1\ s > \Lambda_f > 1,000\ s$ SV=10 s

Note: For units: s: seconds; dp: data points; --: dimensionless; SV: standard value of parameter.

A.3.1   Investigation One: in-depth sensitivity analysis

The in-depth sensitivity analysis was conducted using the data set collected during the field study E2 (17/07/2003) at Eprapah Creek (Southeast Queensland). The ADV performed continuous measurements between 06:26 and 14:10 at 25 Hz. During this study, approximately ten probe adjustment and six navigation events were logged manually.

A.3.1.1   Pre-processing stage parameters

During the pre-processing stage, three different searches were undertaken for probe adjustment events, navigation events and unknown events using: (1) High-pass/low-pass filter parameters; (2) Event threshold parameters; (3) Event search region parameters; (4) Statistical search window parameters; and (5) Data replacement buffer parameters.

The main outcomes of the sensitivity analysis were the number of events found and the number data points replaced. Figures A.9 and A.10 show the results of the pre-processing stage sensitivity analysis. In each case the left vertical axis contains the number of events found and the right vertical axis shows the number of data points replaced/flagged. The horizontal axis shows each parameters' range of variation. Results of all three pre-processing searches are shown on each graph to demonstrate what stages of the pre-processing were affected by a parameters variation.

Figures A.9A-C show the effect that the event threshold parameters (C_{EP}, C_{EN}, C_{EU}) had on the outcome of the pre-processing stage. In Figures A.9A-C the number of events found decreased as each event threshold parameter (C_{EP}, C_{EN}, C_{EU}) increased. The results of varying the statistical search window size (SW) showed that the number of events detected decreased in all pre-processing stages as the size of the statistical search window increased (Figure A.9D). No change to the number of events detected was found by varying the data replacement buffers (B_{FP}, B_{RP}, B_{FN}, B_{RN}, B_{FU}, B_{RU}), because the buffer parameters were being used only after the events were found. Therefore, the data replacement buffers only affected the number of data points replaced/flagged.

Figures A.9E & F show that varying the front (SR_F) and rear (SR_R) search region size had little effect on the number of events detected in all pre-processing stages. The fluctuations that occurred with the variation of both search region parameters were caused by the uneven division of the standard value of SW into the search region (i.e. (SR_F + SR_R)/SW = 2.5).
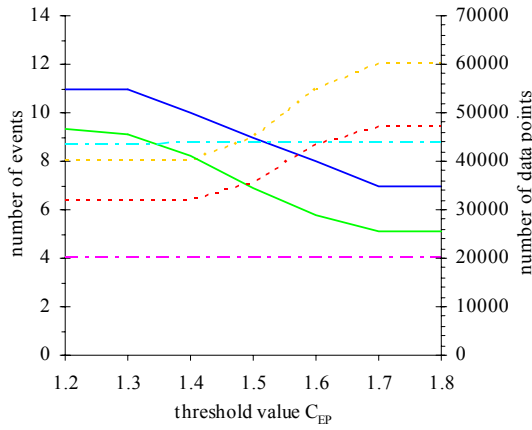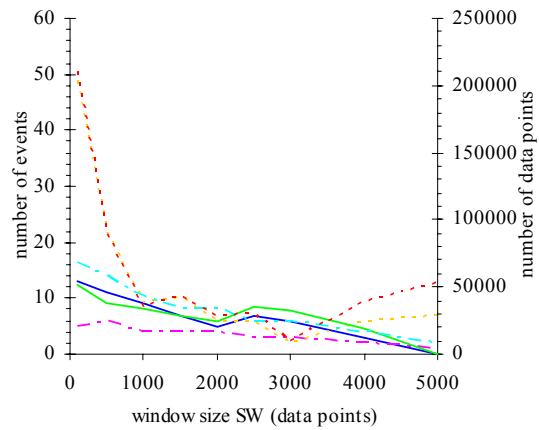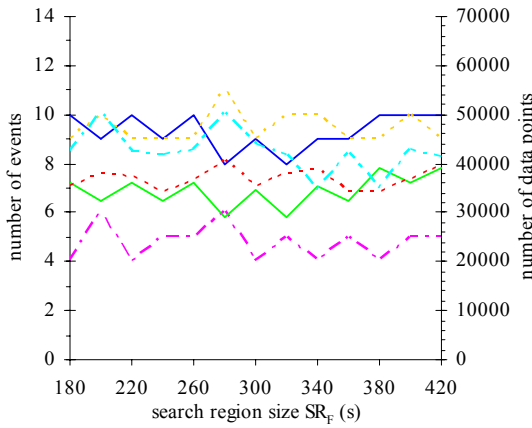
(A) Probe adjustment threshold (C_{EP}).
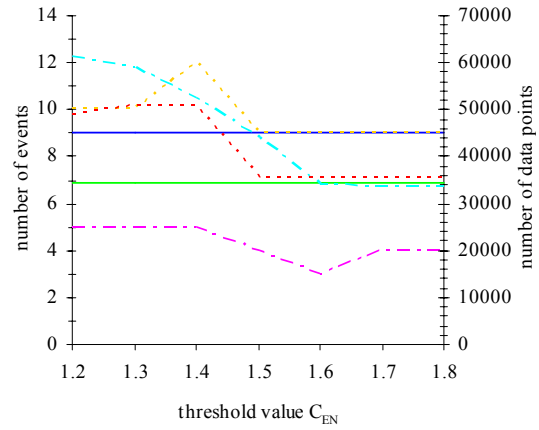
(B) Navigation event threshold (C_{EN}).
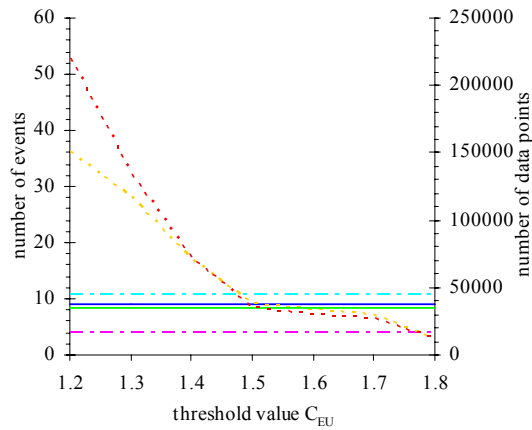
(C) Unknown event threshold (C_{EU}).

(D) Statistical search window (SW).

(E) Front search region (SR_F).
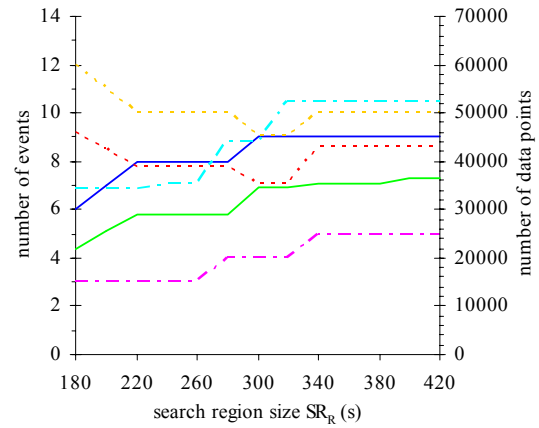
(F) Rear search region (SR_R).

Figure A.9 – Results of sensitivity analysis on parameters of pre-processing stage.

Legend: —— number of events found in "probe adjustment search"; — – — number of events found in "navigation event search"; – – – number of events found in "unknown event search"; —— number of data points replaced in "probe adjustment search"; — – — number of data points replaced in "navigation event search"; – – – number of data points flagged in "unknown event search".

Filtering was used in all pre-processing stages to search for data corrupted by events. Figure A.10 shows that the filtering threshold (Λ_f) chosen caused some changes to pre-processing stage outputs. As the filtering threshold increased the number of events detected in the "probe adjustment search" and "navigation event search" decreased. In the "unknown event search" the number of events detected increased until around 50 s, then decreased after this point. This change in trend highlighted an important turbulence time scale that occurred between 30 and 150 s. This time scale seemed related to the physical characteristics of the system (e.g. cross-section geometry).
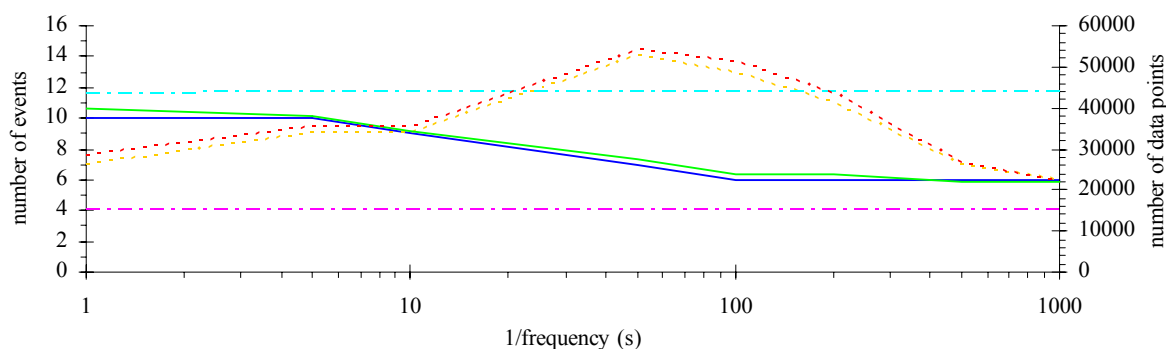

Figure A.10 – Sensitivity analysis results for filtering threshold (Λ_f) in pre-processing stage. Legend: —— number of events found in "probe adjustment search"; — – — number of events found in "navigation event search"; – – – number of events found in "unknown event search"; —— number of data points replaced in "probe adjustment search"; — – — number of data points replaced in "navigation event search"; – – – number of data points flagged in "unknown event search".

A.3.1.2 *De-spiking stage parameters*

De-spiking is a technique developed to find and replace erroneous data points corrupted by spike events, generated by Doppler signal aliasing and Doppler noise primarily (e.g. Goring and Nikora (2002)). Several methods exist and the phase-space thresholding method was deemed the most appropriate for this investigation. In the phase-space thresholding method the high-pass/low-pass filtering threshold parameter may affect the de-spiking outcome. For this sensitivity analysis the number of iterations were set so that it would not affect the outcome of the de-spiking stage.

The outcomes of the de-spiking stage sensitivity analysis were assessed using the number of spike events and erroneous data points found. This analysis used a data set subjected to pre-processing that contained standard values for all parameters. Figure A.11 shows the results

for the variation of the high-pass/low-pass filtering parameter (Λ_f) during the de-spiking stage. The number of spike events are on the left vertical axis and the number of erroneous data points are on the right vertical axis. In Figure A.11 the variation of the filtering threshold during the de-spiking stage had only a small effect on the outcome. For the number of data points and spike events the maxima occurred about the standard value. This indicated that the standard value was a reasonable choice for the filtering threshold.
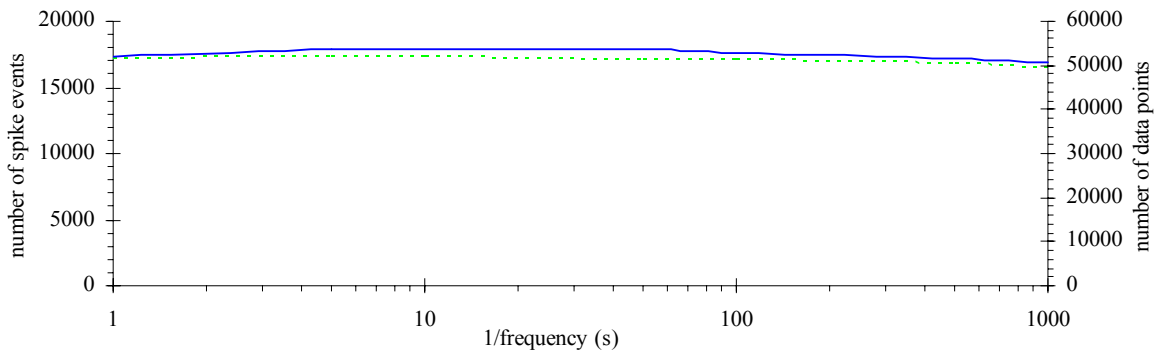

Figure A.11 – Results of sensitivity analysis on high-pass/low-pass filtering threshold parameter (Λ_f) during de-spiking stage.

Legend: – – – number of spike events found; —— number of erroneous data points found.

A.3.1.3 *Comments*

The sensitivity analysis of the pre-processing stage showed that the event threshold constants (C_{EP} and C_{EN}), filtering threshold (Λ_f) and statistical search window (SW) parameters had the greatest effect on the results. Standard values provided reasonable optima for most pre-processing parameters. The exception was the probe adjustment and navigation event thresholds. For these two parameters a lower threshold value could be recommended. Slightly lower values for the probe adjustment and navigation event threshold parameters (C_{EP}, C_{EN}) would allow more of the "known" events to be found, while still not removing good data. This conceivably would increase the effectiveness of the pre-processing stage and therefore the post-processing procedure.

Variation of pre-processing parameters had no significant affect on the de-spiking outcome. Therefore no results were shown. The variation of the filtering threshold parameter for all stages of post-processing also had no significant affect on the de-spiking outcome.

A.3.2 <u>Investigation Two: multiple field study sensitivity analysis</u>

Three independent field study data sets (performed at Eprapah Creek in 2003 and 2004) were used to study the reaction of the post-processing procedure under different field conditions. Table A.2 outlines the date, length and experimental conditions of each field study.

Table A.2 – Description of field studies undertaken at Eprapah Creek used in sensitivity analysis of key post-processing parameters.

Field study	Date	Duration (hours)	Total data points	P/A	N/E	Location AMTD (km)	Probe position (m)	ADV setup data
E2	17/07/03 06:26 to 14:10	7.75	693,129	10	6	2	0.4 to 0.6 bfs	f_{scan} = 25 Hz V_{range} = 100 cm/s
E3	24/11/03 09:18 to 15:55	6.5	593,297	12	9	2.1	0.4 to 0.6 bfs	f_{scan} = 25 Hz V_{range} = 100 cm/s
E4A	2/09/04 07:50 to 13:34	5.75	524,780	0	8	2.1	0.05 ab	f_{scan} = 25 Hz V_{range} = 100 cm/s

Note: P/A: number of probe adjustments; N/E: number of navigation events; V_{range} : maximum velocity range; f_{scan} : sampling frequency; bfs: depth below free surface; ab: elevation above bed; AMTD: Adopted Middle Thread Distance (distance upstream of mouth).

The field trips E2 and E3 were conducted near the free surface, but the data were measured at slightly different longitudinal locations, Sites 2 and 2B (Figure A.12A) respectively. Figures A.12B and A.12C shows that each location had distinct channel cross-sectional geometry characteristics, such as width, depth, and side slope. The field studies E3 and E4 were performed at the same site (Site 2B), but at different positions in the flow field (near free surface and bed respectively, Figure A.12C). Each field work was undertaken at distinct times during the Earth's annual cycle (providing different weather and flow conditions). With a different flow field position or AMTD location in the creek, these field investigations provided a good test of the post-processing procedure.

Only the key parameters that had a significant effect in Investigation One were investigated here.   These were: 1/ High-pass/low-pass filter parameter (Λ_f); 2/ Event threshold parameters (C_{EP}, C_{EN}); and 3/ Statistical search window parameter (SW). The effect of each parameter was assessed based upon the total number of erroneous data points (TEDP) found during post-processing, divided by the total number of data points of each data set (TNDP).

187

This is shown as a percentage in Figure A.13, which allowed the comparison of post-processing performance under different experimental conditions. Figure A.13 shows the impact of parameters Λ_f, C_{EP}, C_{EN} and SW on the results of the post-processing procedure for the field studies E2, E3 and E4.
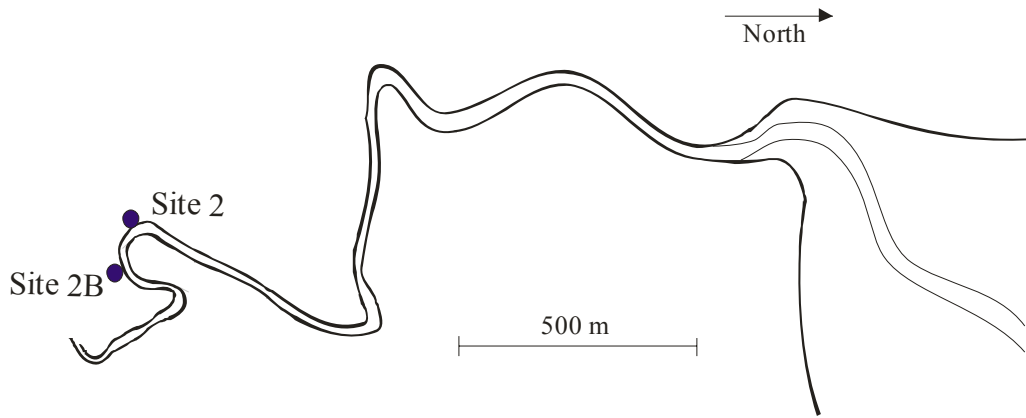
(A) Location of experimental sites used for field studies E2, E3 and E4.
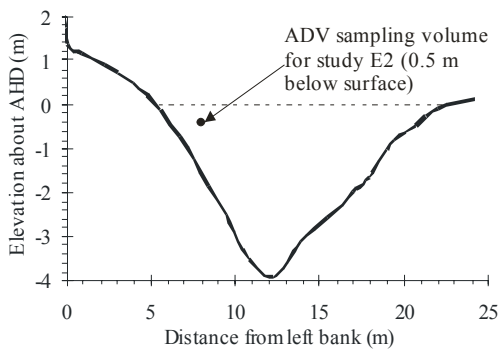
(B) Surveyed cross-section at Site 2 (study E2).
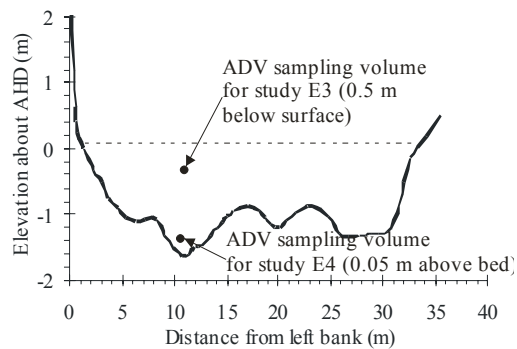
(C) Surveyed cross-section at Site 2B (studies E3 and E4).

Figure A.12 – Key differences between field studies E2, E3 and E4.

No probe adjustments occurred for the study E4, because the sampling volume was at a fixed position above the bed. In Figure A.13A, the magnitude of variation and the variation trend over the probe adjustment event threshold (C_{EP}) parameter range were identical (studies E2 and E3). Figure A.13B shows that for the navigation event threshold the most distinct difference seemed related to the probe position in the flow field. Results measured near the free surface (studies E2 and E3) were similar, but differed from that near the bed (study E4).

In Figure A.13C, the probe position in the flow field caused some differences in the sensitivity analysis outcomes when varying the statistical search window (SW) for the different studies. The magnitude of variation over the investigation range near the bed (study E4) was slightly larger than that at the free surface (studies E2 and E3). Figure A.13D shows
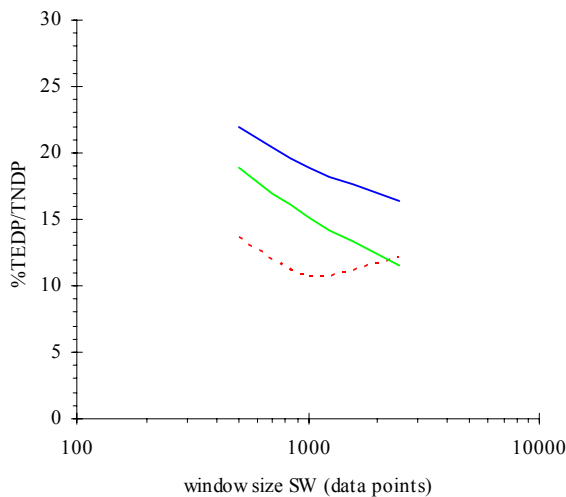
the variation of the filtering threshold had a larger effect near the free surface than near the bed. The results also seemed to indicate that the different cross-sectional geometry for Sites 2 and 2B could change the outcome when varying the filtering frequency.
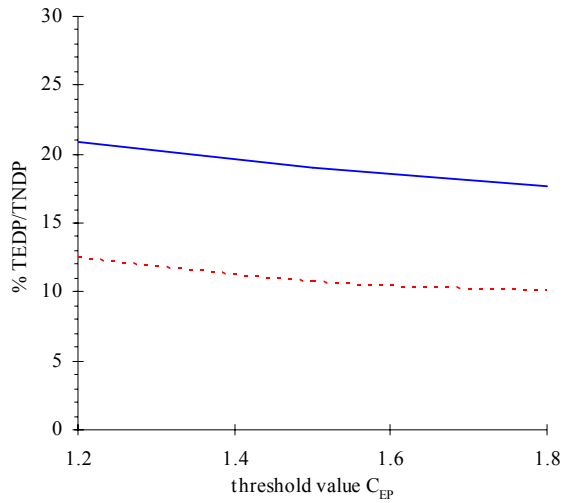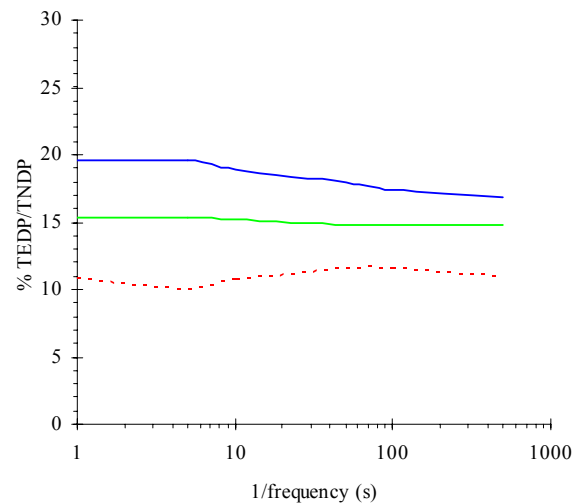

(A) Probe adjustment threshold (C_{EP}).
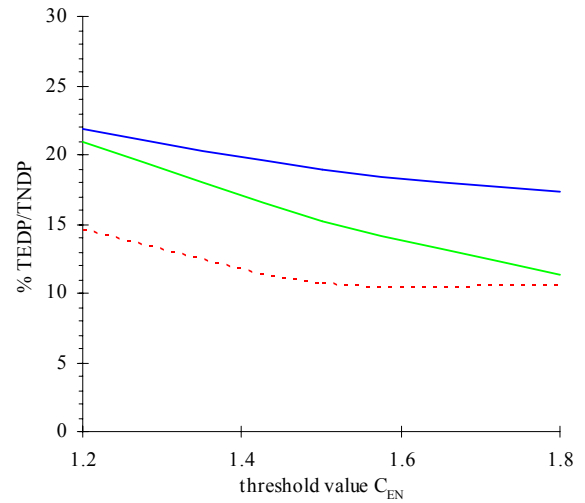
(B) Navigation event threshold (C_{EN}).

(C) Statistical search window size (SW).

(D) Filtering threshold (Λ_f).

Figure A.13 – Comparison of sensitivity analysis on pre-processing and filtering parameters in terms of percentage of erroneous data points for studies E2, E3 and E4.

Legend: —— results for study E2; – – – results for study E3; —— results for study E4.

A.3.2.1 *Comments*

This sensitivity analysis showed that the post-processing procedure provided consistent results for the studies E2, E3 and E4. Some differences in result trends over the variation range seemed related to the probe position in the flow field and to the AMTD location in the creek. The different positions of the probe in the flow field seemed related to different

magnitudes of result variations over the investigation range, between the free surface and near bed investigations.

No one parameter had a significantly large effect on the overall post-processing outcome. The impact of a given parameter seemed to be restricted to the stage of post-processing in which it was used. Although being used in both stages the filtering frequency threshold parameter (Λ_f) had a larger effect on the pre-processing stage than the de-spiking stage.

A.4   DISCUSSION

To investigate the effectiveness of post-processing procedure under different field conditions, three independent experimental data sets were used (Table A.2). All were performed at Eprapah Creek, Southeast Queensland in 2003 and 2004. Post-processing was conducted on each data set. First the data set was passed through the WinADV package. This flagged communication errors and data points when the average signal to noise ratio < 5 dB. Data points with an average correlation below a certain percent were also flagged. For the field studies E2 and E3, average correlations < 70 % were flagged, while for the study E4 average correlations < 60 % were flagged. The difference in threshold values related to the probes position in the flow field. All errors found during this stage were replaced and logged. The time-step, the three velocity components and the error flag data were written to a separate file. Pre-processing and de-spiking stages were performed using this modified file. In each stage of post-processing standard parameter values were used (Table A.1). Figure A.14 shows the data set of the field trip E2 after the velocity signal check errors were repaired.
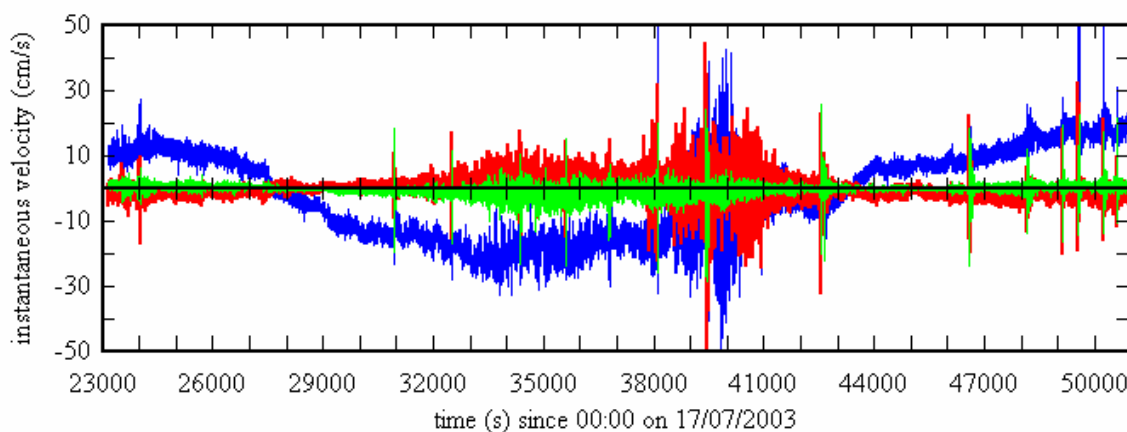

Figure A.14 – Data set of study E2 (17/07/03) after velocity signal check errors found using WinADV were repaired. Data collected at Site 2 Eprapah Creek, approximately 8.0 m from left bank and about 0.5 m below free surface.

Legend: — streamwise velocity V_x ; — transverse velocity V_y ; — vertical velocity V_z.

A.4.1 <u>Effectiveness of pre-processing stage</u>

Table A.3 shows the success of the probe adjustment and navigation event searches in locating known events using the standard parameter values. In the three data sets at least 75 % of the known probe adjustments events were found, while the percentage of navigation events found seemed lower (between 20 and 60 %). However, these values were deceptive, because probe adjustments and/or navigation events that occur close to one another may be found first and the corrupted data of both events replaced. Pre-processing actually removed more than 60 % of all navigation events that occurred during the three field studies. Those not detected tended to be those when the boat passed the probe at a good distance from the probe and at slow speed. The generated search region for the undetected navigation event was flagged for future investigation. The optimisation of both the navigation event and probe adjustment thresholds is vital to maximising the number of known events removed from the data set. Figure A.15 shows the field trip E2 data set after pre-processing was performed.

Table A.3 – Summary of pre-processing results for field study data sets.

Results for C_{EP} = 1.5 and C_{EN} = 1.5	E2	E3	E4A
Number of known probe adjustment events found	9/10	9/12	0/0
Number of known navigation events found	4/6	2/9	3/8
Actual number of known probe adjustments removed	9/10	9/12	0/0
Actual number of known navigation events removed	5/6	6/9	5/8
Total number of data points replaced during pre-processing	78,365	54,058	25,131

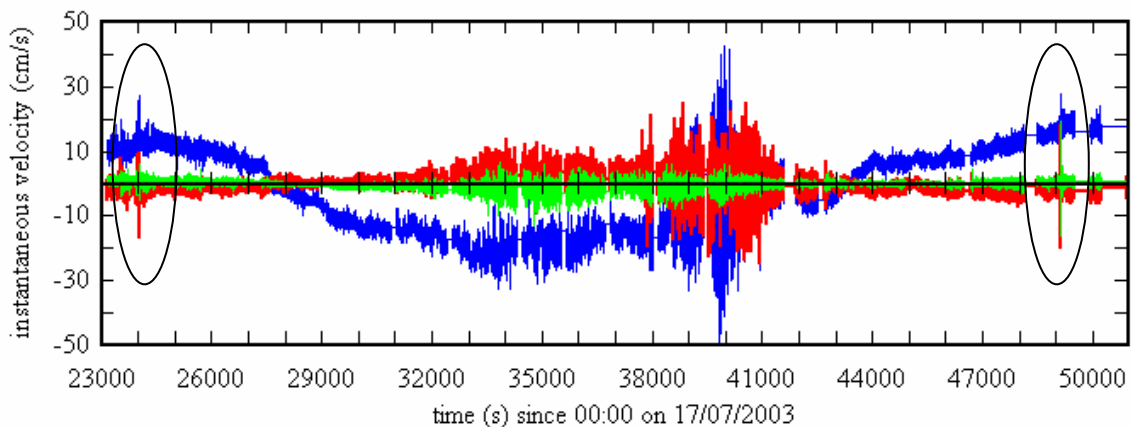Note: A1/A2: number of events found (A1)/number of known events recorded (A2).

Figure A.15 – Data set of study E2 (17/07/03) after probe adjustment and navigation events detected during pre-processing were replaced. Data measured at Site 2 Eprapah Creek, approximately 8.0 m from left bank and about 0.5 m below free surface.

Legend: — streamwise velocity V_x ; — transverse velocity V_y ; — vertical velocity V_z .

Highlighted in Figure A.15 are one probe adjustment and one navigation event that the pre-processing searches missed when using the standard threshold parameter values. Both highlighted events were detected if the probe adjustment and navigation event search thresholds were lowered (i.e. C_{EP}, C_{EN} = 1.4). At this stage optimisation is difficult without independent velocity measurements to compare with those of the ADV. Independent velocity data would allow the true effect of probe adjustments and navigation events to be understood.

A.4.2   Effectiveness of de-spiking stage

Figure A.16 shows the effectiveness of the phase-space thresholding method in detecting and repairing data affected by extreme Doppler noise events for the study E2. One such period of high noise was found between t = 38,000 to 41,000 s from midnight on 17/07/03 (Sample A, Figure A.16). The source of the high noise region in the data set of study E2 is unknown, because of the complex nature of the field site and experimental setup.
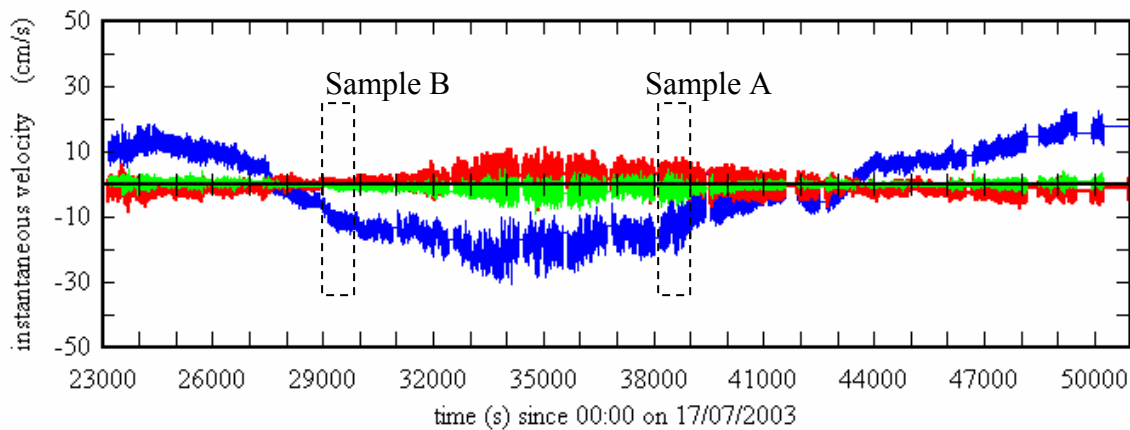

Figure A.16 – Data set of study E2 (17/07/03) after detected "spike events" were repaired. Data collected at Site 2 Eprapah Creek, approximately 8.0 m from left bank and about 0.5 m below free surface.

Legend: — streamwise velocity V_x ; — transverse velocity V_y ; — vertical velocity V_z .

The phase-space thresholding method had a large affect on turbulence statistics in sections of high noise, while regions of little or no noise remain relatively unchanged. Table A.4 demonstrates the effect of the phase-space thresholding method on the turbulence statistics. In Table A.4 the statistics of Sample A (high noise sample) and Sample B (low noise sample) before and after de-spiking are shown. Both Sample A and Sample B (starting at t = 38,000 and 29,000 s since midnight on 17/07/03 respectively) are highlighted in Figure A.16. Sample A contained 62 % erroneous data points caused by "spike events", while Sample B contained no erroneous data points. For Sample A there was a large difference in turbulence

statistics before and after de-spiking. Whereas for Sample B the difference between the turbulence statistics before and after de-spiking was small. This demonstrated that the phase-space thresholding method seemed to operate effectively. It did not find "spike events" where there were none and effectively reduced the influence of data containing a large number of "spike events".

Table A.4 – Comparison of statistics for two data samples of streamwise velocity (study E2). Sample A (high noise region, t = 38,000 s) and Sample B (low noise region, t = 29,000 s). Both data samples contain 5,000 data points.

	$\overline{V_x}$ (cm/s)	v_x' (cm/s)	$Sk(V_x)$	$Ku(V_x)$
Sample A before de-spiking	-4.39	3.39	0.002	5.91
Sample A after de-spiking	-4.59	1.66	-0.095	-0.246
Sample B before de-spiking	-10.17	0.83	0.005	-0.066
Sample B after de-spiking	-10.17	0.83	0.005	-0.066

Note: $\overline{V_x}$: time-averaged streamwise velocity; v_x' : standard deviation of streamwise velocity; $Sk(V_x)$: skewness of streamwise velocity; and $Ku(V_x)$: kurtosis of streamwise velocity.

A.4.3   Effectiveness of post-processing

During post-processing the number of erroneous data points flagged and replaced at each stage are shown in Table A.5. Of special importance, is the effect that the pre-processing stage had on the post-processing outcome. Table A.5 shows that between 10 and 20 % of the data sets (studies E2, E3 and E4) were erroneous. More than 80 % of these erroneous data points were found during post-processing. The pre-processing stage alone found that between 3 and 11 % of the total number of data points to be erroneous in these data sets. This was a significant percentage of the data sets, thereby validating the use of the pre-processing stage.

The number of erroneous data points found through the de-spiking stage was dependent on the quantity of noise present during data collection. Results of the phase-space thresholding method seemed effective in checking that the post-processed data were of an appropriate quality for analysis. The use of the pre-processing stage before the de-spiking stage changed the de-spiking outcome by between 5 and 20 % for the data sets (studies E2, E3 and E4). This highlighted that the pre-processing stage not only removed erroneous data points not found during the de-spiking stage, but also improved the effectiveness of the de-spiking stage in detecting spike events.

Table A.5 – Results of post-processing of three independent field investigations.

Field Study	E2	E3	E4	Description
Total number of data points	696,129	593,297	(A) 524,780 (B) 317,027	
Number of erroneous data points (1)	5,580	12,762	(A) 440 (B) 1	(1) Velocity signal check (WinADV)
Number of erroneous data points (2)	PA 34,518 NE 43,487 TOT 78,005	PA 36,518 NE 17,540 TOT 54,058	NE (A) 25,131 NE (B) 0 TOT(A + B) 25,131	(2) Pre-processing
Number of erroneous data points (3A)	53,596	9,118	(A) 54,398 (B) 6,809	(3A) De-spiking and pre-processing
Number of erroneous data points (3B)	50,489	11,486	(A) 51,519 (B) 6,809	(3B) De-spiking (no pre-processing)
Total number of erroneous data points (1 + 3B)	56,069	24,248	58,769	(1 + 3B) Conventional post-processing
Total number of erroneous data points (1 + 2 + 3A)	137,181	75,938	86,779	(1 + 2 + 3A) Complete post-processing

Note: PA: probe adjustment search; NE: navigation event search; TOT: total for pre-processing stage; (A): first data set of study E4; (B): second data set of study E4.

A.4.4 Summary

Post-processing is an effective and necessary procedure that needs to be conducted before analysis of turbulence data can begin. This is especially true for long duration studies in which continuous measurements were recorded in natural systems. In such studies, probe adjustments and navigation events may occur that affect the recorded data. This study showed that these events needed to be replaced within the data set before analysis. The pre-processing stage of post-processing proved effective in finding and removing these events.

Both the de-spiking and pre-processing stages seemed to work effectively for the low velocity unsteady flows of the estuarine systems under investigation. A lot of this was because of the filtering of data undertaken. In unsteady flows, not performing post-processing on the high-pass filtered data limited the effectiveness of both the de-spiking and pre-processing stages.

B.1   PRESENTATION

This Appendix outlines in detail the data analysis methods used in this investigation of the turbulence properties in a small subtropical estuary. The main focus of this study was the turbulence velocity data measured by acoustic Doppler velocimetry (ADV). For each field study the instantaneous velocity data collected by each ADV underwent a post-processing technique first outlined in Chanson et al. (2005b). Each post-processed data set contained the three instantaneous velocity components V_x, V_y and V_z, where x is the streamwise direction (positive downstream); y is the transverse direction (positive towards left bank); and z is the vertical direction (positive upwards).

All turbulence properties were calculated using the sampling size and sampling technique described in Section B.1.1. Note that a data sample was considered corrupted if more than 20 % of the data points in that sample were erroneous. Corrupted data samples were not analysed (i.e. left blank), so as not to influence the turbulence properties investigated. Section B.2 describes the sensitivity analysis conducted to determine the sampling size used in the turbulence analysis.   The methods used to calculate the turbulence properties under investigation are presented in Section B.3. These included the first four statistical moments of each velocity component and tangential Reynolds stresses and the integral and dissipation time scales. The analysis also yielded the correlation coefficients of Reynolds stress, the horizontal and vertical turbulence intensity ratios, bed shear stress and the triple products of streamwise velocity. Section B.4 describes the spectrum analysis techniques used during this investigation and the technique for generating the spectrum.

B.1.1   <u>Turbulence statistics sampling technique</u>

In natural estuaries, the flow is unsteady and gradually time-variable. The sample size for the calculation of the time-averaged velocity ($\overline{V}$) effectively acts as a low-pass filter threshold. The cut-off frequency affects the calculation of the turbulent velocity fluctuations v ($v = V - \overline{V}$) for a given data set. This cut-off frequency is critical and must provide a sample size that yields statistically meaningful results, be larger than the turbulent velocity fluctuations, yet smaller than the variation of the tides.

For the present study all the turbulence properties were processed over 200 s (5,000 data points at 25 Hz and 10,000 data points at 50 Hz). A sensitivity analysis (Section B.2) found that a sampling period of 200 s allowed approximately 95 % of all data samples to be statistically stationary over several tidal cycles. The statistical properties of stationary data

samples are easier to calculate than those of non-stationary data samples, simplifying the analysis methods used. Turbulence properties were calculated every 10 s along the entire data set to limit the number of samples to be analysed. As the "10 s" interval was smaller than the sample size (200 s), the data points within the neighbouring samples over lap (Figure B.1). Figure B.1 illustrates the data sampling technique.
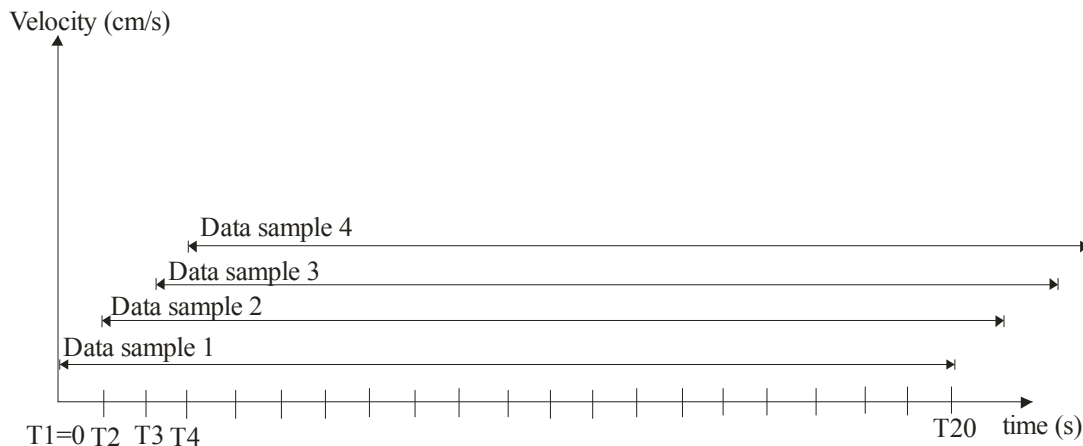

Figure B.1 – Data sampling technique used for calculation of turbulence properties.

B.2   SENSITIVITY ANALYSIS: STATISTICAL WINDOW SIZE FOR TURBULENCE ANALYSIS

A sensitivity analysis was performed to determine an appropriate statistical sampling size for the turbulence data collected at Eprapah Creek. The field studies E5, E6 and E7 conducted at Eprapah Creek were used in this sensitivity analysis, with each study having an investigation period of between 25 and 50 hours. Table B.1 outlines some key information on the field studies E5, E6 and E7. The studies E5 and E6 were undertaken mid estuary under spring and neap tidal conditions respectively, while the study E7 was performed in the upper estuary under neap tidal conditions. Section B.2.1 looks at the variation of water level over different sample periods. In Section B.2.2 the effect of sample size on the mean trend of the time-averaged velocity is investigated, while Section B.2.3 investigates the effect of sample size on the percentage of data samples that are stationary for the data sets of the studies E5 and E6

Table B.1 – Investigation and sampling information for studies E5, E6 and E7.

Study	E5	E6	E7
Date	8-9/03/05	16-18/05/05	5-7/06/06
Focus	Spring tides - middle estuary	Neap tides – middle estuary	Neap tides – upper estuary
Duration (hours)	25	48	50
Tidal range (m)	2.48	1.37	1.52
Rainfall (mm)	0	0	0
Mean depth (m)	1.6	1.6	1.7
Site	2B	2B	3
AMTD (km)	2.1	2.1	3.1
ADV Sampling location	0.1 m above bed, 10.7 m from left bank	0.4 m above bed, 10.7 m from left bank	0.4 m above bed, 4.2 m from right bank
f_{scan} (Hz) 3D-ADV	25	25	25
YSI6600 sampling location	0.1 m above bed, 10.4 m from left bank	0.4 m above bed, 10.4 m from left bank	0.4 m above bed, 3.9 m from right bank
f_{scan} (Hz) YSI6600	0.167	0.083	0.083

Note: AMTD: Australian Middle Thread Distance (upstream from mouth); f_{scan} : sampling frequency; Tidal range: maximum observed at sampling location.

B.2.1   Variation in water level over sample period

The sample size must be larger than the turbulent velocity fluctuations, yet smaller than the variation of the mean properties. In estuaries the flow is unsteady and time-variable predominantly because of the variation in water level from the tides. If the variation of water level over the sampling period is relatively small then the flow behaves in a "pseudo" steady fashion. Therefore, the first test of sampling size was to determine the variation of water level over the sampling period. A YSI6600 collected water level data at the experimental site, sampling every 6 s (study E5) or 12 s (studies E6 and E7) throughout the investigation periods. Figure B.2 shows the maximum and median values of water level variations over each sampling period investigated. In Figure B.2 the maximum and median values of the water level variation over the sampling period increased as the sampling period increased. The water level variations over the sampling period were similar for sampling periods less than 200 s. However, the magnitude of water level variation began to increase for sampling periods larger than 200 s.

For a sampling period of 200 s, the median value of water level variation over the sampling volume was 0.01 m over the investigation periods of the studies E5, E6 and E7. Also the maximum variation in water level over the sampling period was less than 0.04 m for these

field studies. These maximum and median values were significantly smaller than the tidal ranges and mean depths observed at the experimental sites for the field studies E5, E6 and E7.
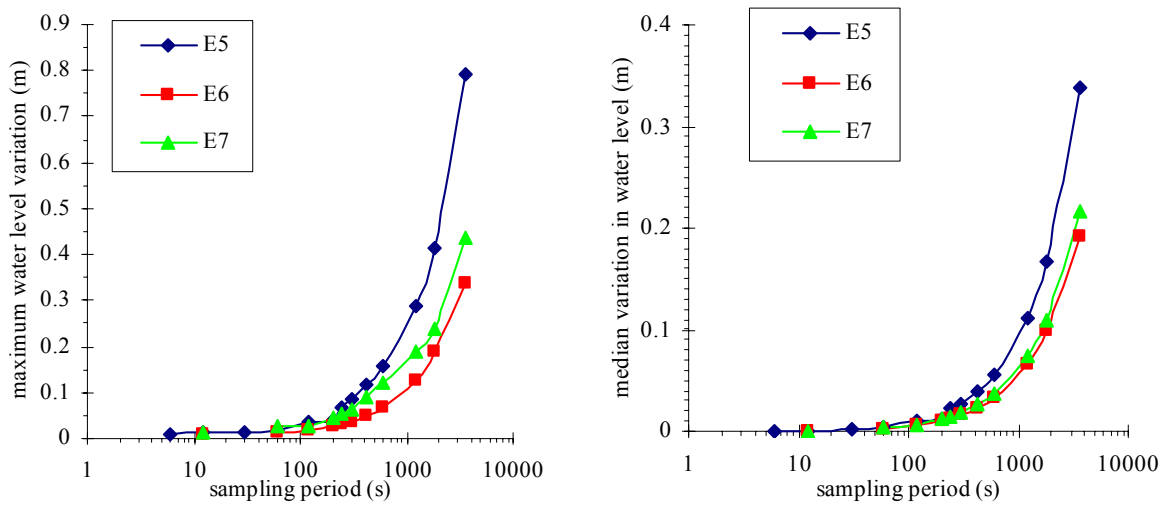
(A) Maximum values of water level variation.

(B) Median values of water level variation.

Figure B.2 – Maximum and median values of water level variation over sampling period. Data collected by YSI6600 probe located at sampling site for studies E5, E6 and E7.

B.2.2   Effect of sample size on time-averaged velocity data

In Figure B.2 the variation in water level over the sampling period was largest for the spring tidal conditions of the field study E5. Therefore, the effect of the sampling size on the time-averaged velocity data will be investigated using the data set of the study E5. The sample size for the calculation of the time-averaged velocity $\overline{V}$ effectively acts as a low-pass filter threshold. Figure B.3 shows the time-averaged streamwise velocity for the sampling sizes 1,000, 5,000, 10,000 and 50,000 data points as functions of time. At a sampling frequency of 25 Hz these samplings sizes are equivalent to sampling periods of 40, 200, 400 and 2,000 s respectively.

In Figure B.3 a sampling size of 1,000 data points seemed to provide too high of a cut-off frequency, as the time-averaged data seemed to still include some higher frequency velocity oscillations. For sampling sizes between 1,000 and 10,000 data points the mean trend of the time-averaged streamwise velocity seemed similar, while for sampling sizes larger 10,000 data points, the difference between the mean trends in time-averaged velocity increased as the sample size increased (e.g. 50,000 data points, Figure B.3).
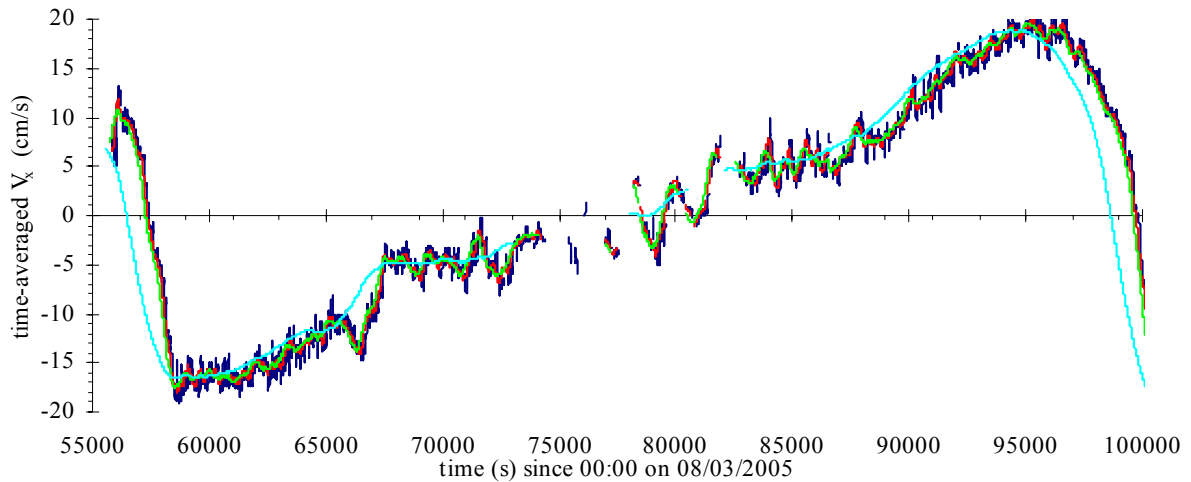
Figure B.3 – Effect of sampling size on time-averaged streamwise velocity of study E5 (8-9/03/05). Data measured by 3D-ADV (10 MHz) 0.1 m above bed at Site 2B Eprapah Creek. Statistical samples taken every 10 s along entire data set.

Legend: — 1,000 data points; — 5,000 data points; — 10,000 data points; — 50,000 data points.

B.2.3 Stationarity test

The stationarity of a data sample indicates whether the mean and variance of the data vary over the length of the sample (Bendat and Piersol (1971)). If the mean and variance of the data do not vary over the sample then that sample is considered stationary. The calculation of statistical properties of a stationary sample are simpler than for a non-stationary data sample. This section uses the "run test" of Bendat and Piersol (1971) to test the stationarity of several sampling sizes for the for three velocity components of the post-processed velocity data of the field studies E5 and E6. Table B.2 presents the average percentage of stationary data of several sampling sizes for all velocity data of the field studies E5 and E6. In Table B.2, the percentage of stationary data was similar for sample sizes less than 5,000 data points, while the number of stationary samples decreased as the sample size increased for sample sizes larger than this.

Table B.2 – Average percentage of stationary samples of all velocity components in data sets of studies E5 and E6 (data sampled at 25 Hz).

Field study	Number of samples	Percentage of stationary samples			
		1,000 dp	5,000 dp	10,000 dp	50,000 dp
E5	8,001	96	95	90	74
E6	16,289	94	94	86	75

Note: dp: data points.

B.2.4 Summary

From this sensitivity analysis the sampling size of 200 s (5,000 data points at 25 Hz) was chosen because it was much larger than the instantaneous velocity fluctuation time scales, contained enough points to yield statistically meaningful results and considerably smaller than the period of the tidal fluctuations. A sample size of 200 s meant approximately 95 % of all data samples for the field studies E5 and E6 were stationary, which simplified the calculation of the turbulence statistics.

B.3 ANALYTICAL METHODS USED

B.3.1 Statistical moments

The first four statistical moments (time-averaged mean, standard deviation, skewness and kurtosis) of the velocity and tangential Reynolds stresses were used. These were calculated using the definition of statistical moments provided in Press et al. (1992). Press et al. defined the time-averaged mean ($\overline{X}$), standard deviation (x'), skewness ($Sk(X)$) and kurtosis ($Ku(X)$) of the instantaneous random variable X as:

$$\overline{X} = \frac{1}{N}\sum_{j=1}^{N} X_j \tag{B.1}$$

$$x' = \sqrt{\frac{1}{N-1}\sum_{j=1}^{N}\left(X_j - \overline{X}\right)^2} \tag{B.2}$$

$$Sk(X) = \frac{1}{N}\sum_{j=1}^{N}\left[\frac{X_j - \overline{X}}{x'}\right]^3 \tag{B.3}$$

$$Ku(X) = \left\{\frac{1}{N}\sum_{j=1}^{N}\left[\frac{X_j - \overline{X}}{x'}\right]^4\right\} - 3 \tag{B.4}$$

where N = number of data points in sample; j = data point number; and X_j = data value at sample number j. The kurtosis is zero for a Gaussian distribution and this definition is known as "excess kurtosis" (Kenney and Keeping (1951)).

The standard deviation characterises the magnitude of fluctuations about the time-averaged mean. Skewness and kurtosis provide some information regarding the temporal distribution of fluctuations around its mean value and the deviations from a Gaussian distribution. A non-zero skewness indicates some degree of temporal asymmetry of the turbulence fluctuations (e.g. sweep versus ejection). A kurtosis larger than zero is associated with a peaky signal (e.g. produced by intermittent turbulent events). Although turbulence is a "random" process and

hence Gaussian, Bradshaw (1971) stated that: "the small departures from a Gaussian probability distribution are the most interesting features of the turbulence".

B.3.2 Instantaneous Reynolds stress

The Reynolds stress tensor included the normal stresses and tangential stresses. A Reynolds stress describes a transport effect resulting from the turbulent motion induced by velocity fluctuations, with its subsequent increase of momentum exchange and mixing (Piquet (1999)). The instantaneous Reynolds stress is defined as:

$$\rho v_l v_m = \rho \left(V_l(j) - \overline{V_l} \right)\left(V_m(j) - \overline{V_m} \right) \tag{B.5}$$

The instantaneous values of $\overline{V_l}$, $\overline{V_m}$ (l, m = direction tensors: x, y, z) were calculated using 200 s samples from the data point being calculated. The first four statistical moments of each tangential Reynolds stress were calculated from this instantaneous Reynolds stress data.

B.3.3 Turbulence time scales

An autocorrelation analysis was used to calculate the Eulerian integral and dissipation time scales. The normalised autocorrelation function R_{ii} for a point measurement was defined as:

$$R_{ii}(\tau) = \frac{R(v_i(t),\ v_i(t+\tau))}{v_i'^2} \tag{B.6}$$

where v is the instantaneous velocity fluctuation ($v = V - \overline{V}$); v' is the standard deviation of velocity; i is a direction tensor ($i = x, y, z$); τ is the time lag; and R is the covariance function. Figure B.4 shows an autocorrelation function and demonstrates how the Eulerian integral and dissipation time scales were calculated from it.
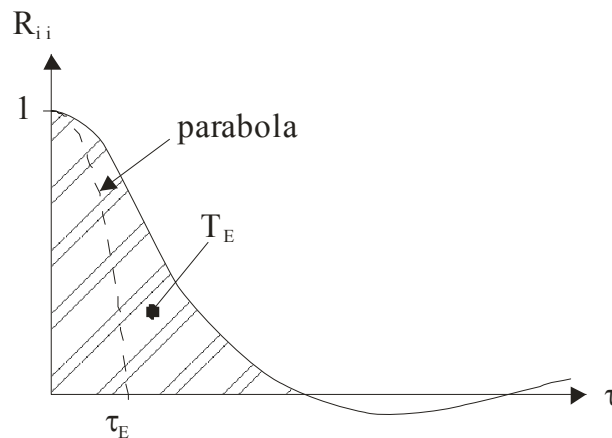
Figure B.4 – Sketch defining an autocorrelation function and Eulerian integral T_E and dissipation τ_E time scales.

B.3.3.1 *Integral time scales*

The integral time scale represents the longest connection in the turbulent velocity fluctuations. Piquet (1999) defined the integral time scale T_E as:

$$T_E = \int_{\tau=0}^{\tau(R_{ii}(\tau)=0)} R_{ii}(\tau)\,d\tau \qquad\qquad (B.7)$$

where τ is the time lag; R_{ii} is the normalised autocorrelation function; i is a direction tensor (i = x, y, z); and $\tau(R_{ii}(\tau)=0)$ is the time lag for which $R_{ii}=0$ (Figure B.5). Integral time scales are equal to the area under the normalised autocorrelation curve up to $R_{ii}(\tau)=0$. Figure B.5 illustrates the calculation of the integral time scale.
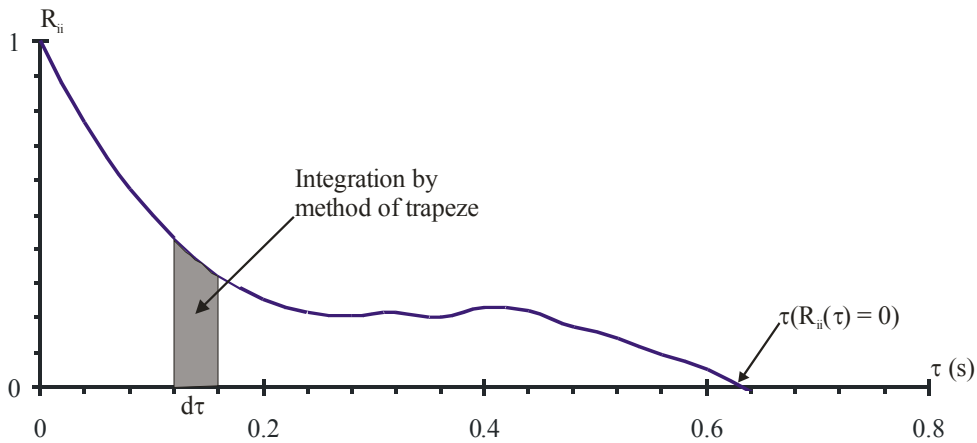
Figure B.5 – Calculation of integral time scale using area under autocorrelation function until $R_{ii}(\tau)=0$. Data in example from field study E2 (17/07/03) for data sample of 200 s.

For each data sample of 200 s (5,000 (25 Hz) and 10,000 (50 Hz) data points), the integral time scale was calculated for each correlation window of 10 s (250 (25 Hz) and 500 (50 Hz) data points). The overall integral time scale of the data sample was calculated by averaging the individual integral time scales of the correlation windows within that sample. At present the individual correlation windows within a statistical data sample window do not overlap. If $\tau(R_{ii}(\tau)=0) < 1/f_{scan}$ then the value of that sample was ignored.

B.3.3.2 *Dissipation time scales*

The dissipation time scale τ_E is a measure of the most rapid changes that occur in the turbulent fluctuations of velocity v(t) (Hinze (1975)). It is related to the curvature of the autocorrelation function at the origin ($\tau = 0$). Using the Taylor series expansion of the autocorrelation function the dissipation time scale τ_E may be expressed as:

$$\tau_E = \sqrt{\dfrac{2\,\overline{v'^2}}{\overline{\left(\dfrac{\partial v}{\partial t}\right)^2}}} \qquad\qquad\qquad (B.8)$$

Hallback et al. (1989), Fransson et al. (2005) and Koch and Chanson (2005) used the above formula to obtain a measured time scale $\tau_E(\delta t)$ based upon the time increment δt:

$$\tau_E(\delta t) = \sqrt{\dfrac{2\,\overline{v'^2}}{\overline{\left(\dfrac{\delta v}{\delta t}\right)^2}}} \qquad\qquad\qquad (B.9)$$

where v' standard deviation of velocity component; δt_{scan} is the experimental scan rate ($1/f_{scan}$, $f_{scan} = 25$ or 50 Hz); and δt is a time increment ($\delta t_{scan} \leq \delta t \leq 4\,\delta t_{scan}$). Following Koch and Chanson (2005) several time increments $\delta t = \delta t_{scan}$, $2\,\delta t_{scan}$ and $4\,\delta t_{scan}$ were used to calculate $\tau_E(\delta t)$ with the results fitted by a quadratic expression:

$$\tau_E(\delta t) = \tau_E(0) + a\,\delta t^2 + b\,\delta t \qquad\qquad\qquad (B.10)$$

where $\tau_E(0)$ is the estimated dissipation time scale; and a and b are constants calculated from best data fit. Figure B.6 explains the calculation of the dissipation time scale through quadratic interpolation.
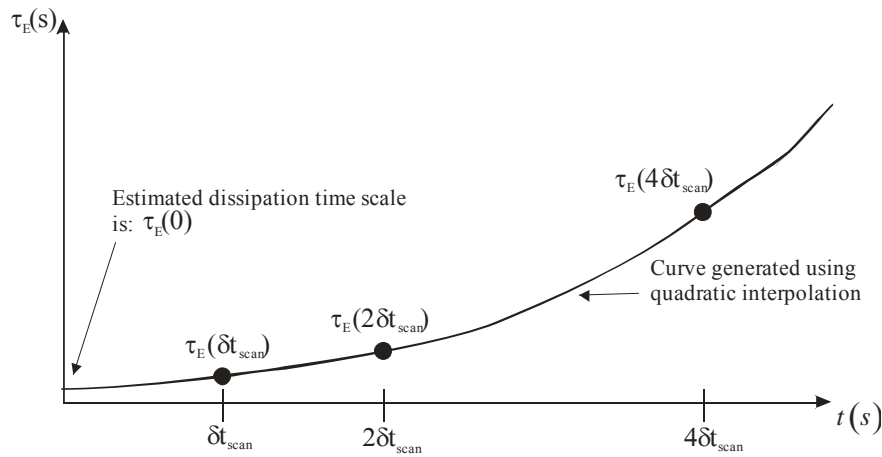
Figure B.6 – Definition sketch for dissipation time scales.

Within the data sample of 200 s (5,000 (25 Hz) and 10,000 (50 Hz) data points), an overlapping correlation window of 10 s (250 (25 Hz) and 500 (50 Hz) data points) in size was used to calculate numerous values of $\tau_E(\delta t)$. These values of $\tau_E(\delta t)$ were averaged to provide a value of $\tau_E(\delta t)$ most representative of that statistical data sample. If during quadratic interpolation $\tau_E(0)$ was negative, that value was ignored.

B.3.4 Dimensionless turbulence parameters

Some dimensionless turbulence properties were investigated during this report. These were the horizontal and vertical turbulence intensity ratios (v'_y/v'_x and v'_z/v'_x) and the correlation coefficients of tangential Reynolds stresses (R_{vxvy} , R_{vxvz} and R_{vyvz}). The turbulence intensity ratios are a dimensionless parameter that describe the structure of the turbulence (Nezu and Nakagawa (1993)). A correlation coefficient of tangential Reynolds stress (e.g. $R_{vxvy} = \overline{v_x v_y}/(v'_x v'_y)$) indicates the degree of similarity of the turbulence (Nezu and Nakagawa (1993)).

B.3.5 Bed shear stress

The bed shear stress τ_b is an important property in the study of sediment transport, as it determines the quantity and size of sediment suspended or transported (Fredsoe and Diegaard (1992)). In this study the bed shear stress was approximated using the magnitude of the horizontal velocity U_{xy} at 0.2 m above the bed:

$$\tau_b = 0.5 \, \rho \, C_D \, U_{xy}^2 \tag{B.11}$$

$$C_D = \left(\kappa/\ln(z_r/z_0) \right)^2 \tag{B.12}$$

where ρ = water density; C_D = coefficient of drag; $U_{xy} = \sqrt{V_x^2 + V_y^2}$ is the horizontal velocity magnitude in the ADV sampling volume; κ = von Karman constant; z_r = distance above the bed; and z_o = (grain diameter)/30. For these calculations a logarithmic velocity profile was assumed and C_D is approximated by Equation B.12 (Bricker et al. (2005)).

B.3.6 Triple-correlations of streamwise velocity

Triple correlations characterise transport of Reynolds stress by velocity fluctuations (Bradshaw (1976)). Here the triple correlations $\overline{v_x v_x v_y}$, $\overline{v_x v_x v_z}$ and $\overline{v_x v_y v_z}$ represent the transport of the tangential Reynolds stresses $\overline{v_x v_y}$, $\overline{v_x v_z}$ and $\overline{v_y v_z}$ in the streamwise direction. These time-averaged triple correlations were calculated using:

$$\overline{v_l v_m v_n} = \overline{(V_l - \overline{V_l})(V_m - \overline{V_m})(V_n - \overline{V_n})} \tag{B.13}$$

where l, m, n = direction tensors (e.g. x, y, z); V = instantaneous velocity; and $\overline{V}$ = time-averaged velocity.

B.4 SPECTRUM ANALYSIS

The frequency spectrum shows how the energy of the fluctuations in a random time series (e.g. velocity) are distributed with frequency (Figure B.7). The amplitude of the peaks in the spectrum show the quantity of energy that the fluctuations of that frequency contributed to the random time series. Analysis of a frequency spectrum effectively decomposes the complex time series into its simplest most basic constituents. Here the aim of the spectrum analysis is to isolate those fluctuation frequencies that contributed most energy to the random time series (e.g. velocity). In a spectrum the frequency peaks with the largest amplitudes in the frequency spectrum are considered the predominant fluctuations in that time series as these contributed the most energy.
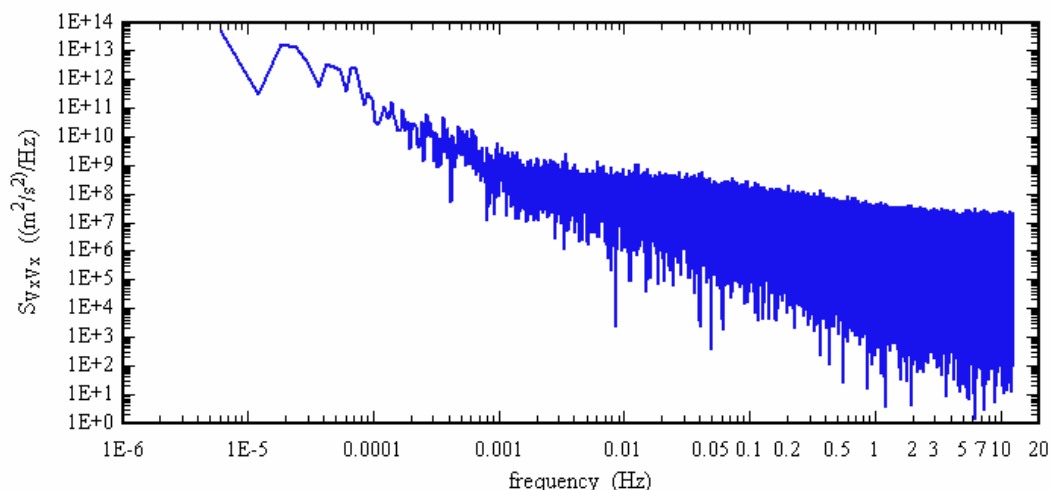
Figure B.7 – Example of frequency spectrum. Frequency spectrum of streamwise velocity $S_{V_x V_x}$ for field study E5 (8-9/03/05) conducted 0.1 m above bed at Site 2B Eprapah Creek.

In this study the frequency spectrum of the velocity and physio-chemistry data time series measured were converted into a frequency spectrum using FORTRAN code adapted from the "spctrm" subroutine of Press et al. (1992). The "spctrm" routine uses FFT to convert the time series into the frequency domain. Texts such as Bendat and Piersol (1993) and Priestley (1981) outline the theory behind the creation of a spectrum using FFT. For each time series, a frequency spectrum was calculated over the entire length of that series (i.e. investigation period). The data series was extended out to the nearest power of two (2^N) using the value of the last data point of the series.

APPENDIX C   FIELD DATA COLLECTED AT EPRAPAH CREEK (AUSTRALIA)

C.1   INTRODUCTION

Nine field investigations were conducted at Eprapah Creek for the period between 2003 and 2007. Eprapah Creek is a small subtropical stream located on the East coast of Australia, near the city of Brisbane. In the estuary the mean water depth is typically 1 to 2 m, and the width is approximately 20 to 40 m. The creek is approximately 12.6 km long with an estuarine zone of about 3.8 km. Figure C.1 shows a sketch of the Eprapah Creek estuarine zone. Table C.1 outlines the nine field investigations undertaken at Eprapah Creek between 2003 and 2007. The experimental sites used at Eprapah Creek are indicated in Figure C.1.
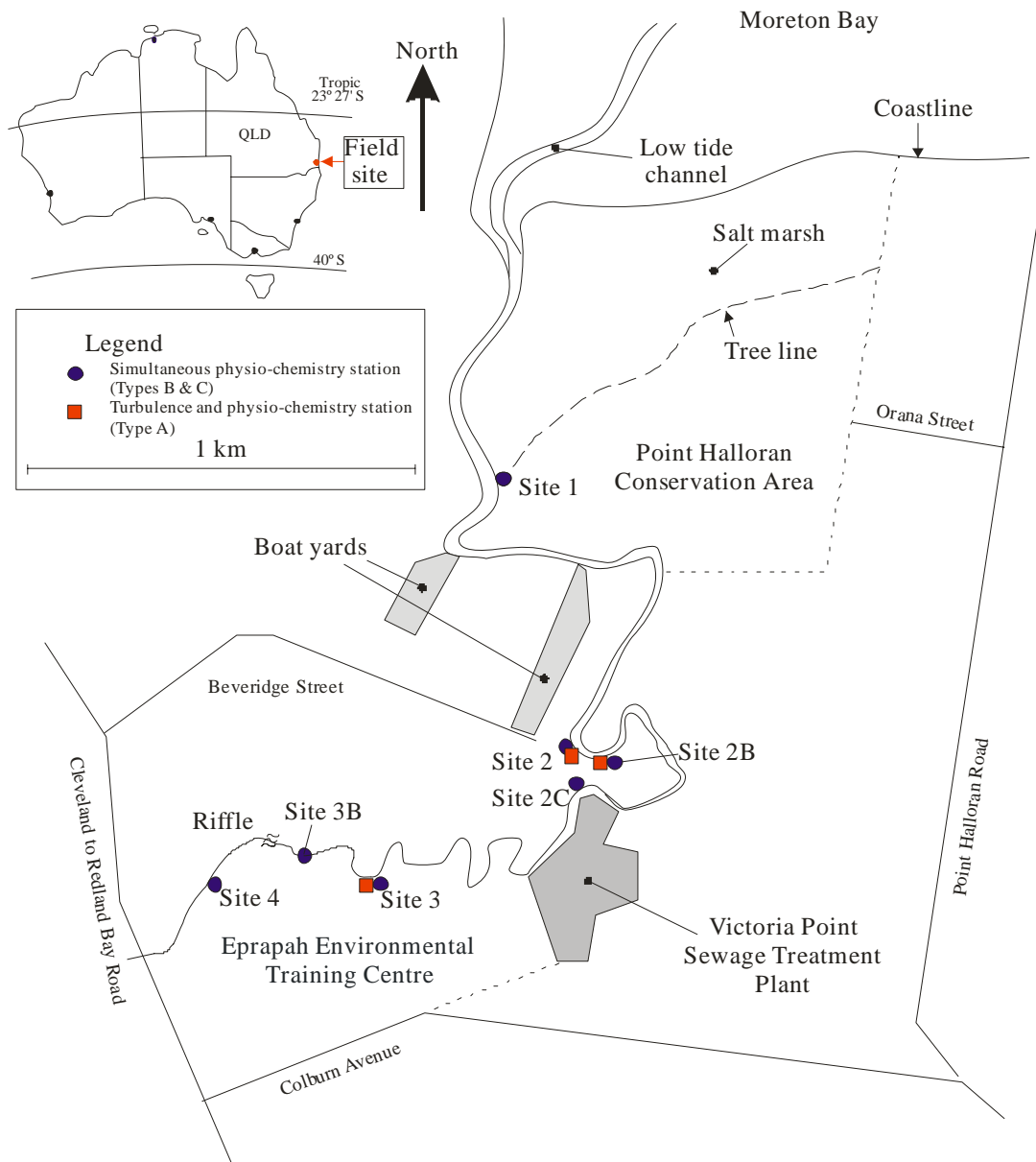
Figure C.1 – Sketch of Eprapah Creek and sampling locations used.

The main data sets for the field studies at Eprapah Creek were the turbulence and physio-chemistry recorded continuously throughout most field studies and the vertical physio-chemical profiles collected during or about each field study. For the field studies E1 to E7 high frequency turbulence and physio-chemistry data were measured at Sites 2, 2B or 3 (Figure C.2). Figure C.2 shows the experimental cross-sections at Sites 2, 2B and 3 and the approximate transverse location of the sampling volumes used in the field studies performed at each site (Table C.1).

Table C.1 – Field studies conducted at Eprapah Creek between 2003 and 2007.

Field study	Date	Duration (hours)	Tidal range (m)	Longitudinal sampling location (km)	Data collected
E1	4/04/03	12	1.84	2.1 (Site 2B) 0.0, 1.0, 2.0, 3.1	A B
E2	17/07/03	8	2.03	2.0 (Site 2) 0.0, 2.0, 2.7	A B
E3	24/11/03	7	2.53	2.1 (Site 2B) 1.0, 2.0, 3.1	A B
E4	2/09/04	12	1.81	2.1 (Site 2B) 1.0, 2.0, 3.1	A B
E5	8-9/03/05	25	2.37	2.1 (Site 2B) 0.0, 2.0, 2.4, 2.7	A B
E6	16-18/05/05	48	1.36	2.1 (Site 2B) 0.0, 1.0, 2.0, 2.7, 3.1	A B
E7	5-7/06/06	50	1.38	3.1 (Site 3) 0.0, 1.0, 2.0, 2.7, 3.1	A B
E8	28/08/06	12	1.51	0.0, 1.0, 2.0, 2.7, 3.1	B
E9	2-4/10/06 11-13/10/06	50 50	1.92 1.86	0.0, 1.0, 2.0, 2.7	B

Note: A: continuous turbulence and physio-chemistry data collected; B: vertical physio-chemistry profile data collected; Tidal range: maximum observed at Victoria Point.

Section C.2 presents the instantaneous velocity data collected through acoustic Doppler velocimetry at Eprapah Creek during the first seven field studies. In Section C.3 the instantaneous physio-chemistry data recorded by YSI6600 probes during the first seven field studies are presented. The vertical physio-chemistry profiles measured by a YSI6920 probe at Eprapah Creek during or about all field studies are presented in Section C.4.
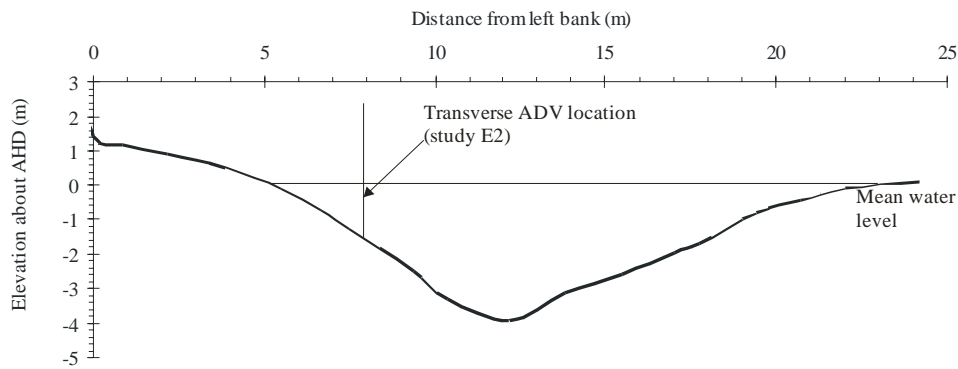
(A) Cross-section at Site 2, located 2.0 km from mouth.
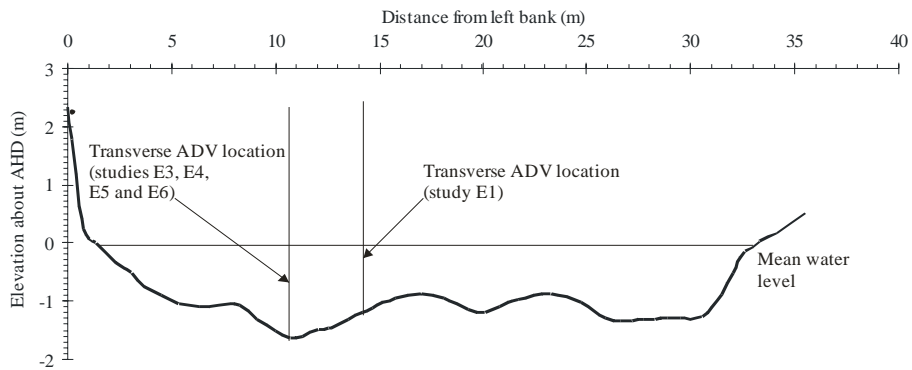
(B) Cross-section at Site 2B, located 2.1 km from mouth.
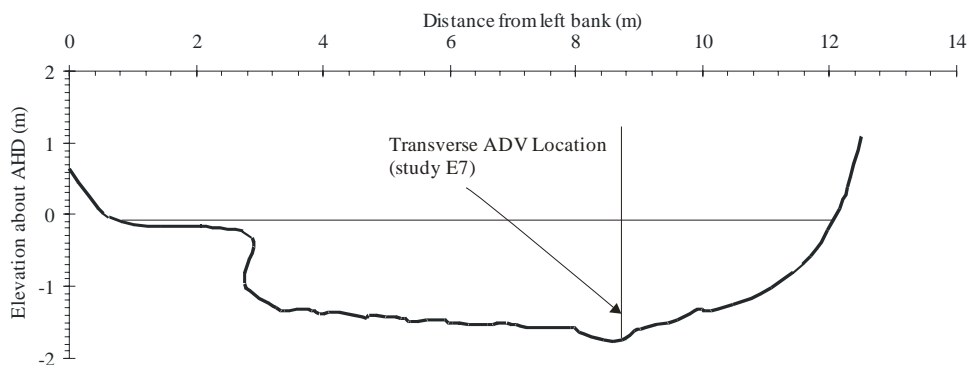
(C) Cross-section at Site 3, located 3.1 km from mouth.

Figure C.2 – Surveyed experimental cross-sections and transverse ADV locations used at Eprapah Creek, looking downstream.

C.1.1   Instrumentation

The turbulent velocity measurements within Eprapah Creek were conducted with two acoustic Doppler velocimeters: (1) a Sontek UW ADV (10 MHz, serial 0510) with a three-dimensional down-looking head; and (2) a Sontek microADV (16 MHz, serial number A641F) with a two-dimensional side-looking head. For both ADVs the sampling volume was located 5 cm from the respective sensors, with the sensor heads being mounted on rigid stems. Here, the ADVs are referred to as the 3D-ADV (10 MHz) and 2D-microADV (16 MHz) respectively. The physio-chemistry data were collected continuously using a YSI6600 probe. The YSI6600 probe used measured water depth, water temperature, conductivity, turbidity, pH, dissolved

oxygen and chlorophyll a levels. The standard configuration for the continuous data collection was to have the sampling volumes of the 3D-ADV and YSI6600 probes horizontally aligned, with the YSI6600 probe 0.3 m towards the bank. Table C.2 describes the field investigations in which continuous high frequency turbulence and water quality data were collected and the equipment deployed.

Table C.2 – Summary of field studies with continuous high frequency data collection.

Field study	E1	E2	E3	E4
Date	4/04/03	17/07/03	24/11/03	2/09/04
Study focus	Near free surface	Near free surface	Near free surface	Near bed
Site	2B	2	2B	2B
ADV sampling location	~0.5 m below free surface, 14.2 m from left bank	~0.5 m below free surface, 8.0 m from left bank	~0.5 m below free surface, 10.7 m from left bank	0.05 m above bed, 10.7 m from left bank
ADV f_{scan} (Hz)	25	25	25	25
V_{range} (m/s)	1.0 and 0.3	0.3	1.0	0.3
YSI6600 sampling location	~0.5 m below free surface, 13.9 m from left bank	~0.5 m below free surface, 7.7 m from left bank	~0.5 m below free surface, 10.4 m from left bank	0.05 m above bed, 10.4 m from left bank
YSI6600 f_{scan} (Hz)	0.2	0.2	0.5	0.3

Field study	E5	E6	E7
Date	8-9/03/05	16-18/05/05	5-7/06/06
Study focus	Near bed – mid estuary – spring tide	Near bed – mid estuary – neap tide	Near bed – upper estuary – neap tide
Site	2B	2B	3
ADV sampling location	0.1 m above bed, 10.7 m from left bank	0.2 (#) and 0.4 m above bed, 10.7 m from left bank	0.2 (#) and 0.4 m above bed, 4.2 m from right bank
ADV f_{scan} (Hz)	25	25 25 (#)	25 50 (#)
V_{range} (m/s)	1.0	1.0 1.0 (#)	0.3 0.3 (#)
YSI6600 sampling location	0.1 m above bed, 10.4 m from left bank	0.4 m above bed, 10.4 m from left bank	0.4 m above bed and 0.3 m below free surface, 3.9 m from right bank
YSI6600 f_{scan} (Hz)	0.167	0.083	0.083

Note: f_{scan} : sampling frequency; V_{range} : ADV velocity range; [#]: indicates information pertaining to 2D-microADV (16 MHz).

For all field investigations undertaken at Eprapah Creek vertical physio-chemistry profiles were collected with a YSI6920 probe. The YSI6920 probe measures water depth, temperature, conductivity, pH, turbidity and dissolved oxygen. During or about the date of the field studies at Eprapah Creek, the EPA (QLD) performed its monthly monitoring program. The monthly monitoring program collected vertical profiles of key physio-chemical properties at certain locations along the creek (Table C.1).

C.1.1.1 *Post-processing of ADV turbulence data*

All ADV velocity data were post-processed using the technique described in Chanson et al. (2005b). The post-processing must be undertaken to ensure the quality of the data set. Corrupted data are inherent to the ADV metrology, and are predominantly caused by poor signal quality (low correlation and low signal to noise ratio) and Doppler noise within the measured signal. Chanson et al. (2005b) found that in natural systems the ADV data could be corrupted by large disturbances such as navigation or fauna activity near the ADV. All turbulence data measured at Eprapah Creek with an ADV underwent three stages of post-processing, these were:

1) – Velocity signal check:

Data points with low-correlation, low signal to noise ratio or communication errors were removed and replaced by the mean of the endpoints about the erroneous data.

2) – Large event detection (pre-processing):

The pre-processing stage searches for large disturbances (e.g. navigation near probe, adjustments of probe) that were observed during a field study. Erroneous data from known large disturbance events were replaced using the mean of the endpoints technique.

3) – Small disturbance detection (de-spiking):

The phase-space thresholding method was used to find small disturbances generated by "spike" events and Doppler noise. Any data point determined to be erroneous was replaced using the mean of the endpoints technique.

C.1.2 Notation

V_x instantaneous streamwise velocity; positive downstream (m/s)

V_y instantaneous transverse velocity; positive towards left bank (m/s)

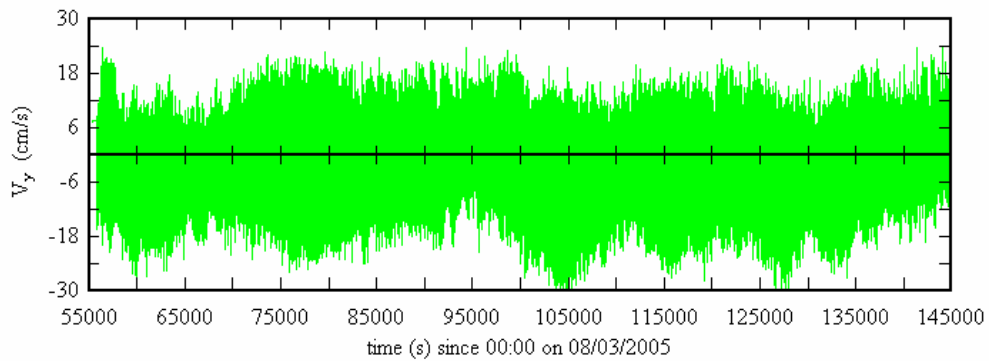V_z instantaneous vertical velocity; positive upwards (m/s)

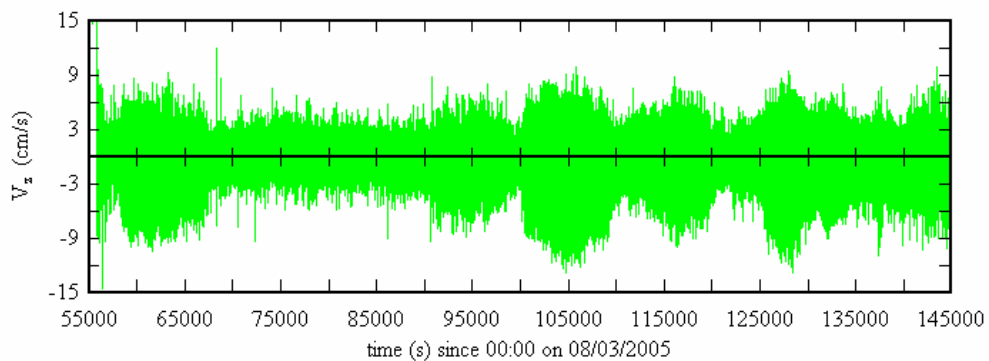## C.2 FIELD OBSERVATIONS: INSTANTANEOUS VELOCITY DATA

C.2.1 Field study E1 (4/04/2003)
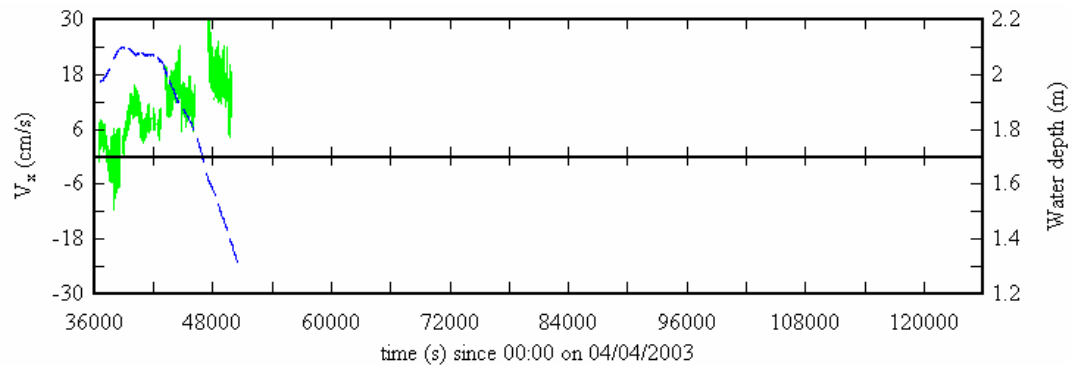
(A) Water depth and instantaneous streamwise velocity data (positive downstream).
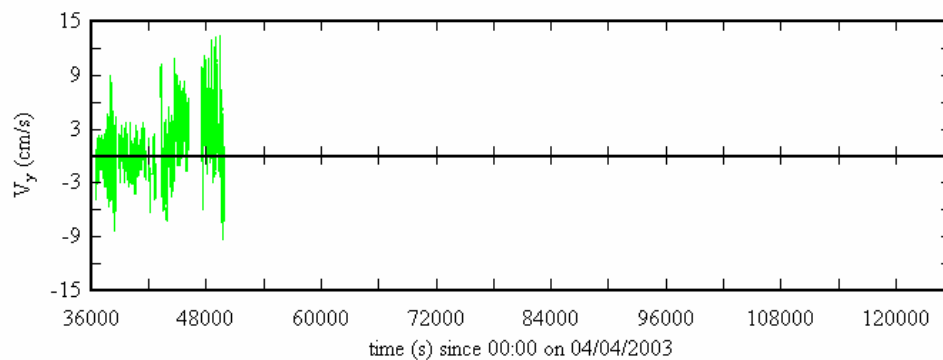
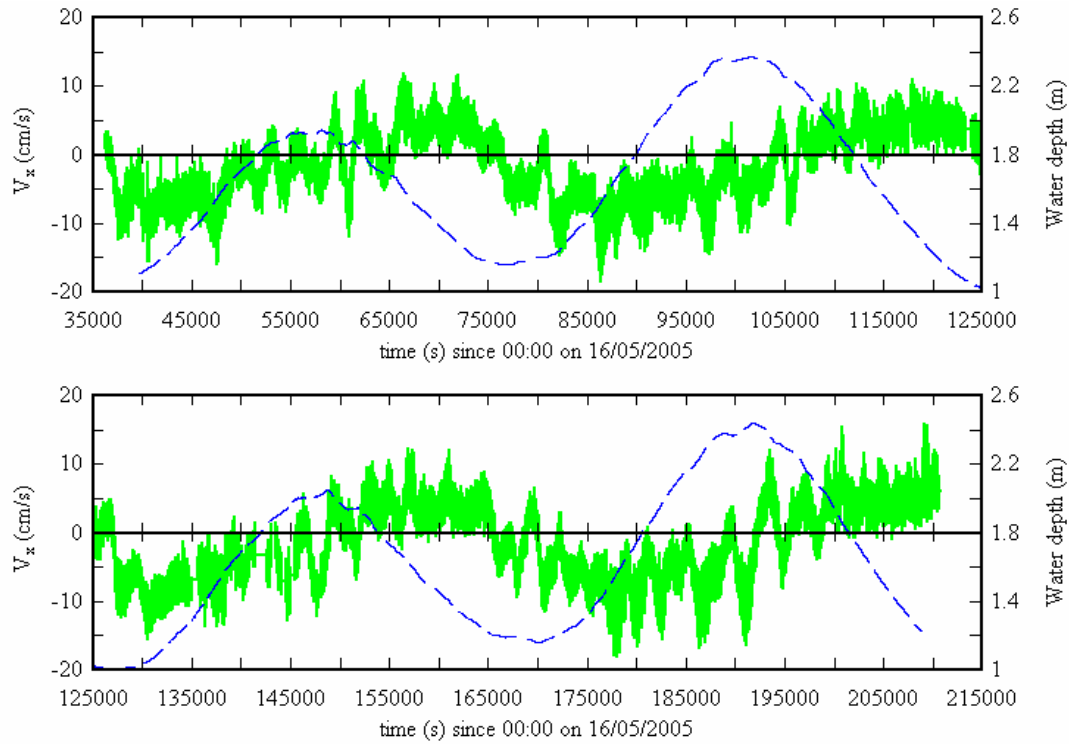(B) Instantaneous transverse velocity data (positive towards left bank).
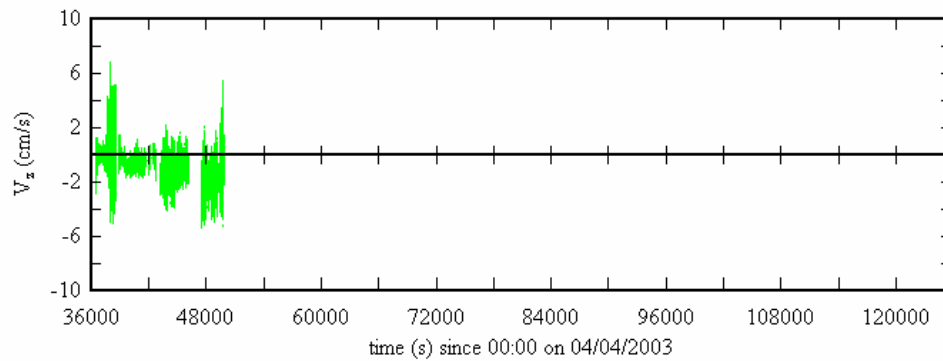
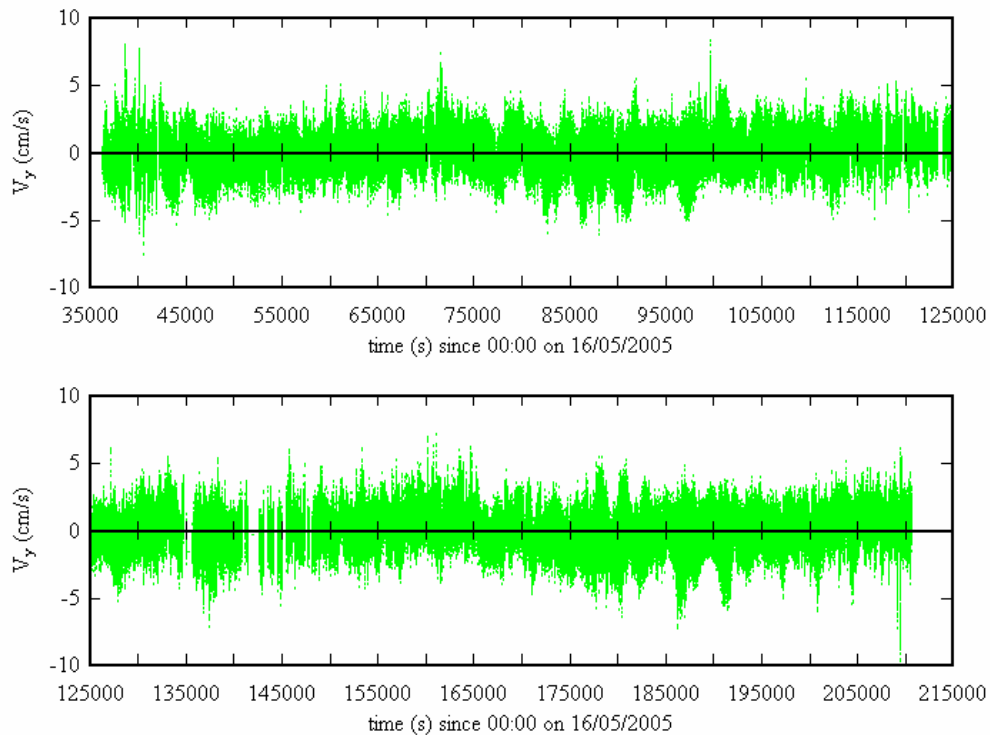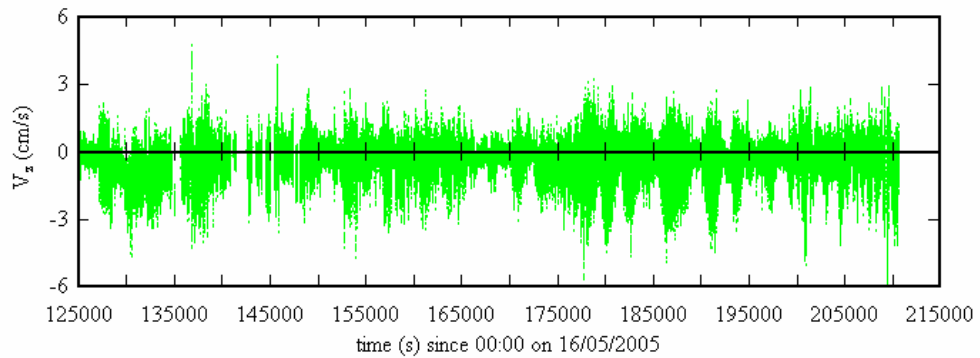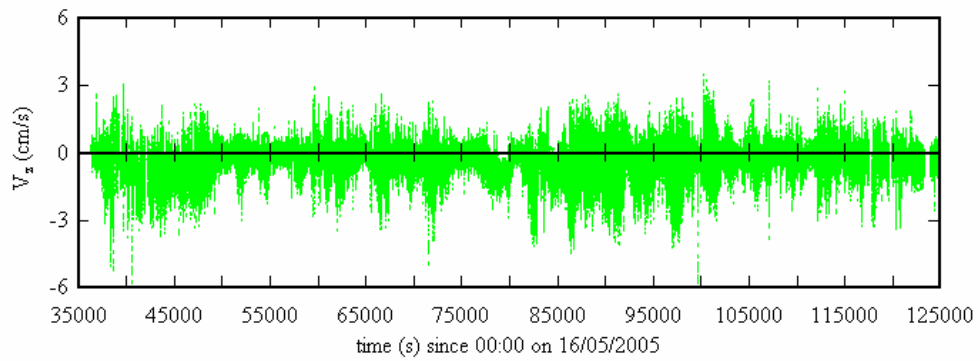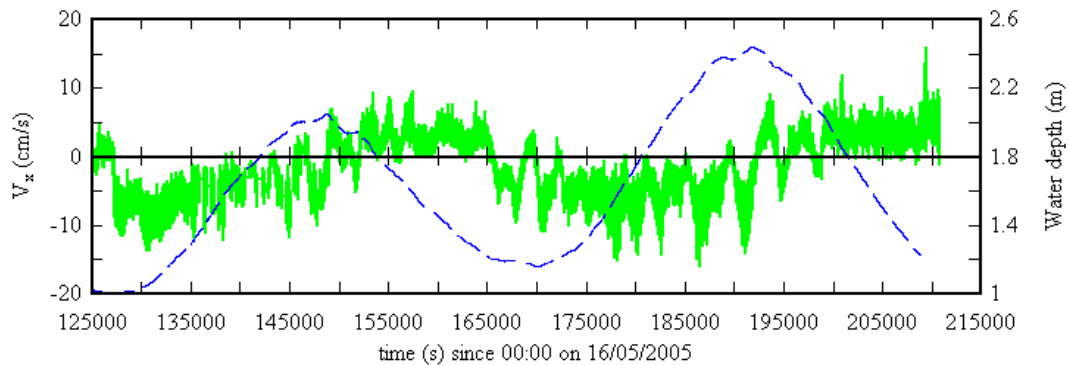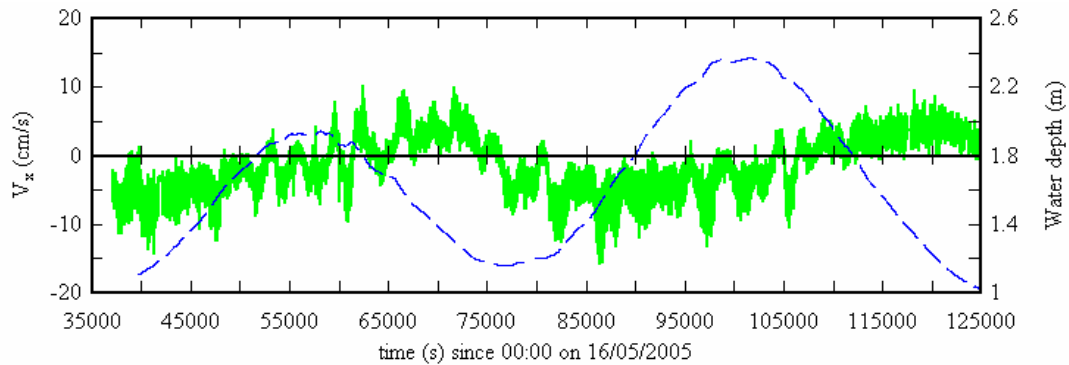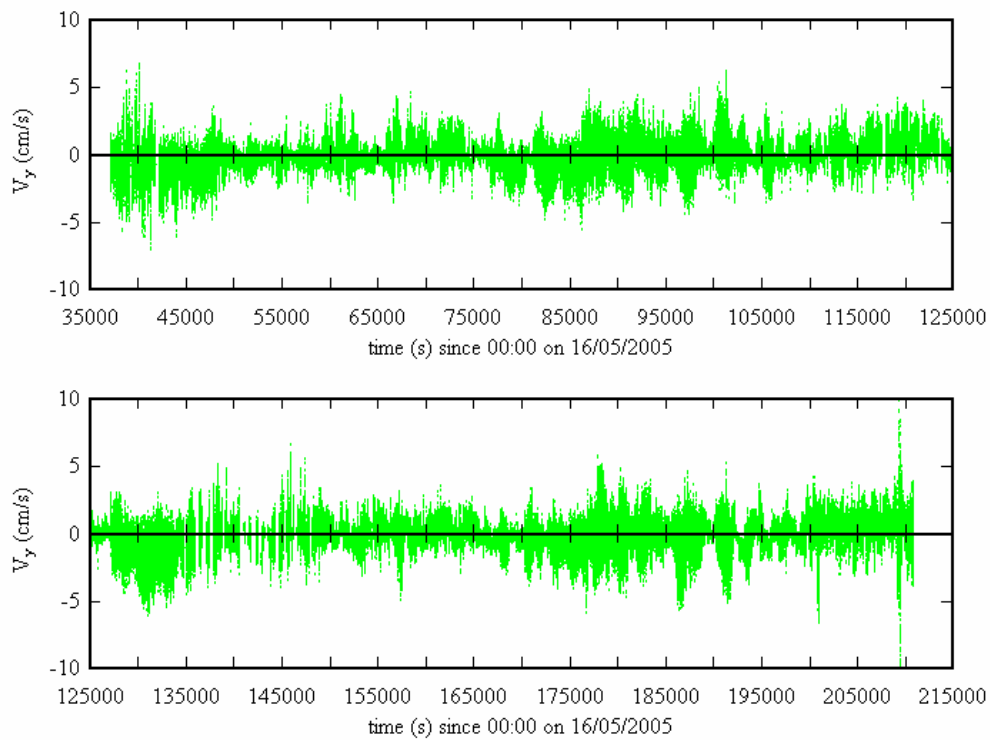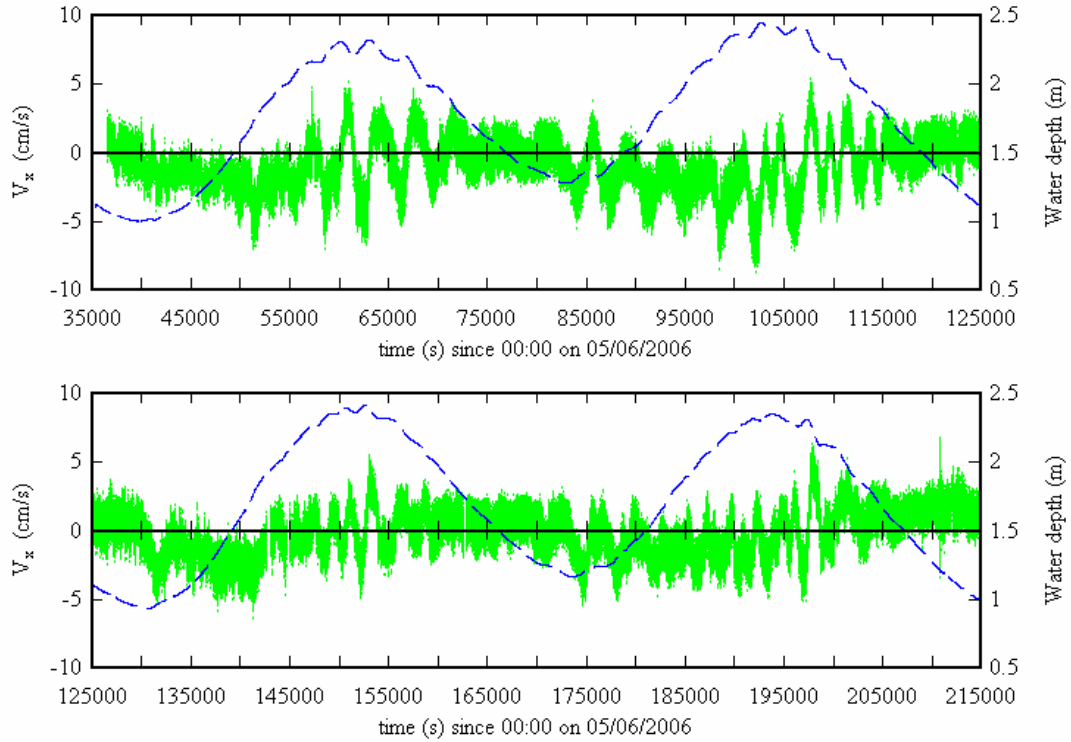(C) Instantaneous vertical velocity data (positive upwards).

Figure C.3 – Instantaneous velocity data collected at Site 2B Eprapah Creek for study E1 (4/04/03). Data collected at 25 Hz by 3D-ADV (10 MHz) located about 0.5 m below surface, 14.2 m from left bank. All velocity data shown were post-processed.

Legend: — instantaneous velocity data; – – water depth.

C.2.2 Field study E2 (17/07/2003)
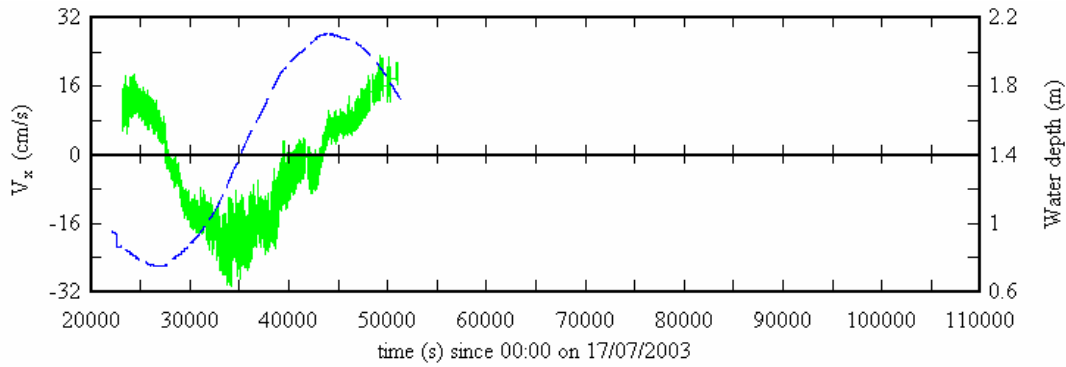
(A) Water depth and instantaneous streamwise velocity data (positive downstream).
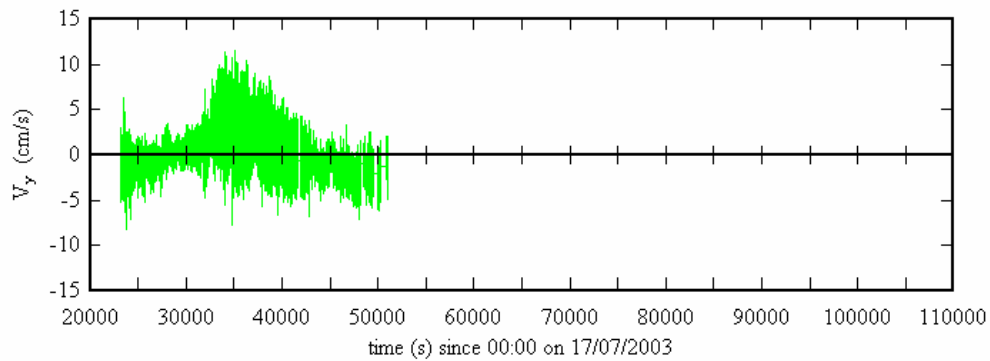
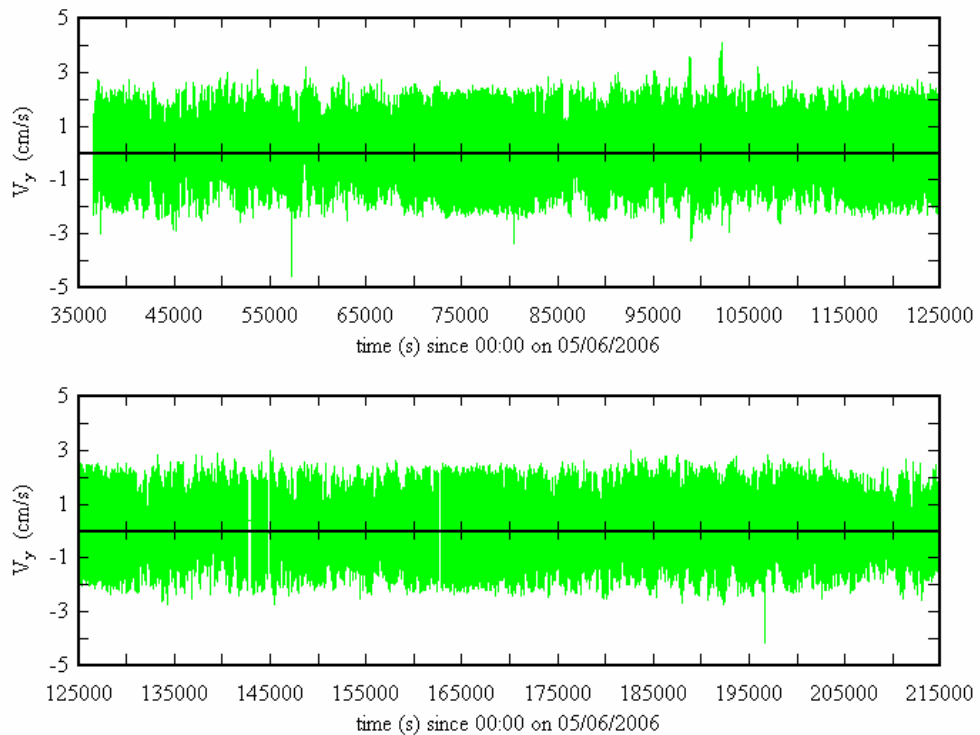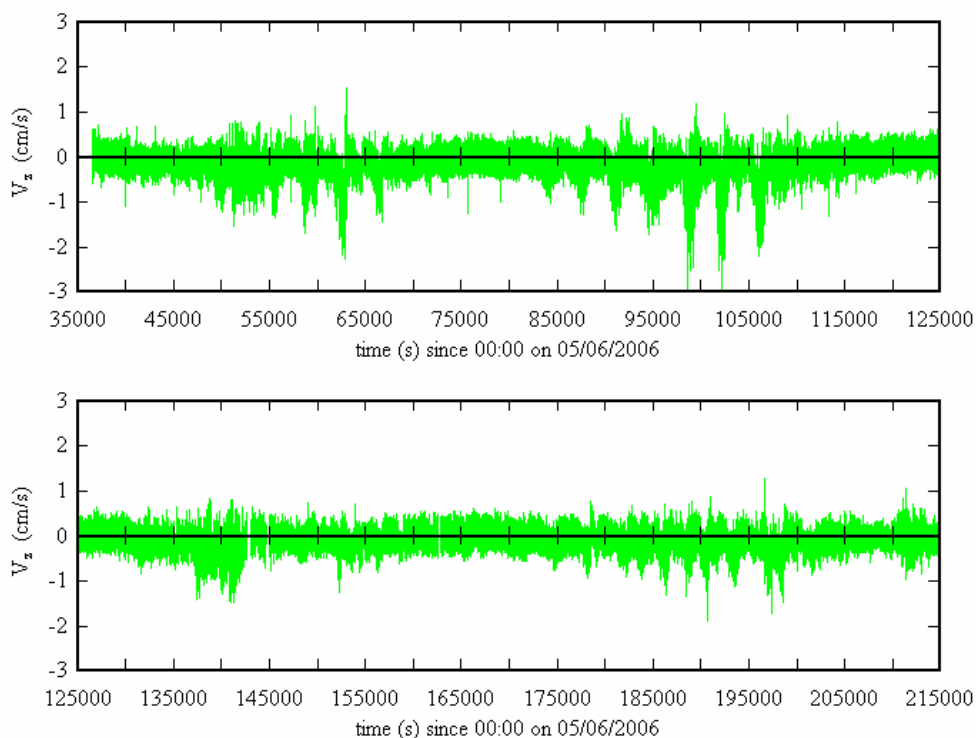(B) Instantaneous transverse velocity data (positive towards left bank).
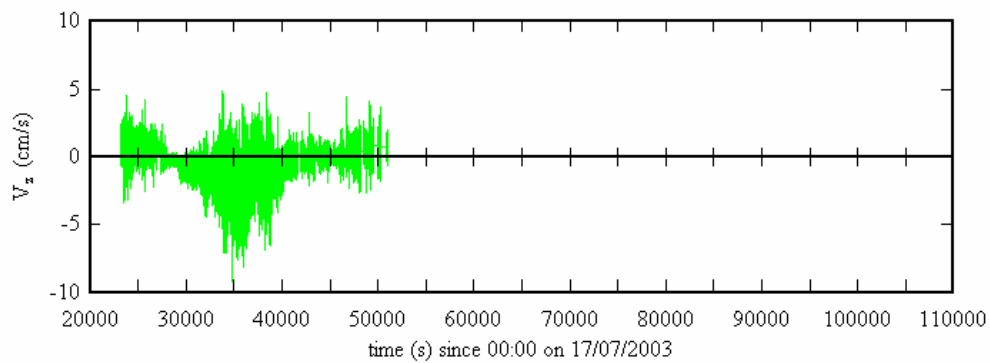
(C) Instantaneous vertical velocity data (positive upwards).

Figure C.4 – Instantaneous velocity data collected at Site 2 Eprapah Creek for study E2 (17/07/03). Data collected at 25 Hz by 3D-ADV (10 MHz) located about 0.5 m below surface, 8.0 m from left bank. All velocity data shown were post-processed.

Legend: —— instantaneous velocity data; – – water depth.

212

C.2.3   Field study E3 (24/11/2003)
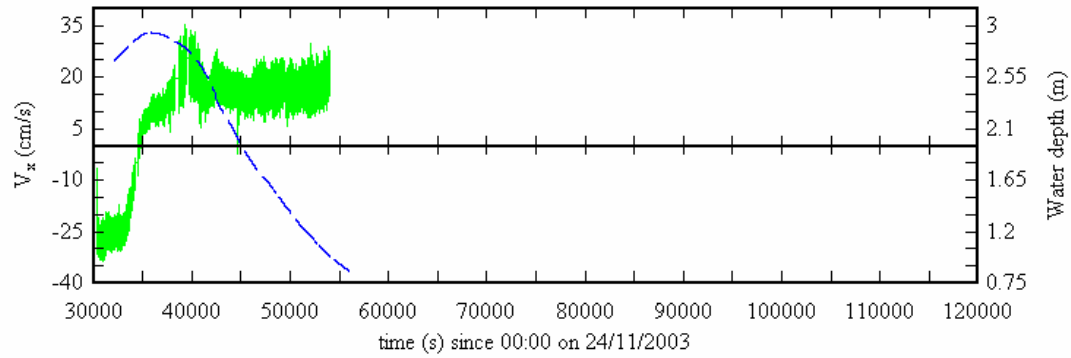
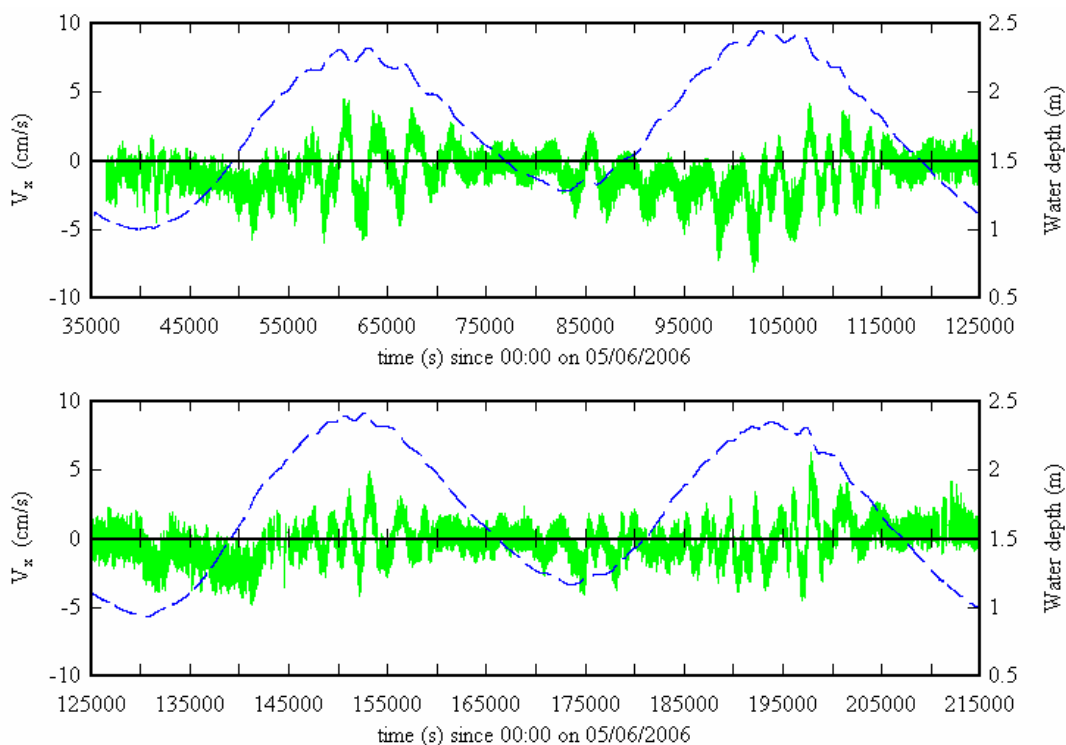(A) Water depth and instantaneous streamwise velocity data (positive downstream).
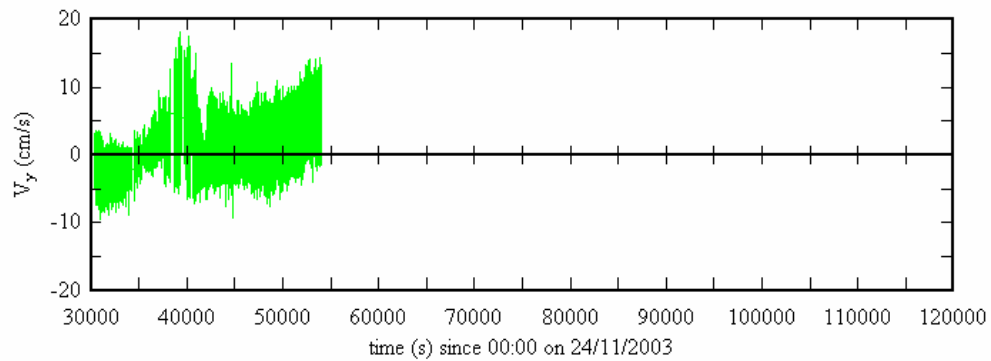
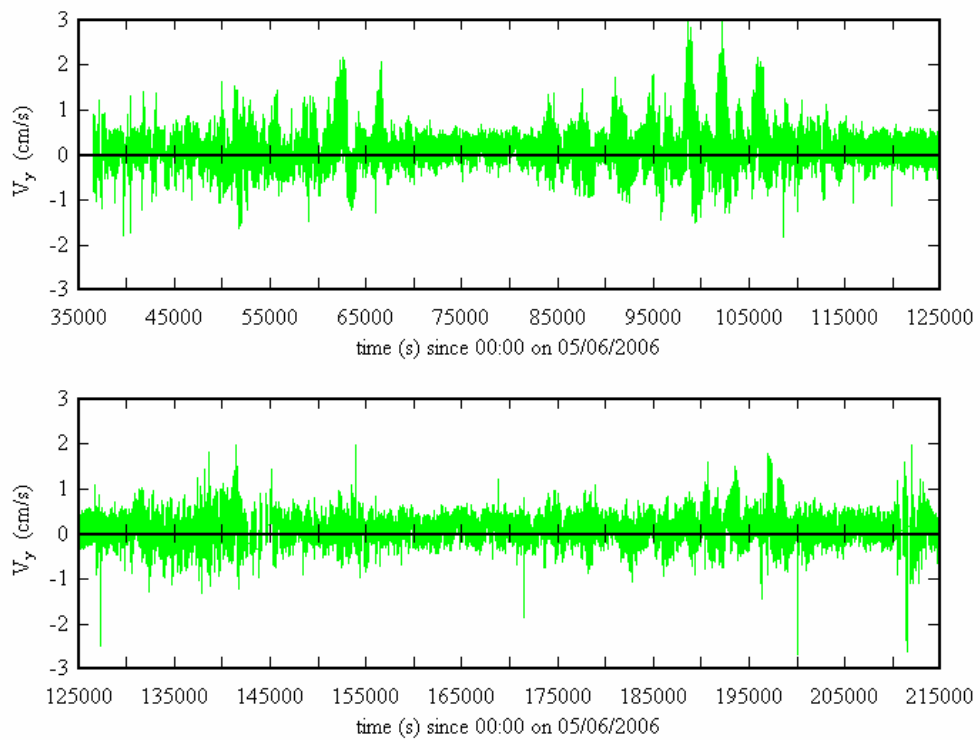(B) Instantaneous transverse velocity data (positive towards left bank).
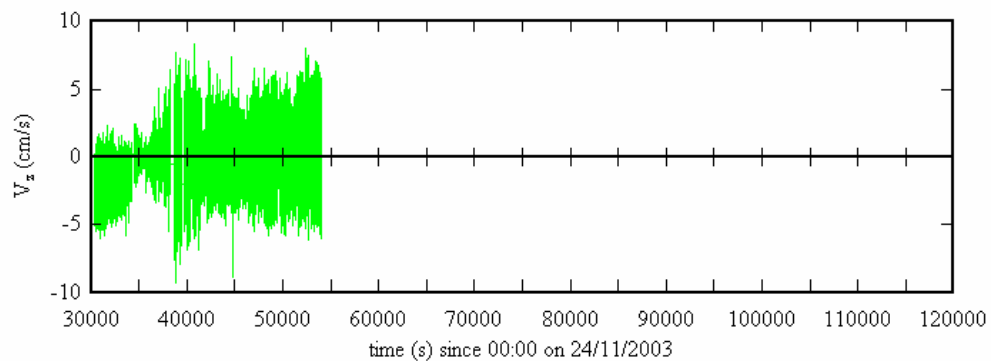
(C) Instantaneous vertical velocity data (positive upwards).

Figure C.5 – Instantaneous velocity data collected at Site 2B Eprapah Creek for study E3 (24/11/03).   Data collected at 25 Hz by 3D-ADV (10 MHz) located about 0.5 m below surface, 10.7 m from left bank. All velocity data shown were post-processed.

Legend: ⎯ instantaneous velocity data; – – water depth.

C.2.4   Field study E4 (2/09/2004)
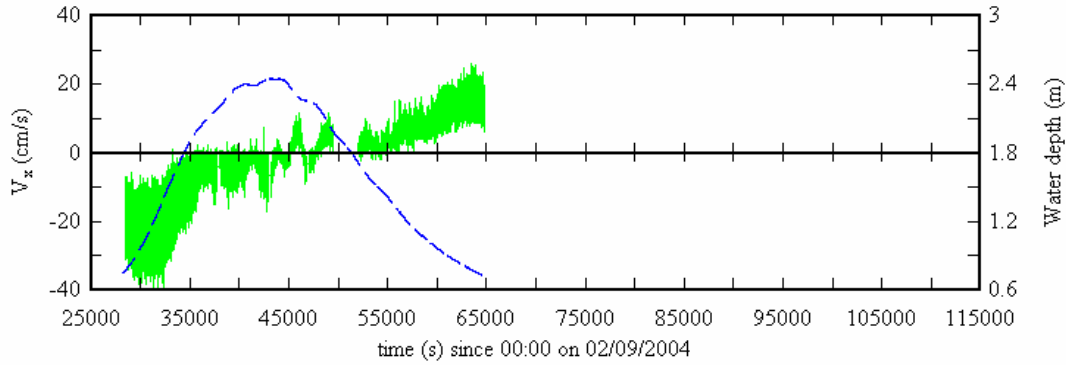
(A) Water depth and instantaneous streamwise velocity data (positive downstream).
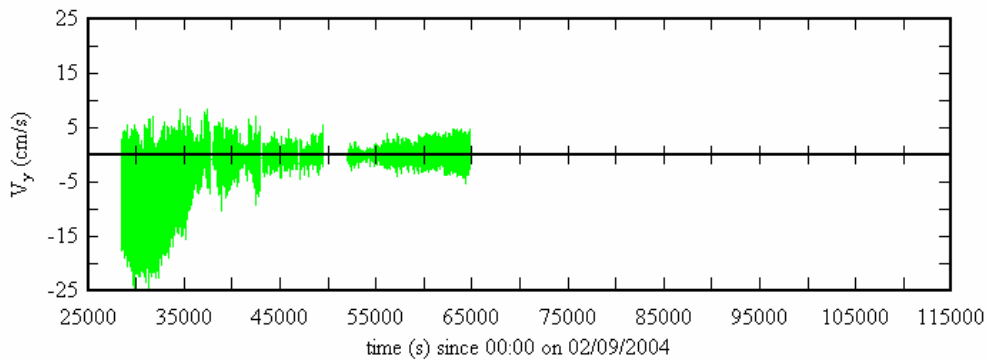
(B) Instantaneous transverse velocity data (positive towards left bank).
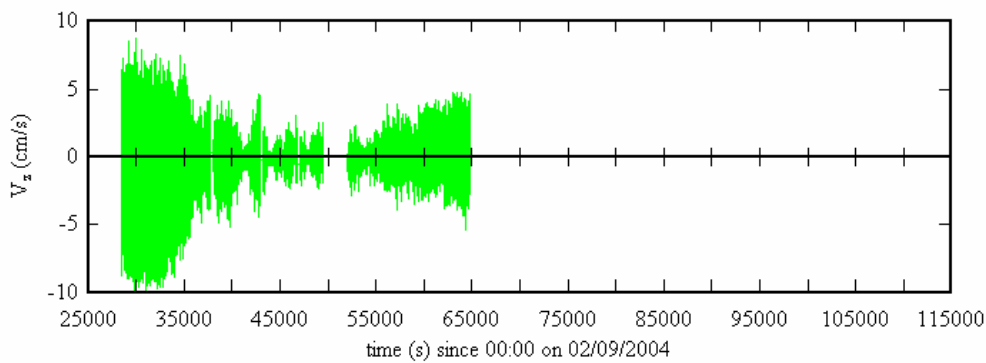

(C) Instantaneous vertical velocity data (positive upwards).

Figure C.6 – Instantaneous velocity data collected at Site 2B Eprapah Creek for study E4 (2/09/04). Data collected at 25 Hz by 3D-ADV (10 MHz) located 0.05 m above bed, 10.7 m from left bank. All velocity data shown were post-processed.

Legend: —— instantaneous velocity data; – – water depth.

C.2.5 Field study E5 (8-9/03/2005)
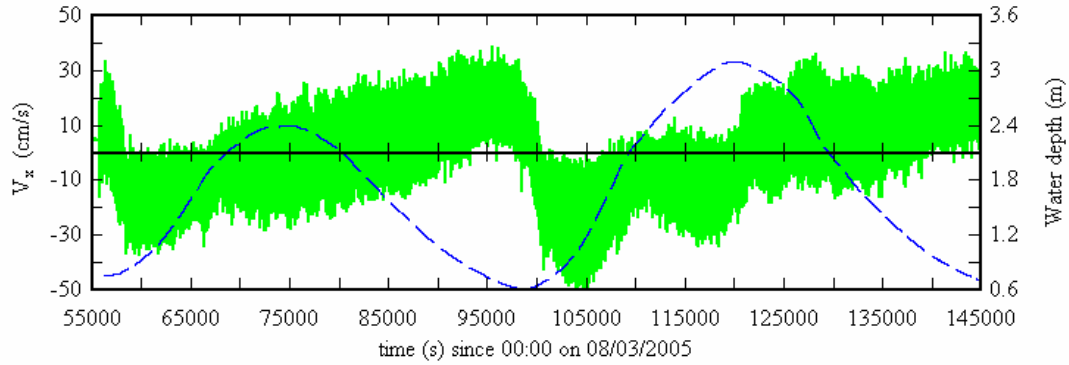
(A) Water depth and instantaneous streamwise velocity data (positive downstream).

(B) Instantaneous transverse velocity data (positive towards left bank).

(C) Instantaneous vertical velocity data (positive upwards).

Figure C.7 – Instantaneous velocity data collected at Site 2B Eprapah Creek for study E5 (8-9/03/05). Data collected at 25 Hz by 3D-ADV (10 MHz) located 0.1 m above bed, 10.7 m from left bank. All velocity data shown were post-processed.

Legend: ⎯ instantaneous velocity data; – – water depth.

(A) Water depth and instantaneous streamwise velocity data (positive downstream).

(B) Instantaneous transverse velocity data (positive towards left bank).

(C) Instantaneous vertical velocity data (positive upwards).

Figure C.8 – Instantaneous velocity data collected at Site 2B Eprapah Creek for study E6 (16-18/05/05). Data collected at 25 Hz by 3D-ADV (10 MHz) located 0.4 m above bed, 10.7 m from left bank. All velocity data shown were post-processed.

Legend: — instantaneous velocity data; – – water depth.

(A) Water depth and instantaneous streamwise velocity data (positive downstream).

217

(B) Instantaneous transverse velocity data (positive towards left bank).

Figure C.9 – Instantaneous velocity data collected at Site 2B Eprapah Creek for study E6 (16-18/05/05). Data collected at 25 Hz by 2D-microADV (16 MHz) located 0.2 m above bed, 10.7 m from left bank. All velocity data shown were post-processed.

Legend: — instantaneous velocity data; – – water depth.

C.2.7 Field study E7 (5-7/06/2006)

(A) Water depth and instantaneous streamwise velocity data (positive downstream).

(B) Instantaneous transverse velocity data (positive towards left bank).

219

(C) Instantaneous vertical velocity data (positive upwards).

Figure C.10 – Instantaneous velocity data collected at Site 3 Eprapah Creek for study E7 (5-7/06/06). Data collected at 25 Hz by 3D-ADV (10 MHz) located 0.4 m above bed, 4.2 m from right bank. All velocity data shown were post-processed.

Legend: — instantaneous velocity data; – – water depth.

(A) Water depth and instantaneous streamwise velocity data (positive downstream).

220

(B) Instantaneous transverse velocity data (positive towards left bank).

Figure C.11 – Instantaneous velocity data collected at Site 3 Eprapah Creek for study E7 (5-7/06/06). Data collected at 50 Hz by 2D-microADV (16 MHz) located 0.2 m above bed, 4.2 m from right bank. All velocity data shown were post-processed.

Legend: ⎯ instantaneous velocity data; – – water depth.

C.3 FIELD OBSERVATIONS: INSTANTANEOUS PHYSIO-CHEMISTRY DATA
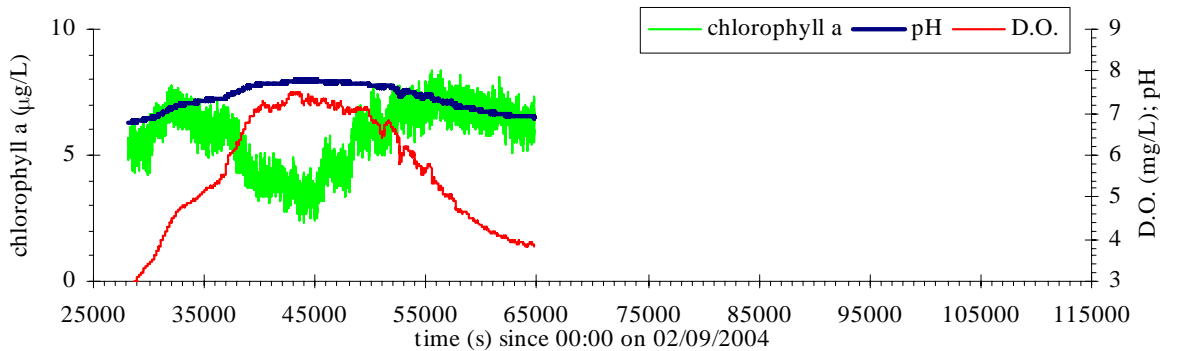
C.3.1 Field study E1 (4/04/2003)
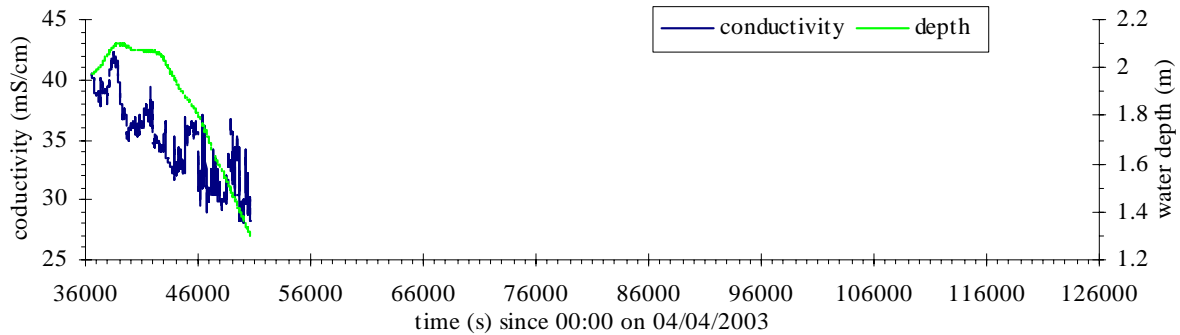
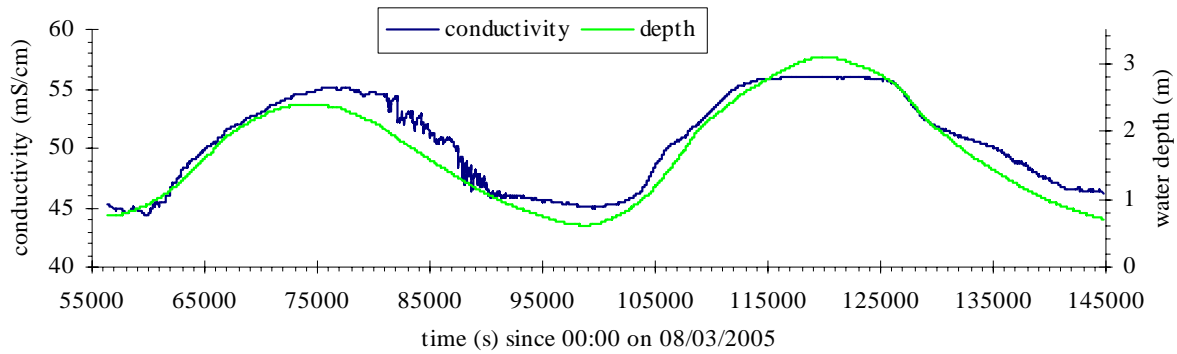(A) Instantaneous water depth and Conductivity data.
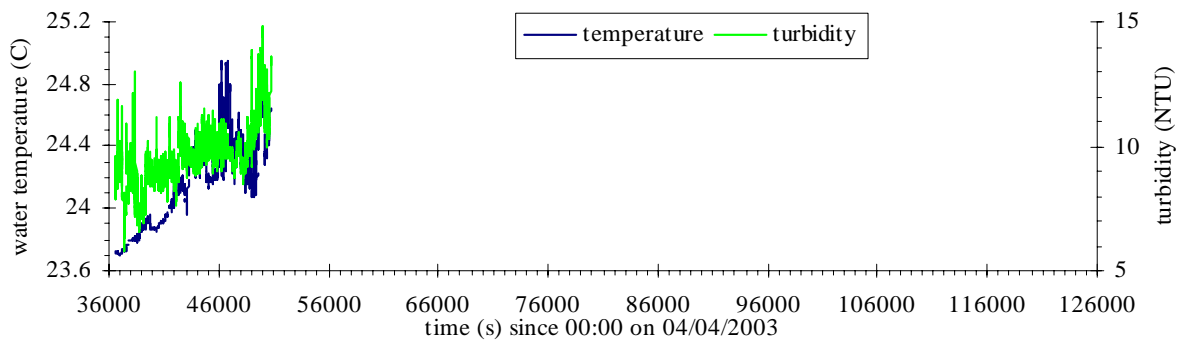
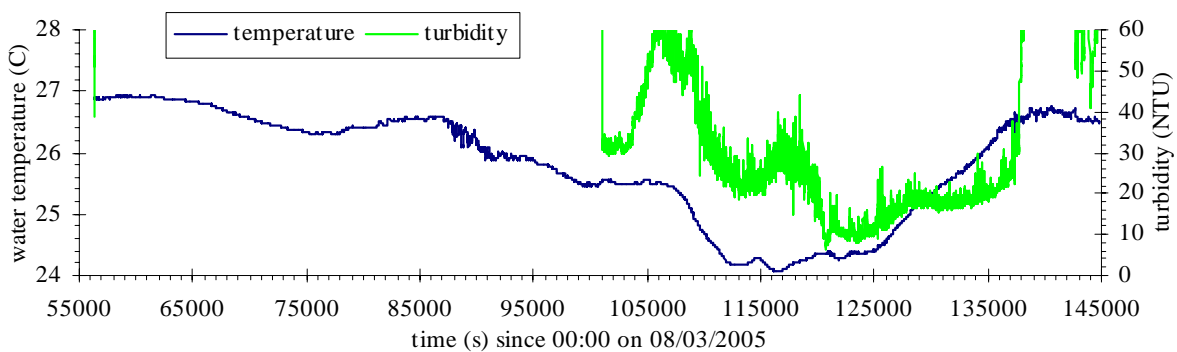(B) Instantaneous water temperature and turbidity data.
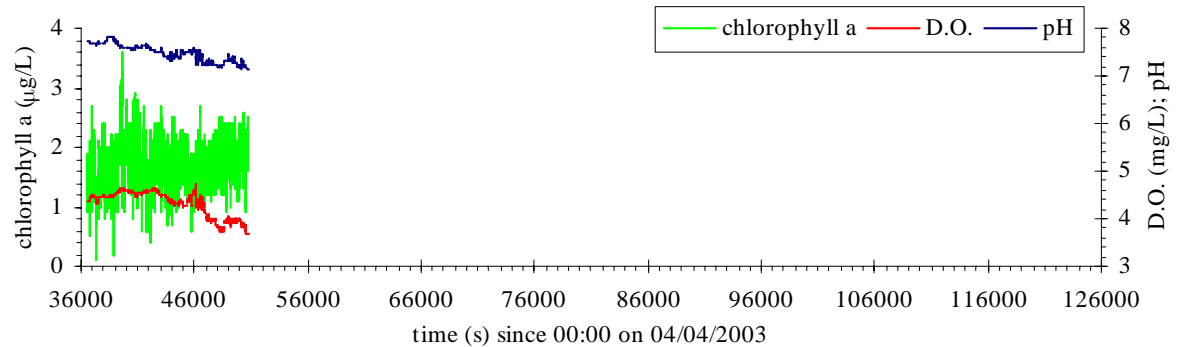
(C) Instantaneous dissolved oxygen, pH and chlorophyll a level data.

Figure C.12 – Instantaneous physio-chemistry data collected at Site 2B Eprapah Creek for study E1 (4/04/03). Data collected at 0.2 Hz by YSI6600 probe located 0.5 m below surface, 13.9 m from left bank. Note water depth reconstructed from YSI6600 probe data.
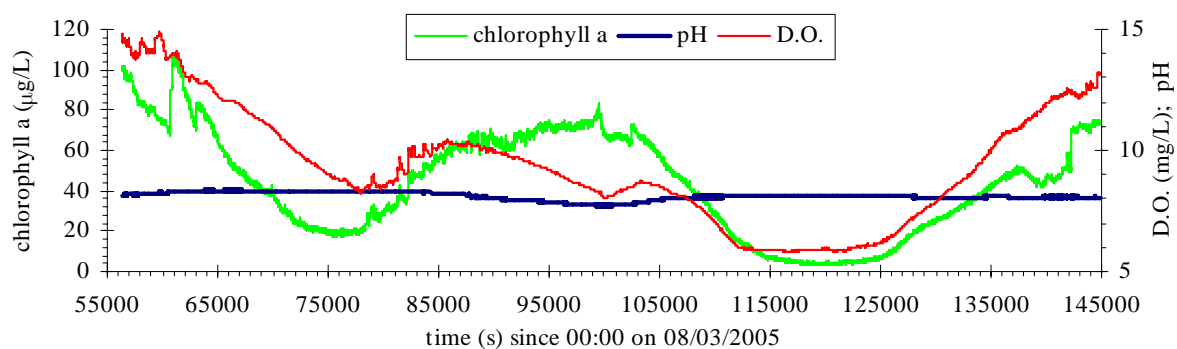
C.3.2   Field study E2 (17/07/2003)
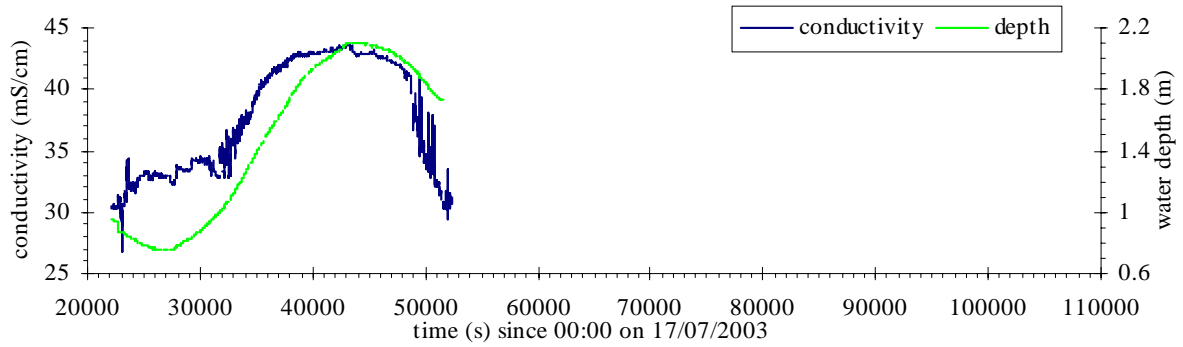
(A) Instantaneous water depth and conductivity data.
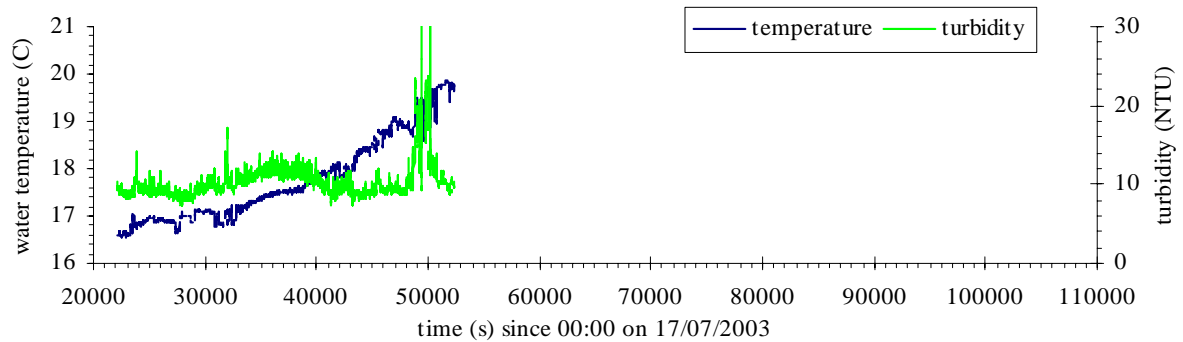
(B) Instantaneous water temperature and turbidity data.
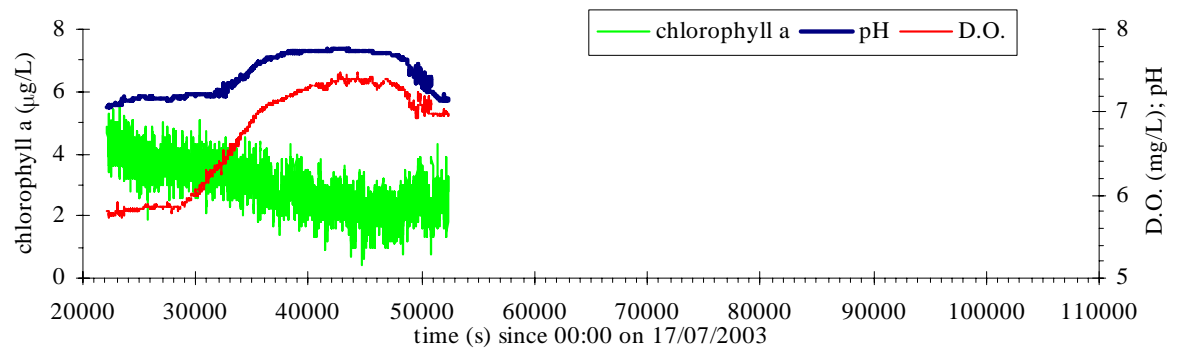
(C) Instantaneous dissolved oxygen, pH and chlorophyll a level data.

Figure C.13 – Instantaneous physio-chemistry data collected at Site 2 Eprapah Creek for study E2 (17/07/03). Data collected at 0.2 Hz by YSI6600 probe located 0.5 m below surface, 7.7 m from left bank. Note water depth reconstructed from YSI6600 probe data.

C.3.3   Field study E3 (24/11/2003)
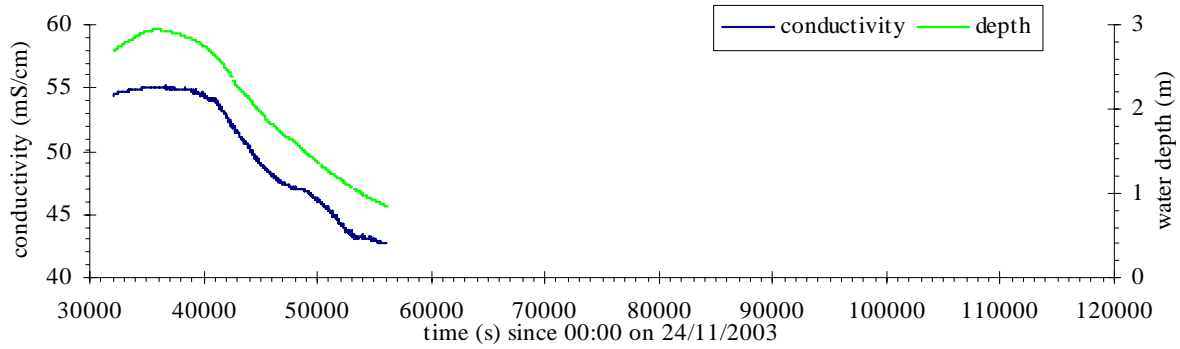
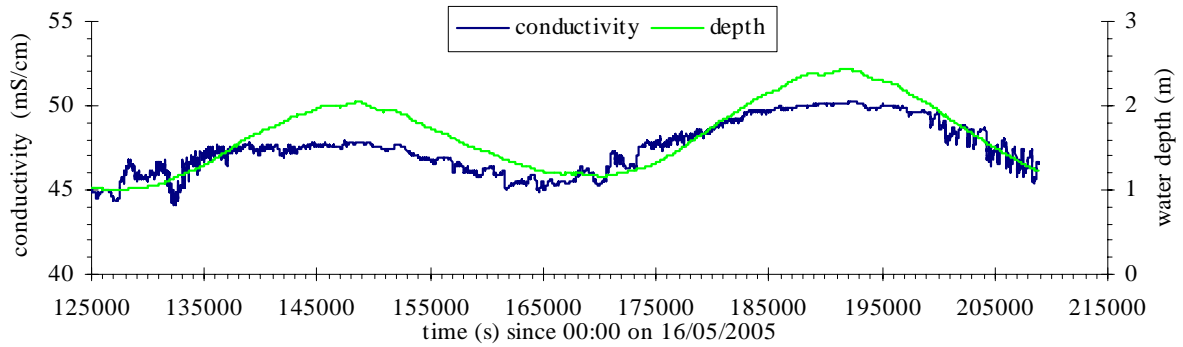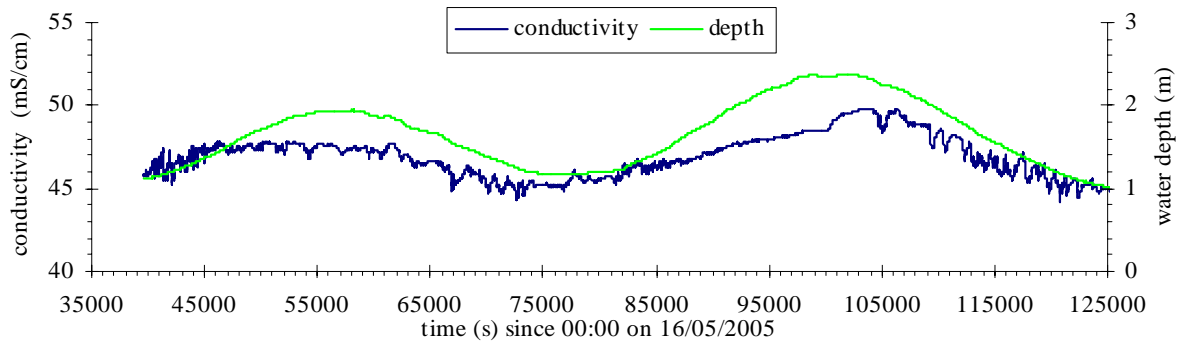(A) Instantaneous water depth and conductivity data.
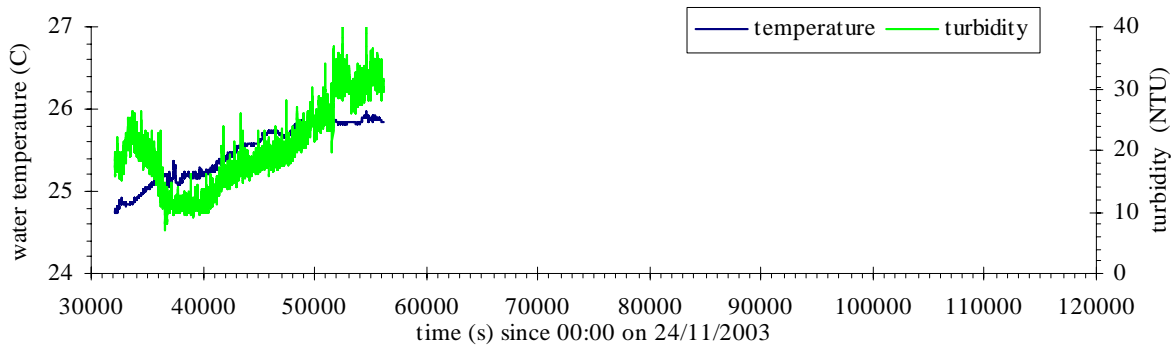
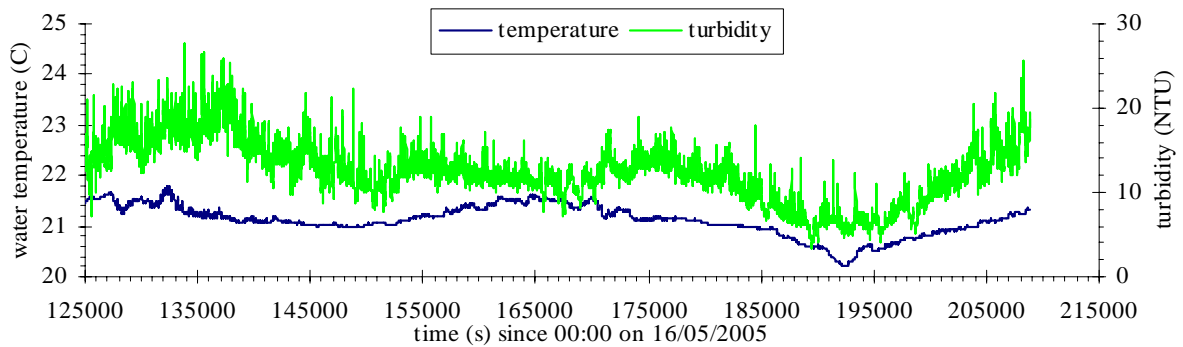(B) Instantaneous water temperature and turbidity data.
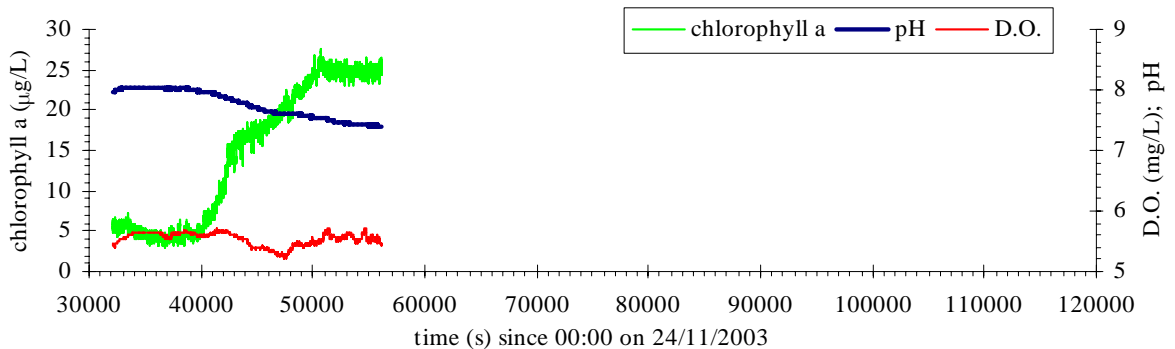
(C) Instantaneous dissolved oxygen, pH and chlorophyll a level data.

Figure C.14 – Instantaneous physio-chemistry data collected at Site 2B Eprapah Creek for study E3 (24/11/03). Data collected at 0.5 Hz by YSI6600 probe located 0.5 m below surface, 10.4 m from left bank. Note water depth reconstructed from YSI6600 probe data.

C.3.4   Field study E4 (2/09/2004)
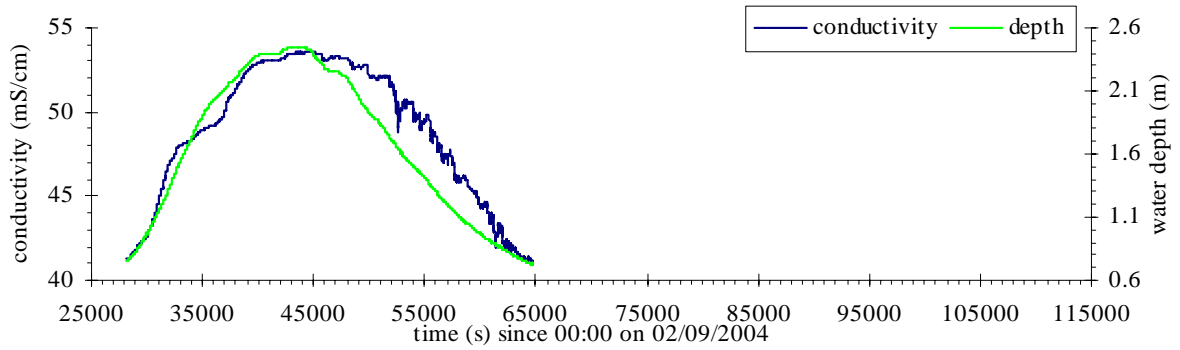
(A) Instantaneous water depth and conductivity data.
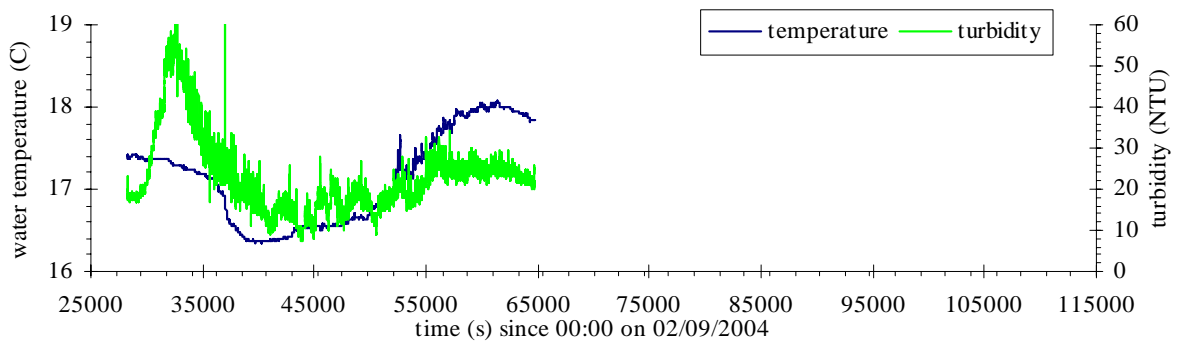
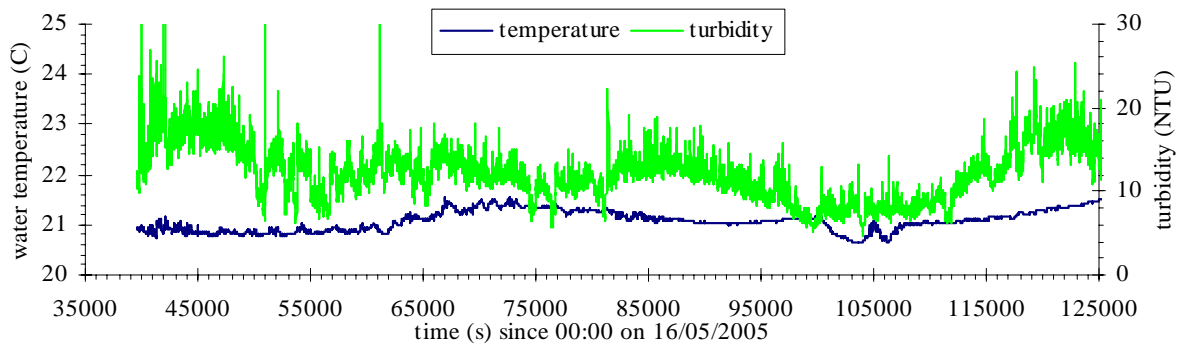(B) Instantaneous water temperature and turbidity data.

(C) Instantaneous dissolved oxygen, pH and chlorophyll a level data.

Figure C.15 – Instantaneous physio-chemistry data collected at Site 2B Eprapah Creek for study E4 (2/09/04). Data collected at 0.3 Hz by YSI6600 probe located 0.05 m above bed, 10.4 m from left bank.

C.3.5   Field study E5 (8-9/03/2005)

(A) Instantaneous water depth and conductivity data.

(B) Instantaneous water temperature and turbidity data.

(C) Instantaneous dissolved oxygen, pH and chlorophyll a level data.

Figure C.16 – Instantaneous physio-chemistry data collected at Site 2B Eprapah Creek for study E5 (8-9/03/05). Data collected at 0.167 Hz by YSI6600 probe located 0.1 m above bed, 10.4 m from left bank.
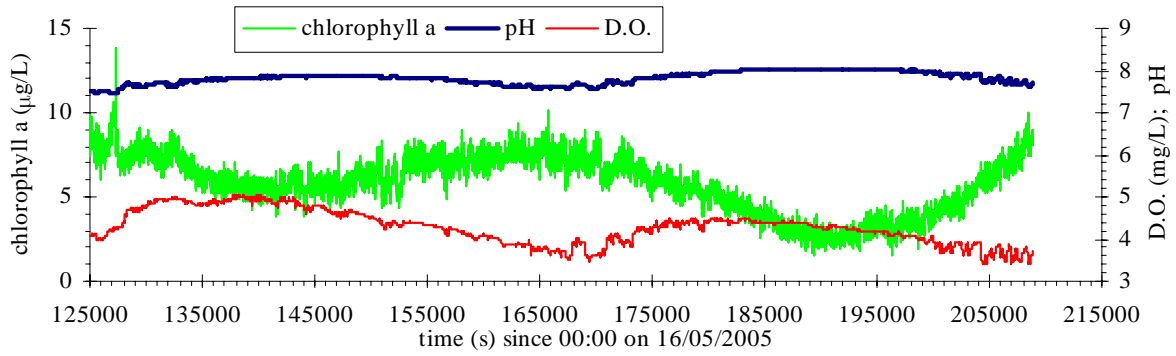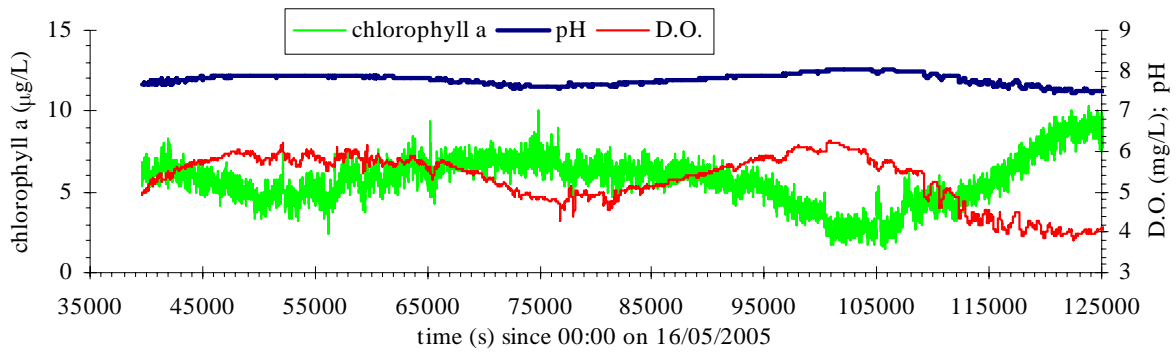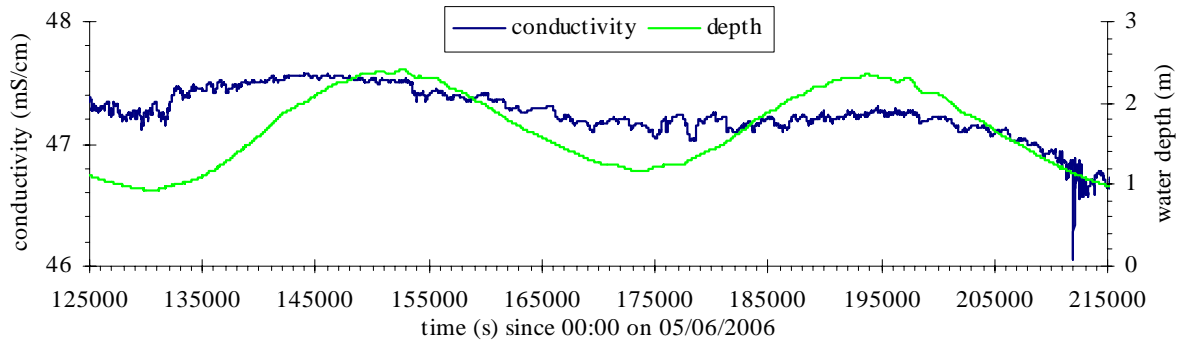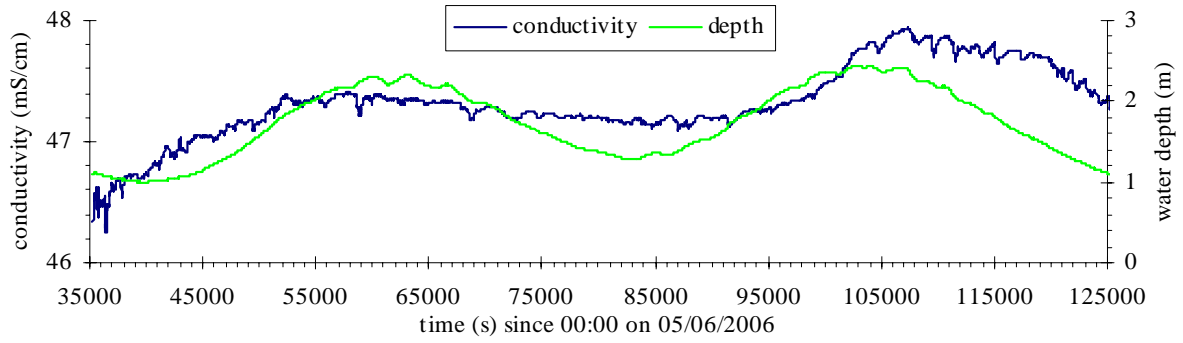
C.3.6   Field study E6 (16-18/05/2005)

(A) Instantaneous water depth and conductivity data.
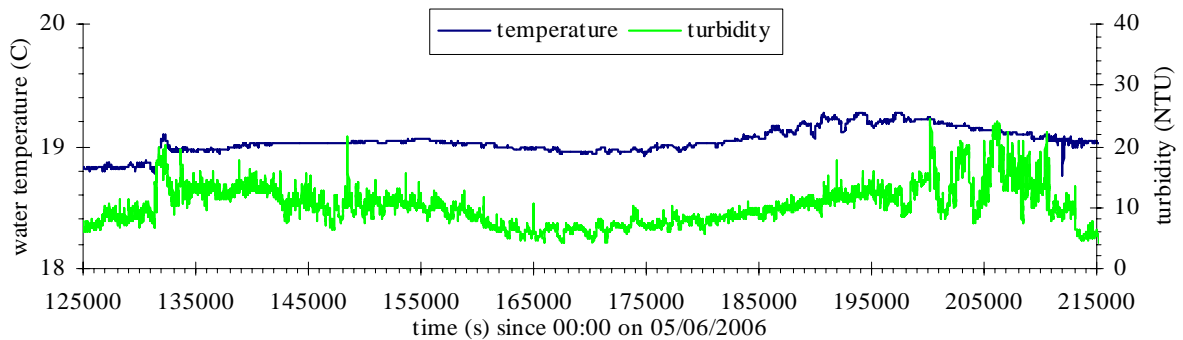

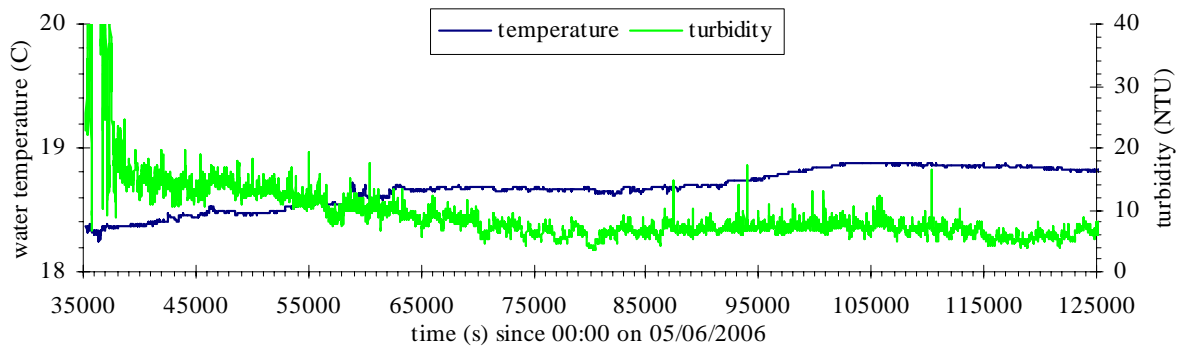(B) Instantaneous water temperature and turbidity data.

227

(C) Instantaneous dissolved oxygen, pH and chlorophyll a level data.

Figure C.17 – Instantaneous physio-chemistry data collected at Site 2B Eprapah Creek for study E6 (16-18/05/05). Data collected at 0.083 Hz by YSI6600 probe located 0.4 m above bed, 10.4 m from left bank.
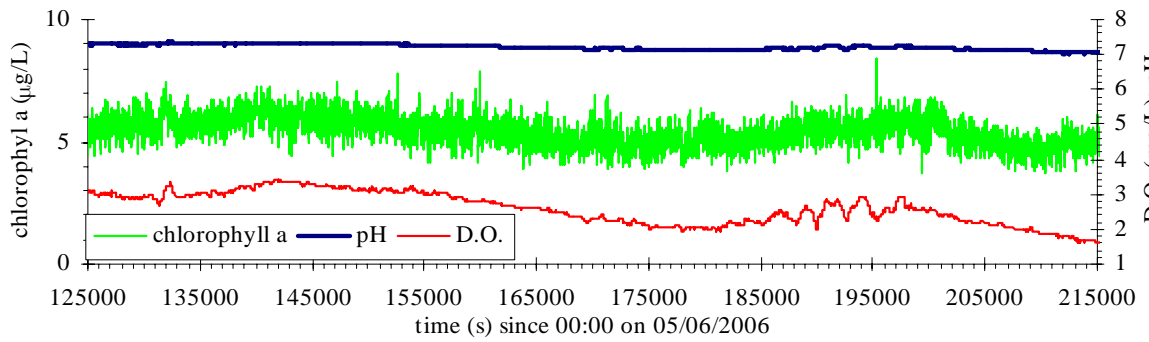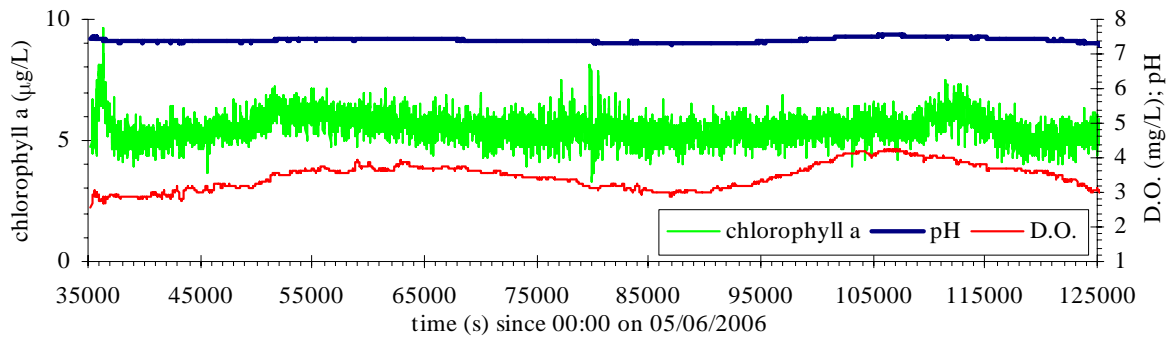
C.3.7 Field study E7 (5-7/06/2006)

(A) Instantaneous water depth and conductivity data.

(B) Instantaneous water temperature and turbidity data.

(C) Instantaneous dissolved oxygen, pH and chlorophyll a level data.

Figure C.18 – Instantaneous physio-chemistry data collected at Site 3 Eprapah Creek for study E7 (5-7/06/06). Data collected at 0.083 Hz by YSI6600 probe located 0.4 m above bed, 3.9 m from right bank.

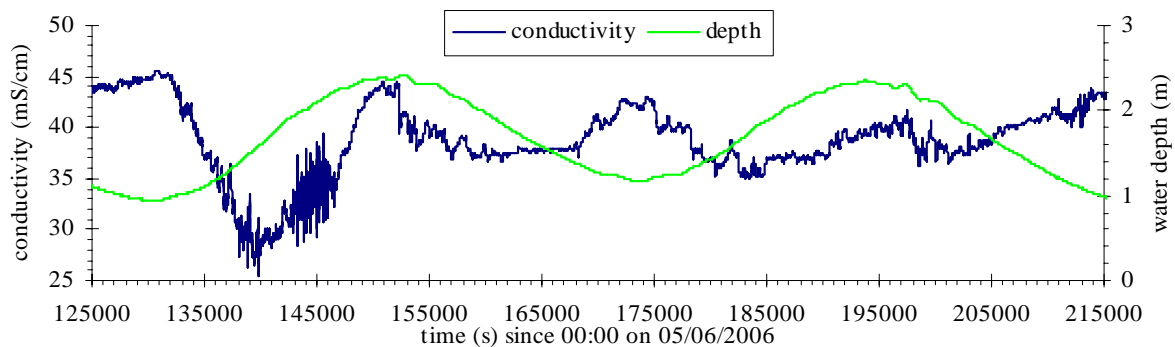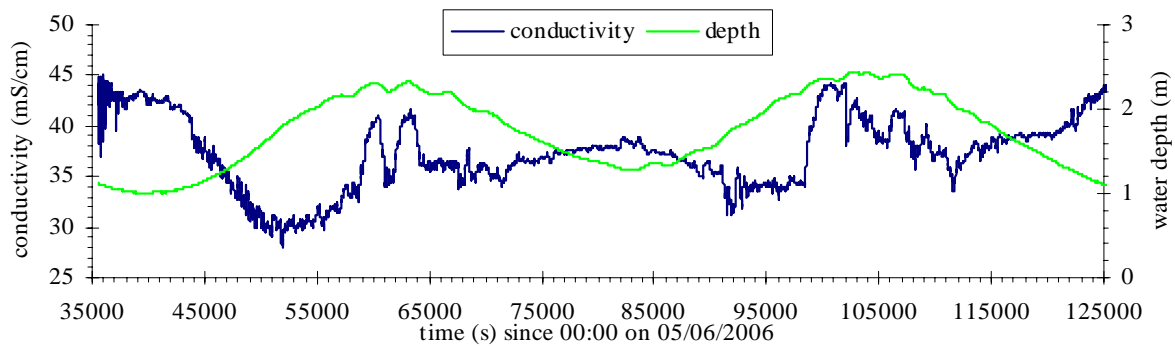(A) Instantaneous water depth and conductivity data.

230

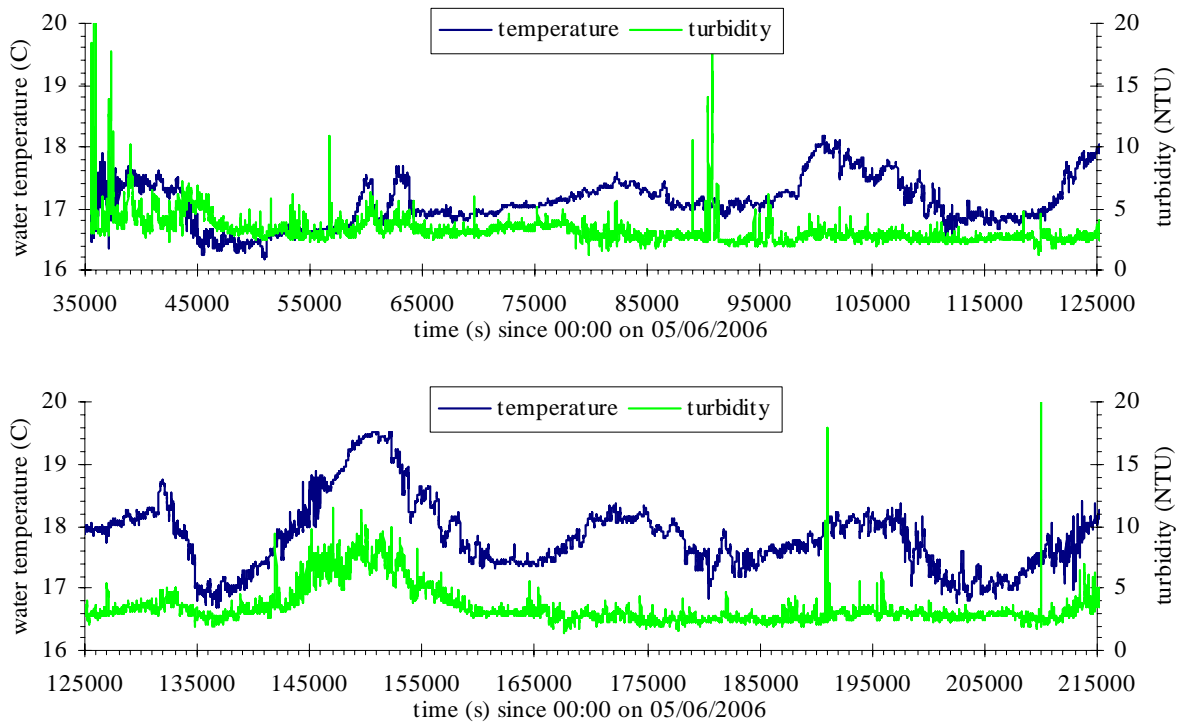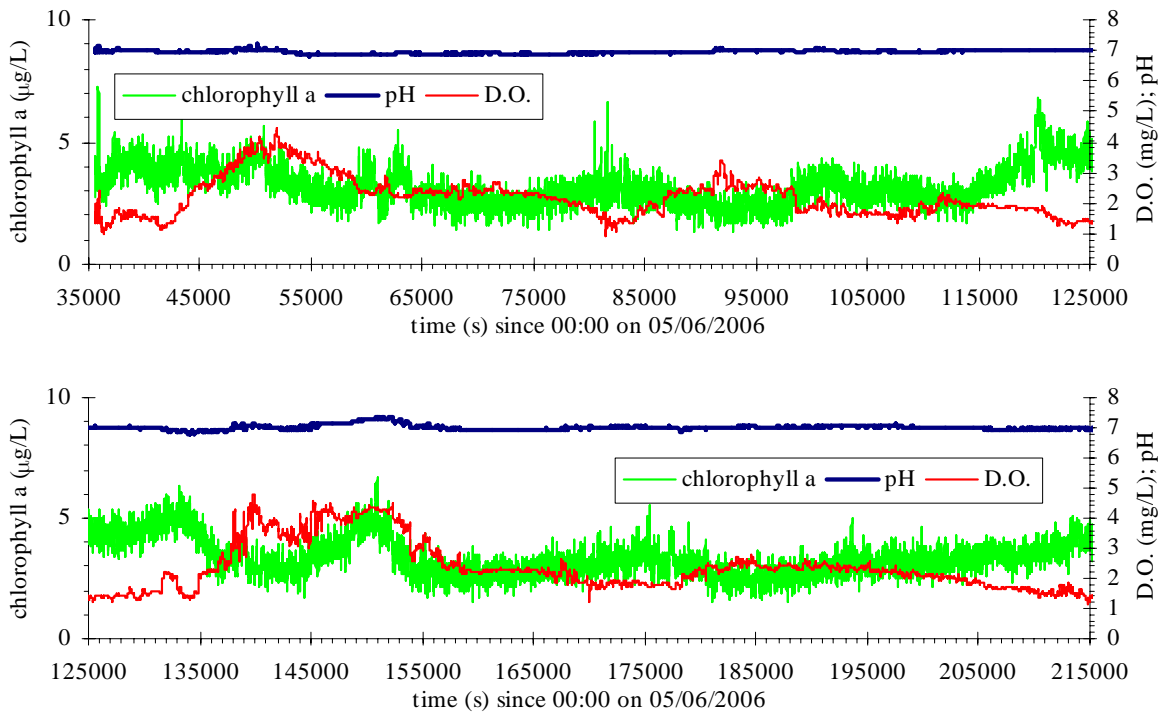(B) Instantaneous water temperature and turbidity data.

(C) Instantaneous dissolved oxygen, pH and chlorophyll a level data.

Figure C.19 – Instantaneous physio-chemistry data collected at Site 3 Eprapah Creek for study E7 (5-7/06/06). Data collected at 0.083 Hz by YSI6600 probe located about 0.3 m below surface, 3.9 m from right bank.

C.4   FIELD OBSERVATIONS: VERTICAL PHYSIO-CHEMISTRY PROFILES

C.4.1   Field study E1 (4/04/2003)
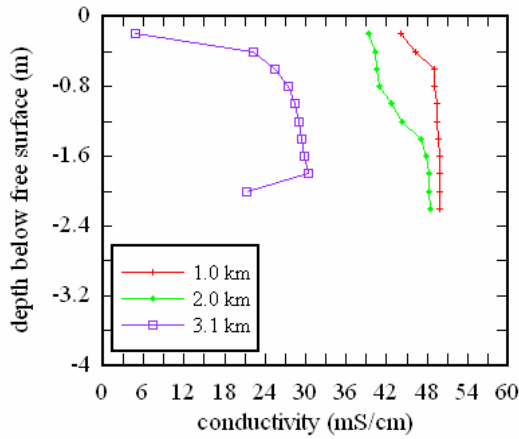
(A) Conductivity data.
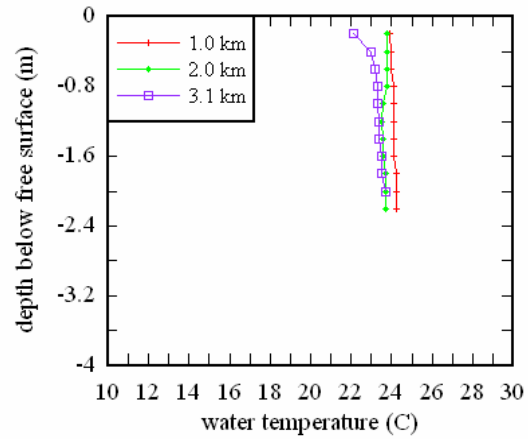
(B) Water temperature data.

(C) Turbidity data.

(D) Dissolved oxygen data.

(E) pH data.

Figure C.20 – Vertical physio-chemistry profiles collected for study E1 (4/04/03). Data collected on 4/04/03 at 1.0 km (10:20); 2.0 km (10:44); & 3.1 km (11:12) from mouth.

(A) Conductivity data.

(B) Water temperature data.

(C) Turbidity data.

(D) Dissolved oxygen data.

(E) pH data.

Figure C.21 – Vertical physio-chemistry profiles collected for study E1 (4/04/03). Data collected on 4/04/03 at 1.0 km (12:31); 2.0 km (12:48); & 3.1 km (13:23) from mouth.

C.4.2 Field study E2 (17/07/2003)

(A) Conductivity data.

(B) Water temperature data.

(C) Turbidity data.

(D) Dissolved oxygen data.

(E) pH data.

Figure C.22 – Vertical physio-chemistry profiles collected for study E2 (17/07/03). Data collected on 17/07/03 at 0.0 km (12:50); 2.0 km (13:16); & 2.7 km (13:34) from mouth.
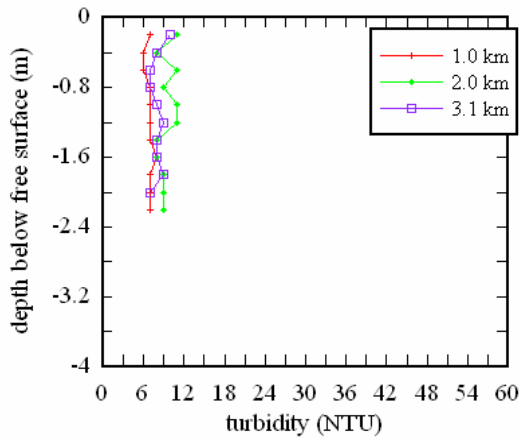
C.4.3 Field study E3 (24/11/2003)

(A) Conductivity data.

(B) Water temperature data.

(C) Turbidity data.

(D) Dissolved oxygen data.

(E) pH data.

Figure C.23 – Vertical physio-chemistry profiles collected for study E3 (24/11/03). Data collected on 23/11/03 at 1.0 km (09:32); 2.0 km (09:45); & 3.1 km (10:12) km from mouth.
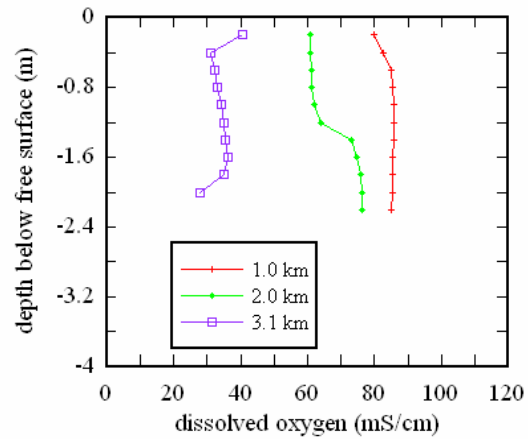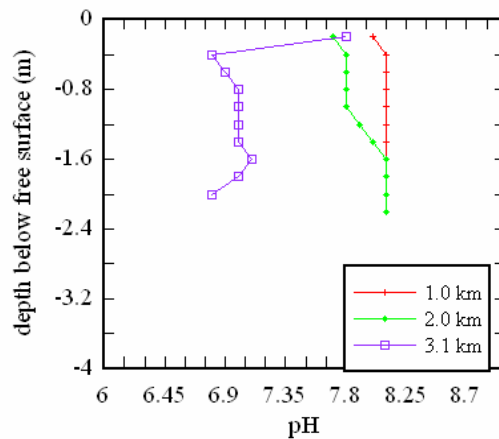
(A) Conductivity data.

(B) Water temperature data.

(C) Turbidity data.

(D) Dissolved oxygen data.

(E) pH data.

Figure C.24 – Vertical physio-chemistry profiles collected for study E3 (24/11/03). Data collected on 23/11/03 at 1.0 km (11:23); 2.0 km (11:41); & 3.1 km (11:55) from mouth.

(A) Conductivity data.

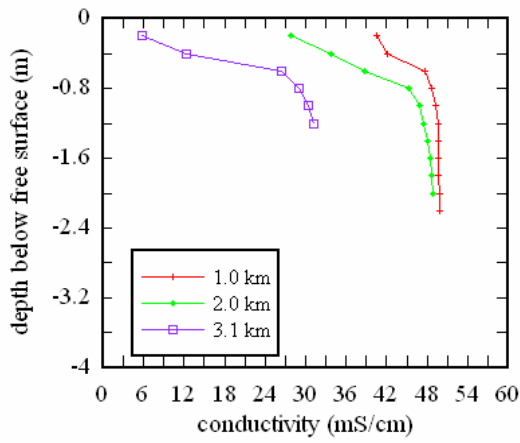
(B) Water temperature data.

(C) Turbidity data.

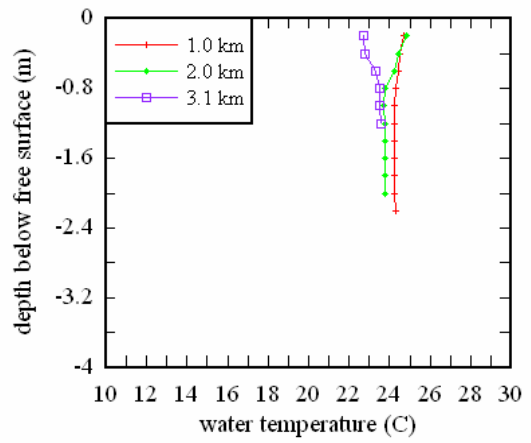(D) Dissolved oxygen data.

(E) pH data.

Figure C.25 – Vertical physio-chemistry profiles collected for study E3 (24/11/03). Data collected on 23/11/03 at 1.0 km (13:04); 2.0 km (13:24); & 3.1 km (13:50) from mouth.

C.4.4   Field study E4 (2/09/2004)

(A) Conductivity data.

(B) Water temperature data.

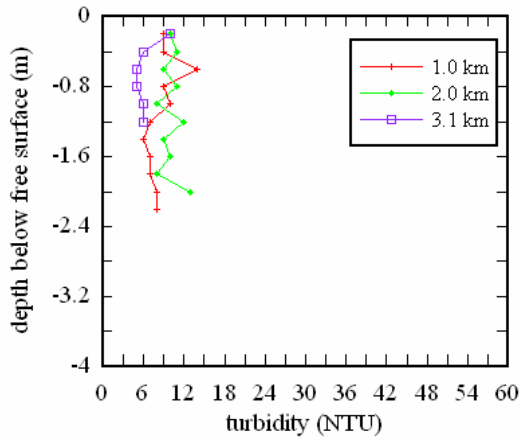(C) Turbidity data.

(D) Dissolved oxygen data.

(E) pH data.

Figure C.26 – Vertical physio-chemistry profiles collected for study E4 (2/09/04).   Data collected on 2/09/04 at 1.0 km (09:05); 2.0 km (09:25); & 3.1 km (09:47) from mouth.
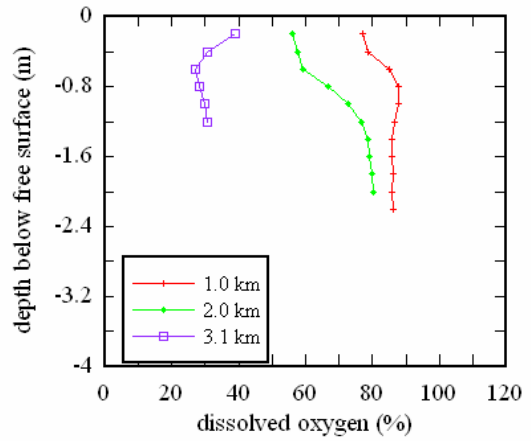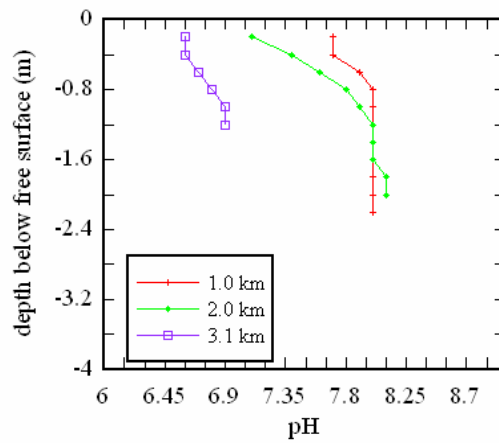
(A) Conductivity data.

(B) Water temperature data.

(C) Turbidity data.

(D) Dissolved oxygen data.

(E) pH data.

Figure C.27 – Vertical physio-chemistry profiles collected for study E4 (2/09/04). Data collected on 2/09/04 at 1.0 km (10:09); 2.0 km (10:29); & 3.1 km (10:47) from mouth.

(A) Conductivity data.

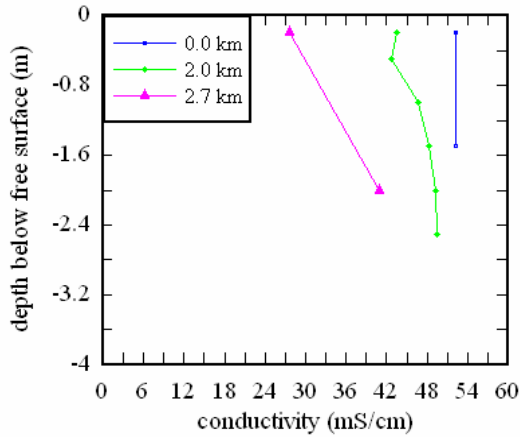(B) Water temperature data.
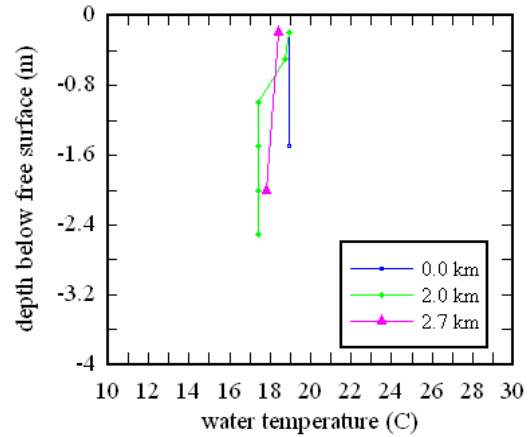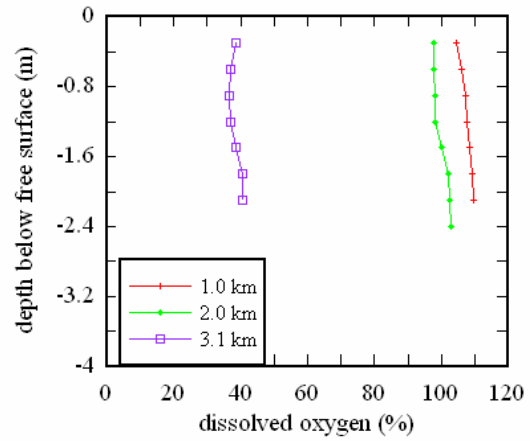
(C) Turbidity data.

(D) Dissolved oxygen data.
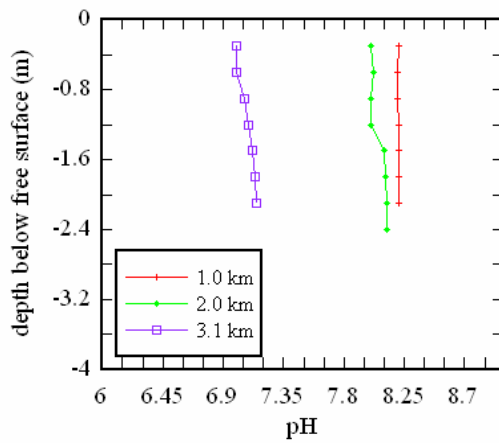
(E) pH data.

Figure C.28 – Vertical physio-chemistry profiles collected for study E4 (2/09/04). Data collected on 2/09/04 at 1.0 km (11:33); 2.0 km (11:55); & 3.1 km (12:24) from mouth.
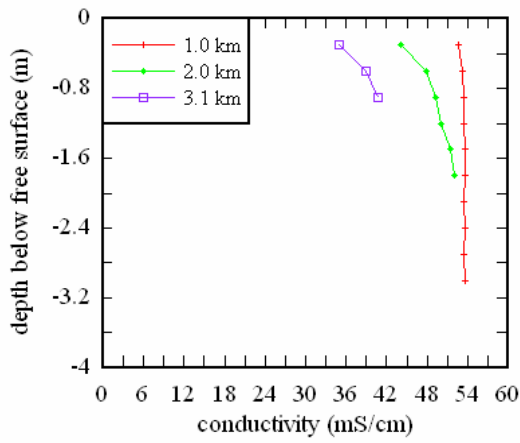
(A) Conductivity data.
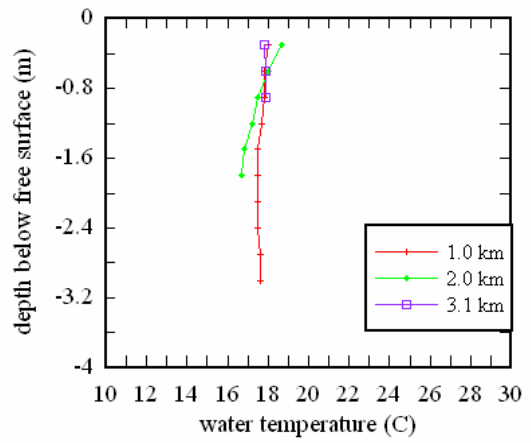
(B) Water temperature data.
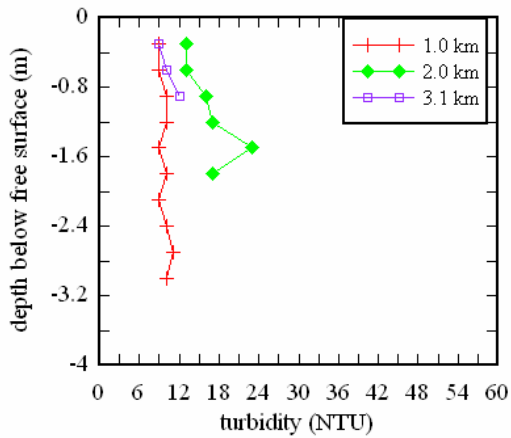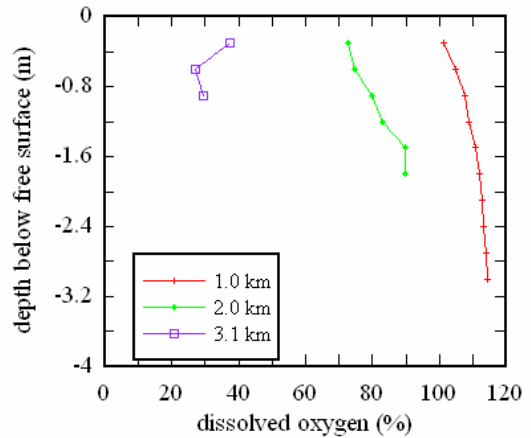
(C) Turbidity data.

(D) Dissolved oxygen data.
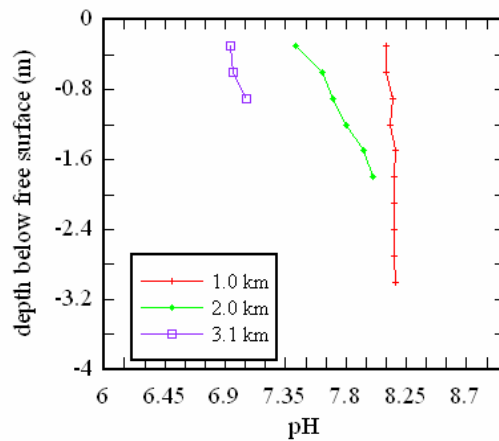
(E) pH data.

Figure C.29 – Vertical physio-chemistry profiles collected for study E4 (2/09/04). Data collected on 2/09/04 at 1.0 km (13:30); 2.0 km (14:00); & 3.1 km (14:30) from mouth.
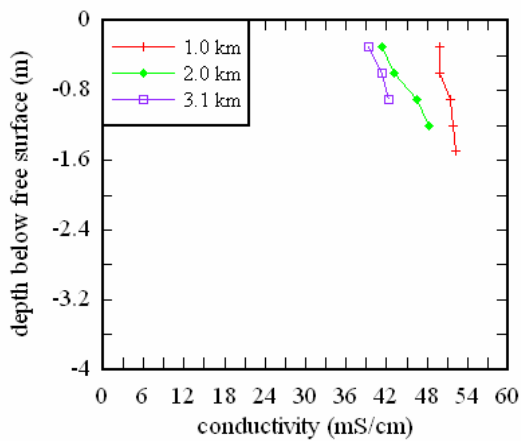
241

(A) Conductivity data.
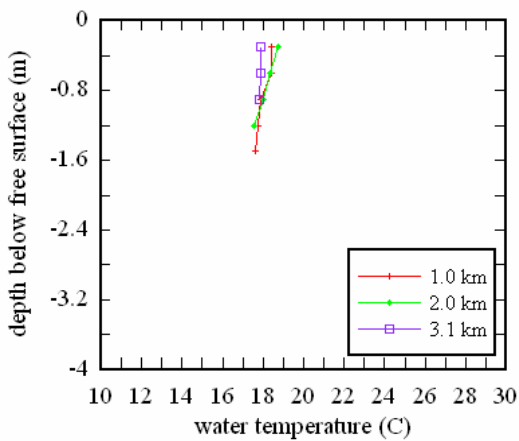
(B) Water temperature data.
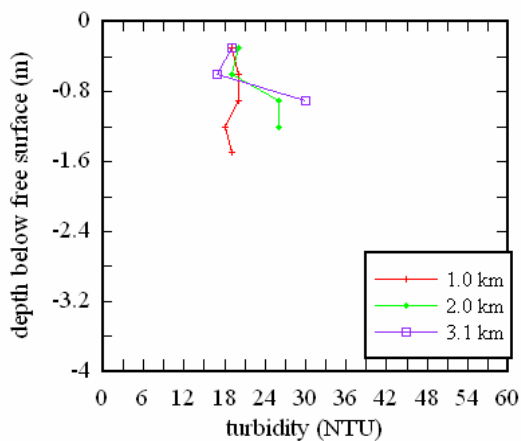
(C) Turbidity data.
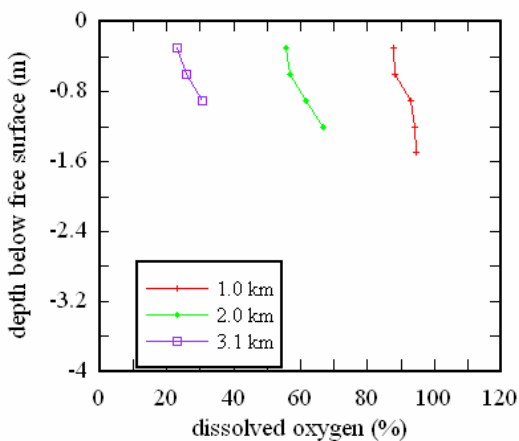
(D) Dissolved oxygen data.
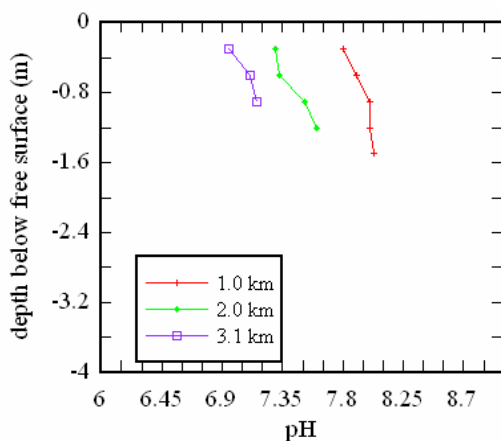
(E) pH data.

Figure C.30 – Vertical physio-chemistry profiles collected for study E4 (2/09/04). Data collected on 2/09/04 at 1.0 km (15:35); 2.0 km (15:46); & 3.1 km (16:16) from mouth.
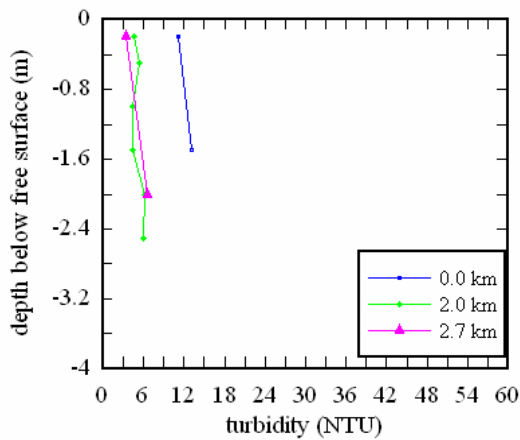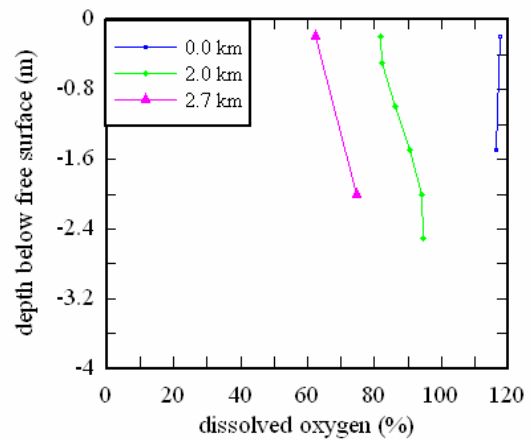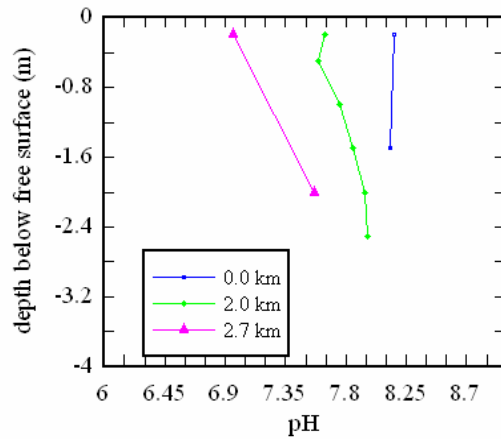
C.4.5   Field study E5 (8-9/03/2005)
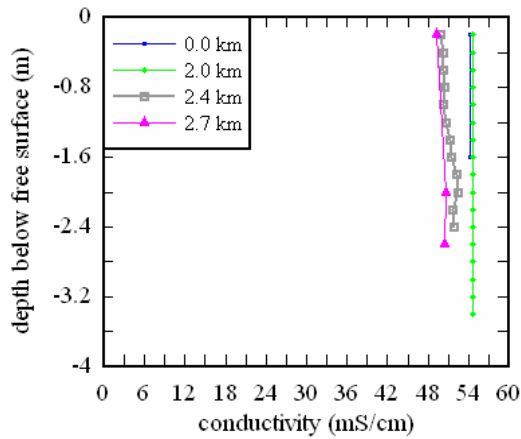
(A) Conductivity data.
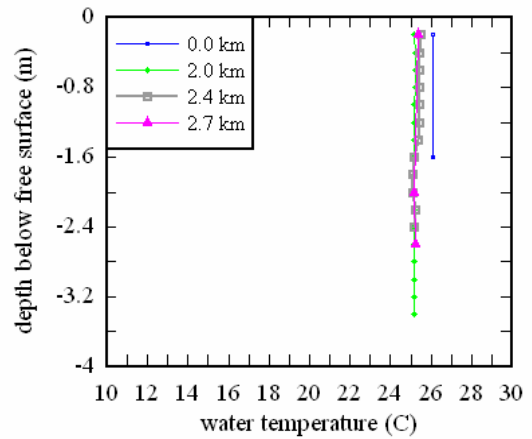
(B) Water temperature data.
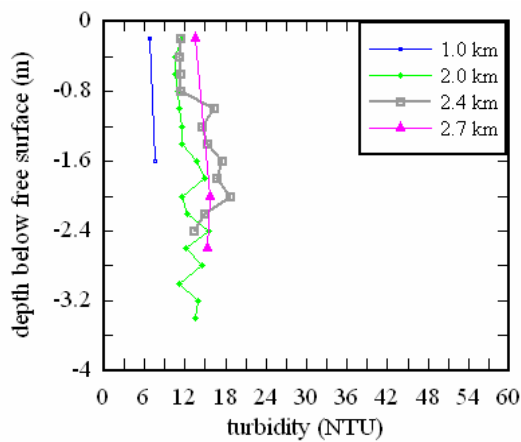
(C) Turbidity data.
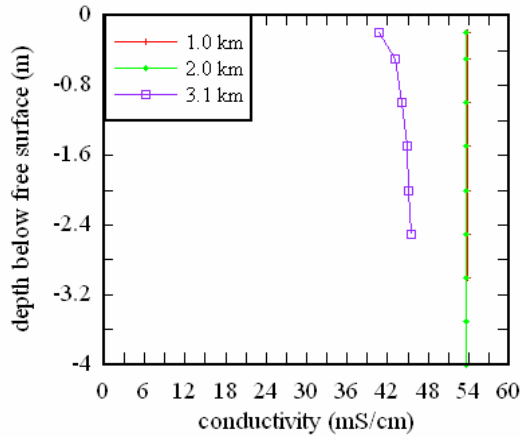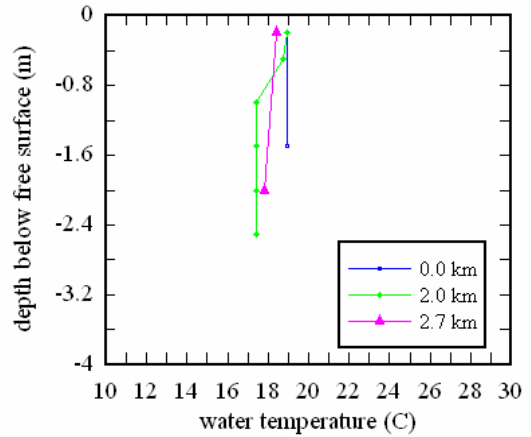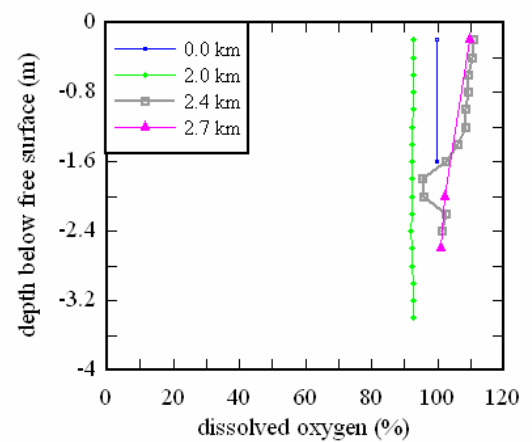

(D) Dissolved oxygen data.
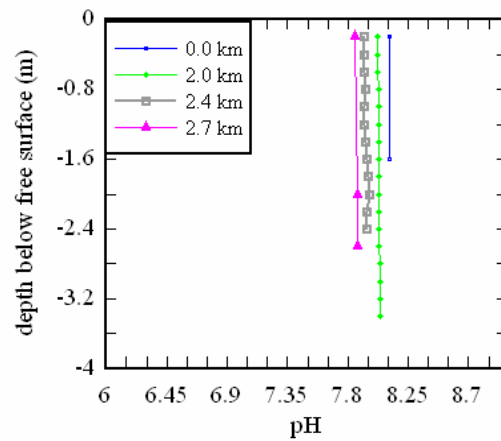
(E) pH data.

Figure C.31 – Vertical physio-chemistry profiles collected for study E5 (8-9/03/05). Data collected on 10/03/05 at 0.0 km (11:05); 2.0 km (11:23); 2.4 km (11:46); & 2.7 km (12:02) from mouth.
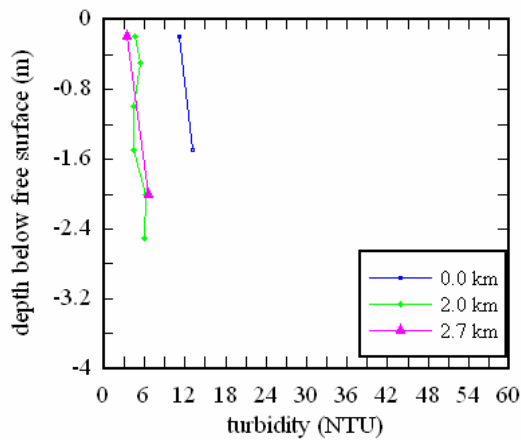
C.4.6 Field study E6 (16-18/05/2005)
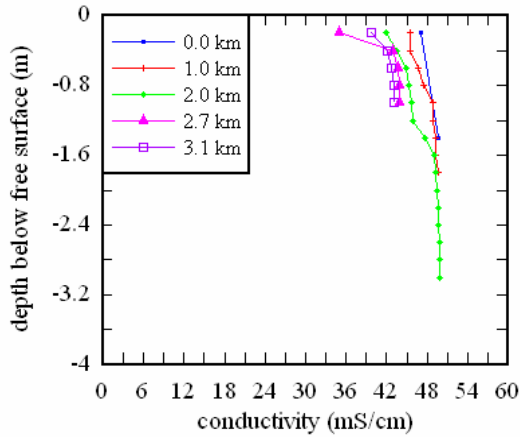
(A) Conductivity data.
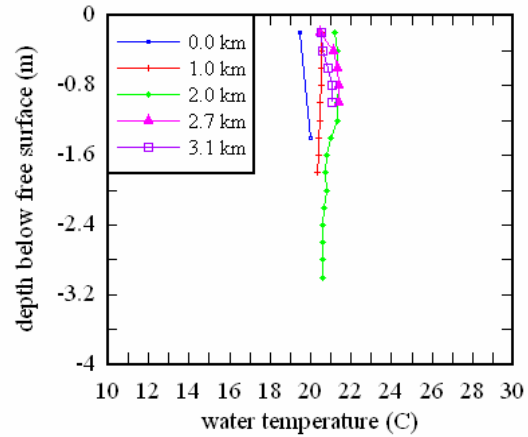
(B) Water temperature data.
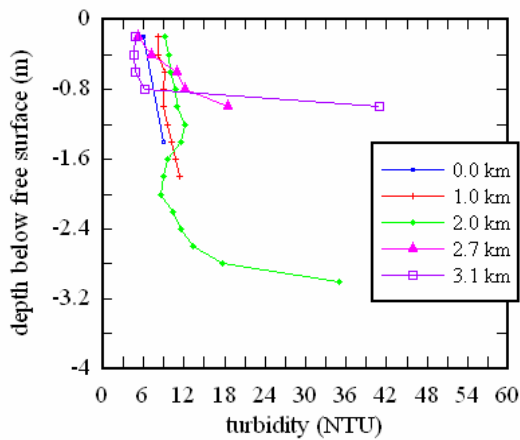
(C) Turbidity data.
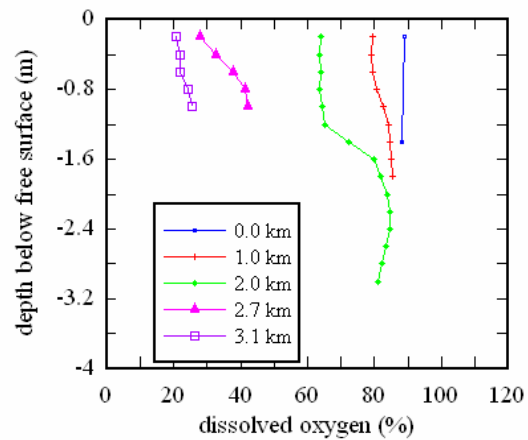
(D) Dissolved oxygen data.
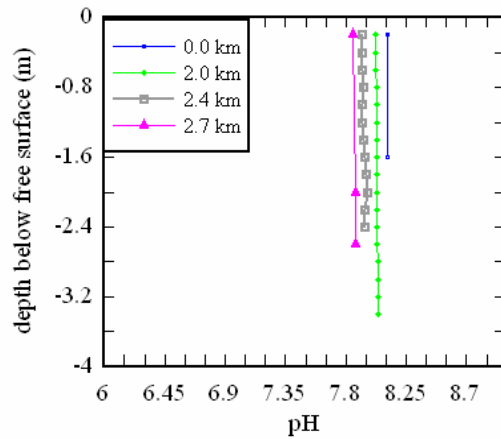
(E) pH data.

Figure C.32 – Vertical physio-chemistry profiles collected for study E6 (16-18/05/05). Data collected on 17/05/05 at 0.0 km (08:14); 1.0 km (08:35); 2.0 km (08:53); 2.7 km (09:34); & 3.1 km (09:53) from mouth.

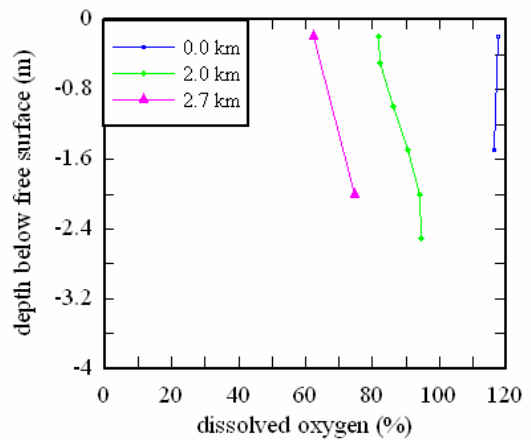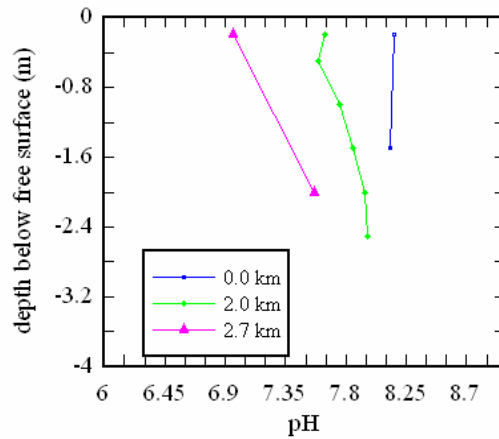C.4.7   Field study E7 (5-6/06/2006)
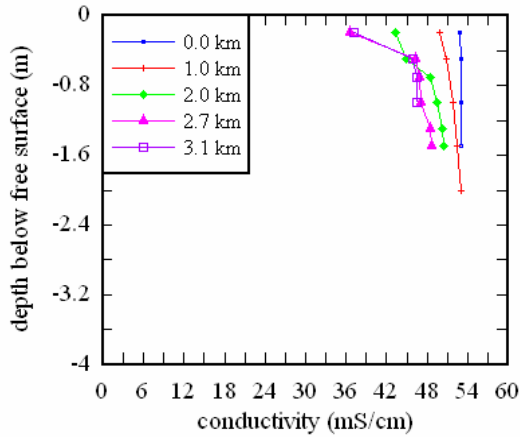
(A) Conductivity data.
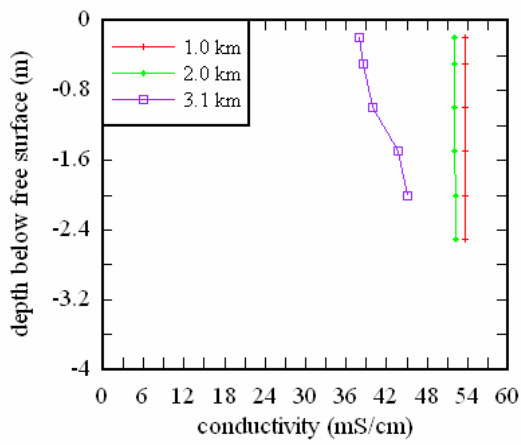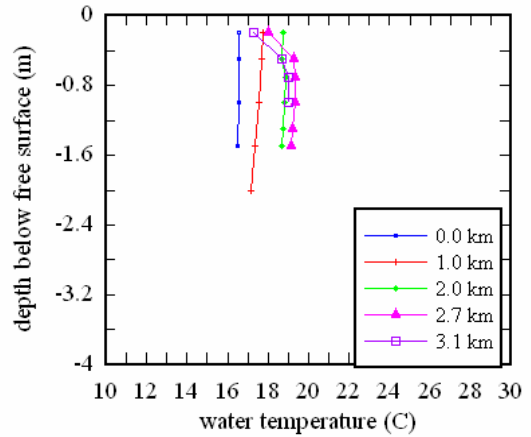

(B) Water temperature data.
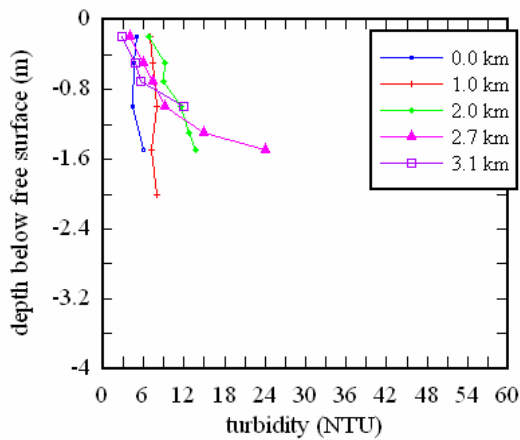
(C) Turbidity data.
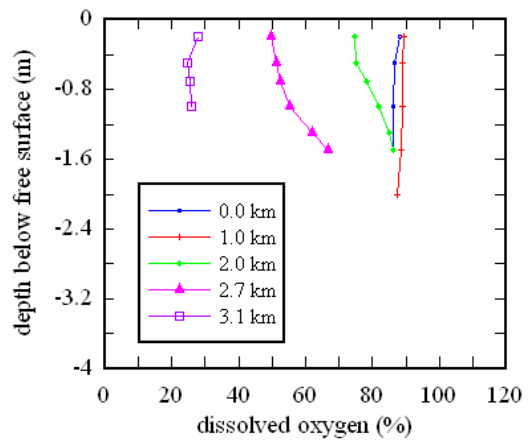
(D) Dissolved oxygen data.
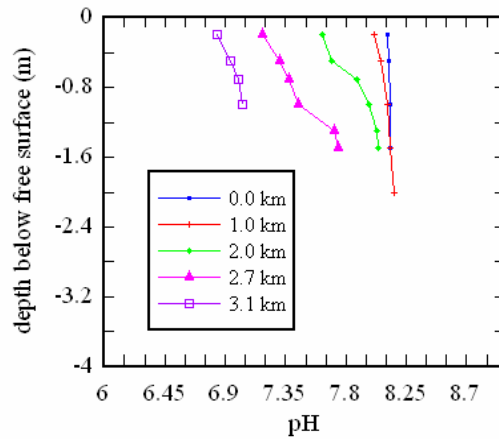
(E) pH data.

Figure C.33 – Vertical physio-chemistry profiles collected for study E7 (5-7/06/06). Data collected on 7/06/06 at 0.0 km (09:09); 1.0 km (09:31); 2.0 km (09:49); 2.7 km (10:17); & 3.1 km (10:35) from mouth.

C.4.8   Field study E8 (28/08/2006)
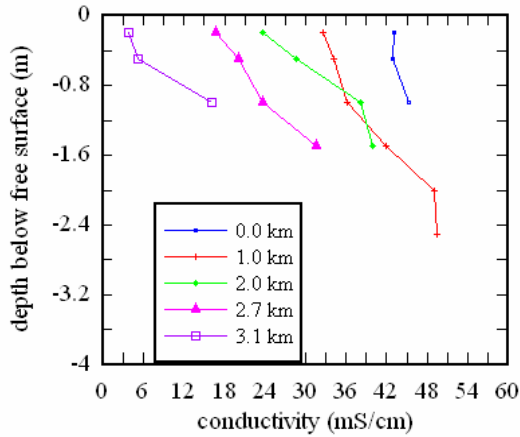
(A) Conductivity data.
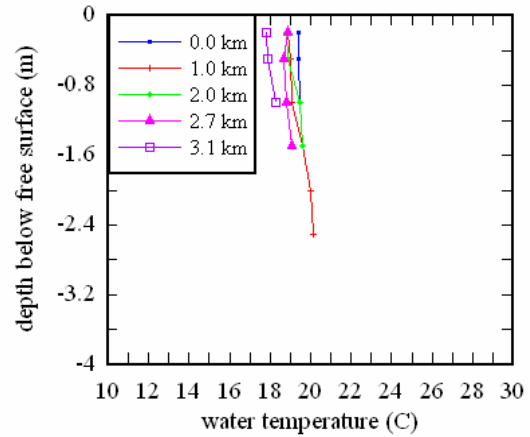
(B) Water temperature data.
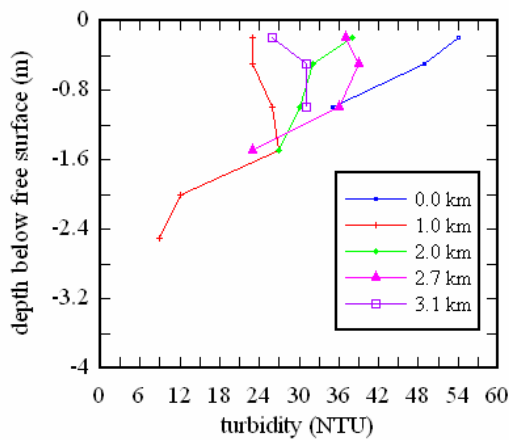
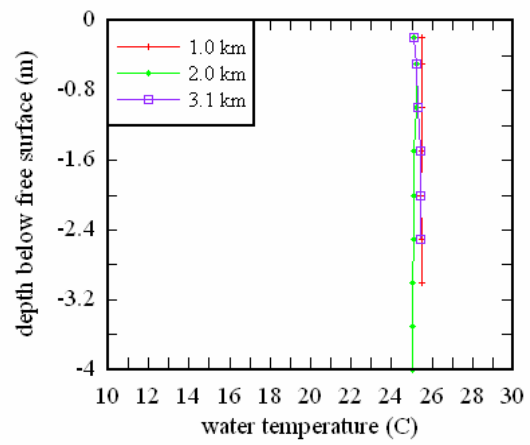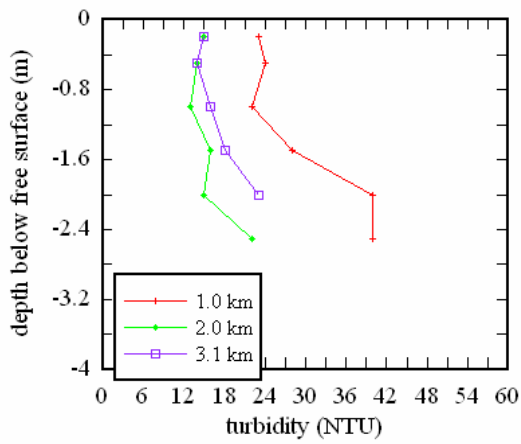(C) Turbidity data.
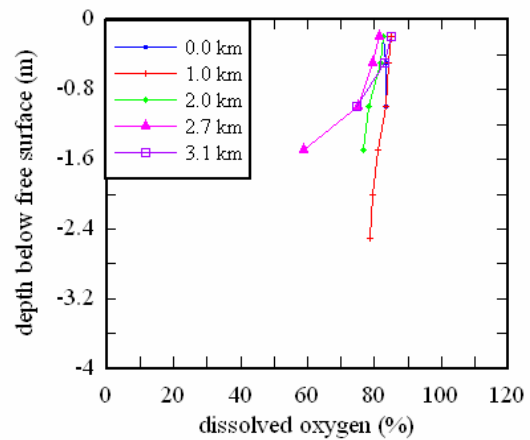
(D) Dissolved oxygen data.
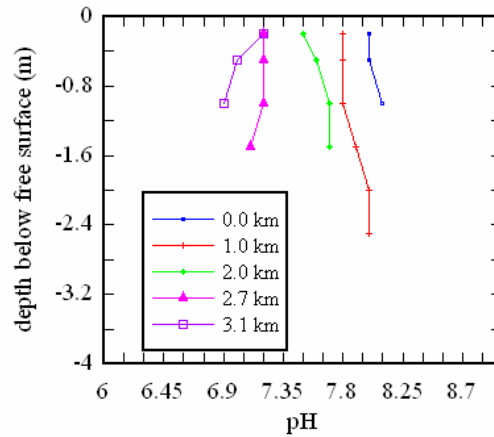
(E) pH data.

Figure C.34 – Vertical physio-chemistry profiles collected for study E8 (28/08/06).   Data collected on 28/08/06 at 0.0 km (08:25); 1.0 km (08:32); 2.0 km (08:50); 2.7 km (09:10); & 3.1 km (09:20) from mouth.
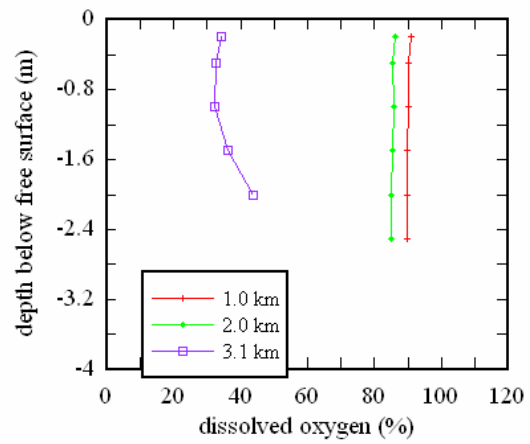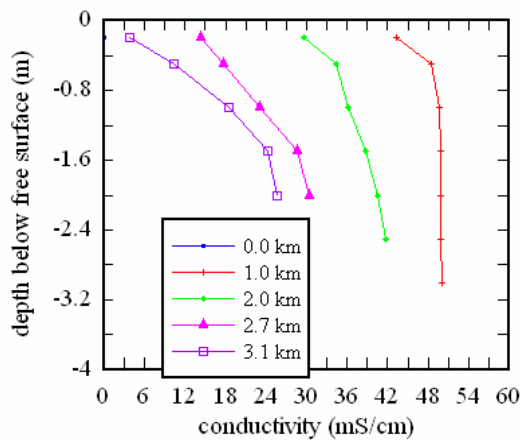
(A) Conductivity data.
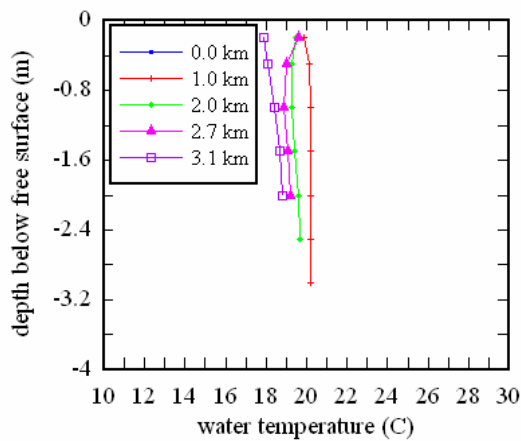
(B) Water temperature data.
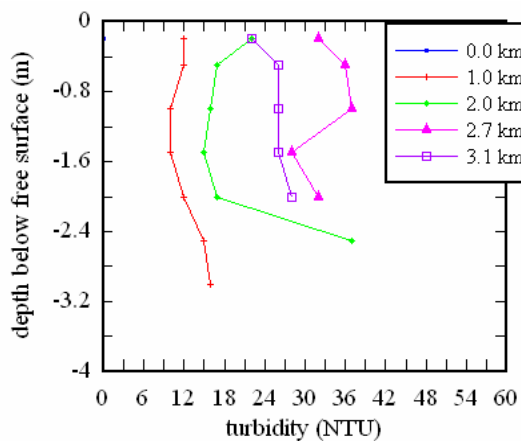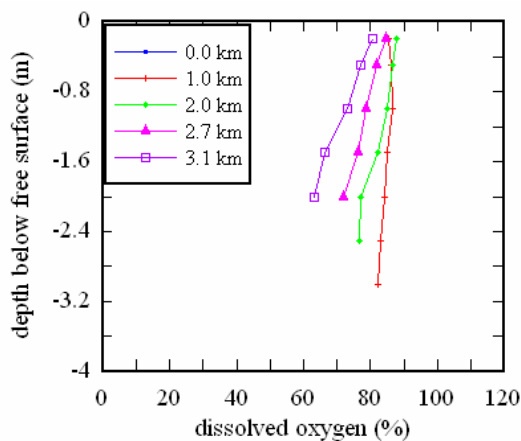
(C) Turbidity data.

(D) Dissolved oxygen data.
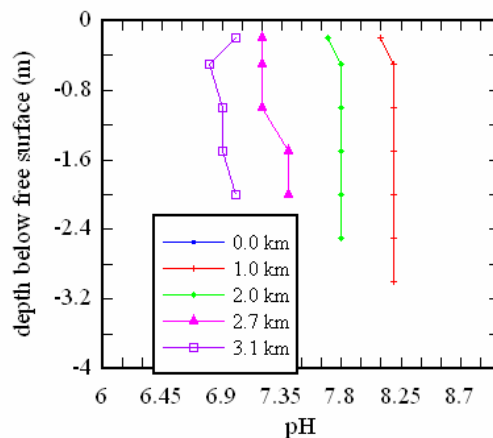
(E) pH data.

Figure C.35 – Vertical physio-chemistry profiles collected for study E8 (28/08/06). Data collected on 28/08/06 at 1.0 km (09:55); 2.0 km (10:16); 2.7 km (10:45); & 3.1 km (10:58) from mouth.
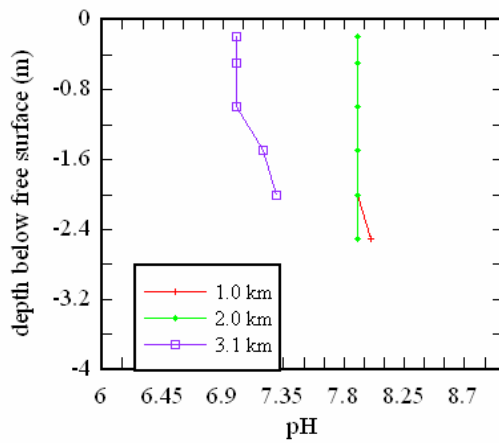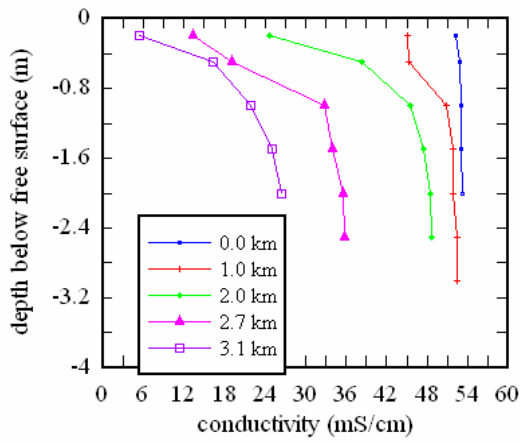
(A) Conductivity data.
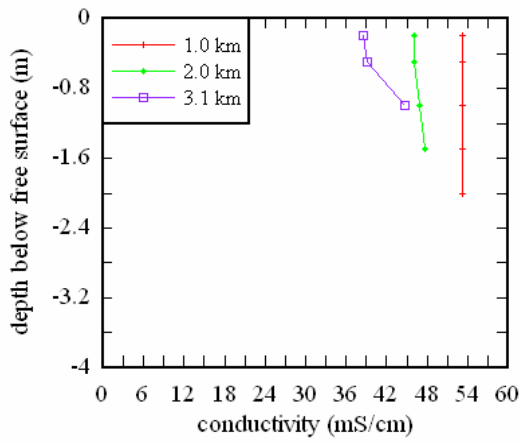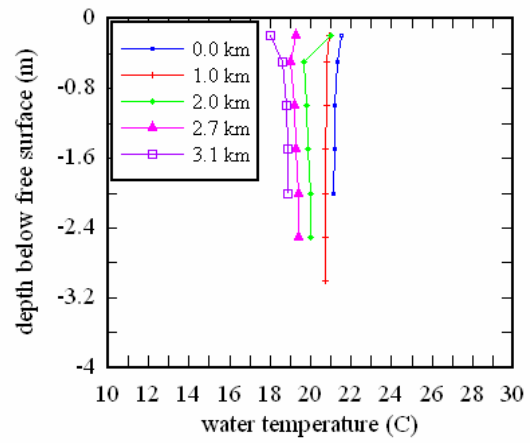
(B) Water temperature data.
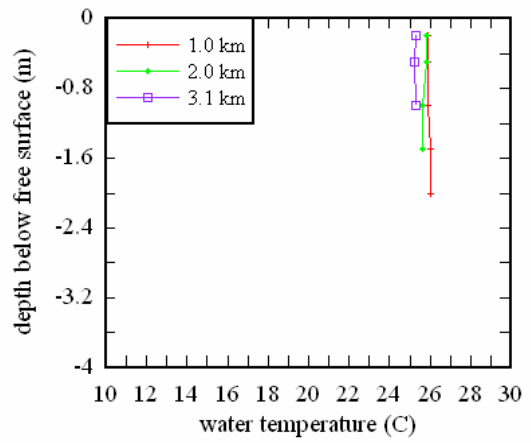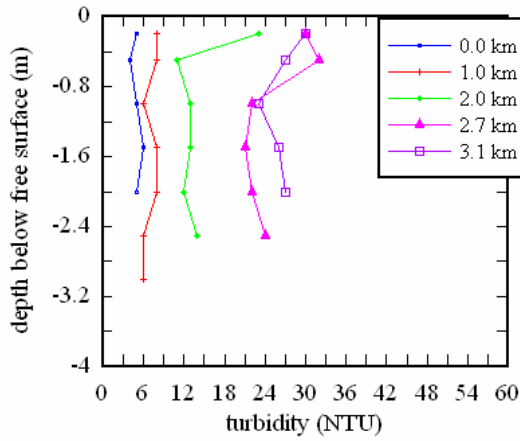
(C) Turbidity data.
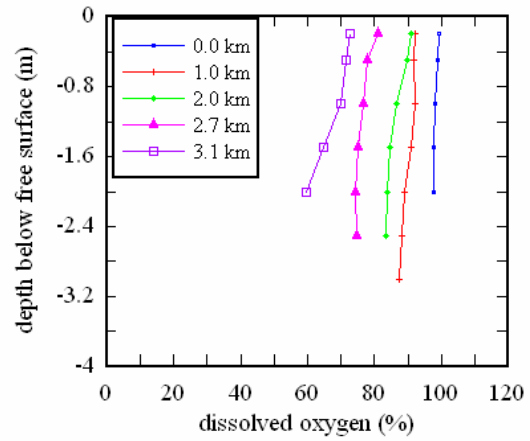
(D) Dissolved oxygen data.
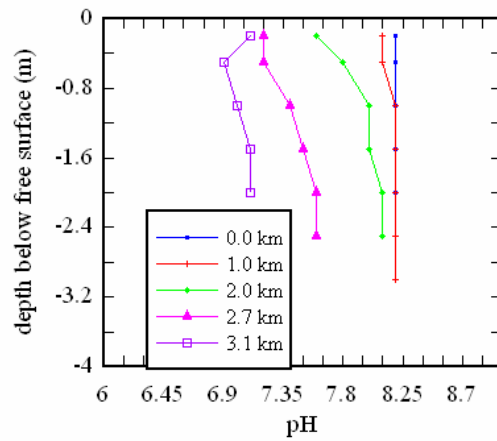
(E) pH data.

Figure C.36 – Vertical physio-chemistry profiles collected for study E8 (28/08/06). Data collected on 28/08/06 at 0.0 km (11:32); 1.0 km (11:46); 2.0 km (12:05); 2.7 km (12:25); & 3.1 km (12:35) from mouth.

C.4.9   Field study E9 (2-13/10/2006)
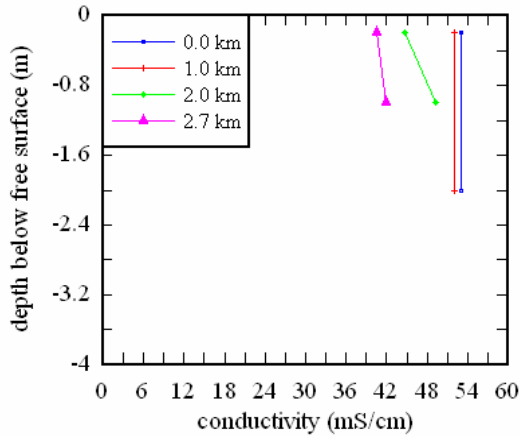
(A) Conductivity data.
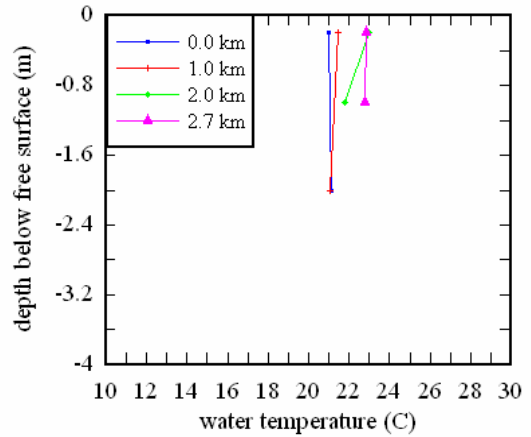
(B) Water temperature data.
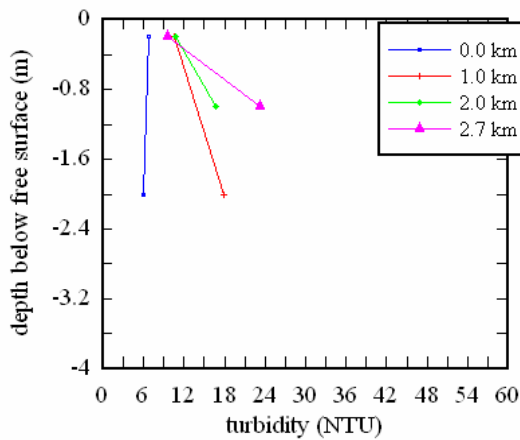
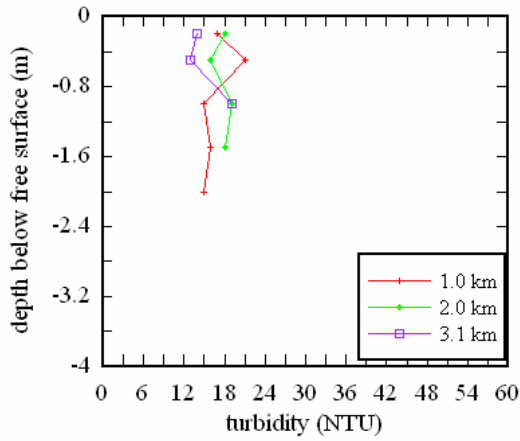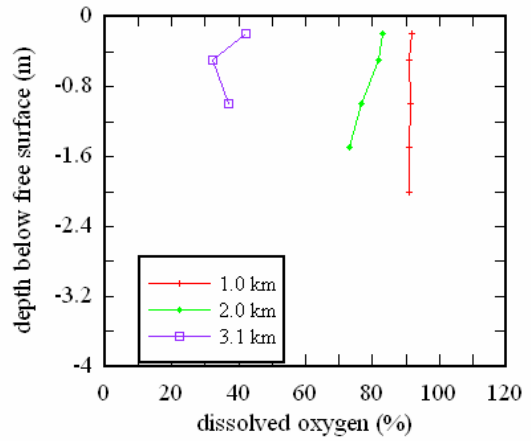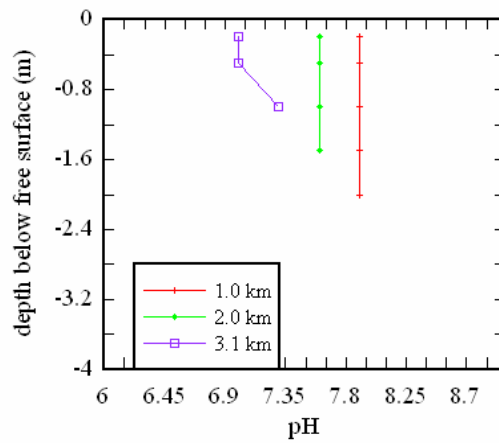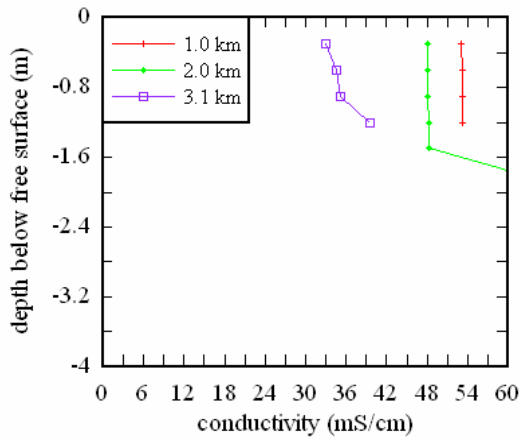(C) Turbidity data.
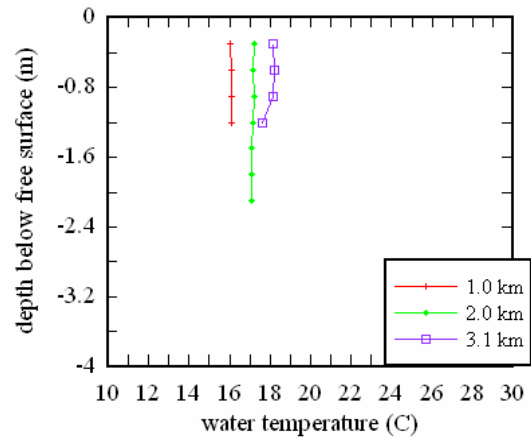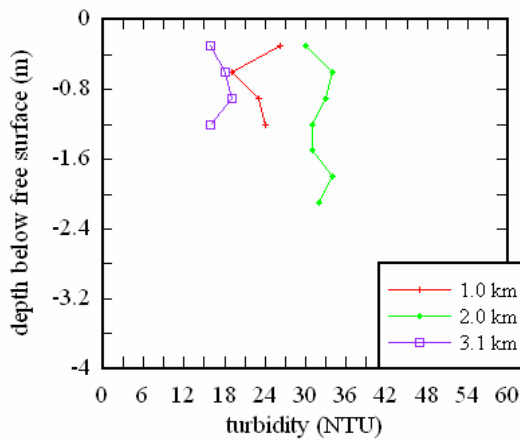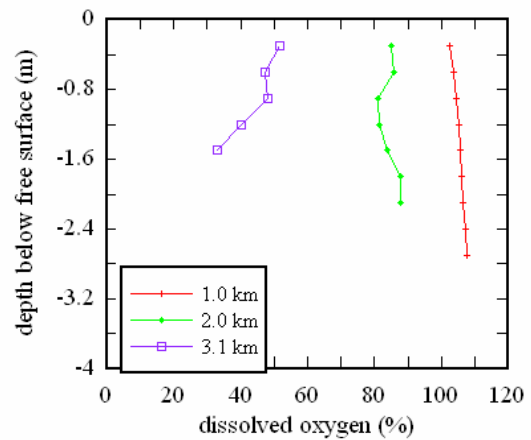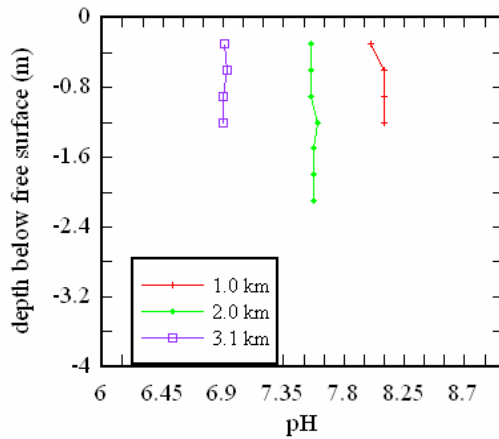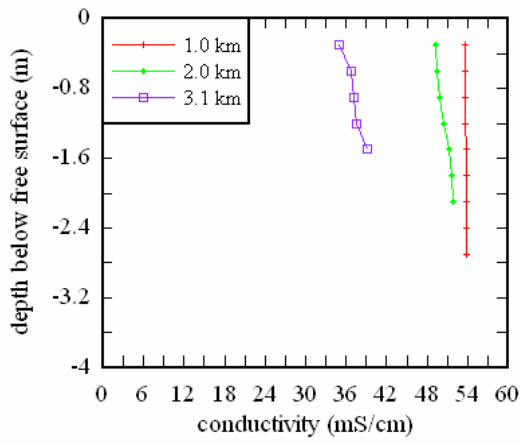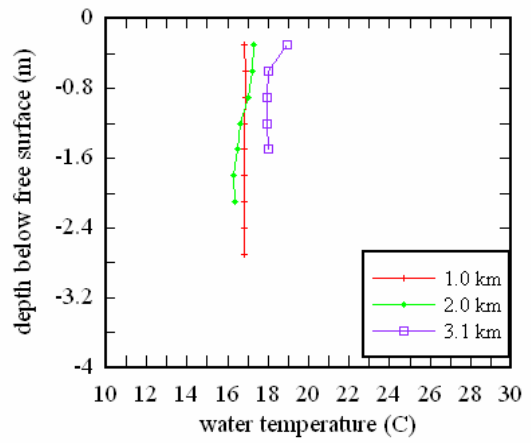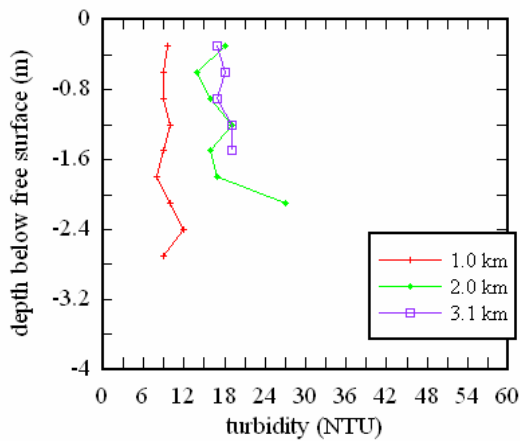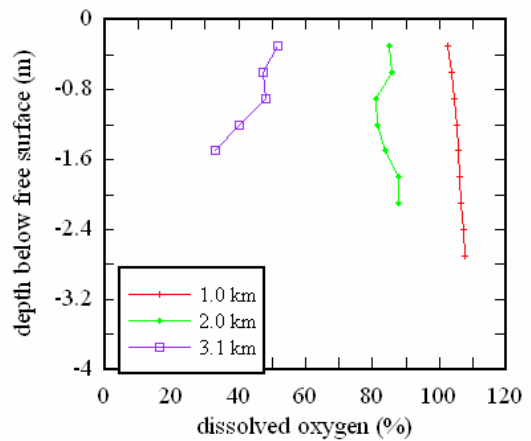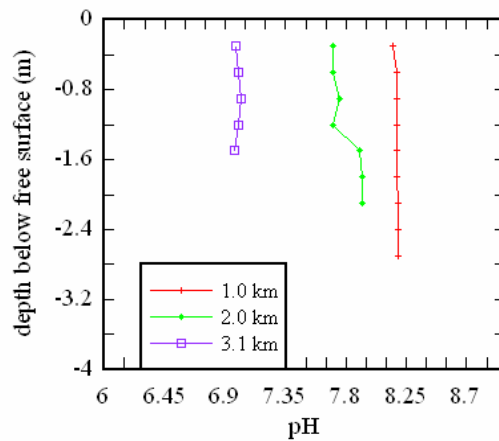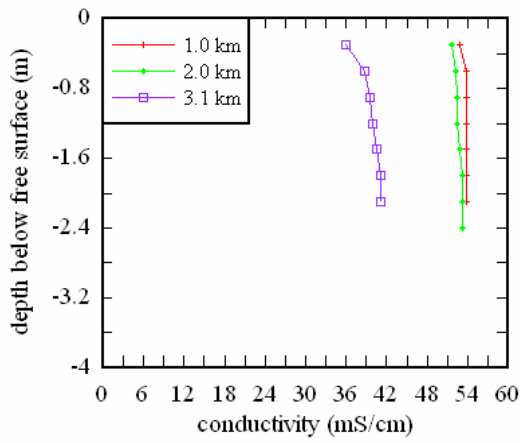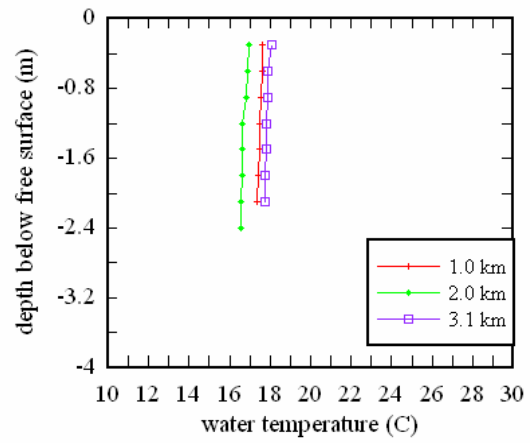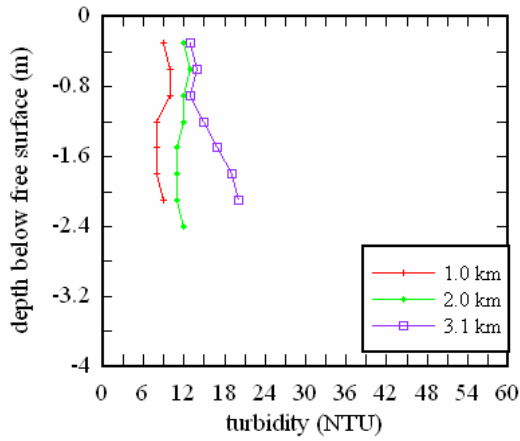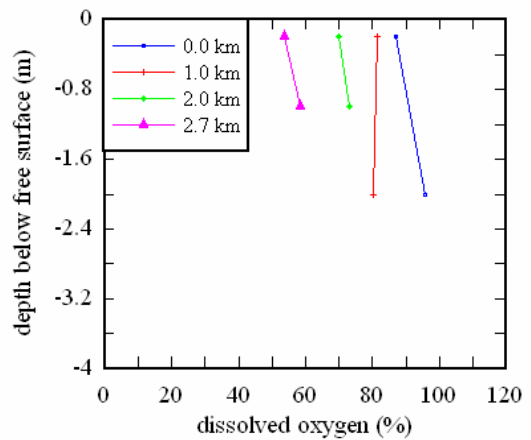

(D) Dissolved oxygen data.
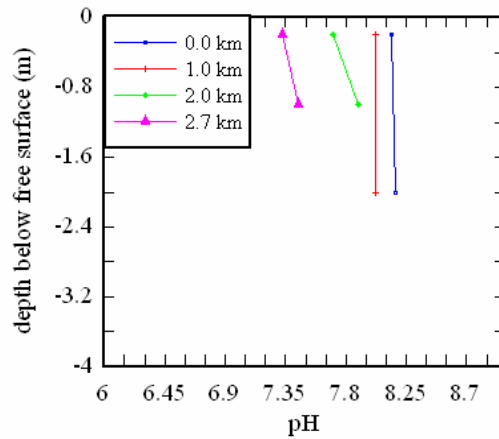
(E) pH data.

Figure C.37 – Vertical physio-chemistry profiles collected for study E9 (2-13/10/06). Data collected on 5/10/06 at 0.0 km (10:22); 1.0 km (10:30); 2.0 km (10:41); & 2.7 km (10:56) from mouth.

APPENDIX D   LABORATORY EXPERIMENT – RELATIONSHIP BETWEEN SUSPENDED SEDIMENT CONCENTRATION AND ADV BACKSCATTER INTENSITY

D.1   INTRODUCTION

The study of the suspended sediment concentration is an important factor for assessing the evolution and health of an estuary. Several studies suggested that acoustic Doppler backscatter and turbidity may be a suitable proxy for measuring the suspended sediment concentration (SSC). In 2006 a laboratory experiment was conducted to calibrate the acoustic Doppler backscatter and turbidity with suspended sediment concentration. This laboratory experiment was performed using the water and sediment collected from a small subtropical estuary (Eprapah Creek) in Southeast Queensland (Australia).

Section D.2 describes the acoustic backscatter intensity and how previous studies have utilised the backscatter intensity to estimate the suspended sediment concentration within the sampling volume. In Section D.3 the experimental technique used, measurements collected and outcomes of the calibration experiment are presented.

D.2   ACOUSTIC BACKSCATTER INTENSITY

Acoustic Doppler devices perform high frequency velocity measurements, but a further output is the signal backscatter intensity (I_B). This intensity is the acoustic signal that is backscattered from small particles within the sampling volume. The backscatter intensity relates to suspended sediment (Lohrmann et al. (1994), Sontek (1997)). Thus acoustic Doppler devices can measure at high frequency (up to 100 Hz) an estimate of the sediment concentration. The backscatter intensity is calculated from the signal amplitude (AMP) of each receiver of the ADV. Measured in counts (one count equals 0.43 dB), the amplitude (AMP) represents the signal strength of the receiver. A count is the number of particles for which the transmitted signal is reflected back to the individual receiver. Lohrmann et al. (1994) outlined a simplified relationship between acoustic signal scatter and concentration of particles in the sampling volume (Equation D.1):

$$I = I_0 \; C_s \; S_f \; S_a \left(\frac{e^{-2 \left(a_w + a_s \right) r}}{r^2} \right) \tag{D.1}$$

where I = backscatter intensity; I_0 = transmitted intensity; a_w = water absorption; a_s = absorption due to particle scattering; r = acoustic propagation path; S_a = holds all particle specific parameters (size; elasticity; and density); S_f = all system specific parameters (transducer size; efficiency; probe geometry; and receive sensitivity); and C_s = suspended

sediment concentration. For low concentrations ($C_s < 1$ g/L) and a known particle size distribution Equation D.1 presents a linear relationship between sediment concentration and ADV backscatter intensity.

Lohrmann et al. (1994) calculated the backscatter intensity (I) from the ADV signal to noise ratio (SNR):

$$SNR = 10 \log_{10}\left(\frac{I}{NL}\right) \tag{D.2}$$

Sontek (1997) recommended against calculating backscatter intensity from signal to noise ratio. The backscatter intensity can be calculated from the signal amplitude by substituting SNR = 0.43(SL - NL) where SL = signal amplitude (AMP); and NL = noise level into Equation D.2. Kawanisi and Yokosi (1997) outlined a relationship between backscatter intensity and signal amplitude:

$$I = 10^{0.043\,SL} - 10^{0.043\,NL} \tag{D.3}$$

Since ADVs operate at high frequencies (10 MHz to 16 MHz) the noise level is small compared to the signal amplitude (Kawanisi and Yokosi (1997)). Kawanisi and Yokosi (1997) deduced the backscatter intensity from the averaged intensity of the three receivers. Nikora and Goring (2002) neglected the effect of noise level (NL) and used:

$$I_a \propto 10^{0.0434\,SL_a} \tag{D.4}$$

where I_a = individual backscatter intensity for the amplitude of receiver a (SL_a). The sum of the individual amplitudes of the three receivers was multiplied by 0.00003 to estimate a backscatter intensity $I_M = 0.00003\,(I_a + I_b + I_c)$. The use of 0.00003 provided Nikora and Goring (2002) with a pseudo intensity average from the three receivers. Other studies, such as Voulgaris and Meyers (2004) and Fugate and Friedrichs (2002) also found linear relationships between suspended sediment concentration and ADV backscatter intensity.

D.2.1   Method used

Since the signal amplitude is a scalar property of the sampling volume, the backscatter intensity I_B of an ADV signal was estimated here by using the averaged amplitude of the ADV signal ($AVAMP$) measured in counts:

$$I_B = 0.00001\,(10^{0.043\,AVAMP}) \tag{D.5}$$

where AVAMP is the averaged amplitude output from the post-processing software (e.g. WinADV). The coefficient 0.00001 was introduced to avoid large values of backscatter intensity. Nikora and Goring (2002) used a constant of similar magnitude (0.00003) to "avoid too large numbers".

D.3   CALIBRATION OF ADV BACKSCATTER, TURBIDITY AND SUSPENDED SEDIMENT CONCENTRATION

D.3.1   Experimental technique

D.3.1.1   Field site: Eprapah Creek

Eprapah Creek (153.30°E, 27.567°S) is a small subtropical stream located on the East coast of Australia, near the city of Brisbane. The creek is approximately 12.6 km long with an estuarine zone of approximately 3.8 km. In the estuary the mean water depth is typically 1 to 2 m mid-stream, and the width is approximately 20 to 40 m. At Eprapah Creek there are mixed semi-diurnal tides, with a range of 1 to 2.5 m (i.e. "micro-tidal" conditions). The catchment area of Eprapah Creek is approximately 39 km^2. Figure D.1 shows a sketch of the Eprapah Creek estuarine zone with the sampling locations indicated.
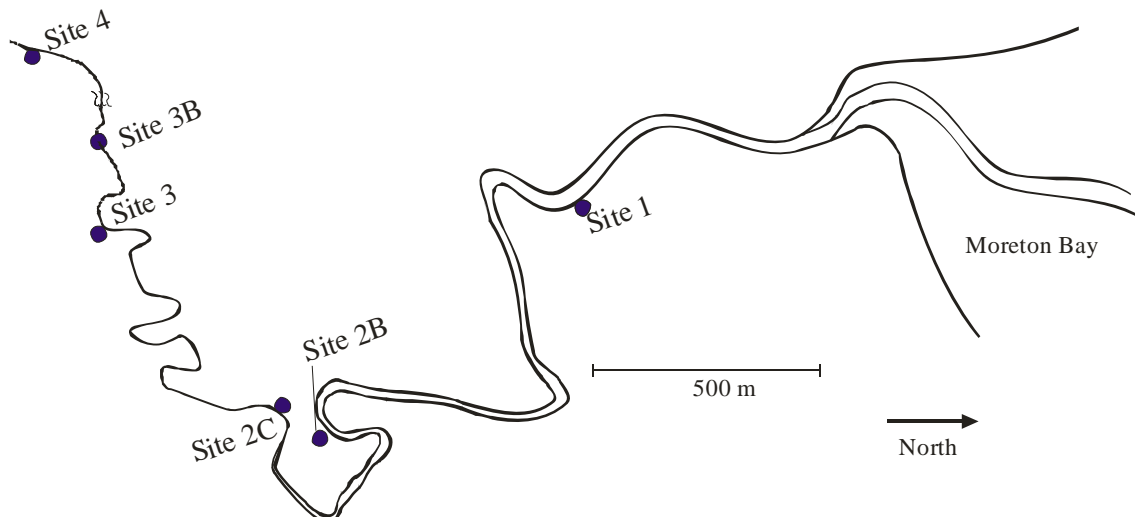
Figure D.1 – Sketch of Eprapah Creek (153.30°E, 27.567°S), located near Brisbane Australia.

Seven field investigations were performed in the Eprapah Creek estuary for which high frequency samples were measured continuously by a turbidity meter (YSI6600) and ADV system(s) (Table D.3). These field studies were detailed in: Chanson (2003); Chanson et al. (2005a); Trevethan et al. (2006); and Trevethan et al. (2007).

Table D.1 – Turbulence and turbidity field measurements conducted at Eprapah Creek.

Study	Date	ADV type	f_{scan} (ADV) (Hz)	f_{scan} (YSI6600) (Hz)	T_{study} (hrs)	ADV Sampling location
E1	4/04/03	(10 MHz)	25	0.2	12	Site 2B, 0.5 m below surface, 14.2 m from left bank
E2	17/07/03	(10 MHz)	25	0.2	8	Site 2, 0.5 m below surface, 8.0 m from left bank
E3	24/11/03	(10 MHz)	25	0.5	7	Site 2B, 0.5 m below surface, 10.7 m from left bank
E4	2/09/04	(10 MHz)	25	0.3	9	Site 2B, 0.05 m above bed, 10.7 m from left bank
E5	8-9/03/05	(10 MHz)	25	0.167	25	Site 2B, 0.1 m above bed, 10.7 m from left bank
E6	16-18/05/05	(10 MHz) (16 MHz)	25 25	0.083	48	Site 2B, 0.2 & 0.4 m above bed, 10.7 m from left bank
E7	5-7/06/06	(10 MHz) (16 MHz)	25 50	0.083	50	Site 3, 0.2 & 0.4 m above bed, 4.2 m from right bank

Note: f_{scan} : sampling frequency; T_{study} : study duration; (10 MHz): Sontek 3D-ADV (10 MHz); (16 MHz): Sontek 2D-micro-ADV (16 MHz); Site 2: AMTD = 2.0 km; Site 2B: AMTD = 2.1 km; Site 3: AMTD = 3.1 km; and AMTD: Australian Middle Thread Distance (upstream of mouth).

D.3.2   Laboratory calibration experiments

Water and sediment samples were collected mid estuary at Eprapah Creek (Sites 2C and 2B, Figure D.1 respectively). Sediment sample 1 was gathered on the creek bed, while sample 2 was collected on the bank just below the high water mark. Both sediment samples consisted of fine "muddy" material, although sample 2 was slightly coarser than sample 1. Note that the size distribution of both sediment samples were not tested as part of this study.

These water and sediment samples were then used in controlled laboratory conditions to calibrate the backscatter intensity and turbidity with a known suspended sediment concentration. All calibration tests were conducted within 28 hours of the samples collection (Table D.2). The calibration experiment was performed with a Sontek 2D-microADV (16 MHz, serial number A641F) system and a YSI6600 probe (Figure D.2). The 2D-microADV and turbidity meter (YSI6600) were calibrated by measuring the signal amplitude and turbidity of known concentrations of suspended sediment from sediment samples 1 or 2.

For each test a known mass of wet sediment was introduced into a tank containing a known volume of water, which was continuously stirred with a submerged pump (Figure D.2). Figure D.2 shows the experimental setup at the beginning (no sediment added) and end

(maximum sediment added) for test A (Table D.2). Some additional manual stirring was undertaken towards the end of each test (high turbid conditions) to keep the sediment in suspension and the concentration profile uniform. The mass of wet sediment introduced was measured with a Sartorius Type1518 balance.
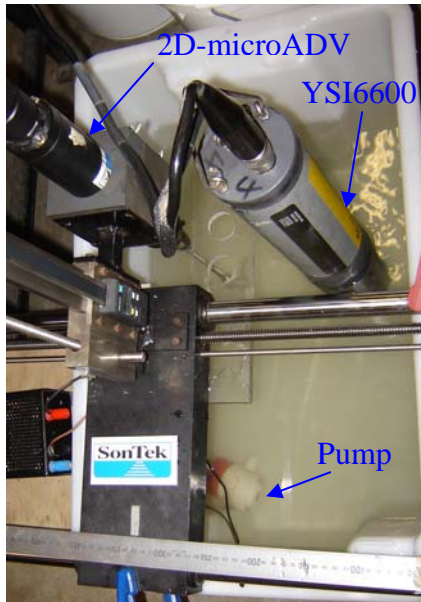
(A) Test tank with 0 g sediment added (SSC $= 0$ g/L). Key equipment labelled.

(B) Test tank with 28.35 g of sediment added (SSC $= 0.71$ g/L).

Figure D.2 – Photographs of laboratory calibration test. Pictures taken during test A, which used Eprapah Creek water and sediment sample 1 (collected on stream bed).

During each test the turbidity sensor of the YSI6600 probe was placed next to the sampling volume of the 2D-microADV (Figure D.2). For each sampling run a set mass of sediment was added. After the sediment was added the 2D-microADV sampled at 50 Hz for 3 minutes, while three turbidity readings were collected by the YSI6600 probe during the same period. The ADV signal amplitude (AVAMP) and turbidity readings were averaged over the 3 minute sampling period. For each SSC the ADV backscatter intensity was calculated using Equation D.5. Note that all ADV data were post-processed with WinADV to remove communication errors.

Table D.2 – Summary of laboratory calibration tests.

Reference	Water	Sediment	SSC range (g/L)	Turbidity range (NTU)	Remarks
Collection	Site 2C	Site 2B	--	6.6 to 8.0	Water and sediment collection at Eprapah Creek; 11/07/06 (10:15)
Test A	Eprapah Creek	Sample 1 (bed)	0 to 0.71	7.2 to 150.4	Date: 11/07/06 Start time: 14:12
Test B	Eprapah Creek	Sample 1 (bed)	0 to 0.54	8.1 to 126.2	Date: 12/07/06 Start time: 08:56
Test C	Eprapah Creek	Sample 2 (bank)	0 to 0.47	7.9 to 148.8	Date: 12/07/06 Start time: 10:26
Test D	Brisbane tap water	Sample 1 (bed)	0 to 0.78	0 to 186.3	Date: 12/07/06 Start time: 13:00

Note: SSC : suspended sediment concentration; bed: sediment sampled from creek bed; bank: sediment sampled from bank (below high water mark); --: no sediment added.

D.3.3 Experimental results

The main focus of this investigation were tests A and B, which used Eprapah Creek water and sediment collected from the stream bed (sample 1). This combination was thought most representative of the actual conditions encountered at Eprapah Creek in previous field studies (Table D.1). Table D.3 presents the averaged ADV backscatter intensity and turbidity data measured for each suspended sediment concentration investigated during tests A and B. For Eprapah Creek water and creek bed sediment (tests A and B) the most appropriate relationships were found to be:

$$SSC = 0.943 \, (1 - \exp(-0.111 \, I_B)) \tag{D.6}$$

$$SSC = 0.00485 \, Turb - 0.035 \tag{D.7}$$

$$Turb = 171.1 \, (1 - \exp(-0.159 \, I_B)) \tag{D.8}$$

where SSC is suspended sediment concentration (g/L); I_B is ADV backscatter intensity (defined in Equation D.5); and Turb is Turbidity (NTU). Each of these relationships (Equations D.6 to D.8) showed correlation with the laboratory test data of R > 0.99 (Figure D.3). However, it should be noted that Equations D.6 to D.8 are only valid within the ranges investigated (0 > SSC > 0.71 g/L; 7 > turbidity > 150 NTU; 0.06 > I_B > 12.21). Chanson et al. (2006) detailed the relationships investigated as part of the laboratory calibration experiment and found Equations D.6 to D.8 to be the most physical meaningful.

Table D.3 – Results of laboratory calibration tests A an B. Tests conducted with sediment collected on stream bed at Site 2B (sample 1) in 40 litres of Eprapah Creek water.

Test	Sampling run	Sediment Mass added (g)	SSC (g/L)	Turbidity (NTU)	AVAMP (counts)	I_B
A	1	0	0	7.25	86.53	0.065
	2	0.875	0.0219	10.80	100.67	0.294
	3	1.799	0.0450	14.57	105.73	0.441
	4	4.238	0.1059	24.60	113.55	0.911
	5	8.322	0.2081	45.92	121.07	1.882
	6	14.497	0.3624	73.13	128.22	3.690
	7	20.606	0.5152	109.30	134.62	6.977
	8	28.385	0.7096	150.43	140.48	12.207
B	1	0	0	8.07	88.10	0.072
	2	0.105	0.00263	8.80	91.81	0.112
	3	0.240	0.0060	9.70	94.87	0.153
	4	0.492	0.0123	11.33	98.02	0.215
	5	0.833	0.0208	13.67	101.98	0.313
	6	1.331	0.0333	17.20	105.78	0.443
	7	2.376	0.0594	22.67	110.07	0.651
	8	4.098	0.10245	32.67	115.26	1.058
	9	6.747	0.1687	46.77	121.20	1.925
	10	12.527	0.3132	77.07	129.32	1.463
	11	21.583	0.4668	126.20	136.22	8.195

Note: SSC : suspended sediment concentration; I_B : ADV backscatter intensity averaged over sampling run; AVAMP : average signal amplitude averaged over sampling run; sampling run: 3 minute sampling period.

Figure D.3 shows the relationships between ADV backscatter intensity, turbidity and suspended sediment concentration for all laboratory tests undertaken (Table D.2). In Figure D.3 the data collected during tests C and D differed from each other and that of tests A and B. Tests C and D were performed as part of another study (Chanson et al. (2006)) to demonstrate the effect of a different sediment sample and a different water quality respectively on the relationships investigated. This difference in the observed relationships between the tests showed the importance of using water and sediment that is most representative of the field site where the calibrated ADV is to be deployed.
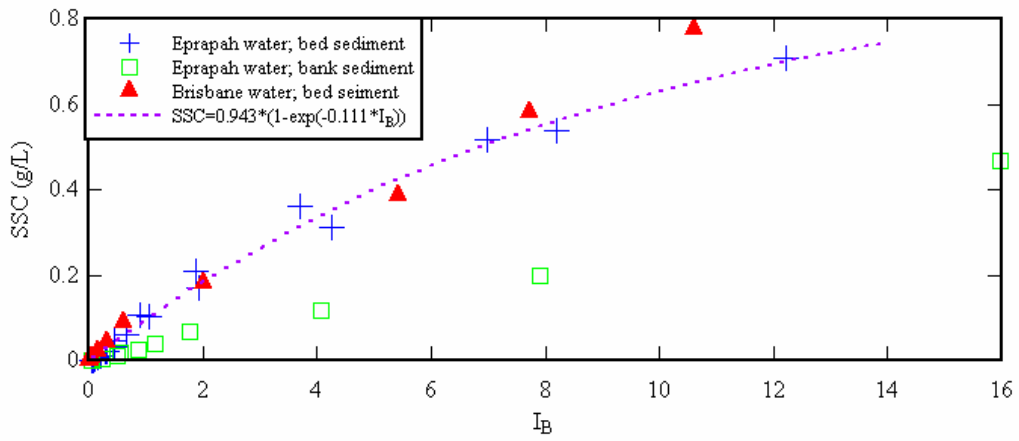
(A) Relationship between SSC and I_B. Data compared to Equation D.6.
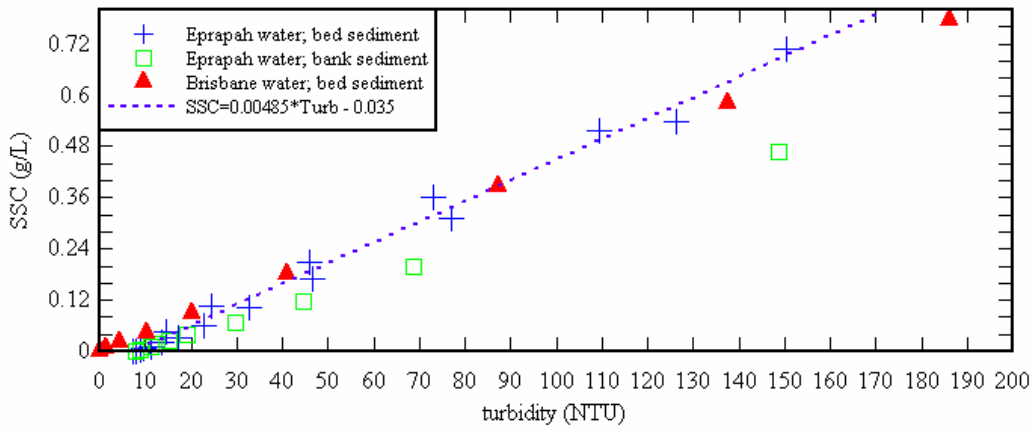
(B) Relationship between SSC and turbidity. Data compared to Equations D.7.
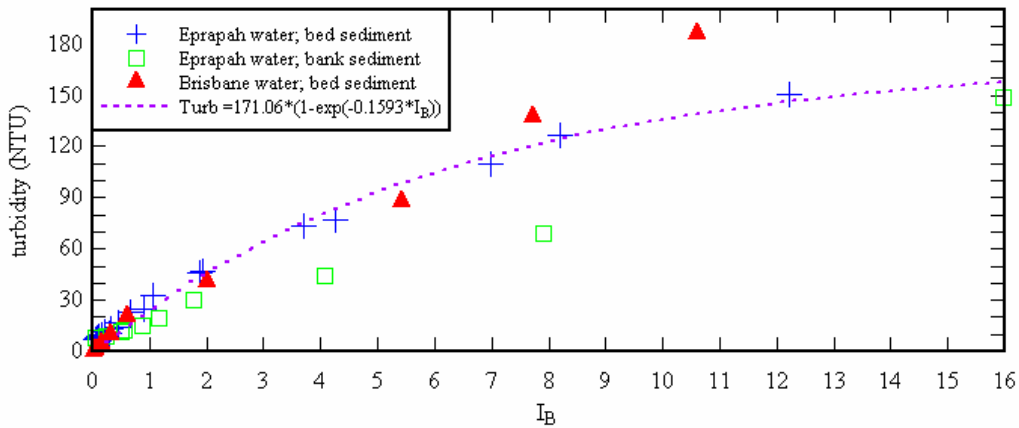
(C) Relationship between turbidity and I_B. Data compared to Equation D.8.

Figure D.3 – ADV backscatter intensity (I_B), turbidity and suspended sediment concentration (SSC) data collected during the laboratory calibration experiment (11-12/07/06). Backscatter data: 2D-microADV (16 MHz, serial number A641F); turbidity data: YSI6600 probe.

APPENDIX E INVESTIGATION OF LONG PERIOD OSCILLATIONS OBSERVED AT EPRAPAH CREEK

E.1 PRESENTATION

Some long period oscillations were observed in the water levels and horizontal velocities of all field investigations undertaken at Eprapah Creek. For spring tidal conditions mid estuary (studies E3 and E5) large velocity fluctuations with a period of approximately 3.5 hours were observed. Under neap tidal conditions in the middle and upper estuarine zones (studies E6 and E7) long period oscillations with periods between 2,000 and 5,000 s caused velocity fluctuations similar to that of the tidal forcing (Figure E.1). Figure E.1 shows the streamwise velocity and water depth as functions of time for the field studies E5, E6 and E7.

Here the long period oscillations observed in Eprapah Creek and some possible causes of these oscillations are investigated. The turbulence and water level data from the field studies E5 (8-9/03/2005), E6 (16-18/05/2005) and E7 (5-7/06/2006) are used to isolate the predominant long period oscillations observed in Eprapah Creek. Table E.1 outlines some information on the field studies E5, E6 and E7. The studies E5 and E6 were performed mid estuary under spring and neap tidal conditions respectively, while the study E7 was conducted in the upper estuary for neap tides.

Table E.1 – Investigation and sampling information for studies E5, E6 and E7.

Study	E5	E6	E7
Date	8-9/03/05	16-18/05/05	5-7/06/06
Focus	Spring tides – middle estuary	Neap tides – middle estuary	Neap tides – upper estuary
Duration (hours)	25	48	50
Tidal range (m)	2.48	1.37	1.52
Rainfall (mm)	0	0	0
Mean depth (m)	1.6	1.6	1.7
Site	2B	2B	3
AMTD (km)	2.1	2.1	3.1
Sampling location	0.1 m above bed, 10.7 m from left bank	0.2 and 0.4 m above bed, 10.7 m from left bank	0.2 and 0.4 m above bed, 4.2 m from right bank
f_{scan} (Hz) 3D-ADV 2D-microADV	25 *	25 25	25 50

Note: AMTD: Australian middle thread distance (upstream from mouth); f_{scan} : sampling frequency; Tidal range: maximum observed at sampling location; *: probe not deployed.
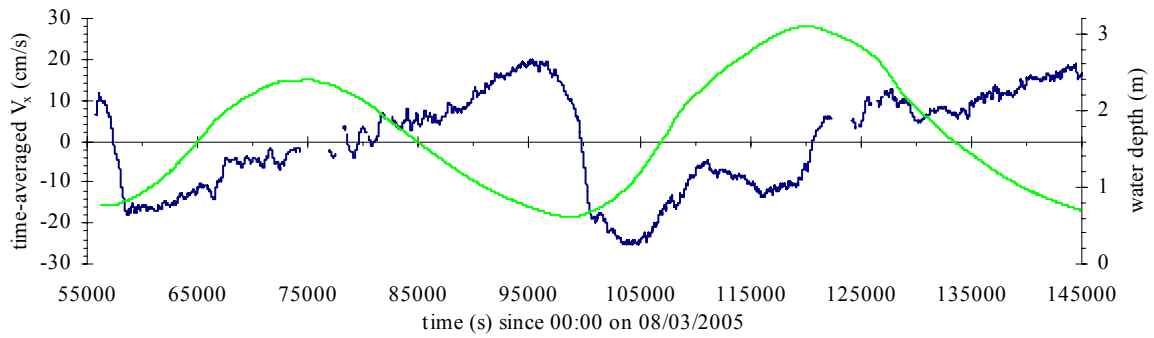
(A) Spring tide data collected by 3D-ADV 0.1 m above bed, 10.7 m from left bank at Site 2B, Eprapah Creek for study E5 (8-9/03/05).
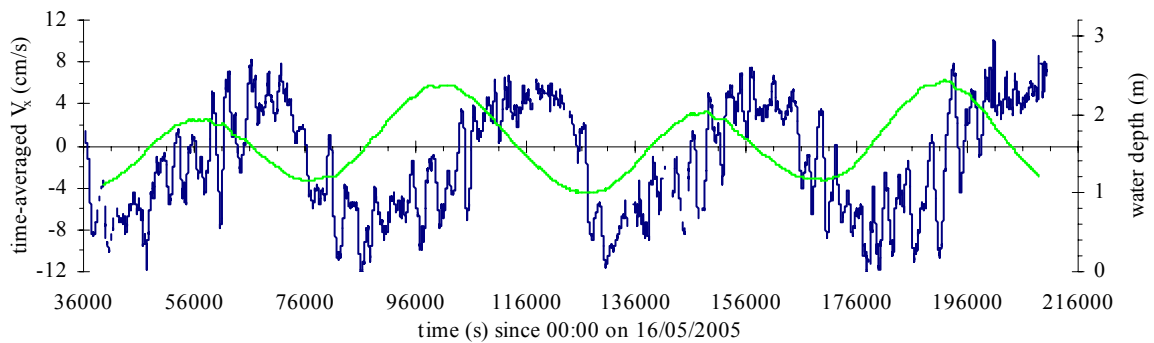
(B) Neap tide data collected by 3D-ADV 0.4 m above bed, 10.7 m from left bank at Site 2B, Eprapah Creek for study E6 (16-18/05/05).
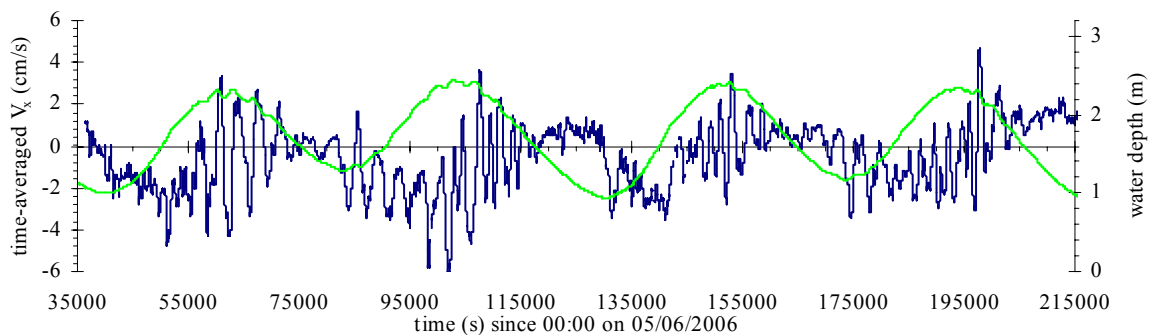
(C) Neap tide data collected by 3D-ADV 0.4 m above bed, 4.2 m from right bank at Site 3, Eprapah Creek for study E7 (5-7/06/06).

Figure E.1 – Time-averaged streamwise velocity and water depth as functions of time for studies E5, E6 and E7. Velocity data averaged over 200 s every 10 s along entire data set. Legend: — water depth; — time-averaged streamwise velocity.

Two different acoustic Doppler velocimeters were used to collect high frequency velocity data at Eprapah Creek, these were a Sontek 3D-ADV (10 MHz) (all studies) and a Sontek 2D-microADV (16 MHz) (studies E6 and E7). When deployed these ADVs measured continuously at high frequency (f_{scan} > 25 Hz) for the duration of each investigation. For the

field studies E5, E6 and E7, water level data were collected along with other physio-chemistry data by a YSI6600 probe located 0.3 m from the sampling volume of the 3D-ADV.

E.1.1 Post-processing of acoustic Doppler velocimetry data

All ADV velocity data were post-processed using the technique described in Chanson et al. (2005b). The post-processing must be undertaken to ensure the quality of the data set. Corrupted data are inherent to the ADV metrology. These are predominantly caused by poor signal quality (low correlation and/or low signal to noise ratio) and Doppler noise within the measured signal. Chanson et al. (2005b) found that in natural systems the ADV data could be corrupted by large disturbances such as navigation or fauna activity near the ADV. All turbulence ADV data collected underwent three stages of post-processing, these were:

1) – Velocity signal check:

Data points with low-correlation, low signal to noise ratio or communication errors were removed and replaced by the mean of the endpoints about the erroneous data.

2) – Large event detection (pre-processing):

The pre-processing stage searches for large disturbances (e.g. navigation near probe, adjustments of probe) that were observed during a field study. Erroneous data from known large disturbance events were replaced using the mean of the endpoints technique.

3) – Small disturbance detection (de-spiking):

The phase-space thresholding method was used to find small disturbances generated by "spike" events and Doppler noise. Any data point determined to be erroneous was replaced using the mean of the endpoints technique.

E.2 TIDAL AND PHYSICAL CHARACTERISTICS OF EPRAPAH CREEK AND MORETON BAY

In small subtropical estuaries (e.g. Eprapah Creek) the major influence on the water level and velocity fluctuations are the tidal forcing and the local topography. Freshwater inflow could also influence the water levels and velocities observed, however, in small subtropical systems the inflow of significant natural freshwater is extremely limited (Digby et al. (1999)). Here possible causes of the long period oscillations observed in the water level and velocity data collected at Eprapah Creek are investigated using the tidal and topographical characteristics of Eprapah Creek and Moreton Bay. Figure E.2 shows topographical sketches of Moreton Bay and Eprapah Creek.

(A) Moreton Bay.   (B) Eprapah Creek.
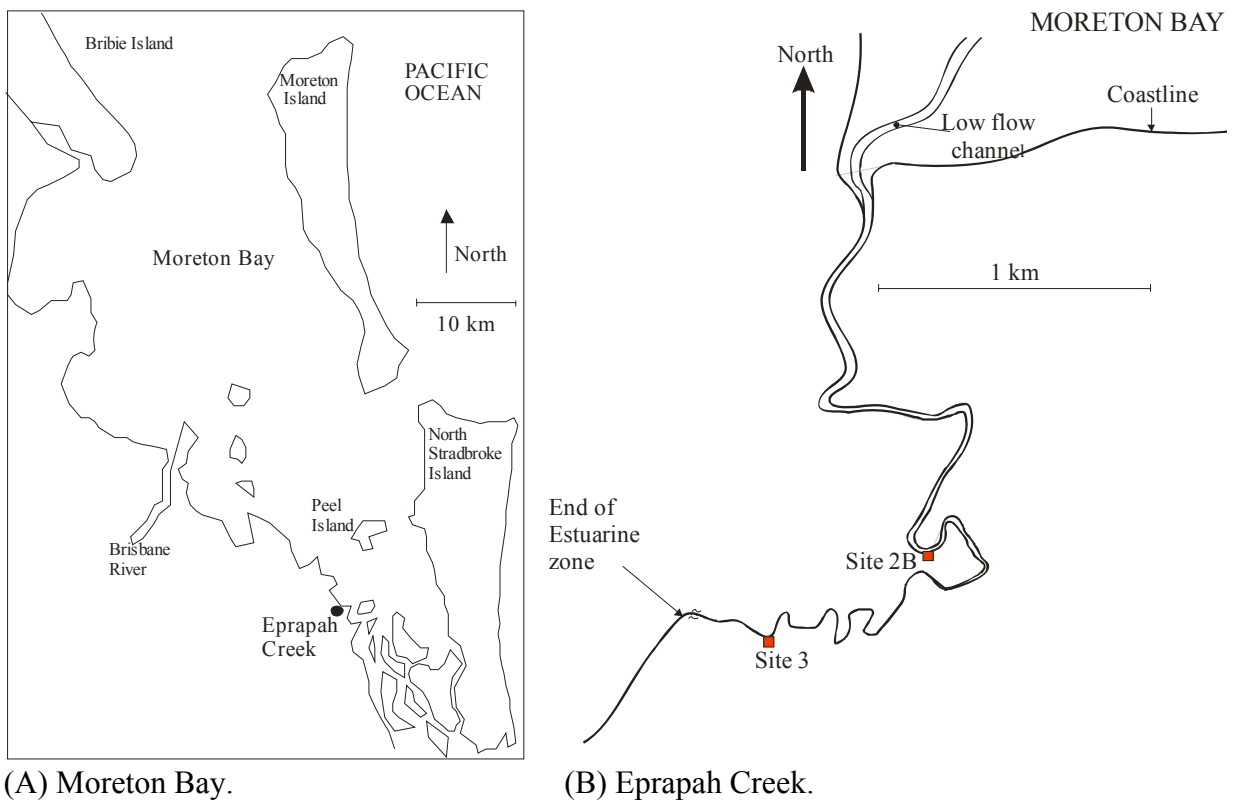
Figure E.2 – Topographical sketch of Moreton Bay and Eprapah Creek.

E.2.1 Major tidal components

The amplitude and period of the tides observed in Eprapah Creek and at the Brisbane Bar in Moreton Bay differed slightly. This seemed related to the different bathymetry of the two locations. During 2001 the Queensland Department of Transport measured the tides at several sites in Southeast Queensland, including at the Brisbane Bar and in Eprapah Creek, and determined the tidal constituents for these locations. Table E.2 outlines the ten most predominant tidal constituents observed in Moreton Bay and Eprapah Creek from the Queensland Department of Transport study.

The predominant tidal constituents in Moreton Bay and Eprapah Creek were mostly the same, with the M2 being the dominant constituent in both locations. However, the tidal amplitude and phase differed in Moreton Bay (Brisbane Bar) and in Eprapah Creek, with many of the constituent amplitudes being larger in Eprapah Creek than at the Brisbane Bar. For all field studies conducted at Eprapah Creek the tidal range measured in Eprapah Creek was larger than that measured at Brisbane Bar (by Queensland Department of Transport). This seemed to indicate that the tides were being amplified upon entering Eprapah Creek. Savenije (2005) commented that tidal amplification was commonly observed in coastal plain type estuaries. Previous studies (e.g. Dyer (1973)) suggested that tidal amplification occurred when the topographical convergence about the estuary entrance was stronger than the local friction.

261

Table E.2 – Predominant tidal constituents in Moreton Bay (Brisbane Bar) and Eprapah Creek. Tidal constituent data courtesy of Queensland Department of Transport.

Brisbane Bar (31/12/00 to 1/01/01)				Eprapah Creek (6/06/01 to 7/07/01)			
Constituent	Period (hours)	Amplitude (mm)	Phase (degrees)	Constituent	Period (hours)	Amplitude (mm)	Phase (degrees)
M2	12.42	703	274	M2	12.42	752	287
K1	23.93	213	171	K1	23.93	207	173
S2	12.00	191	302	S2	12.00	188	312
N2	12.66	138	264	N2	12.66	152	296
O1	25.82	117	131	O1	25.82	112	134
P1	24.07	60	169	P1	24.07	58	171
K2	11.97	57	294	M4	6.21	56	144
SA	8766	50	12	K2	11.97	56	304
L2	12.19	36	262	SA	8766	52	14
NEU2	12.63	31	253	L2	12.19	38	245

Of note, was the amplification of the smaller period constituents (e.g. M4, M6 and M8), which seemed at least 150 % larger within Eprapah Creek than in Moreton Bay. Table E.3 lists the amplitudes of the M4, M6 and M8 constituents in Eprapah Creek and Moreton Bay (Brisbane Bar).

Table E.3 – Amplitude and period of some M2 sub-harmonic constituents.

Brisbane Bar (31/12/00 to 1/01/01)			Eprapah Creek (6/06/01 to 7/07/01)		
Constituent	Period (hours)	Amplitude (mm)	Constituent	Period (hours)	Amplitude (mm)
M4	6.21	13.2	M4	6.21	56.4
M6	4.14	10.9	M6	4.14	15.2
M8	3.11	0.4	M8	3.11	3.1

E.2.2   Resonance fluctuations

Resonance fluctuations (seiching) can form in bays and estuaries by the reflection of tidal forcing from certain geographical landmarks (e.g. banks of bay, meanders in creeks). The natural resonance period T is related to the distance and depth of water between the two topographical landmarks and can be approximated by:

$$T = 2\,L\big/\sqrt{g\,d} \qquad\qquad\qquad (E.1)$$

where L = distance between two topographical landmarks; d = averaged water depth between two topographical landmarks; and g = gravitational acceleration (g = 9.8 m/s^2 in Brisbane).

The period of the long period oscillations in velocity and water level in Eprapah Creek seemed similar to the resonance waves generated by both external (within Moreton Bay) and

internal (within Eprapah Creek) sources. This section investigates the topographical dimensions of Moreton Bay and Eprapah Creek to help classify the possible causes of the predominant long period oscillations observed during the field studies at Eprapah Creek.

E.2.2.1 *Possible resonance periods of Moreton Bay*

Moreton Bay is separated from the Pacific Ocean by three large sand islands (Moreton Island, North Stradbroke Island and South Stradbroke Island). It is approximately 30 km wide North of the Brisbane River and narrows to about 12 km wide near Eprapah Creek, with a mean depth of approximately 5 m. South of Eprapah Creek there are many small mostly uninhabited sand islands in between North and South Stradbroke Islands and the mainland, that extend all the way to the Gold Coast. Only resonance periods for that part of Moreton Bay, North of Victoria Point (Eprapah Creek) were investigated here. Figure E.3 shows some conceivably important dimensions of Moreton Bay, with the insert presenting a close-up of Moreton Bay immediately surrounding Eprapah Creek.
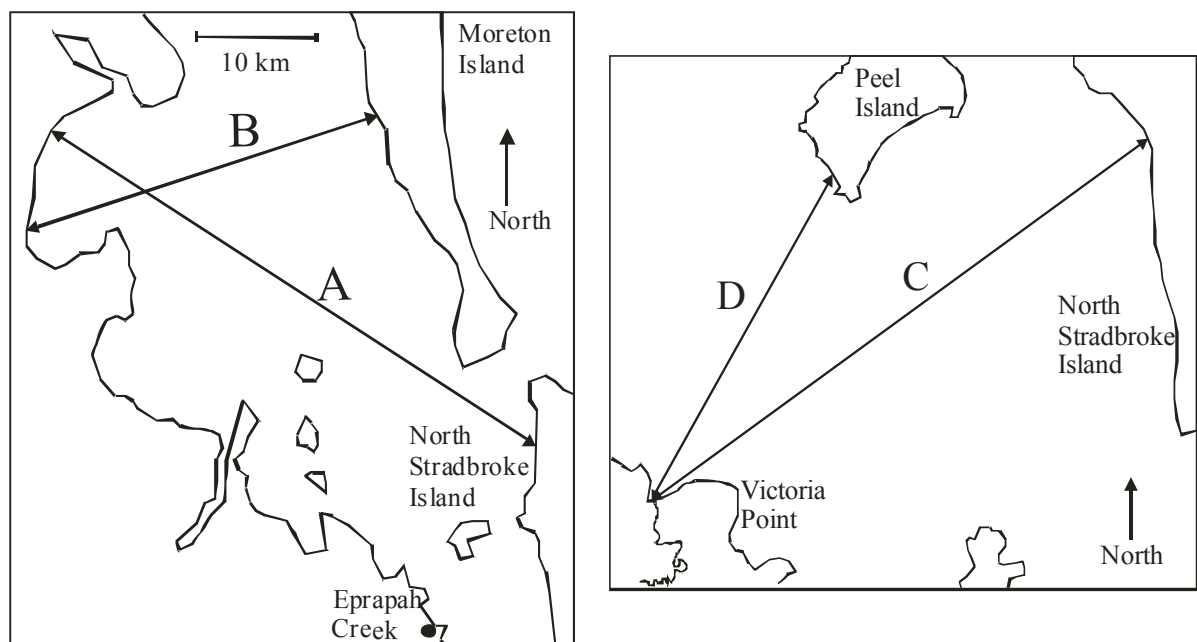
Figure E.3 – Some topographic dimensions of Moreton Bay. Insert shows close-up of Moreton Bay topography near Eprapah Creek.

Table E.4 lists the topographical distances highlighted in Figure E.3 These dimensions provide an approximation of the largest and smallest topographical distances in Moreton Bay that could conceivably be responsible for creating some resonance. Dimensions A and B (Table E.4) approximate the maximum width and unobstructed length of Moreton Bay, which provide an approximation of the largest resonance periods that could be generated. Trevethan

et al. (2006) noted that the resonance periods of dimensions C and D were similar to the half period of some flow reversals caused by long period oscillations in Eprapah Creek. Here, the dimensions C and D were used to approximate the smaller resonance periods generated in Moreton Bay.

Table E.4 – Range of possible resonance periods created in Moreton Bay.

Dimension	Description	L (km)	d (m)	T (s)
A	Maximum unobstructed length – North Stradbroke Island and mainland (Deception Bay)	51,500	5	14,710
B	Maximum width – mainland (Deception Bay) and Moreton Island	32,800	5	9,370
C	Distance between mouth of Eprapah Creek and North Stradbroke Island	11,500	3	4,120
D	Distance between mouth of Eprapah Creek and Peel Island	6,800	3	2,500

Note: L: distance between two topographical landmarks; d: mean depth between topographical landmarks; T: natural resonance period.

E.2.2.2   *Possible resonance periods within Eprapah Creek*

The estuarine zone of Eprapah Creek is approximately 3.8 km long, with a mean depth of about 2 m.   Figure E.4 shows a sketch of the Eprapah Creek estuary, with several topographical landmarks highlighted. Table E.5 presents the distance of water between these landmarks and the possible resonance periods generated. The distances presented in Table E.5 demonstrate the largest and smallest resonance periods that could be created in Eprapah Creek.   Herein the topographical dimensions of Eprapah Creek were derived from those discussed in previous studies (Chanson (2003), Trevethan et al. (2006)). The largest possible resonance wave that could be generated within Eprapah Creek is related to the entire length of the estuarine zone. Trevethan et al. (2006) suggested resonance waves created in Eprapah Creek could also be related to smaller distances such as that between the mouth and Site 2B; and Site 2B to the upper extent of the estuary. Several natural weirs are located mid estuary about Site 2B, which conceivably act as a hydraulic control at low tide. Other possible resonance periods could conceivably be created by the meander lengths and transverse dimensions of the creek (Chanson (2003)).
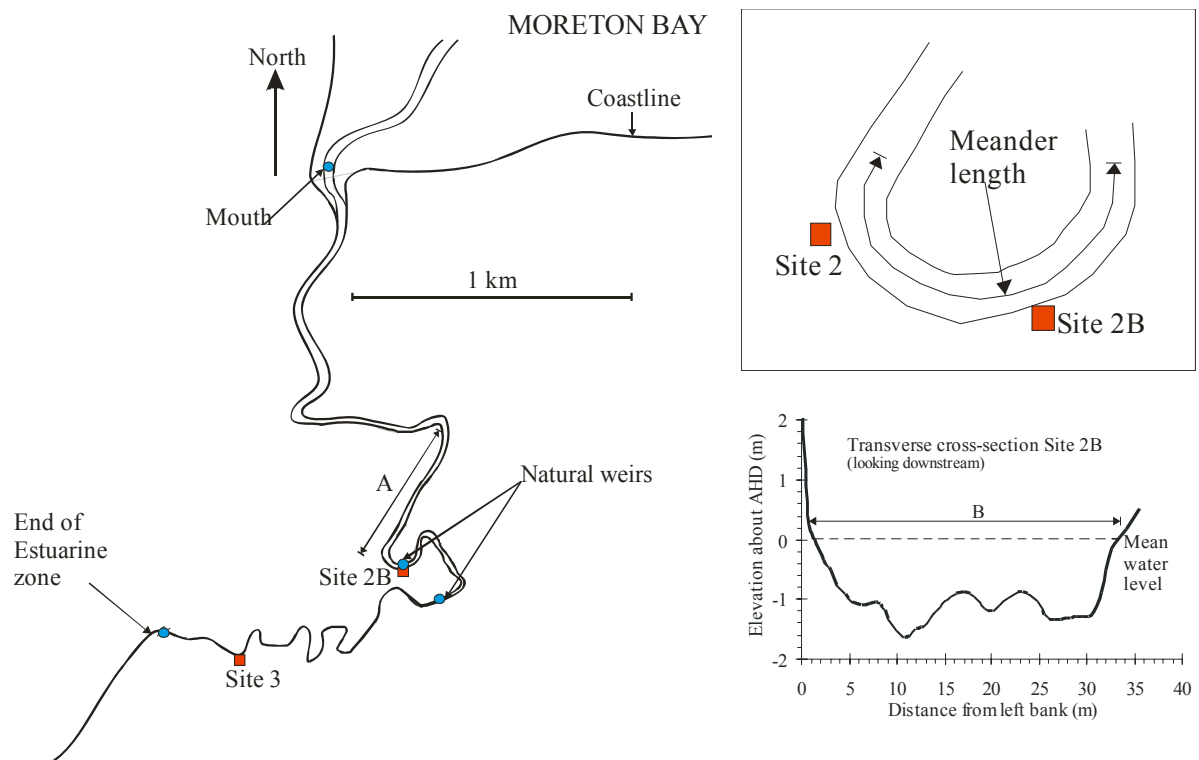
Figure E.4 – Sketch of Eprapah Creek estuarine zone, with some topographical landmarks highlighted.

Table E.5 – Range of possible resonance periods created in Eprapah Creek.

Description	L (m)	d (m)	T (s)
Entire length of estuary (mean depth)	3,800	2	1,700
Entire length of estuary (mean depth extreme low tide)	3,800	1.2	2,200
Entire length of estuary (mean depth extreme high tide)	3,800	4	1,200
Distance from mouth to Site 2B	2,100	2	950
Distance from Site 2B to upper limits of estuary	1,700	2	800
Distance from Site 3 to upper limits of estuary	700	2	300
Distance between 90 ° bends between mouth and Site 2 (e.g. dimension A, Figure E.4)	500	2	220
Length of largest meander	400	2	190
Meander length at Site 2 and 2B (Figure E.4)	250	2	110
Mean transverse distance at Site 1	60	2	30
Mean transverse distance Site 2B (dimension B, Figure E.4)	30	2	15
Mean transverse distance Site 3	10	2	5

Note: L: distance between two landmarks; d: mean depth between landmarks; T: natural resonance period.

E.2.3   Turbulence time scales

An autocorrelation analysis yielded the Eulerian integral time scales T_E (Figure E.5). The integral time scale is a rough measure of the longest connection between turbulent velocity fluctuations. For all field studies conducted at Eprapah Creek the maximum observed integral

265

time scale periods were approximately 2 s (Trevethan et al. (2006)). This seemed to indicate that any oscillation period less than 2 s were generated by turbulence not resonance.
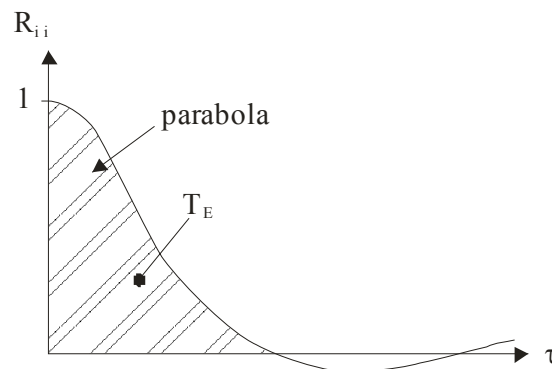
Figure E.5 – Velocity autocorrelation function and integral time scale T_E definition.

E.2.4   Discussion

Six oscillation period groups based on tidal and physical characteristics are outlined in Table E.6. These groups were used to categorise the observed velocity fluctuations and match these with the possible phenomenon that created them.

Table E.6 – Oscillation period groups based on local tidal and physical characteristics.

Group	Period range (s)	Tidal and/or physical characteristics
A	$T_{range} > 14,400$	Tidal components
B	$14,400 > T_{range} > 2,200$	Possible external resonance sources (e.g. Moreton Bay)
C	$2,200 > T_{range} > 1,200$	Extreme range of entire estuary length resonance ($d_L = 1.2$ m; $d_H = 4.0$ m)
D	$1,200 > T_{range} > 200$	Range of possible smaller longitudinal resonance (e.g. Site 2B to upper limits of estuary; distance between 90° bends between mouth and Site 2B)
E	$200 > T_{range} > 2$	Smaller resonances caused by meander lengths or cross-section widths
F	$2 > T_{range}$	Related to turbulence

Note: d_L and d_H are approximate mean depth of entire estuary for extreme low and high tides; T_{range} : oscillation period range for groups investigated.

An analysis of the tidal components in Eprapah Creek by the Queensland Department of Transport showed that some tidal components with periods between 1 year and 14,900 s (M6) caused some significant water level fluctuations in Eprapah Creek. In this study water level

fluctuations were considered significant if larger than 0.01 m. In Eprapah Creek the smallest significant tidal period seemed to be that of the M6 (T = 14,900 s). Therefore, any velocity fluctuations with a period larger than 14,900 s were most probably generated by the tidal forcing. This assumption seemed supported by the fact that the largest conceivable resonance periods in Moreton Bay were approximately 14,700 s.

The resonance periods in Moreton Bay investigated here ranged between approximately 2,500 and 14,700 s. Any velocity fluctuation periods within this range could conceivably be generated by seiching within Moreton Bay.

Three oscillation period groups were used to define the possible resonance created within Eprapah Creek, these were based on the entire length of the estuary; smaller longitudinal distances (e.g. mouth to Site 2B); and meander lengths and cross-section widths. The oscillation period group related to the entire estuary length had a range 2,200 and 1,200 s based on the estimated resonance periods for extreme low and high tides respectively. Oscillation periods within this range could possibly be created by resonance over the entire length of the estuary, as the next longitudinal physically significant longitudinal distances (e.g. Site 2B to end of estuary) all seemed to have resonance periods less than 1,100 s.

The smaller conceivable internal resonances were divided into group D (1,200 to 200 s) and group E (200 to 2 s). Oscillation periods in group D related to longitudinal lengths such as: mouth to Site 2B (natural weir); Site 2B to end of estuarine zone; or the length of a straight section between two 90 ° bends. Group E was based on more site specific dimensions, such as the local meander lengths or the transverse width of the experimental site. The lower limit for this group was determined by oscillation periods known to have been created by turbulence (Section E.2.3). Therefore, fluctuations with periods less than 2 s were considered to be generated by turbulence.

E.3   PREDOMINANT OSCILLATION PERIODS OBSERVED IN EPRAPAH CREEK

A spectrum analysis was performed on the horizontal velocity data to isolate the predominant oscillation periods for the field studies E5, E6 and E7 (Table E.1). For each study the 20 most predominant peaks in the frequency spectrum were isolated for the streamwise and transverse velocity data. The predominant peaks in a frequency spectrum indicate the oscillation periods that contributed the most energy to the fluctuations of the measured data. However, the resolution of the low frequency peaks was limited by the duration of each field study. For this investigation it was considered prudent only to evaluate a predominant peak accurate if it repeated at least 12 times during the investigation period (T < 7,200 s (study E5) and T < 14,400 s (studies E6 and E7)).

E.3.1   Field study E5 (8-9/03/2005)

The field study E5 was performed mid estuary (Site 2B) under spring tidal conditions, with the ADV sampling volume 0.1 m above the bed and 10.7 m from the left bank. Turbulence data were measured with the 3D-ADV (10 MHz) at 25 Hz for a investigation period of 25 hours. Figure E.6 shows the frequency spectrum of the streamwise and transverse velocity data collected for the study E5. For the study E5, the 4 most predominant oscillation periods seemed to have periods similar to tidal constituents observed in Eprapah Creek (Figure E.6). However, the 25 hour investigation period of this study did not allow adequate resolution of fluctuation periods with T > 7,200 s and as such these are not presented in Table E.7. Table E.7 presents the 20 most predominant oscillation periods (T < 7,200 s) observed in the spectra of the streamwise and transverse velocity data for the field study E5 (Figure E.6).

(A) $S_{V_xV_x}$.   (B) $S_{V_yV_y}$.

Figure E.6 – Frequency spectrum of streamwise $S_{V_xV_x}$ and transverse $S_{V_yV_y}$ velocity data for study E5 (8-9/03/05). Data collected at 25 Hz, 0.1 m above bed at Site 2B, Eprapah Creek.

For the field study E5 the predominant streamwise and transverse velocity fluctuations (T < 7,200 s) had periods that were conceivably related to physical characteristics of groups B, C and D (Table E.6). This seemed to indicate that resonance periods within Moreton Bay and Eprapah Creek had some influence on the horizontal velocity fluctuations at Site 2B, Eprapah Creek. Five of the predominant streamwise velocity oscillation periods ranged between 2,200 and 1,500 s. These oscillation periods seemed related to internal resonance generated along the entire length of Eprapah Creek. Those predominant periods between 1,200 and 900 s were most likely caused by resonance generated between the mouth and Site 2B, while the

transverse oscillation period of about 600 s was conceivably generated by resonance between Site 2B and the upstream extent of the estuary.

Table E.7 – Predominant oscillation periods (T < 7,200 s) observed at Site 2B for study E5.

Oscillation period (s)	
V_x	V_y
5,993 (B)	6,214 (B)
3,813 (B)	2,793 (B)
2,796 (B)	4,415 (B)
3,570 (B)	5,593 (B)
5,412 (B)	2,663 (B)
4,194 (B)	6,711 (B)
4,934 (B)	2,046 (C)
4,660 (B)	2,943 (B)
2,124 (C)	2,467 (B)
2,664 (B)	2,581 (B)
1,645 (C)	5,243 (B)
1,824 (C)	3,570 (B)
1,974 (C)	1,103 (D)
3,226 (B)	1,766 (C)
1,553 (C)	2,267 (B)
2,363 (B)	1,598 (C)
2,996 (B)	4,092 (B)
2,504 (B)	1,511 (C)
1,029 (D)	1,271 (C)
953 (D)	603 (D)

Note: (letter in brackets refer to oscillation groups in Table E.6).

E.3.2 Field study E6 (16-18/05/2005)

The field study E6 was conducted mid estuary (Site 2B) under neap tidal conditions. Two ADVs were deployed with the sampling volumes 0.2 and 0.4 m above the bed and 10.7 m from the left bank. Turbulence data were measured with the 3D-ADV (10 MHz) and 2D-microADV (16 MHz) at 25 Hz for a investigation period of 48 hours. Figure E.7 shows the frequency spectrum of the streamwise and transverse velocity data collected for the study E6. The 5 most predominant oscillation periods seemed to have periods similar to tidal constituents observed in Eprapah Creek (Figure E.7). However, the 48 hour investigation period of this study did not allow adequate resolution of fluctuation periods with T > 14,400 s and as such these are not presented in Table E.8. For the spectra of the streamwise velocity at both 0.2 and 0.4 m above the bed a region of increased energy was observed between

269

approximately 2,000 and 4,500 s. A similar phenomenon was not discernible in the transverse velocity spectra at 0.2 and 0.4 m above the bed.
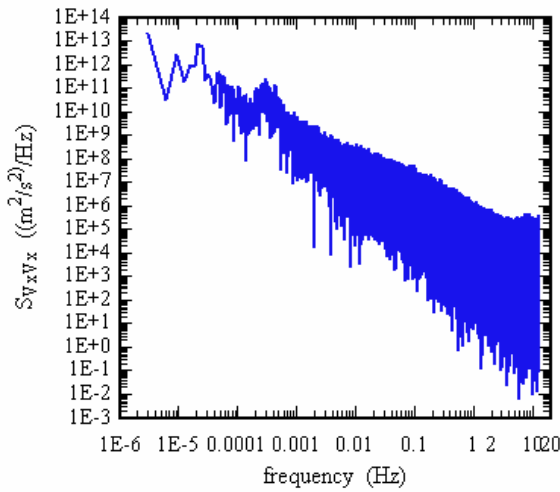
(A) S_{VxVx} data collected at 0.2 m above bed. (B) S_{VxVx} data collected at 0.4 m above bed.
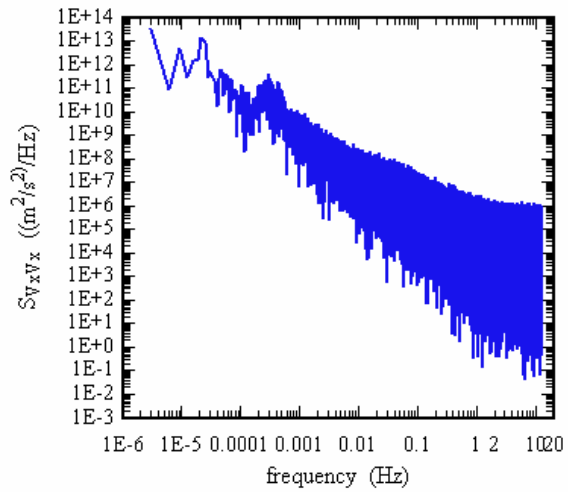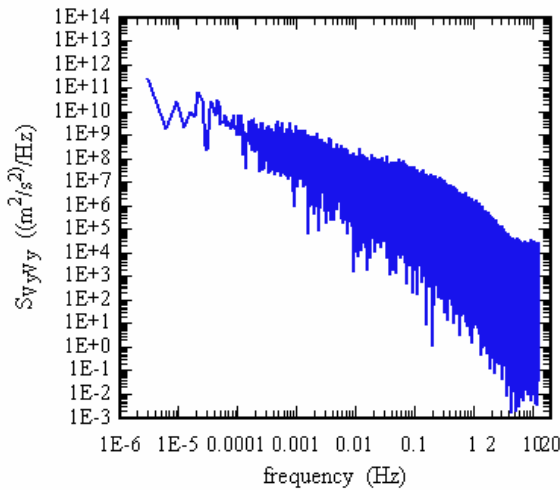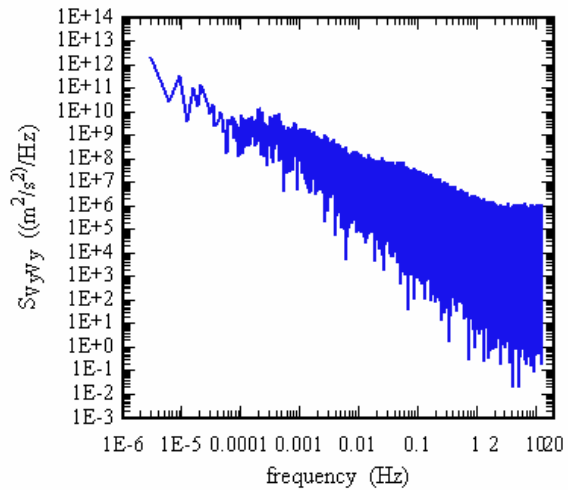
(C) S_{VyVy} data collected at 0.2 m above bed. (D) S_{VyVy} data collected at 0.4 m above bed.

Figure E.7 – Frequency spectra of streamwise S_{VxVx} and transverse S_{VyVy} velocities for study E6 (16-18/05/05). Data collected at 25 Hz, 0.2 and 0.4 m above bed at Site 2B, Eprapah Creek.

Table E.8 presents the 20 most predominant oscillation periods (T < 14,400 s) observed in the spectra of the streamwise and transverse velocity data for the field study E6 (Figure E.7). In Table E.8 the predominant oscillation periods of the horizontal velocities were within the ranges of oscillation groups B, C and D, with the majority being within oscillation group B. This seemed to indicate that the predominant velocity oscillations observed mid estuary under neap tidal conditions were mostly formed outside Eprapah Creek. Only two of the

predominant streamwise velocity oscillation periods could conceivably be associated with resonance generated internally within Eprapah Creek. Many of the predominant streamwise oscillations periods (14/20) were observed at both 0.2 and 0.4 m above the bed. However, only 2 predominant transverse velocity periods were observed at both 0.2 and 0.4 m above the bed. This difference in the periods of the predominant transverse velocity oscillations could lead to the formation of secondary currents.

Table E.8 – Predominant oscillation periods (T < 14,400 s) observed at Site 2B for study E6.

Oscillation periods at 0.2 m.a.b. (s)		Oscillation periods at 0.4 m.a.b. (s)	
V_x	V_y	V_x	V_y
3,355 (B)	9,869 (B)	3,355 (B)	4,944 (B)
3,902 (B)	11,983 (B)	3,902 (B)	4,415 (B)
2,330 (B)	8,830 (B)	3,608 (B)	2,298 (B)
4,043 (B)	5,687 (B)	3,495 (B)	10,168 (B)
9,869 (B)	6,453 (B)	2,330 (B)	2,449 (B)
12,905 (B)	2,124 (C)	4,043 (B)	2,684 (B)
2,969 (B)	6,711 (B)	2,969 (B)	4,247 (B)
3,495 (B)	1,291 (C)	9,869 (B)	6,579 (B)
2,844 (B)	4,043 (B)	4,934 (B)	13,980 (B)
4,934 (B)	1,824 (C)	2,844 (B)	3,258 (B)
3,608 (B)	3,902 (B)	4,534 (B)	2,820 (B)
3,226 (B)	2,237 (B)	4,194 (B)	7,222 (B)
9,321 (B)	4,863 (B)	4,660 (B)	7,457 (B)
4,474 (B)	1,042 (D)	9,321 (B)	2,346 (B)
4,726 (B)	2,996 (B)	2,179 (C)	8,830 (B)
4,194 (B)	3,258 (B)	2,504 (B)	7,989 (B)
2,942 (B)	2,009 (C)	3,226 (B)	5,326 (B)
2,237 (B)	4,596 (B)	4,358 (B)	2,137 (C)
7,457 (B)	2,684 (B)	2,021 (C)	3,136 (B)
2,179 (C)	1,485 (C)	8,339 (B)	1,257 (C)

Note: (letter in brackets refer to oscillation groups in Table E.6); m.a.b.: metres above bed.

E.3.3   Field study E7 (5-7/06/2006)

The field study E7 was performed in the upper estuary (Site 3) under neap tidal conditions. Two ADVs were deployed with the sampling volumes 0.2 and 0.4 m above the bed and 4.2 m from the right bank. Turbulence data were measured with the 3D-ADV (10 MHz) and 2D-microADV (16 MHz) at 25 and 50 Hz respectively, for an investigation period of 50 hours. After collection a hardware fault was found to have occurred in the 3D-ADV (10 MHz), which created some high frequency noise. This hardware fault seemed to affect all data collected with the 3D-ADV (10 MHz) for oscillation periods of T < 200 s and therefore, oscillation periods T < 200 s (groups E and F) measured by the 3D-ADV (study E7) were not

discussed here. Figure E.8 shows the frequency spectrum of the streamwise and transverse velocity data collected for the study E7.
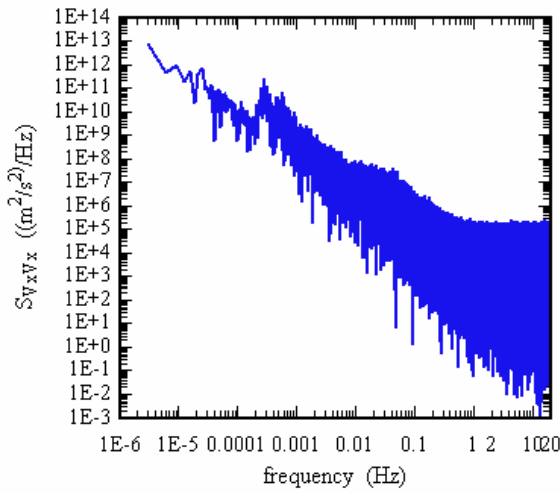
(A) S_{VxVx} data collected at 0.2 m above bed.
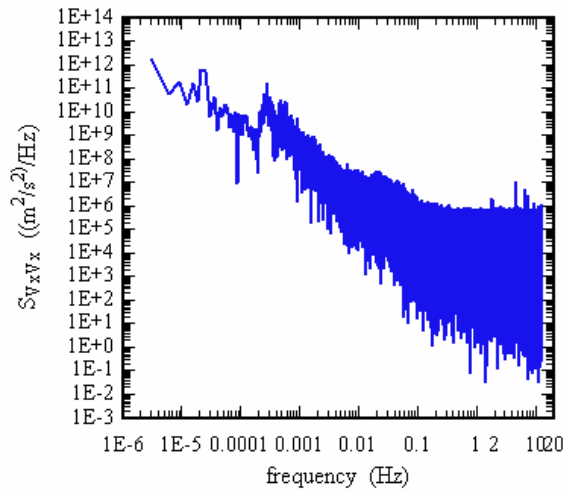
(B) S_{VxVx} data collected at 0.4 m above bed.
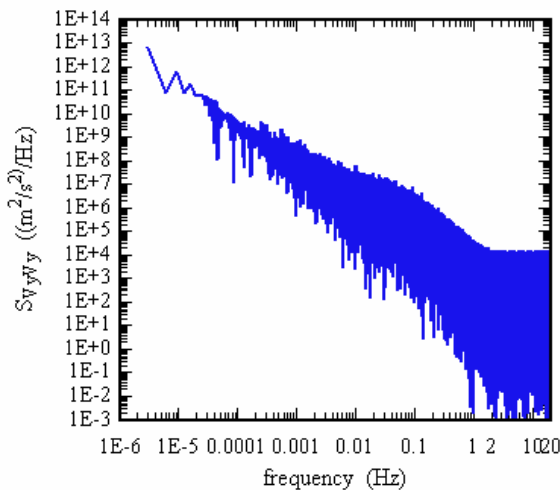
(C) S_{VyVy} data collected at 0.2 m above bed.
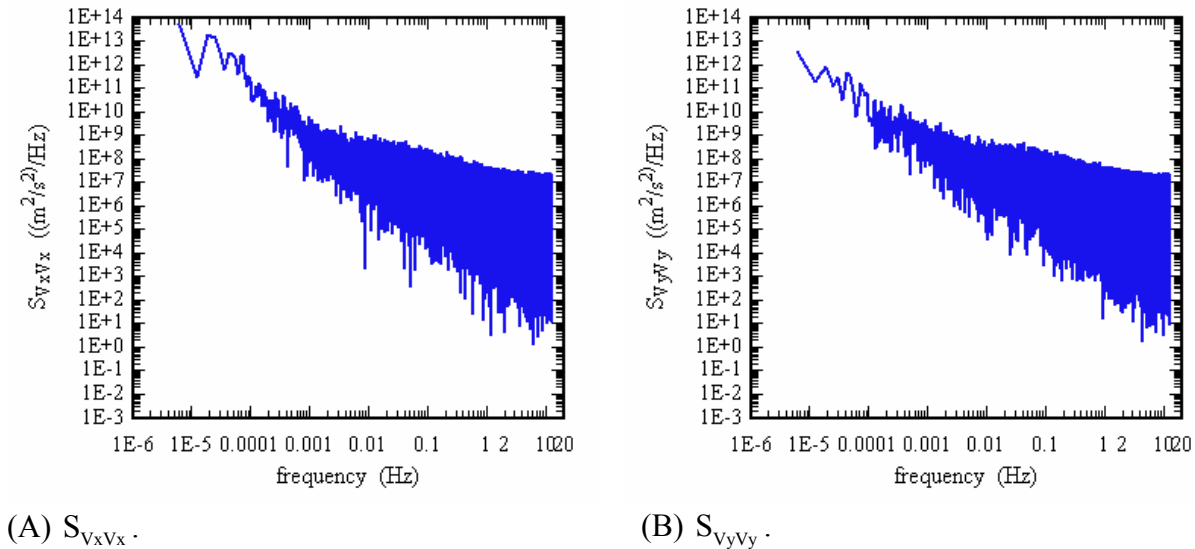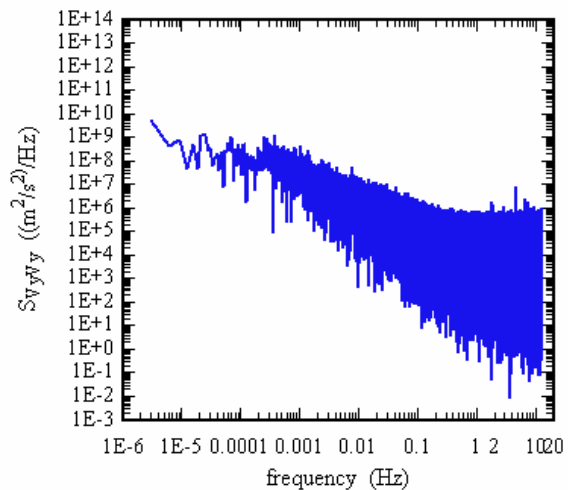
(D) S_{VyVy} data collected at 0.4 m above bed.

Figure E.8 – Frequency spectra of streamwise S_{VxVx} and transverse S_{VyVy} velocities for study E7 (5-7/06/06). Data collected 0.2 m (50 Hz) and 0.4 m (25 Hz) above bed at Site 2B, Eprapah Creek.

For the field study E7, the three most predominant oscillation periods seemed to have periods similar to tidal constituents observed in Eprapah Creek (Figure E.8). However, the 50 hour investigation period of this study did not allow adequate resolution of fluctuation periods with T > 14,400 s, and as such these are not presented in Table E.9. For the spectra of the streamwise velocity at both 0.2 and 0.4 m above the bed a region of increased energy was observed between approximately 1,500 and 4,500 s.

272

Table E.9 presents the 20 most predominant oscillation periods (T < 14,400 s) observed in the spectra of the streamwise and transverse velocity data for the study E7 (Figure E.8). In Table E.9 the predominant streamwise velocity oscillation periods were from groups B and C, while the predominant transverse oscillation periods were from groups B, C and D. Seven of the predominant streamwise velocity oscillation periods were between 2,200 > T > 1,500 s. These velocity oscillation periods were similar to the resonance periods conceivably generated along the entire length of Eprapah Creek (group C, Table E.6). One predominant transverse velocity oscillation period (T = 961 s) seemed related to resonance between the upstream end of the estuary and the natural weirs about Site 2B.

Many of the predominant transverse velocity periods observed at 0.2 and 0.4 m above the bed were different, with only 2 out of 20 oscillation periods being the same. However, the majority (12/20) of predominant streamwise velocity oscillation periods were the same.

Table E.9 – Predominant oscillation periods (T < 14,400 s) observed at Site 3 for study E7.

Oscillation periods at 0.2 m.a.b. (s)		Oscillation periods at 0.4 m.a.b. (s)	
V_x	V_y	V_x	V_y
3,608 (B)	13,421 (B)	3,608 (B)	2,642 (B)
3,290 (B)	12,427 (B)	3,995 (B)	3,995 (B)
3,995 (B)	11,570 (B)	3,728 (B)	3,647 (B)
1,794 (C)	10,824 (B)	3,290 (B)	3,532 (B)
2,820 (B)	3,948 (B)	2,110 (C)	8,830 (B)
1,730 (C)	7,989 (B)	3,107 (B)	11,184 (B)
2,208 (B)	8,830 (B)	1,730 (C)	3,136 (B)
2,110 (C)	6,579 (B)	1,794 (C)	1,864 (C)
3,107 (B)	9,587 (B)	2,208 (B)	2,414 (B)
12,905 (B)	3,290 (B)	4,302 (B)	4,143 (B)
4,302 (B)	3,608 (B)	1,875 (C)	961 (D)
2,009 (C)	6,991 (B)	2,820 (B)	1,216 (C)
2,969 (B)	6,331 (B)	2,009 (C)	3,528 (B)
11,570 (B)	8,389 (B)	2,642 (B)	1,955 (C)
2,642 (B)	5,326 (B)	4,726 (B)	5,083 (B)
4,793 (B)	3,495 (B)	4,534 (B)	2,561 (B)
1,864 (C)	1,907 (C)	12,427 (B)	1,186 (D)
4,143 (B)	1,785 (C)	11,184 (B)	2,110 (C)
1,613 (C)	5,887 (B)	8,830 (B)	12,427 (B)
1,505 (C)	4,534 (B)	8,184 (B)	1,590 (C)

Note: (letter in brackets refer to oscillation groups in Table E.6); m.a.b.: metres above bed.

E.4   EFFECT OF LONG PERIOD OSCILLATIONS IN EPRAPAH CREEK

The effect of the long period oscillations on the flow turbulence observed for the field studies E5, E6 and E7 were investigated by filtering the streamwise and transverse velocity data. Each data set was filtered with band-pass filter thresholds based upon the oscillation period ranges defined in Table E.6. The velocity magnitude and standard deviations were used to assess the impact of each oscillation group on the turbulence. Figure E.9 shows the median values of the magnitude and standard deviations of the streamwise and transverse velocity as functions of frequency for each oscillation group. Median values of the magnitude and standard deviations are presented on the high frequency cut-off for each oscillations group (e.g. 0.005 Hz for group E).

In Figure E.9 the median values of the streamwise and transverse velocity magnitude decreased rapidly with increasing frequencies. This indicated that the predominant influence on the velocity oscillations in the middle and upper estuarine zones of Eprapah Creek came from the tidal forcing. Mid estuary the velocity magnitude generated by the tidal constituents (group A) and resonances generated outside Eprapah Creek (group B) under spring tidal conditions (study E5) were twice as large as those under neap tidal conditions (study E6). Note that the impact of the tides on the horizontal velocity magnitude seemed substantially less for the field study E7 (upper estuary) than the study E6 (middle estuary) under similar neap tidal conditions. At present, the cause of the reduced velocity magnitude for the study E7 is unknown.

Alternatively, the velocity magnitude for all groups related to possible resonance within Eprapah Creek (groups C, D and E) seemed relatively independent of tidal conditions and longitudinal location (AMTD) for the studies E5, E6 and E7. Note that for the studies E6 and E7 (neap tides) the transverse velocity magnitudes of oscillation groups C and D (resonance sources within Eprapah Creek) were similar to those of groups A and B (sources outside Eprapah Creek, e.g. the tides). This indicated that oscillations sources within Eprapah Creek (e.g. internal resonance) could conceivably have a significant influence on the observed velocity fluctuations.

Figures E.9B and E.9D shows that the median values of streamwise and transverse velocity fluctuations ($v_x^'$ and $v_y^'$) increased with increasing frequency for the spring tidal forcing (study E5). This was not the case under neap tidal conditions (studies E6 and E7), when the streamwise and transverse velocity standard deviations were almost constant for oscillation groups D, E and F (f > 0.005 Hz, Figures E.9B and E.9D). The two different patterns in turbulent velocity fluctuations seemed to indicate two different types of energy transfer processes driving the velocity fluctuations under spring and neap tidal conditions.

274
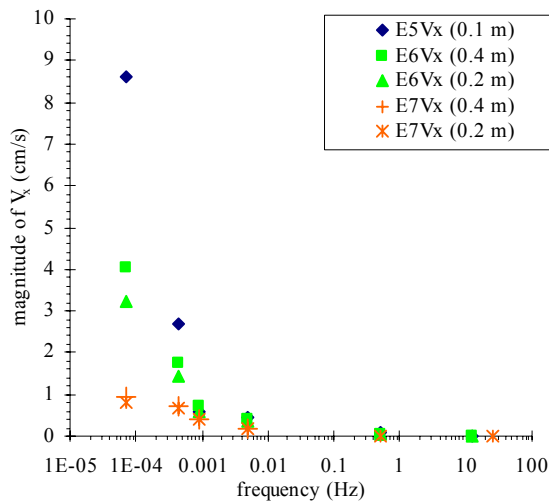
(A) Velocity magnitude of V_x.
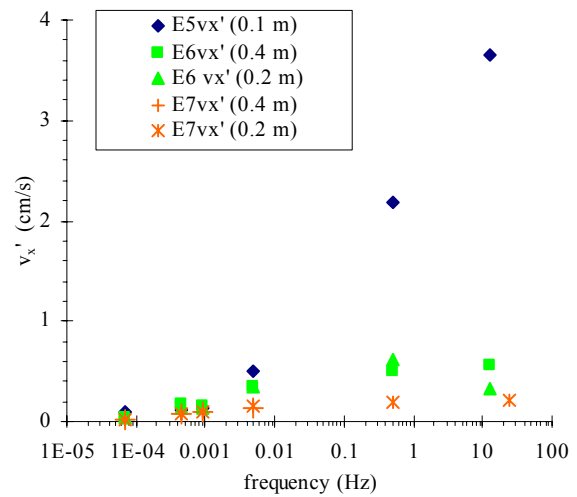
(B) Standard deviations v_x'.
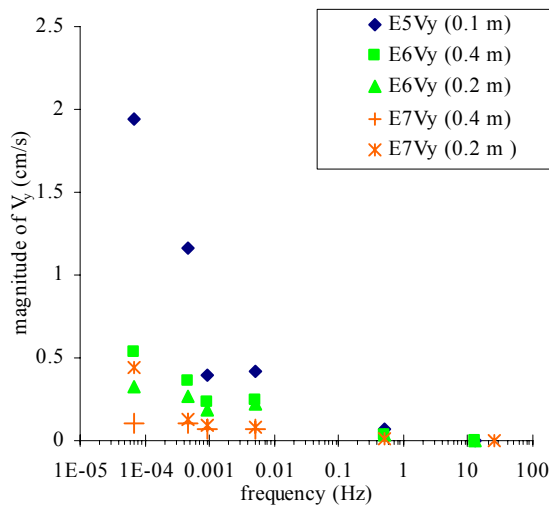
(C) Velocity magnitude of V_y.
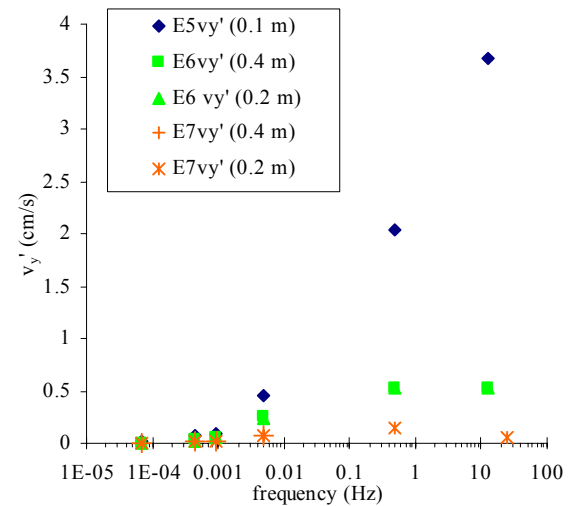
(D) Standard deviations v_y'.

Figure E.9 – Median values of magnitude and standard deviations for streamwise and transverse velocities as functions of high frequency cut-off for each oscillation group. Data collected for field studies E5 (mid estuary, spring tides), E6 (mid estuary, neap tides) and E7 (upper estuary, neap tides). Note: legends in figures indicate field study and sampling elevation above bed.

E.4.1   Transverse velocity fluctuations and associated secondary currents

For both the field studies E6 and E7 the predominant transverse velocity oscillations observed at 0.2 and 0.4 m above the bed were mostly different, with only 2 or less oscillation periods being the same at the two sampling elevations (Tables E.8 and E.9). This difference in transverse velocity oscillation periods at 0.2 and 0.4 m above the bed could lead to the formation of transverse velocity events and associated secondary currents. Some transverse velocity events and associated secondary currents were observed throughout the field studies E6 and E7. One particular transverse velocity event was observed when the transverse

velocities at 0.2 and 0.4 m above the bed were in opposite directions. This type of transverse velocity event is often associated with a specific type of secondary current known as a "reverse cell". Reverse cell secondary currents commonly form near the outer bank of meanders and rotate in the opposite direction to the main transverse flow direction (Bathurst et al. (1977)). In channel meanders the main transverse velocity direction (secondary current) is towards the outer bank at the bed and towards the inner bank near the surface.

In this study the largest of these transverse velocity events were observed at the beginning of the flood tide (e.g. t = 129,000 and 135,000 s of study E6, Figure E.10) in both middle and upper estuarine zones (studies E6 and E7). This is consistent with the findings of West et al. (1984) in a study of the flow patterns of a UK estuary that found shear induced instabilities and secondary flow events were more likely to form on the flood tide. For the field study E7 transverse velocity events with a period of approximately 10 s were manually logged from the instantaneous data display.

The effect of the long period oscillations on the formation of transverse velocity cells (e.g. reverse cells) in the middle and upper estuaries was investigated using two of the largest transverse velocity events for the studies E6 and E7. Figure E.10 shows these two largest transverse velocity events observed for the field studies E6 and E7. The possible reverse cell secondary currents observed are indicated for each transverse velocity event shown in Figure E.10. In Figure E.10 the period and magnitude of the transverse velocity events observed mid estuary (study E6) were larger than those in the upper estuary (study E7).

For both middle (study E6) and upper (study E7) estuarine zones the individual transverse velocity cells were not uni-directional (Figures E.10A, C and D). In Figure E.10A the transverse velocity cells from t = 77,160 to 77,860 s and t = 78,010 to 80,240 s seemed to rotate in the opposite directions (i.e. ($\overline{V_y}$ (0.2 m) > 0; $\overline{V_y}$ (0.4 m) < 0) and ($\overline{V_y}$ (0.2 m) < 0; $\overline{V_y}$ (0.4 m) > 0) respectively). These reversals in the transverse velocity cell direction had periods similar to the long period oscillations observed in Tables E.8 and E.9 (studies E6 and E7 respectively). This seemed to indicate that the interaction of the long period oscillations (not the tides) with the local bathymetry formed these transverse velocity events observed under neap tidal conditions (studies E6 and E7).

The number of individual transverse velocity events, their maximum and minimum durations and the median transverse velocity magnitudes are listed in Table E.10. Table E.10 shows that the duration of these transverse velocity events were similar to half of the period for the long period oscillations in groups B, C and D (Table E.6). This indicated that the long period

oscillations from these groups were conceivably a primary cause of the larger transverse velocity events and associated secondary currents observed in the field studies E6 and E7.
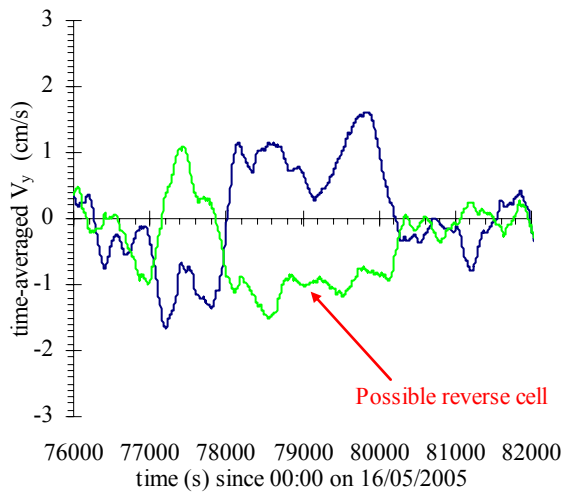
(A) Event E6a (t = 76,000 to 82,000 s, study E6).
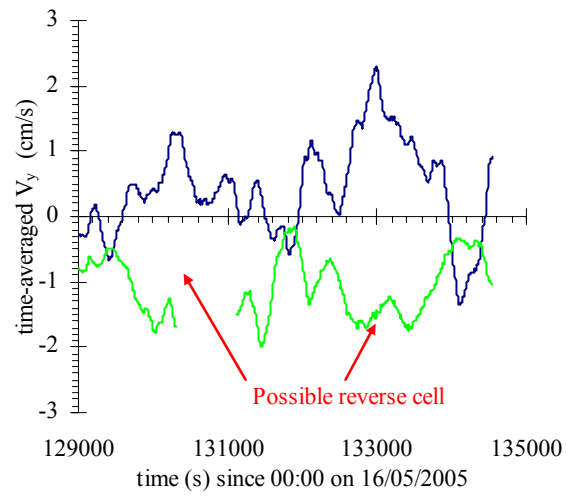
(B) Event E6b (t = 129,000 to 135,000 s, study E6).
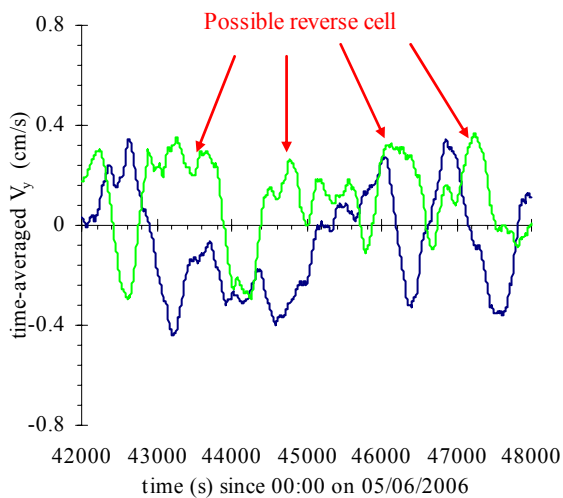
(C) Event E7a (t = 42,000 to 48,000 s, study E7).
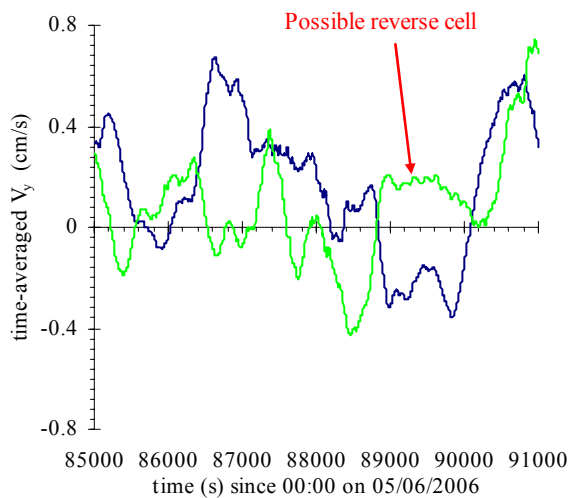
(D) Event E7b (t = 85,000 to 91,000 s, study E7).

Figure E.10 – Time-averaged transverse velocity $\overline{V_y}$ at 0.2 and 0.4 m above bed as functions of time for some transverse velocity events observed for studies E6 and E7. Velocity averaged over 200 s every 10 s along entire data set.

Legend: — $\overline{V_y}$ 0.2 m above bed; — $\overline{V_y}$ 0.4 m above bed.

The median values of transverse velocity magnitude $\left|\overline{V_y}\right|$ for the entire data sets of the studies E6 and E7 were approximately 0.55 and 0.17 cm/s respectively. For each 6,000 s section of data (Figure E.10) the median values of transverse velocity magnitude were equal to or larger

than that of the entire data set for the field studies E6 and E7 (Table E.10). This indicated that during these larger transverse velocity events there was an increased transverse velocity magnitude.

Table E.10 – Description of some transverse velocity events from field studies E6 and E7.

Field study	Event number	Number of events	Maximum event duration (s)	Minimum event duration (s)	$\left|\overline{V_y}\right|$ at 0.2 m.a.b. (cm/s)	$\left|\overline{V_y}\right|$ at 0.4 m.a.b. (cm/s)
E6	E6a	3	2,230	460	0.81	0.66
	E6b	3	2,000	210	0.63	0.71
E7	E7a	7	970	140	0.17	0.18
	E7b	7	1,270	170	0.17	0.26

Note: Event duration: period in which $\overline{V_y}$ at 0.2 and 0.4 m were in opposite directions; m.a.b.: metres above bed; $\left|\overline{V_y}\right|$: median value of time-averaged transverse velocity magnitude for 6,000 s of event shown in Figure E.10.

E.5   SUMMARY

For all field studies undertaken at Eprapah Creek some long period oscillations were observed in the water level and horizontal velocity data. The fact that these long period oscillations were observed in the water level data seemed to indicate that some of these oscillations were created by some form of seiching within Eprapah Creek and/or Moreton Bay. Some of the predominant horizontal velocity oscillations had periods similar to the theoretical resonance periods created both within and outside Eprapah Creek.

For the field studies E5, E6 and E7 predominant velocity oscillation periods between 2,200 and 1,500 s were observed. Oscillations periods between 1,500 and 2,200 s matched the theoretical range of resonance created by resonance over the entire length of the Eprapah Creek estuarine zone. Some predominant oscillation periods between 1,200 and 600 s were also observed for the studies E5, E6 and E7. These velocity oscillation periods were similar to the theoretical natural resonance created between the natural weirs about Sites 2B and the mouth, or the upstream extent of the estuarine zone. The natural weirs located mid estuary could conceivably act as a hydraulic control, splitting the estuary in two at low water.

The predominant velocity oscillations with periods T > 2,200 s were most likely created outside Eprapah Creek. Several of these larger period velocity oscillations had periods similar to some of the major tidal constituents. However, the investigation periods of the field

studies E5, E6 and E7 were not long enough to confirm that these velocity fluctuations had the same period as the major tidal constituents. Another conceivable source for these long period oscillations was seiching created within Moreton Bay. However, a comprehensive study of the possible resonance periods within Moreton Bay is outside the scope of this study. The long period oscillations with periods smaller than those of the major tidal constituents seemed to contribute the different flow and energy transfer systems observed at Eprapah Creek under spring and neap tidal conditions. Under neap tidal conditions the influence of long period oscillations on the velocity data collected seemed significant. For example, some long period oscillations with periods between 2,000 and 5,000 s caused streamwise velocity fluctuations of similar magnitude to that of the tides.

Under neap tidal conditions (studies E6 and E7) the long period oscillations observed seemed to restrict the intensity of the lower period (T < 2,000 s) streamwise and transverse velocity fluctuations. For the studies E6 and E7 the turbulence intensities of T < 2,000 s were nearly constant. However, under spring tidal conditions (study E5) the intensity of the turbulence fluctuations increased as the oscillation period decreased. This seemed to indicate that two different energy transfer and mixing processes occurred under spring and neap tidal conditions.

Long period oscillations in the transverse velocity seemed responsible for the formation and then reversal of some secondary current cells observed at Site 2B and Site 3 for the studies E6 and E7 respectively. The magnitude of the transverse velocities observed during these secondary cell events were close to the maximum transverse velocity observed during the field studies E6 and E7. Therefore, these secondary cells could have a significant impact on the local mixing properties.

APPENDIX F   WAVE-TURBULENCE SEPARATION TECHNIQUE

F.1   INTRODUCTION

In a natural system affected by wind waves such as Hamana Lake there is a need to separate the wave induced and current induced turbulence data (Benilov and Filyushkin (1970)). Bowden and White (1966) found that there was correlation between pressure and velocity spectra in an estuary under the influence of wind waves. Kitaigorodskii et al. (1983) found that a spectral peak occurred in both the velocity and water level spectra around the dominant wave frequency. Several previous investigations (e.g. Benilov and Filyushkin (1970), Jiang et al. (1990), Thais and Magnaudet (1995), Trowbridge (1998)) developed methods for separating "wave noise" from the turbulence data.

Many studies (e.g. Kitaigorodskii et al. (1983), Cioffi et al. (2006)) used the linear filtration technique of Benilov and Filyushkin (1970). The linear filtration technique assumes that fluctuations of a random process correlated with the displacement of the free surface are caused by waves. Other studies (e.g. Jiang et al. (1990)) used different nonlinear wave decomposition methods developed from the work of Dean (1965). The method explained in Dean used a nonlinear least squares time domain resolution of the full kinematic and dynamic equations at the free surface. Thais and Magnaudet (1995) combined the linear filtration technique of Benilov and Filyushkin (1970) and that of Dean (1965) to develop the triple decomposition method. The triple decomposition method distinguishes between the three components of the fluctuating motion, these being the potential and rotational parts of the orbital motion as well as the turbulent fluctuations. Trowbridge (1998) developed a technique that required two or more synchronised measurements in a vertical profile (with measurements less than ¼ depth apart) to separate the wave induced and current induced turbulence data. What frequencies of the data need separating was determined through correlation of the velocity fluctuations at the two measurement positions. This technique could not be applied to the data collected at Hamana Lake because only one ADV was deployed.

F.1.1   Field Studies at Hamana Lake, Japan

Three field investigations collecting continuous high frequency turbulence data were performed at Hamana Lake, Japan in November and December 2005. Figure F.1 shows the locations of these field studies in Hamana Lake and the location of Hamana Lake in Japan. These field studies were designated the field studies HLJ1 (24-25/11/2005), HLJ2 (30/11-1/12/2005) and HLJ3 (21-22/12/2005). Table F.1 outlines the field studies conducted at Site 1 Hamana Lake.
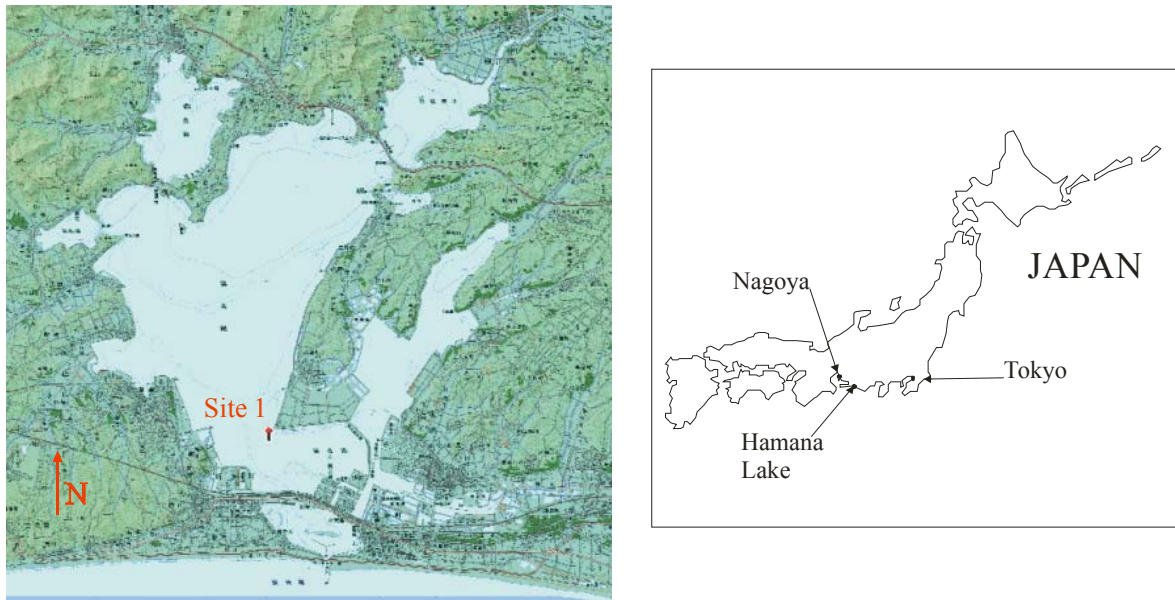
Figure F.1 – Diagram of Hamana Lake (picture courtesy of S. Aoki). Insert shows location of Hamana Lake in Japan.

Table F.1 – Field studies conducted at Site 1 Hamana Lake in 2005.

Field study	**HLJ1**	**HLJ2**	**HLJ3**
Date	24-25/11/05	30/11-1/12/05	21-22/12/05
TR (m)	0.45	0.70	0.6
T_{study} (hrs)	28	25	30
f_{scan} (Hz)	32	32	32
Sampling location	Site 1, 0.25 m above bed, 454 m from left bank	Site 1, 0.25 m above bed, 454 m from left bank	Site 1, 0.25 m above bed, 454 m from left bank
Site cross-section width (m)	1,476	1,476	1,476
Mean depth at Site 1 (m)	0.91	0.92	0.92

Note: f_{scan} : ADV sampling frequency; T_{study} : study duration; TR : maximum tidal range.

During all three field studies at Hamana Lake wind waves were observed about the experimental site. Figure F.2 shows a photograph of some wind waves observed at Site 1 Hamana Lake during the setup of the field study HLJ1. Table F.2 shows the wind velocity range and averaged wind speeds recorded at the Hamamatsu weather station near Hamana Lake for these field studies. During all field trips the wind direction was predominantly Westerly with occasional fluctuations towards the Northwest.

Figure F.2 – Photograph of wind waves observed at Site 1 Hamana Lake taken during installation for study HLJ1 on 24/11/05, with poles holding ADV on far left.

Table F.2 – Wind information recorded at Hamamatsu weather station for studies HLJ1, HLJ2 and HLJ3. Maxima and minima hourly wind velocities for each study, and mean wind velocities are listed.

Field study	Date	Duration (hours)	Wind velocity range (m/s)	Averaged wind velocity (m/s)
HLJ1	24-25/11/05	28	1.2 to 6.5	4.0
HLJ2	30/11-1/12/05	25	1.0 to 6.0	4.2
HLJ3	21-22/12/05	30	1.3 to 11.1	6.3

F.1.2   Notation

$R_{V\xi}(\tau)$ cross-correlation function of velocity and water level data (m^2/s)

$R_{\xi\xi}(\tau)$ autocorrelation function of water level (m^2)

S_{VV} spectrum of velocity (m^{2}s^{-2}/Hz)

S_{VxVx} spectrum of streamwise velocity (m^{2}s^{-2}/Hz)

S_{VyVy} spectrum of transverse velocity (m^{2}s^{-2}/Hz)

S_{VzVz} spectrum of vertical velocity (m^{2}s^{-2}/Hz)

$S_{V\xi}(\omega)$ co-spectrum of velocity and water level (m^{2}s^{-1}/Hz)

$S_{\xi\xi}(\omega)$ spectrum of water level (m^2/Hz)

ξ fluctuations in water level (m)

τ correlation time lag (s)

ω angular frequency (rad/s)

F.2 WAVE-TURBULENCE SEPARATION TECHNIQUE

A simple method was derived from the linear filtration method suggested by Benilov and Filyushkin (1970). It was used to process the wave and turbulence data collected at Hamana Lake during the field studies HLJ1, HLJ2 and HLJ3. With the linear filtration method of Benilov and Filyushkin, any fluctuations in a measured random parameter (e.g. velocity) that correlate with the displacement of the water surface are considered to be caused by the surface waves. The linear filtration method of Benilov and Filyushkin (1970) required that synchronised water level $\xi(t)$ and velocity $V(t)$ data were collected at the same frequency. Under the influence of wind waves the velocity $V(t)$ is made up of turbulent fluctuations $V^T(t)$ and some "noise" generated by the waves $V^W(t)$:

$$V(t) = V^T + V^W \tag{F.1}$$

The random process $\xi(t)$ is related to the wave noise through the linear relationship:

$$V^W(t) = L\,\xi(t) \tag{F.2}$$

where L = unknown linear operator. Equation F.2 is required to establish $V^T(t)$ at any moment of time t, if the correlation function $R_{\xi\xi}(\tau)$, the cross-correlation function $R_{V\xi}(\tau)$ and Equation F.3, or the corresponding spectral densities ($S_{\xi\xi}(\omega)$ and $S_{V\xi}(\omega)$) and Equation F.3 are known:

$$\overline{V^T(t)\,\xi(t)} = 0 \tag{F.3}$$

For this investigation the first step in the separation of the wave and turbulence data was the generation of the spectra for the water level and three velocity components. These spectra were plotted (Figure F.3) and visually inspected to determine the frequency band where the velocity and water level spectra correlated. The wave-turbulence interaction frequency band was that in which the frequencies of the water level spectra that contained more than 3 % of the energy of the dominant wave period. Figure F.3 shows the spectra of the water level and three velocity components measured by the Nortek 3D-Vector field ADV during the field study HLJ2 (30/11-1/12/05). In Figure F.3 the visually interpreted frequency range of correlation between the velocity and water level spectra is highlighted. Note that the spectra shown in Figure F.3 were smoothed to reduce the noise in the higher frequency ranges.
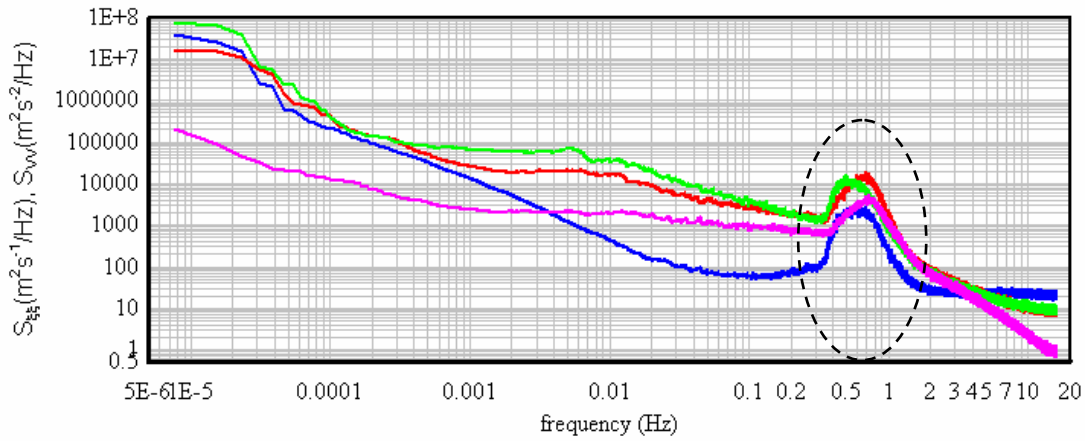
Figure F.3 – Spectra of water level and velocity data measured for study HLJ2 at Hamana Lake (30/11-1/12/05). Spectra smoothed with averaging window of 256 data points.

Legend: — water level spectrum $S_{\xi\xi}$; — transverse velocity spectrum $S_{V_yV_y}$; — streamwise velocity spectrum $S_{V_xV_x}$; — vertical velocity spectrum $S_{V_zV_z}$.

For the field study HLJ2 the range of correlation between the spectra of water level and velocity components was determined visually and found to be approximately 0.3 to 1.2 Hz. Data outside this frequency range were deemed not affected by the waves, while that data within the frequency band were. The turbulence data were separated in two steps: 1) – wave induced data were separated using the filtering limits of 0.3 and 1.2 Hz; 2) – Current induced data were separated by two filtering passes either side of the correlated frequency range (0.3 and 1.2 Hz) using the thresholds of 0 to 0.3 Hz and 1.2 to 16 Hz. The two filtered bands of non-wave velocity data were then combined back together to form the current induced data set. Figure F.4 shows the spectra of the water level and velocity components for the study HLJ2 after the influence of the wind waves was removed. It is acknowledged that by filtering out the wave affected data between the range of 0.3 to 1.2 Hz, all "true" turbulence data within this range were removed (Figure F.4). The removal of turbulence data within this range was deemed acceptable because it covered a narrow frequency band. Further, this narrow frequency range was several orders of magnitude lower than that where viscous dissipation occurs.
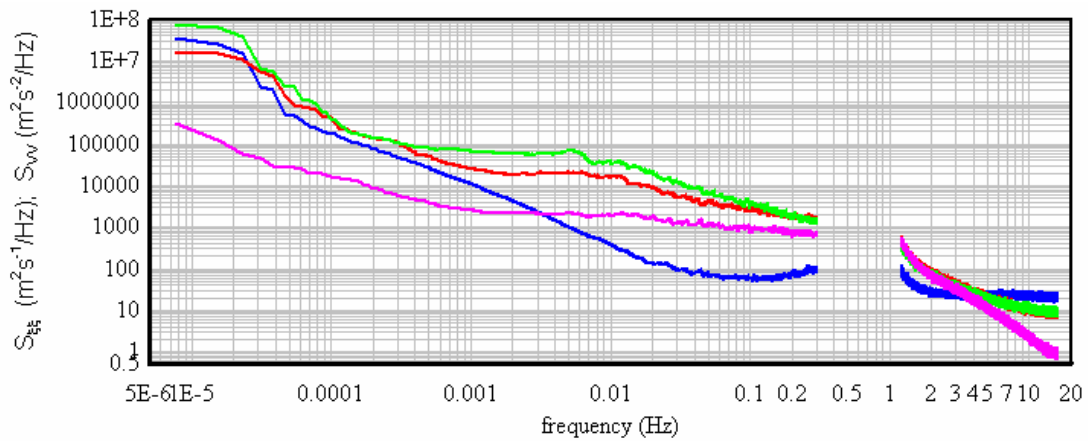
Figure F.4 – Spectra of water level and velocity components with influence of wind waves removed (study HLJ2). Spectra smoothed using averaging window of 256 data points. Legend: — water level spectrum $S_{\xi\xi}$; — transverse velocity spectrum $S_{V_yV_y}$; — streamwise velocity spectrum $S_{V_xV_x}$; — vertical velocity spectrum $S_{V_zV_z}$.

F.3   VALIDATION

The linear filtration method (Benilov and Filyushkin (1970)) uses the correlation between the spectrum of water level and a turbulence property (e.g. velocity) to determine the frequency band in which wave-turbulence interaction occurred. For this investigation a quick and simple method was sort for determining the frequency range influenced by wind waves. Some investigation showed that a visual inspection of the water level and velocity spectra using a percentage of the peak wave energy to determine the frequency range was the quickest and simplest method available. The use of a percentage of the peak wave energy E_{peak} provided a physical basis for determining the frequency range of the velocity data influenced by the wind waves. As Kitaigorodskii et al. (1983) found that a spectral peak occurs in both the velocity and water level spectra around the dominant wave frequency. However, some investigation was required to determine an optimal percentage of the peak wave energy required.

For the linear filtration technique the frequency range of wave-turbulence interaction for a measured turbulence property is that range where there is high correlation between the water level and that turbulence property. Therefore, the threshold percentage of the peak wave energy should be chosen to remove the maximum quantity of high correlation data, while not removing the low correlation data. This threshold percentage was chosen by comparing the frequency range determined by each percentage of the peak wave energy to the correlation within and outside this frequency range. The correlation values used in this study were calculated through the cross-correlation of the spectra for water level and each velocity

285

component for the field studies HLJ1, HLJ2 and HLJ3 (e.g. Figure F.5). Figure F.5 shows the cross-correlation between the spectra of water level and three velocity components as functions of frequency for the field study HLJ2. In Figure F.5 the cross-correlation of water level and all velocity component spectra increased about the dominant wave frequency.
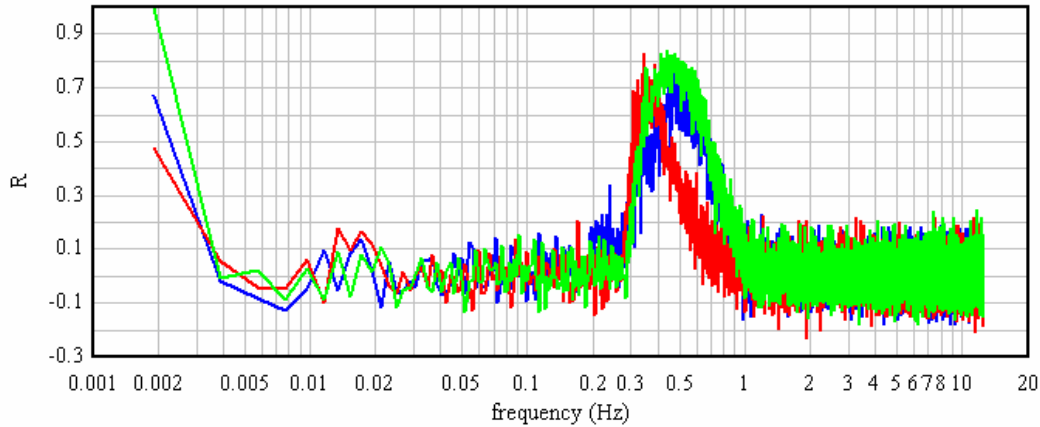
Figure F.5 – Cross-correlation of water level and velocity spectra as functions of frequency for study HLJ2 (30/11-1/12/05). Spectral cross-correlation performed using a correlation window of 256 data points.

Legend: — correlation between $S_{\xi\xi}$ and S_{VyVy} ; — correlation between $S_{\xi\xi}$ and S_{VxVx} ;

— correlation between $S_{\xi\xi}$ and S_{VzVz} .

Table F.3 presents the frequency band determined by the percentage of peak wave energy and the correlation values outside these ranges for the several percentage values tested. In Table F.3 the correlations shown were the average cross-correlation values of the three velocity components and the water level outside the frequency range. For this study some correlation existed between the water level and velocity spectra at a particular frequency if $R > 0.5$.

For the field studies HLJ1, HLJ2 and HLJ3, the use of 3 % of the peak wave energy as the frequency range threshold seemed optimal as the correlation coefficient outside this frequency range was $R < 0.4$. A correlation of $R < 0.4$ could be considered to show little or no correlation between the two spectra at those frequencies. This seemed to indicate that the influence of wind waves was limited outside the frequency range determined by using 3 % of the peak wave energy as a threshold. Threshold percentages larger than 3 % of the peak wave energy show correlations of $R > 0.5$. This indicated that some frequencies influenced by wind waves would have remained in the separated data, affecting turbulence analysis. The use of a threshold percentage smaller than 3 % seemed to eliminate all low frequency data

(e.g. 1 % of E_{peak}, Table F.3) because this percentage of peak wave energy was less than the energy created by the tidal currents.

Table F.3 – Results of optimal percentage E_{peak} threshold investigation for studies HLJ1, HLJ2 and HLJ3.

Field study	Peak wave energy (m^2/Hz)	30 % of E_{peak}		10 % of E_{peak}		5 % of E_{peak}		3 % of E_{peak}		1 % of E_{peak}	
		f_{waves} (Hz)	$\lvert R \rvert$	f_{waves} (Hz)	$\lvert R \rvert$	f_{waves} (Hz)	$\lvert R \rvert$	f_{waves} (Hz)	$\lvert R \rvert$	f_{waves} (Hz)	$\lvert R \rvert$
HLJ1	4,500	0.39	0.66	0.36	0.64	0.33	0.67	0.3	0.4	0	0
		0.78	0.52	0.94	0.30	1.07	<0.1	1.14	<0.1	1.41	<0.1
HLJ2	2,500	0.40	0.63	0.35	0.63	0.33	0.49	0.22	0.33	0	0
		0.83	0.19	1.0	<0.1	1.15	<0.1	1.2	<0.1	2.57	<0.1
HLJ3	13,000	0.33	0.71	0.28	0.70	0.25	0.52	0.22	0.32	0	0
		078	0.50	0.89	0.29	1.02	<0.1	1.2	<0.1	1.35	<0.1

Note: E_{peak}: peak wave energy; f_{waves}: low (upper number)/high (lower number) frequency cut-offs between which wave-turbulence interaction occurred; $\lvert R \rvert$: average correlation between spectra of water level and each velocity component lower (top number) and higher (bottom number) than wave-turbulence interaction frequency range.

F.4   DISCUSSION

For the field studies HLJ1, HLJ2 and HLJ3, the predominant wave period generated by the wind was approximately 2 s. Table F.4 presents the wave periods of the most energetic wind waves and the frequency bands used for each field study to separate the wave induced and current induced components of the gross velocity data. The most energetic wind waves were those which contained more than 3 % of the energy of the dominant wave period.

For each field study the wave-turbulence interaction frequency band was that in which the frequencies of the water level spectra contained more than 3 % of the energy of the dominant wave period. These frequency bands were used to separate the wave induced and current induced components of the gross velocity data using the method outlined in Section F.2. The effect of the wave-turbulence separation process on the dynamics of Hamana Lake at Site 1 is demonstrated in Figure F.6. Figure F.6 presents the wind speed (right vertical axis) and time-averaged streamwise Reynolds stress $\rho \overline{v_x v_x}$ of the gross and current induced data (left vertical axis) for the study HLJ3 as functions of time.

Table F.4 – Frequency bands determined to be influenced by wind waves.

Field study	Date	Wind wave period (s)	Separated frequency band (Hz)
HLJ1	24-25/11/05	0.88 to 3.3	0.3 to 1.14
HLJ2	30/11-1/12/05	0.83 to 3.3	0.3 to 1.2
HLJ3	21-22/12/05	0.83 to 4.5	0.22 to 1.2

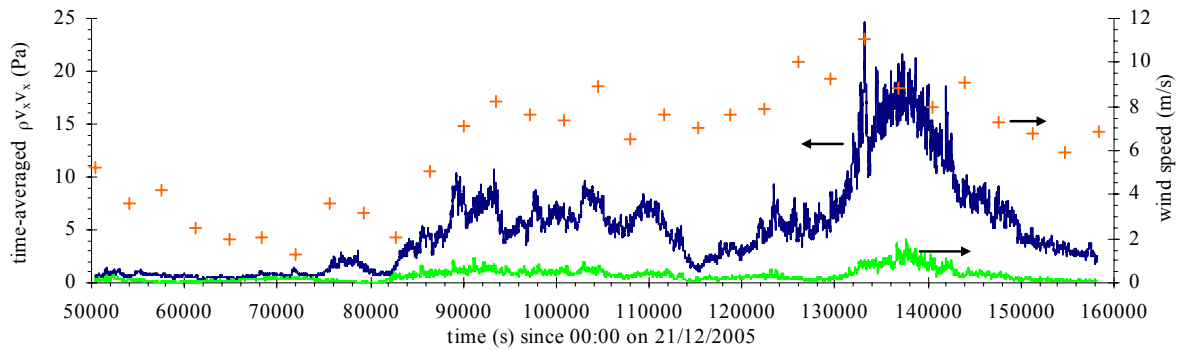Note: Wind wave periods shown contain at least 3 % of energy from dominant wave period.

Figure F.6 – Wind speed and time-averaged Reynolds stress $\rho\overline{v_x v_x}$ of gross and current induced data as functions of time (s) since midnight on 21/12/05 (study HLJ3). Time-averaged Reynolds stress calculated for 5,000 data points every 10 s along entire data set. Wind speeds are hourly average collected at Hamamatsu weather station.

Legend: + wind speed; — $\rho\overline{v_x v_x}$ for gross data ; — $\rho\overline{v_x v_x}$ for current induced data.

In Figure F.6 the streamwise normal Reynolds stress was greatly reduced through the separation process by the removal of the wind wave generated shear. This reduction in time-averaged Reynolds stress $\rho\overline{v_x v_x}$ seemed proportional to the magnitude of the wind speed, with the difference between gross and current induced data increasing with the increased wind speed. The normal Reynolds stress is important as it is analogous to the fluctuations of shear stress and turbulent kinetic energy at the sampling volume and can be used to estimate the bed shear stress (e.g. Bricker et al. (2005)). Thais and Magnaudet (1996) found that wave-turbulence interactions greatly influenced energy transfers over a significant frequency range during experiments undertaken in a laboratory wave flume. The wave-turbulence interaction influenced the energy transfers over this frequency band by imposing a constant time scale related to the wind induced strain. Therefore, wave-turbulence interaction also influenced the turbulent mixing processes that occur beneath these wind waves.

APPENDIX G   FIELD STUDIES CONDUCTED AT HAMANA LAKE IN 2005

G.1   INTRODUCTION

Three series of field investigations were conducted at Hamana Lake (Figure G.1) by Toyohashi University of Technology (Coastal Engineering Group) in November and December 2005. These studies focused on estuarine turbulence and its impact on the local environment. Figure G.1 shows a picture of Hamana Lake and the site of experiments performed. Hamana Lake is located on the Southeast Coast of Honshu Island, Japan in the Shizuoka Prefecture (Insert, Figure G.1).
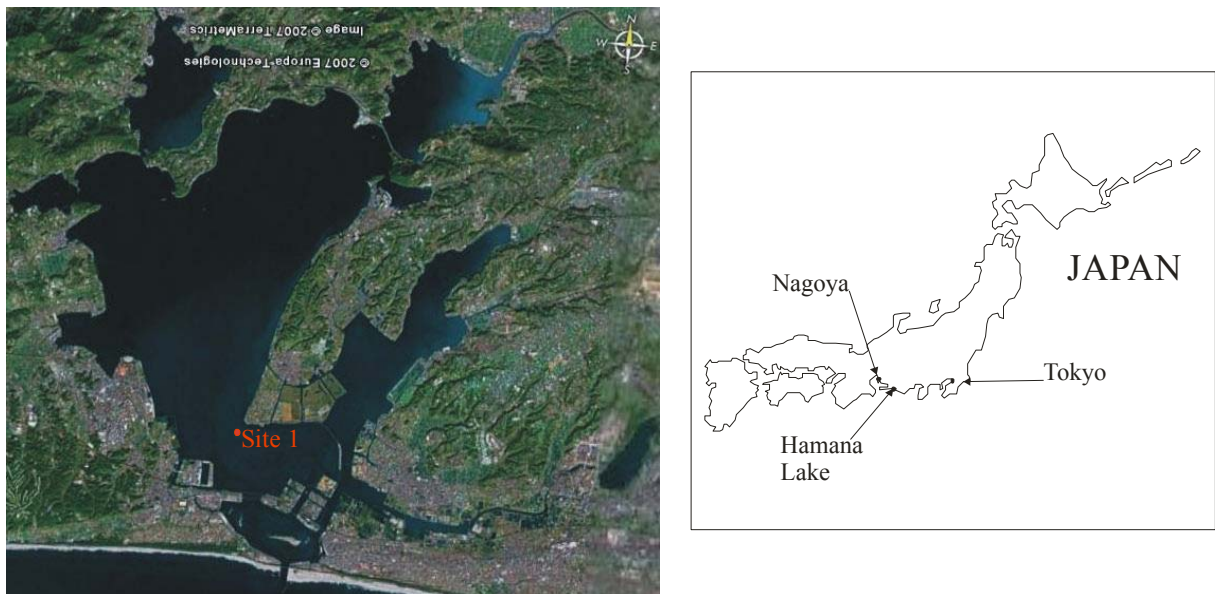

Figure G.1 – Picture of Hamana Lake Japan (picture courtesy of Google Earth). Insert shows location of Hamana Lake in Japan.

Hamana Lake has human settlements around most of its shores and it supports a large marine agriculture industry including eel; fish; shellfish; and seaweed farming. The field studies were carried out in collaboration with the Shizuoka Prefecture Fisheries Department to improve the development of shellfish larvae within Hamana Lake. It was observed that shellfish larvae had difficulty settling on the bed of Hamana Lake, because of high bed shear stress.

Section G.2 outlines the field studies performed at Site 1 Hamana Lake during 2005, the instruments used, some practical issues encountered during the field studies and the post-processing techniques applied to the measured data. In Section G.3 some turbulence properties of the post-processed (gross) data sets are presented. These include the first four statistical moments of velocity and tangential Reynolds stress; the turbulence intensity ratios;

correlation coefficients of Reynolds stress; and integral and dissipation time scales. Section G.4 presents some key differences in the turbulence properties of the gross and current induced data sets, while Section G.5 discusses some of the key outcomes from three field studies undertaken at Site 1 Hamana Lake.

G.2   FIELD STUDIES AND INSTRUMENTATION

Hamana Lake (Figure G.1) is a relatively large tidal lake with a small opening to the Pacific Ocean. It extends approximately 15 km inland and has a surface area of 7.4 x 10^7 m^2. The width of the entrance is approximately 200 m and is controlled by man made structures. The entrance channel is regularly dredged to keep the channel continuously open. The depth of Hamana Lake increases landwards, from less than 1 m near the entrance to more than 12 m further inland.

The three field investigations were performed at Site 1 indicated in Figures G.1and G.2. Site 1 (N34° 42' 27.3", E137° 34' 50.3") was located in a shallow area near the estuary mouth. This shallow region is typical of restricted entrance (bar-built) type estuaries (Dyer (1997)). Site 1 was located approximately 600 m Northeast of main navigation channel, 450 m South of nearest bank and approximately 3.5 km NNW of the entrance (Figure G.2). Figure G.3 shows the experimental cross-section through Site 1. The location of the experimental cross-section is indicated in Figure G.2. At Site 1 the mean depth was approximately 0.9 m for the three field studies. The maximum tidal range during the three field studies was 0.56 m. Throughout all three field investigations wind waves were observed at Site 1, generated by wind speeds V_W > 1 m/s. The sediment in the area surrounding Site 1 was predominantly sand with d_{50} = 0.24 mm.
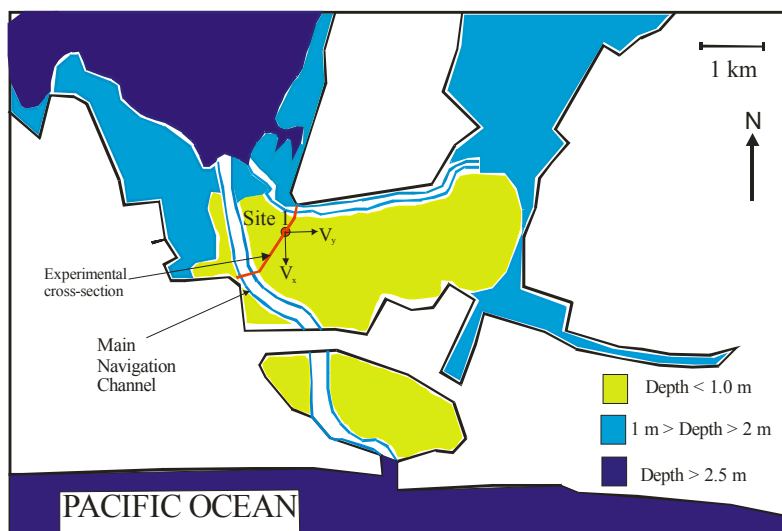

Figure G.2 – Sketch of Hamana Lake near entrance.
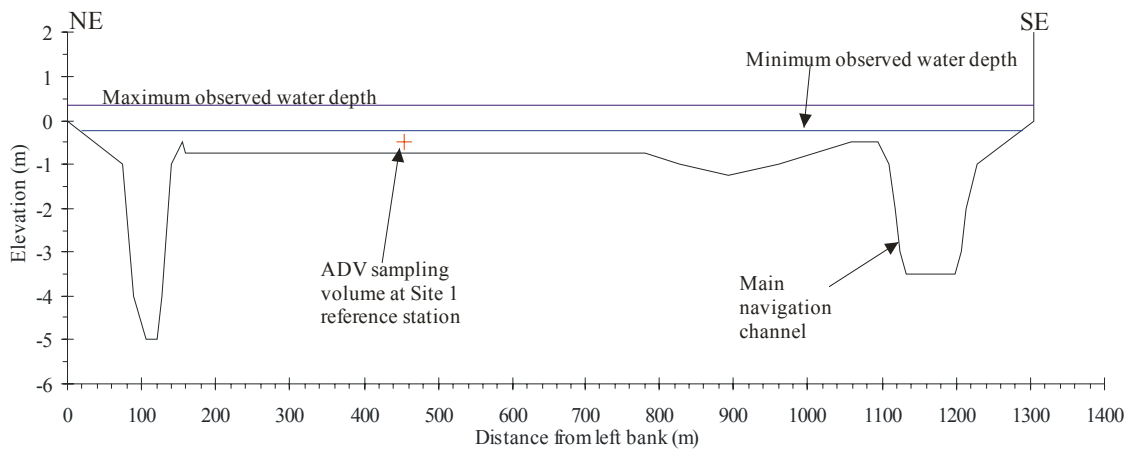
Figure G.3 – Experimental cross-section through Site 1 at Hamana Lake, looking downstream.

Figure G.4 shows a sketch of the experimental setup at Site 1. The field investigations were designated the field studies HLJ1 (24-25/11/2005), HLJ2 (31/11-1/12/2005) and HLJ3 (21-22/12/2005), and are described in Table G.1. For the studies HLJ1, HLJ2 and HLJ3, all velocity measurements at Site 1 reference station (Figure G.4) were sampled continuously at 32 Hz, 0.25 m above the bed for at least one diurnal tidal cycle (25 hours).

Figure G.4 – Sketch of Site 1 at Hamana Lake, for studies HLJ1 (24-25/11/05), HLJ2 (31/11-1/12/05) and HLJ3 (21-22/12/05).

Table G.1 – Summary of field studies undertaken at Hamana Lake in 2005.
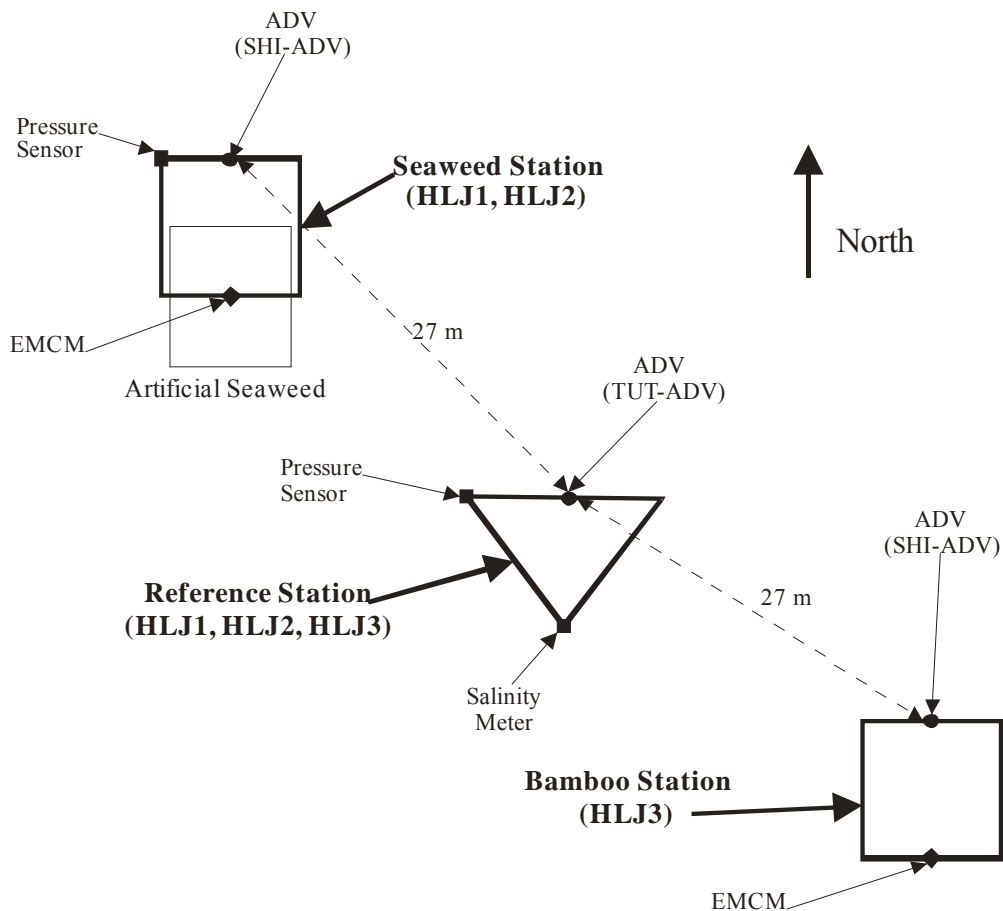
Field Study	HLJ1	HLJ2	HLJ3
Study Details Date	24-25 November 2005	30 Nov. – 1 Dec. 2005	21-22 December 2005
Study period	11:00 (24/11/05) to 15:00 (25/11/05)	14:00 (30/11/05) to 15:00 (1/12/05)	14:00 (21/12/05) to 20:00 (22/12/05)
Focus	Reference and Seaweed stations during neap tide	Reference and Seaweed stations during spring tide	Reference and Bamboo stations during spring tide
Remarks			Large increase in wind speed midway through study
Weather Air temperature (C)	12 [7.3 to 17.1]	9.2 [5.5 to 14.5]	3.6 [-0.9 to 8.8]
Wind speed (m/s)	4.0 [1.2 to 6.5]	4.2 [1.0 to 6.0]	6.3 [1.3 to 11.1]
Predominant wind direction	Westerly	Westerly	Westerly
Tidal range (Site 1) (m)	0.45*	0.7*	0.6*
Acoustic Doppler Velocimetry Equipment type	Nortek Vector ADV	Nortek Vector ADV	Nortek Vector ADV
V_{range} (m/s)	0.3	0.3	0.3
f_{scan} (Hz)	32	32	32
Sampling volume location	Site 1 reference station, 0.25 m above bed	Site 1 reference station, 0.25 m above bed	Site 1 reference station, 0.25 m above bed
Physio-Chemistry Sampling Equipment type	Alec Electronics compact-CT meter	Alec Electronics compact-CT meter	Alec Electronics compact-CT meter
f_{scan} (Hz)	1	1	1
Water temperature (C)	15.5 [13.7 to 18.2]	15.0 [12.5 to 16.9]	7.7 [5.0 to 10.1]
Conductivity (mS/cm)	41.1 [38.6 to 45.3]	37.3 [33.9 to 39.7]	34.3 [31.6 to 36.7]

Note: *: maximum tidal range observations including wind wave effects; []: extreme values in square brackets; V_{range} : ADV velocity range; f_{scan} : sampling frequency.

G.2.1 Instrumentation

The same instruments and experimental setup was used for each field trip conducted at the Site 1 reference station, Hamana Lake (Table G.1). Turbulence data were collected

continuously at 32 Hz throughout the investigation period. An Alec Electronics compact-TD collected the water depth and temperature data, while an Alec Electronics compact-CT meter collected the water temperature and conductivity data at the reference station. Both probes logged continuously at 1 Hz for all three field studies. The compact–CT and compact-TD probes were located next to the bed as shown in Figure G.4. All the instruments used were synchronised from a single laptop. Table G.2 outlines the accuracy of the equipment used during the studies HLJ1, HLJ2 and HLJ3.

Table G.2 – Accuracy of instrumentation used during field studies at Hamana Lake.

Instrumentation	Parameter	Accuracy
Nortek Vector ADV	Velocity (m/s)	1 %
	Pressure (dBar)	0.25 %
	Water temperature (C)	0.1 C
Alec Electronics compact-TD Temp./Depth Sensor	Depth (mH$_2$O)	0.3 %
	Water temperature (C)	0.05 C
Alec Electronics compact-CT Cond./Temp. sensor	Conductivity (mS/cm)	0.05 mS/cm
	Water temperature (C)	0.05 C

G.2.2   Practical experiences

Despite the careful preparation for the field studies HLJ1, HLJ2 and HLJ3, several minors problems were encountered during these field investigations. For example, the isolated location of Site 1 in Hamana Lake did not allow the monitoring of the area for large disturbances to the ADV signal (e.g. navigation or human activity).

G.2.2.1 *Interference to the ADV compass*

After the field studies HLJ1, HLJ2 and HLJ3 were performed, it was determined that the metal frames influenced the compass bearings of the ADV. This was confirmed by Alec Electronics (Nortek distributor for Japan). Tests found that the distorted direction of the compass did not vary during the measurements. It should be emphasised that the distortion of the ADV compass did not influence the quality of the ADV signal but the direction of the horizontal velocity. The ADV data were corrected using the direction of the electromagnetic current meter (EMCM, Figure G.4) during periods of strong currents. The angles of correction (ADV-EMCM) are listed in Table G.3.

Table G.3 – Correction angles for ADV data (influence of metal frames on ADV compass). All angles shown are for ADV located at Site 1 reference station Hamana Lake.

Field study	Date	Correction angle (°)
HLJ1	24-25/11/05	+ 30.00
HLJ2	31/11-1/12/05	+ 60.46
HLJ3	21-22/12/05	+ 63.85

G.2.2.2 *Distortion of vertical velocity component*

With the ADV system, some possible problems were encountered with the vertical velocity component (Aoki (2006) personal communication). It is believed that the ADV emitter, stem and body created some form of wake which adversely affected the vertical velocity. Similar problems were discussed in earlier studies (e.g. Chanson (2003)). Since the probe was mounted vertically with a down-looking head and the vertical velocities were small, the effects on the horizontal velocity were deemed negligible.

G.2.3 Post-processing of ADV data

All ADV velocity data were post-processed using the technique described in Chanson et al. (2005b). The post-processing must be undertaken to ensure the quality of the data set. Corrupted data are inherent to the ADV metrology, and are predominantly caused by poor signal quality (low correlation and low signal to noise ratio) and Doppler noise within the measured signal. Chanson et al. (2005b) found that in natural systems the ADV data could be corrupted by large disturbances such as navigation or fauna activity near the ADV. For the investigations described here a simplified post-processing technique was used for all ADV data sets. Site 1 was left unmanned during the field investigations and a manual log of any disturbances was not kept. The ADV data were post-processed as:

1) – Velocity signal check:

Data points with low-correlation (COR < 60 %); low signal to noise ratio (SNR < 5 dB); or communication errors were removed and replaced by the mean of the endpoints technique.

2) – Unknown event search:

Possible large disturbances were searched for within the turbulence data. Such large disturbances were flagged. Upon manual inspection, if an event appeared to be generated by foreign influences (e.g. navigation), then that section of data were removed and replaced. No large disturbances were found in the data sets of the field studies HLJ1, HLJ2 or HLJ3.

3) – Small disturbance detection (de-spiking):

The phase-space thresholding method was used to find small disturbances generated by "spike" events and Doppler noise. Any data point determined to be erroneous was replaced using the mean of the endpoints technique. The phase-space thresholding technique was performed on the high-pass filtered velocity data of each component using a low-pass/high-pass filtering threshold (0.02 Hz). A sensitivity analysis showed that the filtering threshold used at Eprapah Creek of 0.1 Hz (Trevethan et al. (2006)) was not the optimum value for Hamana Lake. At Site 1 Hamana Lake the optimum value of the low-pass/high-pass filtering threshold was 0.02 Hz and was used for the studies HLJ1, HLJ2 and HLJ3.

G.3   WAVE-TURBULENCE SEPARATION TECHNIQUE

For the studies undertaken at Hamana Lake wind waves were observed. Wind waves interacted with the current induced turbulence changing the turbulence characteristics under the surface (Benilov and Filyushkin (1970), Thais and Magnaudet (1996)). Previous studies (e.g. Benilov and Filyushkin (1970), Thais and Magnaudet (1995) and Trowbridge (1998)) developed techniques for separating the current induced turbulence data from the wave induced turbulence data. A simple method derived from the linear filtration method (Benilov and Filyushkin (1970)) was used. The linear filtration method required that the fluctuations and water level and a turbulent property (e.g. velocity) be sampled at the same frequency. A Nortek Vector 3D-ADV collected the variations in water level above the sensor at the same frequency as the instantaneous velocity. Therefore, the linear filtration method could be applied to the data to separate the current induced data from the wave induced data.

The first step was the generation of water level spectrum and the spectra of the three velocity components. These spectra were visually inspected to determine the characteristic frequencies for which the velocity and water level spectra were correlated. The wave induced frequency band was selected such that the water level spectra contained more than 3 % of the energy of the dominant wave period.

G.4   FIELD OBSERVATIONS: TURBULENCE PROPERTIES

G.4.1   Statistical moments of velocity data

The time-averaged streamwise velocity $\overline{V_x}$ data showed that the maximum flood and ebb velocities occurred mid tide. Figure G.5 shows the variation of time-averaged streamwise velocity (left vertical axis) and water depth (right vertical axis) as functions of time since midnight for the field trips HLJ1 and HLJ2. In Figure G.5 the time-averaged streamwise

velocity flood and ebb tide maxima occurred mid tide under neap (Figure G.5A) and spring (Figure G.5B) tidal conditions. A similar tidal response of streamwise velocity was observed by van der Ham et al. (2001) in a large shallow semi-enclosed bay in the Netherlands. During the field studies HLJ2 and HLJ3 (spring tidal conditions), the time-averaged streamwise (North/South) velocity maxima were larger during the ebb tides than during the flood tides. Under neap tidal conditions (study HLJ1) the streamwise flood and ebb velocity maxima were about the same. This seemed to indicate that a different response to spring and neap tidal forcing was observed at Site 1.
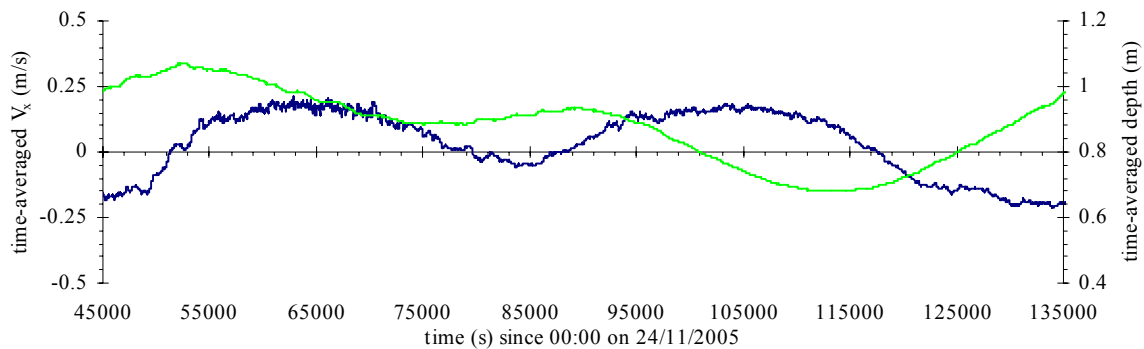
(A) Data collected under neap tidal conditions for study HLJ1 (24-25/11/05).
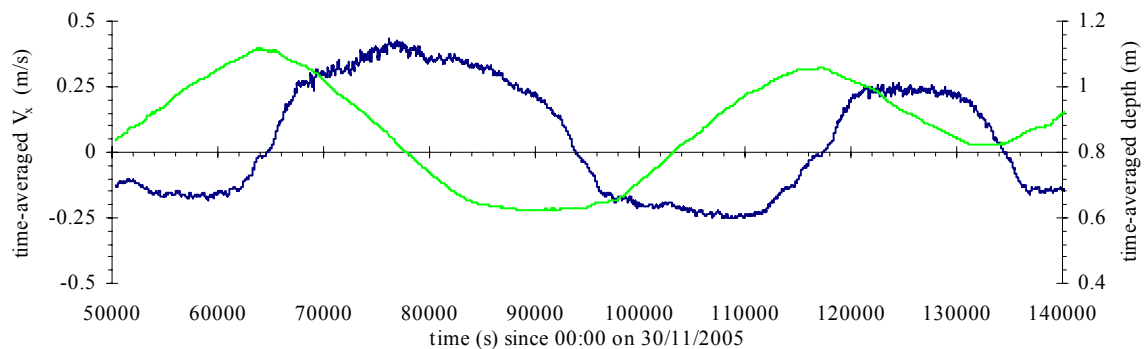
(B) Data collected under spring tidal conditions for study HLJ2 (30/11-1/12/05).

Figure G.5 – Time-averaged streamwise velocity $\overline{V_x}$ (positive downstream) and water depth as functions of time. Data collected 0.25 m above bed at Site 1 for studies HLJ1 and HLJ2. Velocity and water depth averaged over 5,000 data points every 10 s along entire data set. Legend: — time-averaged streamwise velocity (m/s); — water depth (m).

The magnitude and scatter of the time-averaged transverse velocity $\overline{V_y}$ (East/West) were larger during the flood tide than during the ebb tide for all three field studies (Figure G.6A). This is illustrated in Figure G.6A, which shows the time-averaged transverse velocity (positive to East) as a function of the time-averaged streamwise velocity (positive downstream to South) for the field studies HLJ1, HLJ2 and HLJ3. The increased magnitude

and variation of the time-averaged transverse velocity during the flood tide was possibly related to the bathymetry about Site 1.

During the ebb tide the time-averaged transverse velocity direction was predominantly towards the West for the neap tide conditions (study HLJ1), and towards the East under spring tidal conditions (studies HLJ2 and HLJ3) (Figure G.6A). This difference in transverse velocity direction was possibly related to the different flow dynamics at Site 1 between the spring and neap tidal forcing. However, caution is required as this difference in transverse velocity directions could result from the interference between the ADV compass and the mounting frame, and/or the subsequent direction adjustment undertaken (Section G.2.2.1).
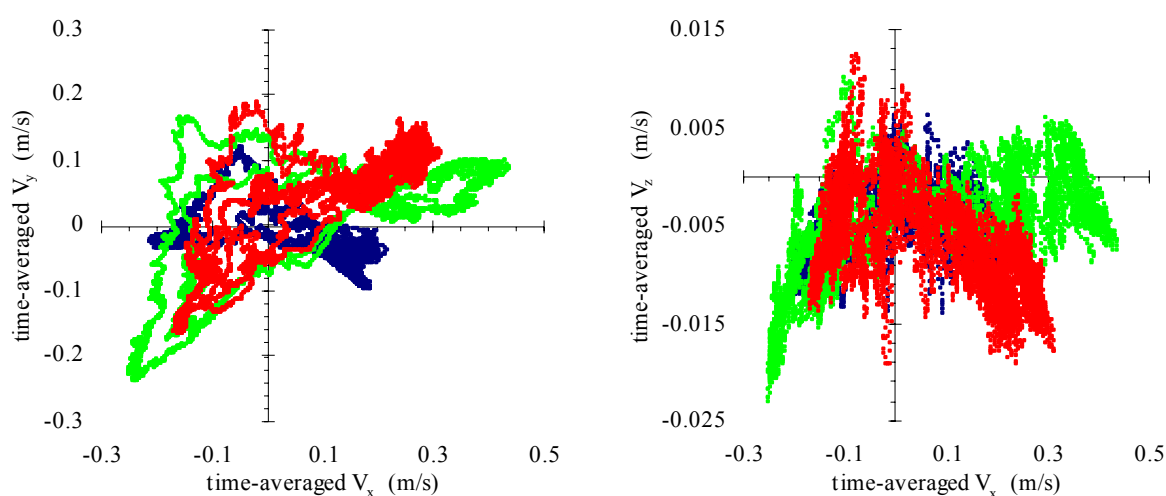
(A) $\overline{V_y}$ data (positive to East).   (B) $\overline{V_z}$ data (positive upwards).

Figure G.6 – Time-averaged transverse $\overline{V_y}$ and vertical $\overline{V_z}$ velocities as functions of time-averaged streamwise velocity (positive downstream). Data collected at 0.25 m above bed at Site 1 for studies HLJ1, HLJ2 and HLJ3. Velocity data averaged over 5,000 data points every 10 s along entire data set for all three studies.

Legend: [•] data for study HLJ1; [•] data for study HLJ2; [•] data for study HLJ3.

The time-averaged vertical velocities were negative (towards the bed) during the flood tide for the field studies HLJ1, HLJ2 and HLJ3. Figure G.6B shows the time-averaged vertical velocity (positive upwards) as a function of the time-averaged streamwise velocity (positive downstream to South). In Figure G.6B the magnitude of negative time-averaged vertical velocity increased with the magnitude of the negative (flood) streamwise velocity. The time-averaged vertical velocities were approximately zero for the remainder of each tidal cycle of the studies HLJ1 and HLJ2. During the field study HLJ3 this was not the case, with the

vertical velocities during the ebb tide being predominantly negative. This difference in $\overline{V_z}$ was possibly related to the increased wind speed observed during the field trip HLJ3. However, it must be stressed that there were some suspicion about the quality of the vertical velocity data (Section G.2.2.2).

The standard deviations of velocity represent the magnitude of velocity fluctuations about a time-averaged mean. It is related to the magnitude of turbulent velocity fluctuations. For the field works HLJ1, HLJ2 and HLJ3 the standard deviations of all velocity components at Site 1 showed no discernible trend during the tidal cycles. Figure G.7 shows the standard deviations of the streamwise v_x' and transverse v_y' velocities as functions of streamwise velocity (positive downstream to South). In Figure G.7A the scatter of the standard deviation data were slightly larger for the field studies HLJ3 and HLJ1 than during the field trip HLJ2.
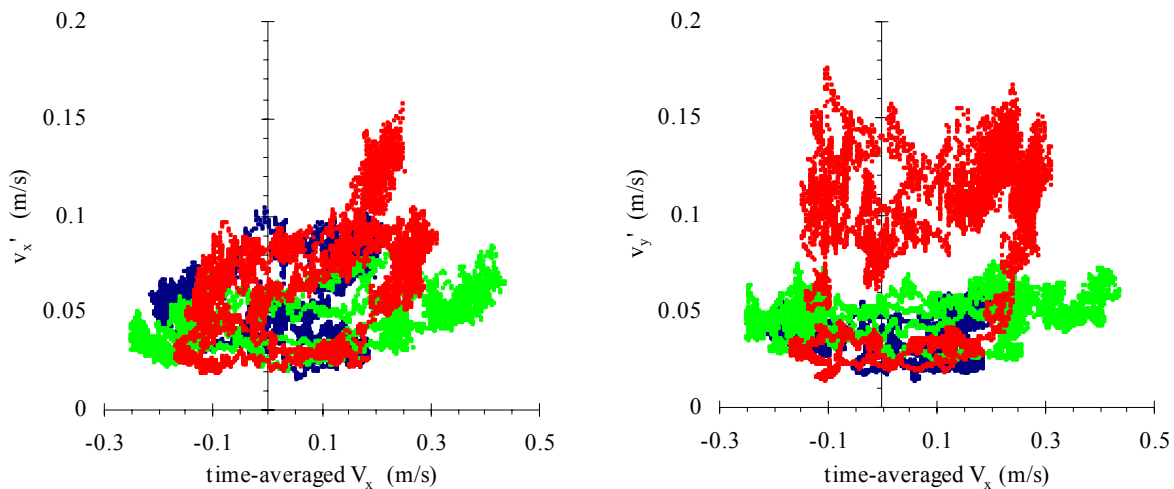
(A) v_x' data.
(B) v_y' data.

Figure G.7 – Standard deviations of streamwise v_x' and transverse v_y' velocities as functions of time-averaged streamwise velocity (positive to South). Data collected 0.25 m above bed at Site 1 for studies HLJ1, HLJ2 and HLJ3. Standard deviations calculated for 5,000 data points every 10 s along entire data set for all three field studies.

Legend: [•] data for study HLJ1; [•] data for study HLJ2; [•] data for study HLJ3.

The scatter of standard deviations for transverse v_y' and vertical v_z' velocities were similar for the studies HLJ1 and HLJ2. In the field study HLJ3 the scatter of standard deviations for transverse and vertical velocities were approximately twice as large as those of the field trips HLJ1 and HLJ2 (e.g. Figure G.7B). This increased magnitude of standard deviations during the study HLJ3 seemed related to the increased wind speed observed. Previous studies

indicated that the effect of the wind waves on turbulence could be greatest in the direction of the wind (e.g. Bowden and White (1966)). During the field studies HLJ1, HLJ2 and HLJ3 the predominant wind direction was Westerly. The transverse velocity component would therefore be expected to be most affected. In Figure G.7B the magnitude of standard deviations for transverse velocity from the study HLJ3 were twice those of the field studies HLJ1 and HLJ2.

For the field trips HLJ1, HLJ2 and HLJ3, 91 % (81,835 samples) of the 89,652 velocity data samples were within reasonable Gaussian limits. That is, the skewness (Sk) and kurtosis (Ku) values were considered reasonably Gaussian when $|Sk| < 4*\sqrt{15/N}$ and $|Ku| < 4*\sqrt{96/N}$, where N is the number of data points per sample (Press et al. (1992)). No easily discernible tidal patterns were observed in the skewness and kurtosis values of all velocity components for the field studies HLJ1, HLJ2 and HLJ3.

G.4.2   Turbulence intensity ratios

The horizontal and vertical turbulence intensity ratios are v_y'/v_x' and v_z'/v_x' respectively. Measurements at Site 1 showed no easily discernible trends over the tidal cycles for the studies HLJ1, HLJ2 and HLJ3. In all three studies the vertical turbulence intensity ratios were the largest around low tide. Median vertical turbulence intensity ratio values for the field studies HLJ1, HLJ2 and HLJ3 were about v_z'/v_x' = 0.45 to 0.65. The horizontal turbulence intensity ratios were approximately twice as large as the vertical turbulence intensity ratios, implying some form of turbulence anisotropy. Median values of the horizontal turbulence intensity ratios were within the range v_y'/v_x' = 0.7 to 1.3 for all three field trips. That is, the turbulence fluctuations in streamwise and transverse directions were of similar magnitude.

G.4.3   Statistical moments of tangential Reynolds stresses

The time-averaged tangential Reynolds stress $\rho \overline{v_x v_z}$ varied with the tides during the studies HLJ1, HLJ2 and HLJ3. Figure G.8A shows the time-averaged Reynolds stress $\rho \overline{v_x v_z}$ as a function of time-averaged streamwise velocity (positive downstream to South). In Figure G.8A the time-averaged Reynolds stress was predominantly positive during the flood tide and negative during the ebb tide. These findings were consistent with the earlier studies of Osonphasop (1983), Kawanisi and Yokosi (1994) and Trevethan et al. (2006) in tidal channels and van der Ham et al. (2001) in a shallow semi-enclosed tidal bay.
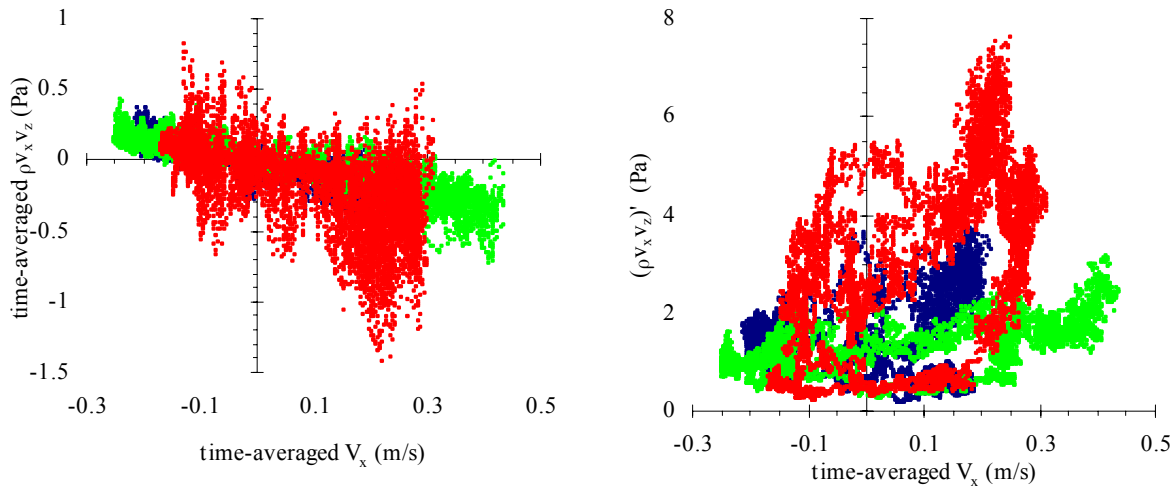
(A) $\rho\overline{v_x v_z}$.

(B) $(\rho v_x v_z)'$.

Figure G.8 – Time-average $\rho\overline{v_x v_z}$ and standard deviations $(\rho v_x v_z)'$ of Reynolds stress $\rho v_x v_z$ as functions of time-averaged streamwise velocity (positive downstream). Data collected 0.25 m above bed at Site 1 for studies HLJ1, HLJ2 and HLJ3. Values calculated for 5,000 data points every 10 s along entire data set for all three field studies.
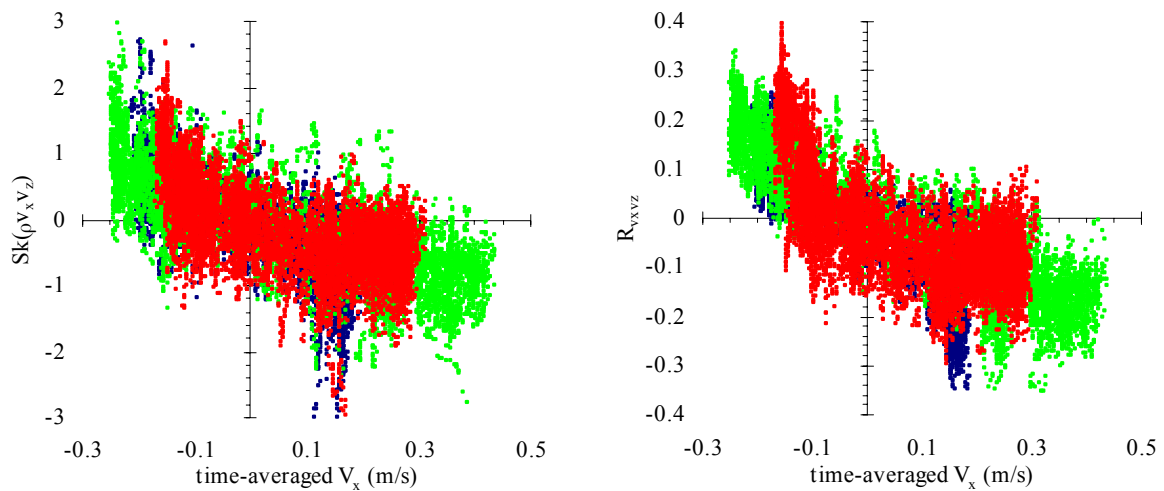
Legend: [•] data for study HLJ1; [•] data for study HLJ2; [•] data for study HLJ3.

Tidal patterns for the time-averaged Reynolds stresses $\rho\overline{v_x v_y}$ and $\rho\overline{v_y v_z}$ were not easily discernible. For the field study HLJ1 the possible tidal trends of time-averaged Reynolds stresses $\rho\overline{v_x v_y}$ and $\rho\overline{v_y v_z}$ seemed different to those of the field trips HLJ2 and HLJ3. This seemed related to the different tidal patterns of transverse velocity discussed in Section G.4.1. The magnitude of time-averaged Reynolds stress $\rho\overline{v_x v_y}$ was 2 to 6 times larger than that of time-averaged Reynolds stresses $\rho\overline{v_x v_z}$ and $\rho\overline{v_y v_z}$ for the field studies HLJ1, HLJ2 and HLJ3. The magnitude of all time-averaged tangential Reynolds stresses were similar under neap (study HLJ1) and spring (study HLJ2) tidal conditions. The magnitudes of all tangential Reynolds stresses for the field trip HLJ3 were larger than those observed in the field studies HLJ1 and HLJ2. This seemed related to the strong wind speed and wind wave climate of the field study HLJ3.

The standard deviations of all tangential Reynolds stresses showed no discernible tidal trend for the studies HLJ1, HLJ2 and HLJ3. Scatter for the standard deviations of all tangential Reynolds stresses were similar during neap and spring tidal conditions (studies HLJ1 and HLJ2). The standard deviations of all tangential Reynolds stresses were about 2 to 5 times larger during the study HLJ3 than those of the field studies HLJ1 and HLJ2 (Figure G.8B).

Figure G.8B shows the standard deviations of the tangential Reynolds stress $(\rho v_x v_z)'$ as functions of time-averaged streamwise velocity (positive downstream to South).

The skewness $Sk(\rho v_x v_z)$ of Reynolds stress $\rho v_x v_z$ varied with the tide during the field studies HLJ1, HLJ2 and HLJ3. Figure G.9A shows the skewness $Sk(\rho v_x v_z)$ as a function of time-averaged streamwise velocity (positive downstream to South). In Figure G.9A the skewness $Sk(\rho v_x v_z)$ was predominantly positive during the flood tide and negative during the ebb tide. Skewness values of the Reynolds stresses $\rho v_x v_y$ and $\rho v_y v_z$ showed no discernible tidal pattern for the studies HLJ1, HLJ2 and HLJ3. The kurtosis values of all tangential Reynolds stresses showed no discernible tidal trends.

(A) $Sk(\rho v_x v_z)$.   (B) R_{vxvz}.

Figure G.9 – Skewness $Sk(\rho v_x v_z)$ of Reynolds stress $\rho v_x v_z$ and correlation coefficient R_{vxvz} as functions of time-averaged streamwise velocity (positive to South). Data collected 0.25 m above bed at Site 1 for studies HLJ1, HLJ2 and HLJ3. Values calculated for 5,000 data points every 10 s along entire data set for all three field studies.

Legend: [•] data for study HLJ1; [•] data for study HLJ2; [•] data for study HLJ3.

For the field studies HLJ1, HLJ2 and HLJ3, approximately 78 % (70,371 samples) of the 89,652 tangential Reynolds stress samples were outside reasonable Gaussian limits for both skewness (Sk) and kurtosis (Ku). The reasonable Gaussian limits of skewness and kurtosis are defined as $|Sk| < 4*\sqrt{15/N}$ and $|Ku| < 4*\sqrt{96/N}$, where N is the number of data points per sample. Only 118 of the 89,652 tangential Reynolds stress samples of the studies HLJ1, HLJ2 and HLJ3 had both skewness and kurtosis values within reasonable Gaussian limits.

This indicated that the tangential Reynolds stress data could be considered non-Gaussian in terms of both skewness and kurtosis.

The kurtosis values for all tangential Reynolds stresses (studies HLJ1, HLJ2 and HLJ3) were between $3 < Ku < 15$, with a median value of approximately 5. Skewness values of all tangential Reynolds stresses during the studies HLJ1, HLJ2 and HLJ3 were $-2 < Sk < 2$. The kurtosis and skewness values of tangential Reynolds stresses were of the same magnitude as those observed by Osonphasop (1983), Shiono and West (1987) and Trevethan et al. (2006) in tidal channels.

G.4.4 Correlation coefficients of Reynolds stress

The correlation coefficient of tangential Reynolds stress is a dimensionless Reynolds stress, defined as: $R_{vxvz} = \overline{v'_x v'_z} / (v'_x v'_z)$. Figure G.9B shows the correlation coefficient of Reynolds stress R_{vxvz} as a function of time-averaged streamwise velocity (positive downstream to South). In Figure G.9B the dimensionless Reynolds stress R_{vxvz} was predominantly positive during the flood tide and negative during the ebb tide. A similar trend was observed by Kawanisi and Yokosi (1993, 1994) and Trevethan et al. (2006) in estuarine tidal channels. The correlation coefficients of Reynolds stresses R_{vxvy} and R_{vyvz} showed no easily discernible tidal trend for the studies HLJ1, HLJ2 and HLJ3.

G.4.5 Turbulence time scales

G.4.5.1 Integral time scales

An integral time scale is a measure of the longest connection in the turbulent velocity fluctuations. For the field investigations HLJ1, HLJ2 and HLJ3 the integral time scales of all velocity components showed no easily discernible tidal patterns. Table G.4 presents the median values of integral time scales observed for the studies HLJ1, HLJ2 and HLJ3. In Table G.4 the median values of all integral time scales were between 0.2 and 0.3 s, while all integral time scales were within the range 0.2 to 0.5 s. These near-constant integral time scales might be related to the interaction of the wind waves with the turbulence within the sampling volume. In laboratory experiments Thais and Magnaudet (1996) determined that the interaction of waves and turbulence imposed a constant time scale on the energy transfers over a significant frequency range. This imposed constant time scale was related to some wave induced strain.

The dimensionless transverse and vertical integral time scales (T_{Ey}/T_{Ex} and T_{Ez}/T_{Ex}) were both approximately equal to 1 for the field studies HLJ1, HLJ2 and HLJ3. This also seemed to indicate that the wind waves imposed a constant time scale on the eddy size at Site 1.

Table G.4 – Median values of integral time scales collected at Site 1 Hamana Lake.

Field study	T_{Ex} (s)	T_{Ey} (s)	T_{Ez} (s)
HLJ1	0.27	0.26	0.24
HLJ2	0.28	0.23	0.22
HLJ3	0.29	0.27	0.24

G.4.5.2 *Dissipation time scales*

The dissipation time scale of a velocity component represents the most rapid changes in the fluctuations of that component. Dissipation time scales of all velocity components showed no easily discernible trend with the tides of the field studies HLJ1, HLJ2 and HLJ3. Table G.5 presents the median values of dissipation time scales for the field studies HLJ1, HLJ2 and HLJ3. For the field studies HLJ1 and HLJ2 the median values of horizontal dissipation time scales τ_{Ex} and τ_{Ey} were between 0.03 to 0.07 s. However, under the large wind speeds observed for the study HLJ3 the median values of the dissipation time scales were between 0.1 to 0.2 s. These dissipation time scales were of the same order of magnitude as the integral time scales observed for the field studies HLJ1, HLJ2 and HLJ3. This conceivably indicated that the wind waves imposed a constant time scale on the energy dissipation cascade at Site 1 Hamana Lake for the study HLJ3.

For the field studies performed at Site 1 Hamana Lake all dissipation time scales were at least an order of magnitude larger than those observed by Trevethan et al. (2006) in a small subtropical estuary where no wind waves were observed. This possibly indicated that the wind waves were responsible for the larger dissipation time scales observed at Site 1 Hamana Lake. In the field trips HLJ1, HLJ2 and HLJ3 the median values of dimensionless transverse and vertical dissipation time scales (τ_{Ey}/τ_{Ex} and τ_{Ez}/τ_{Ex}) were between 0.5 to 1.7 and 1.9 to 3.8 respectively.

Table G.5 – Median values of dissipation time scales collected at Site 1 Hamana Lake.

Field study	τ_{Ex} (s)	τ_{Ey} (s)	τ_{Ez} (s)
HLJ1	0.068	0.047	0.192
HLJ2	0.030	0.055	0.133
HLJ3	0.114	0.192	0.196

G.5   COMPARISON OF GROSS AND CURRENT INDUCED TURBULENCE DATA

The analysis of the post-processed gross velocity data measured at Site 1 Hamana Lake (studies HLJ1, HLJ2 and HLJ3) seemed to indicate that the wind waves were influencing the observed turbulence properties. Therefore, the wave-turbulence separation technique (Section G.3) was applied to the post-processed velocity data of the studies HLJ1, HLJ2 and HLJ3. The wave-turbulence separation technique provided the wave induced and current induced data sets. In this section some turbulence properties of the current induced data are compared to those of the gross velocity data. This section highlights some tidal patterns in the current induced turbulence data that were not easily discernible in the gross data sets. It also compares the median values of some current induced turbulence properties with those of the turbulence properties of the gross data set. Note that all current induced data are shown using the superscript T (e.g. $V_x{}^T$).

For the field studies HLJ1, HLJ2 and HLJ3 the tidal trends for time-averaged velocity data, Reynolds stress $\rho \overline{v_x v_z}$, skewness $Sk(\rho v_x v_z)$ and correlation coefficient R_{vxvz} of the current induced data were similar to those of the gross data set (Section G.4). However, the scatter of these properties varied slightly between the current induced and gross data sets.

G.5.1   Intensity of turbulent velocity fluctuations

The standard deviations of velocity represent the intensity of turbulence velocity fluctuations in the instantaneous velocity data. For the field studies HLJ1, HLJ2 and HLJ3 the standard deviations of all velocity components of the current induced data seemed to vary with the tides (Figure G.10A). This was not the case for the standard deviations of the gross velocity data, in which no easily discernible patterns were observed (Section G.4.1). Figure G.10 shows the standard deviations of transverse velocity for the current induced and gross data sets as functions of time-averaged streamwise velocity (positive to South). Note the different vertical scales in Figures G.10A and G.10B. In Figure G.10A the standard deviations of current induced transverse velocity increased with the increased magnitude of streamwise velocity. A similar pattern was observed by Trevethan et al. (2006) in a small subtropical estuary in Southeast Australia.

Table G.6 presents the median values of the standard deviations for all velocity components of the gross and current induced data sets. In Table G.6 the standard deviations of all velocity components of the gross data set were 2 to 5 times larger than the velocity standard deviations of the current induced data. The largest difference between the velocity standard deviations of the gross and current induced data sets was for the study HLJ3. This increased difference

between the intensity of turbulent fluctuations for the gross and current induced data seemed related to the increased wind speed observed at Hamana Lake for the study HLJ3 (Table G.1).
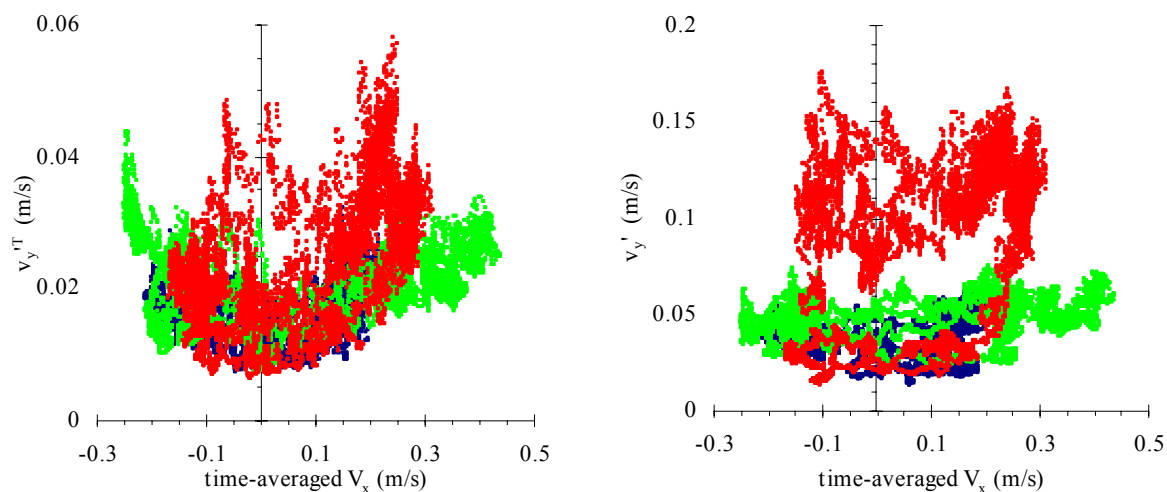
(A) $v_y^{'T}$ for current induced data. (B) $v_y^{'}$ for gross data.

Figure G.10 – Standard deviations of transverse velocity $v_y^{'T}$ and $v_y^{'}$ as functions of time-averaged streamwise velocity (positive to South). Data collected 0.25 m above bed at Site 1 for studies HLJ1, HLJ2 and HLJ3. Values calculated for 5,000 data points every 10 s along entire data set for current induced and gross data.

Legend: [•] data for study HLJ1; [•] data for study HLJ2; [•] data for study HLJ3.

Table G.6 – Median values of velocity standard deviations from gross and current induced data sets.

Field study	Gross data			Current induced data		
	$v_x^{'}$	$v_y^{'}$	$v_z^{'}$	$v_x^{'T}$	$v_y^{'T}$	$v_z^{'T}$
	(m/s)	(m/s)	(m/s)	(m/s)	(m/s)	(m/s)
HLJ1	0.050	0.037	0.025	0.019	0.015	0.010
HLJ2	0.044	0.047	0.047	0.024	0.021	0.014
HLJ3	0.065	0.095	0.095	0.022	0.023	0.013

G.5.2 Intensity of Reynolds stress fluctuations

The standard deviations of the tangential Reynolds stresses represent the intensity of fluctuations in that Reynolds stress. For the field studies HLJ1, HLJ2 and HLJ3 the standard deviations of the current induced tangential Reynolds stresses varied with the tides (Figure G.11A). Figure G.11 shows the standard deviations of Reynolds stress $\rho v_x v_y$ for the current induced and gross data sets as functions of the time-averaged streamwise velocity (positive

305

downstream to South). In Figure G.11A the standard deviations of the current induced Reynolds stress $(\rho v_x v_y)'^T$ increased with the increasing magnitude of streamwise velocity. A similar trend was observed by Trevethan et al. (2006) in a small estuary in Southeast Australia.
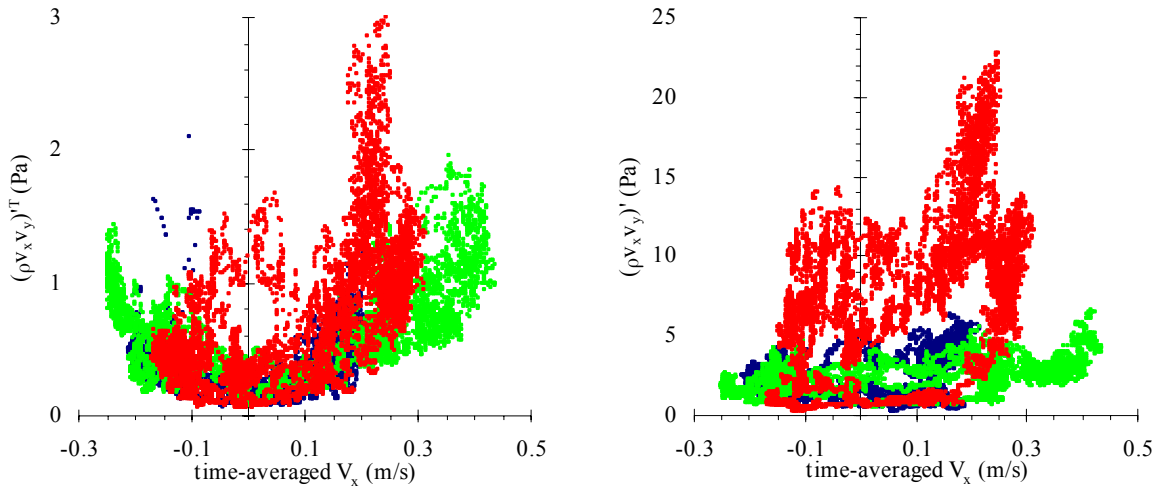
(A) $(\rho v_x v_y)'^T$ for current induced data.   (B) $(\rho v_x v_y)'$ for gross data.

Figure G.11 – Standard deviations $(\rho v_x v_y)'$ and $(\rho v_x v_y)'^T$ of Reynolds stress $\rho v_x v_y$ as functions of time-averaged streamwise velocity (positive to South). Data collected 0.25 m above bed at Site 1 for studies HLJ1, HLJ2 and HLJ3. Values calculated for 5,000 data points every 10 s along entire data set for current induced and gross data.
Legend: [•] data for study HLJ1; [•] data for study HLJ2; [•] data for study HLJ3.

Table G.7 presents the median values for standard deviations of all tangential Reynolds stresses for the current induced and gross data sets from the studies HLJ1, HLJ2 and HLJ3. The median standard deviations of the gross Reynolds stresses were up to an order of magnitude larger than those of the current induced Reynolds stresses. This large difference in the Reynolds stress fluctuation intensities between the current induced and gross data sets highlights the impact that wind waves on the turbulent mixing properties under the surface.

Table G.7 – Median values for standard deviations of Reynolds stresses from gross and current induced data sets.

Field study	Gross data			Current induced data		
	$(\rho v_x v_y)'$ (Pa)	$(\rho v_x v_z)'$ (Pa)	$(\rho v_y v_z)'$ (Pa)	$(\rho v_x v_y)'^T$ (Pa)	$(\rho v_x v_z)'^T$ (Pa)	$(\rho v_y v_z)'^T$ (Pa)
HLJ1	1.26	1.73	0.92	0.20	0.32	0.16
HLJ2	1.28	2.27	1.33	0.36	0.57	0.31
HLJ3	2.67	6.56	3.99	0.31	0.52	0.31

G.5.3   Turbulence time scales

G.5.3.1   *Integral time scales*

An integral time scale is a measure of the longest connection in the turbulent velocity fluctuations. Table G.8 presents the median values of the integral time scales for the current induced and gross velocity data collected at Site 1 Hamana Lake. For the studies HLJ1, HLJ2 and HLJ3 the median values of current induced velocity data were at least twice those of the gross data. The current induced integral time scales ranged between about 0.02 and 2 s, which were larger than the range of the integral time scales of the gross data (Figure G.12). Figure G.12 shows the integral time scales of streamwise velocity for the current induced and gross data of the field studies HLJ1, HLJ2 and HLJ3. In Figure G.12A the scatter of current induced integral time scales T_{Ex}^T spanned several orders of magnitude more than the gross integral time scales (Figure G.12B). This seemed to further indicate that the wind waves were constraining the size of the integral time scales below the surface at Site 1 Hamana Lake.

Table G.8 – Median values of integral time scales for gross and current induced data sets.

Field study	Gross data			Current induced data		
	T_{Ex} (s)	T_{Ey} (s)	T_{Ez} (s)	T_{Ex}^T (s)	T_{Ey}^T (s)	T_{Ez}^T (s)
HLJ1	0.27	0.26	0.24	0.74	0.56	0.60
HLJ2	0.28	0.23	0.22	0.76	0.59	0.42
HLJ3	0.29	0.27	0.24	0.94	0.87	0.62
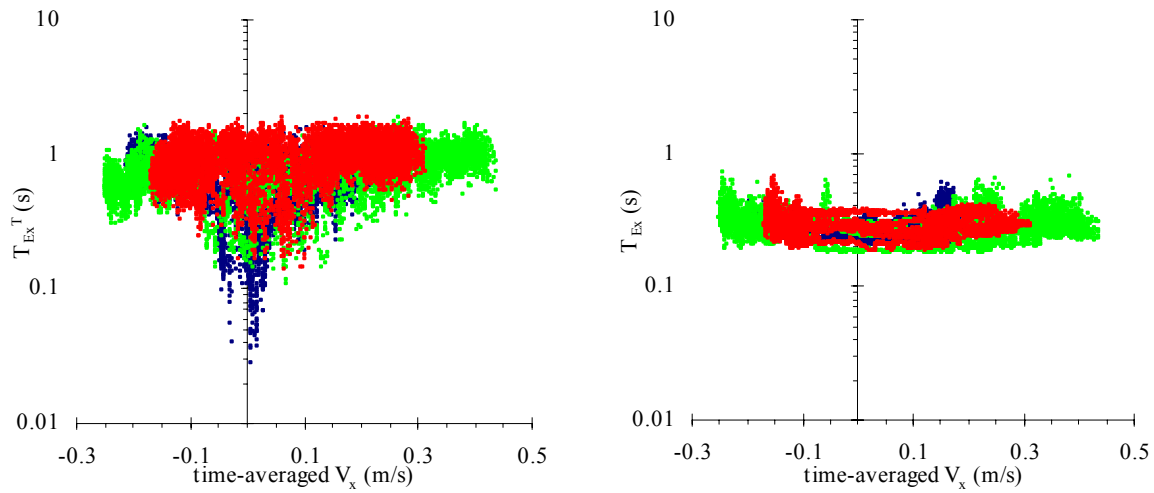
(A) $T_{Ex}{}^{T}$ for current induced data sets.   (B) T_{Ex} for gross data sets.

Figure G.12 – Streamwise integral time scales $T_{Ex}{}^{T}$ and T_{Ex} as functions of time-averaged streamwise velocity (positive to South). Data collected 0.25 m above bed at Site 1 for studies HLJ1, HLJ2 and HLJ3. Values calculated for 5,000 data points every 10 s along entire data set for current induced and gross data.

Legend: [•] data for study HLJ1; [•] data for study HLJ2; [•] data for study HLJ3.

G.5.3.2 *Dissipation time scales*

The dissipation time scale of a velocity component represents the most rapid changes in the fluctuations of that component. Table G.9 outlines the median values for dissipation time scales of the gross and current induced velocity data. The median values of all current induced dissipation time scales were approximately an order of magnitude smaller than those of the gross data. This seemed to indicate that the wind waves possibly had a significant impact on the turbulence energy dissipation cascade down to the eddy sizes represented by the dissipation time scales.

Table G.9 – Median values of dissipation time scales for gross and current induced data sets.

Field study	Gross data			Current induced data		
	τ_{Ex} (s)	τ_{Ey} (s)	τ_{Ez} (s)	$\tau_{Ex}{}^{T}$ (s)	$\tau_{Ey}{}^{T}$ (s)	$\tau_{Ez}{}^{T}$ (s)
HLJ1	0.068	0.047	0.192	0.004	0.006	0.058
HLJ2	0.030	0.055	0.133	0.007	0.011	0.055
HLJ3	0.114	0.192	0.196	0.006	0.007	0.053

308

The dissipation time scales of the horizontal velocities for the current induced data showed a slight tidal pattern (e.g. $\tau_{Ey}{}^{T}$ in Figure G.13A), which was not observed in the dissipation time scales of the gross velocity data (Figure G.13B). Figure G.13 shows the dissipation time scales of transverse velocity for the current induced and gross data sets of the studies HLJ1, HLJ2 and HLJ3. In Figure G.13A the dissipation time scales of the current induced transverse velocity data seemed to decrease about the slack tides ($V_x = 0$).
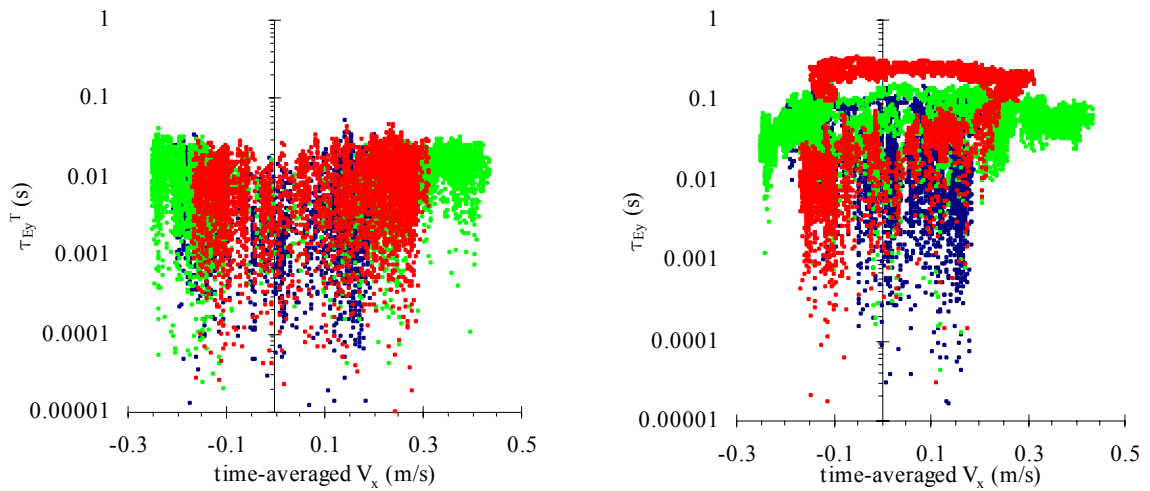
(A) $\tau_{Ey}{}^{T}$ for current induced data sets.

(B) τ_{Ey} for gross data sets.

Figure G.13 – Transverse dissipation time scales $\tau_{Ey}{}^{T}$ and τ_{Ey} as functions of time-averaged streamwise velocity (positive to South). Data collected 0.25 m above bed at Site 1 for studies HLJ1, HLJ2 and HLJ3. Values calculated for 5,000 data points every 10 s along entire data set for current induced and gross data.

Legend: [•] data for study HLJ1; [•] data for study HLJ2; [•] data for study HLJ3.

G.6   SUMMARY

For the field studies conducted at Site 1 Hamana Lake some tidal asymmetries of the streamwise and transverse velocities were observed. Under spring tidal forcing the maximum streamwise velocity of the ebb tide was larger than the flood tide. No tidal asymmetry of streamwise velocity was observed during neap tidal conditions. The time-averaged transverse velocity of the flood tide was larger than during the ebb tide in spring and neap tidal conditions. Different directions of the time-averaged transverse velocity during the ebb tide were observed for spring and neap tidal forcing.

At Hamana Lake, tidal trends were observed for time-averaged Reynolds stress $\rho\overline{v_x v_z}$; skewness of Reynolds stress $\rho v_x v_z$; and dimensionless Reynolds stress R_{vxvz}. These

turbulence properties seemed to be predominantly positive during the flood tides and negative during the ebb tides. Some tidal patterns were also observed in the standard deviations of all velocity components and tangential Reynolds stresses for the current induced data, but not the gross data. The standard deviations of the current induced data varied directly with the magnitude of the streamwise velocity. These tidal trends were similar to those observed by Trevethan et al. (2006) in a small estuary in Australia.

Wind waves were observed at Site 1 Hamana Lake throughout the field studies HLJ1, HLJ2 and HLJ3. These wind waves seemed to have had a substantial effect on the turbulence and mixing properties observed 0.25 m above the bed. The wind waves seemed to increase the intensity of the fluctuations in velocity and Reynolds stresses. This increased fluctuation intensity could have a significant impact on the mixing and sediment transport properties at Site 1 Hamana Lake.

The wind waves also seemed to influence the size of the eddies represented by the dissipation and integral time scales. For the field study HLJ3 with relatively high wind speeds, the median values of integral and dissipation time scales for all velocity components were approximately 0.2 s. This conceivably indicated that the wind waves were imposing a constant time scale on the turbulence energy cascade similar to that observed in the laboratory experiments of Thais and Magnaudet (1996).

These wind wave effects observed highlighted that careful attention must be paid to the collection of high frequency wind data close to the sampling location when conducting field studies on large open bodies of water such as Hamana Lake. High frequency wind data are required to fully understand the localised effect of the wind on and below the surface at the sampling location.

APPENDIX H — EFFECT OF WIND WAVES ON TURBULENCE DATA COLLECTED AT HAMANA LAKE (JAPAN)

H.1 PRESENTATION

Three field investigations collecting continuous high frequency turbulence data were undertaken at Hamana Lake, Japan in November and December 2005. Figure H.1 shows a picture of Hamana Lake, with the experimental site indicated. The insert in Figure H.1 shows the location of Hamana Lake within Japan. These investigations were designated the field studies HLJ1 (24-25/11/2005), HLJ2 (30/11-1/12/2005) and HLJ3 (21-22/12/2005).
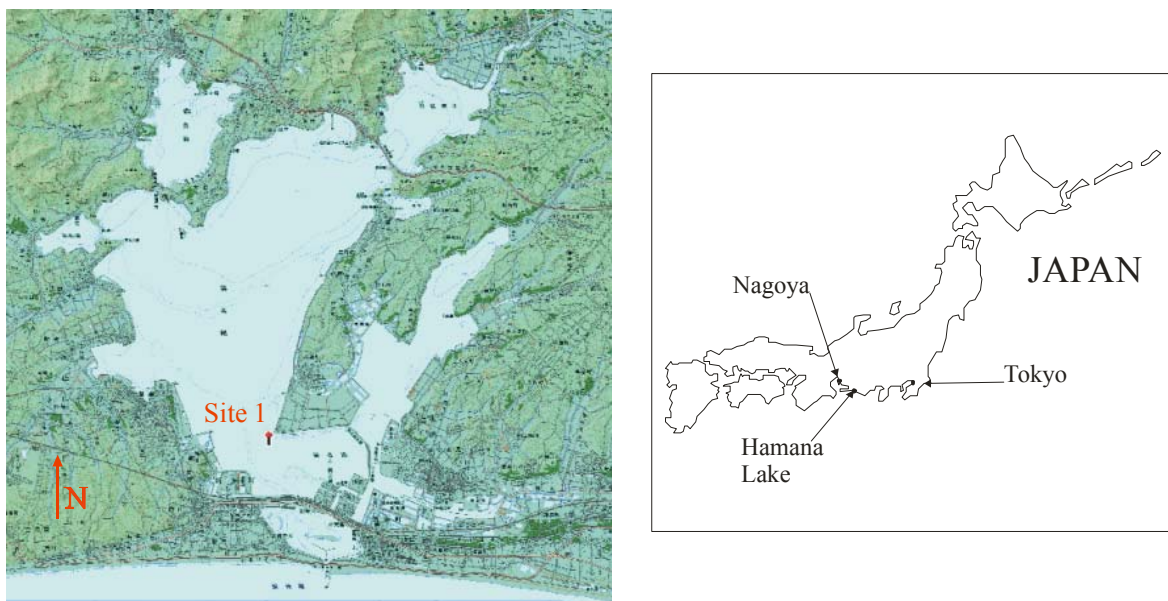
Figure H.1 – Picture of Hamana Lake, Japan (courtesy of S. Aoki). Insert shows location of Hamana Lake in Japan.

For all field studies a predominantly Westerly wind was recorded throughout the investigation period of each study, with occasional fluctuations towards the Northwest. The wind induced some wind waves. Figure H.2 shows a photograph of wind waves observed during the preparation of the study HLJ1 on 24/11/2005. Table H.1 shows the range of wind speeds recorded at the Hamamatsu weather station near Hamana Lake.

Figure H.2 – Photograph of wind waves observed at Site 1 Hamana Lake during installation for study HLJ1 on 24/11/05.

Table H.1 – Wind information recorded at Hamamatsu weather station near Hamana Lake for studies HLJ1, HLJ2 and HLJ3.

Field study	Date	Duration (hours)	Wind velocity range (m/s)	Average wind velocity (m/s)	Predominant wind direction
HLJ1	24-25/11/05	28	1.2 to 6.5	4.0	Westerly
HLJ2	30/11-1/12/05	25	1.0 to 6.0	4.2	Westerly
HLJ3	21-22/12/05	30	1.3 to 11.1	6.3	Westerly

H.1.1   Wave-turbulence separation technique

Wind waves interact with the current induced turbulence changing the turbulence characteristics under the surface (Benilov and Filyushkin (1970), Thais and Magnaudet (1996)). Previous studies (e.g. Benilov and Filyushkin (1970), Thais and Magnaudet (1995), and Trowbridge (1998)) developed techniques for separating the current induced turbulence data from the wave induced turbulence data. A simple method derived from the linear filtration method (Benilov and Filyushkin (1970)) was used. The linear filtration method required that the fluctuations and water level and a turbulent property (e.g. velocity) be sampled at the same frequency. In this study the Nortek Vector 3D-ADV measured the variations in water level above the sensor at the same frequency as the instantaneous velocity. Therefore, the linear filtration method could be applied to the data collected at Hamana Lake to separate the current induced data from the wave induced data.

The first step was the generation of water level spectrum and spectra of the three velocity components. These spectra were visually inspected to determine the characteristic frequencies for which the velocity and water level spectra were correlated. The wave induced frequency band was selected such that the water level spectra contained more than 3 % of the energy of the dominant wave period.

H.1.2   Notation

The data were separated using the wave-turbulence separation technique. The three forms of data used are described using the relationship:

$$V = V^T + V^W \tag{H.1}$$

where V = gross velocity data; V^T = current induced velocity data; and V^W = wave induced velocity data. These superscripts are used throughout this section to characterise each property.

H.2   CASE STUDY: FIELD STUDY HLJ3

This section discusses the effect of wind waves on the turbulence data collected at Site 1 for the study HLJ3 (21-22/12/2005). During the field study HLJ3 the wind velocity greatly increased midway through the study period. Figure H.3 shows the averaged wind speed as a function of time for the study HLJ3. The data were averaged hourly at the Hamamatsu weather station near Hamana Lake. In Figure H.3 the wind speed increased at 86,400 s since midnight on 21/12/05 (approximately 00:00 on 22/12/05) and remained greater than 6 m/s for the rest of the study.
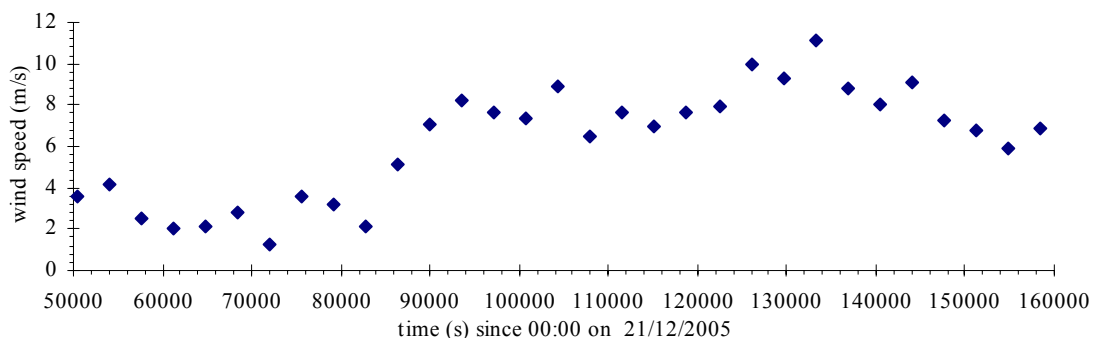
Figure H.3 – Averaged wind speed as a function of time since midnight on 21/12/05 for study HLJ3. Averaged wind speed recorded hourly at Hamamatsu weather station.

Two data segments are analysed here (sections A ands B, highlighted in Figure H.4). Figure H.4 shows the time-averaged water depth at Site 1 Hamana Lake as a function of time since

313

midnight on 21/12/05. In Figure H.4 and Table H.2, the tidal phase and conditions observed for the sections A and B were similar. For section A (t = 50,400 to 70,400 s) the wind conditions corresponded to a mean wind speed of 2.5 m/s. During section B (t = 138,200 to 158,200 s) the wind speed was significantly larger, having a mean wind speed of 7.3 m/s.

A comparison of the data in sections A and B provides some information on the effect of increased wind wave activity on the turbulence properties. Figure H.5 shows the water level spectra of both sections in the frequency domain. In Figure H.5 the peak wave energy of section B was approximately an order of magnitude larger than that of section A. The predominant wave frequencies of sections A and B differed, with the predominant wave periods being approximately 1.3 and 2.0 s respectively.
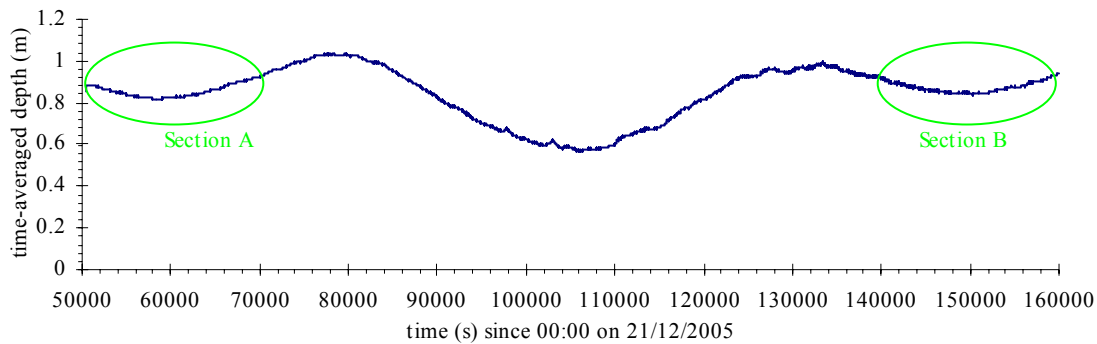
Figure H.4 – Time-averaged water depth at Site 1 Hamana Lake as a function of time since midnight on 21/12/05 (study HLJ3). Data sections A and B are highlighted.

Table H.2 – Summary of sections A and B.

Information	section A	section B
Time (s)	50,400 to 70,400	138,200 to 158,200
Tidal phase	Mid ebb to mid flood	Mid ebb to mid flood
Mean water level (m)	0.86	0.87
Tidal range (m)	0.12	0.10
Averaged wind speed (m/s)	2.5	7.3
Wind speed range (m/s)	2.0 to 4.2	6.0 to 9.1

Figure H.6 shows the time-averaged Reynolds stress $\rho \overline{v_x v_z}$ of the gross data of sections A and B as functions of time. In Figure H.6 the time-averaged Reynolds stress $\rho \overline{v_x v_z}$ was approximately an order of magnitude larger during section B than that observed in section A, although sections A and B experienced similar tidal conditions (Figure H.4). The increased wind speed in section B seemed responsible for the difference in time-averaged Reynolds stress $\rho \overline{v_x v_z}$.
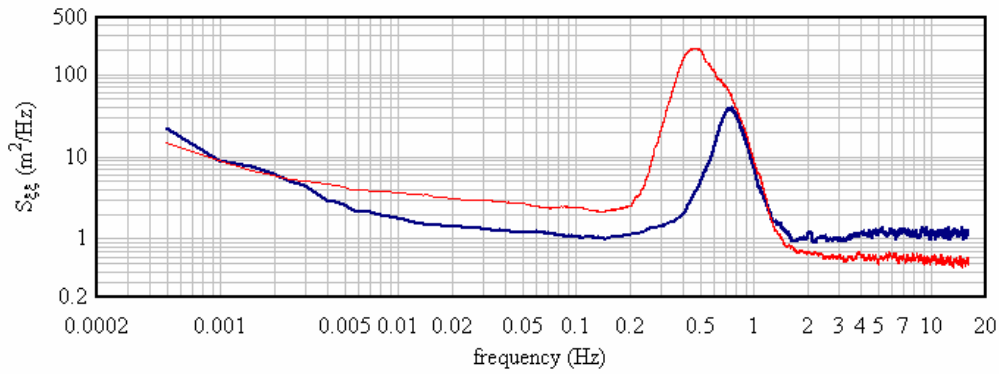
Figure H.5 – Smoothed water level spectra $S_{\xi\xi}$ of sections A and B for water level data collected at Site 1, Hamana Lake for study HLJ3. Spectra smoothed using a window size of 256 data points.

Legend: — $S_{\xi\xi}$ (section A t = 50,400 to 70,400 s); — $S_{\xi\xi}$ (section B t = 138,200 to 158,200 s).
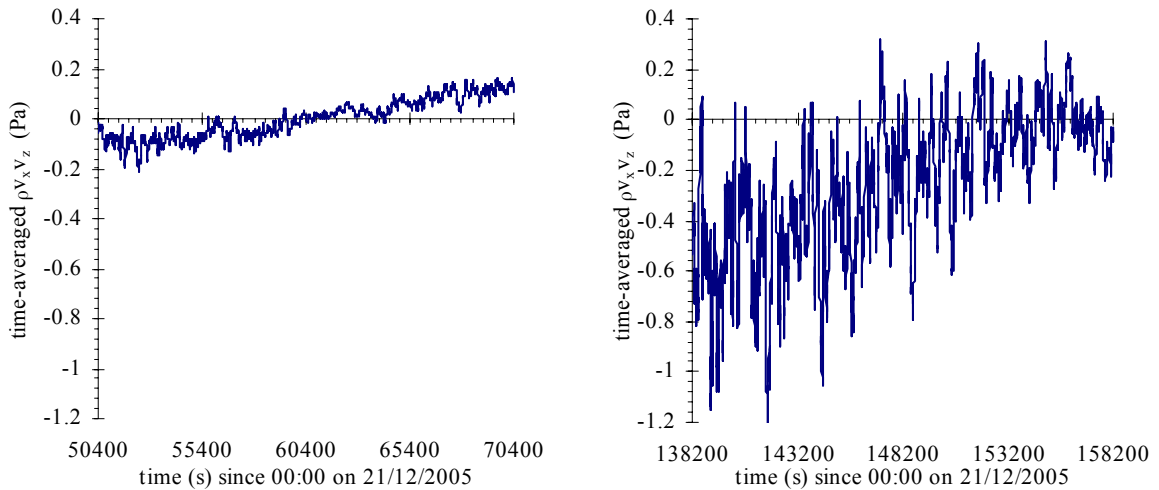
(A) Section A data – "low" wind speed.   (B) Section B data – "strong" wind speed.

Figure H.6 – Time-averaged Reynolds stress $\overline{\rho v_x v_z}$ as a function of time since midnight on 21/12/05. Data collected 0.25 m above bed at Site 1, Hamana Lake for study HLJ3. Reynolds stress averaged over 5,000 data points every 10 s along entire gross data set.

H.2.1   Effect of wind waves on the gross turbulence data: Study HLJ3 (sections A and B)

The gross turbulence data is the raw data measured at Site 1 after ADV after the application of signal post-processing (e.g. Chanson et al. (2005b)). Tables H.3 and H.4 present the median values of the standard deviations for all velocity components and tangential Reynolds stresses of sections A and B. Both gross and wave induced data are shown.

In Tables H.3 and H.4 the differences in median values of all standard deviations between sections A and B were consistent. These indicated that the gross data were predominantly influenced by the wind waves and not by the tidal current for the study HLJ3. For example, the median values of the standard deviations of the gross and wave induced tangential

315

Reynolds stresses of section B were an order of magnitude larger than those of section A. This simple comparison confirmed that the influence of the wind waves dominated the flow turbulence observed 0.25 m above the bed.

Table H.3 – Median values of standard deviations for all velocity components and tangential Reynolds stresses of gross velocity data for sections A and B of study HLJ3. Standard deviations calculated for 5,000 data points every 10 s along entire data set.

Section	$v_x^{'}$ (m/s)	$v_y^{'}$ (m/s)	$v_z^{'}$ (m/s)	$(\rho v_x v_y)^{'}$ (Pa)	$(\rho v_x v_z)^{'}$ (Pa)	$(\rho v_y v_z)^{'}$ (Pa)
A	0.0257	0.0282	0.0186	0.784	0.493	0.532
B	0.0798	0.0982	0.044	8.685	3.606	4.233

Table H.4 – Median values of standard deviations for all velocity components and tangential Reynolds stresses for wave induced data for sections A and B of study HLJ3. Standard deviations calculated for 5,000 data points every 10 s along entire data set.

Section	$v_x^{'W}$ (m/s)	$v_y^{'W}$ (m/s)	$v_z^{'W}$ (m/s)	$(\rho v_x v_y)^{'W}$ (Pa)	$(\rho v_x v_z)^{'W}$ (Pa)	$(\rho v_y v_z)^{'W}$ (Pa)
A	0.0204	0.0205	0.0152	0.456	0.319	0.317
B	0.0768	0.0951	0.0418	7.899	3.243	3.390

H.3 EFFECT OF WIND WAVES ON TURBULENT MIXING AND SEDIMENT TRANSPORT

The effects of wind waves on turbulent mixing are investigated using the time-averaged Reynolds stresses $\rho \overline{v_x v_z}$, $\rho \overline{v_x v_y}$ and the turbulent kinetic energy E_{TK} for the field study HLJ3. Tangential Reynolds stresses describe the transport effects resulting from turbulent motion induced by velocity fluctuations with their subsequent increase of momentum exchange and mixing (Piquet (1999)). Turbulent kinetic energy: $E_{TK} = 0.5 * (v_x^2 + v_y^2 + v_z^2)$ represents the level of turbulence, or the strength of deviations for the instantaneous velocities from the mean velocities (Nikora et al. (2002)).

Bed shear stress and the Shields parameter are important parameters used for investigating sediment transport (Nielsen (1992)). The influences of wind waves on the sediment transport are investigated using the time-averaged bed shear stress $\overline{\tau_b}$ and Shields parameter $\overline{\theta}$. Bed shear stress is a measure of the shear stress being applied to the bed by the fluid motion, while the Shields parameter is the non-dimensional tractive stress due to skin friction.

H.3.1 Time-averaged tangential Reynolds stress $\rho\overline{v_x v_z}$

The time-averaged Reynolds stress $\rho\overline{v_x v_z}$ represents the fluctuations in vertical velocity generated by the fluctuations of streamwise velocity. It is an important property in the study of turbulent mixing in estuaries because it represents the vertical shear stress generated by the streamwise velocity. Previous studies have also noted some strong correlation between the time-averaged Reynolds stress $\rho\overline{v_x v_z}$ and suspended sediment concentration (e.g. West et al. (1984), West and Oduyemi (1989), Kawanisi and Yokosi (1997)).

The time-averaged tangential Reynolds stress $\rho\overline{v_x v_z}$ of both gross and current induced data varied with the tides. For all field studies at Hamana Lake the Reynolds stress $\rho\overline{v_x v_z}$ was predominantly positive during the flood tide and negative during the ebb tide. This same pattern in $\rho\overline{v_x v_z}$ was observed by Osonphasop (1983), Kawanisi and Yokosi (1993) and van der Ham et al. (2001) during independent studies in estuaries. Figure H.7 shows the time-averaged Reynolds stress $\rho\overline{v_x v_z}$ of the gross, wave induced and current induced data as functions of time for sections A and B of the study HLJ3.

During the lower wind speed conditions (section A, Figure H.7A) the correlation between the gross data and current induced data (R ~ 85 %) was slightly larger than that of the gross and wave induced data (R ~ 75 %). This finding may suggest that the current induced velocity dominated the generation of time-averaged Reynolds stress $\rho\overline{v_x v_z}$ during the low wind speed periods. Figure H.7B suggests some correlation between the time-averaged Reynolds stress $\rho\overline{v_x v_z}$ oscillations of the gross and wave induced data throughout the stronger wind period of section B. The correlation coefficient was greater than 90 % throughout all of section B. This result suggests that the effect of wind waves dominated the variation of time-averaged Reynolds stress $\rho\overline{v_x v_z}$ during section B of the study HLJ3.
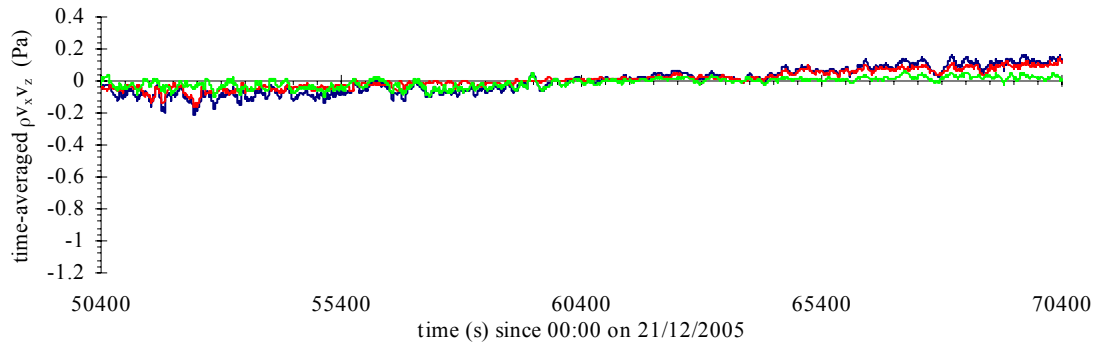
(A) Data section A (t = 50,400 to 70,400 s).
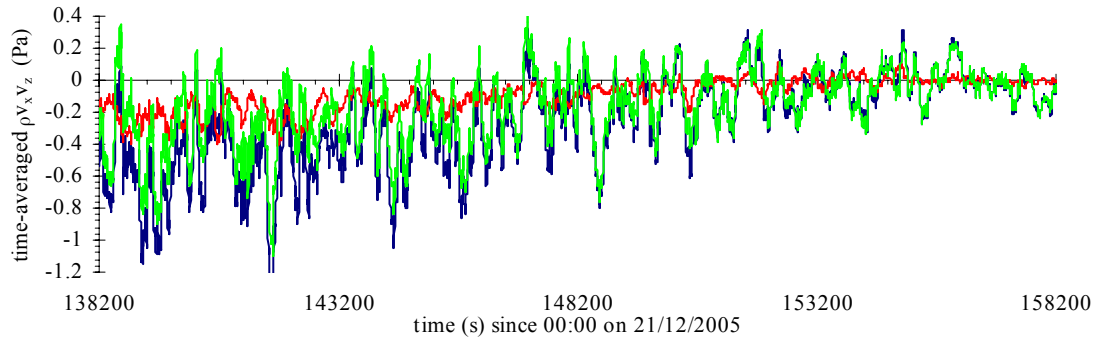
(B) Data section B (t = 138,200 to 158,200 s).

Figure H.7 – Time-averaged Reynolds stress $\overline{\rho v_x v_z}$ as a function of time since midnight on 21/12/05. Data collected 0.25 m above bed at Site 1 Hamana Lake for study HLJ3. Data averaged over 5,000 data points every 10 s along entire data set.

Legend: —— gross data; —— current induced data; —— wave induced data.

H.3.2   Time-averaged tangential Reynolds stress $\overline{\rho v_x v_y}$

The Reynolds stress $\overline{\rho v_x v_y}$ represents the shear stress generated in the horizontal plane at the sampling volume. It provides some information on the horizontal shear stress, turbulent structure and wind shear measured in the sampling volume. Figure H.8 shows the time-averaged Reynolds stress $\overline{\rho v_x v_y}$ of the gross, wave induced and current induced data as functions of time for sections A and B of the study HLJ3.

In section A the magnitude of the time-averaged Reynolds stress $\overline{\rho v_x v_y}$ were similar for the gross, current induced and wave induced data (Figure H.8A). The time-averaged Reynolds stress $\overline{\rho v_x v_y}$ was an order of magnitude larger during the strong wind speeds of section B (Figure H.8B). This increased magnitude of $\overline{\rho v_x v_y}$ seemed directly related to the increased wind speed.

318
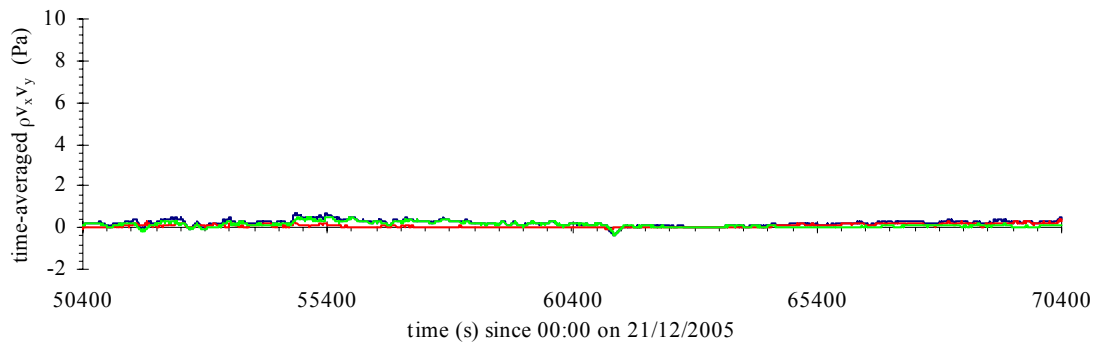
(A) Data section A (t = 50,400 to 70,400 s).
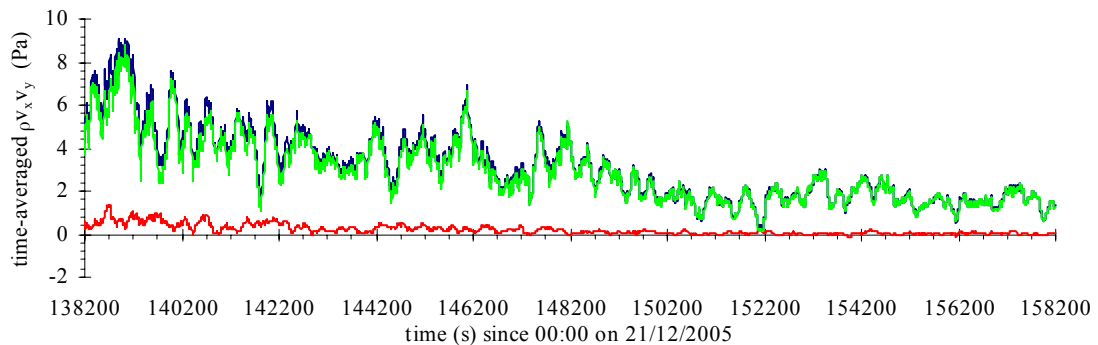
(B) Data section B (t = 138,200 to 158,200 s).

Figure H.8 − Time-averaged Reynolds stress $\rho\overline{v_x v_y}$ as a function of time (s) since midnight on 21/12/05. Data collected 0.25 m above bed at Site 1 Hamana Lake for study HLJ3. Data averaged over 5,000 data points every 10 s along entire data set.

Legend: ── gross data; ── current induced data; ── wave induced data.

H.3.3   Turbulent kinetic energy E_{TK}

The turbulent kinetic energy $E_{TK} = 0.5 * (v_x^2 + v_y^2 + v_z^2)$ represents the level of turbulence observed about the sampling volume. Figure H.9 shows the turbulent kinetic energy E_{TK} of the gross, wave induced and current induced turbulence data as functions of time for sections A and B (study HLJ3). In Figure H.9B the turbulent kinetic energy under strong winds speeds of section B were over an order of magnitude larger than those of section A (Figure H.9A). For strong wind speeds of section B the turbulent kinetic energy magnitude of the gross and wave induced data were an order of magnitude larger than those of the current induced data. In section B there seemed some correlation between the fluctuations of E_{TK} for the gross and wave induced data, with a correlation coefficient of R = 85 %.

319
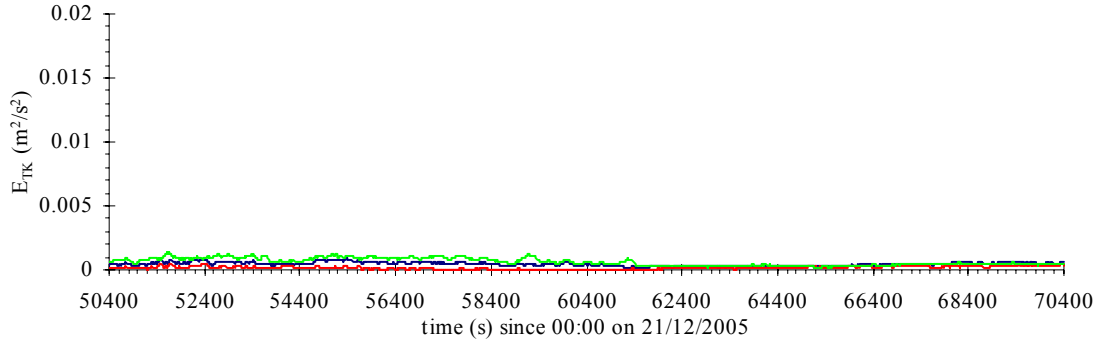
(A) Data section A (t = 50,400 to 70,400 s).
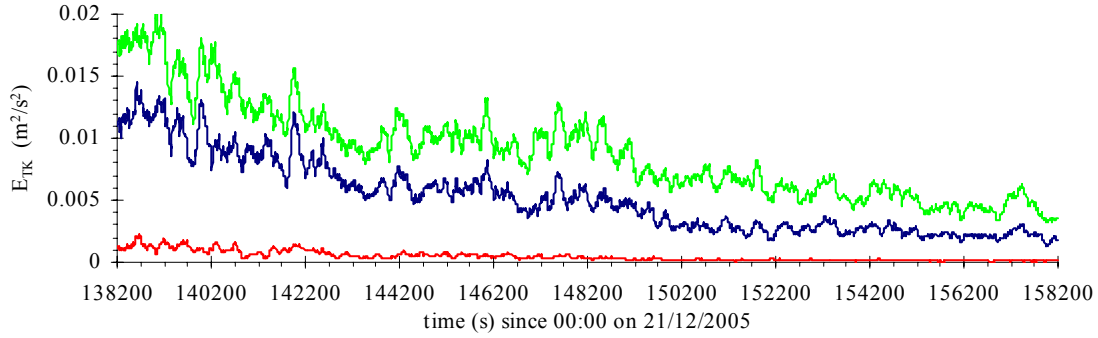
(B) Data section B (t = 138,200 to 158,200 s).

Figure H.9 – Turbulent kinetic energy E_{TK} as a function of time (s) since midnight on 21/12/05. Data collected 0.25 m above bed at Site 1 Hamana Lake for study HLJ3. Turbulent kinetic energy calculated for 5,000 data points every 10 s along entire data set. Legend: — gross data; — current induced data; — wave induced data.

H.3.4   Bed shear stress and Shields parameter

The bed shear stress τ_b and the Shields parameter θ are important properties in the study of sediment transport. Bed shear stress is a measure of the shear stress being applied to the bed by the fluid motion and can be used to find an approximation of the size of sediment suspended (Fredsoe and Deigaard (1992)). The Shields parameter is the non-dimensional tractive stress caused by skin friction and is commonly used to assess whether sediment transport will occur to a particle of a certain size. At Hamana Lake, both tidal currents and wind waves were found to influence the turbulence near the bed, therefore the bed shear stress τ_b was calculated for both currents (Equation H.1) and waves (Equation H.2), using:

$$\tau_b{}^T = \rho \ C_D \ U_{xy} \left| U_{xy} \right| \tag{H.1}$$

$$\tau_b{}^W = 0.5 \ \rho \ f_W \ U_{0.25m}^2 \tag{H.2}$$

where ρ is density of water; Coefficient of drag ($C_D = (\kappa / \ln(z_r/z_o))^2$ Bricker et al. (2005)); $U_{xy} = \sqrt{V_x^2 + V_y^2}$ is horizontal velocity magnitude at 0.25 m above bed; $U_{0.25m}$ is amplitude

320

of wave-orbital velocity at 0.25 m above bed; f_W is wave friction factor ($f_W = \exp(5.213 * ((2.5 * d_{50})/a_W)^{0.194}) - 5.977)$, Nielsen (1992)), d_{50} is grain diameter of 50 percentile ($d_{50} = 0.24$ mm at Site 1 Hamana Lake); κ is von Karman constant ($\kappa = 0.41$ here); z_r is sampling elevation above bed; $z_o = d_{50}/30$; a_W is amplitude of near bed wave-orbital motion. The Shields parameter θ was calculated using the wave induced (τ_b^T) or current induced (τ_b^W) bed shear stress through:

$$\overline{\theta} = \frac{\tau_b}{g \, d_{50} \, (\rho_s - \rho)} \qquad\qquad \text{(H.3)}$$

where g is gravity acceleration; and ρ_s is density of sediment. Figure H.10 shows the time-averaged bed shear stress $\overline{\tau_b}$ and Shields parameter $\overline{\theta}$ values of the wave and current induced data from data sections A and B (study HLJ3) as functions of time. In Figures H.10A and H.10C the time-averaged current induced bed shear stress and Shields parameter varied with the tides for the data of section A. However, in data section B the current induced bed shear stress and Shields parameter showed a similar variation to that of the wave induced data. This seemed related to the increased Westerly wind speed during section B, which increased the transverse velocity magnitude at Site 1.

The magnitude of the wave induced bed shear stress and Shields parameter increased with the wind speed (i.e. larger in section B than section A). However, the magnitude of the current induced bed shear stress and Shields parameter seemed similar for sections A and B. In Figure H.10D the wave induced Shields parameter was larger than the critical Shields parameter value, while the wave induced Shields parameter of section A was lower than the critical value (Figure H.10C). This indicated that during the increased wind speeds of section B, the tractive stress induced by the wind waves alone was enough to facilitate the transportation of sediment.

H.4   DISCUSSION

For the field study HLJ3 the magnitude of the wind speed seemed to determine the dominant effect on the turbulent mixing properties and sediment transport under the surface, that is, the wind waves under strong wind conditions or the tidal current for low wind speeds. From the data of section A (lower wind speed) and section B (strong wind speed) the wind waves seemed to dominate the turbulence properties at 0.25 m above the bed for wind speeds greater than 5 m/s.

This study showed that wind waves have an adverse effect of the measured turbulence properties beneath the surface at Hamana Lake. Therefore, when conducting field studies on large open bodies of water such as Hamana Lake careful attention must be paid to the collection of high frequency wind data close to the sampling location. High frequency wind data is required to fully understand the localised effect of the wind on and below the surface at the sampling location.
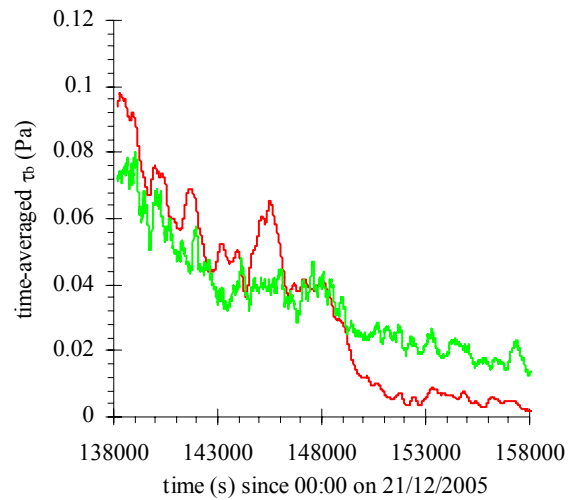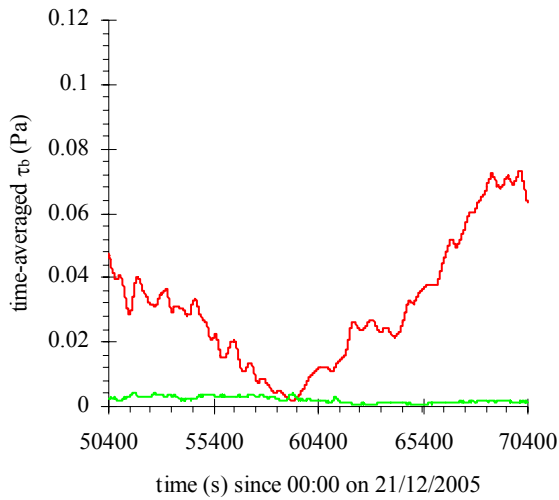
(A) $\overline{\tau}_b$ of section A (t = 50,400 to 70,400 s).   (B) $\overline{\tau}_b$ of section B (t = 138,200 to 158,200 s).
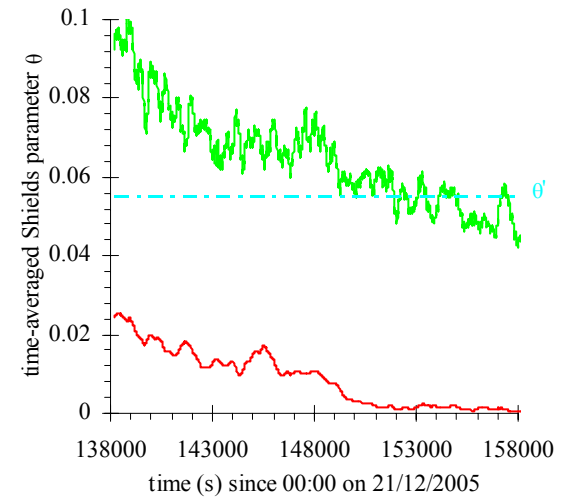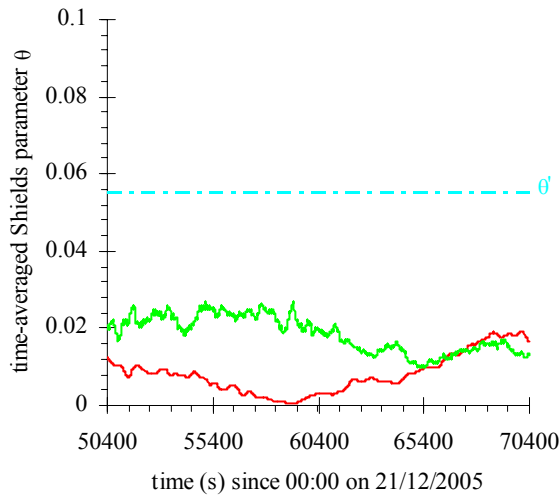
(C) $\overline{\theta}$ of section A (t = 50,400 to 70,400 s).   (D) $\overline{\theta}$ of section B (t = 138,200 to 158,200 s).

Figure H.10 – Time-averaged bed shear stress $\overline{\tau}_b$ and Shields parameter $\overline{\theta}$ values as functions of time. Data collected at 0.25 m above bed at Site 1, Hamana Lake for study HLJ3. Values calculated over 5,000 data points every 10 s along entire data set.

Legend: —— current induced data; —— wave induced data; - - critical value of shields parameter.

APPENDIX I   INVESTIGATION OF CORRELATION BETWEEN WATER QUALITY PROPERTIES AND MOMENTUM

I.1   PRESENTATION

A spectrum analysis was performed on the physio-chemistry data collected at Eprapah Creek by a YSI6600 probe for the field studies E5, E6 and E7 (Table I.1). In each field study the probe sensor was located at 0.1 or 0.4 m above the bed and 0.3 m beside the 3D-ADV (10 MHz). These physio-chemistry spectra were compared to the spectra of the time-averaged velocity data measured by the 3D-ADV (10 MHz). The aim of this comparison was to investigate similar oscillation periods within the velocity and physio-chemistry spectra. A comparison of the velocity and physio-chemistry spectra was conducted by the cross-correlation of two spectra using a technique outlined in Section I.2. Some correlation between the spectra of the velocity component and the physio-chemical property might indicate turbulent momentum mixing of that water quality property occurred.

Table I.1 – Investigation and sampling information for studies E5, E6 and E7.

Study	E5	E6	E7
Date	8-9/03/05	16-18/05/05	5-7/06/06
Focus	Spring tides – middle estuary	Neap tides – middle estuary	Neap tides – upper estuary
Duration (hours)	25	48	50
Tidal range (m)	2.48	1.37	1.52
Rainfall (mm)	0	0	0
Mean depth (m)	1.6	1.6	1.7
Site	2B	2B	3
AMTD (km)	2.1	2.1	3.1
ADV Sampling location	0.1 m above bed, 10.7 m from left bank	0.4 m above bed, 10.7 m from left bank	0.4 m above bed, 4.2 m from right bank
f_{scan} (Hz) 3D-ADV	25	25	25
YSI6600 sampling location	0.1 m above bed, 10.4 m from left bank	0.4 m above bed, 10.4 m from left bank	0.4 m above bed, 3.9 m from right bank
f_{scan} (Hz) YSI6600	0.167	0.083	0.083

Note: AMTD: Australian Middle Thread Distance (upstream from mouth); f_{scan} : sampling frequency; Tidal range: maximum observed at sampling location.

For the field studies E5, E6 and E7 the sampling volumes of the 3D-ADV (10 MHz) and the YSI6600 probe were horizontally aligned with the YSI6600 probe 0.3 m towards the outside

bend (Figure I.1). The YSI6600 probe measured water depth, temperature, conductivity, pH, turbidity, dissolved oxygen and chlorophyll a levels continuously throughout the investigation periods of these studies.
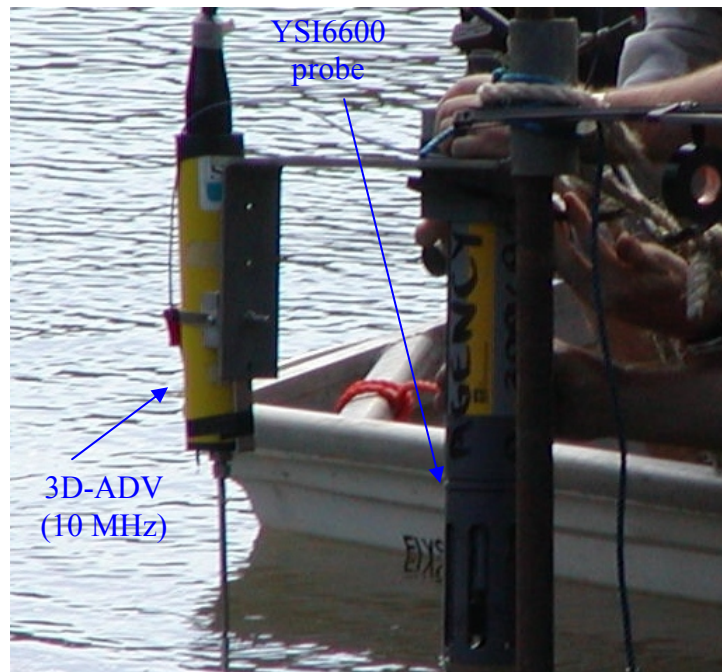
Figure I.1 – Configuration for 3D-ADV (10 MHz) and YSI6600 probe for collecting turbulence and physio-chemistry data. Photograph by H. Chanson for study E2 (17/07/03).

I.2   SPECTRAL CROSS-CORRELATION

Previous studies (e.g. Coy et al. (1997), Arnold and Reilly (1998), Varghese et al. (2000)) used the cross-correlation of spectra to isolate common peaks in energy spectral density. These studies showed that good correlation in the spectra of two independent data sets indicated a common chemical or oscillation frequency within these data sets. Here the cross-correlation between spectra of physio-chemistry and time-averaged velocity data were used to investigate the possible effect of momentum mixing on the measured physio-chemistry. As some correlation between the spectra of a velocity component and a physio-chemistry property might indicate that momentum mixing of that property occurred.

The cross-correlation of the spectra for the synchronised velocity component and physio-chemical property was performed using the "CORREL" function in an excel spreadsheet. A correlation window of 512 data points was applied to the two spectra being analysed with no time lag. The cross-correlation was undertaken at each data point in the frequency domain from the lowest frequency to the highest frequency in the two spectra. Figure I.2 gives a demonstration of the spectral cross-correlation process used.
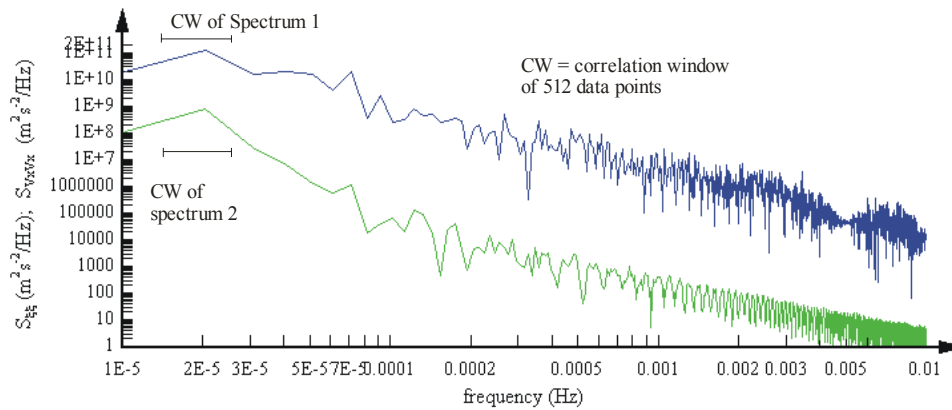
Figure I.2 – Example of cross-correlation between two spectra. Spectrum shown are water level $S_{\xi\xi}$ and streamwise velocity S_{VxVx} data for study E5 (8-9/03/05). Data collected 0.1 m above bed at Site 2B Eprapah Creek.

Legend: — S_{VxVx} ; — $S_{\xi\xi}$.

I.3   RESULTS

Herein the physio-chemistry data were compared to the time-averaged velocity of the field studies E5, E6 and E7. The velocity data were averaged over 200 s and sampled every 6 s (study E5) and 12 s (studies E6 and E7) along the entire data set. This approach provided synchronised time-averaged velocity and physio-chemistry data sampled at the same frequency. A frequency spectrum was generated for each physio-chemistry property and velocity component using a modified version of the "spctrm" sub-routine presented in Press et al. (1992). The spectrum of each physio-chemistry property was then cross-correlated with the spectrum of water level and for each time-averaged velocity component. A possible correlation between two spectra was defined as R > 0.5. Note that no large negative correlations (R < -0.5) were observed for the studies E5, E6 and E7.

In this investigation only oscillation periods between 7,200 and 240 s are discussed, because of a lack of resolution outside this range. The lower limit (7,200 s) was restricted by the 25 hour investigation period of the study E5, while the higher limit (240 s) was restricted by the 12 s sampling frequency of the YSI6600 probe during the studies E6 and E7. In this study each spectrum cross-correlation performed for the field studies E5, E6 and E7 are presented showing the correlation coefficient (R) as a function of frequency.

I.3.1   Field study E5 (8-9/03/2005)

I.3.1.1   *Water level and time-averaged velocity*
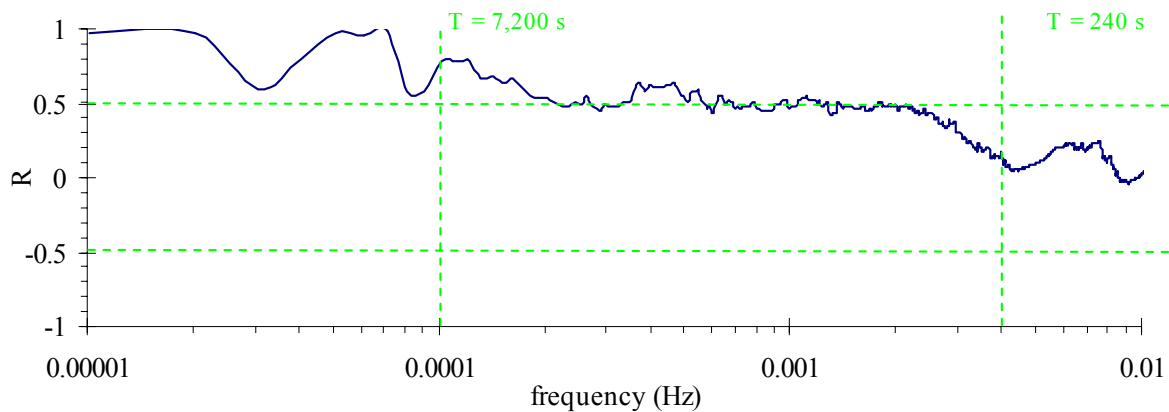
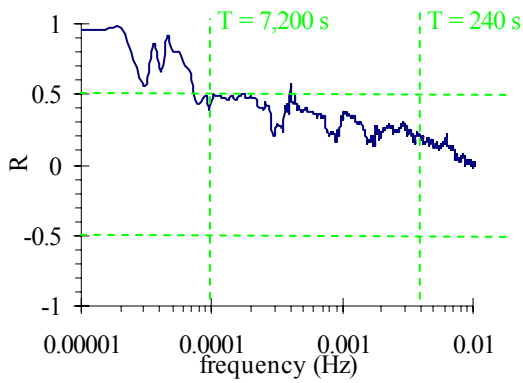(A) Water level and time-averaged streamwise velocity.
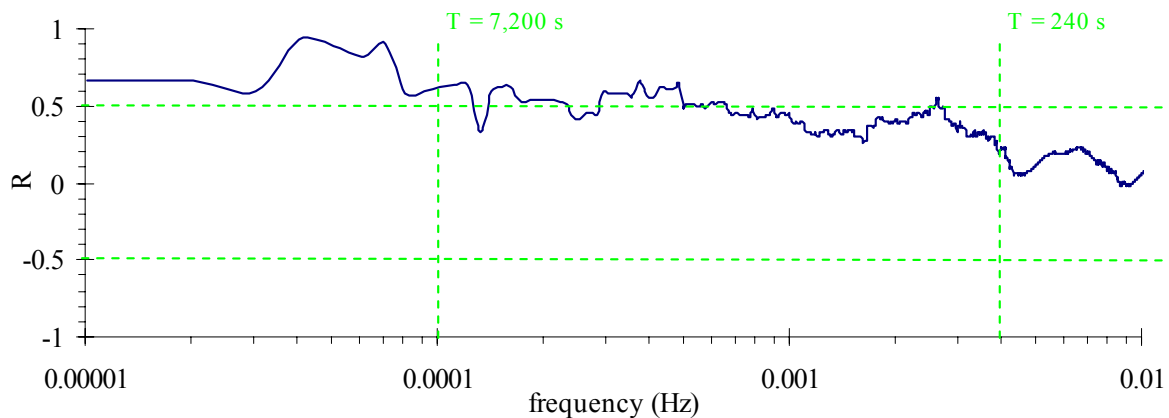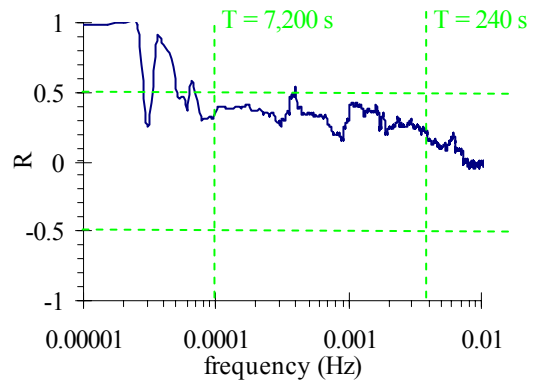

(B) Water level and time-averaged transverse velocity.
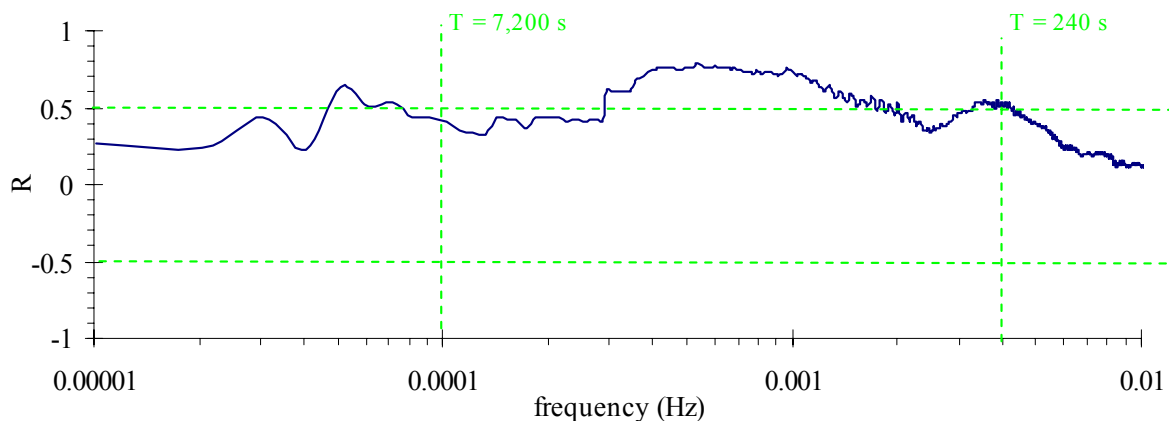
(C) Water level and time-averaged vertical velocity.

Figure I.3 – Cross-correlation between spectra of water level and time-averaged velocities for field study E5 (8-9/03/05). Data collected 0.1 m above bed at Site 2B, Eprapah Creek. Velocity data averaged over 200 s every 6 s along entire data set. Correlation conducted for 512 data points.

I.3.1.2 _Water level and physio-chemistry_
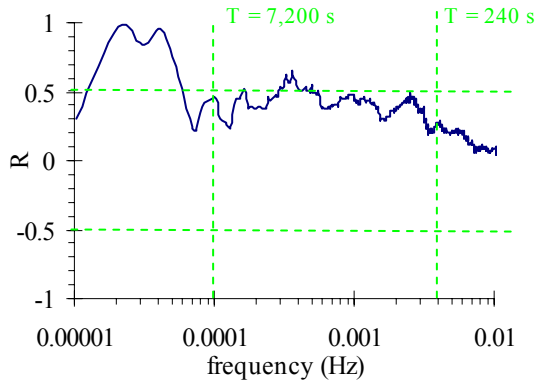
(A) Water level and water temperature.
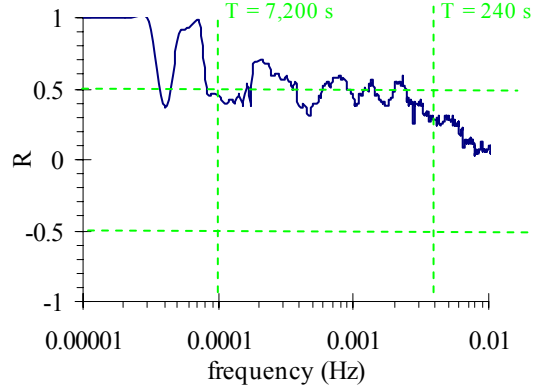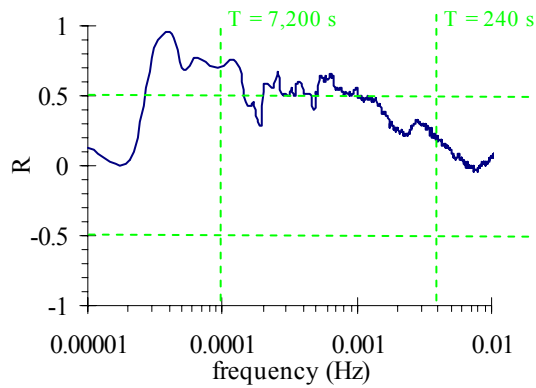
(B) Water level and conductivity.

(C) Water level and turbidity.
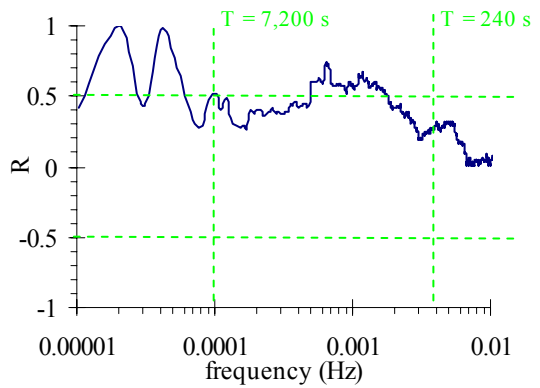
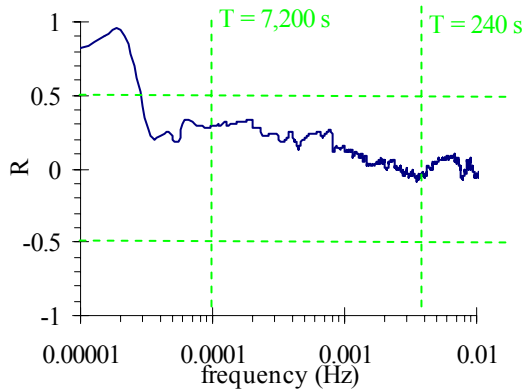(D) Water level and dissolved oxygen.
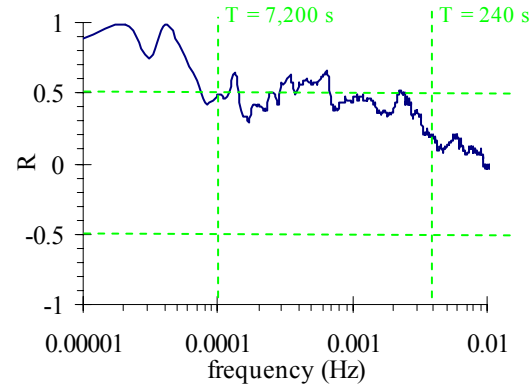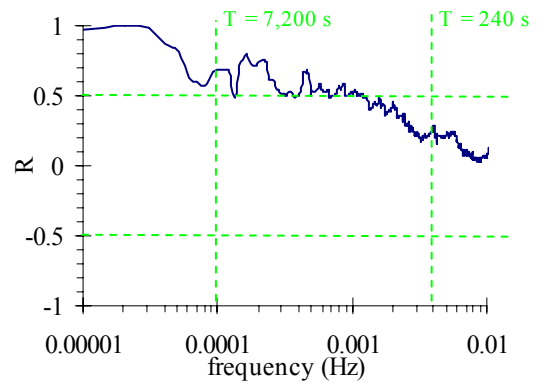
(E) Water level and pH.

(F) Water level and chlorophyll a levels.

Figure I.4 – Cross-correlation between spectra of water level and physio-chemistry data for field study E5 (8-9/03/05). Data collected 0.1 m above bed at Site 2B, Eprapah Creek. Correlation conducted for 512 data points.

I.3.1.3 *Time-averaged streamwise velocity and physio-chemistry*
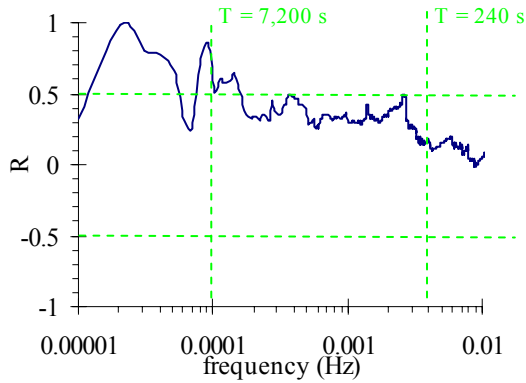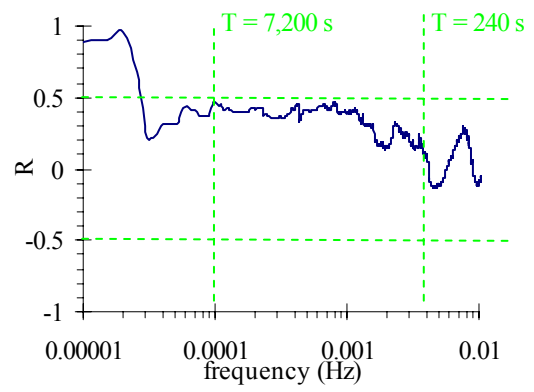

(A) $\overline{V_x}$ and water temperature.
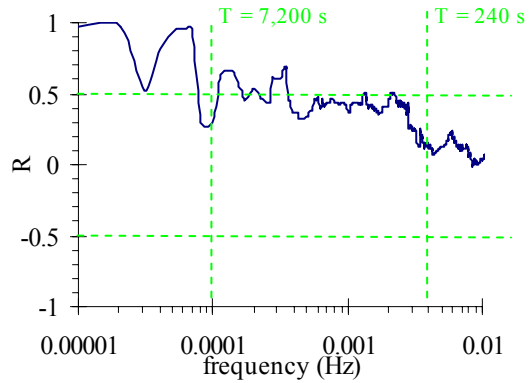
(B) $\overline{V_x}$ and conductivity.
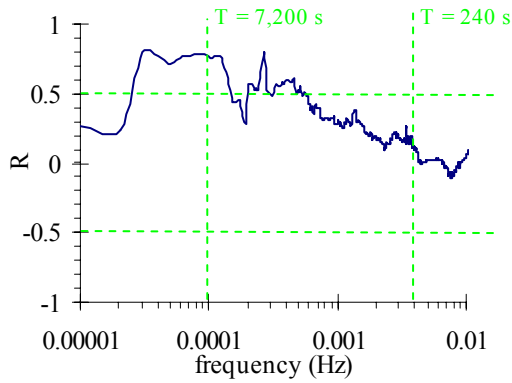
(C) $\overline{V_x}$ and turbidity.
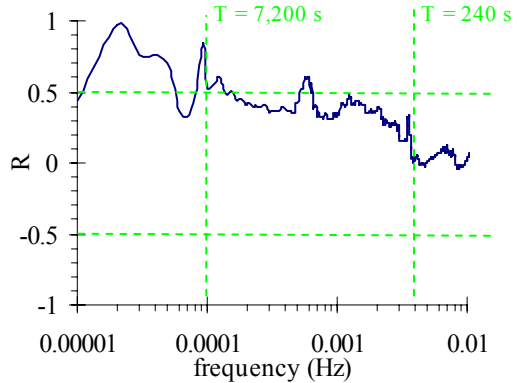
(D) $\overline{V_x}$ and dissolved oxygen.
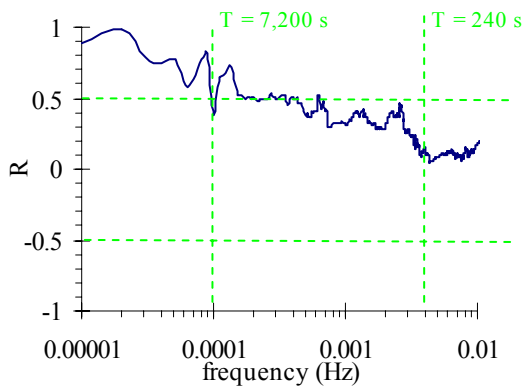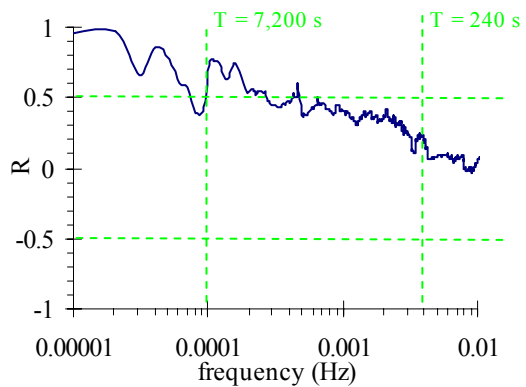
(E) $\overline{V_x}$ and pH.

(F) $\overline{V_x}$ and chlorophyll a levels.

Figure I.5 – Cross-correlation between spectra of time-averaged streamwise velocity $\overline{V_x}$ and physio-chemistry data for study E5 (8-9/03/05). Data collected 0.1 m above bed at Site 2B, Eprapah Creek. Velocity data averaged over 200 s every 6 s along entire data set. Correlation conducted for 512 data points.

I.3.1.4   *Time-averaged transverse velocity and physio-chemistry*
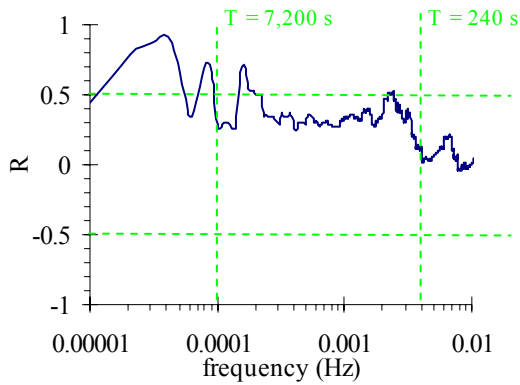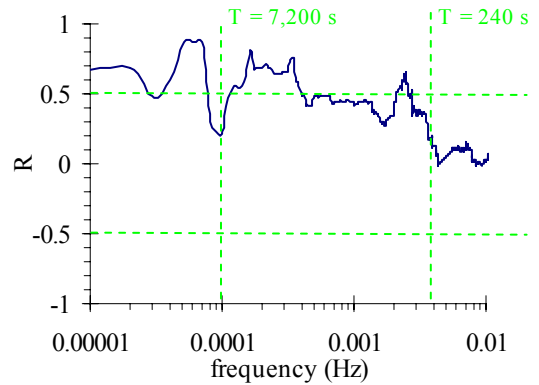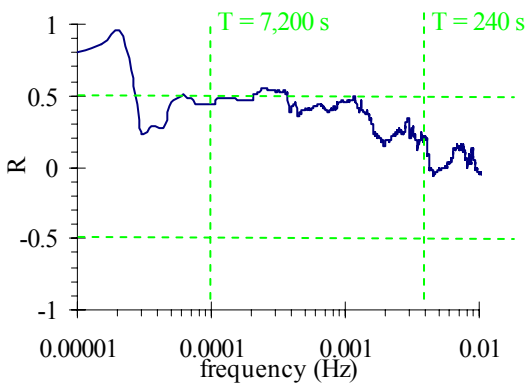

(A) $\overline{V_y}$ and water temperature.

(B) $\overline{V_y}$ and conductivity.
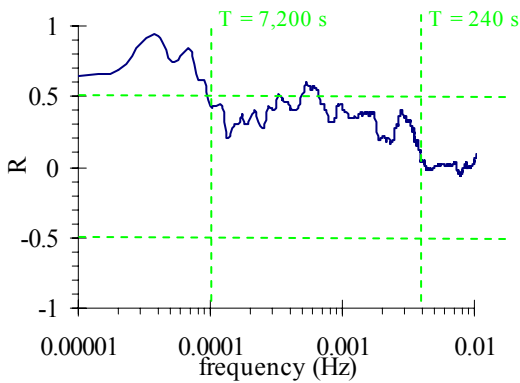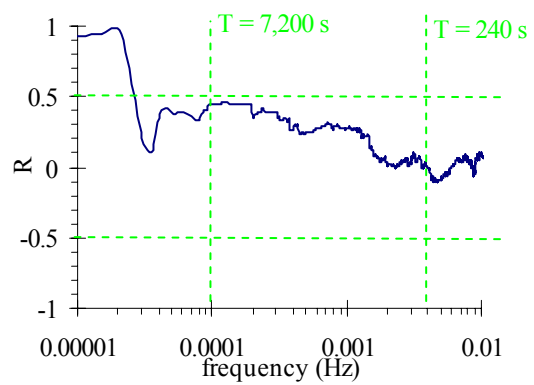
(C) $\overline{V_y}$ and turbidity.
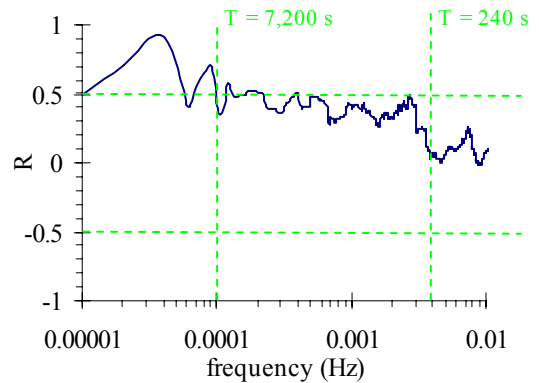
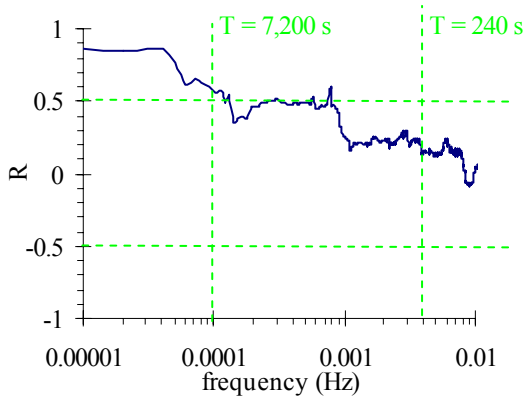(D) $\overline{V_y}$ and dissolved oxygen.
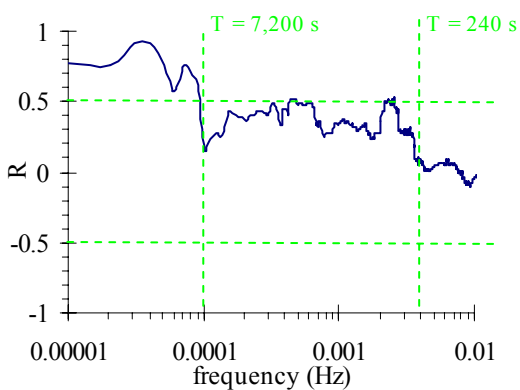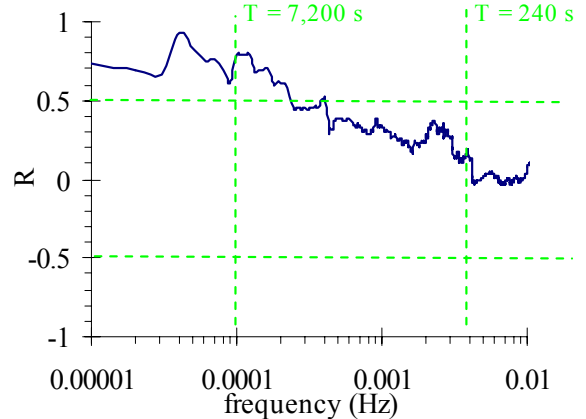
(E) $\overline{V_y}$ and pH.

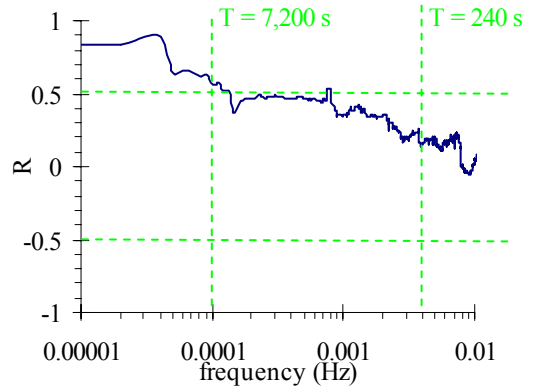(F) $\overline{V_y}$ and chlorophyll a levels.

Figure I.6 – Cross-correlation between spectra of time-averaged transverse velocity $\overline{V_y}$ and physio-chemistry data for study E5 (8-9/03/05). Data collected 0.1 m above bed at Site 2B, Eprapah Creek.   Velocity data averaged over 200 s every 6 s along entire data set. Correlation conducted for 512 data points.
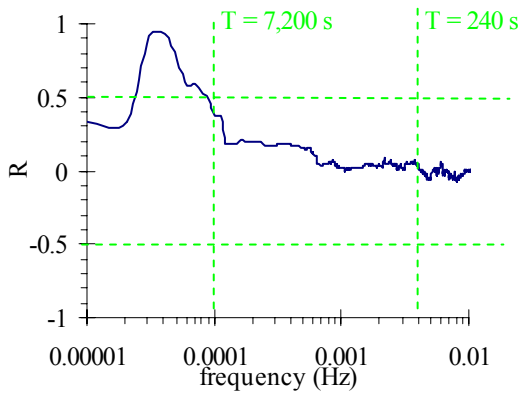
I.3.1.5 *Time-averaged vertical velocity and physio-chemistry*
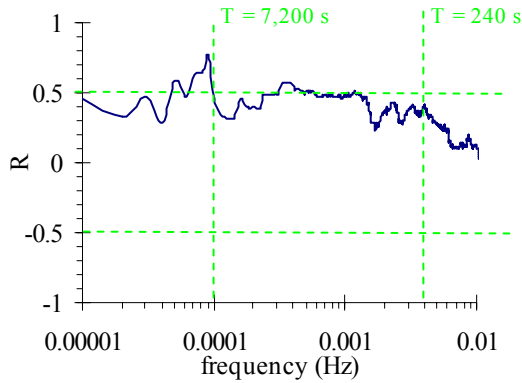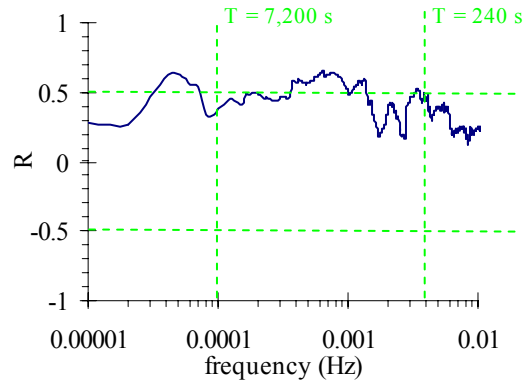

(A) $\overline{V_z}$ and water temperature.

(B) $\overline{V_z}$ and conductivity.
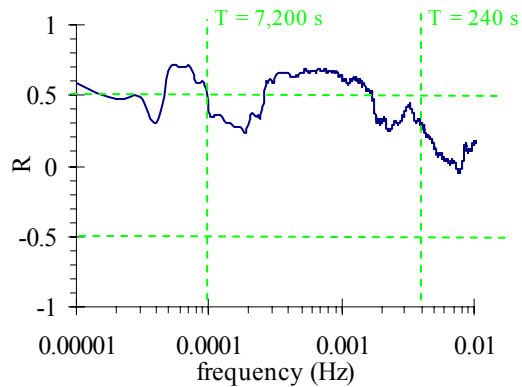
(C) $\overline{V_z}$ and turbidity.
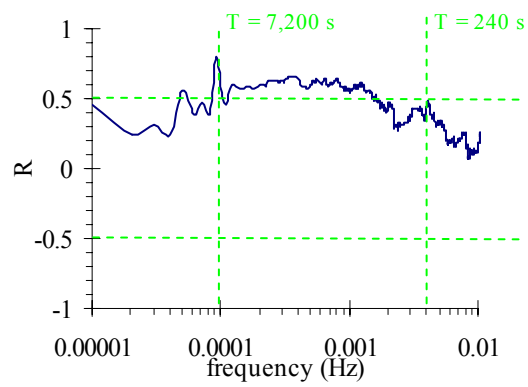
(D) $\overline{V_z}$ and dissolved oxygen.
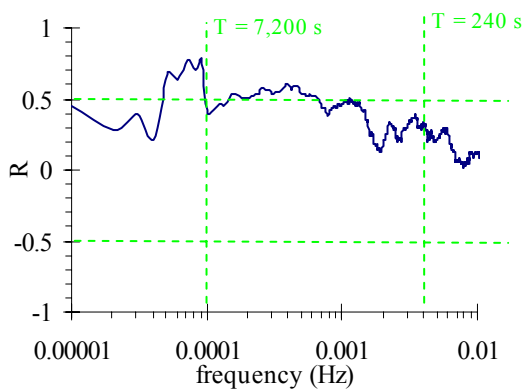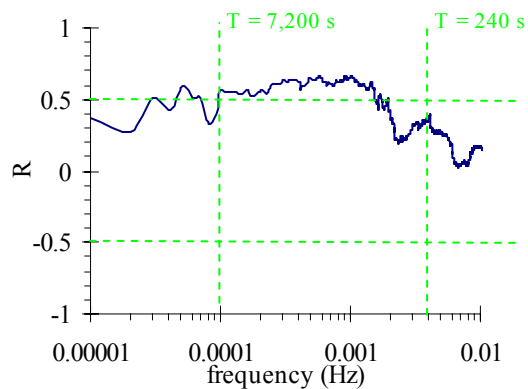
(E) $\overline{V_z}$ and pH.
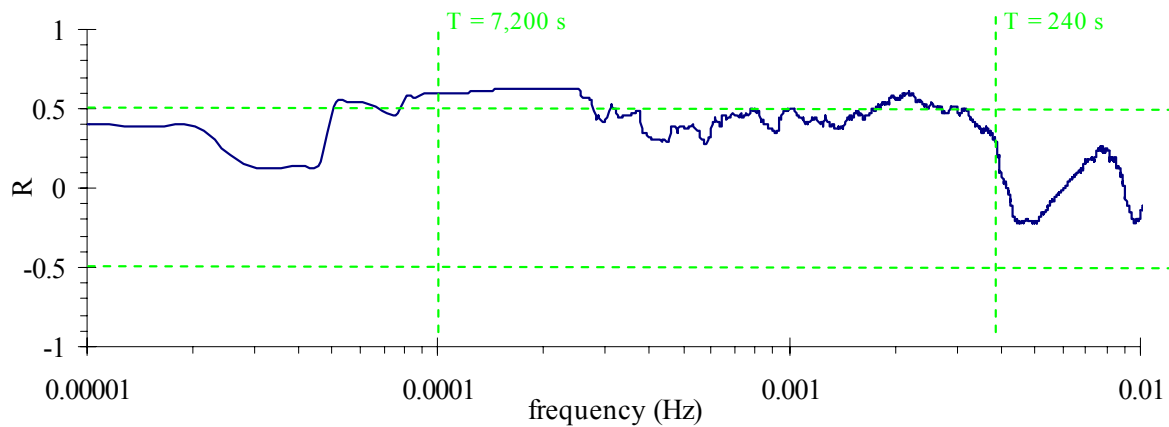
(F) $\overline{V_z}$ and chlorophyll a levels.

Figure I.7 – Cross-correlation between spectra of time-averaged vertical velocity $\overline{V_z}$ and physio-chemistry data for study E5 (8-9/03/05). Data collected 0.1 m above bed at Site 2B, Eprapah Creek. Velocity data averaged over 200 s every 6 s along entire data set. Correlation conducted for 512 data points.

I.3.2.1   Water level and time-averaged velocity
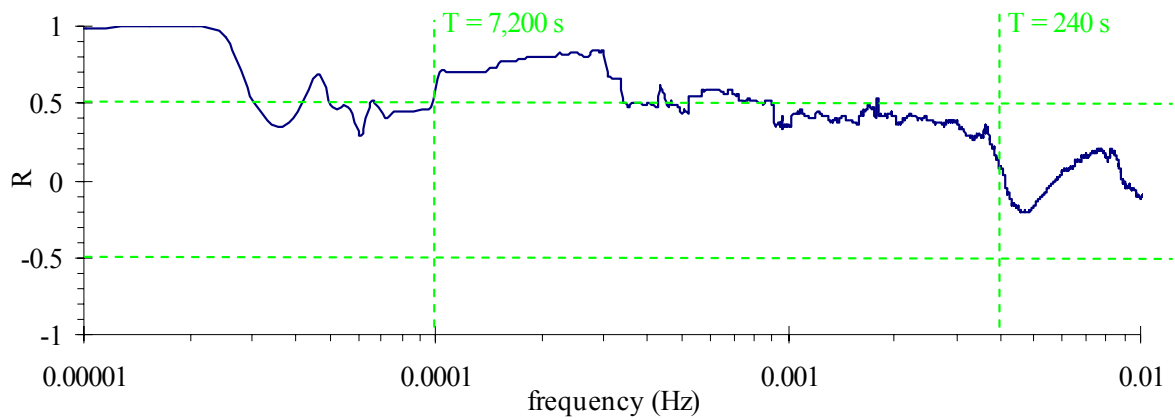
(A) Water level and time-averaged streamwise velocity.

(B) Water level and time-averaged transverse velocity.
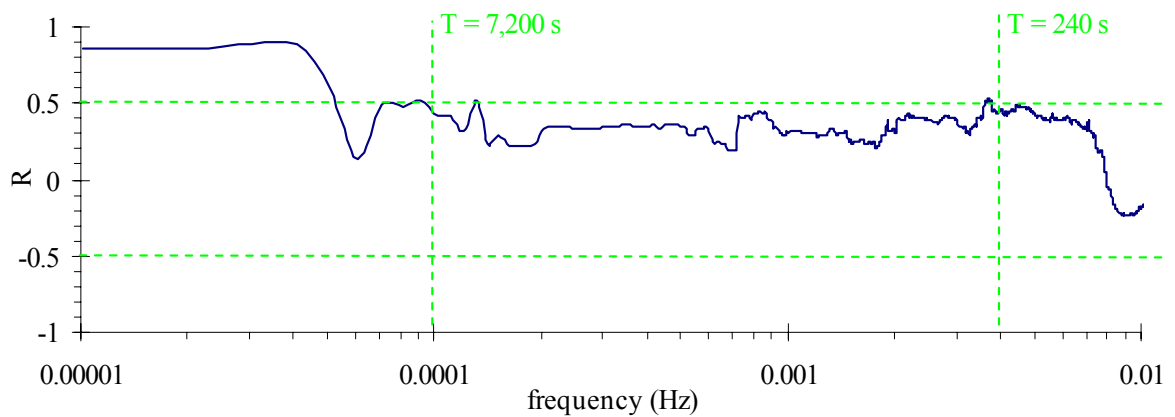
(C) Water level and time-averaged vertical velocity.

Figure I.8 – Cross-correlation between spectra of water level and time-averaged velocities for study E6 (16-18/05/05). Data collected 0.4 m above bed at Site 2B, Eprapah Creek. Velocity data averaged over 200 s every 12 s along entire data set. Correlation conducted for 512 data points.
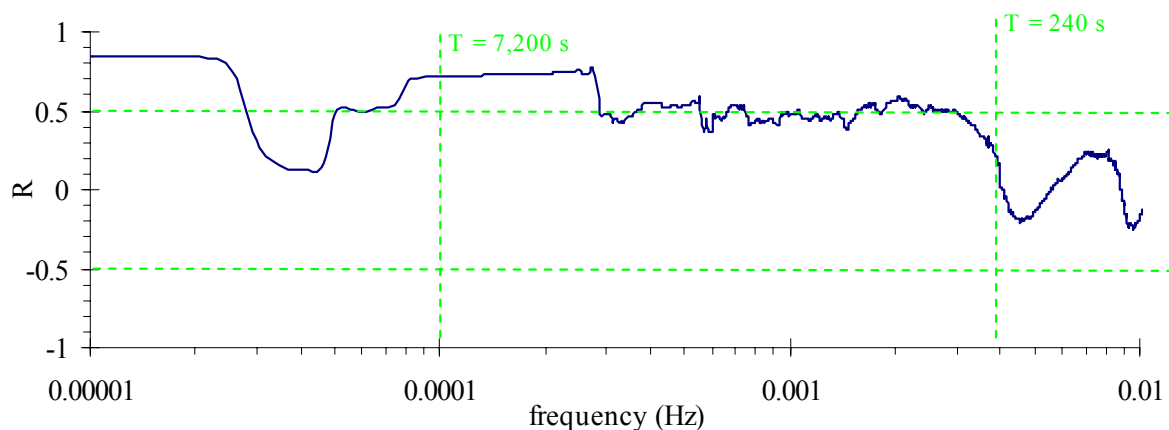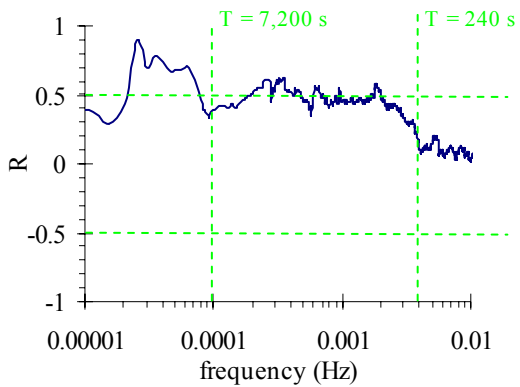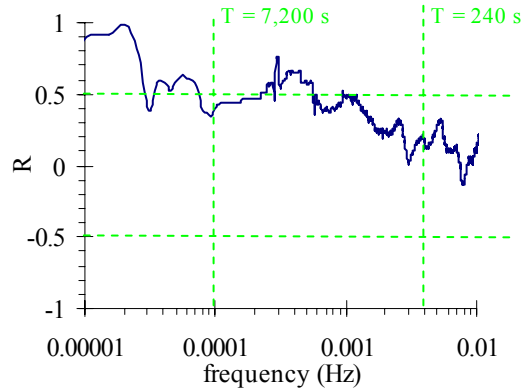
(A) Water level and water temperature.   (B) Water level and conductivity.
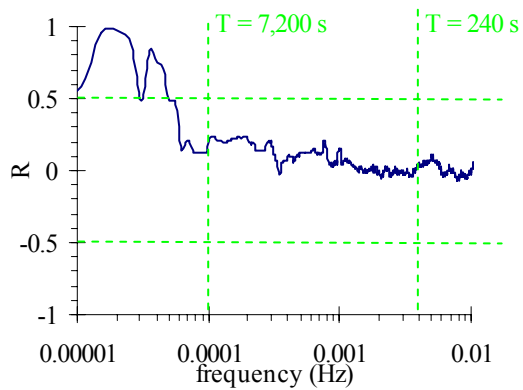
(C) Water level and turbidity.   (D) Water level and dissolved oxygen.
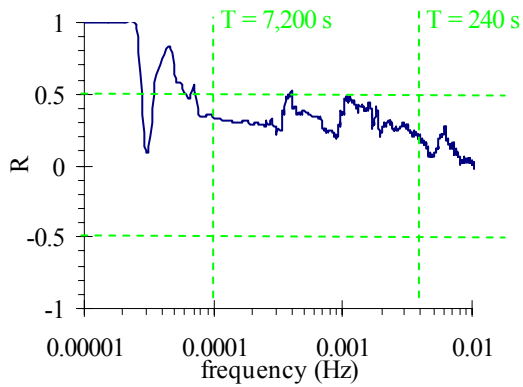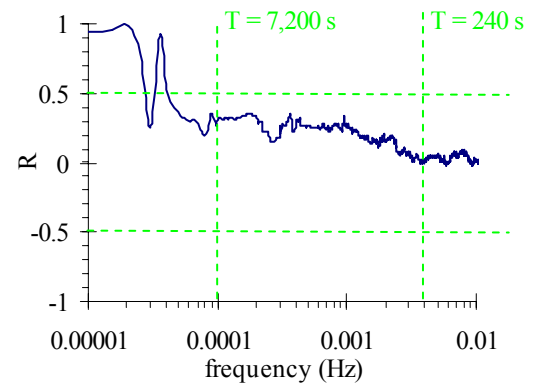
(E) Water level and pH.   (F) Water level and chlorophyll a levels.

Figure I.9 – Cross-correlation between spectra of water level and physio-chemistry data for study E6 (16-18/05/05).   Data collected 0.4 m above bed at Site 2B, Eprapah Creek. Correlation conducted for 512 data points.

(A) $\overline{V_x}$ and water temperature.

(B) $\overline{V_x}$ and conductivity.

(C) $\overline{V_x}$ and turbidity.

(D) $\overline{V_x}$ and dissolved oxygen.

(E) $\overline{V_x}$ and pH.

(F) $\overline{V_x}$ and chlorophyll a levels.

Figure I.10 – Cross-correlation between spectra of time-averaged streamwise velocity $\overline{V_x}$ and physio-chemistry data for study E6 (16-18/05/05). Data collected 0.4 m above bed at Site 2B, Eprapah Creek. Velocity data averaged over 200 s every 12 s along entire data set. Correlation conducted for 512 data points.
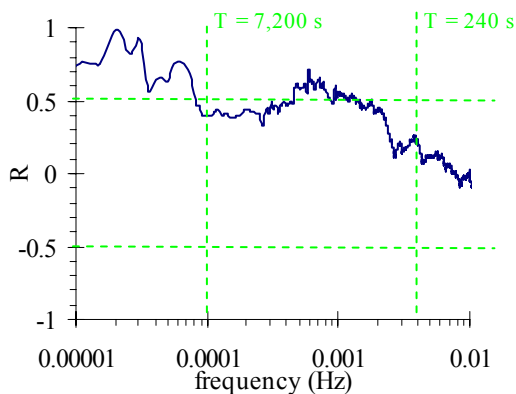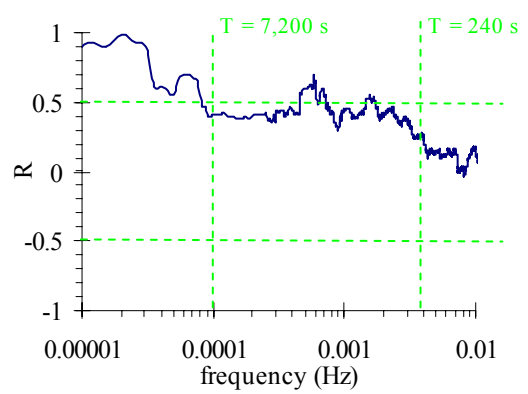
I.3.2.4 *Time-averaged transverse velocity and physio-chemistry*
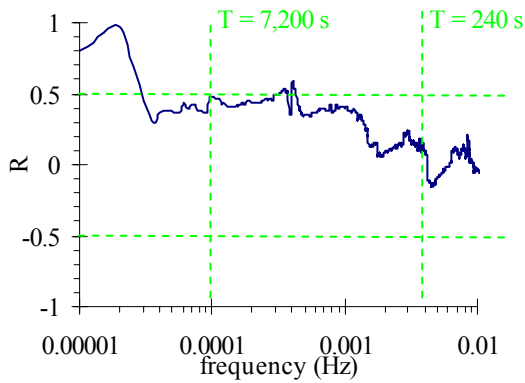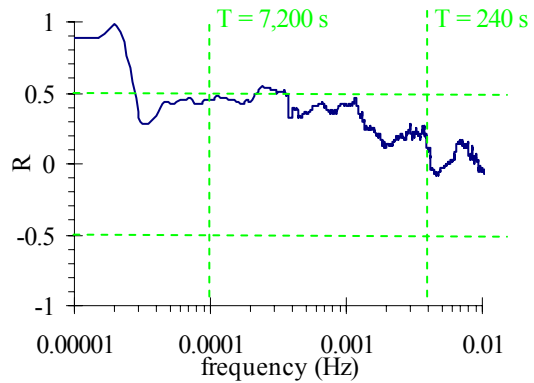
(A) $\overline{V_y}$ and water temperature.

(B) $\overline{V_y}$ and conductivity.

(C) $\overline{V_y}$ and turbidity.

(D) $\overline{V_y}$ and dissolved oxygen.

(E) $\overline{V_y}$ and pH.

(F) $\overline{V_y}$ and chlorophyll a levels.

Figure I.11 − Cross-correlation between spectra of time-averaged transverse velocity $\overline{V_y}$ and physio-chemistry data for study E6 (16-18/05/05). Data collected 0.4 m above bed at Site 2B, Eprapah Creek. Velocity data averaged over 200 s every 12 s along entire data set. Correlation conducted for 512 data points.

I.3.2.5 *Time-averaged vertical velocity and physio-chemistry*

(A) $\overline{V_z}$ and water temperature.

(B) $\overline{V_z}$ and conductivity.

(C) $\overline{V_z}$ and turbidity.
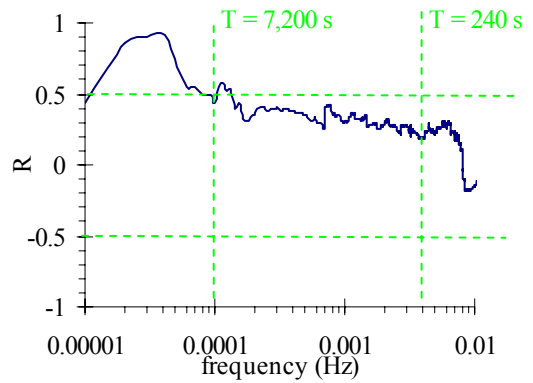
(D) $\overline{V_z}$ and dissolved oxygen.
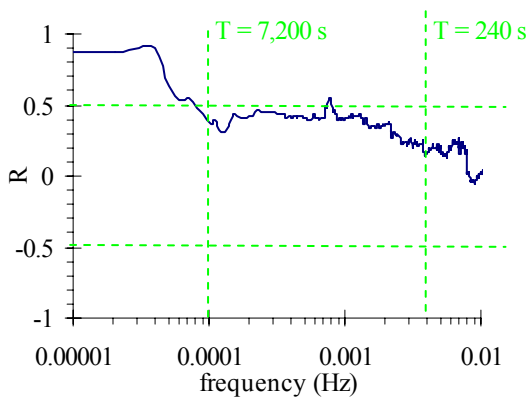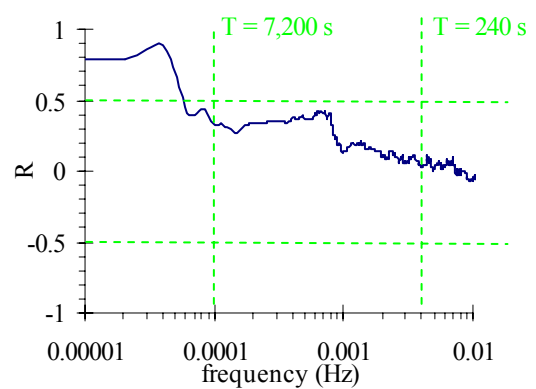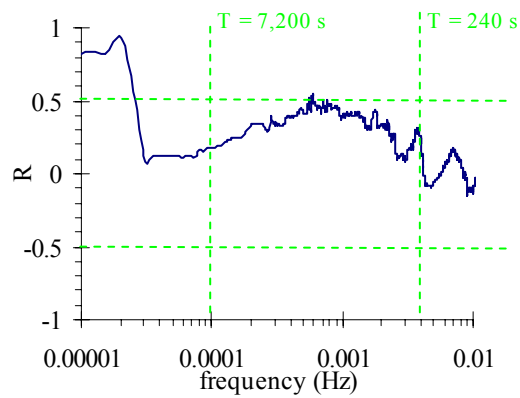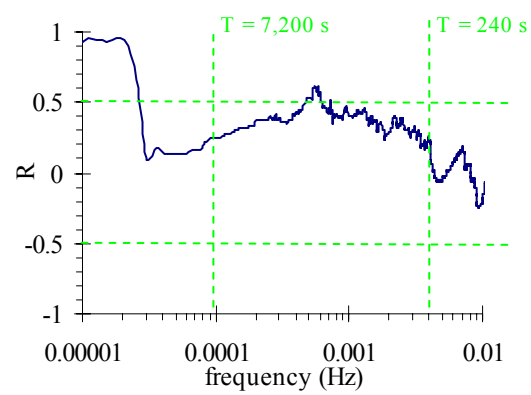
(E) $\overline{V_z}$ and pH.

(F) $\overline{V_z}$ and chlorophyll a levels.

Figure I.12 – Cross-correlation between spectra of time-averaged vertical velocity $\overline{V_z}$ and physio-chemistry data for studyE6 (16-18/05/05). Data collected 0.4 m above bed at Site 2B, Eprapah Creek. Velocity data averaged over 200 s every 12 s along entire data set. Correlation conducted for 512 data points.

I.3.3   Field study E7 (5-7/06/2006)

I.3.3.1   _Water level and time-averaged velocity_
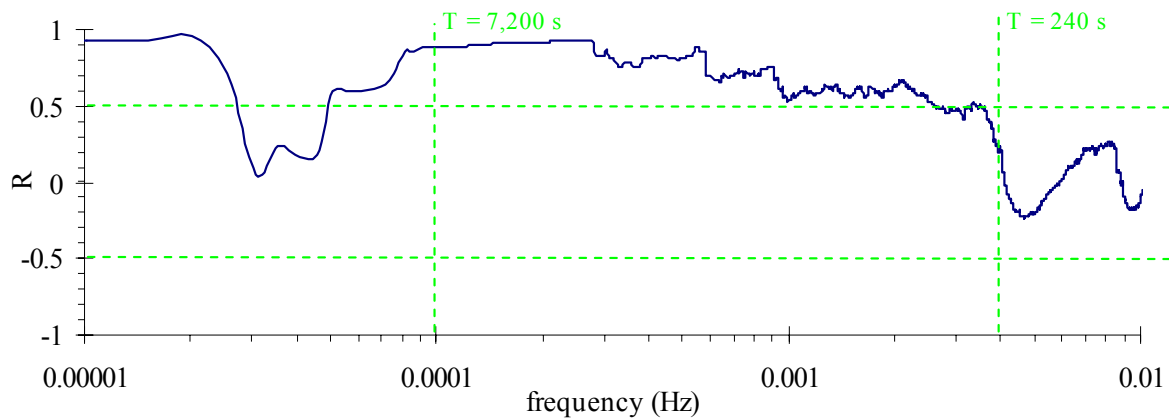
(A) Water level and time-averaged streamwise velocity.

(B) Water level and time-averaged transverse velocity.

(C) Water level and time-averaged vertical velocity.

Figure I.13 – Cross-correlation between spectra of water level and time-averaged velocities for study E7 (5-7/06/06). Data collected 0.4 m above bed at Site 3, Eprapah Creek. Velocity data averaged over 200 s every 12 s along entire data set. Correlation conducted for 512 data points.
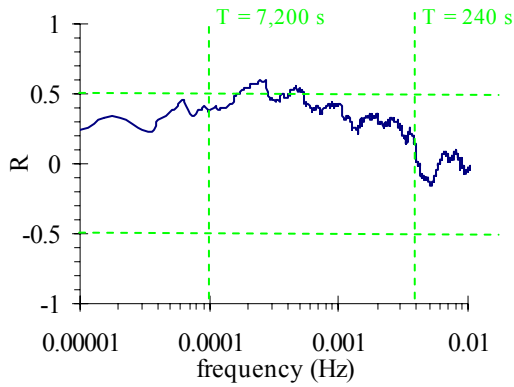
(A) Water level and water temperature.

(B) Water level and conductivity.

(C) Water level and turbidity.

(D) Water level and dissolved oxygen.
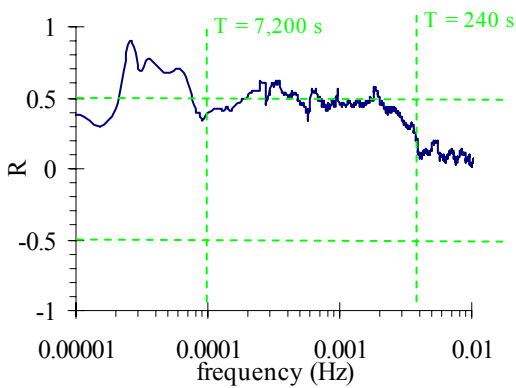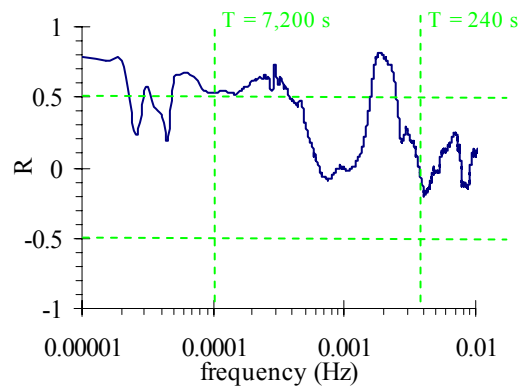
(E) Water level and pH.

(F) Water level and chlorophyll a levels.

Figure I.14 – Cross-correlation between spectra of water level and physio-chemistry data for study E7 (5-7/06/06). Data collected 0.4 m above bed at Site 3, Eprapah Creek. Correlation conducted for 512 data points.

(A) $\overline{V_x}$ and water temperature.

(B) $\overline{V_x}$ and conductivity.

(C) $\overline{V_x}$ and turbidity.

(D) $\overline{V_x}$ and dissolved oxygen.
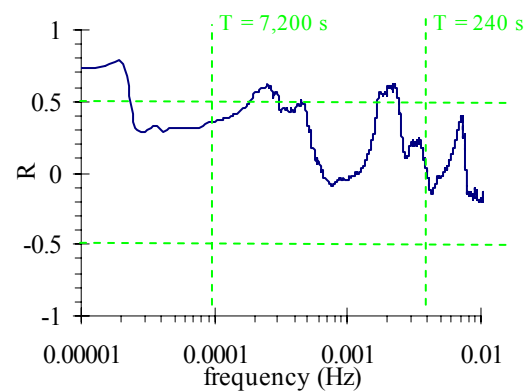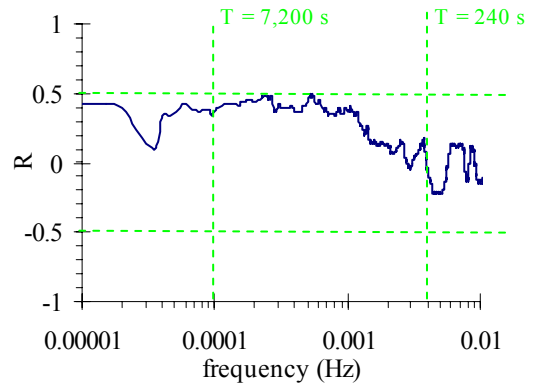
(E) $\overline{V_x}$ and pH.

(F) $\overline{V_x}$ and chlorophyll a levels.

Figure I.15 – Cross-correlation between spectra of time-averaged streamwise velocity $\overline{V_x}$ and physio-chemistry data for study E7 (5-7/06/06). Data collected 0.4 m above bed at Site 3, Eprapah Creek. Velocity data averaged over 200 s every 12 s along entire data set. Correlation conducted for 512 data points.
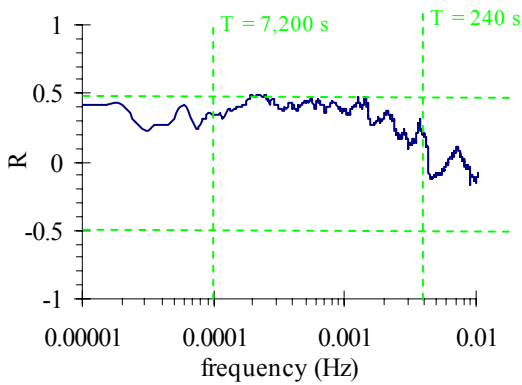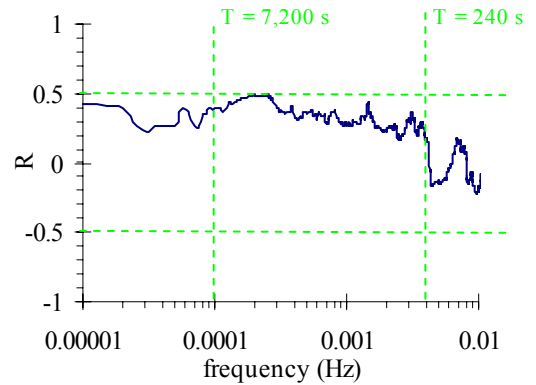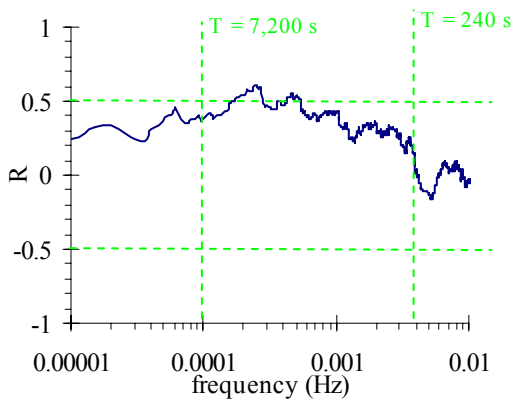
(A) $\overline{V_y}$ and water temperature.

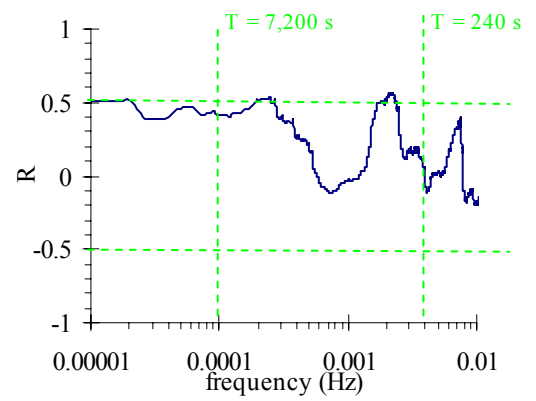(B) $\overline{V_y}$ and conductivity.

(C) $\overline{V_y}$ and turbidity.
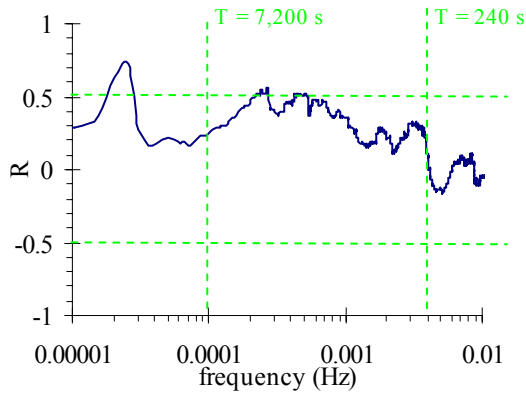
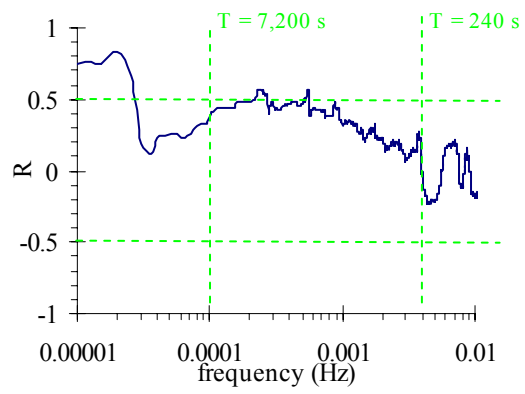(D) $\overline{V_y}$ and dissolved oxygen.

(E) $\overline{V_y}$ and pH.

(F) $\overline{V_y}$ and chlorophyll a levels.

Figure I.16 – Cross-correlation between spectra of time-averaged transverse velocity $\overline{V_y}$ and physio-chemistry data for study E7 (5-7/06/06). Data collected 0.4 m above bed at Site 3, Eprapah Creek. Velocity data averaged over 200 s every 12 s along entire data set. Correlation conducted for 512 data points.

I.3.3.5 *Time-averaged vertical velocity and physio-chemistry*

(A) $\overline{V_z}$ and water temperature.

(B) $\overline{V_z}$ and conductivity.

(C) $\overline{V_z}$ and turbidity.

(D) $\overline{V_z}$ and dissolved oxygen.
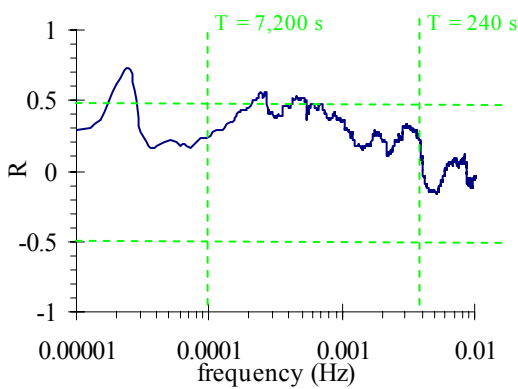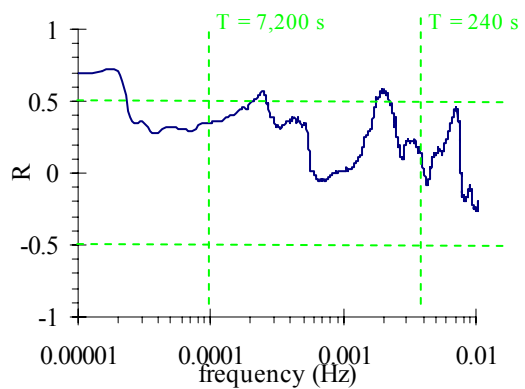
(E) $\overline{V_z}$ and pH.

(F) $\overline{V_z}$ and chlorophyll a levels.

Figure I.17 – Cross-correlation between spectra of time-averaged vertical velocity $\overline{V_z}$ and physio-chemistry data for study E7 (5-7/06/06). Data collected 0.4 m above bed at Site 3, Eprapah Creek. Velocity data averaged over 200 s every 12 s along entire data set. Correlation conducted for 512 data points.
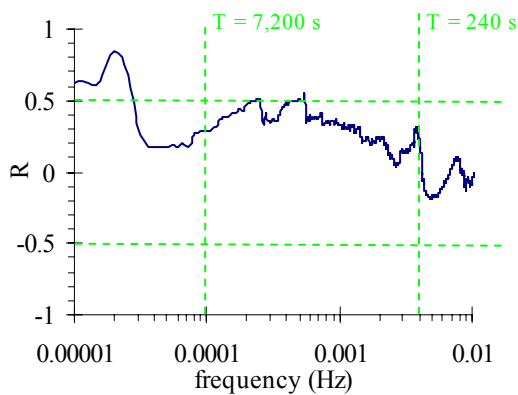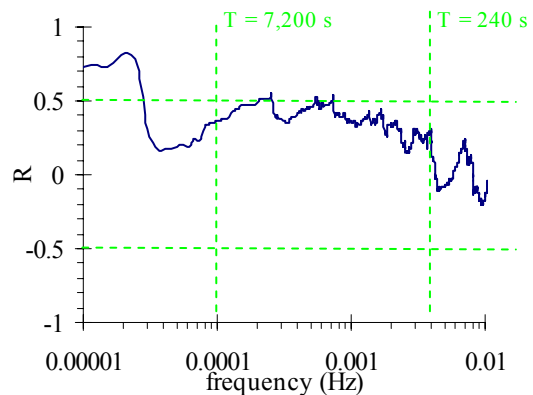
I.4   DISCUSSION

A spectrum cross-correlation analysis of the physio-chemistry and time-averaged velocity data was undertaken to investigate any relationship between momentum and the variation of each physio-chemistry property. In this study the fluctuations in water level and time-averaged velocity were used as a proxy for the fluctuations in momentum. Therefore, some correlation (R > 0.5) between the spectrum of a physio-chemistry property and the spectrum of the water level or a velocity component, conceivably indicated some correlation between momentum mixing and that physio-chemistry property.

Table I.2 presents the oscillation period ranges in which some correlation between momentum and a physio-chemistry property was observed for the field studies E5, E6 and E7. In Table I.2 some correlation between the momentum fluctuations and the fluctuations in all physio-chemistry properties was observed for oscillation periods between 7,200 and 240 s. This indicated that for the field studies E5, E6 and E7 turbulent momentum mixing seemed to be associated with the variations in most physio-chemistry properties for oscillation periods as small as T = 240 s. The impact of turbulent momentum on the mixing of physio-chemistry properties could exist for smaller oscillation periods. However, this investigation was limited by the sampling frequency of the YSI6600 probe.

Table I.2 – Oscillation periods showing some correlation between momentum and physio-chemistry for field studies E5, E6 and E7.

Momentum correlates with:	Study E5 Oscillation periods (s)	Study E6 Oscillation periods (s)	Study E7 Oscillation periods (s)
Water temperature	7,200 to 4,510 3,460 to 1,720 450 to 420	3,310 to 2,240	5,780 to 1,850 1,710 to 1,320 580 to 500
Conductivity	7,200 to 1,000 900 to 700 500 to 280	4,570 to 2,830 1,340 to 1,240	4,650 to 1,790
Chlorophyll a levels	7,200 to 500	##	7,200 to 2,600 620 to 400
Dissolved oxygen	7,200 to 610	7,200 to 2,490 980 to 840	4,950 to 3,880 2,240 to 1,400 680 to 580
pH	6,900 to 1,460 450 to 380	4,830 to 2,710 1,360 to 1,250	5,760 to 1,350 590 to 500
Turbidity	5,010 to 580	##	2,270 to 560

Note: Momentum from fluctuations in time-averaged velocity components and water level; ##: not correlated for periods between 7,200 and 240 s.

The range of correlated oscillation periods between momentum and the physio-chemistry properties seemed larger under spring tidal conditions (study E5) than under neap tidal conditions (studies E6 and E7). Trevethan et al. (2006) found that the intensity of fluctuations of all velocity components and Reynolds stresses were up to an order of magnitude larger mid estuary under spring (study E5) than neap (study E6) tidal conditions. This conceivably indicated that the increased intensity of turbulence fluctuations under spring tides increased the range of physio-chemistry oscillation periods influenced by momentum mixing.

Of note, was that the correlated oscillation period ranges for the field study E7 (Site 3 in upper estuary) were larger than those observed for the study E6 conducted mid estuary at Site 2B under similar neap tidal conditions. The cause of this difference between the correlated oscillation period ranges of the two neap tide studies is presently unknown since the velocity ranges observed for the study E7 were less than those of the study E6.

The results of this investigation seemed to indicate that momentum mixing influenced the variations of all physio-chemistry properties measured by a YSI6600 probe for the range of oscillation periods investigated ($7,200 > T > 240$ s). Theoretically, turbulent momentum could influence the variation of these physio-chemistry properties down to the viscous level, through turbulent energy dissipation. Further investigation is required to prove this, however, any study is limited by the sampling frequency that the physio-chemistry properties or velocity can be measured.